

Interpretation of rock mass yield using apparent stress of microseismic events – examples from  
Glencore's Nickel Rim South Mine, Sudbury, Ontario

by

Oliver Thomas Sousa Carusone

A thesis submitted in partial fulfillment  
of the requirements for the degree of  
Master of Applied Science (M.A.Sc.) in Natural Resources Engineering

Faculty of Graduate Studies  
Laurentian University  
Sudbury, Ontario, Canada

© Oliver Thomas Sousa Carusone, 2018

**THESIS DEFENCE COMMITTEE/COMITÉ DE SOUTENANCE DE THÈSE**  
**Laurentian Université/Université Laurentienne**  
Faculty of Graduate Studies/Faculté des études supérieures

Title of Thesis Titre de la thèse	Interpretation of rock mass yield using apparent stress of microseismic events – examples from Glencore’s Nickel Rim South Mine, Sudbury, ON		
Name of Candidate Nom du candidat	Carusone, Oliver		
Degree Diplôme	Master of Science		
Department/Program Département/Programme	Engineering	Date of Defence Date de la soutenance	May 11, 2018

**APPROVED/APPROUVÉ**

Thesis Examiners/Examineurs de thèse:

Dr. Marty Hudyma  
(Supervisor/Directeur de thèse)

Dr. Phil Dirige  
(Committee member/Membre du comité)

Dr. Shailendra Sharan  
(Committee member/Membre du comité)

Mr. Brad Simiser  
(External Examiner/Examineur externe)

Approved for the Faculty of Graduate Studies  
Approuvé pour la Faculté des études supérieures  
Dr. David Lesbarrères  
Monsieur David Lesbarrères  
Dean, Faculty of Graduate Studies  
Doyen, Faculté des études supérieures

**ACCESSIBILITY CLAUSE AND PERMISSION TO USE**

I, **Oliver Carusone**, hereby grant to Laurentian University and/or its agents the non-exclusive license to archive and make accessible my thesis, dissertation, or project report in whole or in part in all forms of media, now or for the duration of my copyright ownership. I retain all other ownership rights to the copyright of the thesis, dissertation or project report. I also reserve the right to use in future works (such as articles or books) all or part of this thesis, dissertation, or project report. I further agree that permission for copying of this thesis in any manner, in whole or in part, for scholarly purposes may be granted by the professor or professors who supervised my thesis work or, in their absence, by the Head of the Department in which my thesis work was done. It is understood that any copying or publication or use of this thesis or parts thereof for financial gain shall not be allowed without my written permission. It is also understood that this copy is being made available in this form by the authority of the copyright owner solely for the purpose of private study and research and may not be copied or reproduced except as permitted by the copyright laws without written authority from the copyright owner.

## Abstract

Seismic events are manifestations of sudden, inelastic deformations in a rock mass. The characteristics of these deformations are reflected in quantitative descriptors of seismic events, known as seismic source parameters. The seismic source parameter apparent stress ( $\sigma_a$ ) is a relative estimate of co-seismic stress change. This parameter has been used by other authors to infer local stress conditions in a rock mass and how they vary in space and time. This thesis investigates short-term space-time variations in apparent stress in spatially-isolated volumes of a rock mass following open stope blasts. The results are used to infer how the new excavation affects the nearby rock mass. These excavations are expected to cause local stress increases as stress redistributes around the void, and stress decreases as rock mass near the excavation yields and sheds stress.

Data for this research is taken from Glencore's Nickel Rim South Mine (NRSM) in Sudbury, Ontario. This modern operation has a state-of-the-art microseismic monitoring array that consistently locates events with less than 5 m of residual error and provides accurate source parameter estimates for large and small events. NRSM uses a bulk open stoping mining method, which creates large excavations on the order of several thousand tonnes in a matter of a few seconds. The large stress changes and loss of confinement produced by these blasts can generate large seismic responses which provide an abundance of information about rock mass behaviour.

Analysis of apparent stress over time is performed spatially isolating a group of events and tracking apparent stress variation in a moving window. This analysis shows that apparent stress:

- Rapidly increases for a matter of minutes immediately following the blast.
- Gradually decreases for a matter of hours to a lower level than before the blast.
- Slowly increases over a matter of days to weeks.

Based on the mechanics of rock masses near excavations and use of apparent stress to infer local stress conditions, these variations are interpreted to correspond with:

- Mining-induced stress increasing with the creation of a new excavation.
- Stress decreasing as the rock mass near the stope yields and/or enters its post-peak strength.
- Stress increasing farther from the stope as a result of the more damaged rock mass closer to the stope shedding stress onto less damaged regions.

Variations in event-stope distances are also analysed to re-enforce the inferences made based on the variations in apparent stress over time. The analysis of event-stope distances shows that events:

- With high apparent stress tend to locate farther from the stopes than events with low apparent stress.
- Initially move away from the stopes for a matter of hours after the blast.
- Gradually move back towards the stopes for a matter of hours to days.
- Gradually move away from the stopes again for a matter of days to weeks.

The inferred rock mass behaviour based on these variations are:

- Higher stress conditions in more confined and less damaged regions of the rock mass.
- Stress redistributing around the new excavation and creating a new zone of active rock mass yield.
- Yield occurring in a more consistent region of the rock mass as redistribution of stress outside the more damaged regions slows.
- Growth of damaged zones as rock mass yield progresses over time

These observed variations and inferred behaviour are used to propose a conceptual model for rock mass yield which describes the formation of an excavation damage zone following a blast. Further study based on this research may use more detailed aspects of the variations to calibrate constitutive behaviour of rock masses (making it a useful tool for numerical model calibration), or relate variations in apparent stress to the occurrence of large events (making it a useful tool for seismic hazard forecasting).

## Acknowledgements

First, I would like to thank my supervisor Dr. Marty Hudyma for his support, guidance, and patience over the past few years. I have the sincerest appreciation for you giving me the opportunity to conduct this research, and your efforts to provide me with so many interesting experiences and opportunities.

I would also like to thank all the industry professionals who lent me some of their valuable time to answer my questions about all things practical and theoretical, and tour me around their operations.

Financial support for this research was provided by Agnico Eagle's LaRonde Mine, KGHM's Morrison Mine, Vale's Coleman Mine, The Natural Sciences and Engineering Research Council (NSERC), and The Australian Centre for Geomechanics.

Special thanks to Glencore for allowing the publication of this thesis.

Lastly, to my parents, Helen and Joseph, and my fiancé, Melissa, thank you for your constant encouragement, support, and love.

# Table of Contents

Abstract.....	iii
Acknowledgements.....	v
List of Tables .....	x
List of Figures.....	xi
List of Frequently Used Symbols and Abbreviations.....	xxii
1 Introduction.....	1
1.1 Scope.....	2
1.2 Thesis Structure.....	3
2 Literature Review.....	5
2.1 Mechanics of Rock Masses and Application in Mining .....	5
2.1.1 In-Situ Stress.....	5
2.1.2 Mining-Induced Stress.....	5
2.1.3 Constitutive Behavior of Rock Masses.....	7
2.1.4 Excavation damage zones.....	10
2.2 Seismicity and Mining-Induced Seismicity .....	16
2.2.1 Seismic Events.....	16
2.2.2 Mining-Induced Seismicity.....	18
2.2.3 Rockbursts.....	19
2.2.4 Seismic Source Mechanism .....	20
2.2.5 Seismic Monitoring in Mines.....	23
2.3 Seismic Source Parameters .....	26
2.3.1 Location and Time .....	26
2.3.2 Magnitude .....	26
2.3.3 Energy.....	27
2.3.4 Moment.....	28
2.3.5 Apparent Stress.....	29
2.4 Seismic Data Analysis Techniques .....	31
2.4.1 Magnitude-Time Histories .....	31
2.4.2 Frequency-Magnitude.....	32
2.4.3 Diurnal Charts.....	35
2.4.4 Energy-Moment .....	36
2.4.5 Event Locations .....	39
2.4.6 Spatial Variations in Apparent Stress .....	47

2.4.7	Temporal Variations in Apparent Stress.....	49
2.4.8	Energy Index and Cumulative Apparent Volume.....	51
2.5	Seismicity and Constitutive Behaviour of Rock Masses .....	55
3	Nickel Rim South Mine .....	61
3.1	Regional and Local Geology.....	61
3.1.1	Regional Setting.....	61
3.1.2	Local Geology.....	63
3.1.3	In-Situ Stresses.....	69
3.1.4	Faults.....	70
3.2	Mine Design and Mining Methods.....	72
3.2.1	Mine Layout.....	73
3.2.2	Transverse Blasthole Open Stopping.....	75
3.2.3	Stope Sequencing.....	76
3.3	Seismic Monitoring.....	81
3.3.1	Seismic Monitoring Array .....	81
3.3.2	Moment Magnitude Scale.....	83
3.3.3	Location Accuracy .....	84
3.4	Seismic History of NRSM .....	86
3.4.1	Event Locations .....	87
3.4.2	Magnitude-Time Histories .....	91
3.4.3	Diurnal Charts.....	92
3.5	Typical Seismic Responses to Mining at NRSM.....	94
3.5.1	Primary Development .....	94
3.5.2	Secondary/Tertiary Development into Stope Pillars.....	96
3.5.3	Access Pillars .....	98
3.5.4	Toe Slash.....	101
3.5.5	Stope Back .....	102
3.5.6	Northwest-Southeast Stope Corners .....	103
3.5.7	Stope Sidewall .....	105
3.5.8	Temporary Stope Pillars .....	106
3.5.9	Up/Down abutment.....	107
3.5.10	Abutment Cross-Talk.....	108
3.5.11	Structure Daylighting.....	112
4	Methodology .....	114

4.1	Variations in Apparent Stress.....	116
4.1.1	Methods of Tracking Variations and Moving Windows .....	119
4.1.2	Phases of Change in Apparent Stress.....	122
4.1.3	Additional Parameters for Tracking a Distribution .....	124
4.1.4	Determining Beginnings and Ends of Phases .....	126
4.1.5	Justification for a Volumetrically Filtered Approach .....	127
4.1.6	Multiple Interpretations of Phases of Variation.....	130
4.2	Variations in Event Locations and Spatial Distribution of Apparent Stress .....	134
4.2.1	Methods of Tracking Variations in Event Locations.....	134
4.2.2	Phases of Change in Event-Stoppe Distances.....	137
4.2.3	Spatial Variations in Apparent Stress over Time.....	141
4.2.4	Determining Beginnings and Ends of Phases .....	143
4.2.5	Expanding the Interpretation of Spatial Variation in Apparent Stress .....	143
4.2.6	Justification for a Volumetrically Filtered Approach .....	150
4.2.7	Multiple Interpretations of Phases of Variation.....	152
4.2.8	Coupled Interpretation of Apparent Stress and Event-Stoppe Distances .....	155
4.3	Selection of Cases and Compilation of Results .....	158
5	Results.....	159
5.1	Selected Cases .....	159
5.2	Variations in Apparent Stress.....	164
5.2.1	Durations of Phases.....	164
5.2.2	Magnitude of Variations .....	168
5.2.3	Summary of Apparent Stress Variations.....	175
5.3	Variations in Event-Stoppe Distance .....	176
5.3.1	Durations of Phases.....	176
5.3.2	Magnitude of Variations .....	180
5.3.3	Separation between Events with High and Low Apparent Stress.....	190
5.3.4	Summary of Event-Stoppe Distance Variations .....	195
5.4	Comparison of Variations in Apparent Stress and Event-Stoppe Distances.....	196
6	Discussion.....	200
6.1	Inferred Rock Mass Behaviour and Dominant Seismic Responses .....	200
6.2	Typical Behaviour versus Analysed Cases .....	204
6.3	Effects of Time Windows .....	205
6.3.1	Effects of Different Window Sizes.....	205

6.3.2	Use of Fixed-Time Moving Windows .....	210
6.4	Inferring Brittle versus Softening Behaviour .....	213
6.5	Effects of Large Events .....	216
6.6	Additional Stress Changes in the Short Term .....	222
6.7	Effect of Faults .....	227
6.8	Effects of Confinement .....	232
6.9	Scale Effects and Impact on Analysis .....	238
6.10	Non-Similar Behaviour in Mining-Induced Seismogenic Zones .....	252
7	Conclusion .....	255
7.1	Contributions .....	255
7.2	Future Work .....	257
	References .....	259
	Appendix A: Source of Seismic Data .....	266
	Appendix B: Summary of Apparent Stress and MESD Parameters Preceding Blasts .....	267
	Appendix C: Summary of Parameters Taken from Interpretations of Variation in Apparent Stress .....	269
	Appendix D: Summary of Parameters Taken from Interpretations of Variation in Event-Stope Distance .....	275

## List of Tables

Table 2-1: Common strength criteria that integrate minor principal stress into the determination of a failure envelope for hard rock masses.....	10
Table 3-1: List of major lithologies at NRSM and their abbreviations .....	66
Table 3-2: Typical rock mass parameters at NRSM (Jalbout and Simser, 2014).....	69
Table 3-3: Peak rock mass strength and stiffness parameters used for mine-scale stress model (Beck et al., 2012).....	69
Table 3-4: Standard far-field stress regime at NRSM (Jalbout and Simser, 2014; Simser, 2017)	70
Table 4-1: Previously published methods for interpreting variations in apparent stress .....	120
Table 6-1: Analysis of apparent stress phases in 1535-275-P1 SE corner using various window sizes.....	206
Table 6-2: Analysis of MESD phases in 1535-275-P1 SE corner using various window sizes.	208
Table 6-3: Analysis of difference in MESD between high or low apparent stress events and $D_{50}$ for 1535-275-P1 SE corner using different window sizes.....	209
Table 6-4: Proportion of decrease in apparent stress percentiles observed after Phase 1 events leave the moving window in 1535-275-P1 SE corner using various window sizes.....	215
Table 6-5: Proportion of decrease in apparent stress percentiles observed after Phase 1 events leave the moving window in 1475-212-P1 Back using various window sizes .....	215

## List of Figures

Figure 2-1: Streamlines indicating flow of river around bridge pillars (Hoek and Brown, 1980) .	6
Figure 2-2: Stress tangential ( $\sigma_{\theta\theta}$ ) and normal ( $\sigma_{rr}$ ) to a circular opening in an elastic medium subject to a uniform stress field (Brady and Brown, 2006) .....	7
Figure 2-3: Stress-strain curves for samples of Tennessee Marble subjected to various confining pressures in triaxial strength tests (Brady and Brown, 2006; after Wawersik and Fairhurst, 1970) .....	9
Figure 2-4: Visible stress fracturing in wall (a) and floor (b) of a tunnel (Simser et al., 2015a) .	10
Figure 2-5: Stress tangential and normal to a circular opening surrounded by a boundary of fractured rock within an elastic medium subject to a uniform stress field (Brady and Brown, 2006) .....	13
Figure 2-6: Strain cell readings from instruments 50 m (left) and 30 m (right) from a stope following a 5,000 t blast (Hudyma et al., 1994) .....	14
Figure 2-7: Modelled major principal stress ahead of a tabular excavation at selected time increments after a blast (Malan, 1999) .....	15
Figure 2-8: Schematic of different rock mass failure modes around an excavation depending on major and minor principal stress (Diederichs, 2003) .....	16
Figure 2-9: Three-component seismogram from a seismic event in South Africa, vertical units are displacement (m) and horizontal units are time (s) (modified after Mendecki, 1997) .....	17
Figure 2-10: Displacement spectrum of a seismic event in the frequency domain indicating the low frequency plateau ( $\Omega_0$ ) and the corner frequency ( $f_0$ ) (Hedley, 1992) .....	18
Figure 2-11: Rock fragments ejected from left wall of an unsupported opening (Deneka, 2014)	20
Figure 2-12: Six basic mechanisms of mining-induced seismicity in Canadian mines (Hasegawa et al., 1989) .....	21
Figure 2-13: Hypothetical seismic event locations around underground workings (left) and associated seismic sources (right) (Hudyma et al., 2003) .....	21
Figure 2-14: Illustration of a typical underground microseismic monitoring system (Collins et al., 2014) .....	24
Figure 2-15: Dynamic range of various sensors used in seismic monitoring (Mendecki, 1997) .	25
Figure 2-16: P-wave (a) and s-wave (b) radiation patterns for an ideal double-couple seismic source (Aki and Richards, 1980) .....	26

Figure 2-17: Example of a magnitude-time history from a population of events near an open stope .....	32
Figure 2-18: Example of a well-behaved frequency-magnitude relation .....	33
Figure 2-19: Example of a bi-modal frequency-magnitude relation .....	34
Figure 2-20: Example of a diurnal chart with events coloured by magnitude for a population of events near the production area of a mine .....	36
Figure 2-21: Example of an energy-moment graph with a quantile-quantile fitted scaling relation and events coloured by moment magnitude.....	37
Figure 2-22: Example of an energy-moment graph with events coloured by apparent stress.....	38
Figure 2-23: Schematic of major principal stress flow around a stope at Lac Shortt Mine, Chibougamau, Quebec (McCreary et al., 1992) .....	40
Figure 2-24: Plan view of seismic event locations at Lac Shortt mine (Ecobichon et al., 1992) .	41
Figure 2-25: Section view of seismic event locations and stress contours relative to the position of a tabular stope face at East Rand Property Mines, South Africa (McGarr et al., 1975).....	42
Figure 2-26: Locations of seismic events following a stope blast at Lac Shortt (middle) compared to change in major principal stress produced by the blast (top) and overall major principal stress (bottom) (Ecobichon et al., 1992).....	43
Figure 2-27: Number of seismic events (N) and seismic energy (E) in a 10 m window at various distance ahead of and behind an advancing tabular stope face in a Polish coal mine (Syrek and Kijko, 1988) .....	44
Figure 2-28: Locations of seismic events and inferred regions of caved or failed rock mass at Lac Shortt mine (McCreary et al., 1992) .....	45
Figure 2-29: Distribution of apparent stress of $-0.5 < M < 0$ events at various depths in a Canadian mine (Brown and Hudyma, 2017a).....	47
Figure 2-30: Longitudinal view of all seismic event locations in an area of Brunswick Mine, Bathurst, NB (left) and the same event locations with lighter shading indicating lower apparent stress (right) (Simser et al., 2003).....	48
Figure 2-31: Event locations above a sublevel cave at Telfer Gold Mine, Australia (marked by apparent stress) with quartiles of elevation at various eastings for reference (Abolfazlzadeh and Hudyma, 2016) .....	49

Figure 2-32: ASTH of population of seismic events occurring near stope blasts at LaRonde Mine, Preissac, Quebec (Hudyma, 2008).....	50
Figure 2-33: 50-event moving average of apparent stress in a pillar at Golden Giant Mine, Hemlo, Ontario (Coulson, 2009) .....	51
Figure 2-34: Example of an energy-moment graph with events coloured by $\log(EI)$ .....	53
Figure 2-35: EI graph showing sudden change following mass blast at Brunswick Mine (Simser et al., 2003) .....	54
Figure 2-36: EI-CAV graph showing sudden changes in $\log(EI)$ following a blast and a large event at Kidd Creek Mine, Timmins, Ontario (Disley, 2014).....	55
Figure 2-37: Hypothetical stress-strain curves for intact rock samples and rock masses in Hemlo, Ontario (Coulson, 2009) .....	56
Figure 2-38: Contours of deviatoric stress overlain with seismic event locations (left) and interpreted zones of yielded and yielding ground (right) at Creighton Mine, Sudbury, Ontario (Cotesta et al., 2014).....	57
Figure 2-39: Conceptual model of spatial variation in seismicity near an open stope (Mercer and Bawden, 2005; after Bawden and Mercer, 1994) .....	59
Figure 2-40: Five regions of a stress-strain curve for a rock mass with strain-softening behaviour (Cotesta et al., 2014; redrawn from Andrieux et al., 2008) .....	60
Figure 3-1: Regional map of the Sudbury Structure indicating the Sudbury Igneous Complex (SIC) (Rousell and Card, 2009) .....	62
Figure 3-2: Local map of the Sudbury Structure indicating the location of Nickel Rim South (modified after Rousell and Card, 2009) .....	63
Figure 3-3: Section view schematic looking northwest (note a specific grid or coordinate system is not known for this figure) of the main NRSM orebodies from the project's exploration phase (McLean et al., 2005).....	64
Figure 3-4: Section view looking west of main contact and footwall orebodies at NRSM showing mine workings.....	65
Figure 3-5: Stratigraphic column of NRSM (Simser et al., 2015b).....	66
Figure 3-6: Plan view of interpreted geology contacts at 1445 m depth (Glencore, 2017a) .....	67
Figure 3-7: Plan view of interpreted geology contacts at 1625 m depth (Glencore, 2017b).....	68

Figure 3-8: Plan view of interpreted geology contacts at 1445 m depth with superimposed faults (green) (Glencore, 2017a).....	71
Figure 3-9: Longitudinal view of north-south (left) and low-angle (right) mine-scale faults .....	72
Figure 3-10: Longitudinal (left) and section (right) views of level and access designs .....	74
Figure 3-11: Plan view of typical sublevel development (1565).....	75
Figure 3-12: Section view schematic of a typical transverse blasthole stope mined with two blasts (1565-300-P1) (Glencore, 2013).....	76
Figure 3-13: Longitudinal schematic of primary-secondary sequence variants .....	78
Figure 3-14: Longitudinal schematic of primary-secondary-tertiary sequence .....	79
Figure 3-15: Longitudinal view of centre-out sequencing producing a pyramid shape in lower mine (1680 to 1480 levels, January, 2014) .....	80
Figure 3-16: Longitudinal view of a stope taken in a pillarless sequence (1625-337-P1, May 17 <sup>th</sup> , 2014) .....	81
Figure 3-17: Longitudinal (left) and section (left) views of uniaxial (blue cylinders) and triaxial (red pyramids) sensor locations up to late 2017 .....	82
Figure 3-18: Number of sensors used to locate events over time .....	83
Figure 3-19: Moment magnitude as measured by the NRSM microseismic array versus Richter magnitude as measured by the SRSN (2009 to late 2017).....	84
Figure 3-20: Cumulative distribution of location residual errors (2011 to late 2017).....	85
Figure 3-21: Median location residual error by year in different regions of NRSM .....	86
Figure 3-22: Longitudinal views of annual event locations (dots) and extracted stopes (red stars) .....	88
Figure 3-23: Plan view of annual event locations (dots) and extracted stopes in a typical centre-out 1-3-5 primary-secondary sequence (1565 level, 30 m thick horizontal slice).....	90
Figure 3-24: Mine-wide magnitude-time history of events .....	91
Figure 3-25: Mine-wide magnitude-time history of $M \geq 1$ events .....	92
Figure 3-26: Mine-wide diurnal chart of events (2011 to late 2017).....	93
Figure 3-27: Mine-wide diurnal chart of $M \geq 1$ events (2011 to late 2017).....	94
Figure 3-28: Plan view of blast (left) and event (right) locations (coloured and sized by magnitude) over 3 months of primary stope access and footwall development (1595-225 SA, June-August 2010) .....	95

Figure 3-29: Plan view of blast (left) and event (right) locations (coloured and sized by magnitude) over 2 months of tertiary stope access development (1320-192 SA, March-April 2013) .....	97
Figure 3-30: Water wetting shotcrete on the walls and back (dark patches) of a secondary stope access (Simser, 2016).....	98
Figure 3-31: Plan view of blasts (top) and events (bottom) (coloured and sized by magnitude) over a 6-month period, stope blasts marked with red stars (1320 level, January-June 2013) .....	100
Figure 3-32: 1320-300 SA looking north with damage in left and right walls at end of June 2013 (Simser, 2013).....	101
Figure 3-33: Section (left) and longitudinal (right) views of event locations (coloured and sized by magnitude) around a void created by a toe slash over a 24-hour period following the blast (1595-275-P1, October 7 <sup>th</sup> , 2011), also showing the shape of the final stope (pink).....	102
Figure 3-34: Section (left) and longitudinal (right) views of event locations (coloured and sized by magnitude) in the back of the blasted stope (red) over a 24-hour period following the final blast (1445-325-P1, February 8 <sup>th</sup> , 2013) .....	103
Figure 3-35: Plan (left) and oblique northeast (right) views of events (coloured and sized by magnitude) locating in northwest and southeast corners of the blasted stope (red) over a 24-hour period following the final blast (1595-275-P1, October 28 <sup>th</sup> , 2011) .....	104
Figure 3-36: Longitudinal (left) and plan view (right) of event locations (coloured and sized by magnitude) in the sidewall of a blasted stope (red) over a 24-hour period following the final blast (1535-200-P1, October 8 <sup>th</sup> , 2017).....	105
Figure 3-37: Longitudinal (left) and plan (right) views of event locations (coloured and sized by magnitude) in 24 hours following a final stope blast (red) showing events locating in secondary stope pillar (1595-200-P1, October 22 <sup>nd</sup> , 2014).....	106
Figure 3-38: Longitudinal (left) and section (right) views of event locations (coloured and sized by magnitude) over a 24-hour period following a final blast where events located above and below the level of the blasted stope (red) (1535-325-P1, August 21 <sup>st</sup> , 2016) .....	108
Figure 3-39: Plan view of events (coloured and sized by magnitude) locating in the northwest corner of the blasted stope (red) and on east abutment southeast of a previously mined stope over a 24-hour period following the final blast (1535-275-P2, September 15 <sup>th</sup> , 2013).....	109
Figure 3-40: Plan view of event locations (top) and magnitude-time history of events (coloured by date and sized by magnitude) in southeast abutment of 1535-275-P1 (June-September 2013) .	111

Figure 3-41: Longitudinal (left) and oblique northeast view along structure (right) of events (coloured and sized by magnitude) locating along LA2 fault in 24 hours following a final blast (red) (1220-312-P1, June 24 <sup>th</sup> , 2016).....	113
Figure 4-1: Events in 24 hours following 1535-275-P1 final blast (June 19 <sup>th</sup> , 2013) showing SE corner selection volume in longitudinal (left) and plan (right) views .....	117
Figure 4-2: Events in 24 hours following 1535-275-P1 final blast (June 19 <sup>th</sup> , 2013) showing SE corner selection volume looking NE (left) and NW (right) showing only events in volume.....	118
Figure 4-3: Magnitude-time history of events in 1535-275-P1 SE corner volume before and after the final blast.....	119
Figure 4-4: Median apparent stress in 1535-275-P1 SE corner following final blast using 50, 100, 200, and 400-event moving windows .....	122
Figure 4-5: Median apparent stress in 1535-275-P1 SE corner.....	124
Figure 4-6: Determining $AS_{20}$ , $AS_{50}$ , and $AS_{80}$ in a 200-event window in 1535-275-P1 SE corner .....	125
Figure 4-7: Determining end of Phase 1 in 1535-275-P1 SE corner using average peak time of apparent stress percentiles.....	126
Figure 4-8: Events in 24 hours following 1535-275-P1 final blast (June 19 <sup>th</sup> , 2013) showing NW corner selection volume looking NE (left) and SE (right) showing only events in volume.....	128
Figure 4-9: Comparison of apparent stress variation between SE and NW corners of 1535-275-P1 showing end times of phases and number of events in each phase .....	130
Figure 4-10: Three phases of apparent stress variation in the west sidewall of 1680-262-P2 (December 24 <sup>th</sup> , 2011) ending 10.7 hours after blast.....	131
Figure 4-11: Three phases of apparent stress variation in west sidewall of 1680-262-P2 (December 24 <sup>th</sup> , 2011) ending 370 hours after the final blast .....	133
Figure 4-12: Plan view schematic of the use of symmetry in a pillar to simplify the analysis of event-stope distances .....	136
Figure 4-13: Median event-stope distance in 1535-275-P1 SE corner.....	137
Figure 4-14: Examples of MESD decreasing some period after the blast, defining Phase 2 of MESD variation .....	139
Figure 4-15: Determining $D_{50}$ , $D_{50H_{50}}$ , and $D_{50L_{50}}$ in 200-event window in 1535-275-P1 SE corner .....	142

Figure 4-16: Determining end of Phase 1 in 1535-275-P1 SE corner using average peak time of MESDs.....	143
Figure 4-17: Use of $D_{50H_{80}}$ and $D_{50L_{20}}$ to enhance interpretation of spatial gradient of apparent stress in 1535-275-P1 SE corner.....	144
Figure 4-18: Locations of the first 200 events in 1535-275-P1 southeast corner (coloured apparent stress, sized by magnitude) separated by apparent stress .....	146
Figure 4-19: Plan view of 10 m thick horizontal section of 1535-275-P1 SE corner showing event locations (coloured by apparent stress) and cumulative distributions of apparent stress in four quartiles of event-stope distances .....	148
Figure 4-20: Spatial plots of events (coloured by apparent stress, sized by magnitude) occurring in three phases of MESD variation in 1535-275-P1 SE corner .....	150
Figure 4-21: Comparison of MESD variation between SE and NW corner of 1535-275-P1 showing end times of phases and number of events in each phase.....	152
Figure 4-22: Three phases of event-stope distance variation in SE corner of 1535-300-P1 (April 9 <sup>th</sup> , 2014) ending 26.8 hours after blast .....	153
Figure 4-23: Three phases of event-stope distance variation in SE corner of 1535-300-P1 (April 9 <sup>th</sup> , 2014) ending 411.7 hours after blast .....	155
Figure 4-24: Apparent stress and MESD variation in 1535-275-P1 SE corner.....	157
Figure 5-1: Number of stopes, cases, and interpretations by year .....	160
Figure 5-2: Number of stopes, cases, and interpretations by mine level .....	161
Figure 5-3: Number of stopes, cases, and interpretations by easting. Note that 272 corresponds to a line of tertiary stopes in the upper part of the mine only .....	162
Figure 5-4: Number of cases and interpretations by type of seismic response.....	163
Figure 5-5: Distribution of final blast tonnages in selected cases compared to the tonnages of other final blasts taken in 2011 and later .....	164
Figure 5-6: Distributions of phase durations for apparent stress variations .....	165
Figure 5-7: Distributions of ratios of phase durations for apparent stress variations .....	166
Figure 5-8: Distributions of the number of events in each phase of apparent stress variation ...	167
Figure 5-9: Distributions of ratios of numbers of events in each phase of apparent stress variation .....	168

Figure 5-10: Distributions of percentage change in apparent stress observed during Phase 1 (relative to just before the final blast).....	169
Figure 5-11: Distributions of percentage change in apparent stress observed during Phase 2 (relative to the end of Phase 1) .....	170
Figure 5-12: Distributions of percentage change in apparent stress observed during Phase 2 (relative to just before the final blast).....	171
Figure 5-13: Distributions of percentage change in apparent stress observed during Phase 3 (relative to the end of Phase 2) .....	172
Figure 5-14: Distributions of percentage change in apparent stress observed during Phase 3 (relative to just before the final blast).....	173
Figure 5-15: Percentage change in apparent stress from one phase to the next versus the number of events in that phase.....	175
Figure 5-16: Distributions of phase durations for MESD variations.....	177
Figure 5-17: Distributions of ratios of phase durations for MESD variations.....	178
Figure 5-18: Distributions of the number of events in each phase of MESD variation.....	179
Figure 5-19: Distributions of ratios of numbers of events in each phase of MESD variation....	180
Figure 5-20: Distributions of percentage change in MESD observed during Phase 1 (relative to just before the final blast) .....	181
Figure 5-21: Example of high apparent stress events migrating further from stope than low apparent stress events (1415-250-P1 west sidewall, January 20 <sup>th</sup> , 2015).....	182
Figure 5-22: Distributions of percentage change in MESD observed during Phase 2 (relative to the end of Phase 1).....	183
Figure 5-23: Example of high apparent stress events moving closer to the stopes than low apparent stress events during Phase 2 (1535-225-P1 west sidewall, June 30 <sup>th</sup> , 2016).....	184
Figure 5-24: Distributions of percentage change in MESD observed during Phase 2 (relative to just before the final blast) .....	185
Figure 5-25: Distributions of percentage change in MESD observed during Phase 3 (relative to the end of Phase 2).....	186
Figure 5-26: Distributions of percentage change in MESD observed during Phase 3 (relative to just before the final blast) .....	187

Figure 5-27: Distributions of percentage change in MESD between the ends of Phase 1 and 3 (change throughout Phase 2 and 3).....	188
Figure 5-28: Percentage change in MESD from one phase to the next versus the number of events in that phase .....	190
Figure 5-29: Distribution of percentage differences between MESD of events with high or low apparent stress and the MESD for all events at the end of each phase.....	192
Figure 5-30: Distributions of percentage differences between MESD of higher and lower apparent stress events at the end of each phase .....	194
Figure 5-31: End time of Phase 1 of apparent stress variation versus end time of Phase 1 of MESD variation .....	196
Figure 5-32: End time of Phase 2 of apparent stress variation versus end time of Phase 1 of MESD variation .....	197
Figure 5-33: End time of Phase 3 of apparent stress variation versus end time of Phase 2 of MESD variation .....	198
Figure 5-34: End time of Phase 3 of apparent stress variation versus end time of Phase 3 of MESD variation .....	199
Figure 6-1: Schematic of interpreted typical behaviour and inferred rock mass response.....	202
Figure 6-2: Example of time artefacts in apparent stress percentiles defined using fixed time moving windows following a final blast (1535-325-P1 SE corner, August 21 <sup>st</sup> , 2016).....	212
Figure 6-3: Comparison of apparent stress variation in 1535-275-P1 SE corner (June 19 <sup>th</sup> , 2013) and 1475-212-P1 Back (December 29 <sup>th</sup> , 2015) indicating duration of Phase 2 when Phase 1 events are leaving window .....	214
Figure 6-4: Longitudinal view looking north (left) and section view looking west (right) of event locations (coloured by magnitude and sized by time) in 25 hours following 1445-300-P1 final blast (August 6 <sup>th</sup> , 2012).....	217
Figure 6-5: Magnitude-time, apparent stress, and MESD graphs of 1445-300-P1 east sidewall (August 6 <sup>th</sup> , 2012).....	218
Figure 6-6: Magnitude-time and apparent stress percentiles in large volume between 1445 and 1320 east of 275 stopes (May to September 2017).....	220
Figure 6-7: Magnitude-time and apparent stress percentiles in large volume between 1445 and 1320 east of 275 stopes (September 2 <sup>nd</sup> to 5 <sup>th</sup> 2017) .....	222

Figure 6-8: Section view looking east of event location (coloured and sized by magnitude) over 24 hour periods following blasts in 1565-200-P1 and 1625-187-P1 .....	223
Figure 6-9: Magnitude-time, apparent stress, and MESD graphs of 1565-200-P1 west sidewall (May 6 <sup>th</sup> , 2017) .....	225
Figure 6-10: Longitudinal view looking north (left) and plan view (right) of event locations (coloured and sized by magnitude) in first day (top) and next 30 days (bottom) following 1535-250-P2 final blast (July 7 <sup>th</sup> , 2015) showing LA5 (pink) and NS-200 (brown) faults .....	228
Figure 6-11: Comparison of frequency-magnitude relations for events in 1535-250-P2 west sidewall in first day following blast versus next 30 days .....	229
Figure 6-12: Magnitude-time and apparent stress graphs for 1535-250-P2 west sidewall up to 25 hours after blast (July 7 <sup>th</sup> , 2015) .....	230
Figure 6-13: Magnitude-time and apparent stress graphs for 1535-250-P2 west sidewall up to 750 hours after blast (July 7 <sup>th</sup> , 2015) .....	231
Figure 6-14: Magnitude-time, apparent stress, and MESD graphs for 1595-200-P1 pillar (October 22 <sup>nd</sup> , 2014).....	233
Figure 6-15: Longitudinal views looking north of event locations in pillar formed by 1595-200-P1 (October 22 <sup>nd</sup> , 2014) up to one month after blast coloured by apparent stress (top) and event-stope distance (bottom) showing all events (left), $\sigma_a > 15$ kPa (centre), and $\sigma_a < 4$ kPa (right).....	235
Figure 6-16: Magnitude-time, apparent stress, and MESD graphs for 1535-275-P2 east abutment (September 15 <sup>th</sup> , 2013).....	237
Figure 6-17: Magnitude-time and apparent stress graphs in 1535-275-P1 SE corner indicating times when larger events occur.....	240
Figure 6-18: Frequency-magnitude relations for events in each phase of apparent stress variation in 1535-275-P1 SE corner and 200 events in SE corner prior to blast .....	241
Figure 6-19: Energy-moment relations for events in each phase of apparent stress variation in 1535-275-P1 SE corner and 200 events in SE corner prior to blast .....	242
Figure 6-20: Apparent stress and log(EI) percentiles in first 5 hours after blast in 1535-275-P1 SE corner .....	244
Figure 6-21: apparent stress and log(EI) percentiles in first 85 hours after blast in 1535-275-P1 SE corner .....	245

Figure 6-22: Comparison of frequency-magnitude relations of events closest and farthest from stopes in each phase of MESD variation in 1535-275-P1 SE corner. \*Phase 2 frequency-magnitude relations were determined by inspection due to lack of events for algorithmic determination in mXrap ..... 247

Figure 6-23: Comparison of energy-moment relations of events closest and farthest from stopes in each phase of MESD variation in 1535-275-P1 SE corner..... 249

Figure 6-24: MESD graphs using apparent stress (top) and log(EI) (bottom) in 1535-275-P1 SE corner in the first 85 hours following the final blast..... 251

Figure 6-25: Apparent stress percentiles in 1535-225-P1 NW corner (June 30<sup>th</sup>, 2016)..... 253

Figure 6-26: MESD in 1355-275-P3 west abutment (October 7<sup>th</sup>, 2015)..... 254

## List of Frequently Used Symbols and Abbreviations

AS	Apparent Stress
$\sigma_a$	Apparent Stress
ASR	Apparent Stress Ratio
D <sub>50</sub>	Median event-stope distance of a population of events
EDZ	Excavation Damage Zone
ESD	Event-Stope Distance
m	Metre
M	Magnitude
MESD	Median Event-Stope Distance
NRSM	Nickel Rim South Mine
Pa	Pascal
t	Tonne

# 1 Introduction

The association between mining-induced stresses and mining-induced seismicity has been known for decades. Underground mining in higher stress conditions, such as those encountered at greater depths, is often associated with elevated levels of seismicity and seismic hazard. Seismic monitoring has become a valuable tool for mitigating seismic risk in underground mines. The technology applied to monitor mining-induced seismicity has also progressed over several decades. The advent of digital systems and automated processing algorithms has enabled the collection of much greater quantities of high precision, high accuracy seismic data throughout a mine. Although mine operators are primarily concerned with using this data for forecasting seismic hazard and mitigating risks to the workforce, this vast volume of data can also be used to understand the rock mass response to mining.

In a mining environment, the creation of excavations for access to the orebody and extraction of ore cause stresses to redistribute. The manner in which stresses redistribute may cause them to exceed the strength of the rock mass, resulting in localized yield or failure of the material. The creation of a new excavation is often accompanied by the creation of a region of damaged and disturbed rock around it as a result of the induced-stresses. Understanding the formation and properties of these damaged and disturbed regions is essential to designing safe excavations for mining operations.

Seismic events are manifestations of sudden, inelastic strains in a rock mass. The characteristics of seismicity are controlled by the conditions under which it occurs. Accordingly, the characteristics of seismicity can be used to infer certain rock mass conditions. High quality seismic data offers an opportunity to study how the creation of mining excavations damages and disturbs the rock mass. The results of such analysis can be used to make inferences on the constitutive behaviour of the rock mass in the seismically active areas, leading to a better understanding of how a rock mass responds to mining.

The manner in which excavations are created depends on the mining method being employed. For hard rock mines with competent ground, the method of choice almost always involves fragmentation and throw from the use of explosives. Blasts cause nearly instantaneous changes to static stresses in a rock mass. Some of the largest excavations are produced by open stoping

techniques, which create voids on the order of several thousand or tens of thousands of tonnes of rock in just a few blasts. These large blasts have the potential to cause large, sudden stress changes and large seismic responses. The scale of the stress changes, damage to the nearby rock mass, and seismic responses make them useful subjects for the study of how seismicity can be used to infer rock mass behaviour in a mining environment.

This thesis focuses on the short-term seismic responses produced by stope blasts. Spatially-isolated populations of seismic events are studied in order to make inferences on rock mass behaviour resulting from a single isolated induced stress change in a specific region of the rock mass. The source of data for this research is Glencore's Nickel Rim South Mine in Sudbury, Ontario. Nickel Rim South (NRS) is a relatively modern operation, employing an open stoping mining method at depths between 1 and 2 km below surface. The mine's seismic monitoring system produces exceptionally high-quality data and has been in operation for the complete duration of production mining. These aspects of the data set make it an attractive source of data for this thesis.

Study of seismicity and inferences on rock mass behaviour will lead to an improved understanding of non-linear behaviour of rock masses. This improved understanding translates to practical knowledge for mine operators related to excavation stability and where mining-induced stress changes create ground-related hazards. This knowledge may also be useful for calibrating numerical models of mining-induced stress, which are a commonly employed tool for designing mines.

## 1.1 Scope

This thesis studies seismic responses to large, open stope blasts at Nickel Rim South between 2011 and late 2017. The parameters describing seismicity analysed in this these are the location, time, and apparent stress of seismic events. Apparent stress is an estimate of relative co-seismic stress change derived from an event's energy and moment. As has been done by other authors, apparent stress is used to infer local stress levels in a rock mass. This thesis develops a method to analyse space-time variations in apparent stress following stope blasts. Results of this analysis are used to infer rock mass behaviour related to stress and yielding across multiple case studies at NRS. The combined results of multiple case studies are used to develop a model for short-term rock mass yield near excavations as inferred based on the space-time behaviour of apparent stress of local seismic events.

This thesis does not:

- Analyse seismic source parameters other than location, time, and apparent stress.
- Use numerical modelling to interpret stress-strain behaviour.
- Attempt to calibrate any constitutive behaviour or mechanical properties of rock masses.
- Account for potential structural influences on seismic events in analysis (some discussion of this topic is given).
- Consider seismic responses outside the context of stope blasts (some discussion of this topic is given).
- Consider non-production related blasting (e.g. development/tunnel blasts, raise mining, de-stressing).
- Relate patterns, trends, or variations in seismicity or inferred rock mass behaviour to seismic hazard or risk (e.g. occurrence of large events, rock bursts, damage to excavations).

## 1.2 Thesis Structure

Chapter 1 provides context for the research, as well as a scope and objectives.

Chapter 2 is a literature review that covers basic principles of mining-induced stress, constitutive behaviour of rock masses in the context of mining, mining-induced seismicity, parameters used to describe seismic events, seismic data analysis techniques, and seismicity as it relates to the constitutive behaviour of rock masses.

Chapter 3 provides background on Nickel Rim South mine including its geological setting, mining methods, seismic monitoring, history of seismic activity, and common seismic responses to mining.

Chapter 4 develops a method for analysing space-time variations in apparent stress using case examples and presents inferred rock mass behaviour based on the observed variations.

Chapter 5 presents key results related to space-time variations in apparent stress observed across multiple case studies using the methodology described in the previous chapter.

Chapter 6 discusses the proposed model for rock mass yield based on the results presented in the previous chapter and discusses other observed behaviours in specific case examples.

Chapter 7 summarizes the key conclusions of this thesis and recommends possible improvements on the methodology and opportunities for further study.

## 2 Literature Review

### 2.1 Mechanics of Rock Masses and Application in Mining

#### 2.1.1 In-Situ Stress

Natural pressures in the Earth's crust are responsible for in-situ stress conditions in a rock mass with vertical and horizontal components. The vertical stress ( $\sigma_v$ ) increases linearly with depth and is proportional to the weight of the overlying rock. The local horizontal stress ( $\sigma_h$ ) is some multiple of the vertical. In Canada, the major principal stress ( $\sigma_1$ ) is typically horizontal and in the range of 1.5 to 3.0 times that of the vertical, which is typically the minor principal stress ( $\sigma_3$ ). The ratio between major and minor principal stresses is referred to as the k-ratio (Brown and Hoek, 1978; Herget, 1973).

#### 2.1.2 Mining-Induced Stress

The creation of voids in a rock mass, which is an inherent aspect of mining, reorients and redistributes stress in a rock mass. Load that was once carried by the rock mass that was removed to create the excavation is placed on the surrounding rock to maintain equilibrium. Hoek and Brown (1980) represent this concept using the analogy of bridge pillars blocking the flow of a stream (Figure 2-1). The stream lines represent the major principal stress ( $\sigma_1$ ). The stream lines bend to flow around the pillars, resulting in higher concentrations of stream lines near the side edges of the pillars. The reorientation of the streamlines also created a reduction in front of and behind the pillars. Mining-induced stresses behave in a similar manner. The "flow" of stress reorients and redistributes around excavations, resulting in regions of elevated and reduced stress.

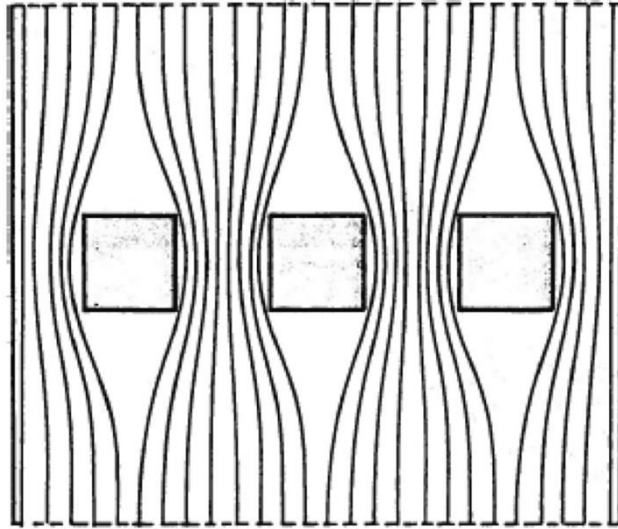


Figure 2-1: Streamlines indicating flow of river around bridge pillars (Hoek and Brown, 1980)

Stress can not flow normal to an excavation boundary. Figure 2-2 depicts a schematic of an analytical solution for radial ( $\sigma_{rr}$ ) and tangential ( $\sigma_{\theta\theta}$ ) stress at a distance  $r$  from a circle of radius  $a$  in an elastic medium subjected to a uniform stress field of magnitude  $p$ . The stress tangential to the opening is highest at the excavation boundary and decreases with distance, approaching the in-situ level  $p$ . The stress radial to the opening is zero at the excavation boundary and increases with distance, approaching the in-situ level  $p$ . In a two-dimensional simplification of mining geometry, the loading of the rock mass near the excavation is nearly uniaxial, but is increasingly biaxial at greater distances. Mining-induced stresses effectively increase the k-ratio for stress in the rock mass (higher  $\sigma_1$  and lower  $\sigma_3$ ). The analytical solution also shows that the scale of the stress redistribution depends on the scale of the excavation. Larger excavations will produce larger regions of elevated stresses and reduced confinement.

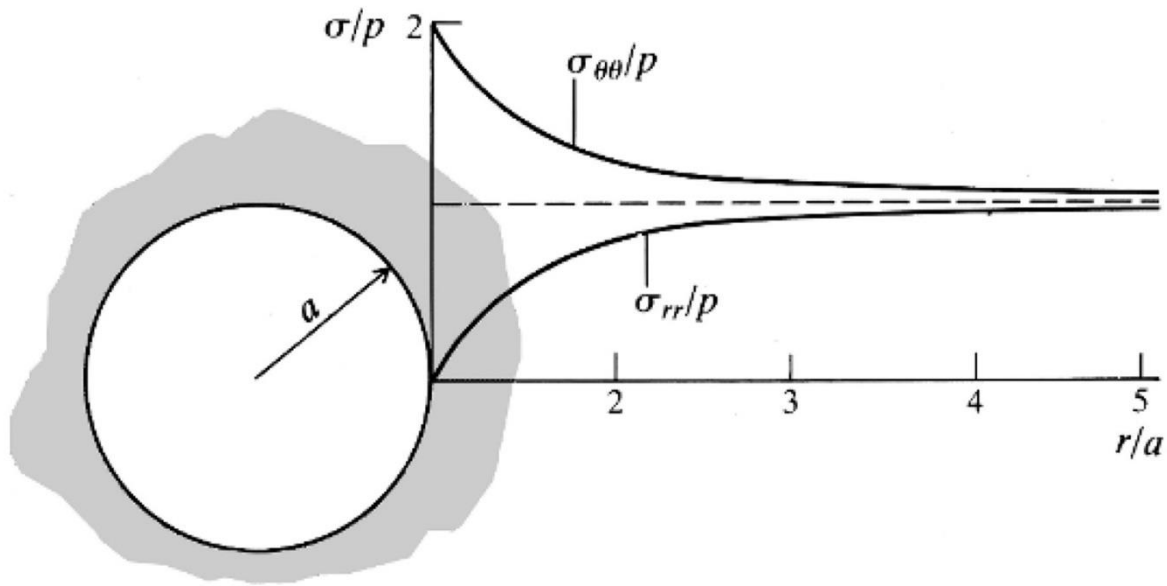


Figure 2-2: Stress tangential ( $\sigma_{\theta\theta}$ ) and normal ( $\sigma_{rr}$ ) to a circular opening in an elastic medium subject to a uniform stress field (Brady and Brown, 2006)

### 2.1.3 Constitutive Behavior of Rock Masses

A rock mass is a natural assemblage of ground with discontinuities (e.g. joints, fractures, etc.) and variations in material properties. In general, the strength of a rock mass is related to the strength of the intact rock as well as the quantity and strength of the discontinuities. On a large enough scale, the rock mass can be treated as a continuum with a uniform, isotropic strength if the discontinuities are random and distributed evenly throughout it. The scale at which the strength becomes uniform and isotropic depends on the density of discontinuities (Hoek, 2006).

Stress-strain behaviour of rock masses depends on the loading conditions. Figure 2-3 shows examples of stress-strain curves for hard rock samples subjected to different confining pressures. Higher confining pressures essentially make the loading condition less uniaxial. All samples have a nearly linear relation at low strains, which corresponds with the elastic behaviour of the material. At a certain point, the slope will begin to decrease and the relation ceases to be linear, which is known as the yield point. The yield point signifies the end of elastic behaviour, and the beginning of inelastic behaviour. Yield occurs at higher levels of stress with increasing confining pressure. The highest stresses on the curve for each sample is known as the peak strength, after which the sample begins to fail. Like yield, peak strength occurs at higher levels of stress with increasing confinement.

The samples have different post-peak behaviour depending on the level of confinement. The samples fail in a brittle manner under low confinement, and a more ductile manner under high confinement. At intermediate levels of confinement, the samples exhibit strain-softening behaviour. The existence of ductile behaviour in hard rock is debateable. Ductile failure depends on the ability of confinement to prevent dilation, which is difficult in a mining environment where there is an abundance of openings for fractured rock to expand into. In lab specimens (like the ones exhibited in Figure 2-3), apparent ductile behaviour may be an artefact of the stiffness of the loading apparatus in conjunction with how stress and strain are measured.

Coulson (2009) tested a hypothesis that the transition from brittle to ductile behaviour occurs at k-ratios less than 3.4, but found evidence of strain softening at ratios as low as 2.0. These results indicate that the brittle-ductile transition must occur below this point. Coulson stated that high-confinement is difficult to replicate in a mining environment where geometry and confinement are frequently changed by the creation of new excavations. Given that typical in-situ stress regimes in Canada have k-ratios of 1.5 to 3.0, an undisturbed rock mass is already near Coulson's theorized brittle-ductile transition of 2.0. As stated previously, mining-induced stresses effectively increase k-ratios (increased major principal stress tangential to excavations and decreased minor principal stress/confinement radial to them), so it would be difficult to replicate the stress conditions favourable to ductile failure in a Canadian hard rock mine. Accordingly, there are multiple works that describe the brittle or strain-softening behaviour of jointed hard rock masses found in the Canadian Shield (Coulson, 2009; Fairhurst, 2004; Hajiabdolmajid et al., 2002). Strain-softening constitutive behaviour is also used extensively in mine-scale numerical stress models of Canadian hard rock mines (Andrieux et al., 2008; Cotesta et al., 2014).

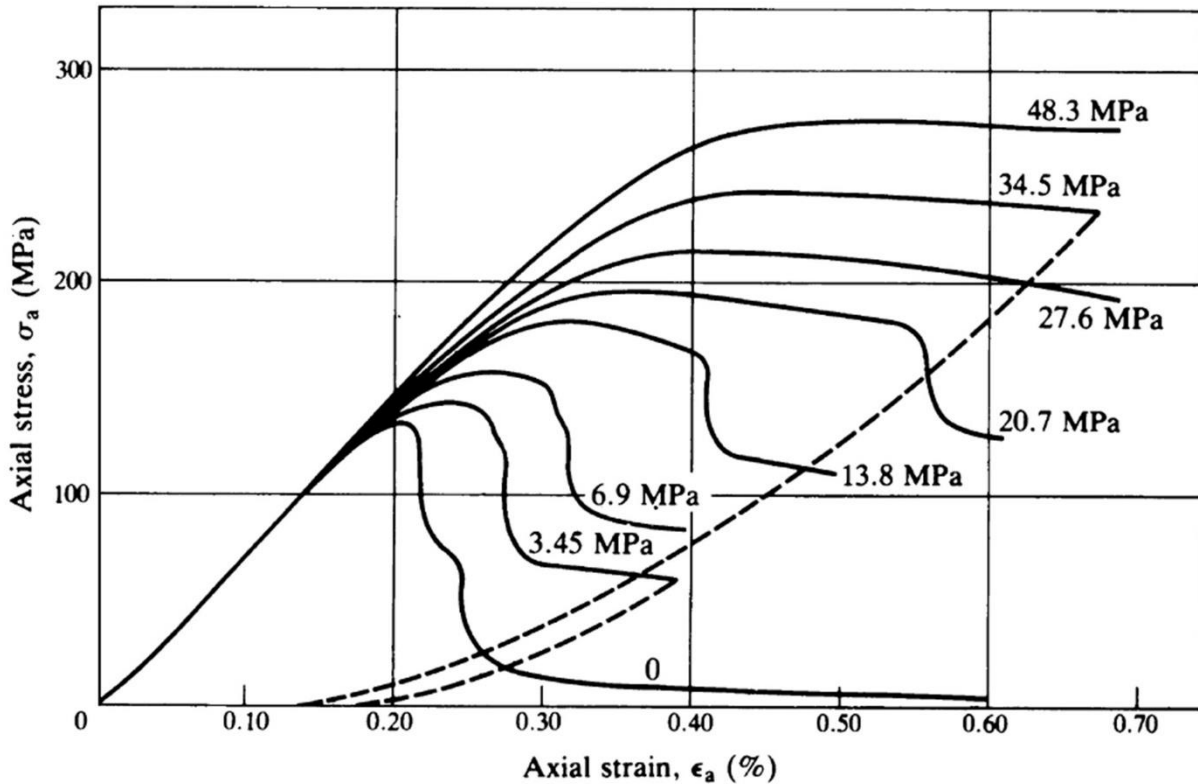


Figure 2-3: Stress-strain curves for samples of Tennessee Marble subjected to various confining pressures in triaxial strength tests (Brady and Brown, 2006; after Wawersik and Fairhurst, 1970)

Multiple rock mass strength criteria have been used to account for how increased confinement contributes to increased rock mass strength. Several commonly used strength criteria are summarized in Table 2-1. With each of these criteria, an increase in  $\sigma_3$  (or  $\sigma_2$  in the case of Griffith (1924) who used a two-dimensional criteria) also increases the maximum  $\sigma_1$  the material can be subjected to before failure. Many of these criteria also incorporate a ratio of the major and minor stress to the uniaxial intact rock strength ( $\sigma_c$ ).

Table 2-1: Common strength criteria that integrate minor principal stress into the determination of a failure envelope for hard rock masses

Criteria	Damage or Failure Criteria Equation	Constants
Coulomb (1776)	$\sigma_1 = \frac{2c \cos \phi + \sigma_3(1 + \sin \phi)}{1 - \sin \phi}$	Internal cohesion and friction angles
Griffith (1924)	$(\sigma_1 - \sigma_2)^2 - 8T_0(\sigma_1 + \sigma_2)$	Tensile strength of intact rock
Bieniawski (1974)	$\frac{\sigma_1}{\sigma_c} = 1 + A \left( \frac{\sigma_3}{\sigma_c} \right)^{0.75}$	Empirical, based on rock type
Hoek-Brown (1997)	$\sigma_1 = \sigma_3 + \sigma_c \left( m_b \frac{\sigma_3}{\sigma_c} + s \right)^{0.5}$	Empirical, based on jointing and disturbance of rock mass

#### 2.1.4 Excavation damage zones

Mining-induced stresses can cause the stress condition in the surrounding rock mass to exceed its strength, leading to yield and/or failure of the material. The zone of yielded ground around an excavation created by mining-induced stresses is known as an excavation damage zone (EDZ). Two visual examples of EDZs in Canadian hard rock mines are shown in Figure 2-4. In these pictures, expansion of the excavations (by either widening the walls or deepening the floors) reveals a cross section of the rock mass immediately adjacent to the original excavations. In both pictures, there are fractures running tangential to the profile of the excavation. Such fractures are unlike natural jointing observed in Canadian hard rock mines, and are attributed to the flow of induced stresses around the excavations (i.e. the major principal stress flowing tangential to the excavation boundary).

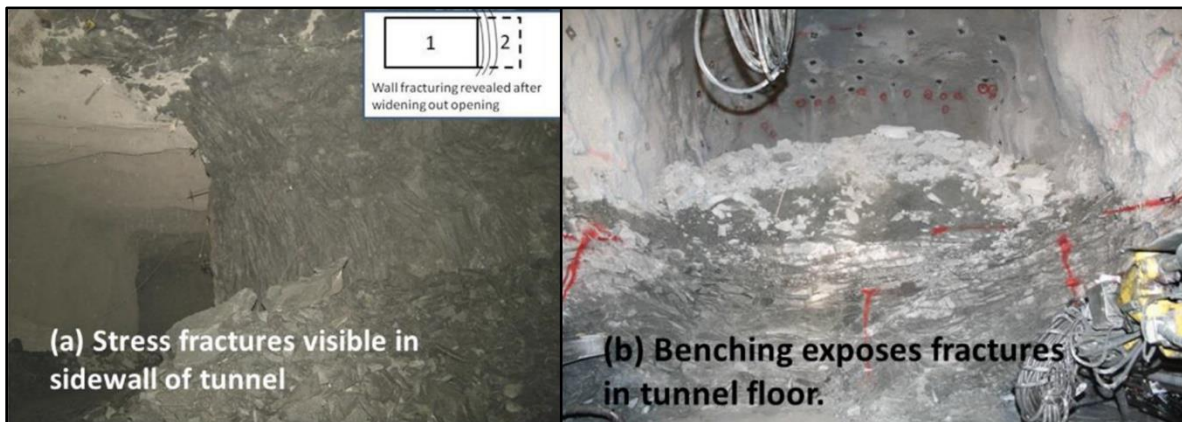


Figure 2-4: Visible stress fracturing in wall (a) and floor (b) of a tunnel (Simser et al., 2015a)

Castro (1996) proposed that damage to rock masses near excavations in moderately-jointed hard rock is initially a result of elevated stress and reduced confinement causing intact rock to fracture. Similar to the rock mass strength criteria presented previously, Castro proposed a damage initiation criteria based on a difference between  $\sigma_1$  and  $\sigma_3$ . He also postulates that movement along pre-existing discontinuities constitutes a secondary rock mass damage effect which becomes an increasingly relevant mechanism with reduced confining stress.

Matrino and Chandler (2004) provide detailed observations on disturbance and damage to rock masses near excavation from an experiment at the Underground Research Laboratory (URL) in Manitoba. Within the rock mass subjected to mining-induced stress changes, they observed an EDZ near the excavation, and an excavation disturbed zone beyond it. They remark that while the excavation disturbed zone is affected by mining-induced stresses, no permanent stress-induced damage could be measured. This zone has been abbreviated as the EdZ by Tsang et al. (2005), and has also been referred to as the excavation influence zone (EIZ) by Perras and Diederichs (2016). Subsequent changes to the rock mass could cause the EDZ to expand into the EIZ.

Within the EDZ itself, Martino and Chandler (2004) also observed a variation in the degree of rock mass damage between they referred to as the inner and outer damage zones (referred to as EDZ<sub>i</sub> and EDZ<sub>o</sub> respectively by Perras and Diederichs (2016)). The rock mass closer to the excavation was more damaged than the rock mass farther away. The inner EDZ is characterized by failed, loosened rock which may detach from the walls, while the outer EDZ is characterized by a gradual transition to what appears to be rock that is unaffected by stress-induced damage. Perras and Diederichs (2016) elaborate on these differences by stating that the EDZ<sub>i</sub> has macroscopic, interconnected fractures with significant dilation, and the EDZ<sub>o</sub> has isolated fractures without significant dilation.

It is important to consider that the URL was constructed in a massive region of rock with almost no natural jointing. Therefore, the observed mechanisms of excavation damage are relevant to intact rock, but potentially less so to a more jointed rock mass. A more jointed rock mass contains planes of weakness which enable other mechanisms of rock mass damage to occur, such as the structurally controlled mechanisms described by Castro (1996). Joints enable movement and damage to occur in areas where the strength of the intact rock has not been exceeded, such as in what Martino and Chandler (2004) referred to as the excavation disturbed zone.

Brittle and strain-softening materials shed stress as they fail. The stress shed from the EDZ is redistributed to the surrounding rock mass. As a result, the region of greatest mining-induced stress is some distance away from the excavation, as opposed to immediately adjacent to as was depicted in Figure 2-2. A conceptual model of how stress redistributes in and around an EDZ is shown in Figure 2-5. This analytical solution is similar to the one shown in Figure 2-2, but accounts for a region of fractured rock mass around the excavation. In this case, the material's strength is defined with a Mohr-Coulomb criterion, and the fractured rock is assumed to have some frictional strength but no cohesion. The excavation is also given an internal pressure ( $p_i$ ) which might represent the artificial pressure given by ground support. The applied internal pressure results in a non-zero radial stress at the excavation boundary. Tangential stress increases throughout the fractured domain, peaks at the interface with the elastic material, and then decreases to the in-situ level  $p$ . Radial stresses also increase through the fractured zone (which contributes to the higher frictional strength and resulting higher tangential stress), inflect at the fractured-elastic interface, and then approach in in-situ level  $p$ .

The model shown in Figure 2-5 makes several simplifications to rock mass behaviour. First, as described by Martino and Chandler (2004), the EDZ is not simply a domain of uniformly fractured rock interfaced with an elastic medium at a discrete boundary. There is variation in the degree of damage throughout the EDZ. Therefore, there should also be variation in the level of stress that the rock mass can maintain. Second, a damaged and disturbed rock mass has a lower modulus than an in-situ rock mass (Hoek and Diederichs, 2006). Consequently, the more damaged material closer to the excavation is less stiff and will deform more readily, offering less confinement to nearby material than less damaged material farther away. Increased confinement at greater distances should also contribute to higher stress levels. Third, the varying levels of confinement throughout the EDZ will also create varying post-peak behaviours (i.e. brittle or strain-softening). Sharan (2008) shows multiple examples of how altering the post-peak behaviours (brittle-plastic or perfectly-plastic i.e. ductile) of a Hoek-Brown material will in turn alter the analytically and numerically resolved size of the EDZ and stress conditions throughout it. In summary, there are multiple complexities to rock mass behaviour that make modelling stress in excavation damage zones difficult. Nevertheless, the schematic and analytical solution shown in Figure 2-5 effectively conceptualizes how an EDZ effects the state of stress near an excavation.

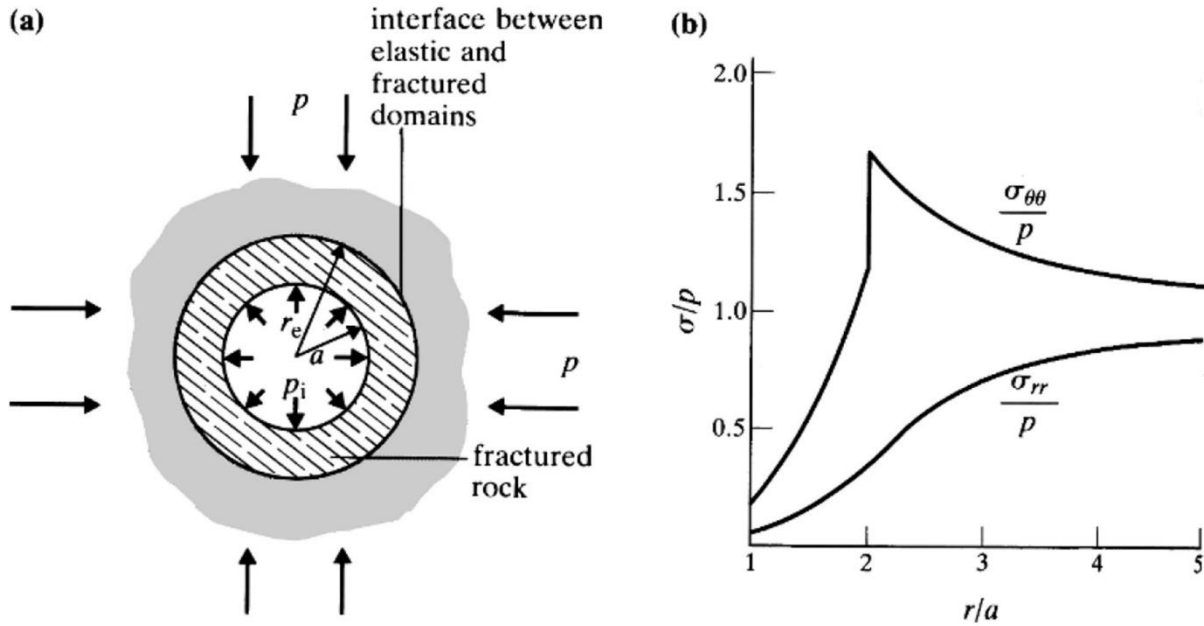


Figure 2-5: Stress tangential and normal to a circular opening surrounded by a boundary of fractured rock within an elastic medium subject to a uniform stress field (Brady and Brown, 2006)

Excavations created by blasting are formed in a matter of seconds, but stress changes and the formation of the EDZ may occur for some period of time afterwards. This effect is related to the time-dependent nature of fracture growth that occurs in brittle rocks (Costin, 1987). Hudyma et al. (1994) present strain readings from two instruments at different distances from a production blast in a Canadian mine as evidence of time-dependent yield in the rock mass. The strain cell readings are shown in Figure 2-6, and depict the change in strain observed over 6 hours following a 5,000 t blast. The readings indicate a sudden stress increase immediately after the blast, with the instrument closer to the blast reading a larger change. Within a matter of minutes of the blast, the reading on Strain Cell #9 begins to gradually decrease, indicating that the rock mass near the stope shedding stress in its post-peak strength. The reading on this instrument begins to level off after several hours. Simultaneously, strain on the instrument farther from the stope (#1) gradually increases over the hours following the initial spike. Like the readings from the instrument closer to the stope, the changes become more gradual over time. This instrument indicates that the stress being shed from the yielding rock mass near the stope is redistributing to the rock mass farther away. Both instruments show that changes occur rapidly immediately after the blast, and more slowly afterwards.

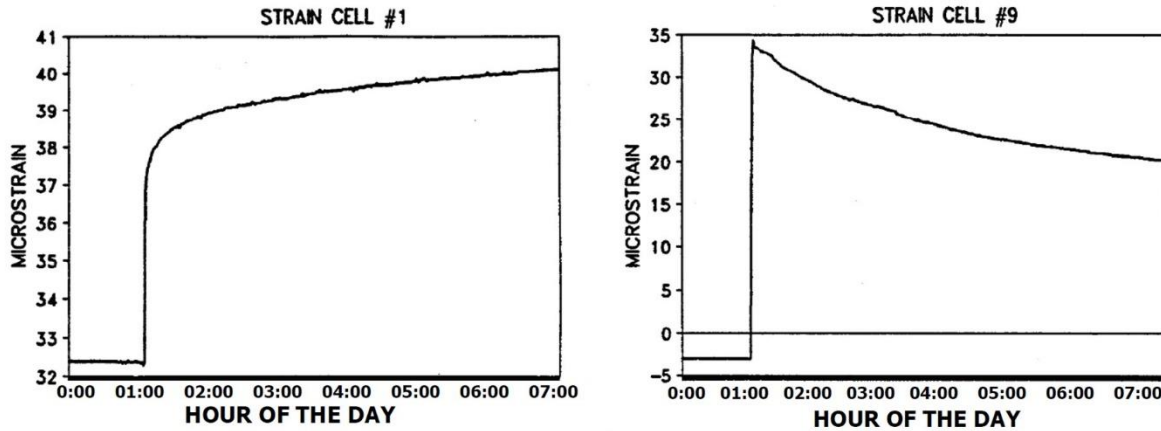


Figure 2-6: Strain cell readings from instruments 50 m (left) and 30 m (right) from a slope following a 5,000 t blast (Hudyma et al., 1994)

Malan (1999) modelled the distribution of stress in front of a tabular excavation using a time-dependent Mohr-Coulomb failure criteria. In his model, failed rock is subjected to an instantaneous loss of cohesive strength, followed by a time-dependent reduction in frictional strength consistent with observed behaviour in South African gold mines. The results of the modelled major principal stress at varying distances from the excavation face are shown in Figure 2-7. As with the analytical model shown in Figure 2-5, there is a region of lower stress immediately adjacent to the excavation which is consistent with a region of damaged rock (the EDZ). In Malan's model, the EDZ grows over time, causing the location with the highest stress to be progressively further from the excavation face. Regions of the rock mass initially under higher stress are subjected to lower stress as they fail. Consequently, regions of the rock mass initially under lower stress are subjected to gradually greater stress as stress is shed out of failed regions closer to the excavation. The largest major principal stress also decreases over time, as stress is distributed throughout a larger EDZ. The migration of the high-stress front also occurs more slowly over time, moving over 0.5 m in the first hour following the blast, but less than that over the next 4 hours. Although it is based on a relatively simple excavation geometry and assumed constitutive behaviour, Malan's model conceptualizes how time-dependent growth of an EDZ will affect the distribution of stress near and excavation.

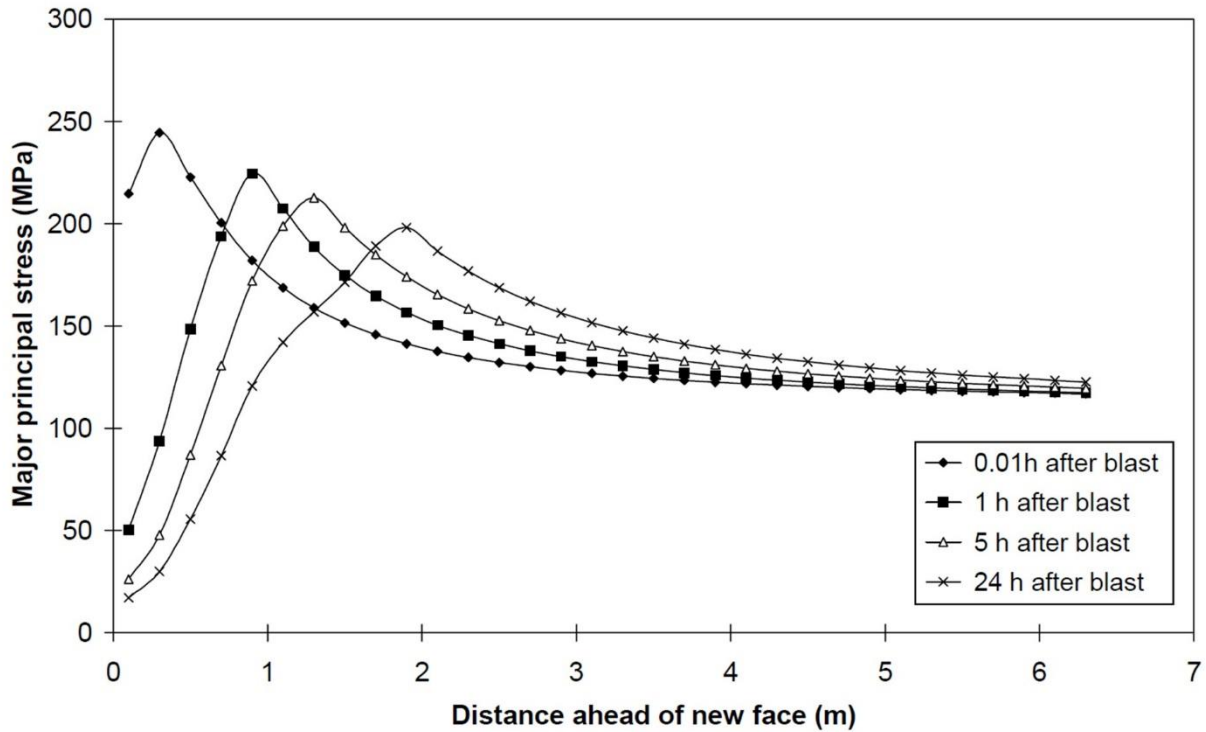


Figure 2-7: Modelled major principal stress ahead of a tabular excavation at selected time increments after a blast (Malan, 1999)

As discussed previously, stress conditions can alter the constitutive behaviour of rock masses. Figure 2-8 shows a schematic by Diederichs (2003) which illustrates the varying mechanisms of rock mass failure observed in the vicinity of excavations. Rock masses under low confinement will unravel or spall. At higher levels of confinement, brought on by greater distance from the excavation or different excavation geometries, the rock mass will have shear failure mechanisms.

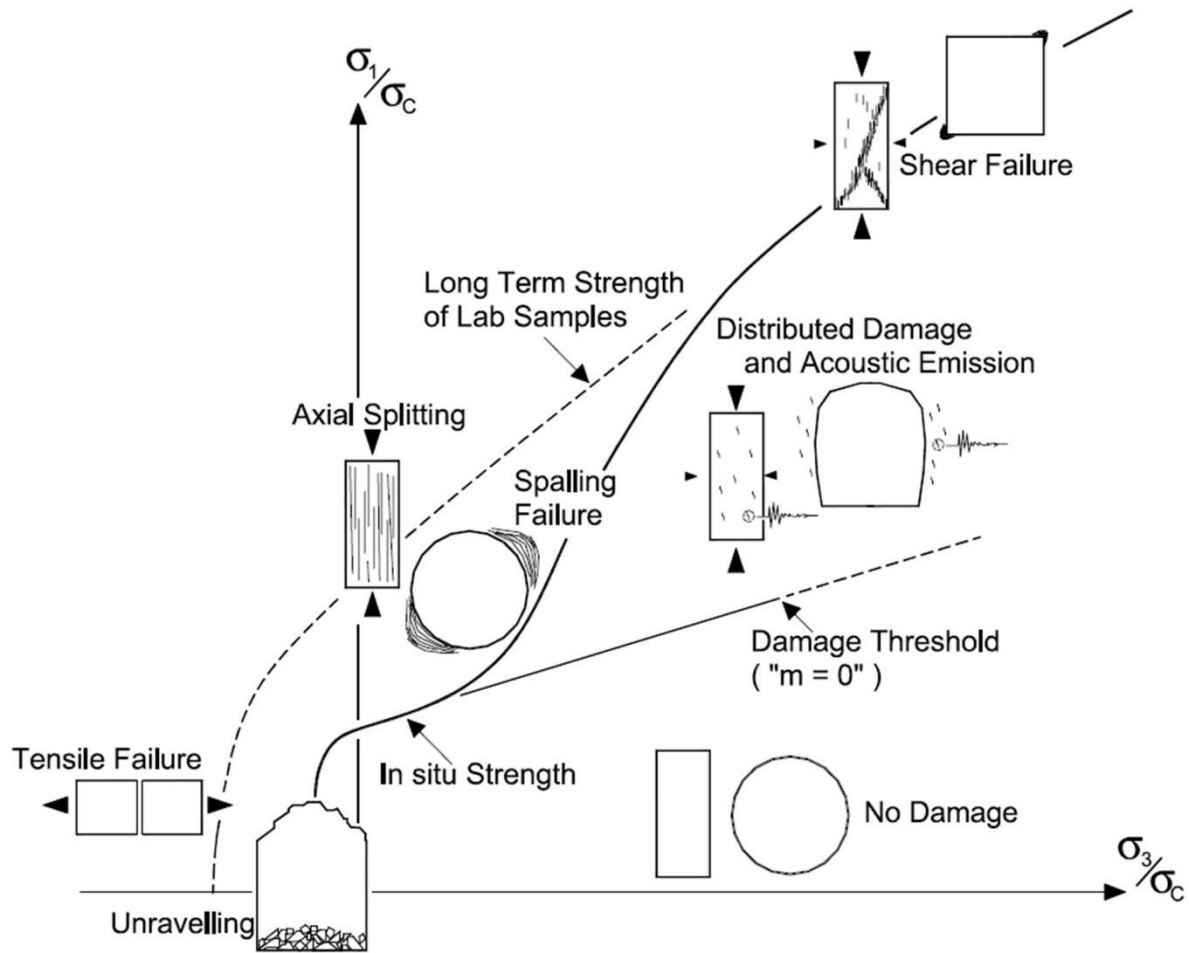


Figure 2-8: Schematic of different rock mass failure modes around an excavation depending on major and minor principal stress (Diederichs, 2003)

## 2.2 Seismicity and Mining-Induced Seismicity

### 2.2.1 Seismic Events

A seismic event is a sudden, inelastic strain in a rock mass that results in elastic wave energy radiating from its source. In the field of crustal seismology, natural seismic events are commonly referred to as earthquakes. The two principal types of waves from seismic events in mines are p-waves and s-waves. P-waves are compressional and oscillate parallel to the direction of travel. S-waves travel slower than p-waves and oscillate normal to the direction of travel. Figure 2-9 shows an example of a seismogram of an event in South Africa recorded by a triaxial sensor. Three components capturing the full motion produced by the waves are shown. The amplitude of the p-wave relative to the s-wave varies between the different directional components of the seismogram, indicating a different direction for the oscillation of each wave.

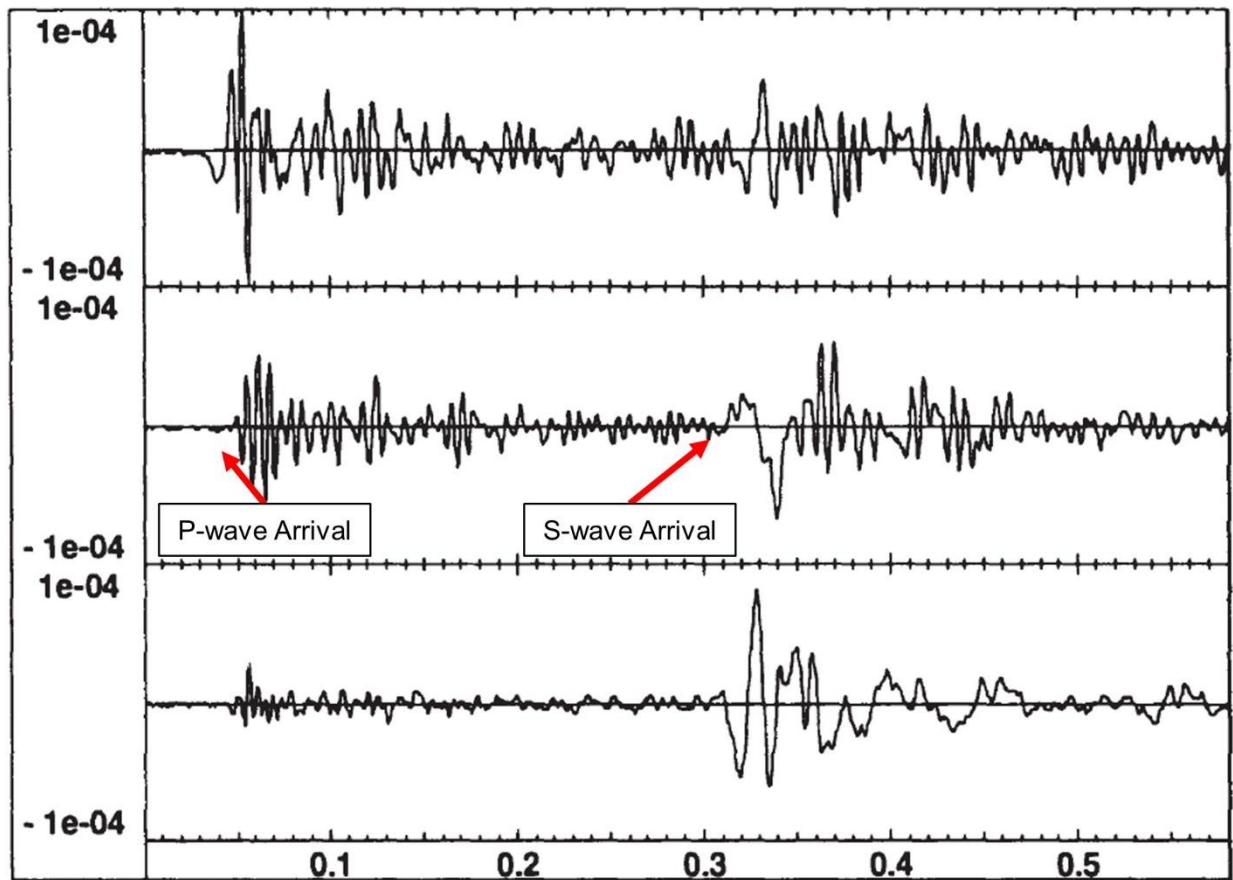


Figure 2-9: Three-component seismogram from a seismic event in South Africa, vertical units are displacement (m) and horizontal units are time (s) (modified after Mendecki, 1997)

Seismic waves can also be visualized in the frequency spectrum, an example of which is shown in Figure 2-10. The frequency spectrum shows other useful properties of the waveform which are used to derive fundamental parameters used to describe the event, namely the low frequency plateau ( $\Omega_0$ ) and the corner frequency ( $f_0$ ). The fundamental parameters derived from the waveform and frequency spectra are referred to as seismic source parameters.

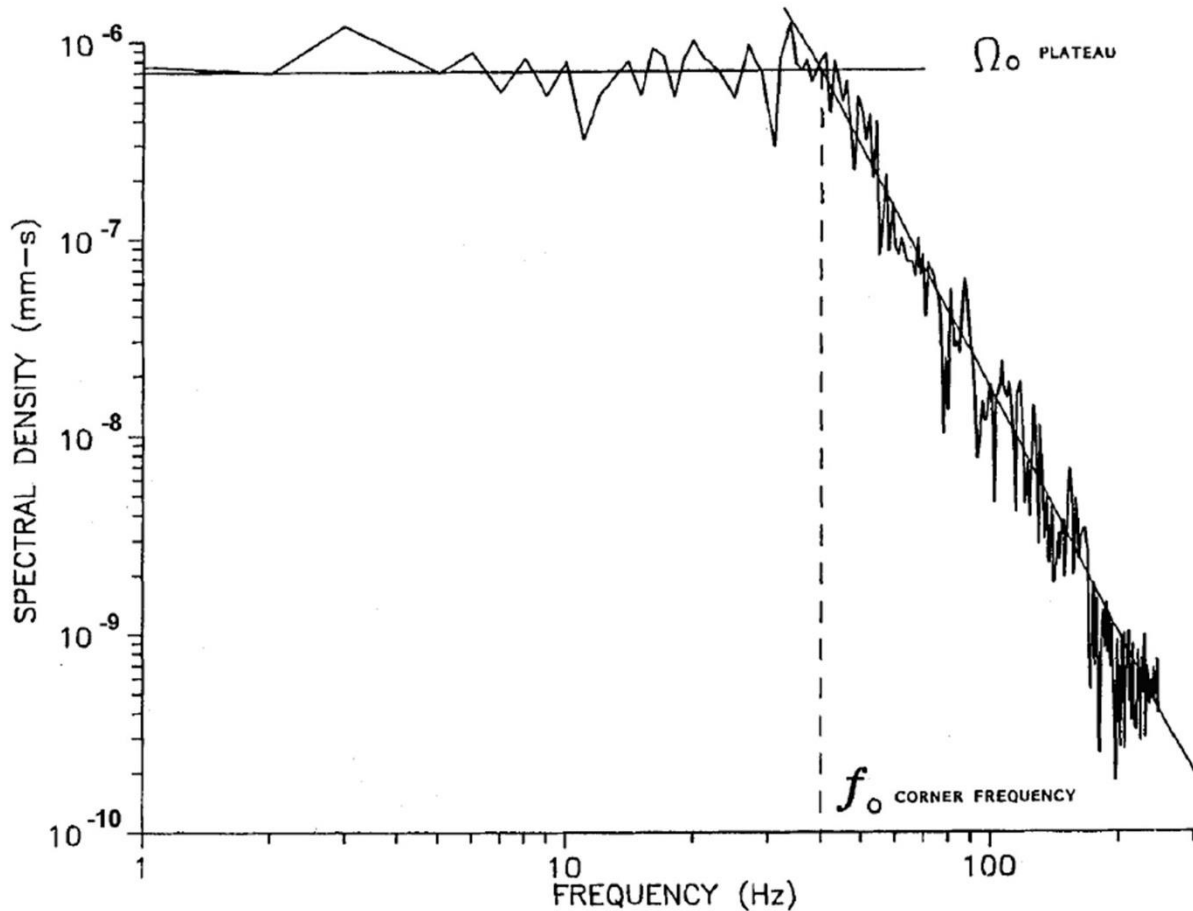


Figure 2-10: Displacement spectrum of a seismic event in the frequency domain indicating the low frequency plateau ( $\Omega_0$ ) and the corner frequency ( $f_0$ ) (Hedley, 1992)

### 2.2.2 Mining-Induced Seismicity

Mining-induced seismicity is the phenomena of excavation-induced stresses causing instability in a rock mass which results in seismic events (Cook, 1976). This phenomena occurs in many underground mines in Canada (Hedley, 1992) and around the world (Gibowicz and Kijko, 1994). Mining-induced seismicity is influenced by several factors including stress, mining geometry, geologic structure, and geologic discontinuities (Gibowicz and Kijko, 1994). Seismicity poses a hazard in underground mines, which is why many mines install systems to monitor seismic events.

Gibowicz and Kijko (Gibowicz and Kijko, 1994) present two broad classifications for mining-induced seismic events: events associated with formation of fractures around excavations, and events associated with geologic discontinuities. The former can be spatially and temporally associated with induced-stresses and stress changes around excavations (i.e. occurring near excavations and when a new excavation is created resulting in a stress change). The size and

quantity of these events is also proportional to the stress change induced by the excavation. The latter is less well defined, but is generally characterized by erratic time distributions, difficulty associating the events with a specific active mining area, and a potentially larger size that is disproportionate to changes in mining-induced stresses. These classifications create two groups of mechanisms of rock mass failure that result in seismic events. Differences in these classifications introduce the concept of non-self-similarity in mining-induced seismicity. The differences in mechanisms leads to a breakdown in the relation between the events caused by each process (i.e. the events associated with one process are not related to and therefore can not be used to describe the process that is causing the other events).

### 2.2.3 Rockbursts

The phenomena of rockbursts and mining-induced seismicity are interconnected but not identical occurrences, so it is important to distinguish the former from the latter. The term “rockburst” refers to sudden, violent damage to an excavation caused by a seismic event. However, while all seismic events are manifestations of sudden inelastic strains in a rock mass, not all seismic events result in violent damage to an excavation (Hedley, 1992). The hazardous nature of rockbursts make them the primary concern related to mining-induced seismicity for mine operators.

Rockbursts are more visual evidence of seismic events damaging intact rock near an excavation. Figure 2-11 shows rock fragments in midair after being ejected from the wall of an excavation. Stress near the excavation surface caused the rock to fracture, and some of the strain energy released during the failure was released as kinetic energy of the fragments.



*Figure 2-11: Rock fragments ejected from left wall of an unsupported opening (Deneka, 2014)*

#### **2.2.4 Seismic Source Mechanism**

A seismic source mechanism refers to the mode of rock mass failure that generates seismic events. Seismic source mechanisms and the local modes of rock mass failure they are associated with depend on various combinations of stress, geology, and mining geometry. There are a variety of seismic sources in mines, some general examples of which are illustrated in Figure 2-12 and Figure 2-13. Each of these mechanisms may fit into one of the two broad categories discussed by Gibowicz and Kijko (1994): stress-driven volumetric fracturing around excavations or shear slip on a geological feature (e.g. a fault).

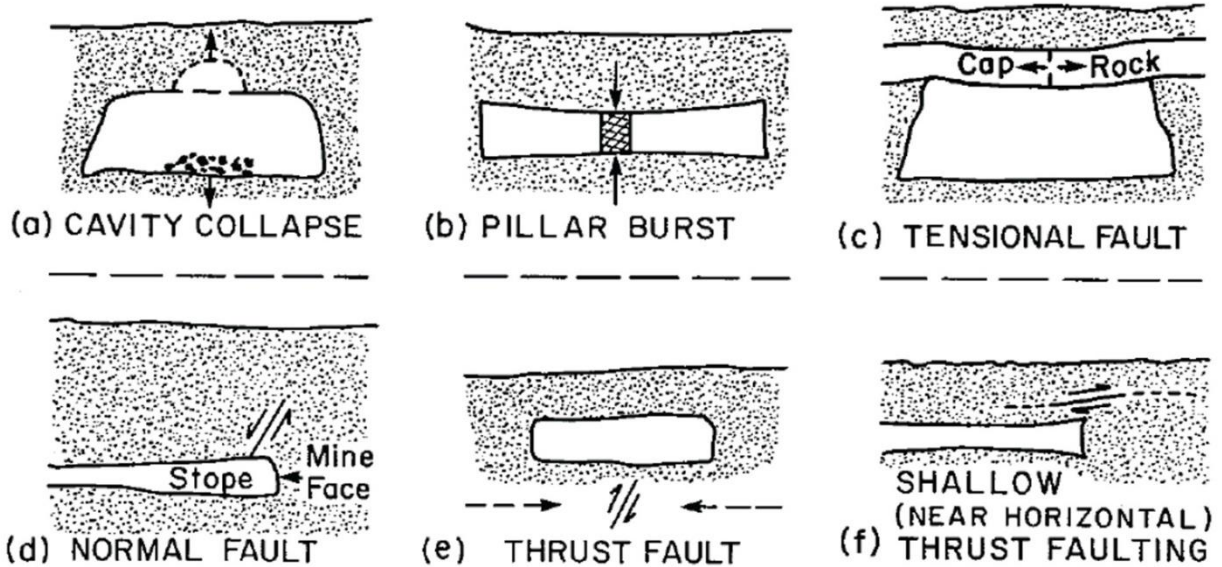


Figure 2-12: Six basic mechanisms of mining-induced seismicity in Canadian mines (Hasegawa et al., 1989)

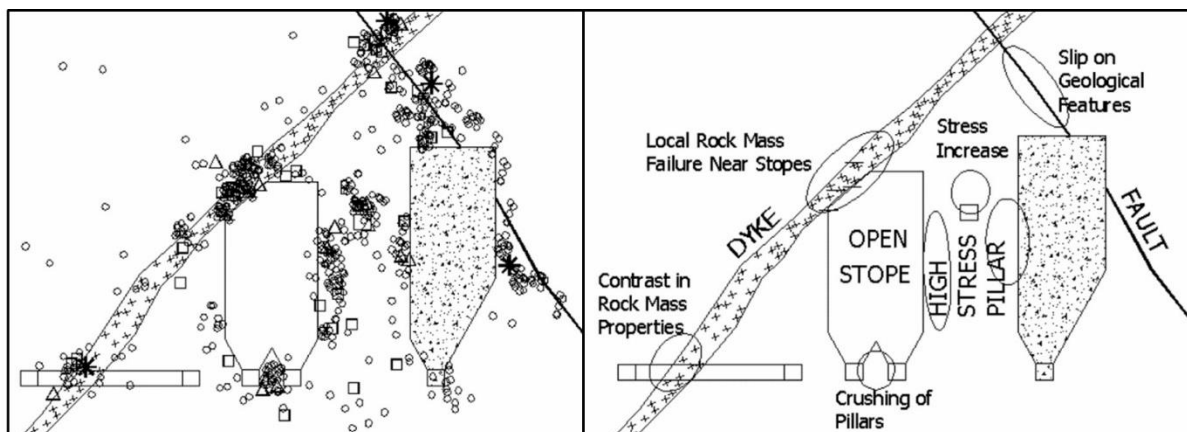


Figure 2-13: Hypothetical seismic event locations around underground workings (left) and associated seismic sources (right) (Hudyma et al., 2003)

If seismic events are accurately located, individual seismic sources can be studied by spatial filtering or clustering. Analysis of these groups of events can be used to infer characterize the local mode of rock mass failure that is generating them (Hudyma, 2008).

In a discussion of the diverse mechanisms of mining-induced seismicity, McGarr (2005) expands the classification of mining-induced seismicity to three categories of mechanisms:

1. Pure shear slip on a geologic feature that is close enough to the mine to be triggered by a small change in stress, but far enough away that it is controlled by the in-situ stresses rather than the mining-induced stresses.

2. Strong interaction between mining-induced stresses and a geologic feature near an excavation resulting in a shear and volumetric component.
3. Stress-driven volumetric fracturing of a rock mass as a result of the formation of an excavation damage zone.

Similar to the classifications of seismic events by Gibowicz and Kijko (1994), events associated with some sort of geologic feature (1 and 2) are larger than those that are not (3). McGarr's classification of seismic source mechanisms implies a more transitional nature from one type of source to another. Recall Figure 2-8 which showed the varying modes of rock mass failure around an excavation under different levels of major and minor principal stress. Such variation has also been demonstrated in seismic source mechanisms. The variation in seismic source mechanisms in mining environments is attributed to the lack of self-similarity of mining-induced seismicity (different populations of events being controlled by different processes and not being directly related to one another).

Urbancic and Young (1993) studied the source mechanisms of seismic events near an open stope in a Sudbury mine and concluded that source mechanism varied with distance from the excavation. The events with non-shear mechanisms located close to the stope face, and events with shear mechanisms located farther away. Between these two regions, there was a transition zone with mixed shear and non-shear mechanisms. Similar results were also found by Abolfazlzadeh and Hudyma (2016) who identified an increasing quantity of events with shear mechanisms at greater elevations above a caving zone in an Australian mine. These studies indicate that different seismic source mechanisms may overlap in the vicinity of a stope face. These results also agree with those of Diederichs (2003) who described the different mechanisms of failure around excavations at varying levels of confinement (Figure 2-8). Volumetric mechanisms may also vary from compression to extension around a stope (Smith-Boughner et al., 2017). These varying mechanisms may be related to the variation between fractures in the inner (fractures with significant dilation) and outer (fractures without significant dilation) excavation damage zones discussed by Perras and Diederichs (2016).

A common theme throughout the investigation of source mechanisms of mine-induced seismic events is the discussion of varying mechanisms for large and small events. The discussions on the general types of seismic events in mines by Gibowicz and Kijko (1994) and McGarr (2005) both

mention size discrepancies between the events related to fracturing around an excavation and events which involve a geologic structure. Young et al. (1992) also reported that non-shear failure mechanisms are more prevalent with smaller events. For this reason, an event's size alone may have implications as to what mechanism of rock mass failure it is associated with.

#### 2.2.5 Seismic Monitoring in Mines

Mine operators use local arrays of time-synchronized sensors to record seismic events occurring near their mine. Modern seismic monitoring systems automatically digitize sensor readings and identify wave arrival times in order to locate events and determine their source parameters. A generic layout of a seismic monitoring system in a underground mine is shown in Figure 2-14. Sensors on different levels of the mine record ground motions and transmit the signals over copper cable to a digitizer on the level (referred to by its proprietary name, Paladin, in Figure 2-14). Analog signals that travel less distance before being digitized pick up less noise and provide a cleaner signal for processing. The digitizer sends the signal to a computer on surface which processes the data (determines wave arrival times, locates events, calculates other source parameters).

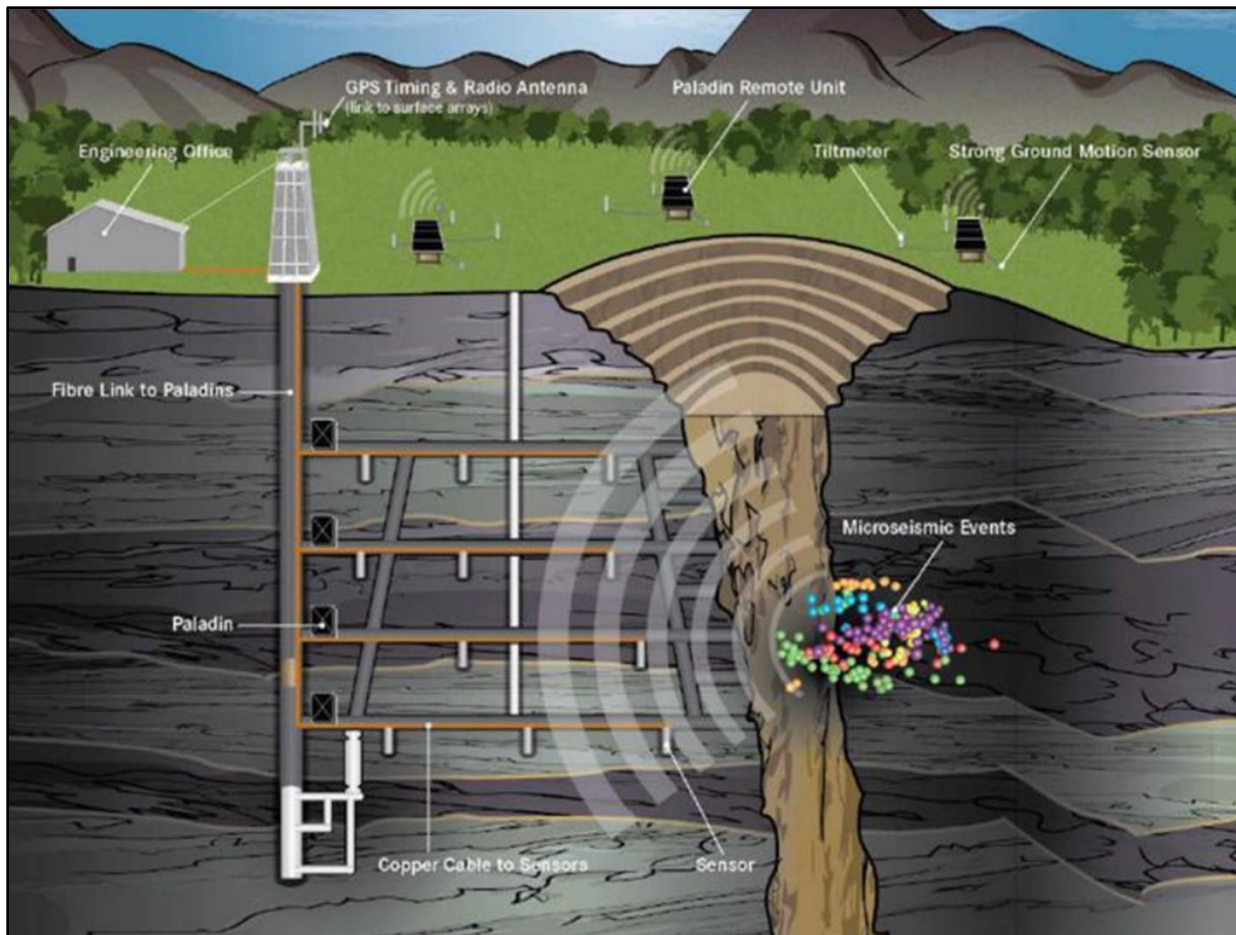


Figure 2-14: Illustration of a typical underground microseismic monitoring system (Collins et al., 2014)

Different types of sensors detect different amplitudes and frequency ranges. Figure 2-15 shows the dynamic range of an accelerometer and various geophones. Each sensor can not reliably detect motion lower than its noise limits, and motion above its clip limits will be saturated and not an accurate representation of the ground motions produced by the event. If a sensor is too close to the seismic source, the motion will be above the clip limit and the sensor will saturate. If the sensor is too far from the source, the waves will have attenuated and the motion will be below the noise limit. Ideally, a seismic monitoring array will have a variety of sensors placed at different distances from seismic sources.

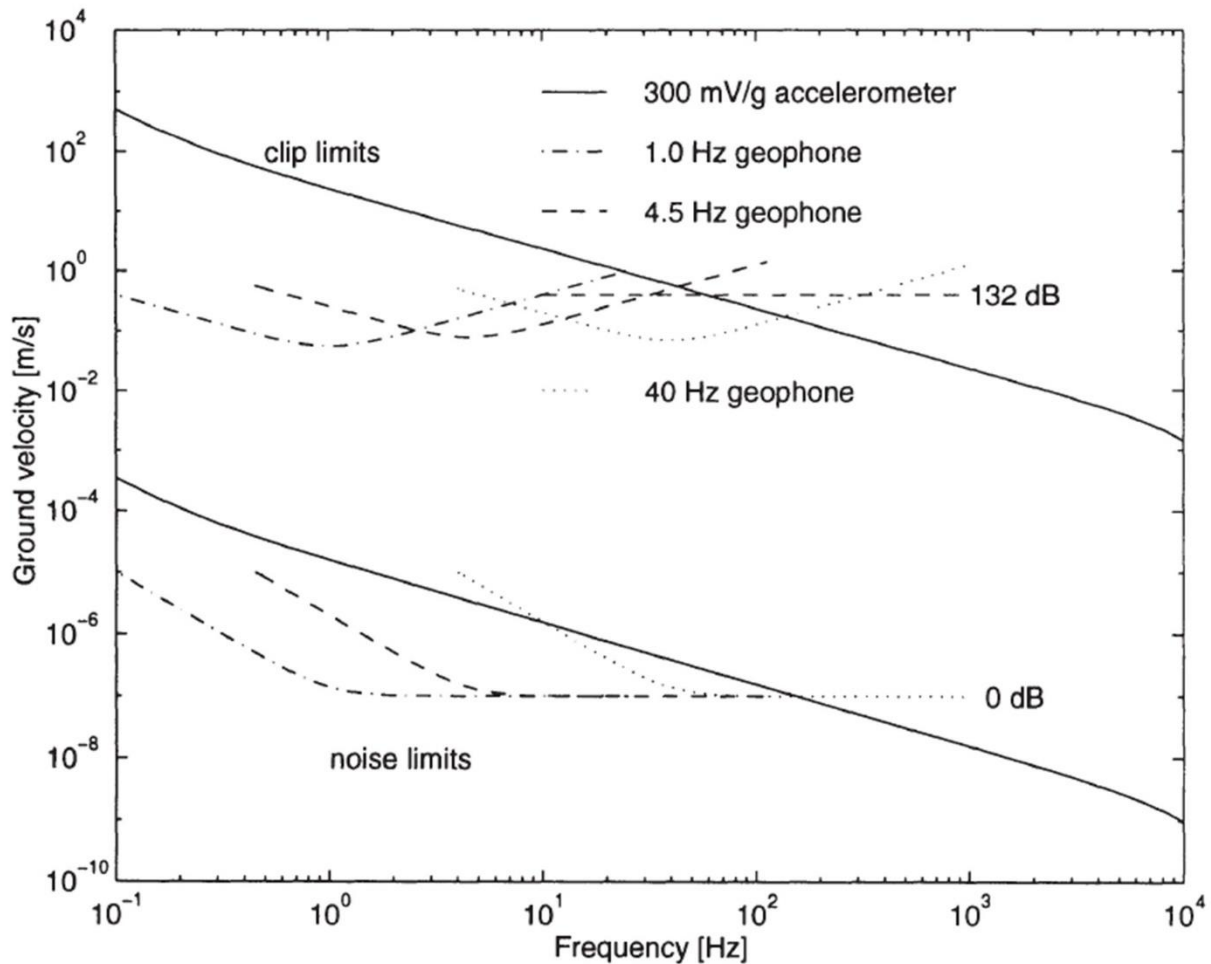


Figure 2-15: Dynamic range of various sensors used in seismic monitoring (Mendecki, 1997)

Sensors may capture a single component (uniaxial) or three components (triaxial) of ground motion. Triaxial sensors provide a complete record of the ground motion which makes calculation of seismic source parameters more accurate. However, there is a cost trade-off between recording the complete ground motion at one location versus a single component of ground motion at three locations.

Amplitudes and polarities of seismic waves are not radiated uniformly in all directions. Figure 2-16 illustrates radiation patterns for an ideal shear seismic source. Seismic sensors should be located in as many directions around the seismic source as possible in order to most adequately sample the radiation patterns of the ground motions produced by the event. More complete sensor coverage around the event also improves location accuracy by increasing the “uniqueness” of a solution to its location (Mendecki, 1997).

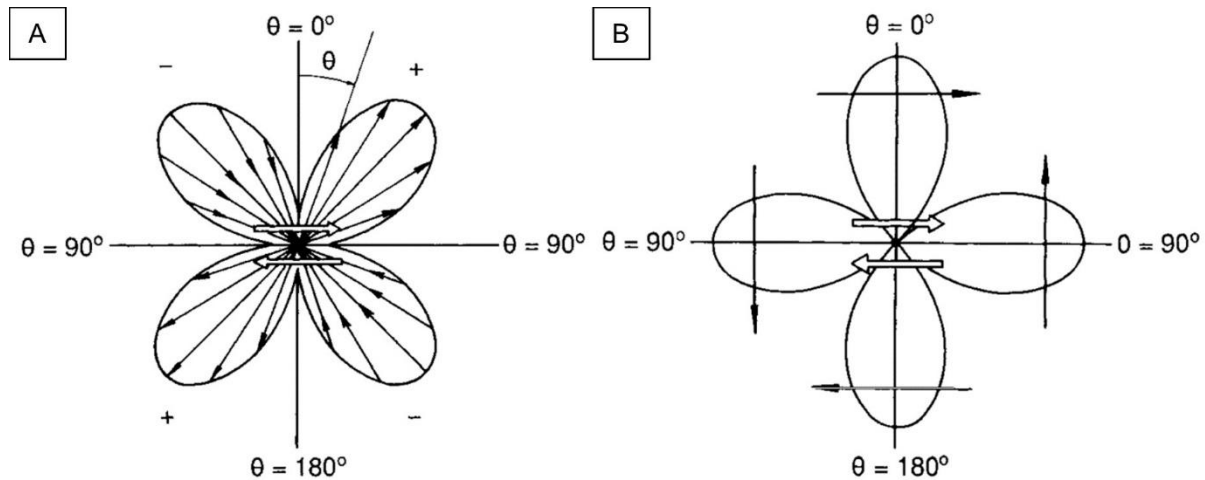


Figure 2-16: P-wave (a) and s-wave (b) radiation patterns for an ideal double-couple seismic source (Aki and Richards, 1980)

## 2.3 Seismic Source Parameters

### 2.3.1 Location and Time

Location is determined using wave arrival times and travel velocities. Once an event's location is known, the time can be determined based on the velocity of the waves and how far they had to travel to the sensors. The simplest methods for determining an event's location assume constant velocities for the p and s-waves and straight-line travel paths from the source to the sensor. However, wave velocities vary between different travel mediums, refract when changing mediums, travel around voids, and reflect and scatter off free surfaces (Mendecki, 1997). These complications are problematic in mining environments which have an abundance of excavations that create free faces and voids, and multiple geologic domains with varying wave velocities. Three-dimensional velocity models can improve location accuracy (Collins et al., 2014), or more sensors around the source location would increase the number of sensors that the waves can travel to in an unobstructed straight line from their source.

### 2.3.2 Magnitude

The magnitude ( $M$ ) of a seismic event is a relative measure of its size based on one of more of its source parameters. These scales are typically logarithmic and serve to give a general measure of how big or small an event is. One of the most commonly referred to magnitude scales is the Richter Scale ( $M_R$ ) which is based on a peak ground motion amplitude (Richter, 1935). The Nuttli Scale ( $M_N$ ) is also based on peak amplitude and is more common in Eastern Canada because it was

designed around the attenuation characteristics of seismic waves in Eastern North America (Nuttli, 1973).

The moment magnitude scale ( $M_w$ ) is based on the seismic moment (Hanks and Kanamori, 1979). This scale is commonly used in the study of mining-induced seismicity. It is considered more robust as it accounts for more complete waveform information rather than a peak amplitude.

### 2.3.3 Energy

Seismic energy ( $E$ ) refers to the total energy radiated in the form of seismic waves from a single event. The total seismic energy for an event is the sum of the energy associated with the p and s-waves  $E = E_p + E_s$ . The ratio of s to p-wave energy has been used as an indicator of seismic source mechanism, with a lower ratio (more p-wave energy for the same s-wave energy) being an indicator of a non-shear source mechanism (Gibowicz et al., 1991, 1990; Urbancic and Young, 1993).

Boatwright and Fletcher (Boatwright and Fletcher, 1984) calculate the energy for each wave as:

$$E = 4\pi\rho c \langle F_c \rangle^2 \left( \frac{R}{F_c R_c} \right)^2 J_c$$

[2.1]

where

$E$  = Seismic energy of the p or s-wave (J)

$\rho$  = Density of the wave transfer medium ( $\text{kg/m}^3$ )

$c$  = Wave velocity (m/s)

$R$  = Distance from the location of the seismic source (m)

$F_c$  = Radiation pattern coefficient

$R_c$  = Correction factor for free face surface amplification

$J_c$  = Integral of the square of the ground velocity spectrum

The seismic energy is a small fraction of the total energy released by the inelastic deformation that caused it. The fraction of the total energy ( $E_T$ ) that is released in the form of seismic waves is referred to as the seismic efficiency  $\eta$  where  $E = \eta E_T$ . For seismic events in natural and mining environments, the seismic efficiency is typically less than 6% (McGarr, 1999).

The seismic efficiency depends on the seismic source mechanism. McGarr (1976) estimated the efficiency seismic events associated with volumetric closure of a mine excavation at around 0.24%. By comparison, an area with higher shear stresses was found have efficiencies in the range of 0.26 to 3.6% (McGarr et al., 1979). Across various South African mines, efficiency was also found to be higher for events with shear focal mechanisms, and lower for events with a non-shear and volumetric focal mechanism (McGarr, 1994). Using a definition for seismic efficiency proposed by Beeler et al. (2003) based on work by Savage and Wood (1971), other authors have also found that events with shear mechanisms have higher seismic efficiency than those with non-shear mechanisms. Based on the definition by Beeler et al., Gibowicz et al. (1990) found higher efficiencies for large events ( $M > 1$ ) with shear mechanisms in a German coal mine, and Urbancic and Young (1993) found the same for small events ( $M < 0$ ) in a Sudbury nickel mine.

### 2.3.4 Moment

Moment ( $M_o$ ) is proportional to the area of slip and magnitude of displacement for shear-type events (Aki and Richards, 1980) and volumetric strain (Mendecki, 2016). Moment can essentially be used as an analog for co-seismic deformation. Gibowicz and Kijko (1994) show seismic moment calculated as:

$$M_o = \frac{4\pi\rho c^3 R\Omega_o}{F_c R_c S_c} \quad [2.2]$$

where

$M_o$  = Moment of the p or s-wave (Nm)

$\rho$  = Density of wave transfer medium ( $\text{kg/m}^3$ )

$c$  = Wave velocity (m/s)

$R$  = Distance from location of the seismic source (m)

$\Omega_o$  = Low-frequency plateau of displacement from the frequency spectra

$F_c$  = Radiation pattern coefficient

$R_c$  = Correction factor for free face surface amplification

$S_c$  = Sensor site correction factor

### 2.3.5 Apparent Stress

Apparent stress ( $\sigma_a$ ) is a relative measure of co-seismic stress change. It is one of multiple parameters used to estimate stress drop of seismic events. Its advantage over others is that its calculation is relatively simple and does not rely on any one failure model (e.g. square or circular shear failure surfaces). The apparent stress is proportional to stress change, but not a direct measure of it (Madariaga, 1976). Wyss and Brune (1968) calculate apparent stress as:

$$\sigma_a = \mu \frac{E}{M_o}$$

[2.3]

where

$\sigma_a$  = Apparent stress (Pa)

$\mu$  = Shear modulus of the rock mass (Pa)

$E$  = Seismic energy (J)

$M_o$  = Moment (Nm)

The contribution of p-wave energy to the total seismic energy makes apparent stress independent of other stress release estimates. The prevalence of non-shear seismic source mechanisms in mining environments makes this aspect of apparent stress particularly useful and distinct from other stress drop estimates (Gibowicz and Kijko, 1994).

Apparent stress can be used to interpret stress in a rock mass. A rock mass under higher stress may release more seismic energy because more strain energy is stored in the rock. However, high stress may not allow for much deformation, leading to lower moment and a higher apparent stress. However, Urbancic and Trifu (1998, 1996) have shown that apparent stress is also highly

dependent on normal stresses (i.e. confinement) and in some cases is quasi-independent of the maximum shear stress. Of course, higher normal stresses contribute to resisting failure, leading to higher shear stresses when failure eventually occurs.

Apparent stress is also proportional to seismic efficiency (fraction of the total energy associated with an event that is radiated as seismic waves). Urbancic and Trifu (1996) presented an observed dependence of apparent stress on seismic efficiency as the reason the parameter was quasi-independent of the maximum shear stress. The correlation between apparent stress and seismic efficiency implies the parameter is also related to the seismic source mechanism. Recall that shear failures have higher seismic efficiency than non-shear failures, and that higher seismic efficiency results in more stored strain energy being released in the form of radiated seismic energy. It is evident that an event with a shear source mechanism may have higher apparent stress than an event with a non-shear mechanism occurring under similar stress conditions. The dependence of radiated seismic energy and apparent stress on seismic source mechanism was demonstrated by Perez-Campos and Beroza (2001) with worldwide population of natural earthquakes. This dependence of apparent stress on mechanism complicates the use of apparent stress as an indicator of stress in a rock mass.

However, there is clearly an interplay of factors that coincide and contribute to higher or lower apparent stress. Under conditions with higher normal stress/confinement:

- The rock mass has higher peak strength (higher stress at the time of failure).
- There is less capacity for deformation (lower seismic moment).
- There are shear failure mechanisms (higher seismic efficiency and seismic energy release).

Under conditions with lower normal stress/confinement:

- The rock mass has lower peak strength (lower stress at time of failure).
- There is more capacity for deformation/dilation (higher seismic moment).
- There are non-shear failure mechanisms (lower seismic efficiency and energy release).

Therefore, apparent stress may be a practical indicator of areas of a rock mass under elevated stress conditions.

## 2.4 Seismic Data Analysis Techniques

### 2.4.1 Magnitude-Time Histories

Magnitude-time histories serve as a visual chronological record of when events of a specific size occurred. In populations of induced seismicity, the time that events occurred can be used to associate them with the mining activity occurring at the same time or just before (e.g. a specific blast). Visualizing how events occur over time, with each event representing an inelastic deformation in the rock mass, indicates rock mass failure is a gradual or continuous process rather than instantaneous and discrete occurrence. Magnitude-time histories also incorporate a line for the cumulative number of events over time. The slope of this line indicates the rate at which events are occurring (steeper slope indicates higher event rate).

Figure 2-17 shows an example of a magnitude-time history from a population of events near an open stope. There is no local mining activity at the beginning of the time history, and few events occur which have lower magnitudes. The first mining activity in the history is development of an access to the stope. Small, incremental blasts are followed by small numbers of intermediate-magnitude events. There are small steps in the cumulative number of events over a period of approximately 6 weeks, indicating the events induced by each individual development blast (each around 200 t). There is 6-week pause while blasting stops and the stope is drilled off. There are few events during this period, all of which have low magnitudes. Production blasting starts with a 5,000 t blast that induces more events than any of the individual development blasts. Lastly, a 19,000 t blast is taken which induces more events than the first production blast. There are many intermediate magnitude events that follow immediately after this blast, and the largest event in the time history occurs within a few days of this largest blast. The event rate remains elevated for approximately 4 weeks while blasted rock is removed from the stope. Multiple other intermediate magnitude events occur during this time, indicating that the rock mass continues to yield. The event rate decreases after the stope is backfilled in early January 2017, and mostly smaller magnitude events occur after this time.

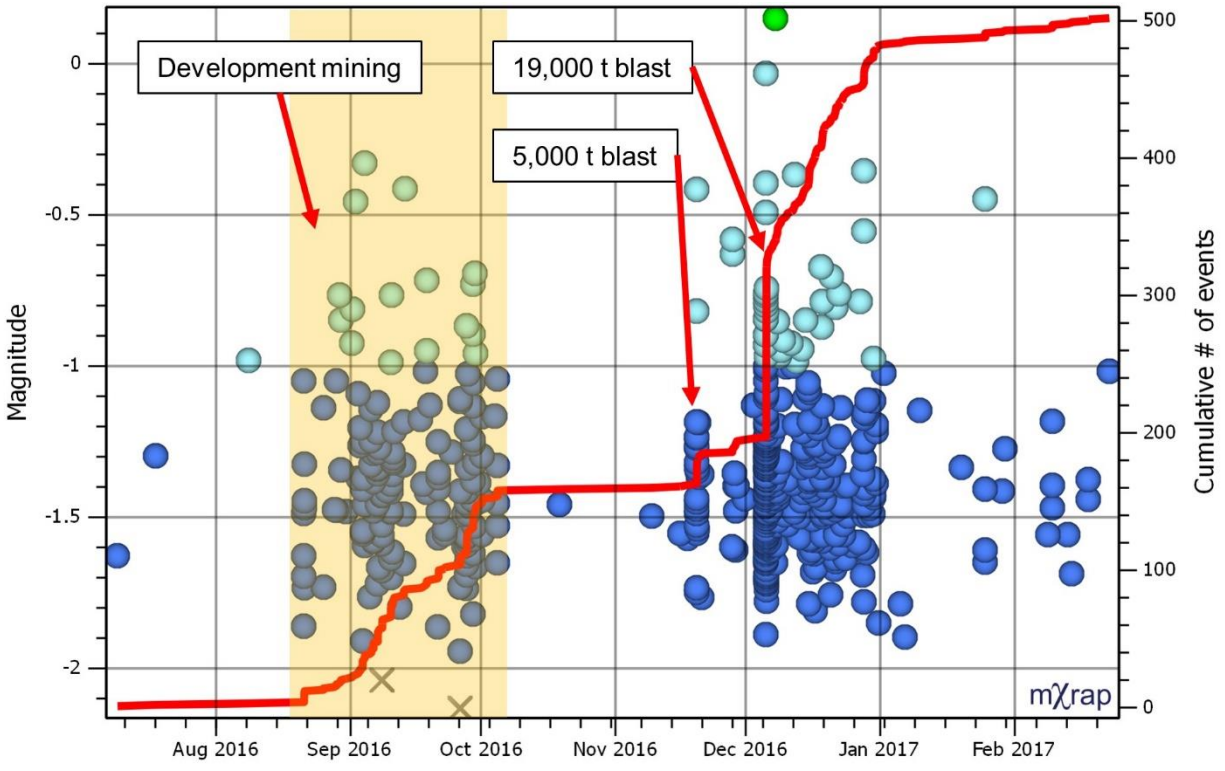


Figure 2-17: Example of a magnitude-time history from a population of events near an open stope

### 2.4.2 Frequency-Magnitude

Gutenberg-Richter frequency-magnitude relations are logarithmic scaled plots that show the number of events greater than a certain magnitude. Well-behaved data should follow a linear trend over several orders of magnitude, such as the relation shown in Figure 2-18.

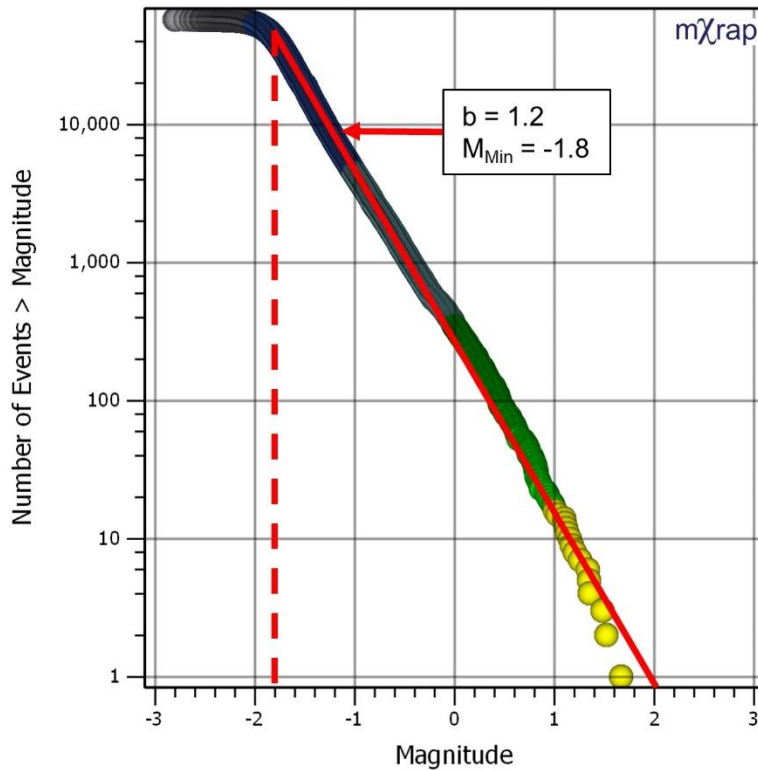


Figure 2-18: Example of a well-behaved frequency-magnitude relation

Well-behaved data should follow a linear relation, indicating a power-law relation between events of different sizes (Richter, 1935). The linear relation takes the form:

$$\log N = a - bM$$

[2.4]

Where

$N$  = Number of events

$a$  = Vertical axis intercept

$b$  = Slope of the line

$M$  = Magnitude

In addition to following a linear relation, well-behaved data should also have the horizontal axis intercept close to the magnitude of the largest observed event. The point on the plot where the data ceases to follow a linear relation at smaller magnitude events is the sensitivity, or  $M_{\text{Min}}$ . The  $M_{\text{Min}}$

in Figure 2-18 is approximately -1.8. Theoretically, the relation should continue to follow a linear trend below this point, but not all of the smaller events are detected.

The slope of the linear relation or b-value indicates the proportion of large and small events. The b-value of the data in Figure 2-18 is 1.2. b-values can be determined by inspection, or a quantitative process that balances fitting the lesser number of large events with the greater number of small events. One such process is described by Wesseloo (2014). A shallower slope indicates that there are fewer small events for every larger one. The proportion of large and small events varies between different seismic sources in mining environments, with more stress-driven sources (e.g. fracturing around excavations) having higher b-values (Hudyma, 2008). b-values in mining environments are also known vary in both space and time (Urbancic et al., 1992b). When populations with different b-values overlap, the combined populations may produce a frequency-magnitude relation with two distinct slopes, known as a bi-modal frequency-magnitude relation. One such example is shown in Figure 2-19. The relation has two distinct slopes, indicating that two mechanisms are present.

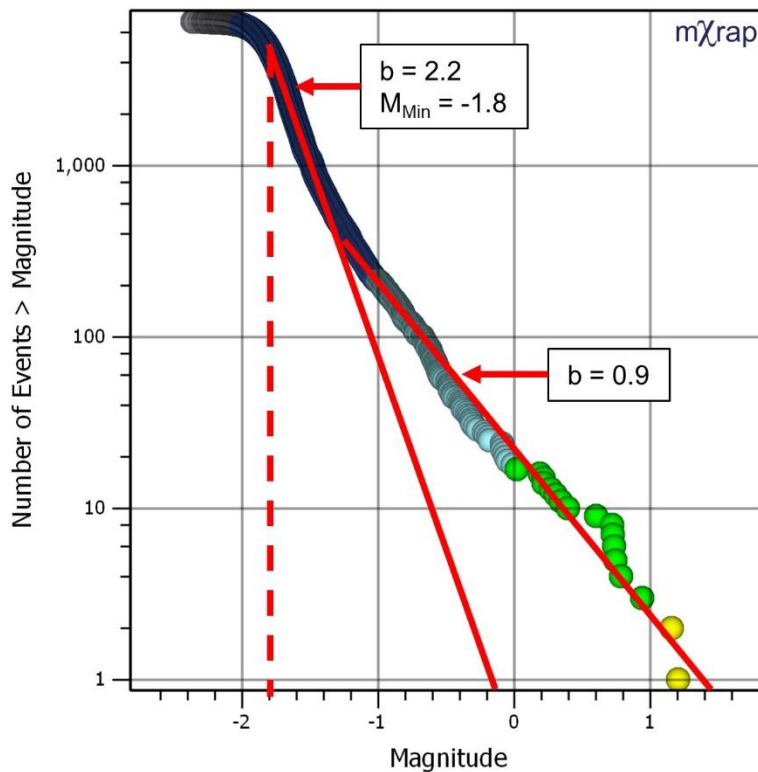


Figure 2-19: Example of a bi-modal frequency-magnitude relation

### 2.4.3 Diurnal Charts

Diurnal charts indicate the time of day events occur at. In populations of induced seismicity, the time of day events occur at can be used to associate them with the action that induced them (Cook, 1976). Higher event rates are often associated with the time of day blasts are taken. Seismic source mechanisms associated with increased mining-induced stresses tend to generate the largest numbers of events. It follows that the highest rates of events correspond with when these induced stress changes occur (i.e. when a new excavation is created by blasting). An example one such population is shown in Figure 2-20. There are two distinct spikes at the 6<sup>th</sup> and 18<sup>th</sup> hours of the day. These times correspond with when blasts are taken at the end of shifts. The spike at 6:00 PM is larger, presumably because more blasts or larger blasts are taken at this time. The larger and/or greater number of induced stress changes at this time of day result in more events occurring. The number of events after the blasts times decreases over a period of several hours, indicating how event rates decrease following blasts. During the hours towards the middle and end of the shift (around 4 hours after each blast time) the number of events is relatively constant. The chart shows events occurring throughout the day, indicating a continuous process of rock mass failure. Lastly, it is notable that the largest events ( $M > 2$ ) do not occur during blast times.

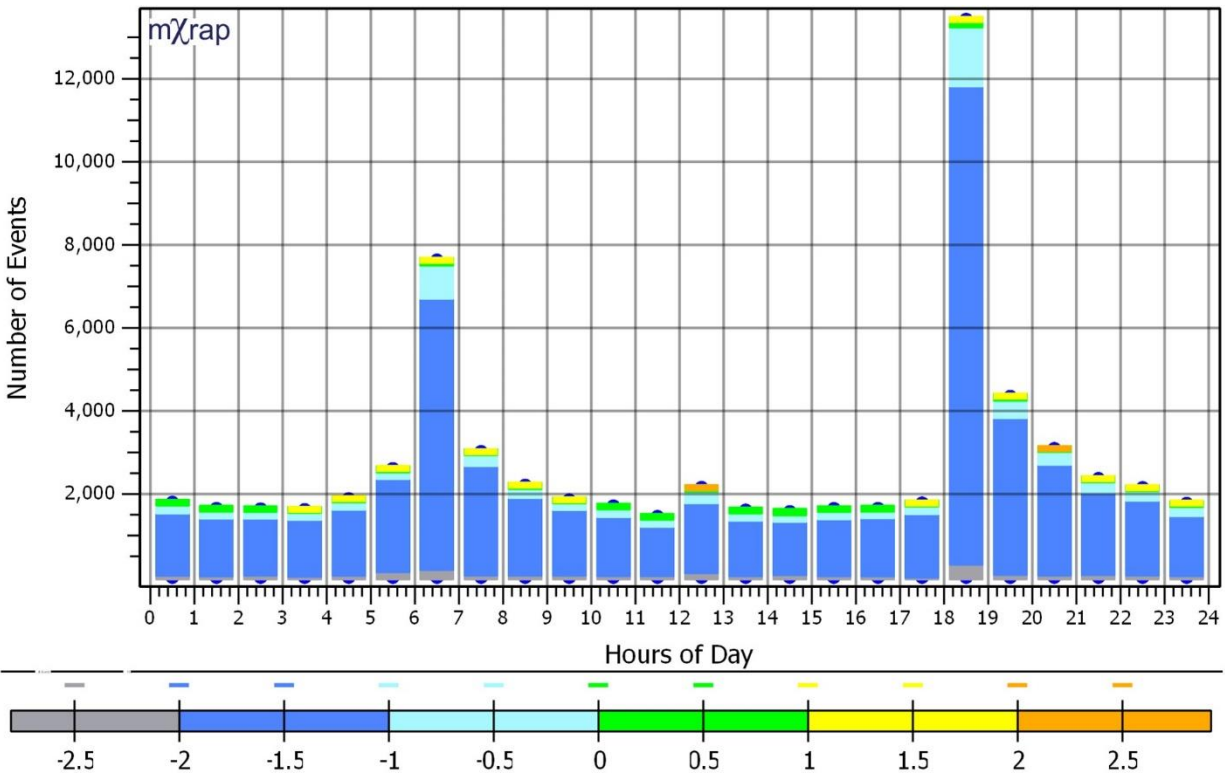


Figure 2-20: Example of a diurnal chart with events coloured by magnitude for a population of events near the production area of a mine

#### 2.4.4 Energy-Moment

Energy-moment graphs are used to show a scaling relation (how the size of one source parameter correlates with another) and are typically plotted with logarithmic axes. Based on van Aswegen and Mendecki (1999), the fitted scaling relation takes the form:

$$\log E = c + d \log M_o$$

[2.5]

where

$E$  = Seismic energy

$c$  = Vertical axis intercept

$d$  = Slope of line

$M_o$  = Moment

Any attempt to fit the relation using a linear regression will give a result that is biased by the smaller events (which have lower energy and moment) and may not be an accurate scaling relation for larger events. Quantile-quantile fitting processes have been shown to generate results that are more representative of the scaling for large and small events (Wesseloo et al., 2014).

An example of an energy-moment graph is shown in Figure 2-21. The graph shows that events with higher moment also have higher energy. The energy also varies by approximately two orders of magnitude for any given seismic moment. This amount of energy variation is typical for populations of seismic events in mine (van Aswegen and Butler, 1993). However, greater variation in energy for any given seismic moment has been suggested to be associated with greater variability in stress and rock mass properties (Mendecki, 1993).

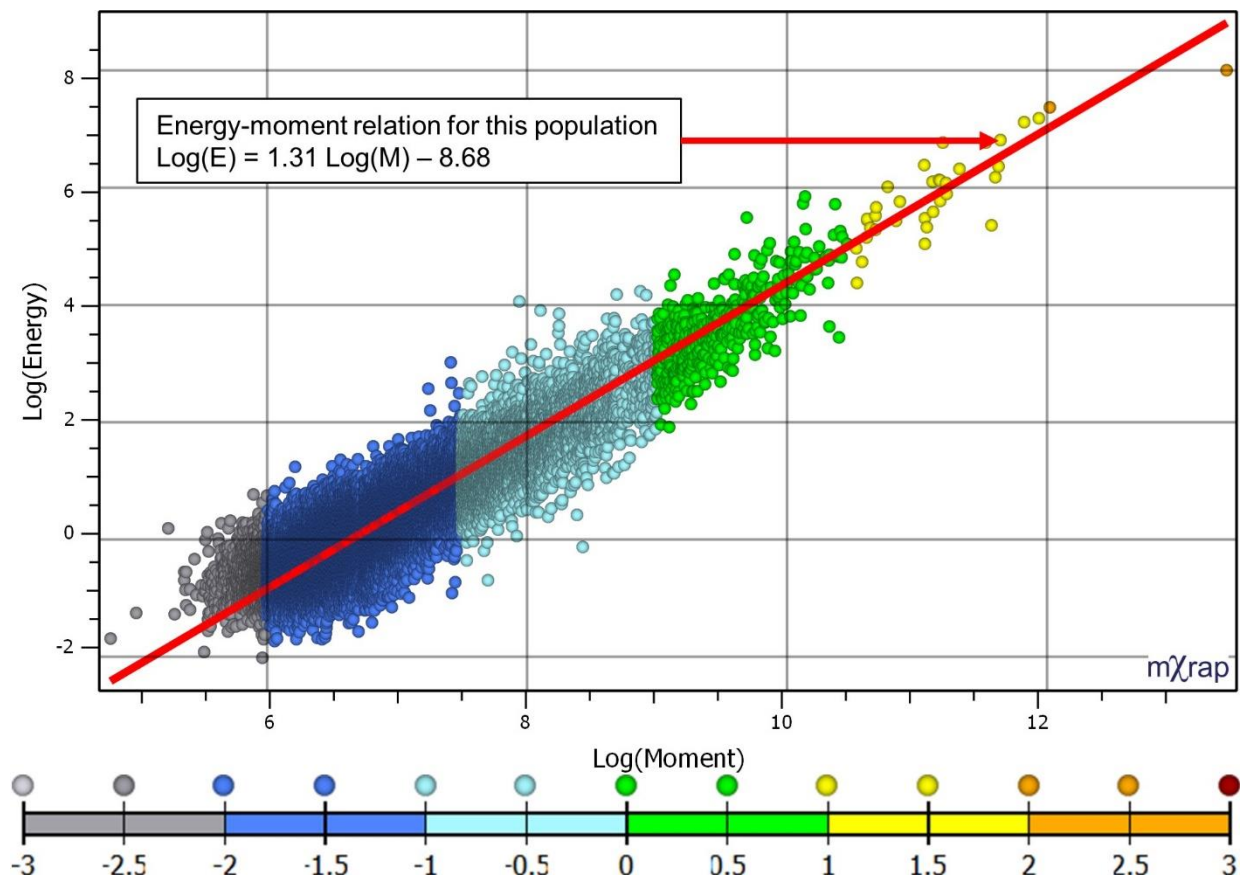


Figure 2-21: Example of an energy-moment graph with a quantile-quantile fitted scaling relation and events coloured by moment magnitude

Energy-moment graphs are particularly useful for visualizing apparent stress because they incorporate the two parameters that are used to calculate it. Figure 2-22 plots the same data shown in Figure 2-21, but events are coloured by apparent stress. As shown in the equation for the source

parameters, events with higher energy for the same moment have higher apparent stress. The graph also shows that larger events tend to have higher apparent stress than smaller events. This feature is also evident in the energy-moment scaling relation for the population, which has a slope greater than 1. The relation in Figure 2-21 indicates that for every order of magnitude increase in moment, energy should increase by 1.31 orders of magnitude. The energy-moment relation shows that apparent stress is scale-dependent in this population. Energy-moment relations with scale dependence to apparent stress have been noted in other mining environments (Amidzic, 2001; Hudyma, 2008; Mendecki, 1993; van Aswegen and Butler, 1993).

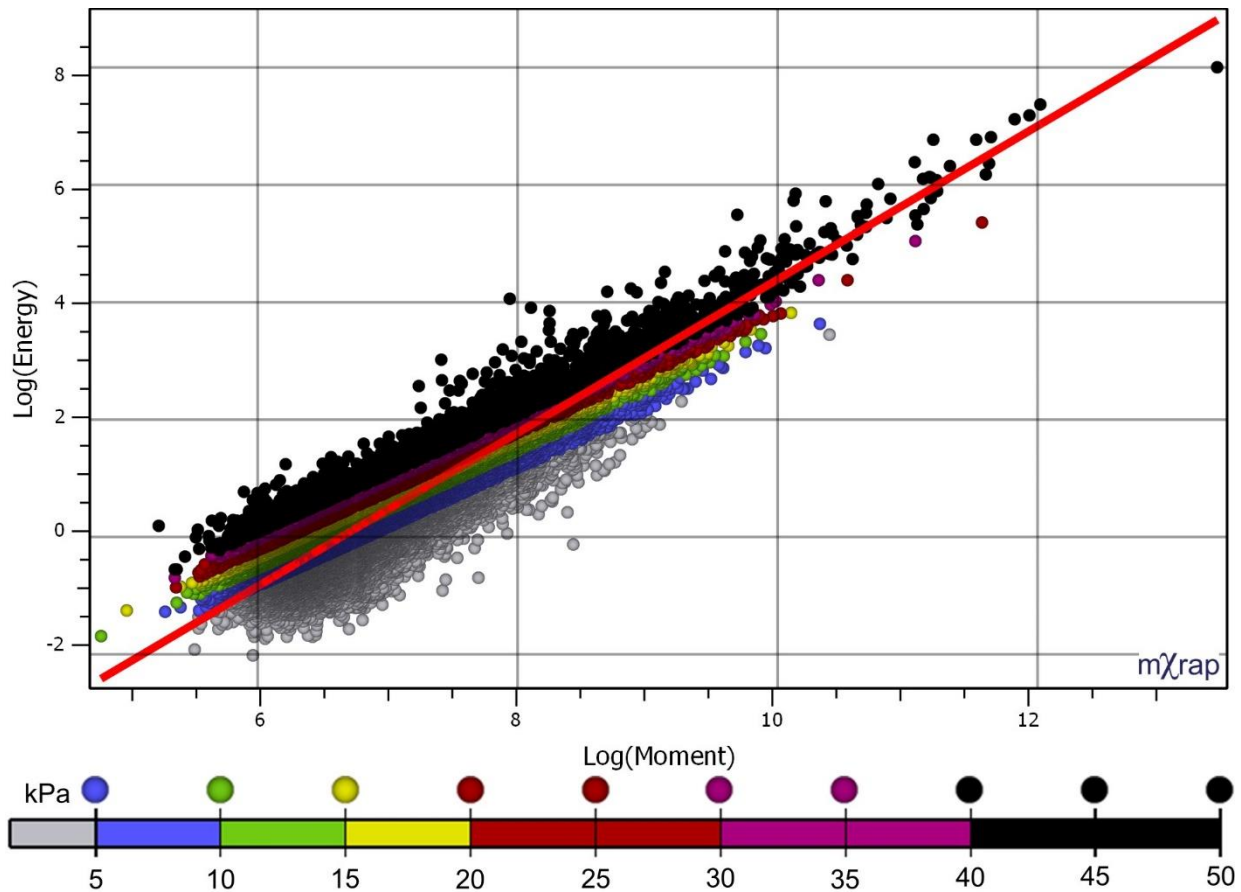


Figure 2-22: Example of an energy-moment graph with events coloured by apparent stress

The scale dependence of apparent stress and other stress release estimates is a point of contention in the field of seismology. Some researchers argue that the apparent scaling in apparent stress is related to the underestimation of energy for smaller events, which radiate a significant portion of their seismic energy at frequencies above the dynamic range of most sensors (Ide and Beroza, 2001). However, the presence of fractures in a rock mass, which are abundant in the highly stressed

regions of rock around mine excavations, has been associated with non-similar scaling behaviour for stress release parameters (Cichowicz et al., 1990; Urbancic et al., 1992a). Furthermore, the diversity of seismic source mechanisms in mining environments and the associations between source mechanism, event size, seismic efficiency, and energy release makes truly scale-dependent populations entirely plausible. This diversity of source mechanisms may be scaled down to the rock mass around a single excavation. Extensional and compressional strains are more dominant in the inner and outer damage zones respectively (Perras and Diederichs, 2016), and may be more or less prevalent in different regions around an excavation (Smith-Boughner et al., 2017). Mercer (1999) attributed difficulty with associating stress release estimates of certain events with modelled local stress conditions with the diversity of seismic source mechanisms. Non-constant energy-moment scaling has even been noted among populations of natural earthquakes (Mayeda et al., 2005).

If a parameter is scale-dependent, the size distribution of events may also influence the distribution of the parameter. In the case of apparent stress, higher apparent stress may be related to the occurrence of more large events, or a population with more large events for every small one (i.e. a frequency-magnitude relation with a higher b-value).

#### 2.4.5 Event Locations

The location of events indicates where inelastic deformations are occurring, making locations a valuable tool for interpreting the constitutive behavior of a rock mass. An area of a rock mass where active stress changes result in seismic events is referred to as a seismogenic zone (after Duplancic, 2001). In mining environments, seismogenic zones typically exist where the creation of new voids results in regions of elevated induced stress.

Events will locate around excavations in the rock mass and correspond with areas of elevated induced stresses. Lac Shortt mine in Quebec had an east-west striking orebody subjected to a NW-SE major principal stress. The mining geometry and stress orientation resulted in elevated stresses in the NE and SW corners of stopes, in the hanging wall and footwall respectively. A schematic of this stress distribution is illustrated in Figure 2-23. Seismic events also tended to locate in the NE and SW corners of stopes. A plan view of event locations at Lac Shortt is shown in Figure 2-24. These corners were also the main sources of unplanned stope dilution on the order of several metres. Access development on the west side of the orebody also frequently encountered poor

quality, heavily fractured ground. These observations exemplify the association between seismicity and local damage to a rock mass. Furthermore, it was noted that the abundance of events of varying size, rather than the magnitude of events, was the principal indicator of a visibly damaged rock mass (Ecobichon et al., 1992).

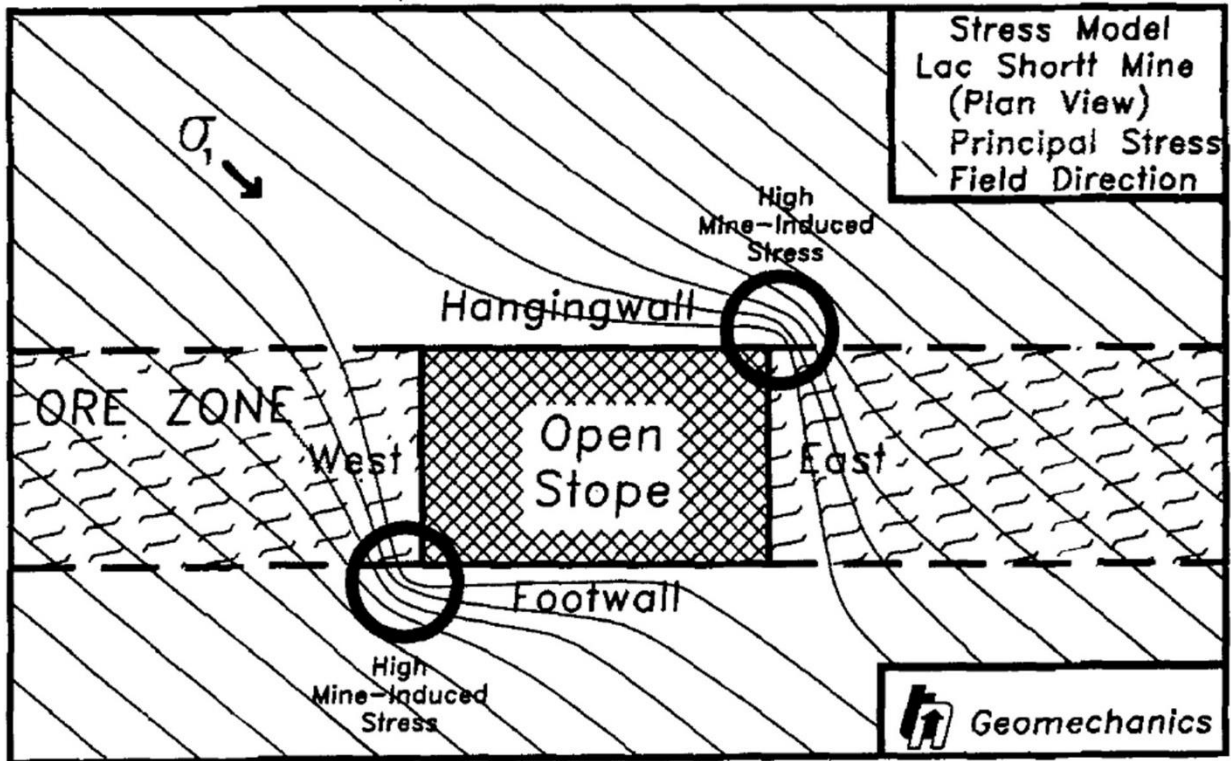


Figure 2-23: Schematic of major principal stress flow around a stope at Lac Shortt Mine, Chibougamau, Quebec (McCreary et al., 1992)

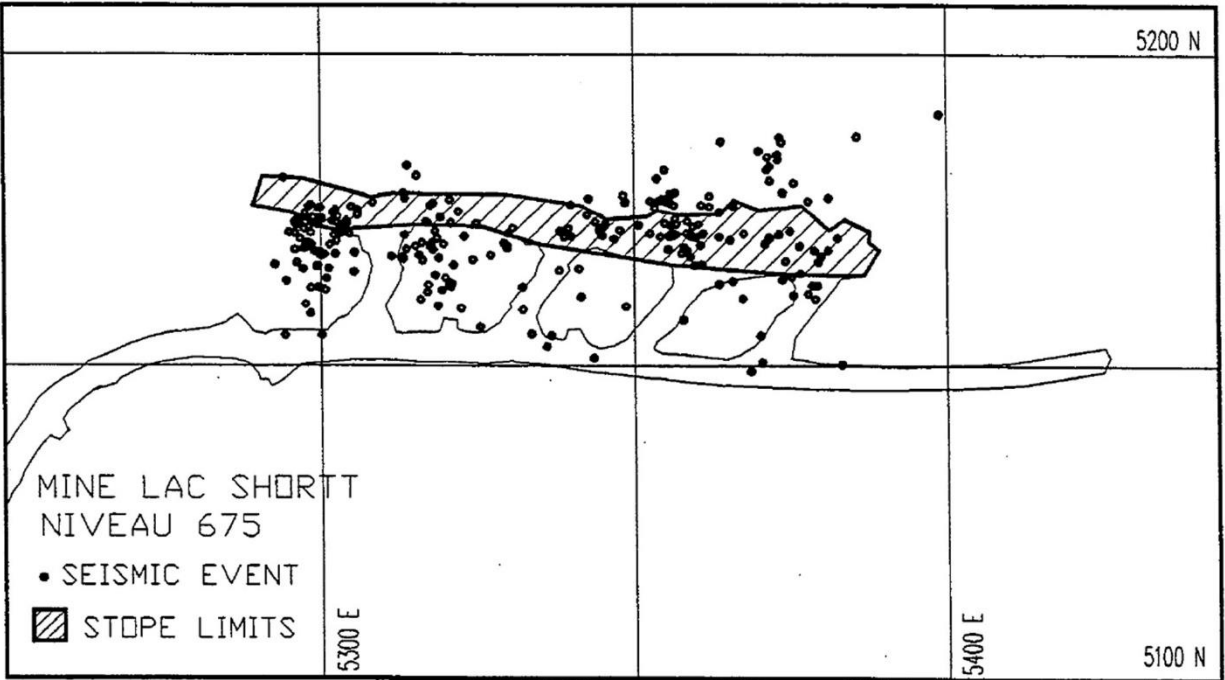


Figure 2-24: Plan view of seismic event locations at Lac Shortt mine (Ecobichon et al., 1992)

Mining-induced seismicity may occur under a combination of elevated stress and reduced confinement. Figure 2-25 shows the locations of seismic events and stress contours relative to the position of a tabular stope face. The stress parameter  $F$  is related to the difference between the major and minor principal stresses, similar to the deviatoric stress (difference between  $\sigma_1$  and  $\sigma_3$ ). Seismic events tend to occur in regions with high major principal stress relative to the minor principal stress (i.e. high deviatoric stress). They also occur in conditions where induced stresses create a tensile or shear loading regime (left or right of the dashed line in Figure 2-25). Events also occur in areas of the rock mass that are not loaded beyond the failure envelope of the intact rock (outside the hatched areas near the stope). The presence of events outside these regions indicates that they are not necessarily associated with the yield of intact rock, rather they are associated with yield of the rock mass. Seismicity in this mine also tended to locate above the stope where the rock mass was stronger (McGarr et al., 1975).

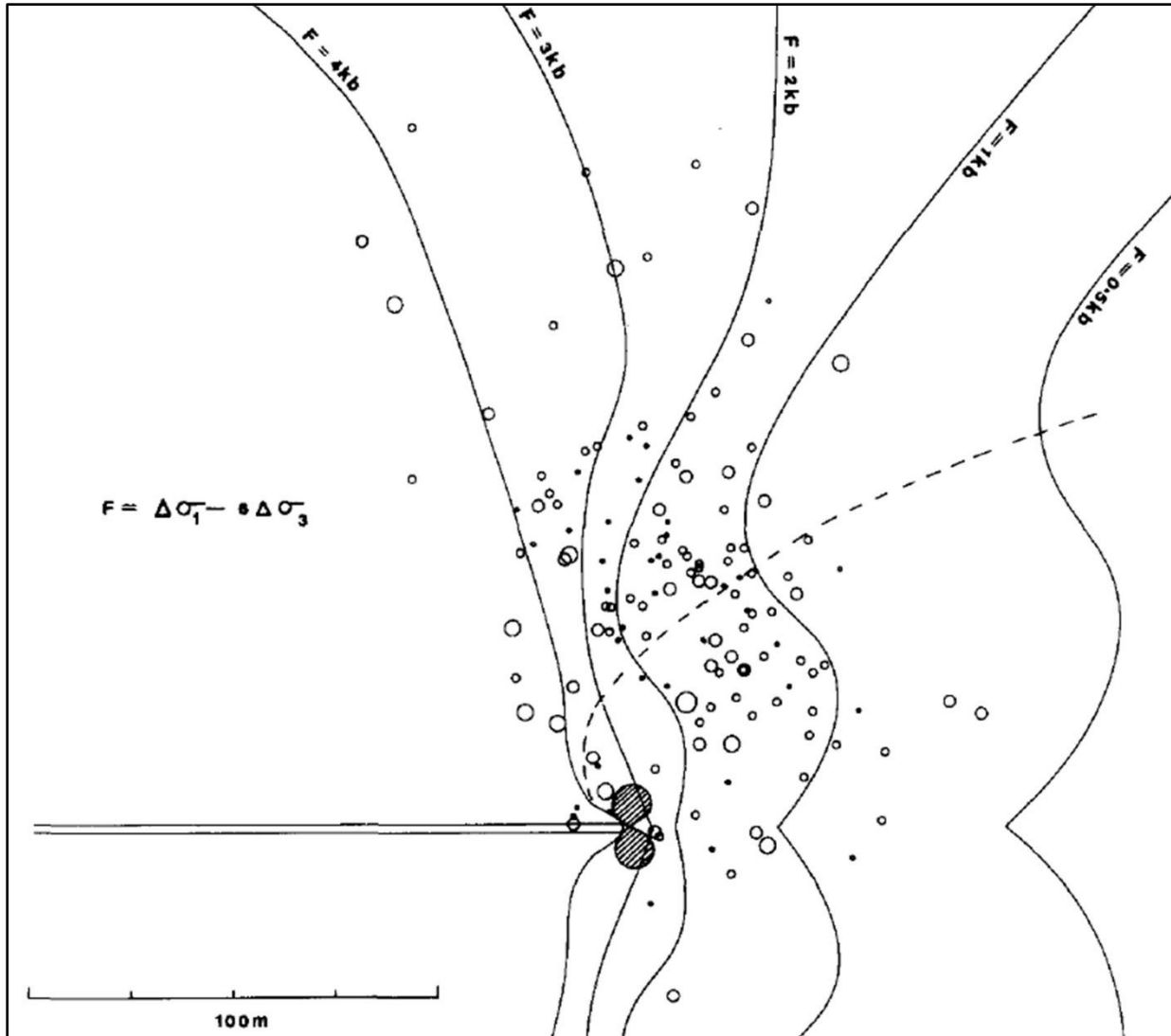


Figure 2-25: Section view of seismic event locations and stress contours relative to the position of a tabular stope face at East Rand Property Mines, South Africa (McGarr et al., 1975)

Ecobichon et al. (1992) noted that seismicity at Lac Shortt was often associated with a change in stress produced by an incremental mining step, rather than elevated stress in general. Figure 2-26 illustrates one such example where seismic events following a stope blast tend to locate where the major principal stress increases following the blast, rather than throughout areas with elevated stress. Most events are located in a zone of intermediate stress near the recent blast, and few events locate in a much more highly stressed areas on a level above the blast. In this case, the induced seismicity is related to localized instability caused by a recent mining step. Areas under elevated stress that are stable should not generate seismic events unless they become unstable.

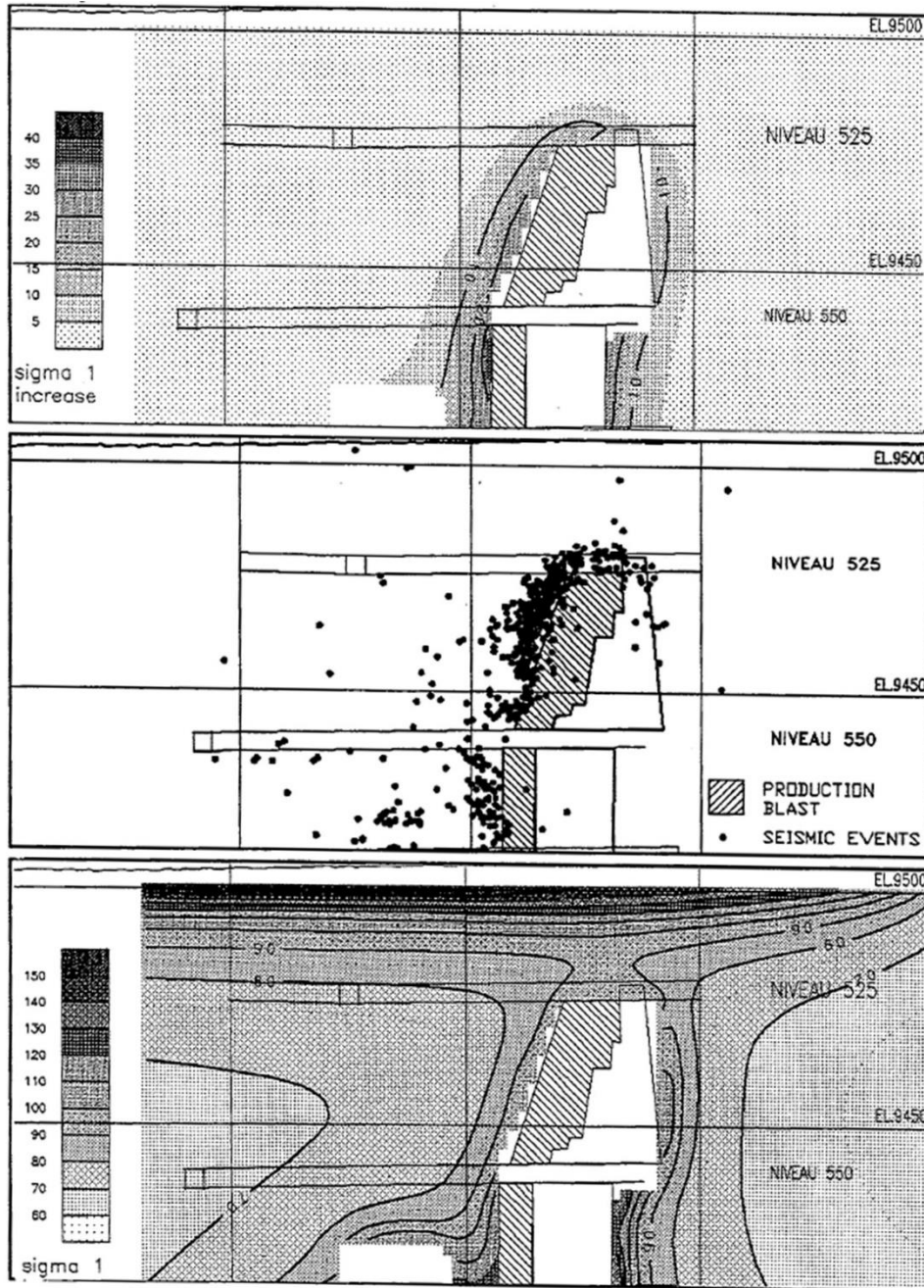


Figure 2-26: Locations of seismic events following a stope blast at Lac Shortt (middle) compared to change in major principal stress produced by the blast (top) and overall major principal stress (bottom) (Ecobichon et al., 1992)

The distribution of events will depend on where rock mass failure is occurring. In general, more seismicity is expected in areas where the rock mass is under higher stress and yield is occurring. However, events of different sizes represent individual strains of different sizes, so the size of events must be considered when characterizing inelastic strain in different locations. Figure 2-27 shows the distribution of events and seismic energy release relative to the position of a tabular

stope face in a Polish coal mine. The number of events and seismic energy release are both greatest immediately in front of the face, where there is the greatest stress and active stress changes are occurring. However, the greatest number of events is slightly closer to the face than the greatest energy release, indicating that the number of events alone is not necessarily the sole indicator of where the rock mass is releasing the greatest amount of strain energy.

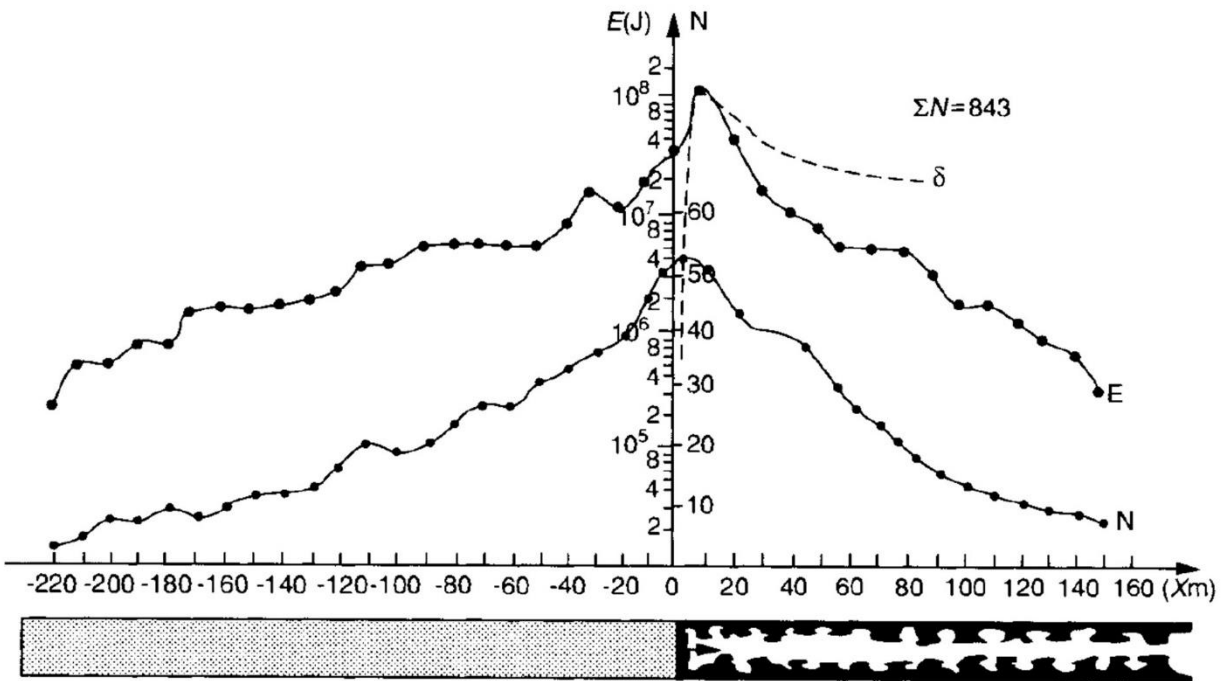


Figure 2-27: Number of seismic events ( $N$ ) and seismic energy ( $E$ ) in a 10 m window at various distance ahead of and behind an advancing tabular stope face in a Polish coal mine (Syrek and Kijko, 1988)

Seismogenic zones may move without the occurrence of induced stress changes associated with the creation of new excavations. As an area of a rock mass fails, it sheds stress to the areas around it. The migration of stress is followed by the migration of seismicity into a new zone of active rock mass yield. Similar to how the locations of seismic events can be used to infer regions of elevated stress and active rock mass yield around excavations, they can be used to infer regions of the rock mass that have undergone significant yield or failure. Figure 2-28 shows an example of how seismic event locations can be used to infer regions of the rock mass that have failed or caved around extracted open stopes. The absence of seismic events in the shaded regions indicates that those parts of the rock mass can not store enough energy to generate detectable seismic events. Therefore, it can be inferred that the rock mass in those regions has significantly yielded or failed. The migration of seismic events over a period of days also indicates that the failed region of the

rock mass is growing and stresses are migrating out of the damaged zones (McCreary et al., 1992). Simser et al. (1998) present a similar example of how the location of seismic events were used to infer the progression of a caving area above an open stope at Brunswick Mine, New Brunswick.

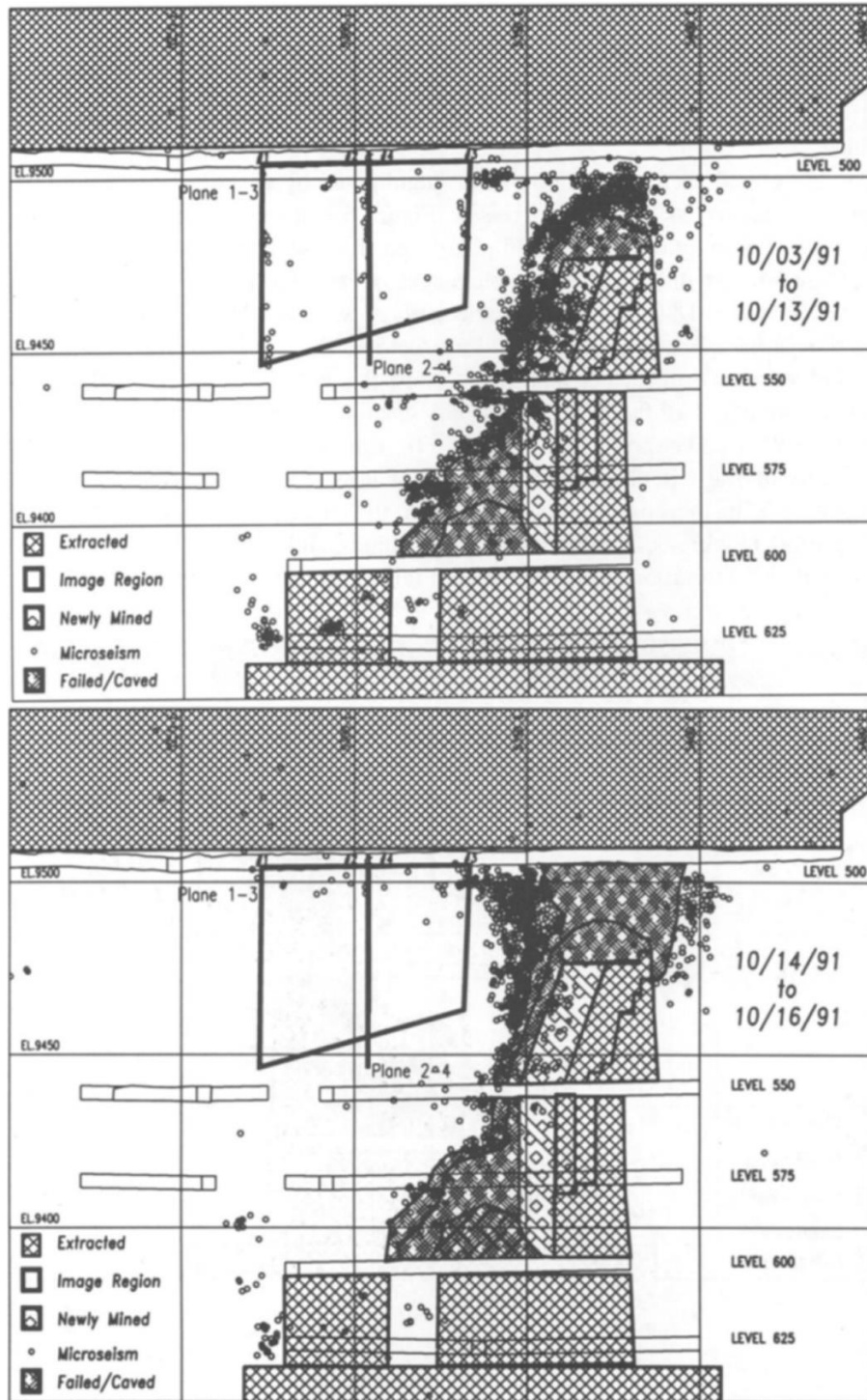


Figure 2-28: Locations of seismic events and inferred regions of caved or failed rock mass at Lac Shortt mine (McCreary et al., 1992)

The analysis of seismic event locations is a common tool to infer the progression of caves in caving mines (Abolfazlzadeh and Hudyma, 2016; Duplancic, 2001; Duplancic and Brady, 1999; Glazer, 2016; Hudyma et al., 2008a, 2008b). After blasting to initiate the caving process, rock mass failure in these mines is driven by a combination of gravity, stress, and removal of confinement from the draw of broken rock. The lack of surveyed or planned excavation shapes in caved regions of a rock mass make the location of seismogenic zones a useful piece of information for interpreting the progression of rock mass failure in the absence of incremental blast-induced stress changes.

Migration of seismicity is not necessarily caused by caving. Multiple open stoping mines observe seismicity migrating away from open stopes, or occurring some distance away from the stopes without excessive caving of the surrounding rock mass into the stopes, such as at Goldex mine (Hudyma et al., 2010). Seismogenic zones in open stoping mines have also been observed at some distance away from recently blasted stopes rather than immediately adjacent to them. This separation indicates the presence of an area of yielded rock mass adjacent to the open stopes. This behaviour is particularly observed in open stoping mines where the overall sequence of stopes is intended to “push” stress outwards such as at Brunswick (Andrieux and Simser, 2001) and LaRonde (Heal et al., 2005) mines. Separation of the seismogenic zone from extracted stopes has also been observed in areas where no active mining is taking place. The separation may be attributed to larger scale stress redistribution and progressive damage to the rock mass that is not necessarily associated with any single mining step. One such example is Creighton Mine, Sudbury, Ontario where a deep, wide, and thick orebody has been mined for over a century. Large yielded zones exist around the orebody, and as a result, the seismogenic zone lies several tens of metres away from the stopes in both the hanging wall and footwall (Cotesta et al., 2014; Snelling et al., 2013).

Abolfazlzadeh (2013) lists the following challenges with analysing seismogenic zones in a sublevel caving mine:

- The zone is three-dimensional.
- The zone moves at different rates at different times.
- The size of the zone varies over time.
- The accuracy with which the zone can be defined depends on how accurately events can be located.

Each of these challenges may also be applicable to the analysis and interpretation of seismogenic zones in open stopping mines.

#### 2.4.6 Spatial Variations in Apparent Stress

Apparent stress varies throughout space and can be used to infer higher or lower stress conditions within a rock mass. Figure 2-29 shows distributions of apparent stress at varying depths in a Canadian mine. In general, apparent stress is higher at greater depths where in-situ stresses are also greater. This result matches that of Mendecki (1997, 1993) who shows a similar trend of increasing apparent stress with depth in a South African mine. Mendecki (1997, 1993) also remarks that variation in apparent stress may also be related to variation in rock mass properties, with stronger rock masses producing seismic events with higher apparent stress.

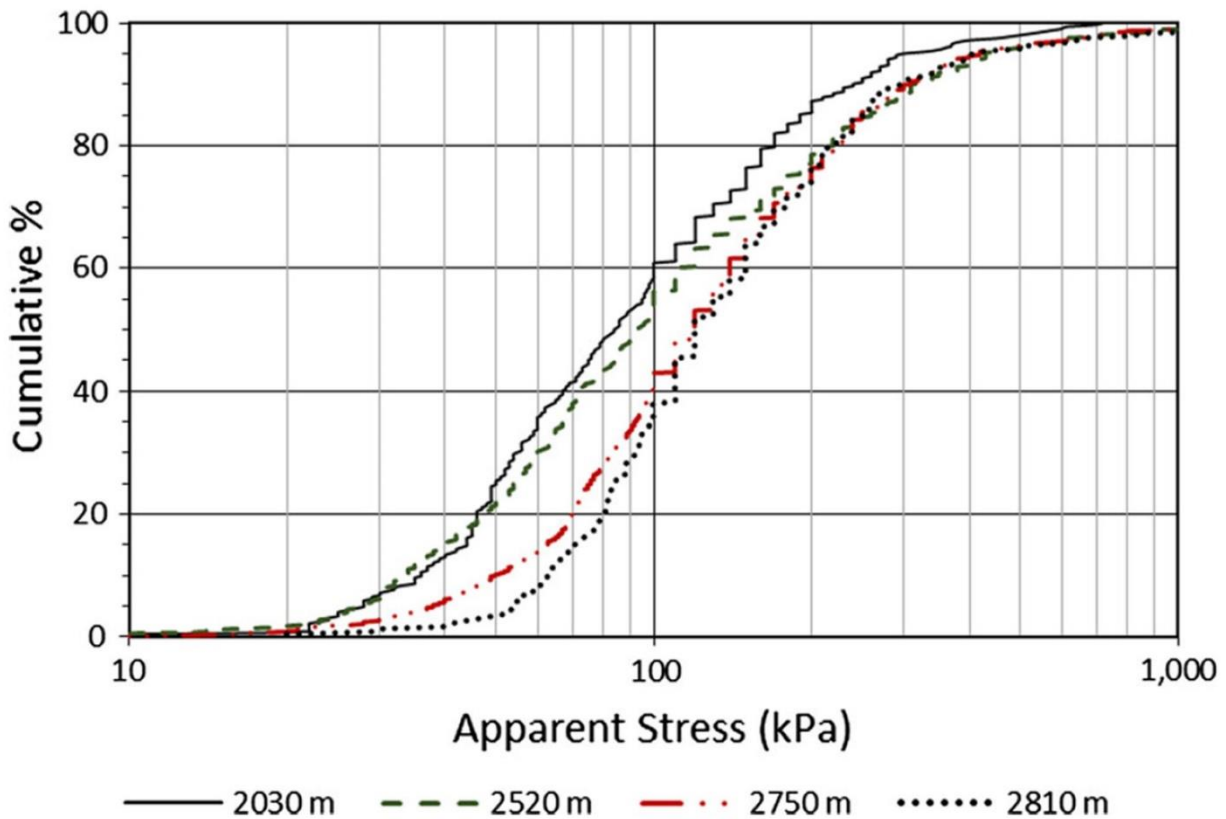


Figure 2-29: Distribution of apparent stress of  $-0.5 < M < 0$  events at various depths in a Canadian mine (Brown and Hudyma, 2017a)

Apparent stress is an estimate of co-seismic stress change and is assumed to be proportional to the stress change occurring in the rock mass. Creation of new excavations subjects the rock mass to elevated stress changes, causing seismic events with higher apparent stress to occur as the rock

mass near the excavations yields. As a result, regions of a rock mass with elevated apparent stress often correspond with regions where active mining is taking place (Brown and Hudyma, 2017a; Simser and Falmagne, 2004). There is an implied temporal effect within this generalization of spatial variation in apparent stress. An area with active mining may induce events with elevated apparent stress due to events occurring in high-stress areas around new excavations. However, when there is not active mining in the same area (i.e. no active induced stress changes), apparent stress of local seismic events may be lower (Brown and Hudyma, 2017a). Therefore, it is important to consider the context of local changes in the rock mass and what they may be caused by (i.e. active mining nearby or some other process).

Apparent stress also depends on the extent of rock mass fracturing. Figure 2-30 shows an example by Simser et al. (2003) of event locations shown in greyscale by apparent stress (lighter shade indicates lower apparent stress). Events with lower apparent stress locate in sill pillar regions where concentrated stresses cause damage to the rock mass and heavy fracturing is observed. Similar results are shown by Dunn (2005), who discussed variation in apparent stress between different tabular stope faces in a South African mine. Dunn observed that the stopes with heavier fracturing tended to generate events with lower apparent stress than stopes with less fracturing. A similar effect was noted by Kwiatek et al. (2011) who observed events with higher apparent stress locating in a dyke distant from active mining and events with lower apparent stress in the face of an active stope.

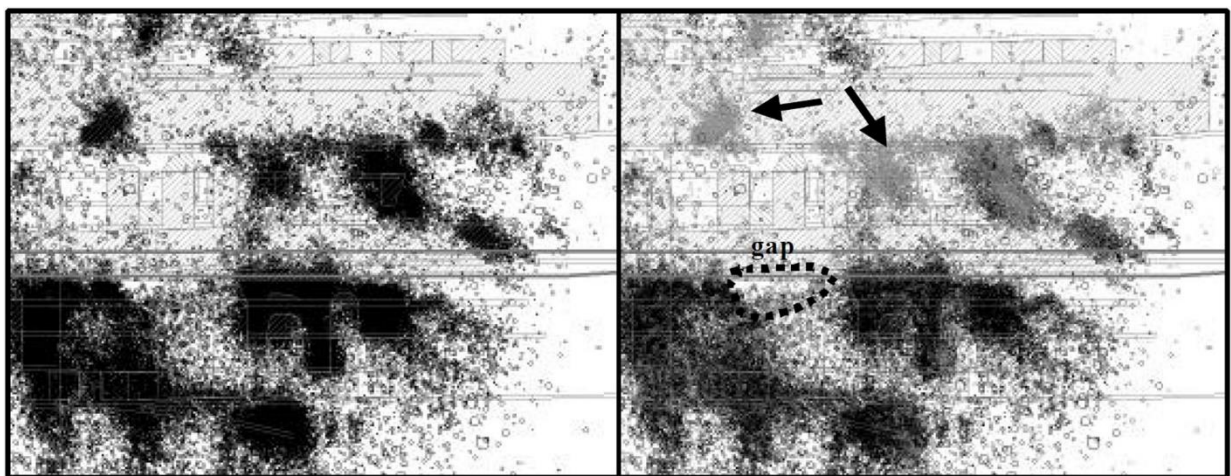


Figure 2-30: Longitudinal view of all seismic event locations in an area of Brunswick Mine, Bathurst, NB (left) and the same event locations with lighter shading indicating lower apparent stress (right) (Simser et al., 2003)

Spatial variation in apparent stress was also observed in the seismogenic zone above a sublevel caving mine in Australia (Abolfazlzadeh and Hudyma, 2016). Figure 2-31 shows a longitudinal view of event locations in this mine. Lines indicate the different quartiles of elevation for events at varying cross sections throughout the mine. Events with higher apparent stress tend to locate above the median elevation of all events. According to Duplancic's (2001) caving model, the rock mass farther above the cave is more intact and the rock mass closer to the cave is more fractured and loosened. Accordingly, Abolfazlzadeh and Hudyma (2016) show that the supposedly less fractured rock mass generates events with higher apparent stress than the rock mass that is closer to the cave and supposedly more fractured. Based on these results, apparent stress can be used to infer the degree of fracturing in different regions of a rock mass.

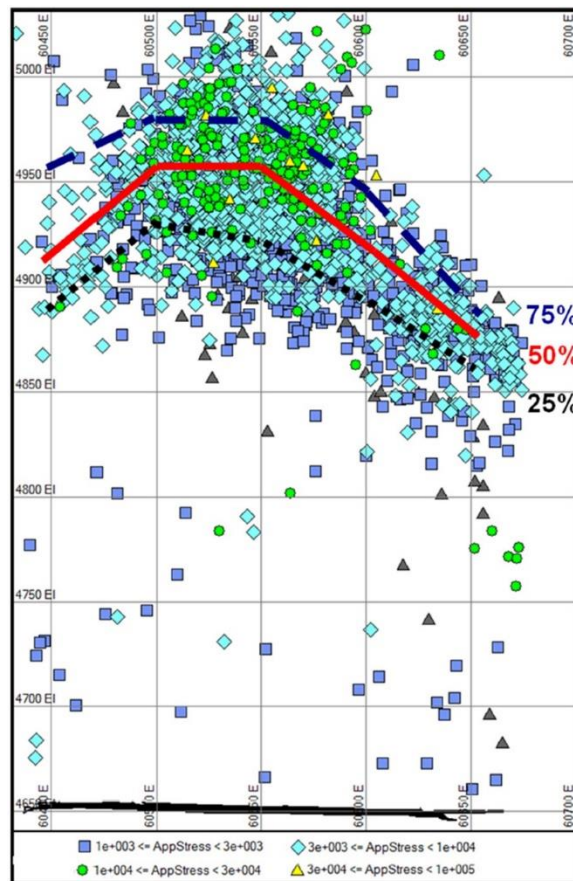


Figure 2-31: Event locations above a sublevel cave at Telfer Gold Mine, Australia (marked by apparent stress) with quartiles of elevation at various eastings for reference (Abolfazlzadeh and Hudyma, 2016)

#### 2.4.7 Temporal Variations in Apparent Stress

Apparent stress also varies throughout time in a mining environment. As mentioned previously, areas with active mining tend to have events with higher apparent stress. This effect is related to

the creation of new excavations causing the rock mass to yield under higher stress conditions. The tendency for mine blasts to generate events with higher apparent stress can be shown with an apparent stress time history (ASTH), an example of which is shown in Figure 2-32. ASTH (Hudyma, 2008) show the frequency of events with an apparent stress greater than a certain threshold, usually the 80<sup>th</sup> percentile for the population (i.e. showing the rate of events with high apparent stress). Figure 2-32 shows an ASTH for a population of events near a production area. The frequency of events with high apparent stress is highest following production blasts (indicated with red stars), indicating that blasting causes a greater number of large stress changes to occur as the rock mass yields. Young (2012) replicated these results at Coleman Mine, Sudbury, Ontario. ASTH however, does not distinguish between an elevated rate of events with high apparent stress and an overall higher distribution of apparent stress for the population at any given time.

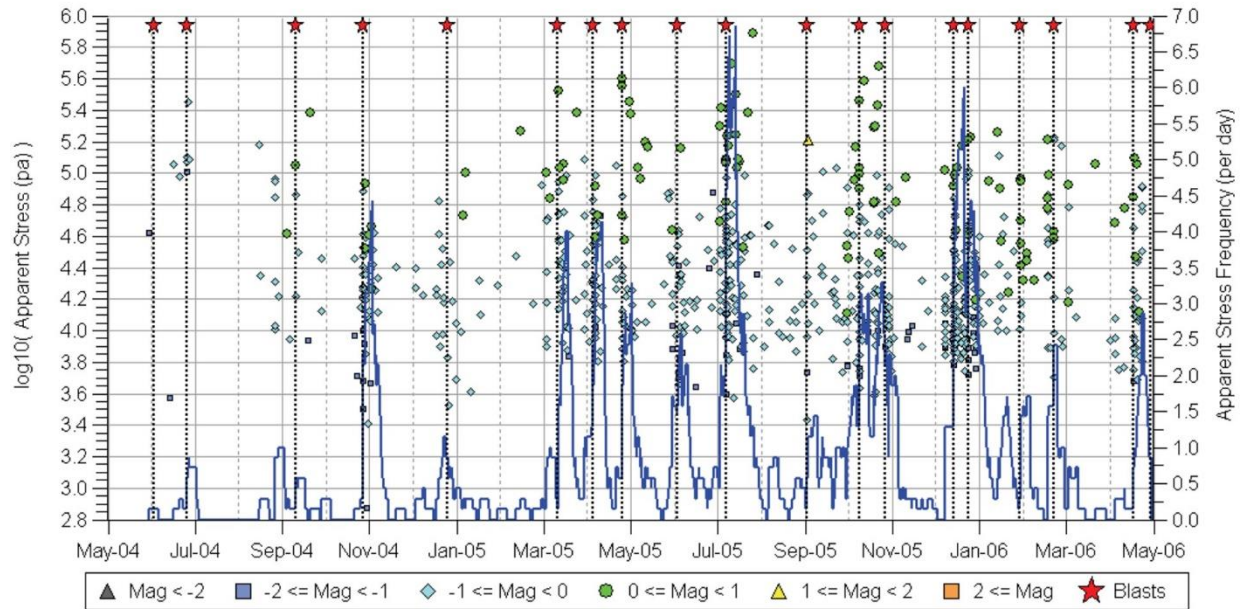


Figure 2-32: ASTH of population of seismic events occurring near stope blasts at LaRonde Mine, Preissac, Quebec (Hudyma, 2008)

Brown (2015) used a relative ratio of apparent stress call the apparent stress ratio (ASR) to infer local stress increase. ASR was calculated as the ratio of the 80<sup>th</sup> to the 20<sup>th</sup> percentile of apparent stress and served to make the analysis of the parameter dimensionless. This method removes the need to define the 80<sup>th</sup> percentile of apparent stress for ASTH analysis. ASR was determined to be a useful indicator of potential for large events to occur as a result of elevated local stress increase.

Apparent stress has also been tracked using a moving average. Coulson (2009) used the average apparent stress (among other parameters) to infer when large-scale rock mass yield occurred in a shaft pillar. The average apparent stress increased as stopes were mined near the pillar, decreased as the pillar yielded, and remained low afterwards. These results are shown in Figure 2-33. Yield in the pillar was validated with field observations of stope drilling in the pillar. Before the inferred yield of the pillar, drilling would trigger flurries of seismic activity, and the drill holes would crush shut in the highly-stressed rock. After the inferred yield of the pillar, drilling was relatively easy and did not result in flurries of seismic activity or crushed holes, indicating that the pillar had fractured and relieved stress. Accordingly, the drop in apparent stress indicated that the rock mass was under less stress.

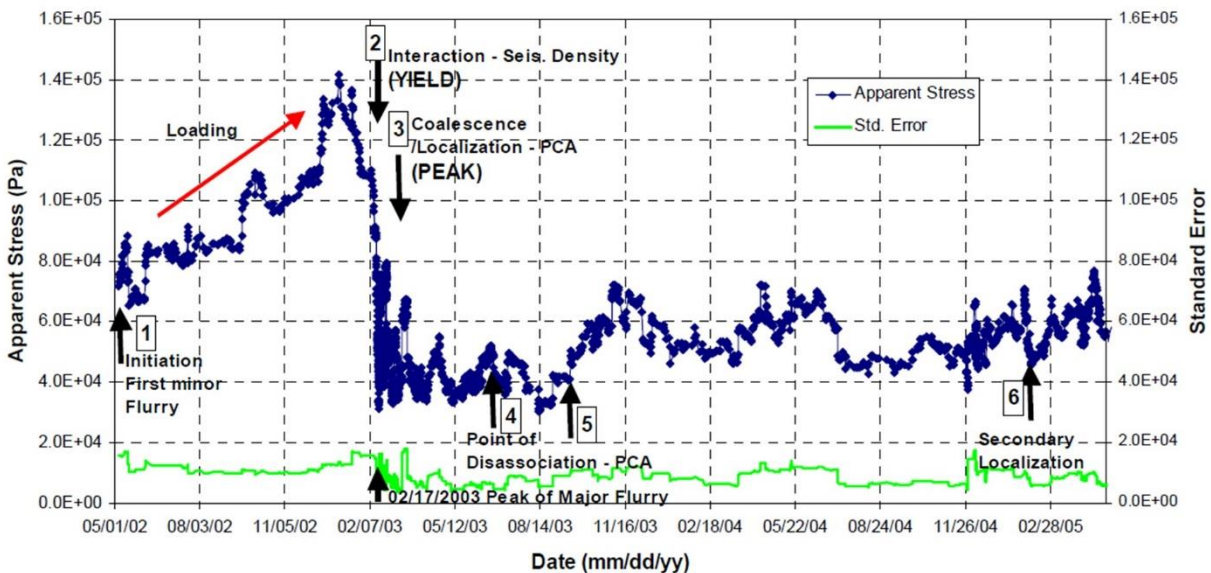


Figure 2-33: 50-event moving average of apparent stress in a pillar at Golden Giant Mine, Hemlo, Ontario (Coulson, 2009)

#### 2.4.8 Energy Index and Cumulative Apparent Volume

Energy Index (EI) after van Aswegen and Butler (1993) is conceptually similar to apparent stress in that it serves to indicate a level of energy for a given moment, but seeks to eliminate influence of scale dependence in energy-moment scaling. Accordingly, variations in EI are driven by variations in energy-moment scaling, rather than variation in event size.

Energy index is calculated as a ratio of an event's observed energy to the typical energy of an event with the same moment. The typical energy is based on the energy-moment relation for the population of events. Therefore, the EI of a single event is not an absolute parameter defined by the properties of a single event. Rather, it is a relative comparison to other events (e.g. from the

same mine, same level, same time period, etc.). The population of events from which individual values of EI are calculated depends on the goals of the analysis (i.e. what each event is being measured relative to). To normalize the distribution of energy for any given moment, the log of EI can be used. log(EI) essentially indicates how many orders of magnitude an event's energy is above or below the expected energy for an event with the same moment. log(EI) is calculated as:

$$\log EI = \log \frac{E_{Obs}}{E_{Exp}} = \log \frac{E_{Obs}}{c + d \log M_{Obs}}$$

[2.6]

where

- $E_{Obs}$  = Observed seismic energy of the event
- $E_{Exp}$  = Expected energy for an event with the same moment
- $c$  = Vertical axis intercept of energy-moment relation
- $d$  = Slope of energy-moment relation
- $M_{Obs}$  = Observed moment of the event

The lack of scale dependence of EI can be visualized in an energy-moment relation. Figure 2-34 shows an energy-moment relation with the same data as shown in the energy-moment relations in Figure 2-21 and Figure 2-22. The events in Figure 2-34 are coloured by log(EI). The figure shows that events with higher moment do not have higher EI than events with lower moment. Therefore, the parameter is not scale-dependent like apparent stress.

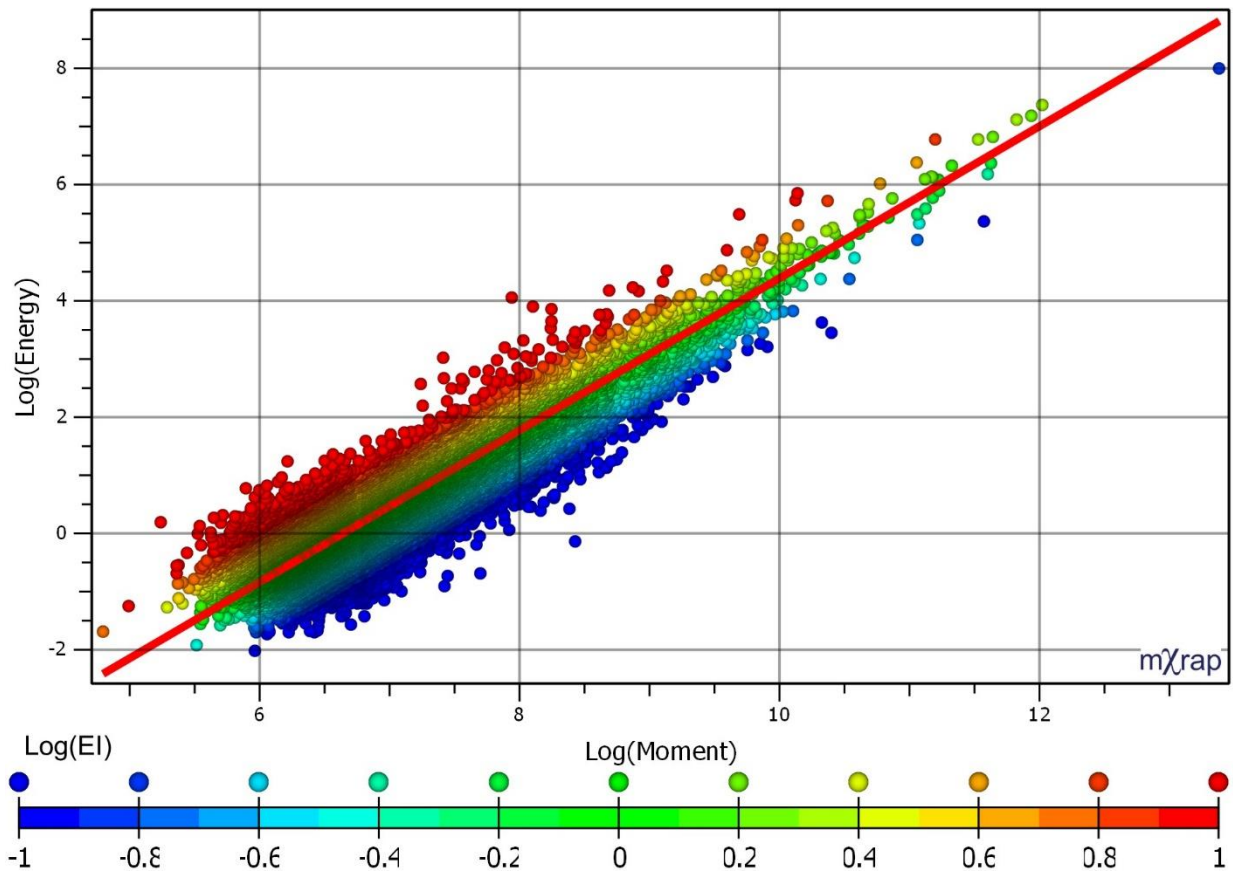


Figure 2-34: Example of an energy-moment graph with events coloured by  $\log(EI)$

Energy index is often shown alongside cumulative apparent volume (CAV). CAV is an estimate of total co-seismic deformation, which has been shown to correlate with measured fault deformation (Mendecki, 1993; van Aswegen and Butler, 1993). AV for a single event is calculated as:

$$AV = \frac{M_o^2}{2\mu E} \quad [2.7]$$

where

$M_o$  = Moment (Nm)

$\mu$  = Shear modulus of the rock mass (Pa)

$E$  = Seismic energy (J)

EI is often tracked in time as a moving average to infer a relative level of stress in the rock mass over time. Variations in EI are interesting to consider alongside apparent stress because, being conceptually similar parameters, their respective analysis may show similar results. Two examples of moving averages of EI are shown in Figure 2-35 and Figure 2-36. Within the scope of this thesis (short-term variations in apparent stress following blasts), it is interesting to note that both of the exemplified studies show sudden changes in EI following blasts. Figure 2-35 by Simser et al. (2003) shows a sudden decrease in EI following a blast that was intended to stress shadow a large region of the mine. This variation was also shown to correspond with a downward shift in the distribution of apparent stress in two spatially isolated populations of events near the blast. Figure 2-36 by Disley (2014) shows a sudden spike and drop in EI following a blast, as well as a sudden drop associated with a large event over a day later. These sudden shifts are often noted, but seldom studied in detail, which is what this thesis seeks to achieve with the study of apparent stress.

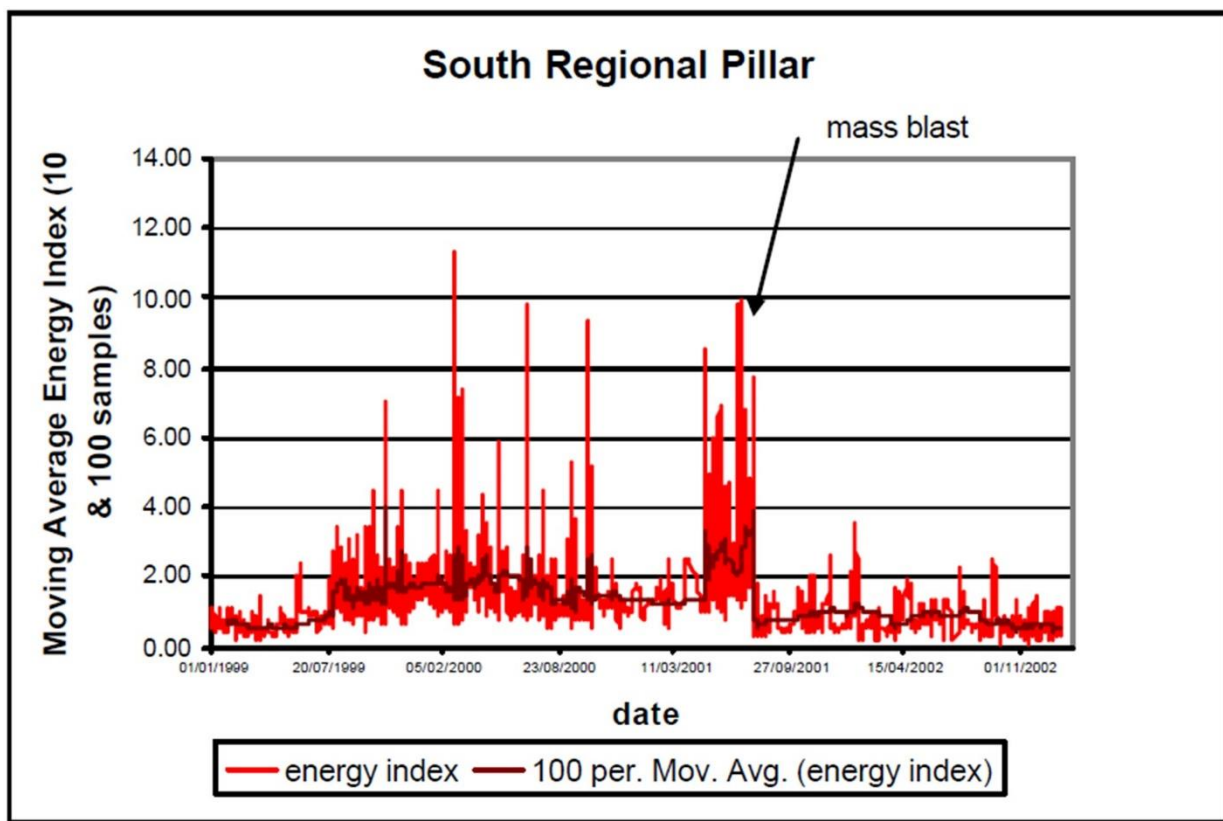


Figure 2-35: EI graph showing sudden change following mass blast at Brunswick Mine (Simser et al., 2003)

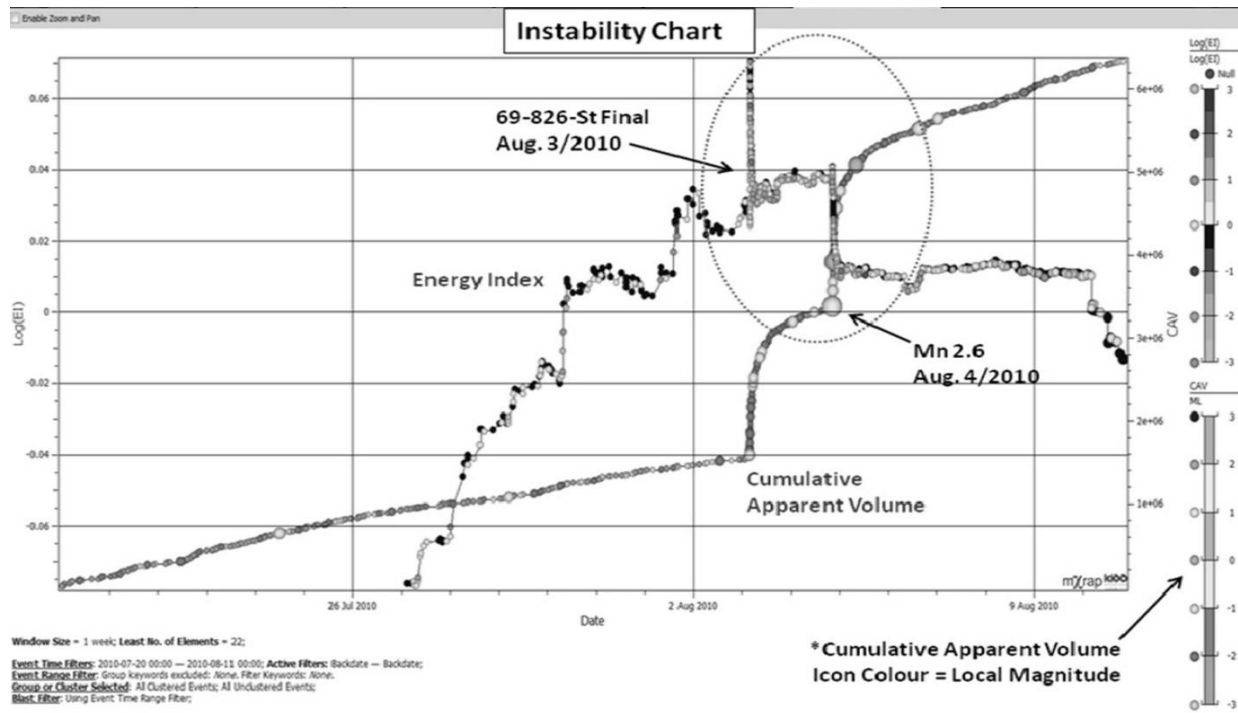


Figure 2-36: EI-CAV graph showing sudden changes in  $\log(EI)$  following a blast and a large event at Kidd Creek Mine, Timmins, Ontario (Disley, 2014)

## 2.5 Seismicity and Constitutive Behaviour of Rock Masses

Seismic events are related to inelastic strains in a rock mass, and seismogenic zones indicate where and when the rock mass is undergoing inelastic strains. The characteristics of seismic events (i.e. their source parameters) are controlled by local conditions. Characteristics of a population of seismic events can be used to make inferences on the characteristics of inelastic strains occurring in a given space and time. Such inferences may be based on relatively simple aspects of seismicity, such as where or when events happen, but may also be related to more complex descriptions of the population such as the spatial distribution of events, the rate at which they occur, or their source parameters. The “Holy Grail” of sorts is to find a concrete, quantitative relationship between these descriptions of a population of events and the constitutive behaviour of the rock mass.

Seismic events indicate where and when an inelastic strain occurred. The onset of seismic activity essentially represents that the rock mass is yielding. Figure 2-37 by Coulson (2009) shows hypothetical stress-strain curves for intact rock samples and rock masses under varying levels of confinement. The schematic shows varying failure mechanisms under different levels of confinement similar to those shown in Figure 2-8 by Diederichs (2003). The onset of microseismic activity signifies the stress at which cracks begin to form ( $\sigma_{ci}$ ). Depending on the level of

confinement, stress increases to the point where the cracks interact to damage the rock mass ( $\sigma_{cd}$ ). Finally, the rock mass reaches its peak strength ( $\sigma_f$ ), then proceeds to yield to an aseismic state at its residual strength.

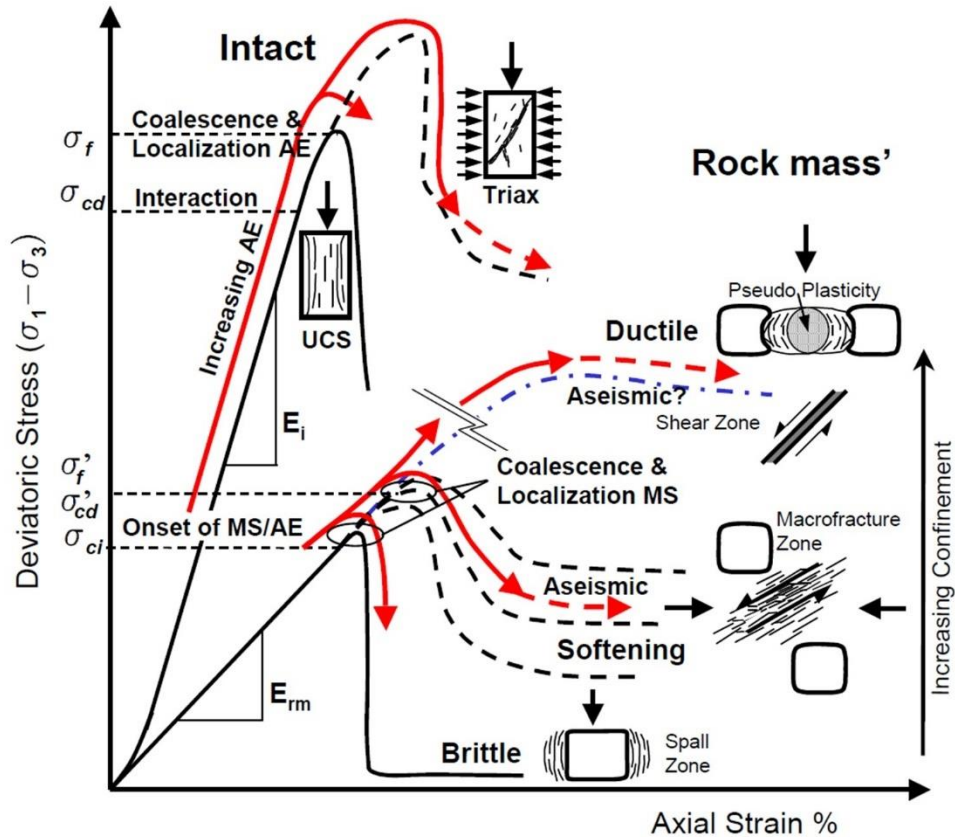


Figure 2-37: Hypothetical stress-strain curves for intact rock samples and rock masses in Hemlo, Ontario (Coulson, 2009)

Because seismicity indicates where rock mass yield is occurring, it can be used to calibrate numerical models. One such example by Cotesta et al. (2014) is shown in Figure 2-38. The figure shows contours of modelled deviatoric stress (difference between  $\sigma_1$  and  $\sigma_3$ , which as discussed previously are incorporated into a variety of rock mass failure criteria) overlain with seismic event locations. Cotesta et al. explain that elevated stresses cause yield to occur near the stopes, and the yield zones expand as mining progresses downwards. Accordingly, in the numerical model there is a:

- Yielded zone near the stopes with low stress and no seismic events, indicating the rock mass is in an aseismic state.
- Zone of elevated stress just outside the yielded zone where there are many seismic events, this is the seismogenic zone where rock mass yielding is occurring.

- Region outside the seismogenic zone in which there are few seismic events and is assumed to be not significantly affected by the mining-induced stresses.

The model shown by Cotesta et al. (2014) demonstrates on a large scale how the locations of seismic events indicates where the rock mass has yielded.

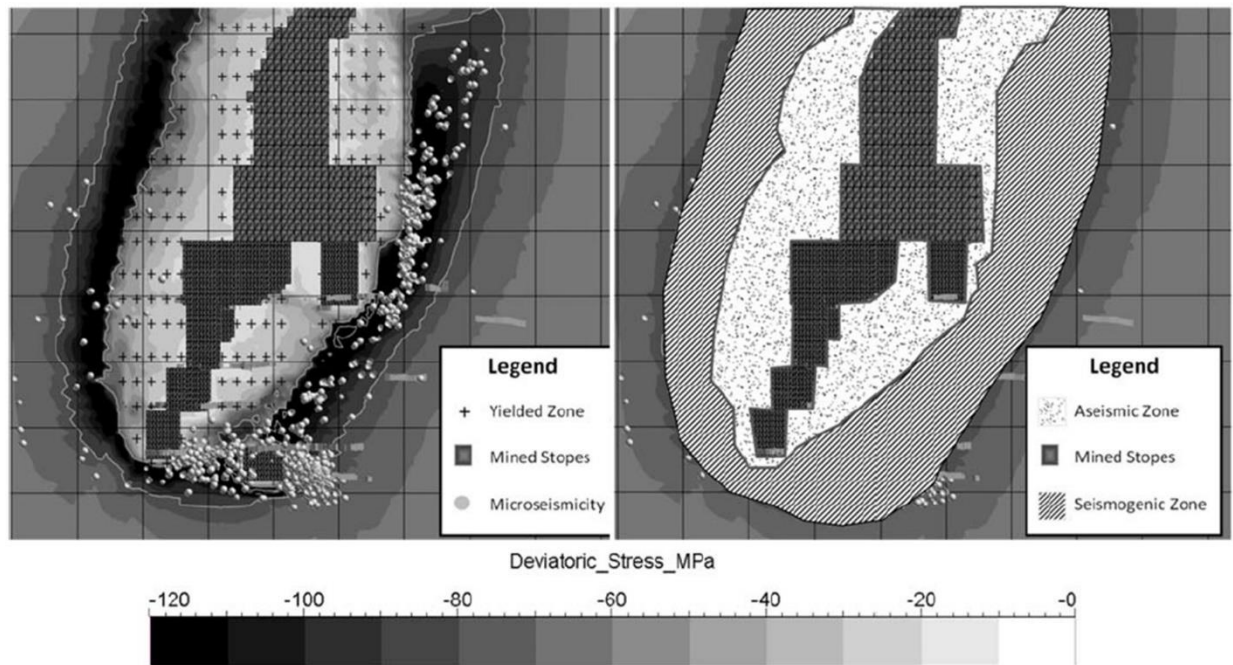


Figure 2-38: Contours of deviatoric stress overlain with seismic event locations (left) and interpreted zones of yielded and yielding ground (right) at Creighton Mine, Sudbury, Ontario (Cotesta et al., 2014)

On the scale of a single stope, Bawden and Mercer (1994) propose a three-region model to describe seismogenic zones near open stopes which is illustrated in Figure 2-39. The first region closest to the stope contains few events which release little energy. This region corresponds with a zone of yielded rock which has been subjected to elevated induced stresses and a loss of confinement. The second region is where most of the events occur and release moderate amounts of energy. This region is where rock mass yield is occurring. The third region, which is farthest from the stopes, had fewer events but individual events have greater energy release. This region is where the rock mass is under elevated stress, but not yet in a state at which it is actively yielding like the second region. Bawden and Mercer's model essentially eludes to how the spatial distribution of events and their source parameters may be used to provide a detailed description of a seismogenic zone. This more detailed description may be used to infer which regions have just started to be affected by stress (third region with higher energy events) and which regions are closer to an aseismic state

(lower energy events). However, the greatest number of events occurring in the second region (active rock mass yield) poses a challenge for analysis of the seismogenic zone. The greater quantity of events in this region will tend to dominate a population of events near open stopes, making it more challenging to delineate regions one and three. Fortunately, accurate event locations and source parameter estimates enable more refined inferences on rock mass behaviour throughout a seismogenic zone and the delineation of different regions within it.

Note that Bawden and Mercer's (1994) model also refers to velocity in the different regions. This velocity refers to that of seismic waves, which travel faster in regions of a rock mass where elevated stresses keep fractured closed. The subject of seismic tomography will not be discussed in this thesis.

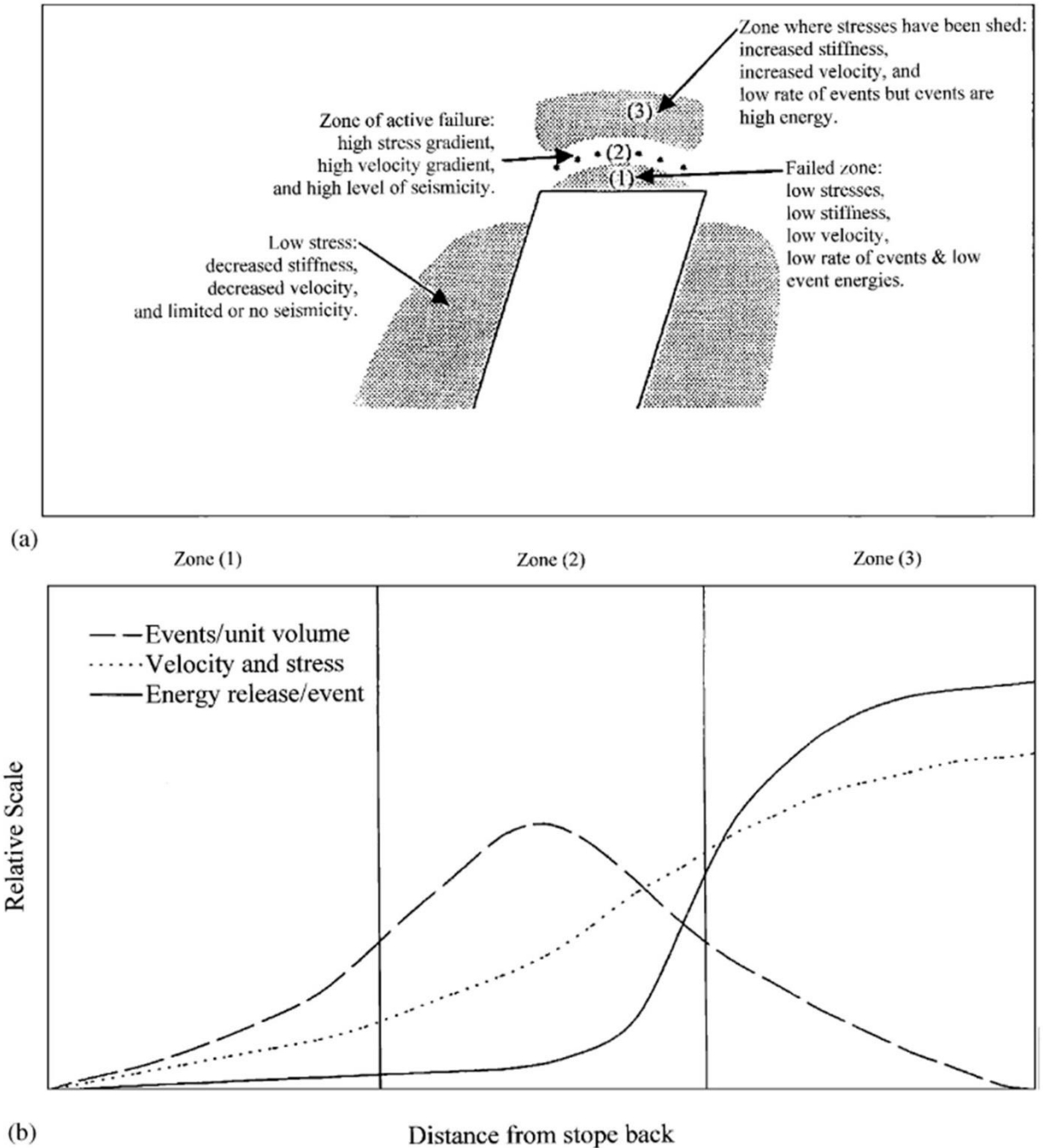


Figure 2-39: Conceptual model of spatial variation in seismicity near an open slope (Mercer and Bawden, 2005; after Bawden and Mercer, 1994)

Because seismic events are controlled by local modes of rock mass failure, they can be used to interpret the mechanisms and constitutive behavior of the failure process they are associated with. Bawden and Mercer (1994) explained how not only the number of events, but their source parameters vary throughout a seismogenic zone. Andrieux et al. (2008) describe seismic responses corresponding to the five regions of a strain softening curve indicated in Figure 2-40. The seismic

response in each region has unique characteristics related the quantity and size of seismic events. These characteristics are used to make inferences on the amount of strain the rock mass is experiencing and how much stress it is under. The five regions shown in the figure are:

1. Low-level seismicity associated with loading heterogeneities, usually undetected by mine-wide arrays, a comparatively aseismic response.
2. Onset of permanent damage past the yield point, high apparent stress.
3. Brittle response past the peak strength, moderate apparent stress and greatest number of events, typically larger events also occurring in this region.
4. Softening response, low apparent stress.
5. Residual strength, few events that usually go undetected by a mine-wide array (essentially aseismic).

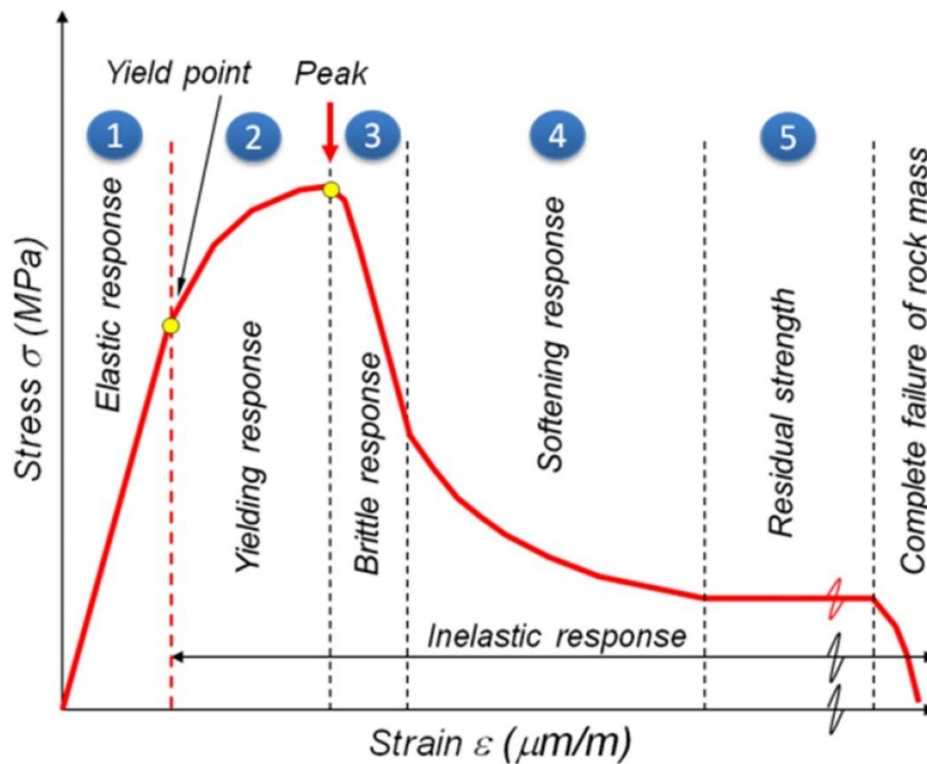


Figure 2-40: Five regions of a stress-strain curve for a rock mass with strain-softening behaviour (Cotesta et al., 2014; redrawn from Andrieux et al., 2008)

### 3 Nickel Rim South Mine

Glencore's Nickel Rim South Mine (NRSM or Nickel Rim South) is a copper-nickel mine in the East Range of the Sudbury Basin. Production started in 2009, making it a relatively modern operation in a camp that has been operating for over a century. The modernity of the operation is reflected in the mine's design and technologies that support the operation, including a state-of-the-art seismic monitoring system. NRSM produces an average of 3,000 tonnes per day from between 1 and 2 km deep. These depths are considered intermediate in the Sudbury Camp, where production has been achieved below 2 km by past and current operations, and several future projects are targeted below this depth. Nevertheless, mining-induced seismic activity is also prevalent at intermediate and shallower depths in the Sudbury Camp (see work on Strathcona mine by Urbancic (1991) which operated shallower than 1 km). The level of seismic activity and modernity of seismic monitoring technologies makes NRSM an attractive research subject.

#### 3.1 Regional and Local Geology

##### 3.1.1 Regional Setting

Nickel Rim South is located on the East range of the Sudbury Structure, a regional structure measuring 58 km long and 28 km wide whose location is shown in Figure 3-1. This structure was formed by a meteorite impact approximately 1850 Ma ago, which is referred to as the Sudbury Event. The impact and resulting melt created a series of the world's largest magmatic sulphide nickel-copper-platinum group element deposits around the perimeter of and just below the Sudbury Igneous Complex (SIC) (Rousell and Card, 2009). The region has undergone various phases of metamorphism resulting in faults, shears, and joints that pre and post-date the Sudbury Event (Rousell, 2009).

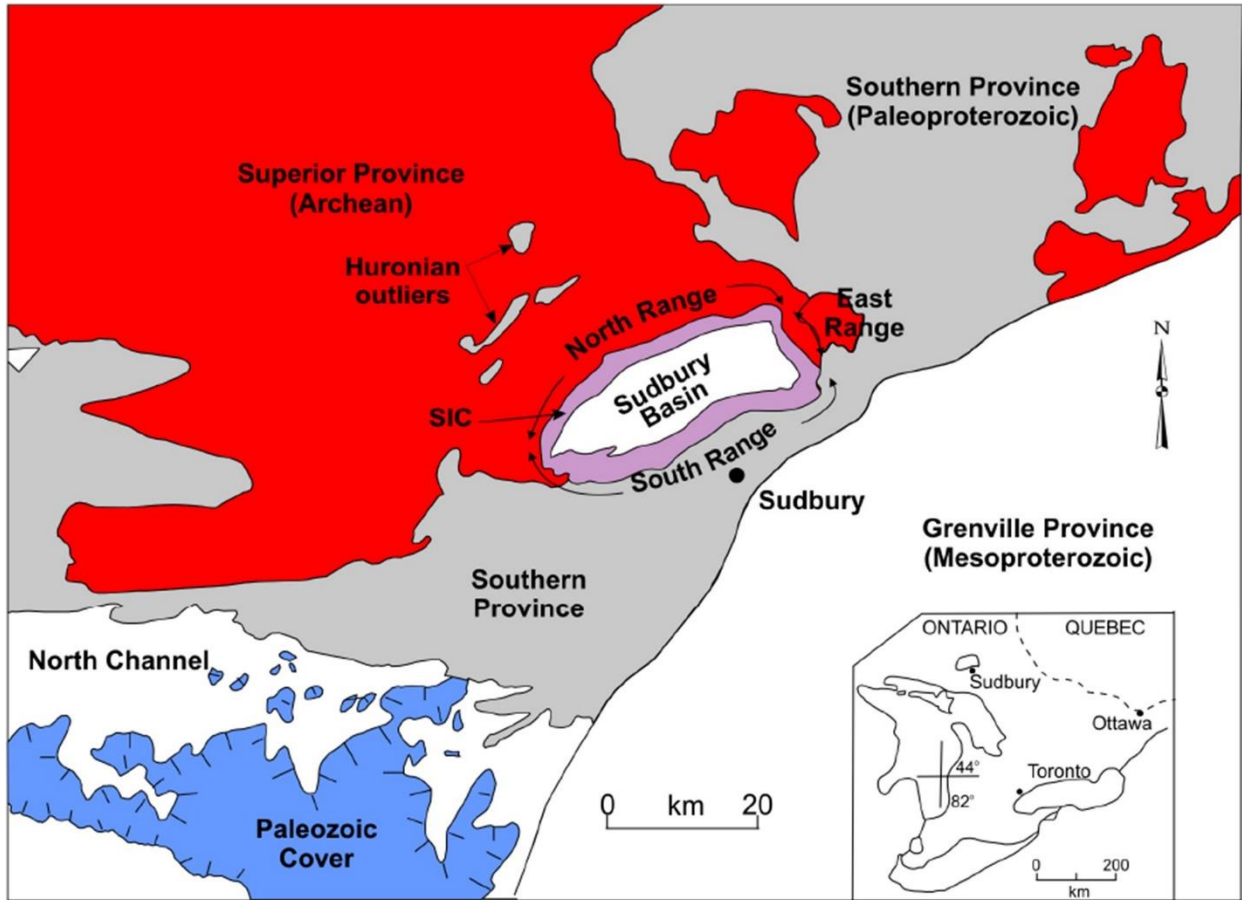


Figure 3-1: Regional map of the Sudbury Structure indicating the Sudbury Igneous Complex (SIC) (Rousell and Card, 2009)

The region is also home to a relatively young (37 Ma) meteorite impact on the East Range which give it a concave shape and formed Lake Wanapitei (Dressler, 1984). The location of Nickel Rim South is shown between the two craters in Figure 3-2.

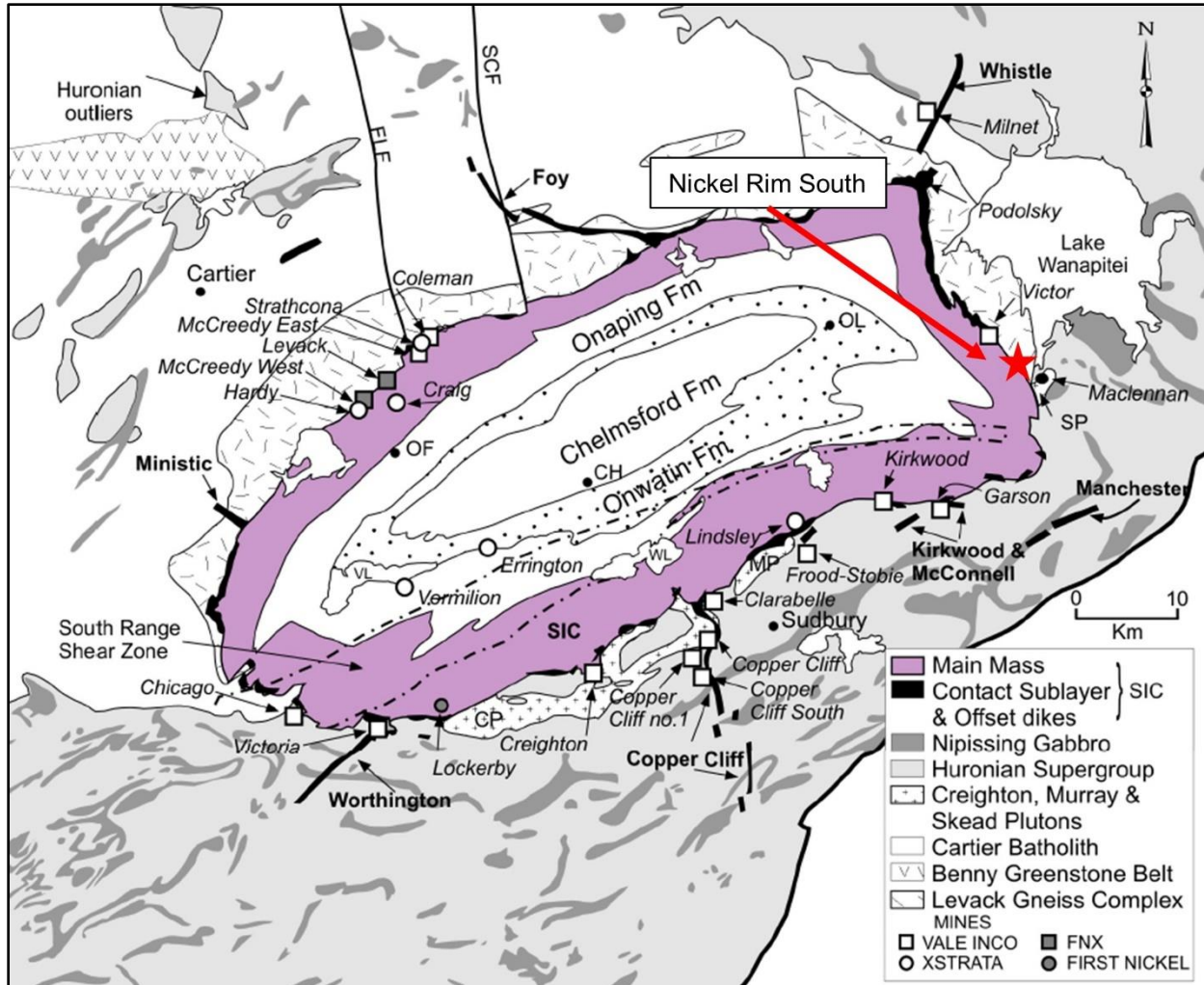


Figure 3-2: Local map of the Sudbury Structure indicating the location of Nickel Rim South (modified after Rousell and Card, 2009)

### 3.1.2 Local Geology

The main ore zones at Nickel Rim South extend from 1.2 to 1.7 km deep. The two main zones are a contact deposit, rich in nickel, and a footwall deposit, rich in copper and precious metals. These are illustrated with section views in Figure 3-3 and Figure 3-4. Figure 3-3 shows a conceptual schematic of the mineralization and surrounding rock mass from the project’s exploration phase, and Figure 3-4 shows the interpreted mineralization contacts and mine workings from the production phase. The nickel and copper zones are in close proximity to each other. There is a transition zone between them at shallower depths, and a sub-economic waste gap between them which widens with depth. The contact deposit is approximately 360 m along strike and ranges from 5 to 80 m thick, with an average thickness of 60 m. The footwall deposit is approximately 300 m along strike and averages 50 m thick. Both deposits dip approximately 70° degrees to the

south. Note that the geometry of mineralization does not necessarily correspond with the geometry of mining (i.e. mineralization rather than ore). Mineralization occurs in the form of massive, semi-massive, and disseminated sulphides. Several smaller zones with economic importance exist along strike and down dip from these zones. These zones are not the focus of this thesis.

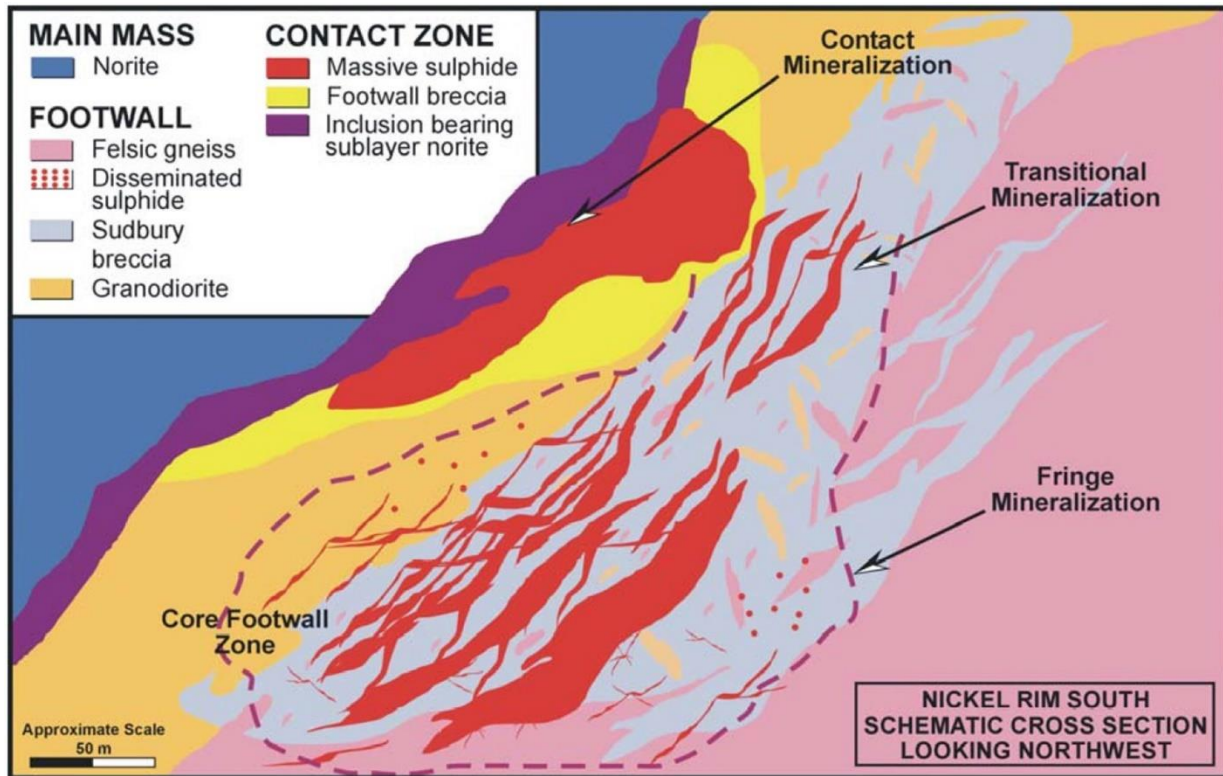


Figure 3-3: Section view schematic looking northwest (note a specific grid or coordinate system is not known for this figure) of the main NRSM orebodies from the project's exploration phase (McLean et al., 2005)

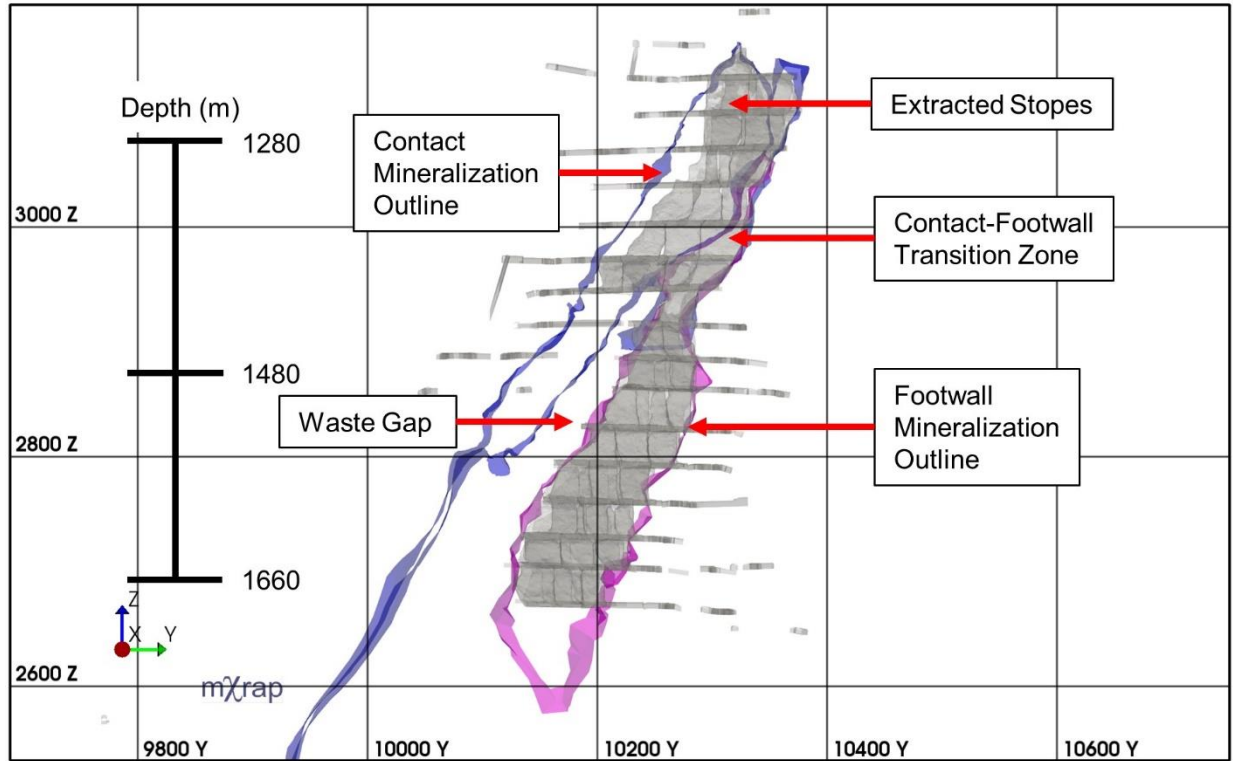


Figure 3-4: Section view looking west of main contact and footwall orebodies at NRSM showing mine workings

Figure 3-5 shows the position of the ore zones relative to the overlying units of the SIC and Sudbury Basin, and underlying country rocks. Late granite breccia is the main host for contact mineralization, and Sudbury breccia is the main host for footwall mineralization. The mineralization in the transition zone is hosted in gabbro. Note that the transition zone indicated in Figure 3-5 does not refer to the transition zone between the contact and footwall deposits, rather, it refers to the transition from granophyre to felsic norite in the SIC. The stratigraphy in Figure 3-5 is similar to the conceptual schematic in Figure 3-3. The major lithologies in the vicinity of the mine workings and their abbreviations are listed in Table 3-1.



Figure 3-5: Stratigraphic column of NRSM (Simser et al., 2015b)

Table 3-1: List of major lithologies at NRSM and their abbreviations

Lithology	Abbreviation
Felsic Norite	FNOR
Dark Norite	DNOR
Dark Norite Breccia	DNBX
Late Granite Breccia	LGBX
Felsic Gneiss	FGN
Sudbury Breccia	SUBX
Granodiorite	GRDR
Diabase	DIA
Gabbro	GAB or TRZN

Figure 3-6 shows a plan view of interpreted geology contacts at a depth of 1445 m. This level typifies the geology at NRSM showing the layering of the geologic units, mineralization hosts, and a slight separation between the contact and footwall ore. Inclusions of diabase and granodiorite are also visible within the felsic gneiss unit. The size and quantity of such inclusions varies

between levels. The presence of granodiorite is notably less than suggested in the schematic by McLean et al. (2005) (Figure 3-3).

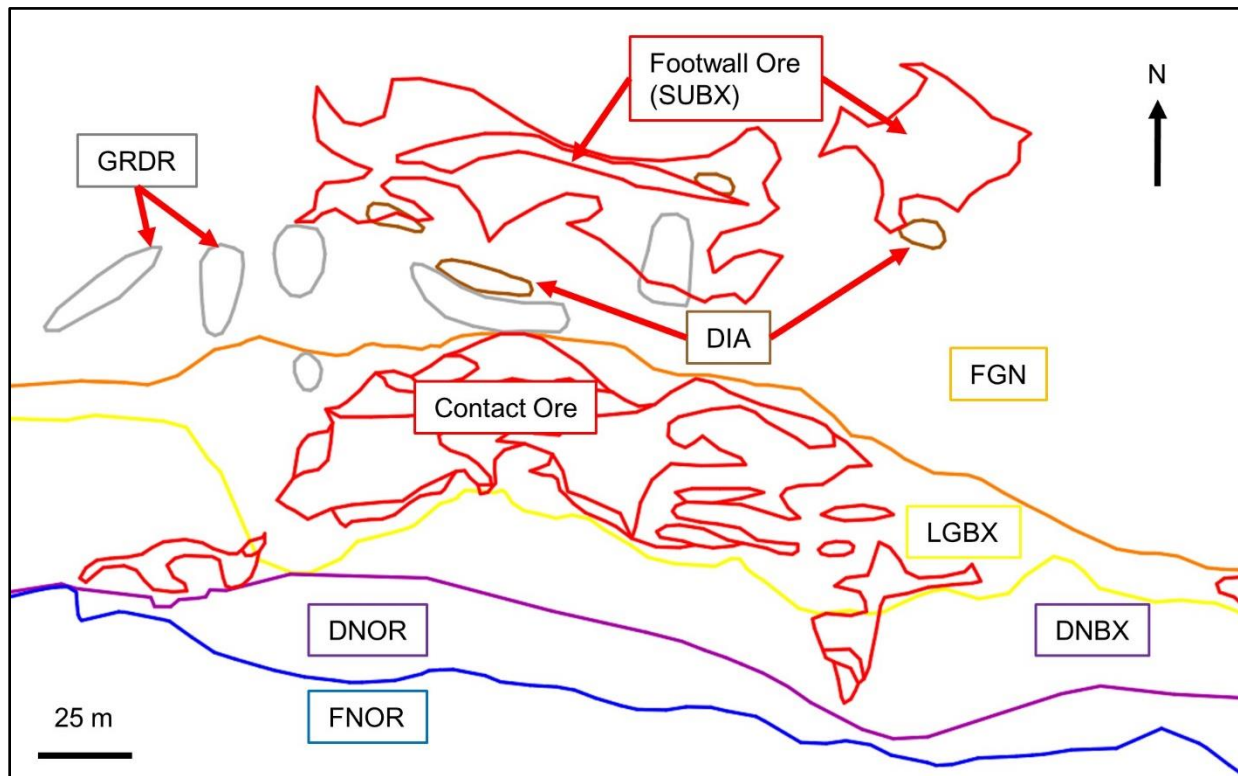


Figure 3-6: Plan view of interpreted geology contacts at 1445 m depth (Glencore, 2017a)

Figure 3-7 shows a plan view of interpreted geology contacts at a depth of 1625 m. Diabase fragments occur in greater size and quantity on this level. This level shows the typical geometry where most mining of the footwall ore has taken place. The footwall is more separated from the SIC contact units which host little ore at this depth. The footwall ore is thicker in the middle of the deposit, but thinner at the edges. The deposit also has a horseshoe shape which is also present in the upper levels. The footwall ore zone has a large trunk vein (inner ore outline) which is thinner on upper levels. The trunk vein is higher-grade massive sulphide copper ore, while the surrounding ore is comprised of semi-massive veins and disseminated mineralization.

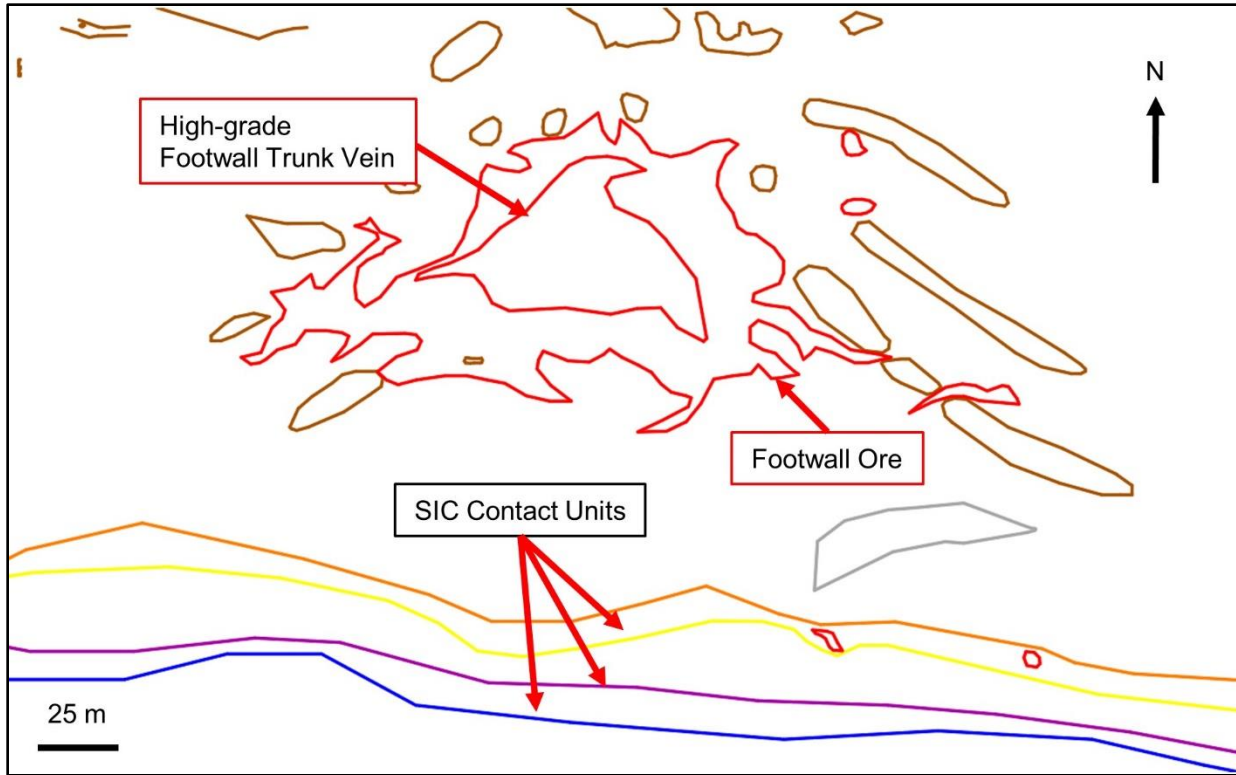


Figure 3-7: Plan view of interpreted geology contacts at 1625 m depth (Glencore, 2017b)

Table 3-2 summarizes intact rock strengths and rock mass quality parameters. As with other Sudbury mines, the host rocks are moderately jointed and have high intact strength. However, the strength of rocks depends on the amount of sulphide mineralization. Higher grade ores have a higher sulphide content and tend to be weaker in terms of both intact rock and rock mass strength, as is the case with the footwall trunk vein.

Table 3-2: Typical rock mass parameters at NRSM (Jalbout and Simser, 2014)

Lithology	UCS (MPa)		Rock quality tunneling index Q parameters				
	Point Load	Core Test	RQD	Jn	Jr	Ja	Jw
FNOR	263	215	75-100	6-9	1-3	1	1
DNOR	234	160	75-100	6-9	1-3	1	1
DNBX	229	160	75-100	6-9	0.5-3	1-3	1
LGBX	190	206	75-100	6-9	1-3	1	1
SDBX	200	383	75-100	6-9	1-3	1	1
FGN	178	250	75-100	6-9	1-3	1	1
Semi-massive Ni Sulphide	153	196	75-100	6-9	0.5-3	1	1
Massive Ni Sulphide	84	89	75-100	6-9	0.5-3	1-3	1
High Grade Copper	49	28	50-75	6-9	0.5-3	1-3	1
DIA	290	-	75-100	6-9	1-3	1	1
GAB	284	279	75-100	6-9	1-3	1	1

Table 3-3 summarizes the calibrated peak moduli and Hoek-Brown strength parameters used in the mine-scale numerical stress model. The calibrated rock mass parameters also indicate weaker and lower modulus (softer) material in copper mineralized zones. Beck et al. (2012) presents a more detailed list of parameters used in the mine-scale stress model which incorporates reductions in strength and stiffness parameters as yielding and post-peak regions of the rock mass soften and transition to their residual strength.

Table 3-3: Peak rock mass strength and stiffness parameters used for mine-scale stress model (Beck et al., 2012)

Lithology	Moduli (GPa)		Rock Mass Scale UCS (MPa)	Hoek-Brown Parameters	
	Bulk	Shear		mb	s
FNOR	16.3	9.77	72.3	3.45	0.0117
DNBX	13.2	7.92	59.9	3.01	0.0111
LGBX	22.7	13.6	93.5	6.02	0.0150
FGN	51.9	31.1	213	6.58	0.0357
Copper zones	14.7	8.79	65.0	3.11	0.0106

### 3.1.3 In-Situ Stresses

Table 3-4 summarizes the orientations and magnitudes of the major principal stresses at NRSM. The regional stresses in the Sudbury basin are generally east-west. The NRSM mine grid is rotated 35° east of UTM north to align with the strike of the orebody and facilitate resource calculations, resulting in an approximately northeast-southwest oriented major principal stress.

The orientation of the far-field major principal stresses were verified using seismic stress inversion by Abolfazlzadeh and McKinnon (2017), and similar orientations were found at the neighboring Nickel Rim Depth deposit using borehole breakout orientations (Goodfellow et al., 2017). Both the seismic stress inversion and borehole breakout results indicate a slight northeast plunge to the major principal stress, and “flipping” of the minor and intermediate principal stresses due to their close magnitude.

Table 3-4: Standard far-field stress regime at NRSM (Jalbout and Simser, 2014; Simser, 2017)

Component	Regional Orientation	Location Orientation (dip/dip direction)	Magnitude (MPa)
$\sigma_1$	East-West	16/24 (NE-SW w/slight northward plunge)	$1.6 \times \sigma_3$
$\sigma_2$	North-South	0/114	$1.3 \times \sigma_3$
$\sigma_3$	Vertical ( $\sigma_3 = \sigma_v$ )	74/204 (near vertical)	$0.026 \times \text{depth (metres)}$

### 3.1.4 Faults

The orebody is intersected by multiple faults, the majority of which are steeply dipping and trend north-south. Figure 3-8 shows the interpreted geology contacts at a depth of 1445 m (same as Figure 3-6) with faults superimposed on top of them. The number of faults varies between levels, but they are typically spaced at 5 to 20 m in ore zones. Many of the smaller faults are not traced between levels.



Figure 3-8: Plan view of interpreted geology contacts at 1445 m depth with superimposed faults (green) (Glencore, 2017a)

Several mine-scale faults are traced between levels. The ones which intersect the mineralization are superimposed on the mine workings in Figure 3-9. Faults at NRSM are brittle in nature, as opposed to more ductile shear structures. There are three major fault sets that intersect mineralization (Jalbout and Simser, 2014):

1. North-south trending and steeply dipping.
2. Low-angle faults with a shallow dip.
3. Northeast to southeast striking and steeply aplite dykes.

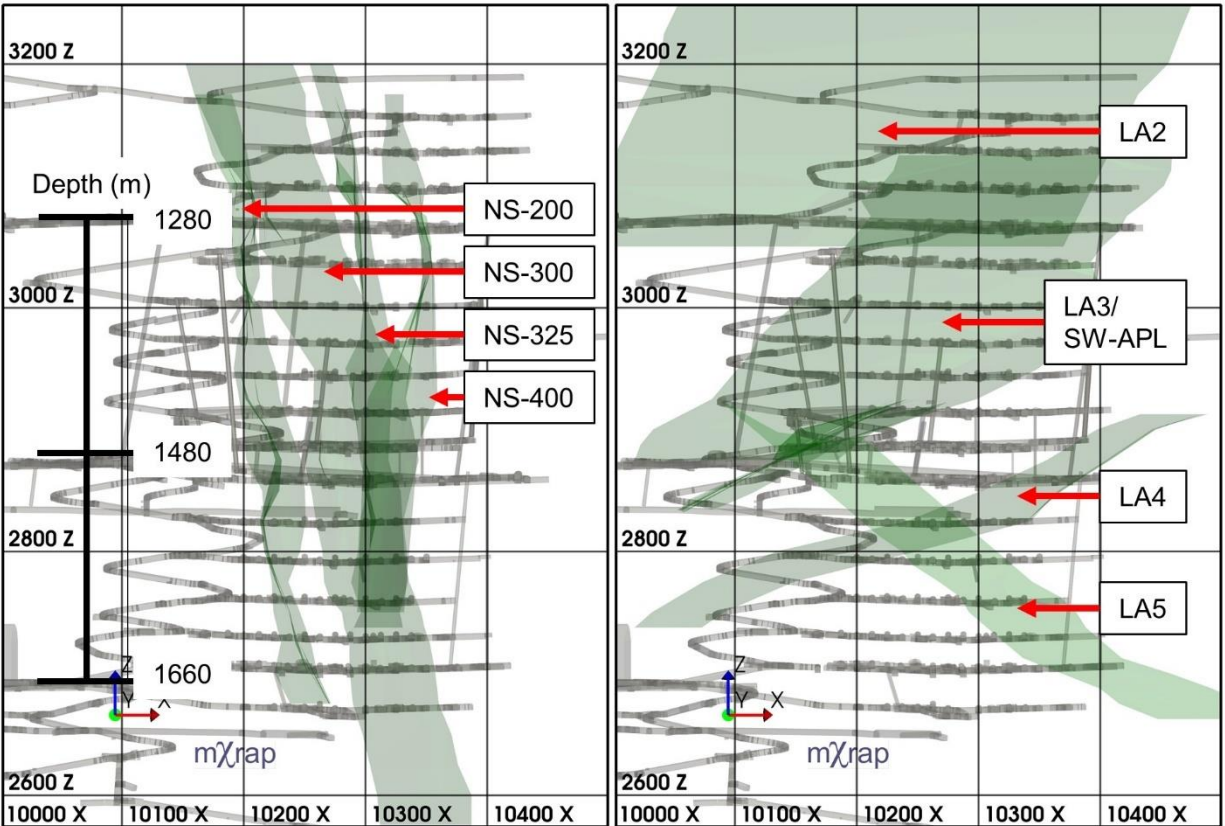


Figure 3-9: Longitudinal view of north-south (left) and low-angle (right) mine-scale faults

Faults play a significant role in the stress field at NRSM. Local stress rotations near geologic structures cause change in the orientation of breakouts in boreholes and excavations. There is also an apparent “stress channeling” effect between faults and excavations and pairs of adjacent faults. Elevated seismic activity are often observed in these stress channels (Jalbout and Simser, 2014). Abolfazlzadeh and McKinnon (2017) also reported non-uniform seismic stress inversion results near larger faults. The role of geologic structures on the magnitudes and orientations of stresses in a rock mass can be simulated in numerical models to provide a more realistic representation of a pre-mining stress field (McKinnon and Garrido de la Barra, 1998). However, such models demand detailed information about each feature being modelled and require extensive calibration (Beck et al., 2012).

### 3.2 Mine Design and Mining Methods

Nickel Rim South employs bulk mining methods to efficiently exploit the thick orebody. The mine layout is intended to enable production on multiple horizons. Multiple production horizons are necessary to maintain the 3,000 t/day production rate and enable independent extraction of nickel

and copper ore. The mine's extraction sequence is also intended to maximize productivity while also strategically managing geomechanical risks associated with stress and seismicity.

### 3.2.1 Mine Layout

The naming convention of development and stopes is intuitive to the description of their locations. The names are based on the mine's coordinate system which is in metric units. Levels are named based on their depth below surface (e.g. 1320 is 1320 m below surface). Accesses are numbered by their level and last three digits of their easting (e.g. the stope access on 1480 that runs along 10300 easting is 1480-300 SA). Stopes are named in based on their undercut stope access (mucking horizon), and each panel is numbered chronologically as mining retreats along the access towards the hanging wall or footwall (e.g. the second stope taken on 1625-225 SA as mining retreats towards the footwall is 1625-225-P2).

Views of the mine-wide development designs are shown in Figure 3-10. Nickel Rim South has three main levels that connect to the shafts: 1280, 1480, and 1660. Ramps are driven from the main levels to access the sublevels which are spaced at 30 m vertical intervals. Stopes are accessed via drifts that run along the strike of the orebody. These drifts may be located in the hanging wall or the footwall. The combination of hanging wall/footwall access was intended to minimize development distances in wide sections of the orebody and where there is a waste gap between the contact and footwall ore zones. The combined access also enables more independent sequencing of the nickel and copper ore. Stopes are accessed exclusively from the hanging wall on levels 1415 and above. As of late-2017, stopes on 1445 and below have been accessed exclusively via the footwall. However, hanging wall access is planned for future stopes in the contact zone below this depth.

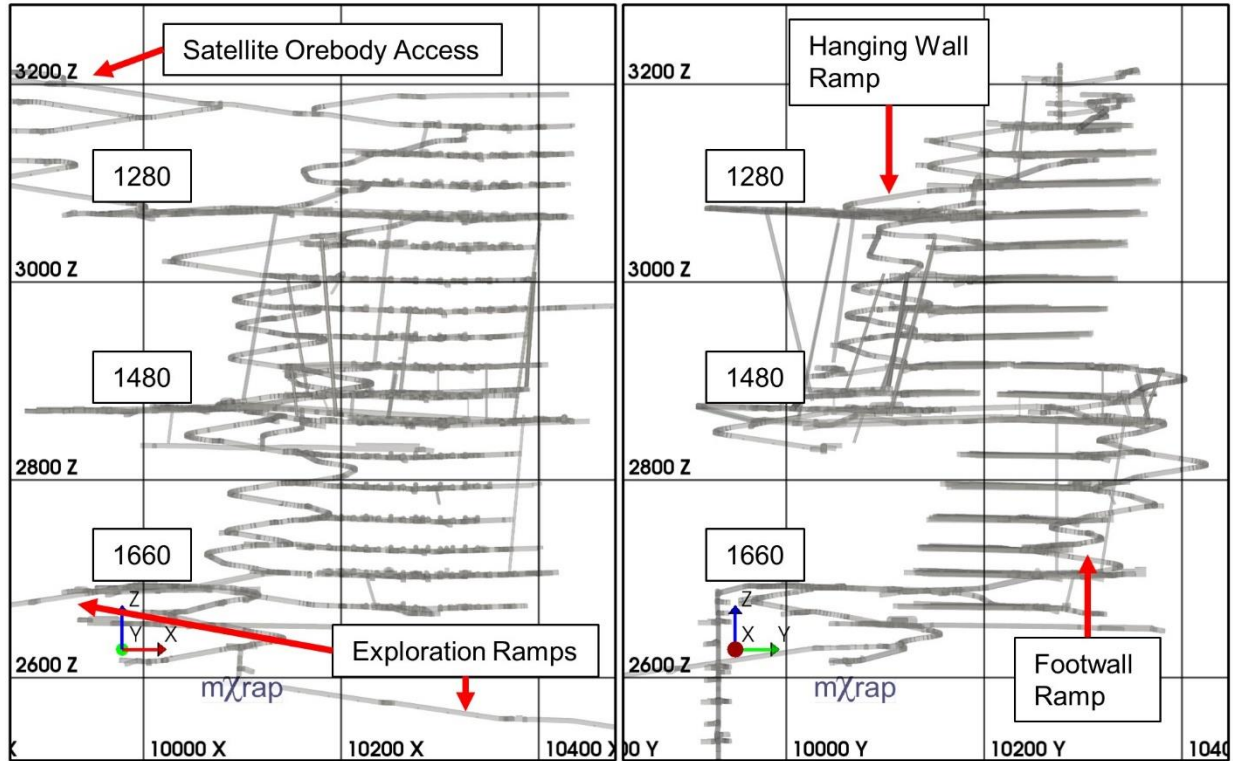


Figure 3-10: Longitudinal (left) and section (right) views of level and access designs

Figure 3-11 shows an example of typical sublevel development for accessing the footwall zone. A drift is driven along the footwall from the ramp. Stope accesses are developed perpendicular to the drift into the ore, and stopes are mined along the access. The pattern of gaps between the stopes shown in the figure is a result of the mining sequence which will be explained later in this chapter. Once all the stopes along an access are mined and backfilled, mining commences along the adjacent access. Nearby accesses are developed off an adjacent one to reduce the length of development and the number of intersections with the footwall drift. The layout of levels with hanging wall access is identical, but with the level's drift located to the south of the ore zone.

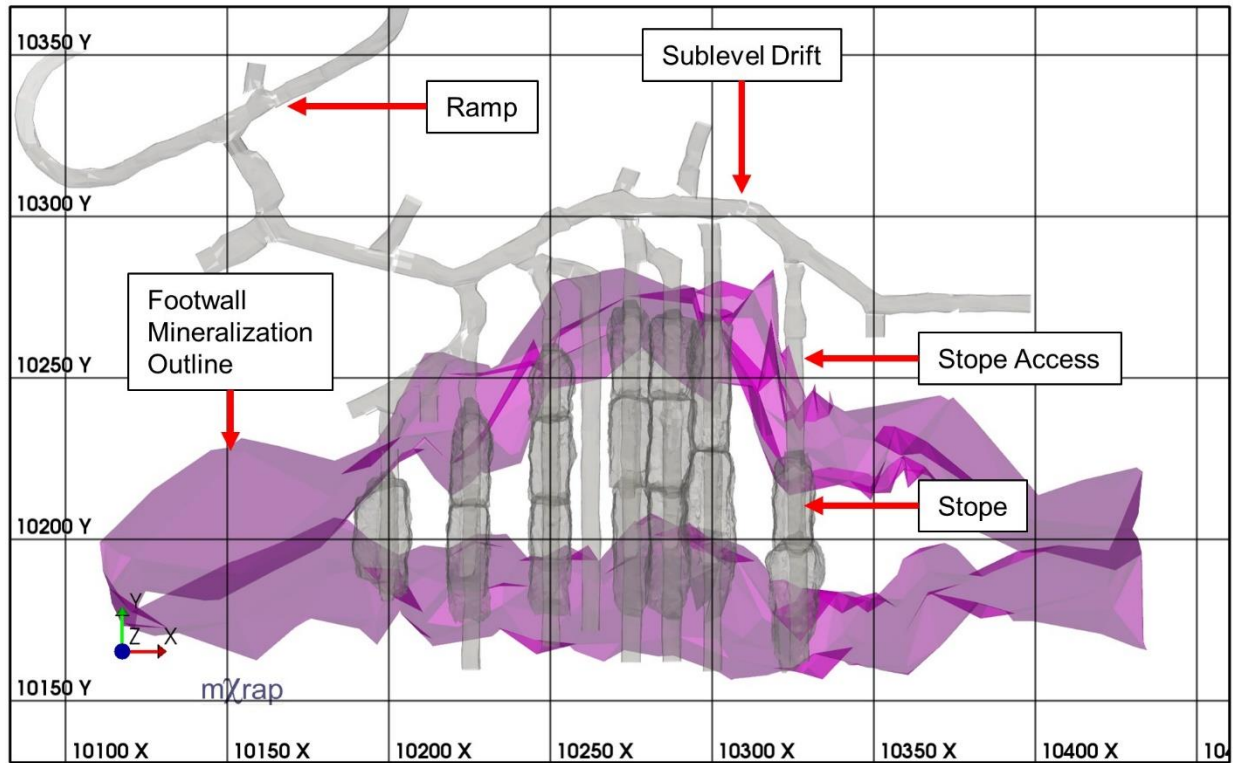


Figure 3-11: Plan view of typical sublevel development (1565)

### 3.2.2 Transverse Blasthole Open Stopping

Nickel Rim South uses transverse blasthole open stopping, a naturally-supported, non-entry mining method typically employed in thick orebodies with competent ore and country rock. The method is highly mechanized and uses large blasts to maximize productivity.

A schematic of a typical stope is shown in Figure 3-12. Accesses to the ore are developed perpendicular to the strike of the orebody from a sublevel that runs along the strike. Blastholes are drilled and loaded from the upper access. NRSM uses 114 mm diameter blastholes drilled in a fan shape (referred to as “rings”). At NRSM, stopes are usually taken in two blasts. A 1.2 m diameter raisebore and the lower access is used as a void for the initial blast, referred to as the “toe slash”. This blast typically extracts the bottom third of a stope and does not extend to the hanging wall or footwall limits. After the blasted rock is removed from the toe slash via the lower access, a second larger blast uses the toe slash as a void takes the remaining two thirds of the stope’s height (sometimes referred to as a “crown” or “daylight” blast). This blast also extends the stope’s lengths to the hanging wall and footwall limits, and is referred to as the “final”. After the stope is emptied, it is filled with a cemented hydraulic fill which must cure before adjacent stopes are mined. If the

orebody is thick (as is shown in Figure 3-12), multiple stopes are mined in a retreating sequence towards the sublevel drift.

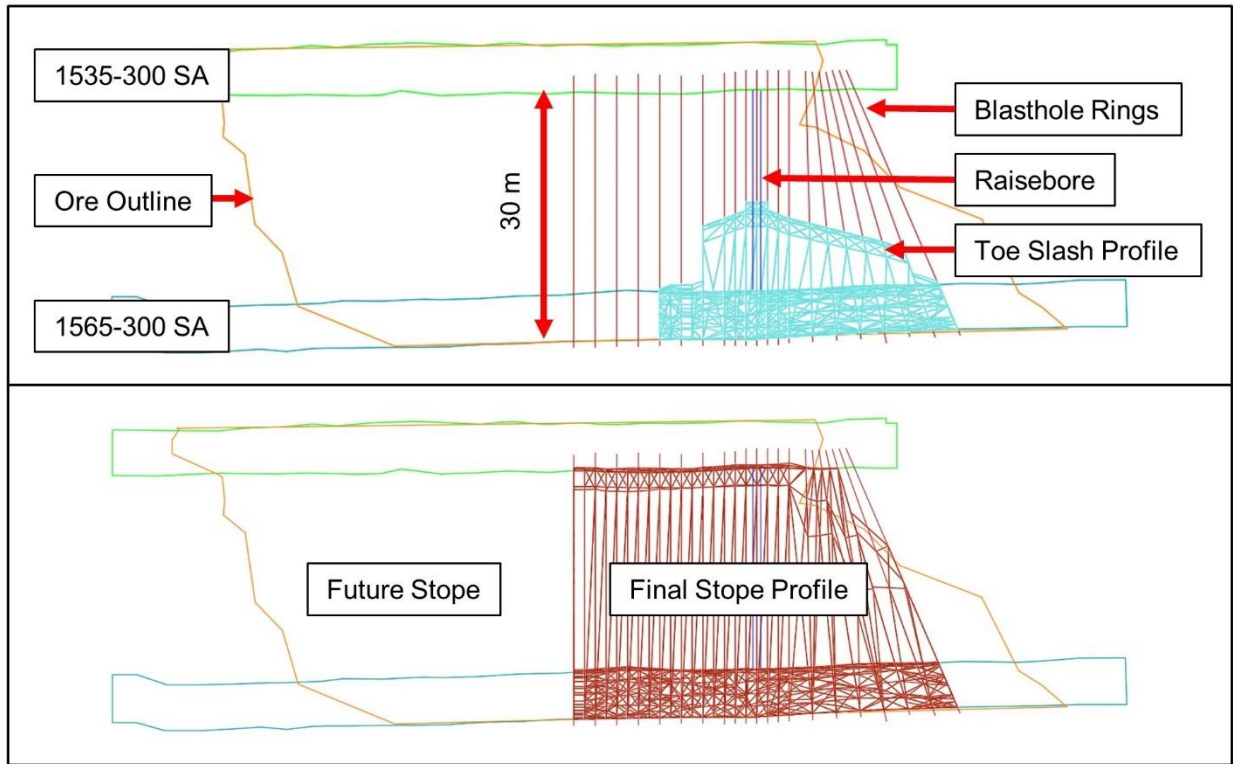


Figure 3-12: Section view schematic of a typical transverse blasthole stope mined with two blasts (1565-300-P1) (Glencore, 2013)

A typical stope at NRSM measures 12.5 m wide (along strike) by 30 m tall (same as the spacing between sublevels) and is up to 30 m long (across strike). A typical toe slash blasts approximately 7,000 t of rock, while a typical final blasts 21,000 t.

### 3.2.3 Stope Sequencing

Mining at NRSM commenced on three primary horizons on the 1320, 1480, and 1660 levels. The horizons were advanced upwards towards two sill pillars, one on 1355 and the other on 1535. A fourth horizon mines downwards from 1660, and a future horizon will mine downwards in the contact zone from 1355 after the sill pillar is mined upwards from the footwall zone. The sill pillars concentrate stress from the mined-out stopes above them and the upward advancing mining front below them. The stope sequencing is designed to strategically manage these stresses to mitigate geomechanical risks such as seismicity and rockbursting.

Two basic sequences are employed at NRSM: primary-secondary, and primary-secondary-tertiary. Primary-secondary sequencing involves mining every other stope first (primaries), leaving

temporary pillars between them which will be mined with secondary stopes after the backfill in the adjacent primaries has cured. The restriction on this sequence is that a primary can not be mined until the adjacent primary is filled, but the backfill in nearby primaries does not necessarily need to have cured. There are two key advantages to this sequence. First, primary stopes can be mined quickly without needing to wait for backfill in adjacent primaries to cure. Second, the pillars have a slender geometry which promotes yielding. The thickness of the orebody combined with the width of the stopes provides relatively little confinement at the core of these pillars, giving them little capacity to store stress before yielding. The result is secondary stopes being mined in a relatively low state of stress. The primary geomechanical hazard during secondary mining is gravity-driven failure, which is considered a more predictable and easily managed challenge when compared to active stress-driven rock mass yield and potential rockbursting (Falmagne et al., 2004).

Two variants of primary-secondary sequences were employed. These sequences are illustrated in Figure 3-13 and are most easily conceptualized by numbering the stopes across the level. The first variation, the 1-3-5, involves mining each adjacent primary sequentially, initially forming 12.5 m wide pillars. The second variation, the 1-5-9, involves mining every other primary on the level, initially forming 37.5 m wide pillars. These wider pillars are then cut into two 12.5 m wide pillars when the primary in the center is mined. The 1-5-9 sequence is intended to circumvent the restriction that two adjacent primaries can not be mined at the same time. This sequence was less restrictive and improved productivity earlier in the mine life when fewer levels were developed. However, the wider pillars did not promote yielding and could pose a greater hazard in elevated stress conditions. Primary-secondary mining was transitioned to exclusively 1-3-5 patterns in 2011 to avoid creating these wide temporary pillars when mining eventually reached the sill pillars.

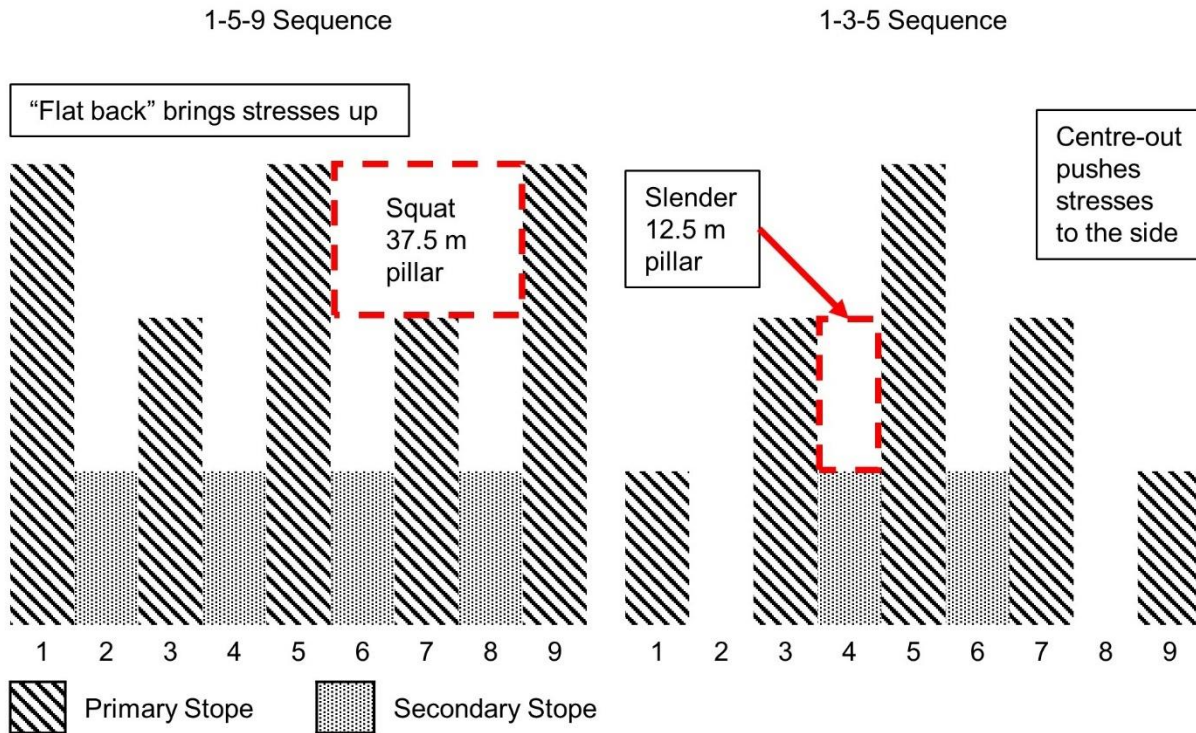
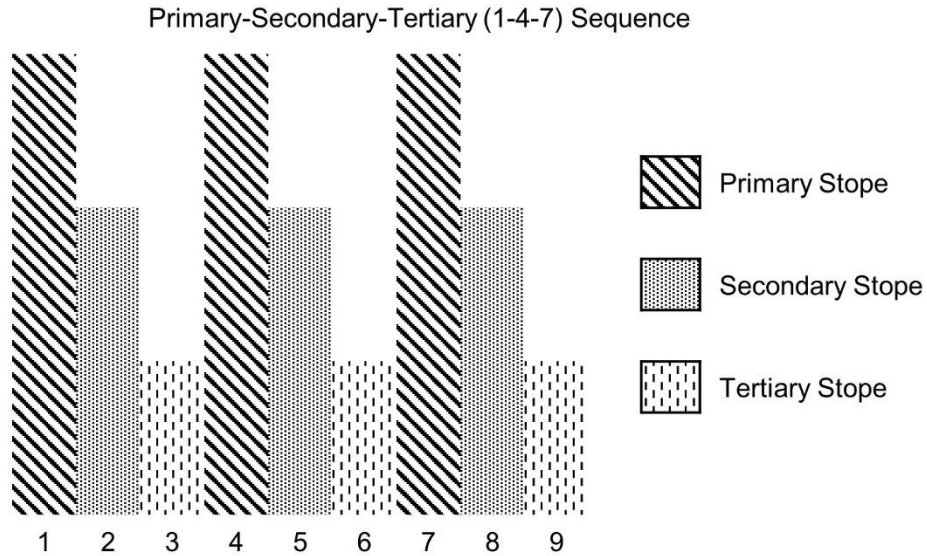


Figure 3-13: Longitudinal schematic of primary-secondary sequence variants

The second type of sequence, primary-secondary-tertiary, is used in the upper part of the mine (levels 1320 and above). Like primary-secondary, this sequence involves the creation of temporary pillars. As per the previous explanation of primary-secondary sequences, primary-secondary-tertiary mining can be thought of as a 1-4-7 sequence. This type of sequence has been illustrated in Figure 3-14. The primary stopes in 1-4-7 sequences are slightly larger than the standard stope size for the rest of the mine, measuring 15 m wide as opposed to 12.5 m wide.



*Figure 3-14: Longitudinal schematic of primary-secondary-tertiary sequence*

On each level, the sequences are executed in a “centre-out” fashion which forms a pyramid shape. The excavation geometry that results from this approach is shown in Figure 3-15. The intention is to evenly move stresses out towards the abutments as opposed to concentrating them in squat pillars. This strategy requires one line of primary stopes be one level “taller” than the adjacent one, and secondary stopes being extracted once the primaries are at least two levels tall on each side.

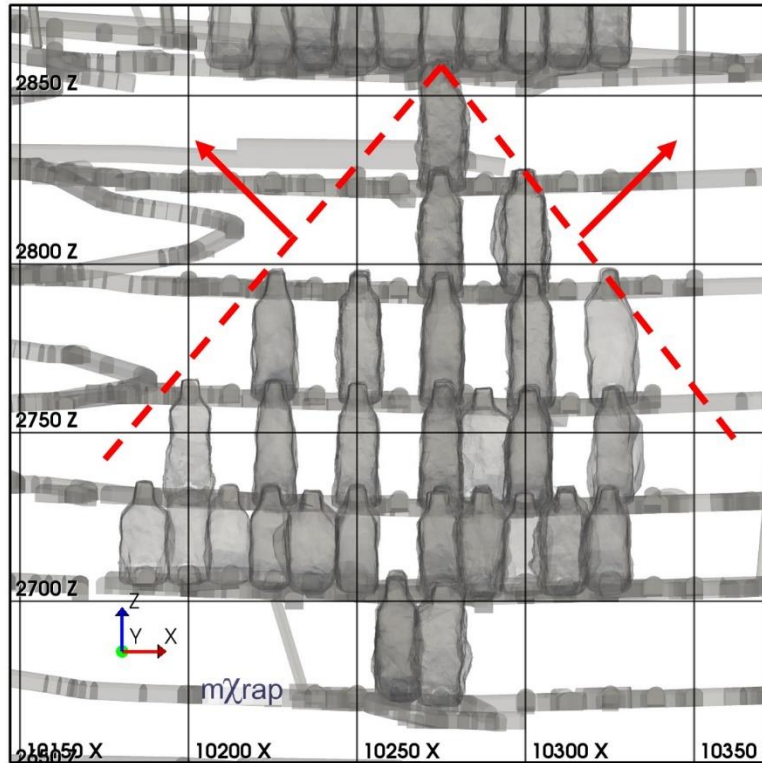


Figure 3-15: Longitudinal view of centre-out sequencing producing a pyramid shape in lower mine (1680 to 1480 levels, January 2014)

Stopes on the edges of the orebody are occasionally mined in a “pillarless” fashion (i.e. mined against a single primary rather than between two adjacent primaries). An example of a pillarless sequence is shown Figure 3-16. This approach is usually taken because the economic limits of the ore do not justify a stope farther away.

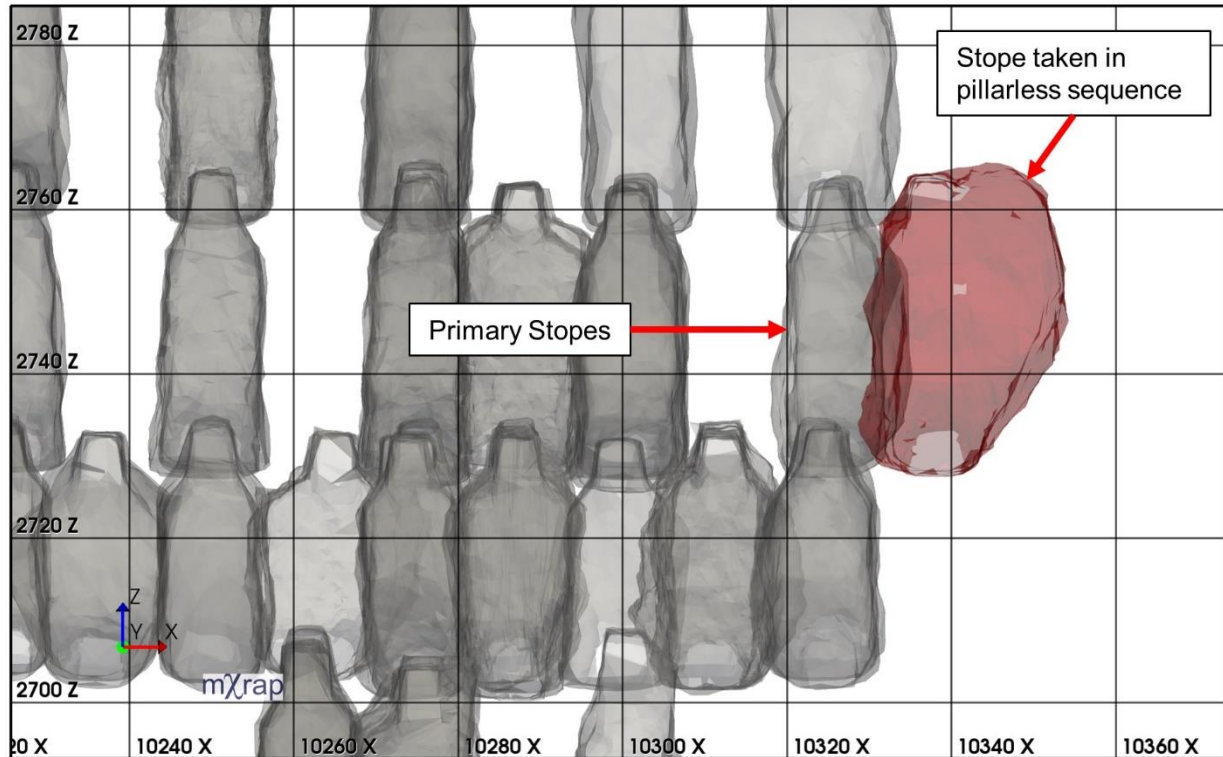


Figure 3-16: Longitudinal view of a stope taken in a pillarless sequence (1625-337-P1, May 17<sup>th</sup>, 2014)

### 3.3 Seismic Monitoring

#### 3.3.1 Seismic Monitoring Array

Nickel Rim South has a state-of-the-art underground array of microseismic sensors. The array was functional before the first stope was mined in 2009, so a complete seismic record of production mining is available. The array has been expanded multiple times since its inception. As of late 2017, the array included 40 uniaxial accelerometers, and 18 15Hz triaxial geophones. A separate array is composed of two 4.5 Hz triaxial geophones: one located near the 1660 shaft station and the other off the production shaft several hundred metres above the orebody. This secondary array is intended to improve source parameter calculation for larger events whose larger ground motions may saturate the microseismic array and must be measured by lower frequency sensors at greater distances. Digitizers are placed on the majority of sublevels which have sensors. Their proximity to the sensors reduces signal noise by minimizing the distance analog signals must travel over copper cable.

Sensors are located along the entire strike of the orebody on multiple levels. Development in the hanging wall and footwall enables sensors to be placed on both sides of the orebody, which

improves location accuracy and source parameter estimates by providing more complete coverage of the event’s radiation pattern. Sensors are also located near the shaft stations which provides additional coverage in the orebody’s western abutment. The locations of sensors in late 2017 are shown in Figure 3-17. The sensors provide the most complete coverage towards the west of the orebody, and near the lower and middle production horizons.

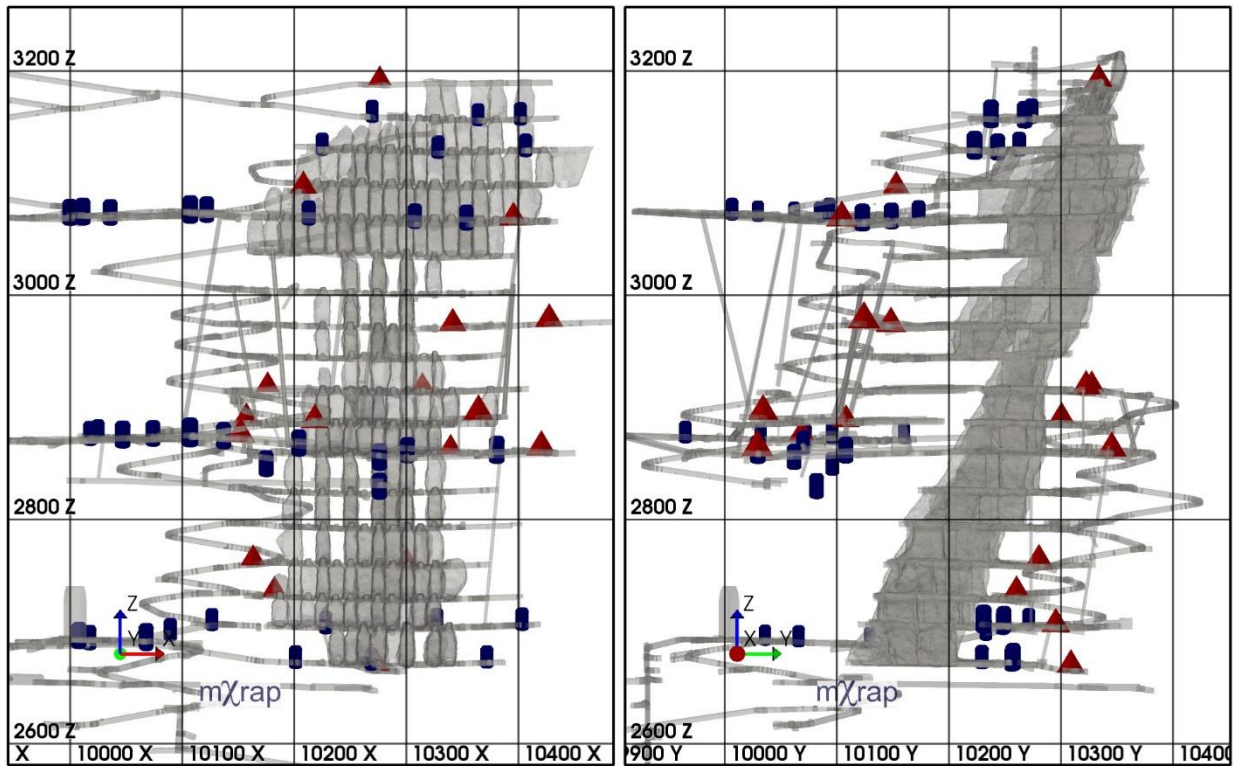


Figure 3-17: Longitudinal (left) and section (left) views of uniaxial (blue cylinders) and triaxial (red pyramids) sensor locations up to late 2017

Figure 3-18 shows the number of sensors used to locate events over time. Array expansions have allowed more sensors to be used over time. The array was significantly expanded in 2010. These expansions added a large number of triaxial geophones and improved the estimation of event magnitudes and other source parameters (Simser et al., 2015a). For this reason, this thesis focuses on the higher quality seismic data collected in 2011 and later.

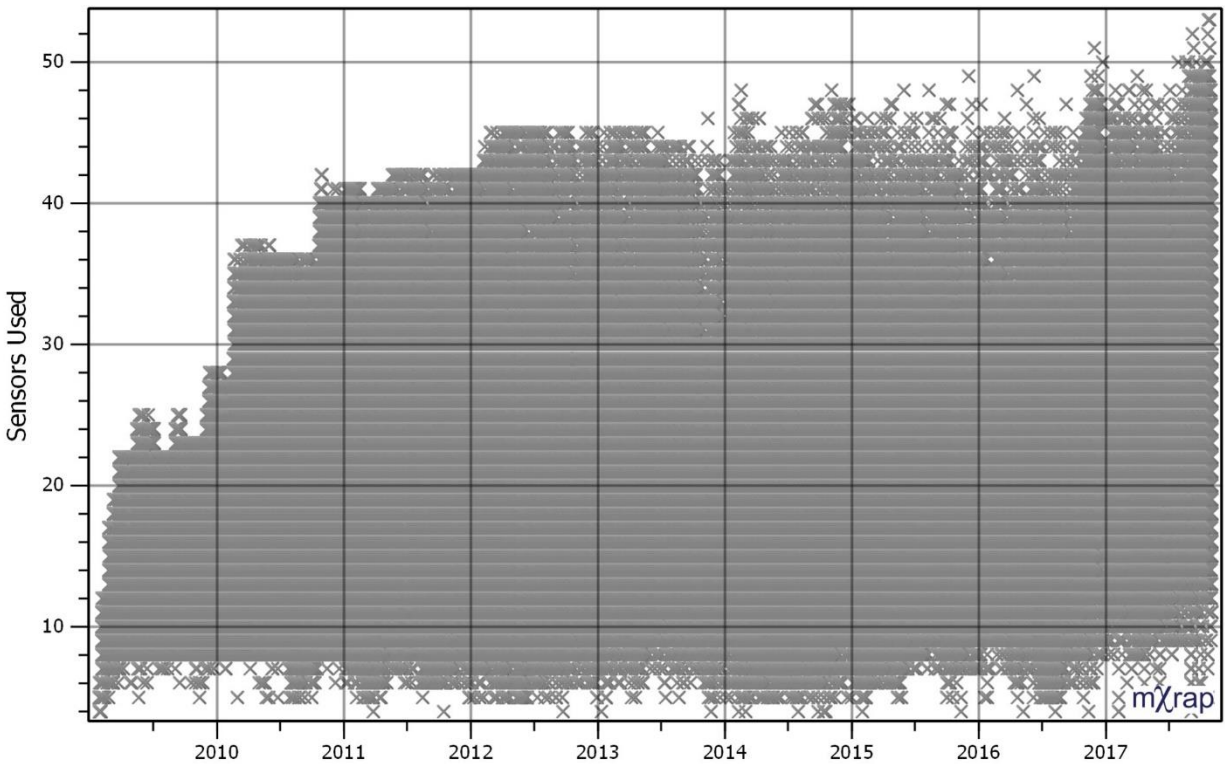


Figure 3-18: Number of sensors used to locate events over time

### 3.3.2 Moment Magnitude Scale

Nickel Rim South uses the moment magnitude scale which was developed by Hanks and Kanamori (1979). The moment magnitude (more typically denoted as  $M_w$  to distinguish it from other magnitude scales) is calculated as follows:

$$M = \frac{2}{3}M_o - 6$$

[3.1]

The moment magnitude is well correlated with Richter Magnitudes estimated by the Sudbury Regional Seismic Network (SRSN). The SRSN is a regional network of 4.5 Hz triaxial geophones intended to estimate the magnitudes of larger events which may saturate the local arrays for mines in the Sudbury Basin. Figure 3-19 shows a comparison of the two magnitude scales. The moment magnitude is slightly less than the Richter magnitude. Some larger magnitude events (greater than Richter 2.0) appear to have been underestimated by the NRSM array. However, the graph indicates a descent correlation between Richter magnitudes 0.5 and 2.0 (note that the SRSN is not intended to detect smaller magnitude events like the local NRSM array). It is expected that the NRSM

microseismic array is providing accurate source parameter estimates for the vast majority of events at the mine which are typically smaller and therefore less likely to saturate the sensors.

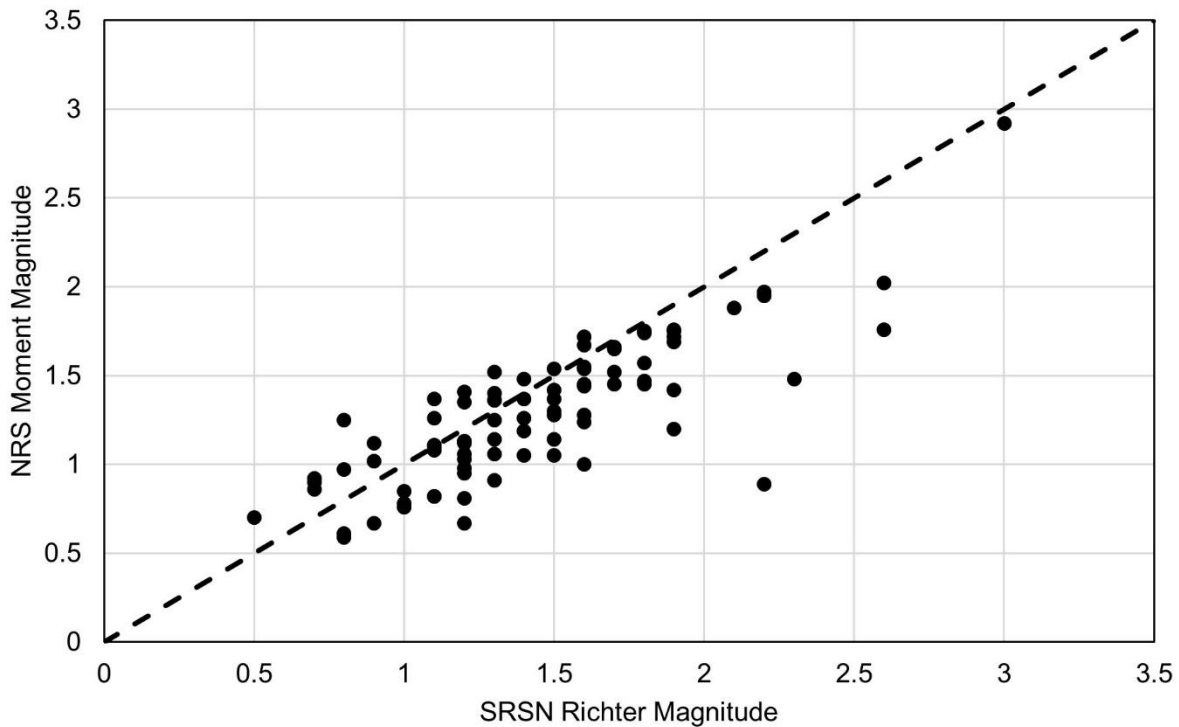


Figure 3-19: Moment magnitude as measured by the NRSM microseismic array versus Richter magnitude as measured by the SRSN (2009 to late 2017)

### 3.3.3 Location Accuracy

As mentioned previously, the hanging wall-footwall coverage of the microseismic array provides superior location accuracy compared to an array that has sensors on only one side of the orebody. Location accuracy can be quantified in terms of a residual distance. This parameter is calculated using the difference between observed and expected wave arrival times based on an event's calculated source location. Cumulative distributions of location residuals are shown in Figure 3-20. Since the 2010 array expansions, most events are located with a residual error less than 3 m, and over 80% of events are located with a residual error less than 5 m. This level of location accuracy enables highly detailed analysis of event locations. Events can be isolated to individual levels, areas around a 12.5 m wide stope, and even individual development headings.

Figure 3-20 also shows that smaller events tend to be located with less residual than larger events. Larger events are typically located less accurately because location algorithms assume point sources. Larger events are caused by larger volumes of the rock mass deforming, essentially

making them less of a point source. Nevertheless, the NRSM array locates larger events with reasonable accuracy, with approximately 70% of  $M \geq +1$  events located with a residual error less than 5 m.

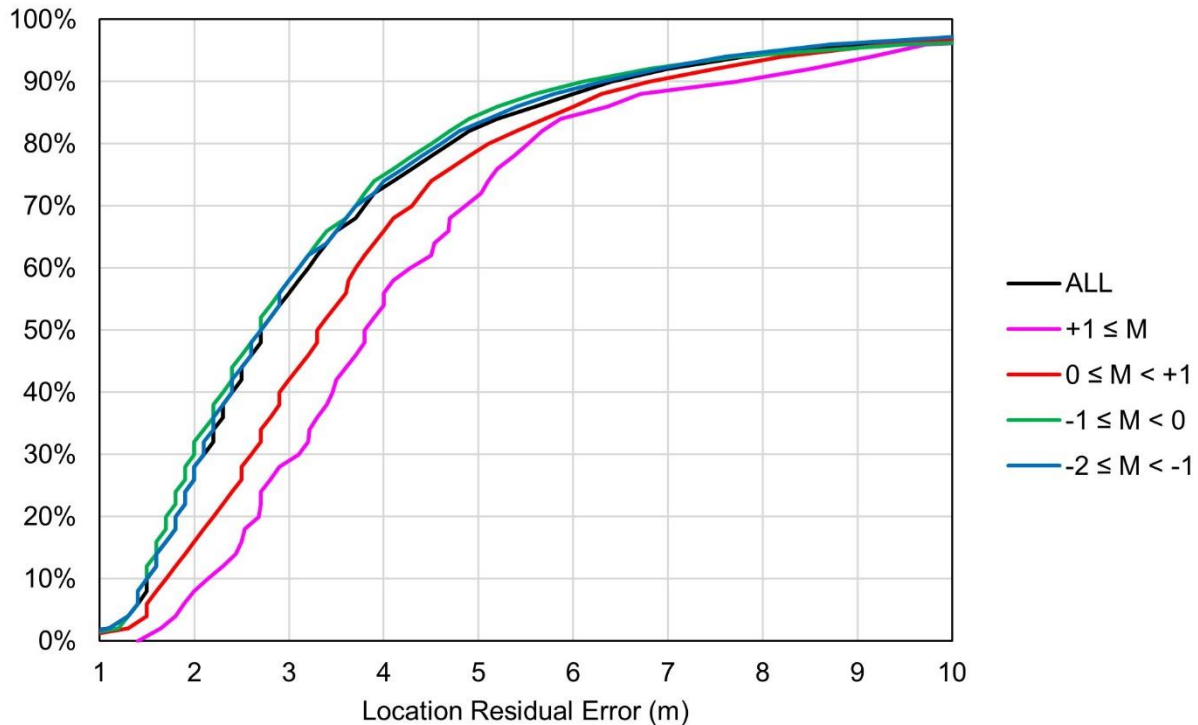


Figure 3-20: Cumulative distribution of location residual errors (2011 to late 2017)

Figure 3-21 shows the median location residual error on an annual basis in different regions of the mine. Residual errors have decreased over time, most substantially after 2012. Before this time, there was substantially more development of ramps and levels which are located outside the volume covered by the array. Seismic events in these areas tended to have higher residual errors than events located near the orebody, which has more complete spherical coverage. The middle and lower production horizons (starting on 1480 and 1660 respectively) tend to have lower residual errors than the upper horizon (1320). Again, this effect is related to greater spherical coverage. Ramp development outside the array led to higher residual error on the west side of the orebody until 2013. In 2013 and later, the western half of the orebody has slightly lower residual error than the east. This disparity is related to sensors near the shaft stations providing more coverage towards the west. The mine’s seismic monitoring supplier has also made improvements to the processing

software’s automated wave arrival picking and location algorithms over time. These improvements also contributed to the reduced residual errors later in the mine life.

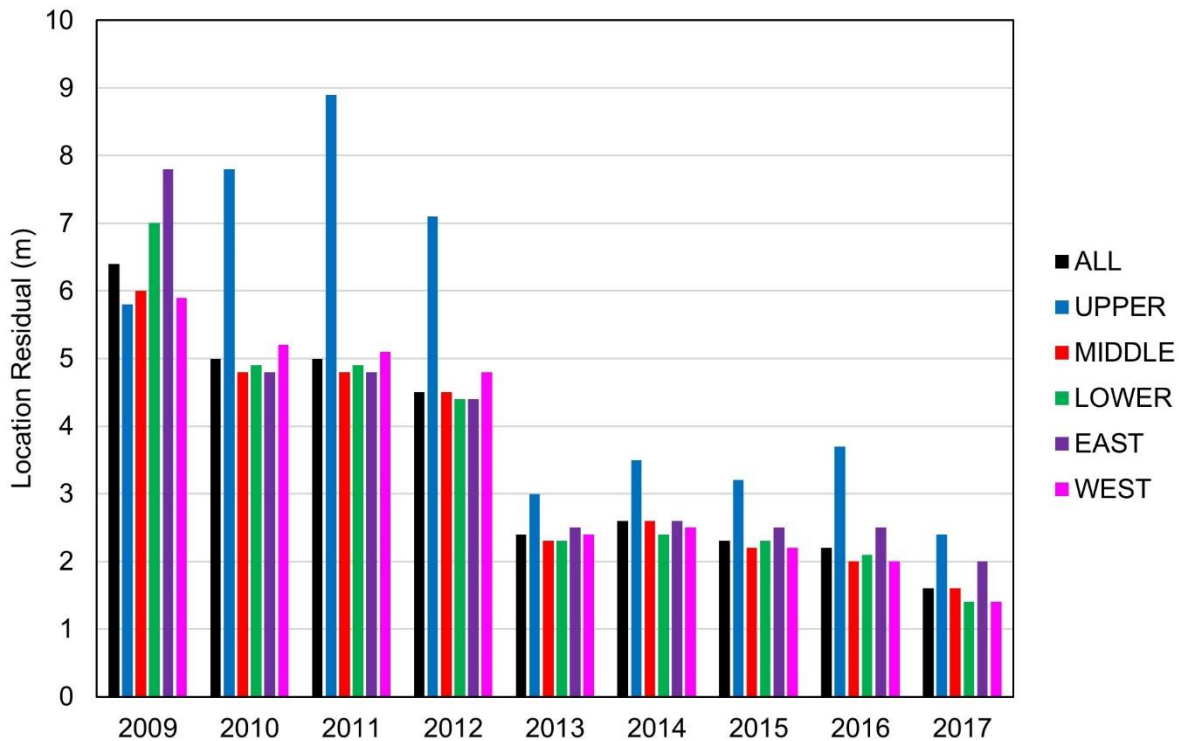


Figure 3-21: Median location residual error by year in different regions of NRSM

The high location accuracy produced by the NRSM array is also evidenced by how closely events and blasts that trigger the seismic system follow the surveyed location of development mining (Jalbout and Simser, 2014; Simser et al., 2015a). Several examples of such seismic data are shown later in this chapter.

### 3.4 Seismic History of NRSM

Throughout the majority of Nickel Rim South’s history, seismicity has been closely linked with active mining areas. Within the broad classifications proposed by Gibowicz and Kijko (1994), this type of seismicity is closely linked in space and time with the creation of new excavations. However, the abundance of faults at NRSM suggests that McGarr’s (2005) classification of mechanisms related to strong interaction between faults and excavations may also be present. Seismicity related to larger scale geologic features and shows little association with active mining in space and time may be present at NRSM but is difficult to distinguish in broad analysis of

seismicity at the mine. The majority of seismicity at NRSM is closely linked in space and time with active mining areas.

### 3.4.1 Event Locations

Figure 3-22 shows longitudinal views of event locations on an annual basis. The locations show a clear association with active mining areas. Earlier in the mine life, events locate along drifts, ramps, and raises which were developed extensively until around 2012. Near the stopes, seismicity progresses upwards and outwards with primary extraction, with little activity in pillars which will be extracted later by secondary and tertiary stopes. The locations of events in the stoping areas show how the sequence redistributes stresses to the abutments of the mining front and leaves behind yielded pillars which produce little or no seismic activity. The NE-SW orientation of the major principal stress causes events to wrap around the footwall on the west side of the orebody, and around the hanging wall on the east side of the orebody. Later in the mine life, the sequence has clearly pushed stresses to the abutments, and there is little activity near the centre of the orebody which is mined out or yielded.

Figure 3-22 also indicates the drastic improvement in location accuracy brought on by array expansions in 2010. Prior to 2011, there are substantially more events scattered around the mine where no development or stoping is taking place. In 2011 and later, the events are more isolated to areas near the active mine development and stopes. There is no strong explanation as to why events might be scattered in areas more distant from active mining earlier in the mine life, but more consistently located near active mining later on. This empirical observation is interpreted to be the effect of improved location accuracy provided by the expanded microseismic array, and further justifies the focus of this thesis on data in 2011 and later.

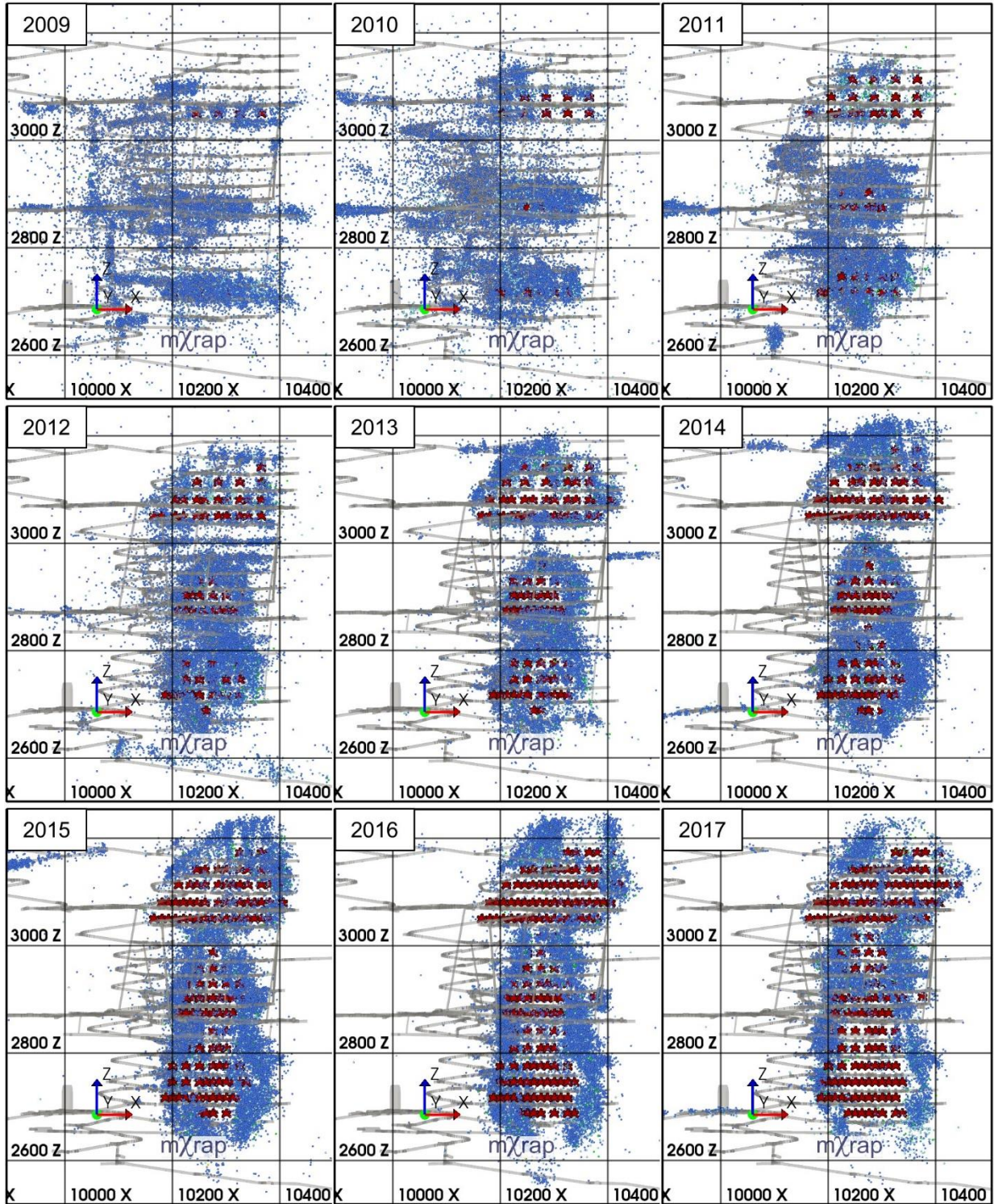


Figure 3-22: Longitudinal views of annual event locations (dots) and extracted stops (red stars)

Figure 3-23 shows plan views of annual event locations on a sublevel with a 1-3-5 primary-secondary sequence. This level exemplifies the typical pattern of seismicity observed on a sublevel

at NRSM. The footwall drift was developed prior to 2012, and the first stopes mined on the level were in the centre of the orebody (275).

- In 2012 there is a large amount of seismicity near the 275-SA stopes as well as to the east where stopes are being mined on the level below.
- In 2013 there is more seismicity near the footwall as the 275-SA stopes progress towards it, and there is seismicity towards the east associated with mining the 300-SA stopes.
- In 2014 primary stoping is complete between 250-SA and 300-SA. There is little seismicity inside the pillars that will be mined along the 262-SA and 287-SA. Seismicity in this year is also associated with primary stoping on the level above.
- In 2015 seismicity progresses further towards the east and west with the extraction of stopes along the 225-SA and 325-SA. Secondary stoping begins along 287-SA, but there is little activity near that area.
- In 2016 further mining of stopes along the 287-SA generates little seismicity nearby. There is some seismicity to the east and west of the primary stopes associated with mining stopes on the levels above and below, but there is substantially less than when stopes are blasted on the level.
- In 2017 the extraction of a primary stope along 200-SA causes seismicity further towards the west. There is some seismicity on the eastern abutment associated with mining on other levels, and there is effectively no activity in the pillars which will be extracted with secondary stopes.

The history of event locations demonstrates how seismicity tends to follow active mining areas and occur at a greater rate with nearby mining.

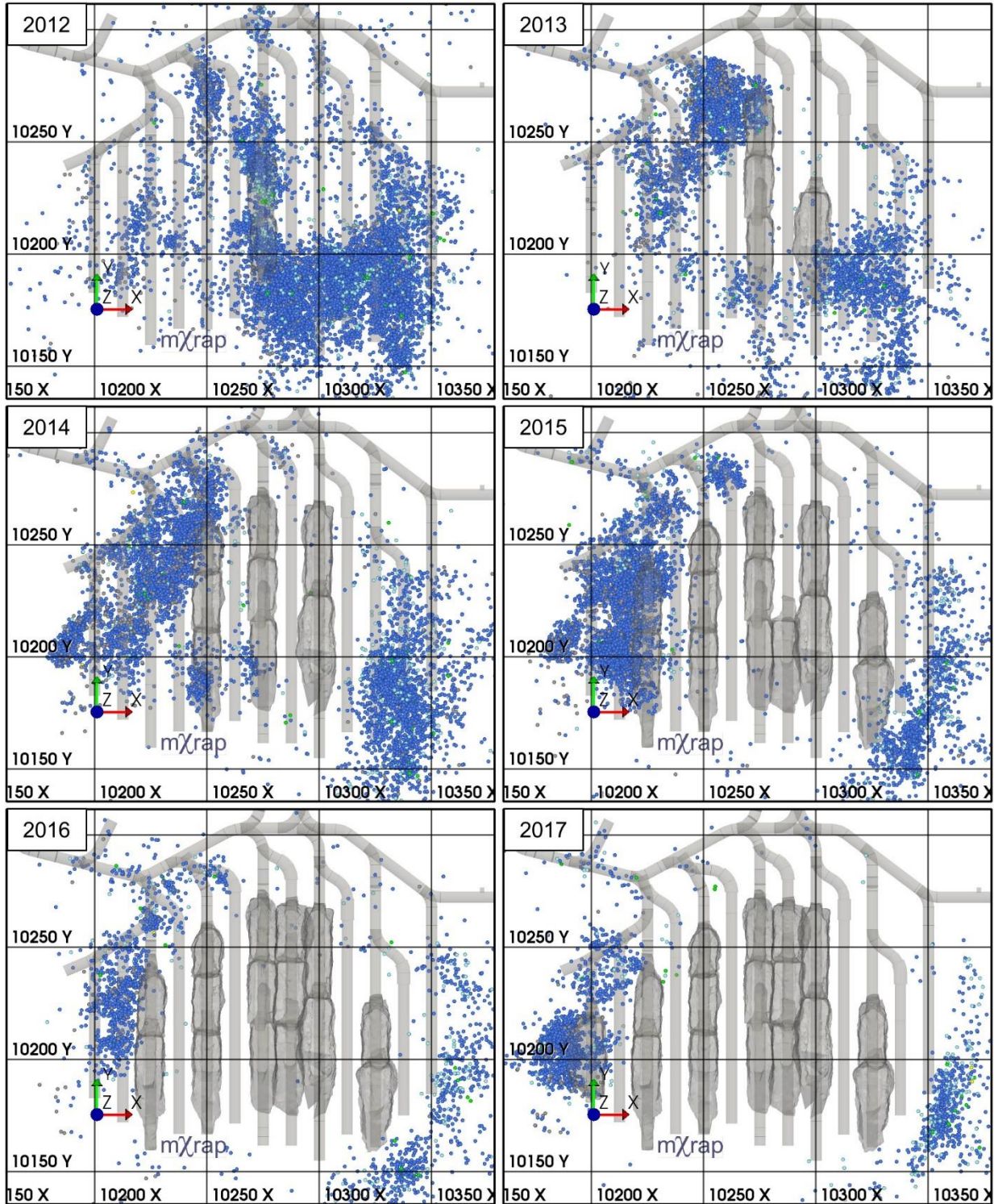


Figure 3-23: Plan view of annual event locations (dots) and extracted stopes in a typical centre-out 1-3-5 primary-secondary sequence (1565 level, 30 m thick horizontal slice)

### 3.4.2 Magnitude-Time Histories

Seismicity at NRSM is relatively consistent over nearly a 9-year period. The magnitude-time history in Figure 3-24 includes all events recorded throughout the mine from when the array became operational in early 2009 up to late 2017. There are no significant gaps in the data, and the array has detected events as small as  $M = -2$  (note that is not the sensitivity of the array, which typically lies between  $M = -1.5$  and  $M = -2.0$ ). The event rate is fairly consistent, with some short periods of elevated activity. Few  $M \geq 0$  events occur early in the mine life. Magnitudes of the largest events increase until around 2012 when  $M \geq 1$  events become more common. Events are typically smaller than  $M = 2$  until late 2017 when two  $M \geq 2$  events occur.

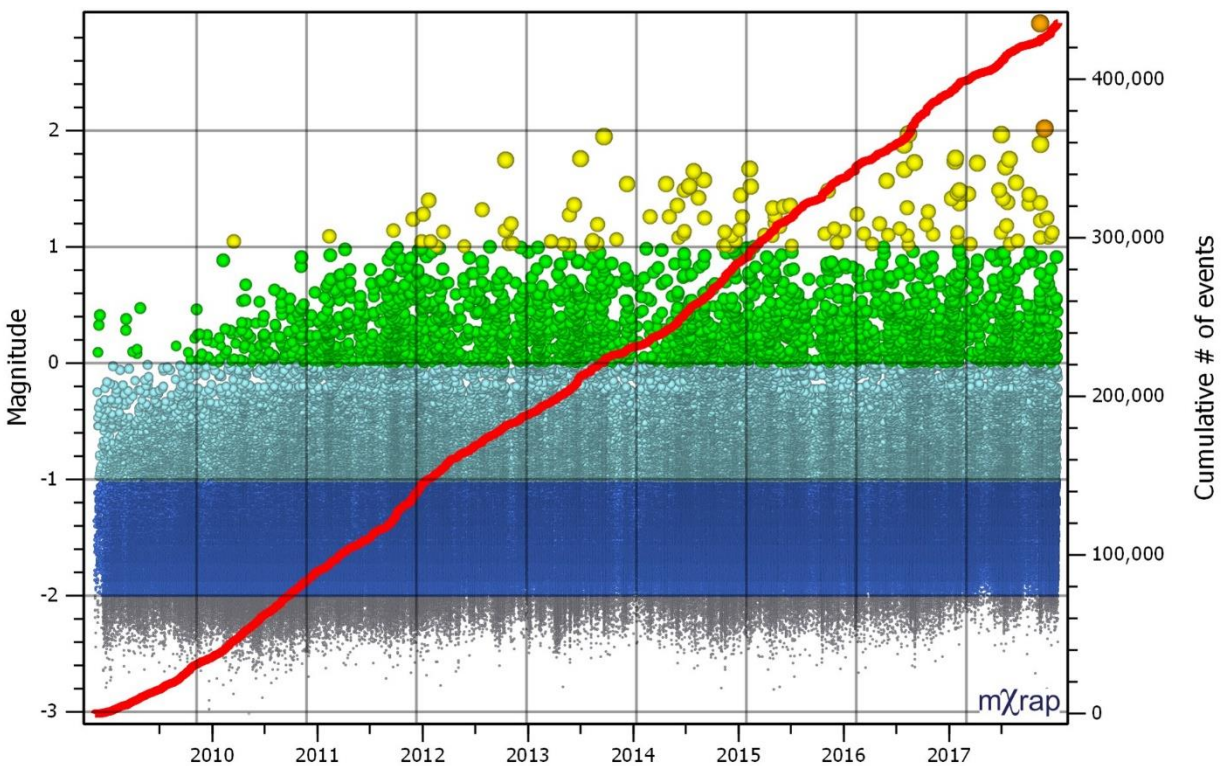


Figure 3-24: Mine-wide magnitude-time history of events

Figure 3-25 shows a magnitude-time history of  $M \geq 1$  events throughout the mine. As stated previously, events larger than this magnitude are relatively infrequent until 2012. The rate of these larger magnitude events increases gradually over time. Slightly more than half the  $M \geq 1$  events occur in 2015 and later.

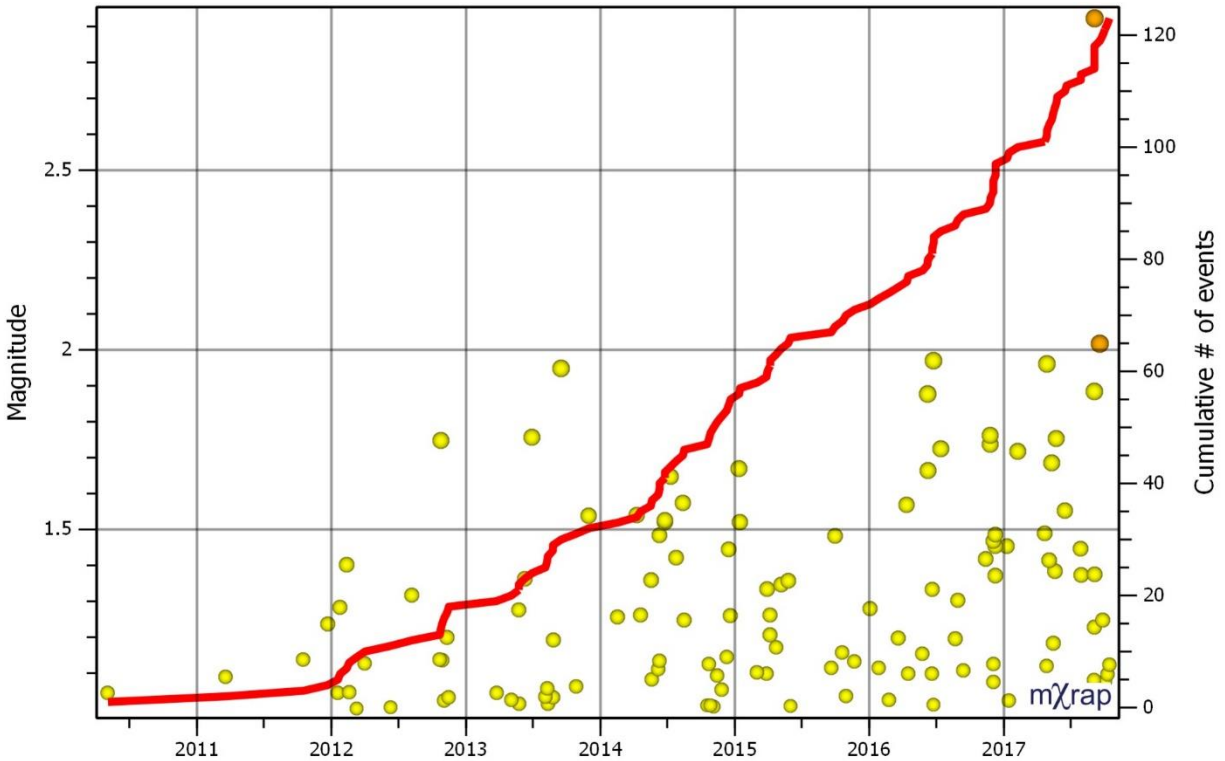


Figure 3-25: Mine-wide magnitude-time history of  $M \geq 1$  events

### 3.4.3 Diurnal Charts

Diurnal charts also speak to the largely blast-driven nature of seismicity at NRSM. Figure 3-26 shows a diurnal chart of all events recorded at NRSM between 2011 and late 2017. 2009 and 2010 were excluded from this chart because different blast times were used during the mine’s development phase. The diurnal chart clearly shows two peaks at 06:00 and 18:00. These times correspond to the times between shifts during which blasts are taken. The peak at 18:00 is larger because stope blasts (which are larger and tend to generate more seismicity than development blasts) are usually taken at the end of the day shift. Note that the apparent slight increase in event rate prior to 6:00 and 18:00 is related to some blasts being taken slightly earlier depending on the time that the workers return to surface and the blast is taken. Flowing the blasts at shift change, the event rates are elevated for 2 to 3 hours. Also of note is that the largest events (two  $M > 2$  events) do not occur at blast times.

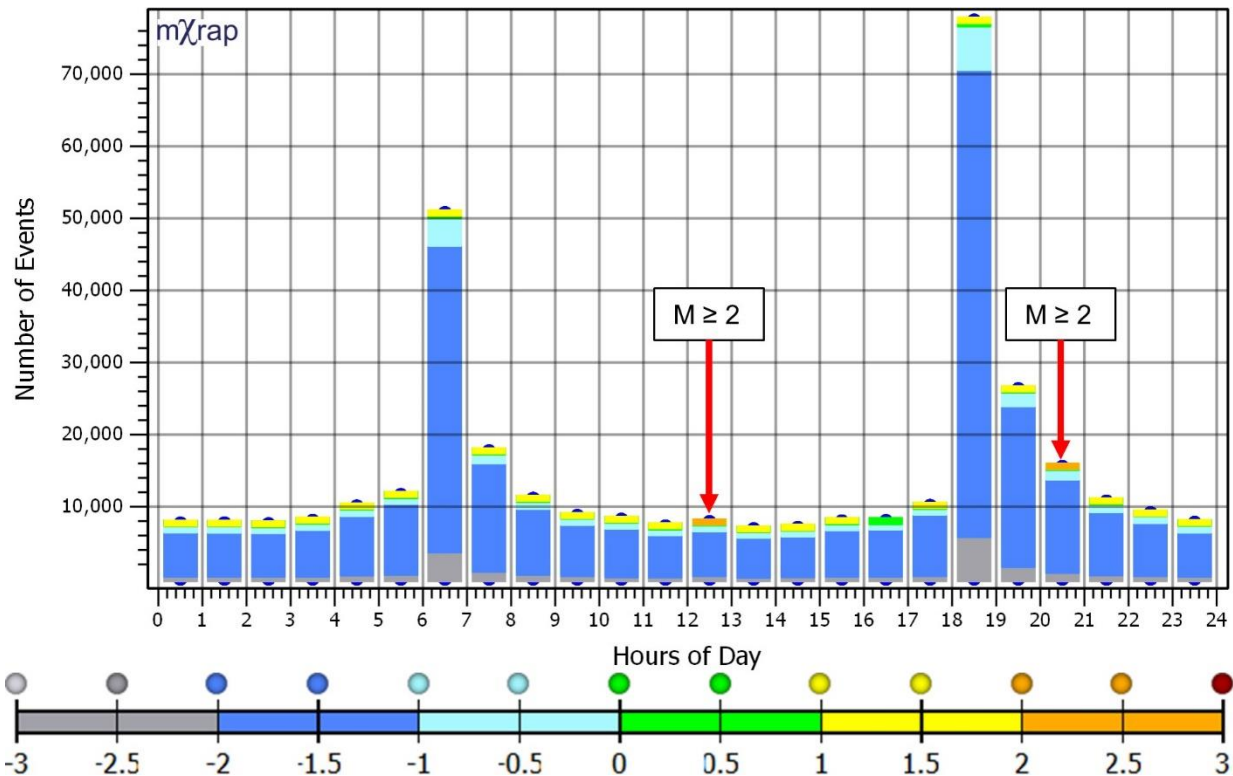


Figure 3-26: Mine-wide diurnal chart of events (2011 to late 2017)

Figure 3-27 shows a diurnal chart of  $M \geq 1$  events over the same period as the events shown in Figure 3-26. Larger magnitude events tend to be less correlated with mining in both space and time (Gibowicz and Kijko, 1994). The peaks at 06:00 and 18:00 are less pronounced in Figure 3-27 than Figure 3-26, indicating a weaker association between the occurrence of larger magnitude events and the times blasts are taken. However, the peaks at 06:00 and 18:00 are still apparent, indicating that there is at least some association between larger magnitude events and mine blasts.

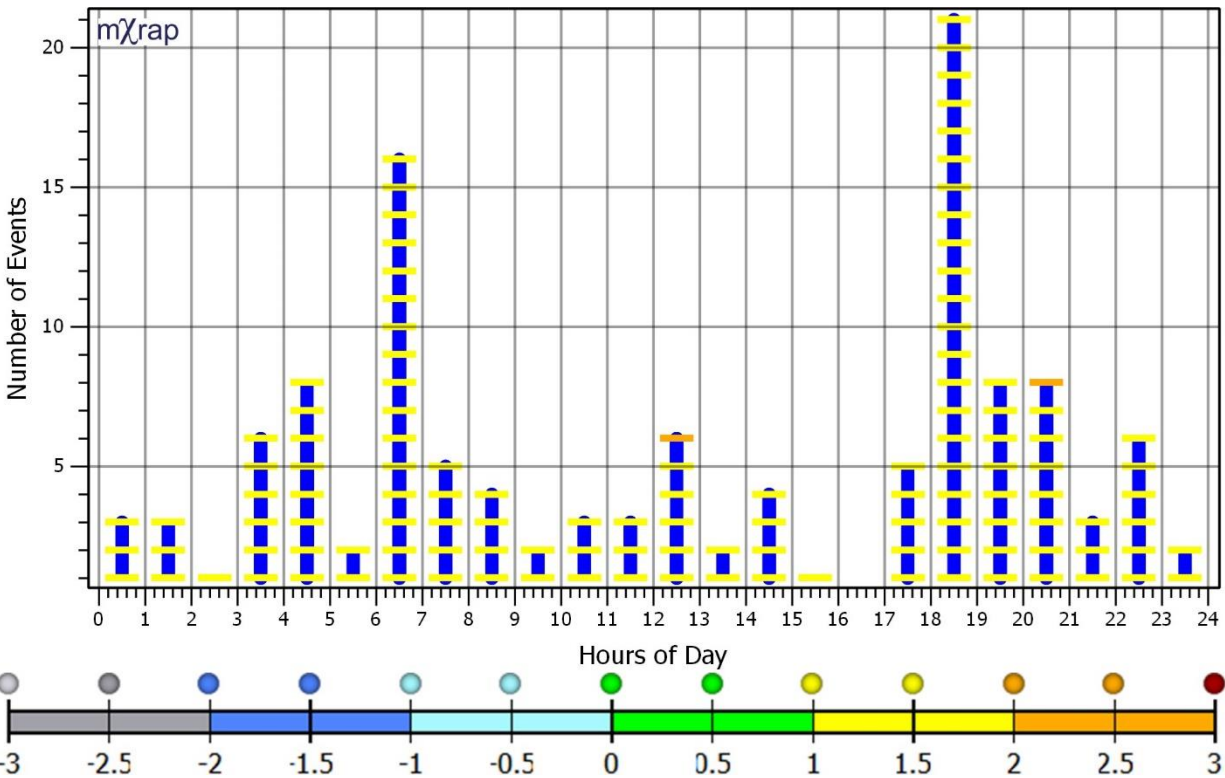


Figure 3-27: Mine-wide diurnal chart of  $M \geq 1$  events (2011 to late 2017)

### 3.5 Typical Seismic Responses to Mining at NRSM

As was shown in the previous section, seismicity at Nickel Rim South follows mining in both space and time. As a result, there are several typical seismic responses observed with each mining activity which are presented in this section. These typical seismic responses are primarily discussed with regard to event locations rather than other aspects of the observed seismicity (e.g. number of events, event magnitude, other source parameters, etc.). Note that the figures in this section use planned development surveys. Not all drifts and accesses depicted were developed during or before the period of seismicity shown. Mined and backfilled stopes are shown in grey, and current stopes being mined are shown in red.

#### 3.5.1 Primary Development

Figure 3-28 shows an example of seismicity observed when developing a primary stope access. This access, 1595-225 SA, was developed relatively early in the mine life, and was the first stope access developed on the level. No stopes had been mined on the level below, 1625, prior to this development, so induced stresses from other excavations are expected to be relatively low. With

other primary accesses, elevated induced stresses and stress shadows from adjacent stopes influence the patterns of observed seismicity.

When blast vibrations trigger the seismic system, the events locate along the access being developed. Events also followed the development of the access and are associated with the induced stresses around the advancing access. The events are close to the access, which is expected due to its relatively small profile and corresponding small area of induced stress. The proximity of the seismic events to what is assumed to be a small area of elevated mining-induced stress speaks to the high accuracy of event locations produced by the NRSM array. Also of note is a small area along the access with a relatively small number of seismic events. This area corresponds with the location of the copper trunk vein. Less seismicity is observed in this softer, weaker region of the rock mass. Some blasts and seismicity are also visible to the upper right of the figures, which are associated with continuing development of the footwall drift.

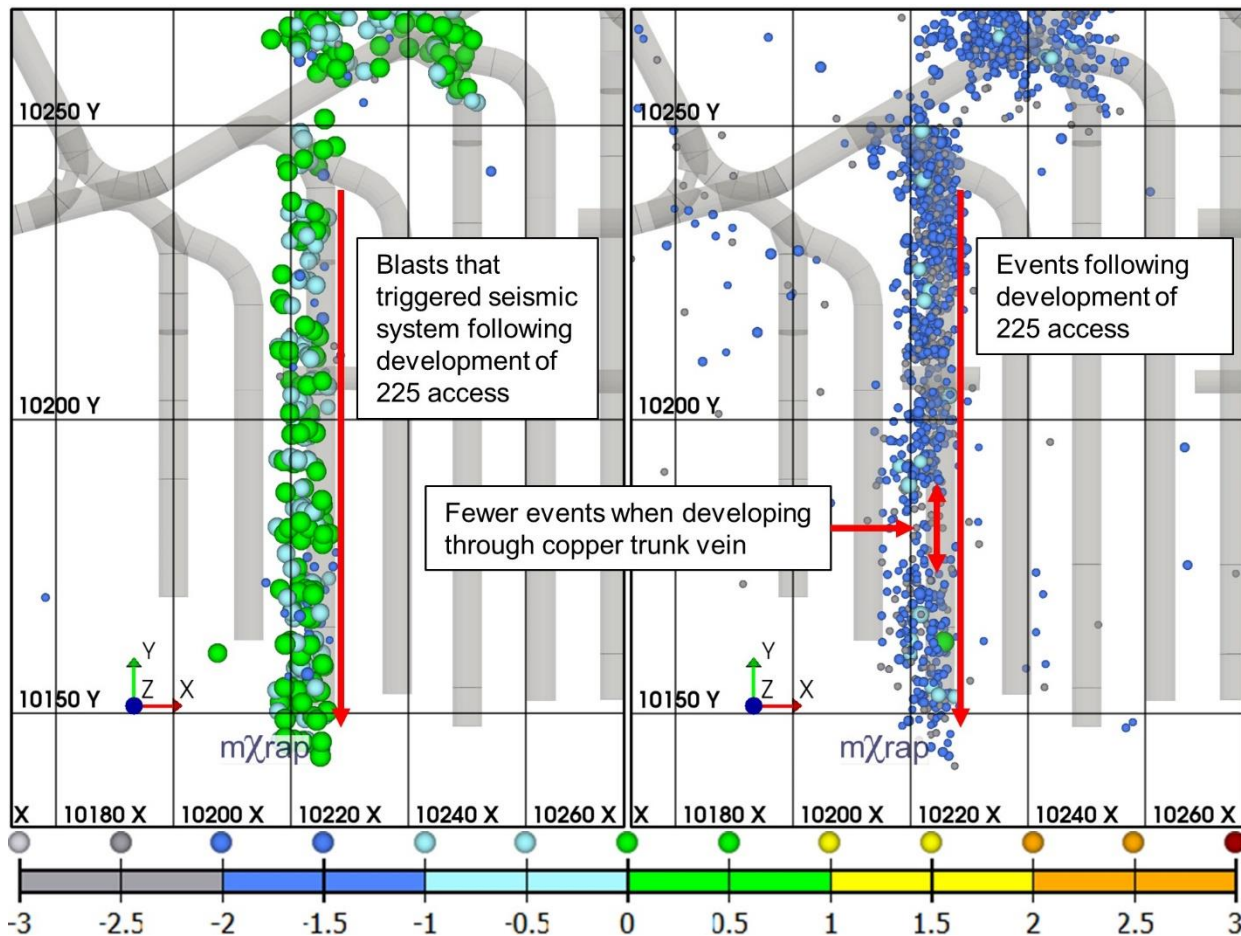


Figure 3-28: Plan view of blast (left) and event (right) locations (coloured and sized by magnitude) over 3 months of primary stope access and footwall development (1595-225 SA, June-August 2010)

### 3.5.2 Secondary/Tertiary Development into Stope Pillars

Development for secondary or tertiary stope accesses has a different seismic response than primary access development. Figure 3-29 shows one such case where a tertiary stope access is driven into a pillar created by the adjacent mined out primary and secondary stopes. As with primary accesses, blasts are detected along the length of the development. However, there are noticeably fewer events when developing through the pillar compared to when the access was entering and exiting it.

The reduction in located seismic events is not necessarily caused by a reduction in system sensitivity in the presence of more voids.  $M > -1$  events are still detected in the pillar, but there are fewer of them. The events in the pillar are also lower magnitude than those outside of it. Production blasts for secondary and tertiary stopes produce similar low levels of seismicity.

Also of note in Figure 3-29 is that the blast locations do not track along the development as closely as with the primary development example (Figure 3-28). The presence of voids in the rock mass contributes to seismic waves reflecting and scattering, making events more difficult to accurately locate. However, the locations are less than 10 m from the development and are “shifted” rather than scattered. These aspects of the event locations imply that the array is capable of consistently producing precise and reasonably accurate event locations despite the presence of a significant number of voids.

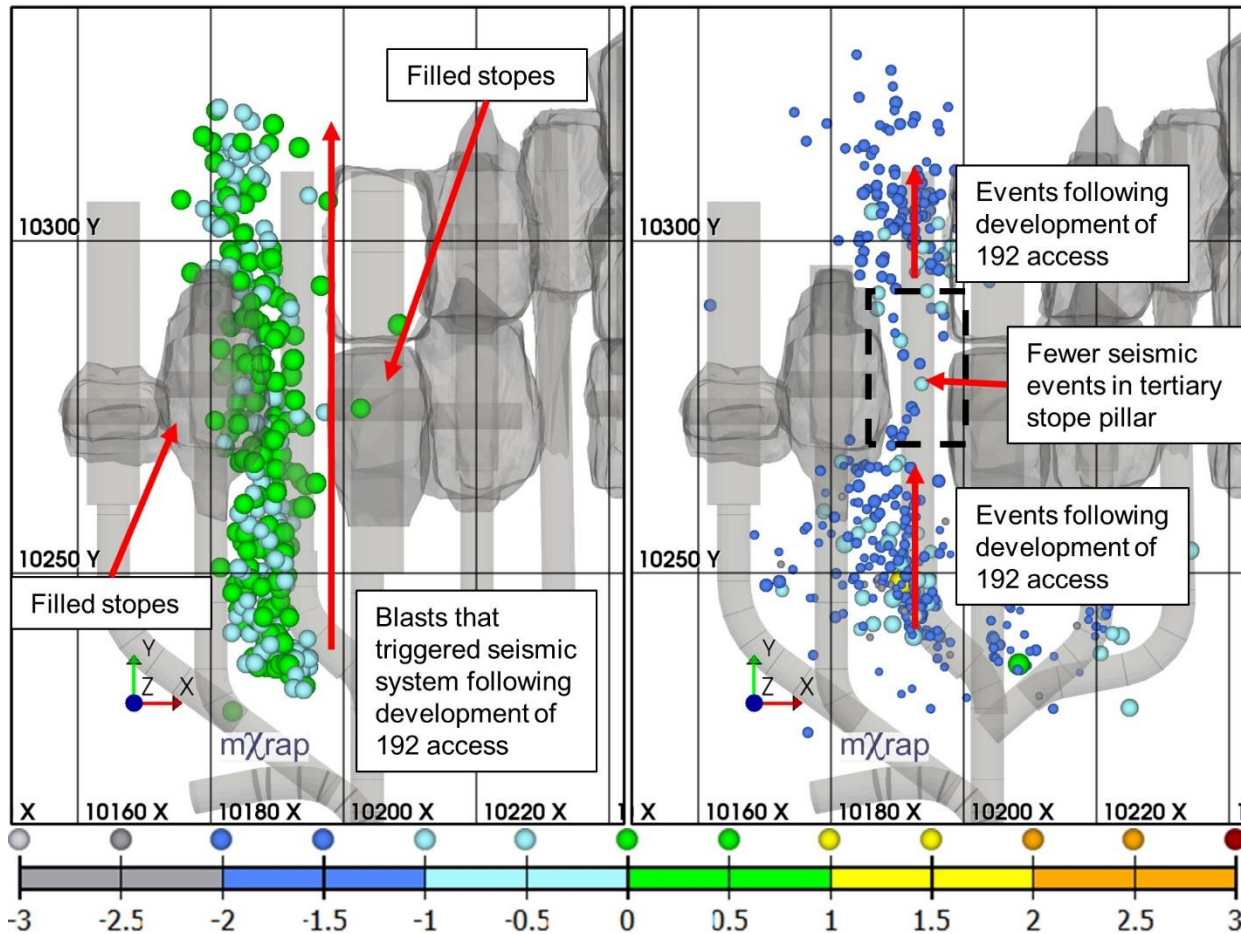


Figure 3-29: Plan view of blast (left) and event (right) locations (coloured and sized by magnitude) over 2 months of tertiary stope access development (1320-192 SA, March-April 2013)

The lack of seismicity in secondary and tertiary stope pillars is attributed to a combination of stress shadowing from the adjacent stopes and the fractured and relaxed ground around the mined out stopes. Stopes are large excavations that produce a large area of induced stresses and reduced confinement, resulting in a larger excavation damage zone than typical mine development. Recall that the geometry and sequence of the stopes are designed to promote yielding of the pillars. The lack of seismicity when developing accesses into the pillars is evidence that the rock mass has yielded and might be approaching an aseismic state at its residual strength.

Increased water inflow in the accesses is also evidence of a yielded rock mass. Figure 3-30 is a picture taken in part of a secondary stope access inside a pillar. The dark patches on the walls and back are caused by water flowing in from the surrounding rock mass. More fracturing and relaxation of the rock mass enables the inflow ground and mine process water. A similar effect was noted by Souley et al. (2001) in granites at the URL in Manitoba. Based on the presence of

water and the absence of seismicity, secondary and tertiary stope accesses likely lie within the excavation damage zone of the adjacent stopes, which lie approximately 4 m from the access walls. Water is not typically observed in primary development. The absence of water is attributed to fewer fractures in the rock mass, and stresses keeping natural fractures clamped shut.



*Figure 3-30: Water wetting shotcrete on the walls and back (dark patches) of a secondary stope access (Simser, 2016)*

### 3.5.3 Access Pillars

The geometry of transverse mining results in the creation of pillars between adjacent stope accesses. These pillars are typically 5.5 m tall (same height as the stope access) and 7.5 m wide (based on 5 m wide accesses and 12.5 m wide stopes). These pillars are subjected to induced stresses from the adjacent stope accesses as well as nearby stopes which cut off the horizontal major principal stress and cause it to flow through these pillars. As a result, these pillars are often seismically active when they are formed by developing an access or when a nearby stope is mined. Figure 3-31 shows several examples seismicity in access pillars. Seismic events locate in the pillars

adjacent to four stope accesses being developed. Events also locate in pillars without adjacent development mining. Seismically active pillars without adjacent development mining may be subjected to induced stresses from nearby stope blasts or the shedding of stress from a nearby stope pillar that is yielding. However, this type of access pillar seismicity is more difficult to associate with a specific recent and nearby stress change.

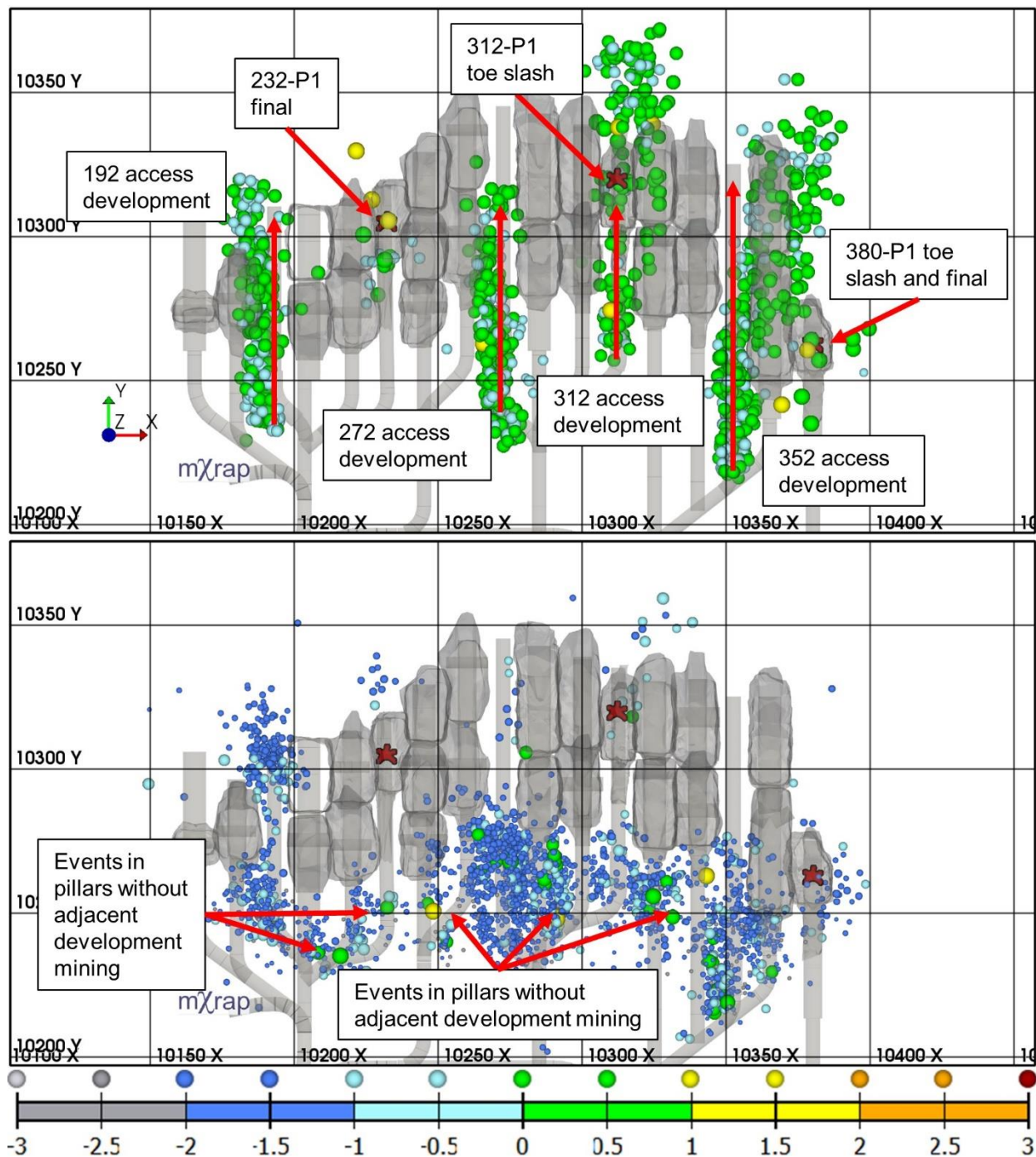


Figure 3-31: Plan view of blasts (top) and events (bottom) (coloured and sized by magnitude) over a 6-month period, stope blasts marked with red stars (1320 level, January-June 2013)

Figure 3-32 shows damage to the walls of a stope access that occurred during the same time period depicted in Figure 3-31. The access, 1320-300 SA, has access pillars on both sides. Development and stope mining occurred along the access that formed the pillar on the right wall (300-312 SA) in early 2013. Development and stope mining along the access that formed the pillar on the left

wall (285-300 SA) was completed in 2009. Seismicity in early 2013 resulted in damage to both pillars. This example demonstrates how a rock mass can be subjected to stress changes that result in seismicity and rock mass damage both recently and a longer time after adjacent mining has taken place.



*Figure 3-32: 1320-300 SA looking north with damage in left and right walls at end of June 2013 (Simser, 2013)*

#### 3.5.4 Toe Slash

The void produced by a toe slash is not typically surveyed, but the locations of the events are used to infer its shape (Jalbout and Simser, 2014). Events locate around the void produced by the toe slash. The locations of these events correspond with an area of stress-induced rock mass damage around the new excavation. The example in Figure 3-33 shows events locating in the top 20 m of the stope which implies the toe slash removed the bottom 10 m of the stope as intended. The events also do not extend far beyond the hanging wall and footwall limits of the stope. These locations are also expected as the hanging wall and footwall limits are usually achieved with the final blast. Events also occur in the walls of the toe slash and around the raisebore. A toe slash may also induce stresses around the upper stope access, resulting in additional seismic events.

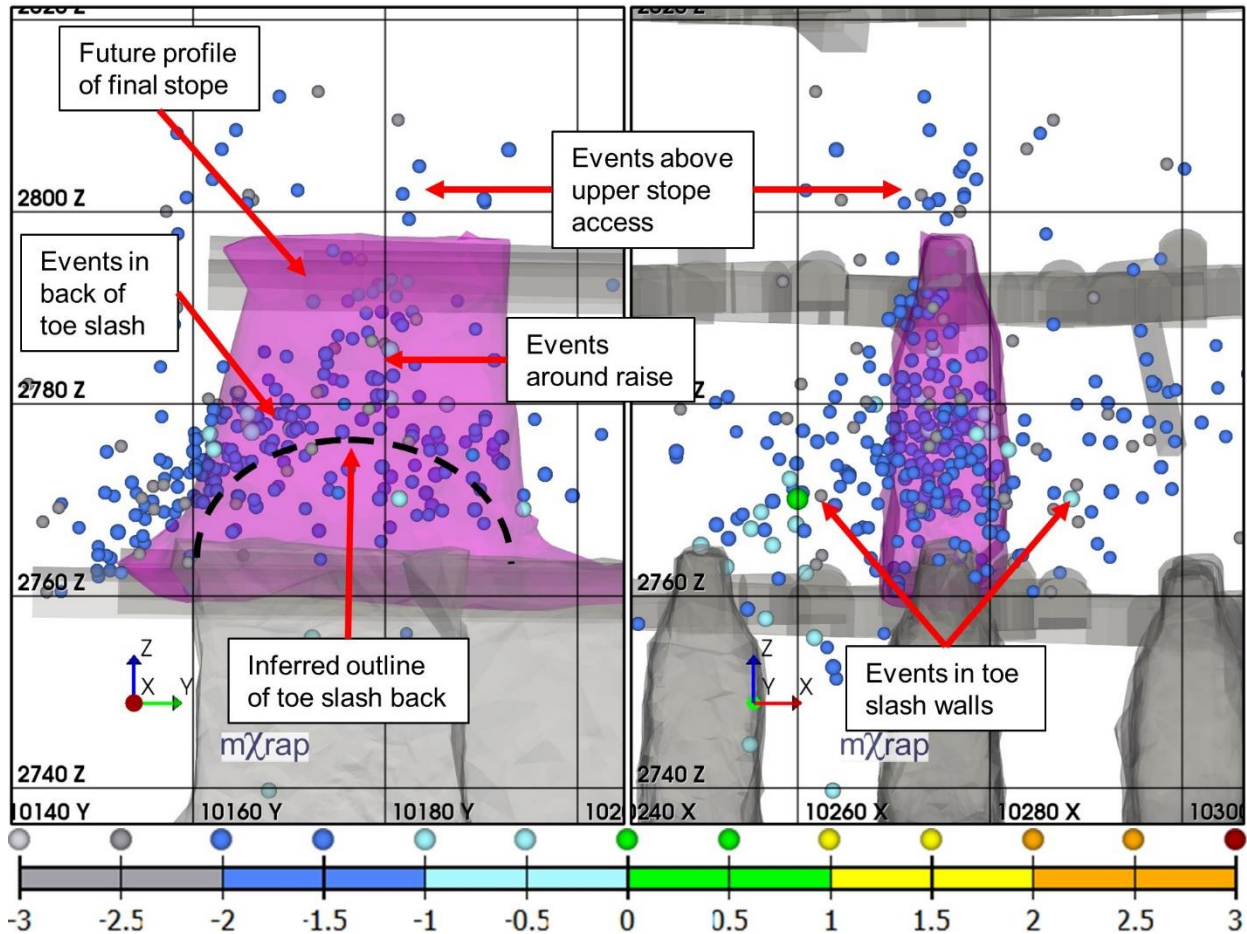


Figure 3-33: Section (left) and longitudinal (right) views of event locations (coloured and sized by magnitude) around a void created by a toe slash over a 24-hour period following the blast (1595-275-P1, October 7<sup>th</sup>, 2011), also showing the shape of the final stope (pink)

### 3.5.5 Stope Back

Events may locate in the back of a stope following the final blast. The final blast cuts off the horizontal major principal stress and forces some of it to flow over the top of the stope, resulting in seismicity in the back of the stope. An example of this behaviour is shown in Figure 3-34. This behaviour is similar to the effect of events locating above the void created by a toe slash. It is worth noting that the stope back has an existing excavation damage zone from the development of the upper stope access. Unlike the walls of the stope, the back is partially supported from the upper stope access. However, the support is designed for the 5 m span of the access and not the 12.5 m span of the stope.

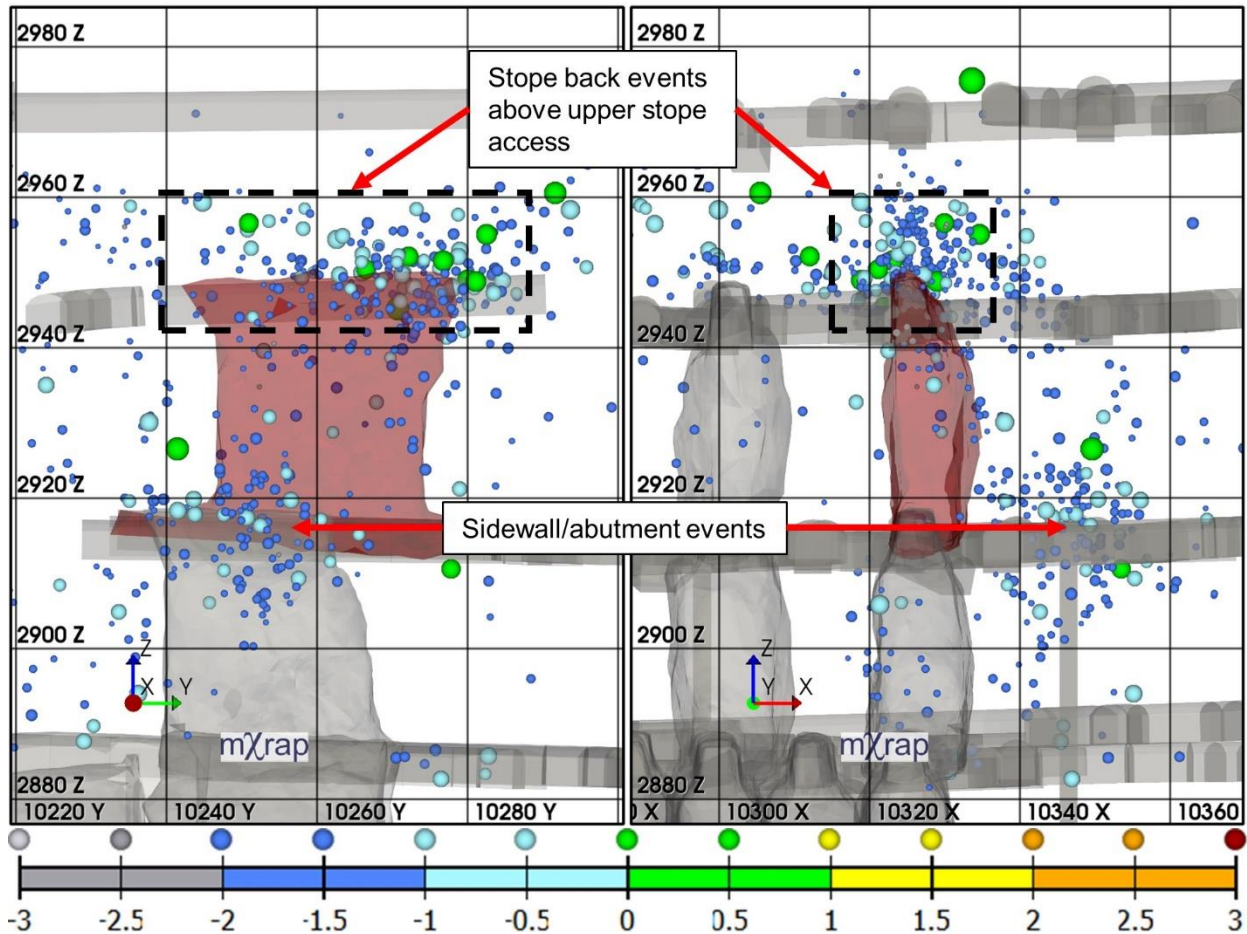


Figure 3-34: Section (left) and longitudinal (right) views of event locations (coloured and sized by magnitude) in the back of the blasted stope (red) over a 24-hour period following the final blast (1445-325-P1, February 8<sup>th</sup>, 2013)

### 3.5.6 Northwest-Southeast Stope Corners

Stresses also flow around stopes after the final blast. The events often locate in the northwest and southeast corners of the stope, as is shown in Figure 3-35. The locations of the events are attributed to the northeast-southwest orientation of the major principal stress, which is oblique to the strike of the orebody. As the stress flows around the stope, it concentrates in the northwest and southeast corners which is where the majority of seismic events are located following final blasts in primary stopes.

Recall that a similar effect was observed at Lac Shortt mine, where an east-west striking orebody was subjected to a northwest-southeast major principal stress. The mining geometry resulted in stress concentrations in the northeast and southwest corners of stopes, which was associated with increased rock mass damage and unplanned dilution in these areas (Ecobichon et al., 1992; McCreary et al., 1992). Examples from these studies have been presented in Chapter 2.4.

This distribution of seismicity following stope blasts justifies the “just-in-time” approach to developing stope accesses. Events in the northwest and southeast corners of the stope in Figure 3-35 locate near planned stope accesses to the east (287 SA) and west (262 SA). If these accesses were in place at the time of the stope blast, the surrounding rock mass would have been subjected to stress-induced damage. The more distant planned accesses (250 and 300 SA) may have been subjected to stresses shed out of the damaged regions near the recently blasted stope. The accesses’ exposure to seismicity, rock mass damage, and stress changes is minimized if development is delayed until after nearby primary mining is complete.

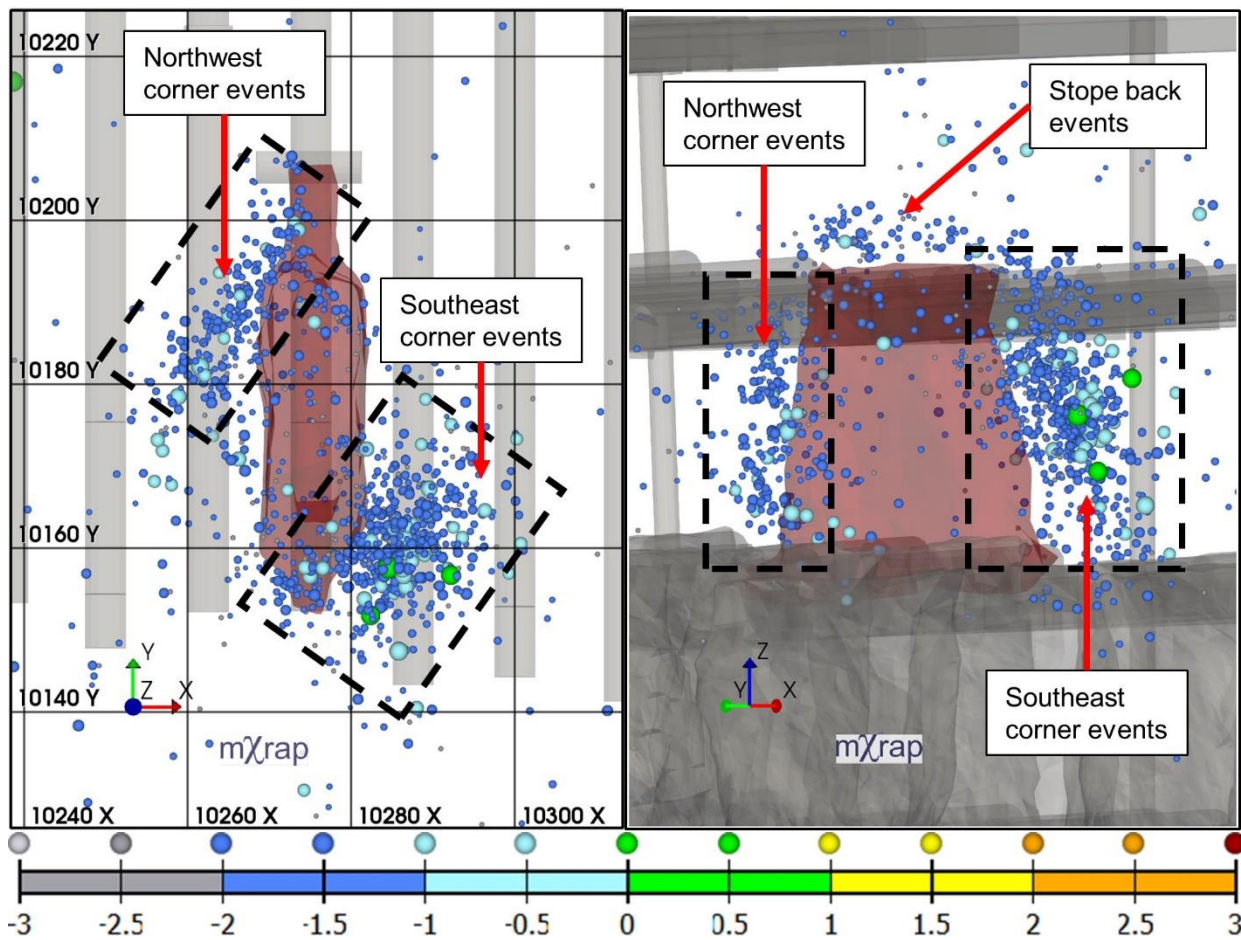


Figure 3-35: Plan (left) and oblique northeast (right) views of events (coloured and sized by magnitude) locating in northwest and southeast corners of the blasted stope (red) over a 24-hour period following the final blast (1595-275-P1, October 28<sup>th</sup>, 2011)

Seismicity is not always observed in both the northwest and southeast corners of the stope. The center-out sequence combined with the center of the orebody having the greatest thickness produces large stress shadows after the first line of panels is mined (along the 275 access in most parts of the mine). Subsequent stopes tend to generate significant amounts of seismicity when they

protrude from these shadows. As per the horseshoe shape of the orebody, said protrusions typically occur with P1 stopes in the eastern half of the mine, and panels which reach the footwall limit of the ore in the western half of the mine. Accordingly, seismicity in the southeast corners of stopes is common in the eastern half of the mine, and seismicity in the northwest corners of stopes is common in the western half of the mine.

### 3.5.7 Stope Sidewall

Events may also locate in the sidewall of a stope as is shown in Figure 3-36. Deviation from the typical northwest-southeast corner may be caused by rotation of the major principal stress around and over or under other mined stopes. Furthermore, the sidewalls of the stope are the largest face of the excavation and correspondingly have the lowest confinement. The lower confinement may contribute to rock mass yield in the sidewalls.

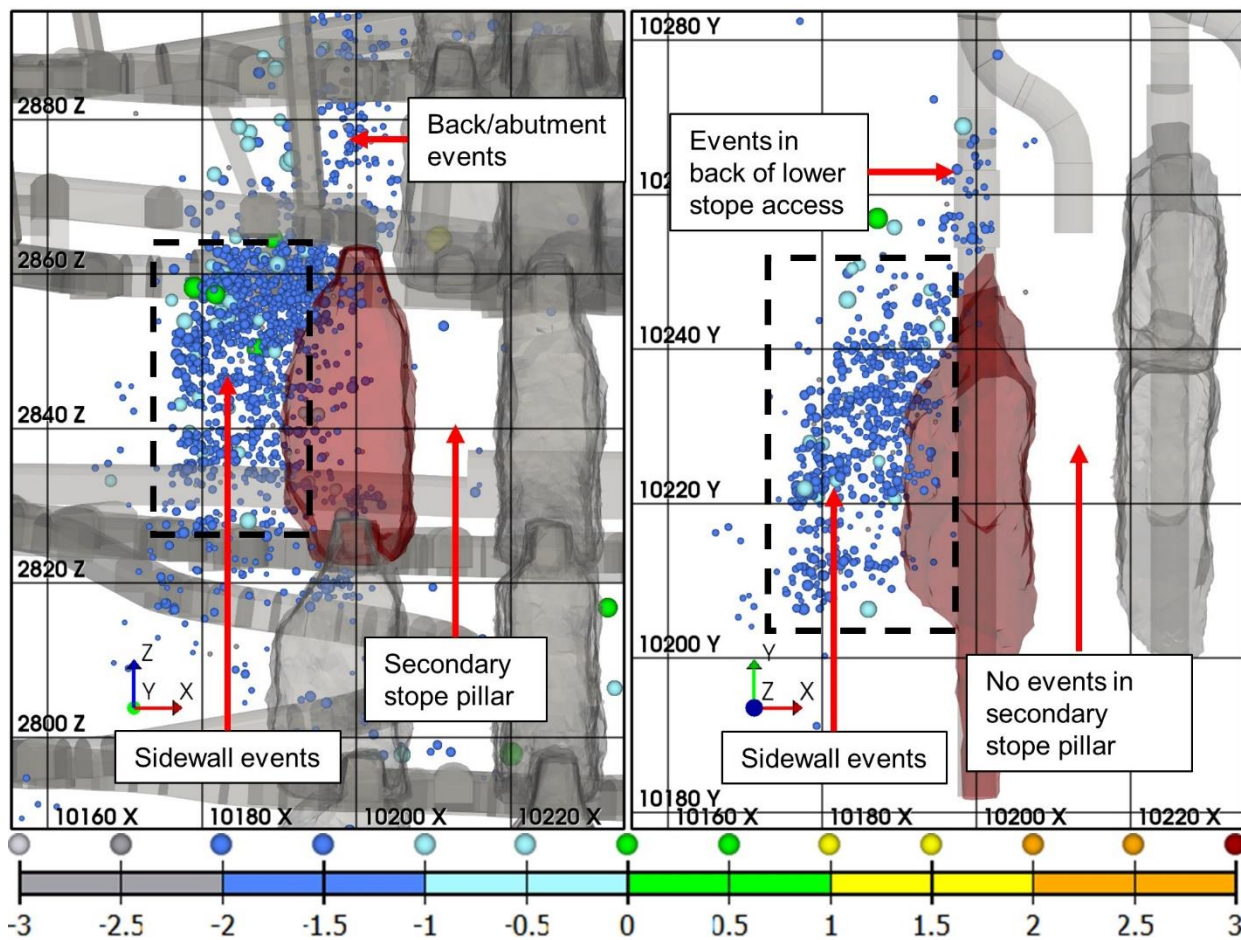


Figure 3-36: Longitudinal (left) and plan view (right) of event locations (coloured and sized by magnitude) in the sidewall of a blasted stope (red) over a 24-hour period following the final blast (1535-200-P1, October 8<sup>th</sup>, 2017)

### 3.5.8 Temporary Stope Pillars

Seismicity may be associated with the creation of temporary stope pillars in the primary-secondary or primary-secondary-tertiary sequence. Figure 3-37 depicts one such example where a temporary pillar is created by mining a primary stope. Events locate in part of the rock mass that will be extracted by a future stope. These pillars are designed such that their geometry promotes rock mass yield, and the occurrence of seismic events when the pillar is formed indicates that the design is effective. The occurrence of seismicity in temporary stope pillars is further justification of the just-in-time development strategy, as it eliminates the exposure of the secondary or tertiary stope access to stress changes and yielding in the pillar.

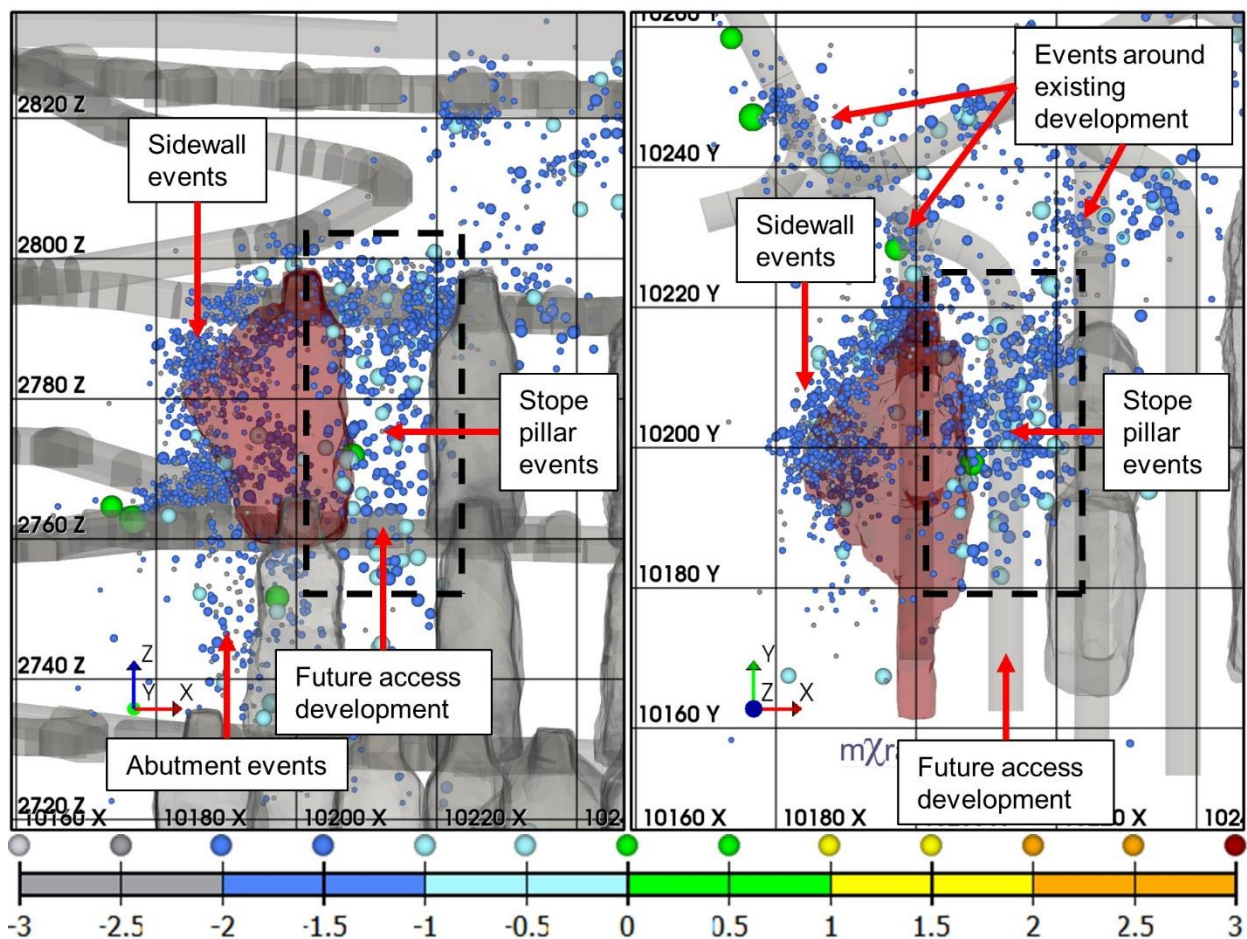


Figure 3-37: Longitudinal (left) and plan (right) views of event locations (coloured and sized by magnitude) in 24 hours following a final stope blast (red) showing events locating in secondary stope pillar (1595-200-P1, October 22<sup>nd</sup>, 2014)

The occurrence of seismicity when forming a pillar is contrasted by the seismic response (or lack thereof) when accesses are developed into the pillars. The lack of seismicity indicates that the pillars are significantly yielded and may be at their residual strength as discussed earlier in this

section. Despite the abundance of temporary stope pillars at NRSM, this type of pillar seismicity is not a major source of seismic activity for the mine. Many of these pillars exhibit little or no seismic activity when they are formed, such as the pillar formed in Figure 3-36. The first set of primary stopes may cause sufficient damage to the adjacent rock mass that it is incapable of generating events of a detectable size before the pillar is formed. The thick orebody and orientation of the major principal stress also results in significant stress shadows which may place the rock mass in a relatively low state of stress before the pillar is formed.

Temporary stope pillar seismicity is more common in thin sections of the orebody where the pillar geometry is less slender and does not promote yielding. The thin sections of the orebody are also farther away from the trunk vein and lower grade (semi-massive or disseminated sulphides), which corresponds with greater rock mass strength and greater potential for seismic activity. Seismicity in temporary stope pillars is also more common in sequences that initially create broader pillars (such as the 1-5-9 or 1-4-7 sequences) whose geometry does not promote yielding and are more difficult to stress shadow.

### 3.5.9 Up/Down abutment

Stope blasts can also induce events on abutments above or below their level. Figure 3-38 shows an example of a final blast that was followed by events in the stope's sidewall as well as in the abutments on the levels above and below. Unlike previous examples of seismic responses following stope blasts, events in abutment are not occurring in an area adjacent to an open stope where confinement was reduced by a recent blast. These events are a result of increased stresses on a confined rock mass or geologic structure. They occur near a pre-existing EDZ, where the rock mass is confined by backfill in the mined-out stopes and any aseismic regions of the rock mass that may be adjacent to them. This type of response is more common in stopes closer to the east and west strike limits of the orebody, especially when a stope is taken in a pillarless sequence on an abutment.

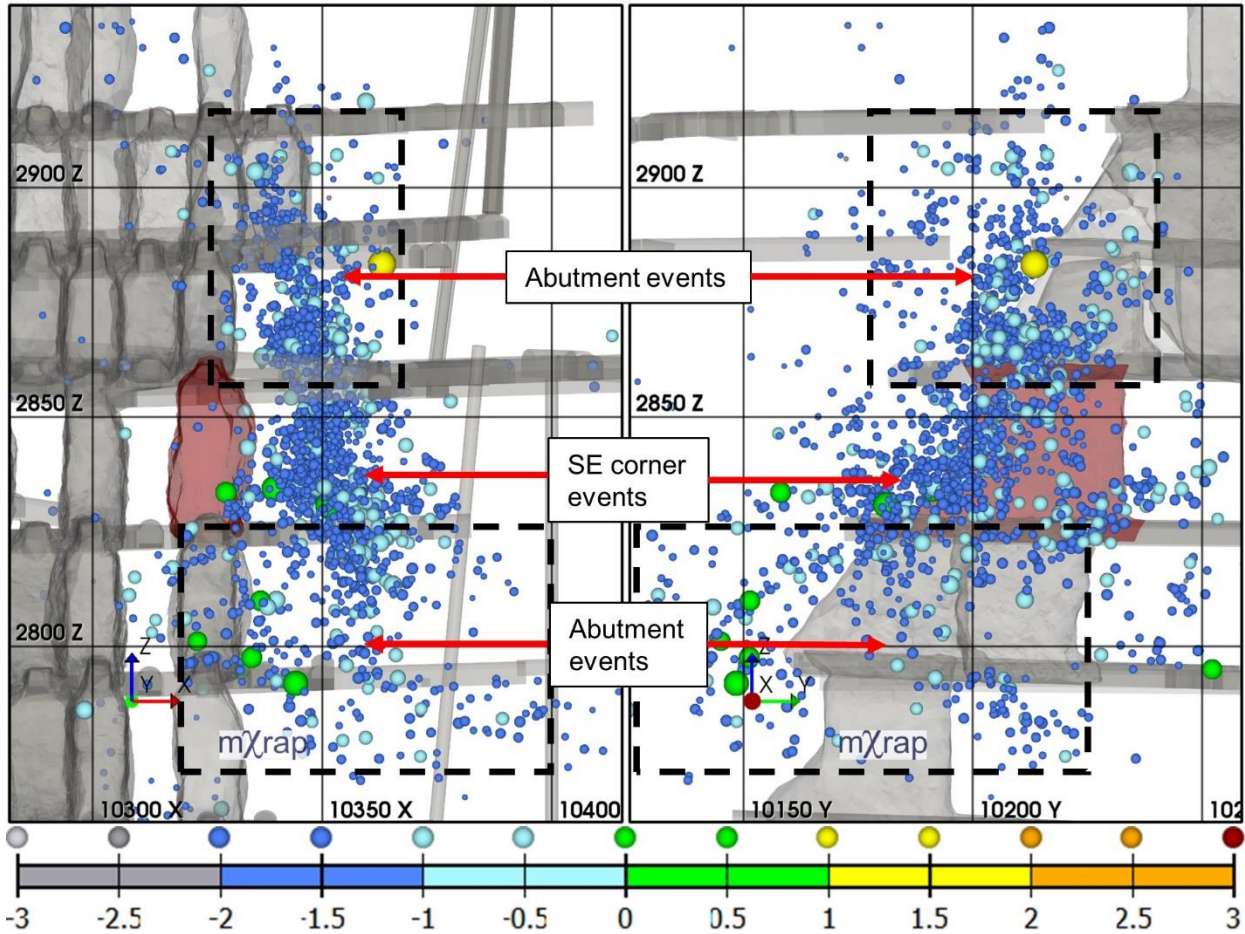


Figure 3-38: Longitudinal (left) and section (right) views of event locations (coloured and sized by magnitude) over a 24-hour period following a final blast where events located above and below the level of the blasted stope (red) (1535-325-P1, August 21<sup>st</sup>, 2016)

### 3.5.10 Abutment Cross-Talk

Stope blasts are also known to induce events in the opposite abutment of the orebody. Figure 3-39 shows an example where the final blast in 1535-275-P2 was immediately followed by events in its northwest corner as well as events in the southeast corner of 1535-275-P1, a stope that had been mined and filled three months prior. Similar to the up/down abutment events, events occurring as a cross-talk response are not associated with a loss confinement resulting from a stope blast. These responses also tend to follow the northwest-southeast corner pattern but on a larger scale (the entire orebody rather than an individual stope). The cross-talk effect is also observed over greater distances such as events occurring next to stopes on the 250 line after a blast on the 300 line.

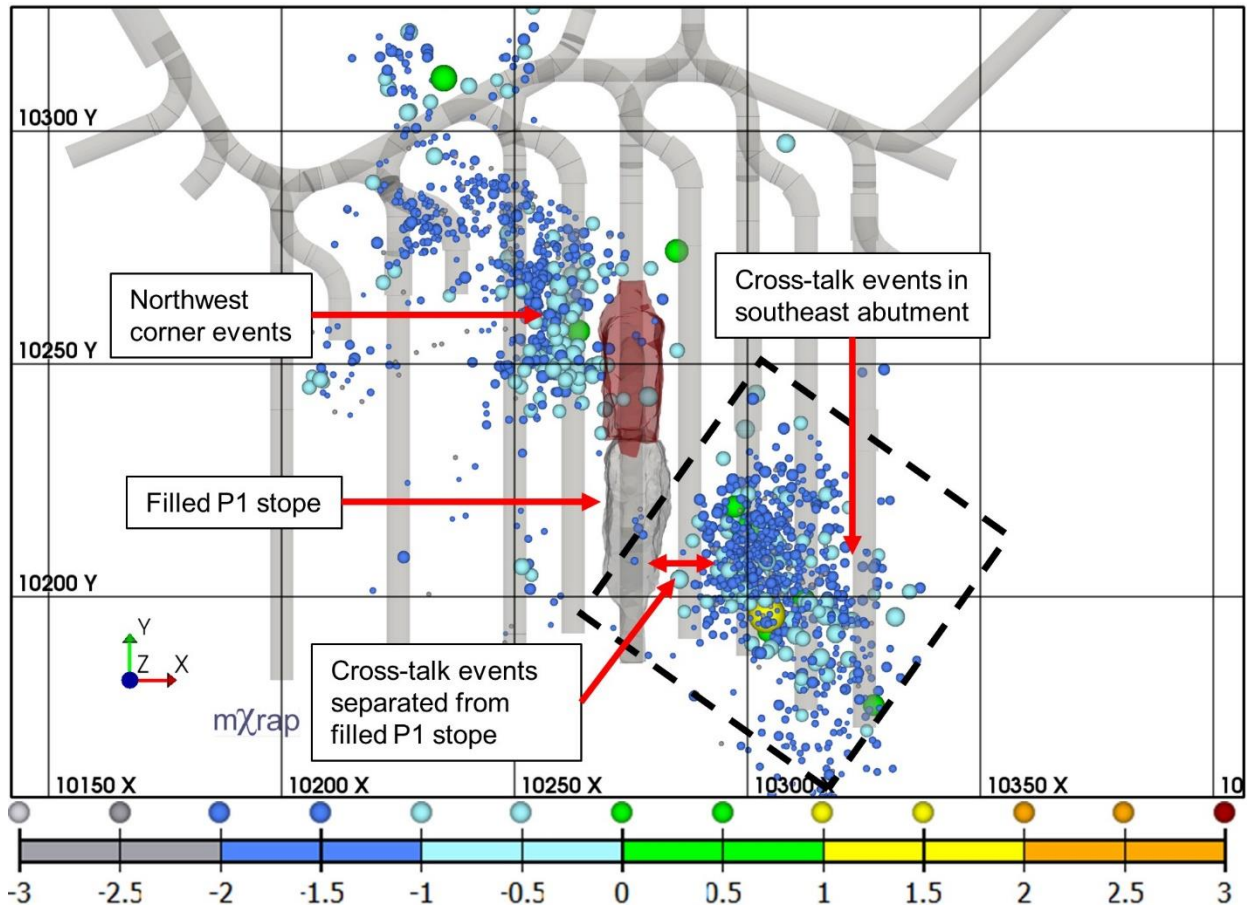


Figure 3-39: Plan view of events (coloured and sized by magnitude) locating in the northwest corner of the blasted stope (red) and on east abutment southeast of a previously mined stope over a 24-hour period following the final blast (1535-275-P2, September 15<sup>th</sup>, 2013)

Also of note in Figure 3-39 is that the cross talk events do not occur immediately adjacent to the mined out P1 stope. The separation between abutment events and previously mined out stopes can also be see in Figure 3-38. As mentioned previously, abutment events are occurring near an existing EDZ which may include part of the rock mass which is at its residual strength and aseismic. The abutment events occur further away from the extracted stopes, indicating that the EDZ is growing. Unlike caving mines where seismogenic zones migrate continuously with the progression of the cave, open stoping operations are stable by design and stress changes (and corresponding growth of EDZs) occur more incrementally.

Figure 3-40 illustrates how events migrate away from a stope with successive induced stress changes. The data in this example covers the time period between the extraction of 1535-275-P1 and P2. A stope adjacent to the analysis area one level below, 1565-300-P1 was also extracted during this time period. When the first stope was extracted in the sequence (1535-275-P1), the

events occurred immediately against its southeast corner (blue events). These events are associated with the formation of an EDZ adjacent to 1535-275-P1. With the next two stopes in the sequence (1565-300-P1 followed by 1535-275-P2), the events in the southeast abutment occur farther away from the southeast corner of 1535-275-P1 (green and red events). These events occurred under higher confinement conditions than the events that occurred with blasts in 1535-275-P1 and are associated with the growth of the EDZ with successive stress changes. It should be noted that some of the events following blasts in 1565-300-P1 occurred near the back of that stope and may be associated with some level of confinement loss (albeit significantly less than the confinement loss in the corner or sidewall of a stope).

This behaviour is not observed with every stope blast, nor does it only occur with successive stope blasts. Additional induced stress changes and migrating seismogenic zones might also be associated with development mining in abutments, a time-dependent failure processes, or caving around open stopes.

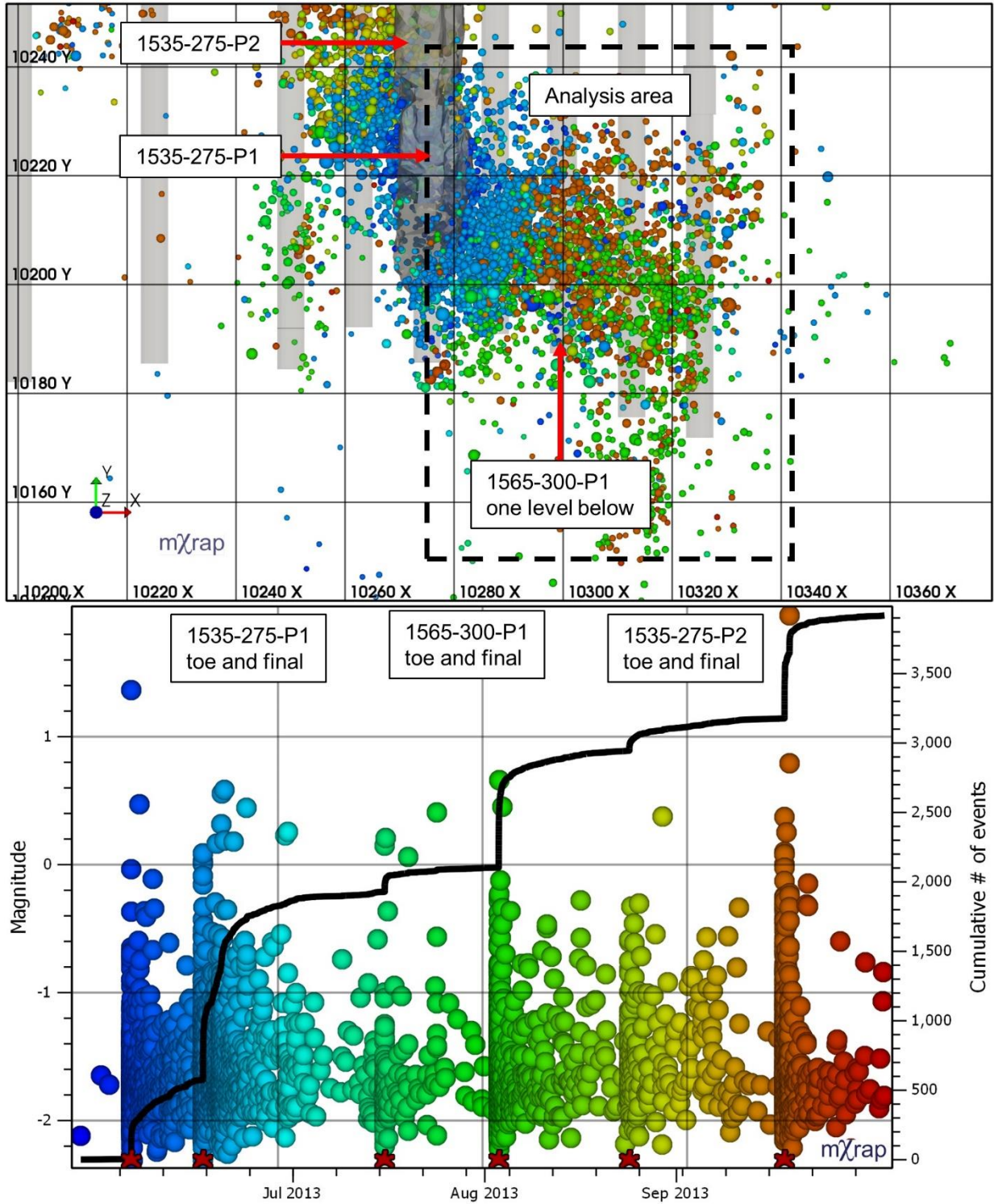


Figure 3-40: Plan view of event locations (top) and magnitude-time history of events (coloured by date and sized by magnitude) in southeast abutment of 1535-275-P1 (June-September 2013)

### 3.5.11 Structure Daylighting

Multiple faults intersect the NRSM orebodies at a variety of orientations. Elevated levels of seismicity are often observed when stopes are mined near major structures. Structure-driven seismic responses are also observed when a stope is mined adjacent to or through a fault, referred to as daylighting the structure. Daylighting a structure removes normal stress and allows it to slip. This type of response is observed with stopes throughout the sequence, including secondary or tertiary stopes which generate little to no seismic activity when not in the presence of a larger scale geologic structure.

An example of a structural response is shown in Figure 3-41. The final blast in 1220-312-P1 daylighted the LA2 fault which immediately generated a large seismic response. 1220-312-P1 is a tertiary stope, which is typically expected to generate little seismicity due to the yielding pillar geometry. The event locations follow the planar trend of the mapped structure rather than the typical flow of stress over and around excavations. The planar trend of the event locations and their distance from mined out stopes imply that they are not necessarily associated with stress-driven yield and the formation or growth of an EDZ. Most of the events are also far from 1220-312-P1. Therefore, their mechanisms may not be associated with a loss of confinement created by that stope.

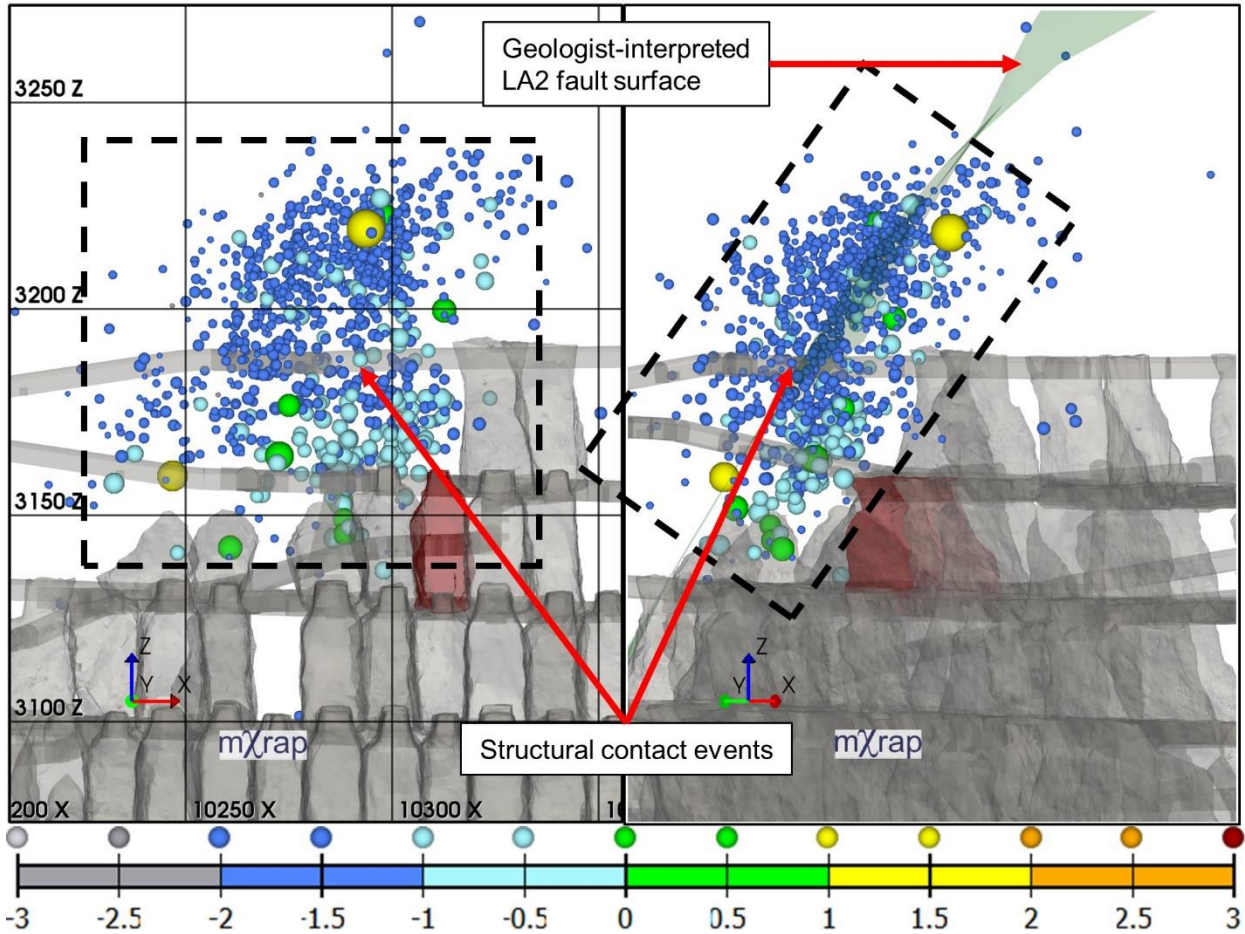


Figure 3-41: Longitudinal (left) and oblique northeast view along structure (right) of events (coloured and sized by magnitude) locating along LA2 fault in 24 hours following a final blast (red) (1220-312-P1, June 24<sup>th</sup>, 2016)

Despite the abundance of geologic structures at NRSM, this type of clearly structure-driven response is relatively rare in comparison to the large number of responses associated with induced stresses and loss of confinement around voids. Suspected fault slip seismicity that occurs in the absence of nearby mining usually occurs with small numbers of events. Structure-influenced seismic responses at NRSM are often associated with stress channeling between faults and excavations rather than a fault slipping and events plotting along a planar surface.

## 4 Methodology

This thesis focuses on investigating short-term space-time variations in apparent stress ( $\sigma_a$ ) following final blasts in open stopes. Analysis of the parameter in space and time can be used to infer how an excavation damage zone forms. Apparent stress is used as an indicator of local stress levels, and event locations indicate a regions of active rock mass yield. Within these regions, sometimes referred to as seismogenic zones (after Duplancic, 2001), the variations in apparent stress can reveal how local stress levels may increase following a blast and decrease in regions where the rock mass has yielded or failed. These three source parameters (location, time, and apparent stress) will be used to develop a method for interpreting rock mass yield near excavations following blasts. This method will then be used to characterize the response of the rock mass at Nickel Rim South following final stope blasts.

The methodology for analysing space-time trends in apparent stress will take a spatially-constrained approach to analysing data. Seismic responses following each blast were spatially separated into different groups as per the types of responses to stope blasts presented in Section 3.5. Spatially filtered volumes are used in order to interpret variations under a consistent set of local conditions that drive rock mass yield and seismicity. Volumetric filtering is often achieved with three-dimensional polygons (van Aswegen, 2005; Wesseloo et al., 2014), and in a somewhat subjective manner intends to delineate and isolate areas of interest in a rock mass for analysis (Mendecki et al., 1999). This approach will produce results that show variations within a seismogenic zone, rather than between different seismogenic zones.

The objective of this work is to isolate and study the short-term effects of a single stope blast on the rock mass. With regard to the time periods for analysis, “short-term” can have a variety of interpretations depending on the behaviour being analysed and the physical processes that control it. Within the context of mining-induced seismicity, van Aswegen (2005) defines the short term as hours and days, and medium term as months. Based on van Aswegen’s definition, any variations occurring up to a month after a blast may be considered “short-term”. Alternatively, this thesis considers the short term as the period between local induced stress changes. The goal of the analysis is to interpret the effects of a single, isolated blast on the nearby rock mass. The rock mass behaviour resulting from one induced stress change may be tracked until another induced stress change “interrupts” the behaviour that resulted from the previous induced stress change.

This interpretation of what constitutes the short term emphasises this thesis's focus on final blasts. There is a longer period between final blasts and subsequent nearby blast-induced stress changes than other mining activities (e.g. development blasts which occur every 1-2 days, or toe slashes which are followed by a final blast in 1-2 weeks). Therefore, the rock mass behaviour resulting from the final blast can be tracked for a longer period before being interrupted by another local induced stress change.

Any other induced stress changes that may influence the volume following the final blast are not considered in this thesis. This simplification is considered reasonable because of the sequencing restrictions at NRSM (i.e. just-in-time development, filling nearby stopes before blasting another one). These restrictions generally result in a period of several weeks to months between the final blast in a stope and blasting in adjacent stopes on the same level or the level above or below it. The prolonged spatial separation between a final blast and other blast-induced stress changes supports interpreting its resulting seismic response(s) in the isolated context of that single blast for a period of weeks or even months.

Another reason why case studies were limited to final blasts was so that event locations could be compared to a surveyed excavation shape. Only blasts in 2011 and later were considered, so as to utilize the higher data quality produced by the microseismic array expansions in 2010. Only cases with the greatest quantity of available data were analysed. The reason for this focus was that sufficient data is required to interpret any trends that might be present, and cases with more data might have more potentially useful information to extract. Furthermore, cases are considered from a wider area of the mine, making the results representative of a broader mine-wide behaviour rather than the behaviour of a single level with more uniform characteristics.

The methodology for tracking variations over space and time will affect how the trends can be assessed qualitatively, and what quantitative information can be drawn from them. Scatterplots (e.g. apparent stress versus time or location versus time) show a great deal of information in the form of individual data points, but do not enable objective assessments of shifts or changes in a population. Similarly, spatial plots of events may not reveal subtle differences in highly scattered or erratic data. Variations throughout a seismogenic zone may be subtle and difficult to visualize through hundreds of events. Furthermore, it is difficult to create appropriate "snapshots" of seismicity over short time intervals that illustrate changes from one state to the next. For example,

two snapshots are meant to illustrate the change from A to B, but the time periods A and B occur over are unknown. Snapshots that are too short may show multiple views of period A when no significant variation is occurring. Conversely, snapshots that are too long might blend A and B together and hide the variation. Therefore, snapshots should only be used with knowledge of the time periods over which changes occur.

Due to the aforementioned difficulties with various scatterplot techniques, the proposed methodology will use a trend smoothing approach to demonstrate how distributions shift or skew over time. Trend smoothing with a moving window of data allows time periods of increases or decreases to be easily identified, quantified, and compared between different cases. Similar approaches have been used by other authors (Coulson, 2009; Mendecki, 1993; Urbancic et al., 1992b) to track variations in seismic source parameters over time. This thesis will make justified modifications to past methodologies based on the author's understanding of the data and interest in certain behaviours.

#### 4.1 Variations in Apparent Stress

Temporal variations in apparent stress can be used to infer when stress is increasing or decreasing. The variations also provide a relative magnitude of stress increase or decrease. These inferences help interpret the stress change produced by a blast, rock mass yield, and redistribution of stress outside an excavation damage zone.

The methodology for analysing variations in apparent stress will be approached through the analysis of case histories. The primary case history used in this section is the southeast corner of 1535-275-P1. The stope and volumetric filter used is shown in Figure 4-1 and Figure 4-2. This stope was blasted in mid-2013 and was the first stope to break the lower sill pillar. The majority of events in the 24 hours following this blast locate in the northwest and southeast corners of the stope. Events are also located in the eastern abutments above and below 1535, in the sill below the 1480 stopes, and in the footwall to the west of the stopes. The multiple spatially distinct sources of seismic activity following this blast demonstrate the need to analyse a spatially filtered population of events. This spatially filtered population presumably occurs under a more consistent set of local rock mass conditions.

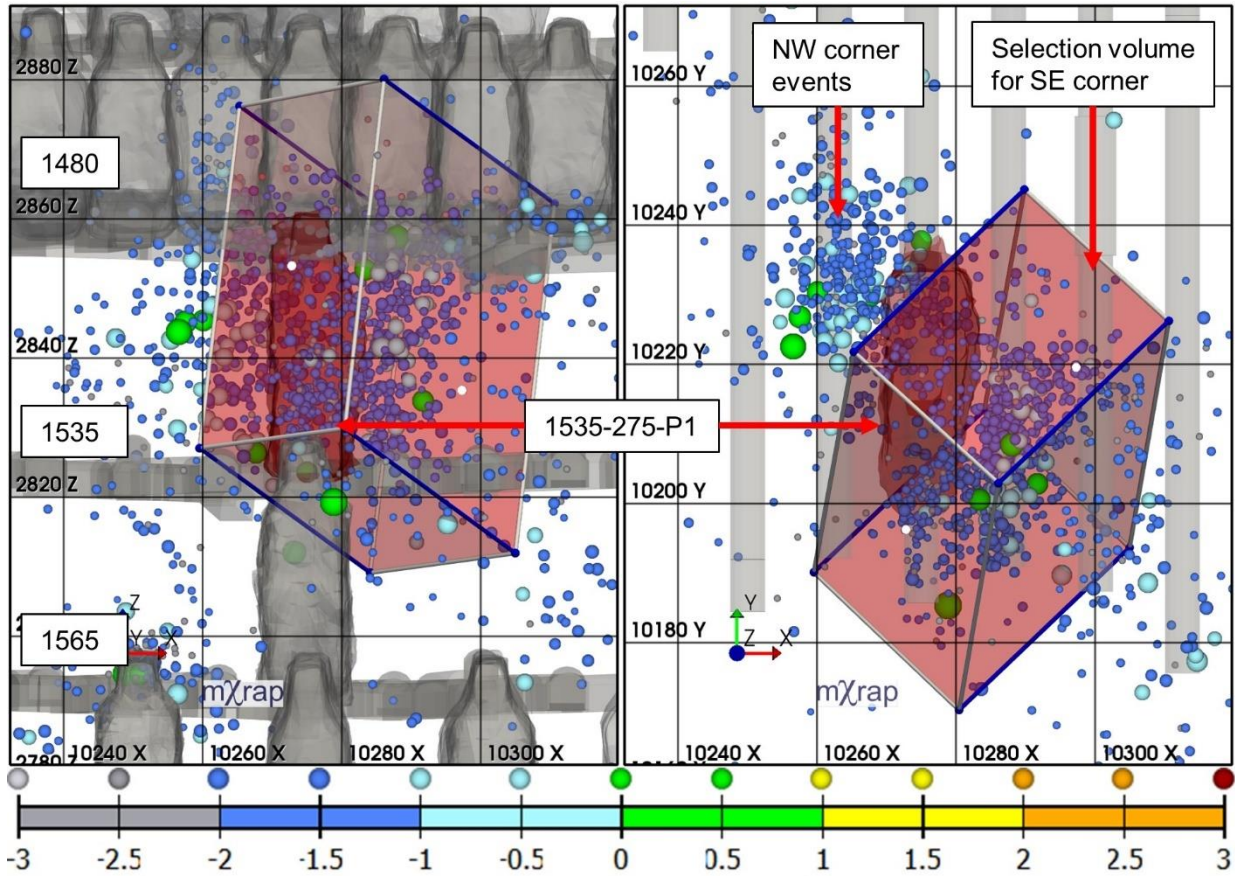


Figure 4-1: Events in 24 hours following 1535-275-P1 final blast (June 19<sup>th</sup>, 2013) showing SE corner selection volume in longitudinal (left) and plan (right) views

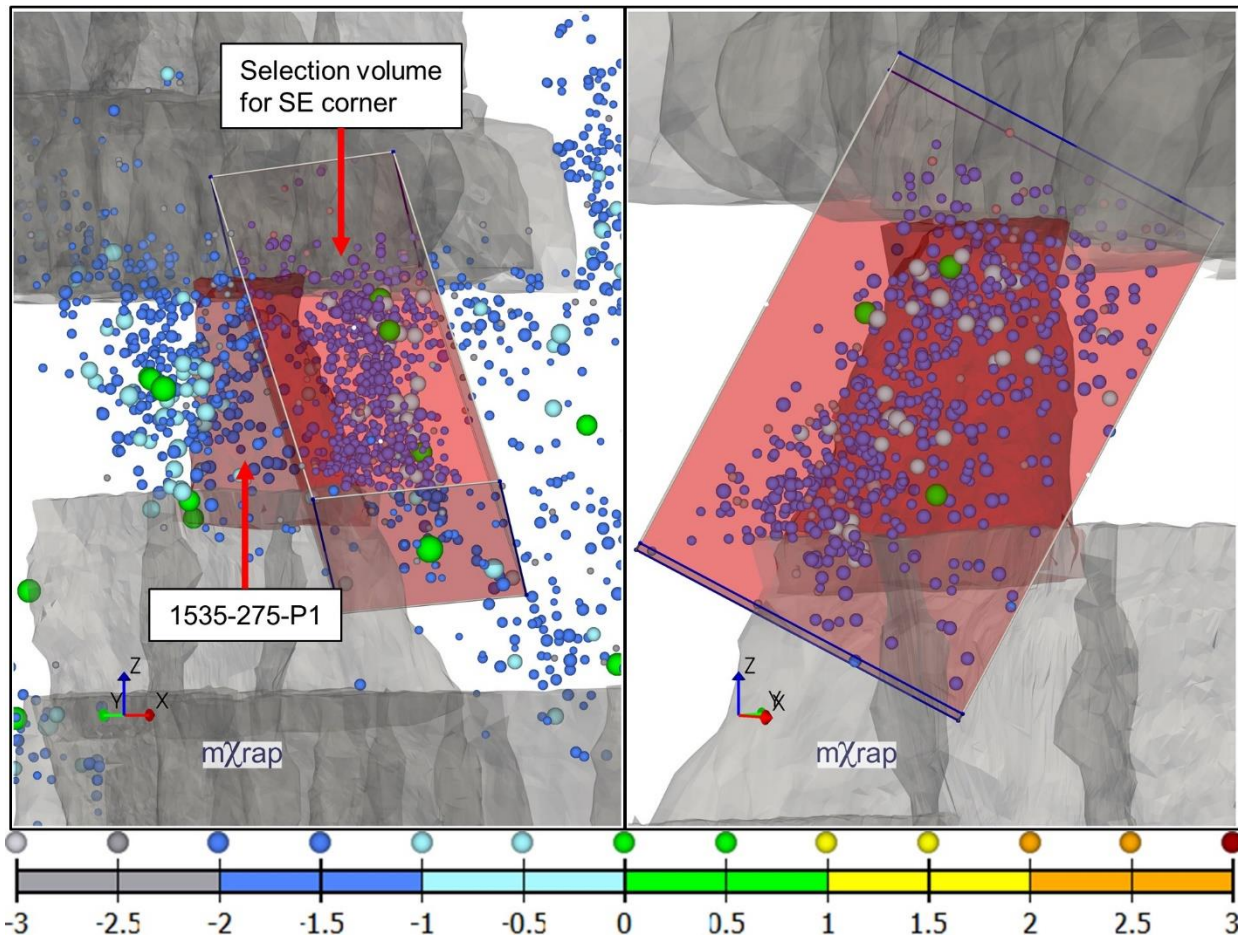


Figure 4-2: Events in 24 hours following 1535-275-P1 final blast (June 19<sup>th</sup>, 2013) showing SE corner selection volume looking NE (left) and NW (right) showing only events in volume

A magnitude-time history of events in the volume is shown in Figure 4-3. Approximately 500 events occur in the volume following the toe slash on June 8<sup>th</sup> (11 days prior). These events are used to form a base line for the conditions in the volume before the final blast. Any change in apparent stress produced by the blast will be immediately reflected by the subsequent events. In the magnitude-time history, some other characteristics of the seismic response to the two blasts can be observed:

- Nearly half the events occur within a matter of hours after the blast
- The largest event, a  $M = 1.3$ , occurs within 6 minutes of the toe slash
- The rate of  $M > -1$  events is highest immediately after the blasts, and decreases over several days
- There is a dramatic increase in the rate of small ( $M < -2$ ) events in the few hours after the blast

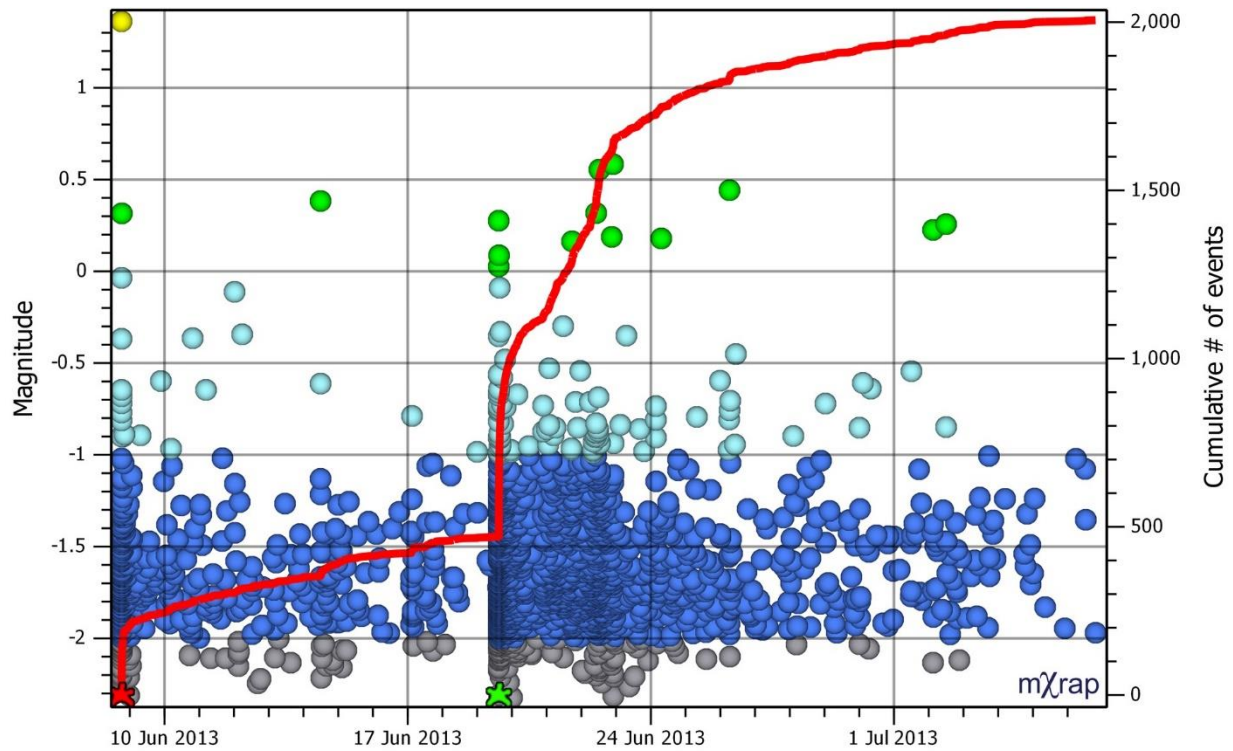


Figure 4-3: Magnitude-time history of events in 1535-275-P1 SE corner volume before and after the final blast

#### 4.1.1 Methods of Tracking Variations and Moving Windows

There are different approaches to tracking variations in apparent stress over time, some of which are listed in Table 4-1. While these methods were effectively implemented in other published works and have advantages in their respective applications, the author chose not to apply any of them. Rather, an alternate method is proposed that attempts to mitigate some of the disadvantages listed alongside the methods in Table 4-1. The proposed methodology attempts to account for a population whose distribution may simultaneously shift and skew. The variations in such a population may not be effectively represented by a single measure of central tendency.

Table 4-1: Previously published methods for interpreting variations in apparent stress

Method	Applied By	Disadvantages
ASTH	Hudyma (2008) Young (2012)	Does not distinguish between higher distribution of apparent stress and higher frequency of events
ASR	Brown (2015) Brown and Hudyma (2017b)	Can be affected by population variance rather than an actual shift in the data
Moving average	Coulson (2009) Urbancic et al. (1992b)	Central tendency of population can be skewed by non-normally-distributed data
Statistical comparison of discrete groups	Simser and Falmagne (2004)	Can not compare appropriate time periods when the rate at which changes occur is unknown, assumes Gaussian distribution

The proposed method uses a moving median as a measure of central tendency. The median is less skewed by non-normally-distributed data than the average and does not require the definition of bins which are required to determine a mode. A key variable in the analysis is the size of the moving window. There are no specific guidelines for defining the size of a moving window. The size of the window depends on the intent of the analysis being performed. The general approach is to smooth out variations that occur over a period shorter than the analysis is concerned with or are believed to be insignificant noise. Figure 4-4 shows the median apparent stress in 1535-275-P1 SE corner following the final blast using four different window sizes. In this example, approximately 400 events occurred in the volume in the first 3 hours after the blast. The windows are defined based on a fixed number of events. This approach gives a consistent sample size despite changing event rates and does not make any assumptions about the time periods over which changes may occur (e.g. using a 1-hour window would smooth out changes that occur over minutes). The different window sizes produce different behaviours in the trend lines such as:

- Different initial starting points of apparent stress (level at 0 hours after blast). The starting point will change depending on the events included before the blast. Shorter windows offer limited sample sizes but include a more recent set of events, which may be more relevant to current rock mass conditions. Longer windows may provide larger sample sizes but reach farther back in time, which may be less relevant to current rock mass conditions.
- The amplitude of variations. Longer windows smooth out the peaks and valleys in the trendline. For example, the initial increase does not reach as high with the longer window because more prior events with lower apparent stress are included, keeping the median

lower. The subsequent decrease does not drop as much because the initial events with higher apparent stress are still in the window, keeping the median higher.

- The slope of the line. Shorter windows allow variations to happen faster, resulting in steeper slopes. For example, with a 50-event window there is a rapid drop within 10 minutes of the blast. With the 200-event window, the drop appears to occur more gradually over about 30 minutes.
- The presence and timing of peaks and valleys. With a 50 or 100-event window, the apparent stress appears to be increasing starting around 1 hour after the blast. The 400-event window shows apparent stress is still decreasing 3 hours after the blast, because the events entering the window still have lower apparent stress than the events leaving it.

To reiterate, the interpretation drawn from any trend line depends on how the data was smoothed. What constitutes a significant variation depends on the intent of the analysis, which may be subjective, and change based on what variations are observed. In this case, it appears that a 200-event window would be suitable for interpreting short-term variations in apparent stress. This window size limits the more erratic variations that occur over minutes, gives higher confidence as to when apparent stress is increasing or decreasing, and will be helpful in the next steps of the proposed methodology which rely on smaller proportions of events in this window.

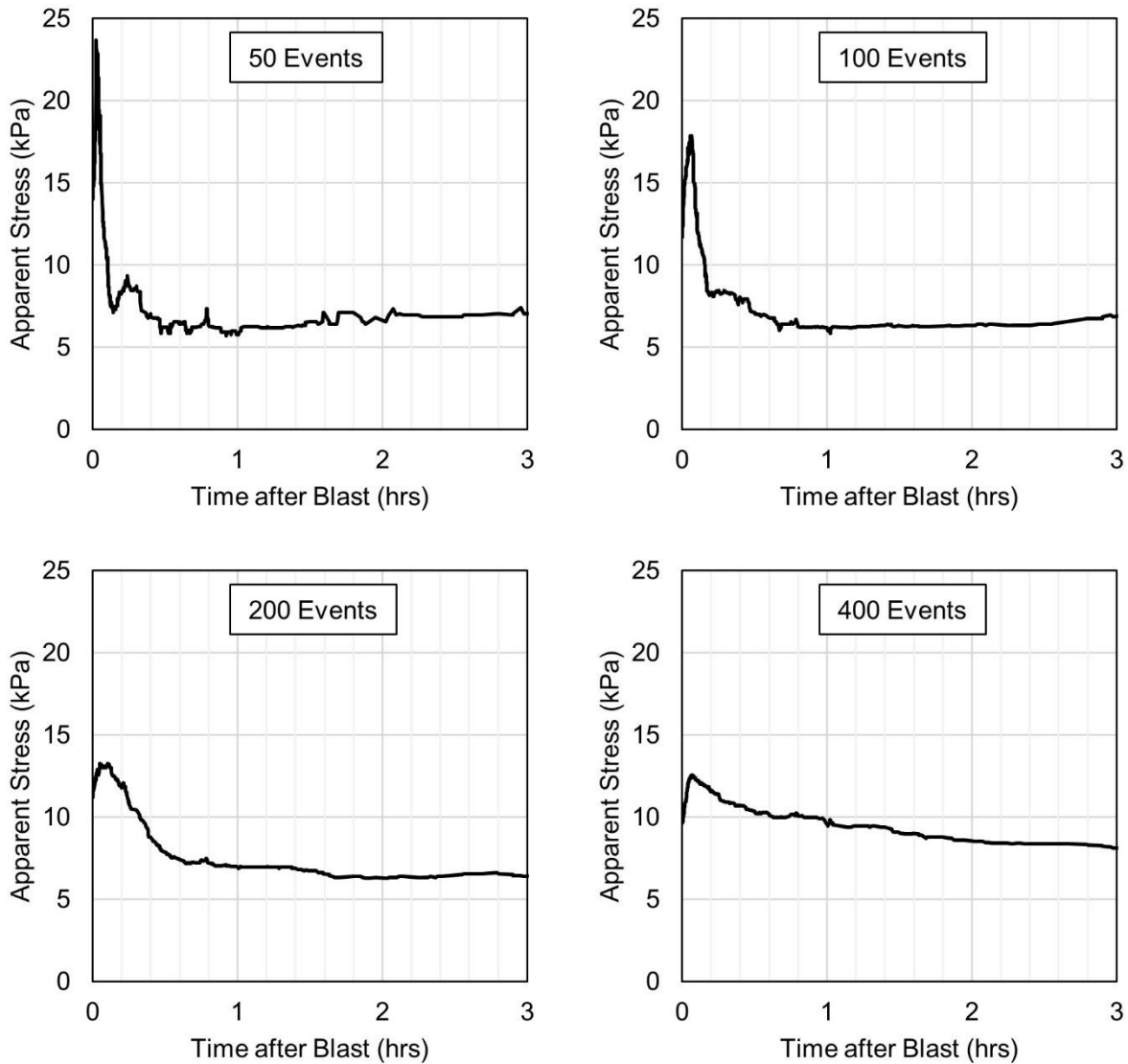


Figure 4-4: Median apparent stress in 1535-275-P1 SE corner following final blast using 50, 100, 200, and 400-event moving windows

#### 4.1.2 Phases of Change in Apparent Stress

In Figure 4-4 there are two extremes in the median apparent stress that occur in a short time after the blast. First, the apparent stress rapidly climbs to a peak which is reached in a few minutes. Second, it more gradually falls to a low point over an hour or so. The transitions between these two extremes will be referred to as Phase 1 and Phase 2 respectively. Figure 4-5 shows a longer time period covering several days after the blast, over which apparent stress rises from the low point at the end of Phase 2. Note that this increase is more gradual than the decrease observed during Phase 2. This period of gradual increase will be referred to as Phase 3. Phase 3 ends when

apparent stress beings to drop again. This may occur around 40 or 80 hours after the blast depending on the interpretation of the overall trend. The drop at 40 hours occurs over a small number of events and does not drop below the level at the end of Phase 2. The drop at 40 hours might be interpreted as insignificant, and the end of the phase at 80 hours would be considered a valid interpretation. Other examples of multiple interpretations of trend lines will be presented and discussed later in this chapter.

From the three observed phases in apparent stress variation following the blast, three corresponding rock mass responses can be inferred:

1. Increasing stress immediately after the blast.
2. Decreasing stress inside the stope's excavation damage zone (EDZ) as it forms.
3. Increasing stress as load sheds from the EDZ onto more intact and confined ground.

Several parallels can be drawn between these inferences and the readings of strain cells near an open stope blast presented by Hudyma et al. (1994) which were discussed in Chapter 2.

1. A sudden increase in stress that occurs within minutes of the blast
2. Decreasing stress as the rock mass yields which occurs quickly at first, and more slowly later on
3. Gradually increasing stress as load is shed from the yielded ground

Of course, the analysis of apparent stress alone does not give the context of where events are occurring. The results shown by Hudyma et al. (1994) validate that the rock mass near the stope yields, while stress increases farther away by using two instruments at different distances. Further analysis of spatial variations in apparent stress will be discussed in the next section.

Changes occurring at greater lengths of time after a blast are more difficult to associate with it due to the continuous process of induced stress changes related to recurring blasts throughout the mine. Therefore, variations in apparent stress occurring more distant in time from the blast are more difficult to directly associate with isolated changes produced by it, and may demand more complex, larger scale interpretations of rock mass behaviour. For this reason, the scope of this thesis will be limited to the aforementioned three phases occurring immediately after the blast. This three-phase model can also be reconciled with existing theories on the formation of excavation damage zones.

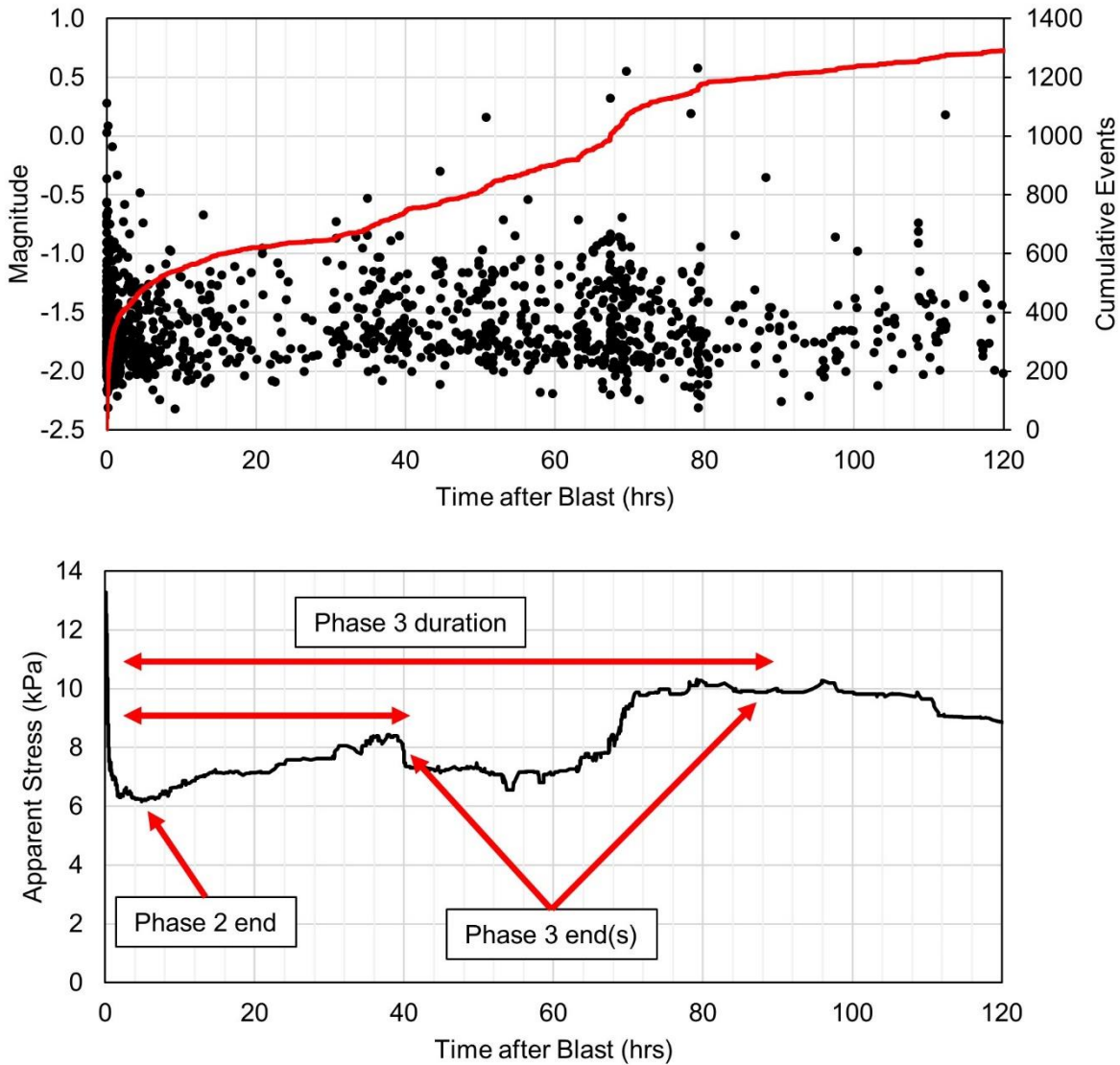


Figure 4-5: Median apparent stress in 1535-275-P1 SE corner

#### 4.1.3 Additional Parameters for Tracking a Distribution

The interpretation of variations in apparent stress can be made more robust by considering other aspects of the distribution. Median is only one measure of central tendency and considering additional points on the distribution can reveal how it shifts and skews. The additional points used in this methodology are the 20<sup>th</sup> and 80<sup>th</sup> percentiles of apparent stress. These were selected after Brown (2015) who used them to calculate apparent stress ratio (ASR), the ratio between the 80<sup>th</sup> and 20<sup>th</sup> percentiles of apparent stress in a population of events. It should be noted that ASR is recommended to be used with larger events only. The inclusion of smaller events may cause results related to ASR to differ from those of Brown (2015).

Following Brown's (2015) notation, the three values used to track apparent stress will be referred to as  $AS_{20}$ ,  $AS_{50}$ , and  $AS_{80}$ , which correspond to the 20<sup>th</sup>, 50<sup>th</sup> (median), and 80<sup>th</sup> percentiles respectively. An example of how these values are determined in the moving window is shown in Figure 4-6. The  $AS_{20}$  and  $AS_{80}$  are plotted alongside the  $AS_{50}$  (median) and also indicate increases and decreases at both ends of the distribution. The  $AS_{20}$  and  $AS_{80}$  are essentially defined based on 40 events each (the top and bottom 20% of events in the 200-event window), so it is clear how a larger window is required to use these measures of the distribution (e.g. they would only be defined by 20 events each with a 100 event window, and 10 events each with a 50 event window).

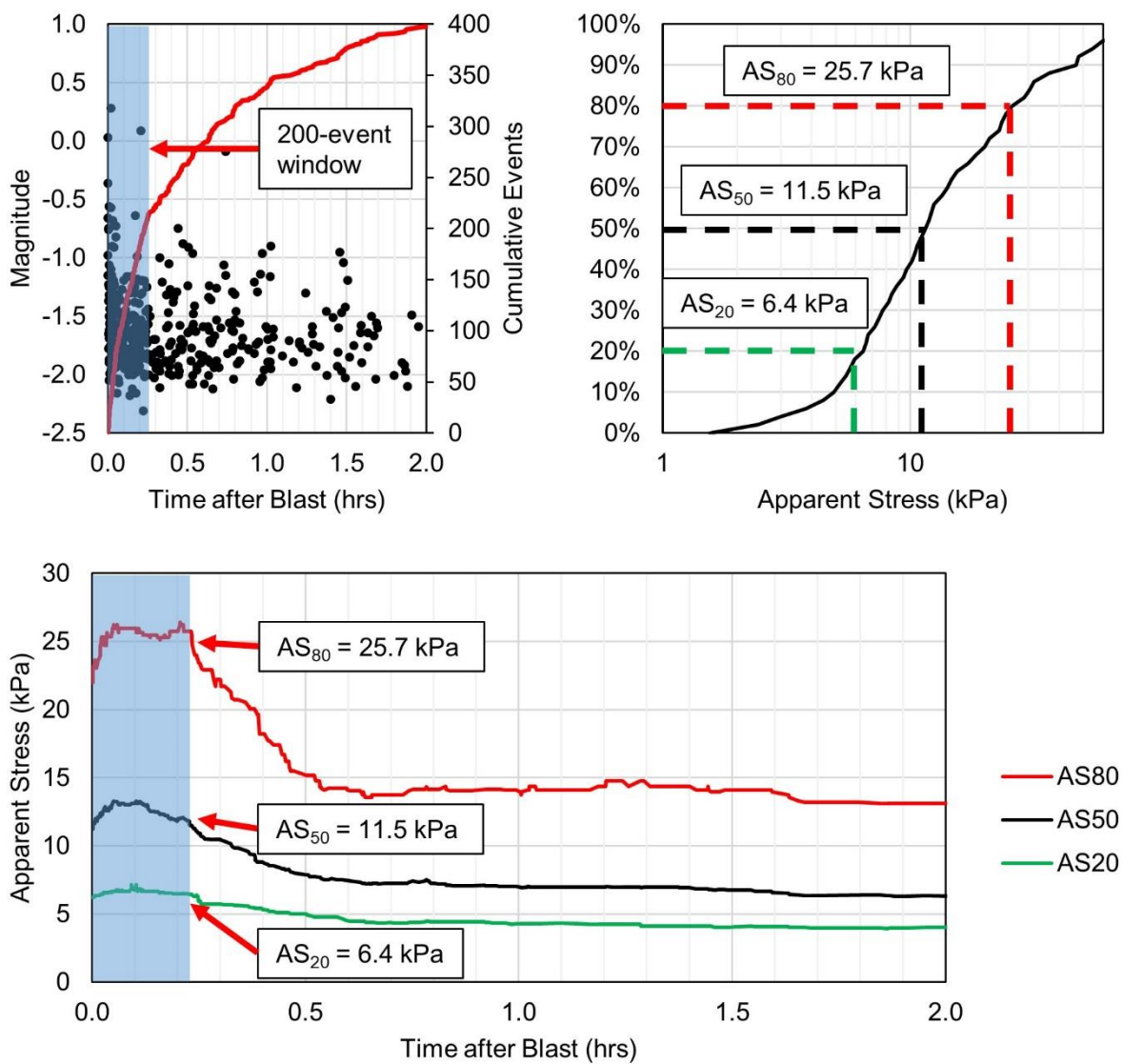


Figure 4-6: Determining  $AS_{20}$ ,  $AS_{50}$ , and  $AS_{80}$  in a 200-event window in 1535-275-P1 SE corner

#### 4.1.4 Determining Beginnings and Ends of Phases

Figure 4-7 shows that the timing of extreme points of AS<sub>20</sub> and AS<sub>80</sub> do not necessarily match up with AS<sub>50</sub>. The end of Phase 1 may lie between 3 and 12 minutes after the blast depending on which trend line is considered. This behaviour shows that the distribution does not simply shift up or down, rather, it simultaneously shifts and skews. There is also always some level of noise in the trend lines that can not be perfectly smoothed out. The average time of a peak or valley in all three trend lines is used to give a more robust definition of the end of each phase. In the example shown in Figure 4-7, Phase 1 is considered to end 7 minutes (0.12 hours) after the blast (blue dashed line). This method considers more points on the distribution than just the centre and is less sensitive to a single data point on any one trend line. This approach also provides a sort of range of the end time of each phase, in this case between 3 and 12 minutes after the blast. The same process is used to define the ends of phases 2 and 3.

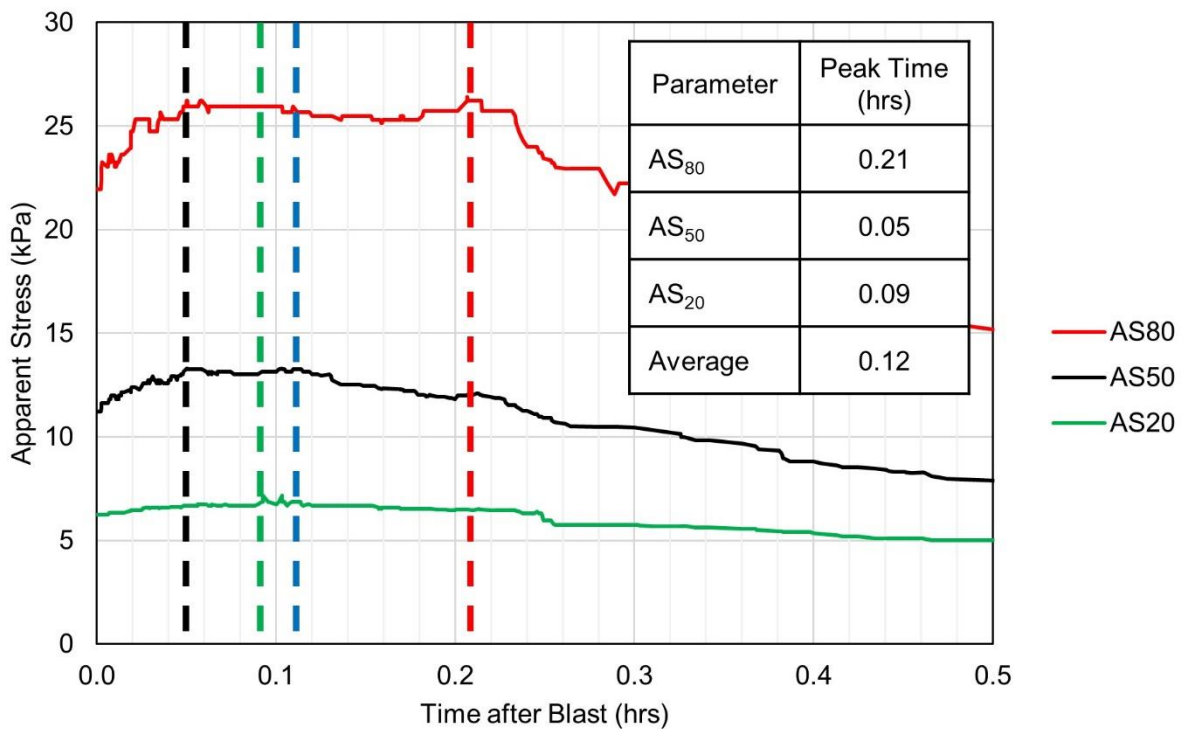


Figure 4-7: Determining end of Phase 1 in 1535-275-P1 SE corner using average peak time of apparent stress percentiles

Only trend line values at the average time will be considered when analysing changes that occur during each phase. This approach disregards individual peaks in each trend line and assumes that each trend line may still be somewhat noisy despite being smoothed with a moving window. Considering the values at the average time is a more robust approach and simplifies analysis of

changes that occur during each phase. Of course, this approach also relies on at least some homogeneity in the movement of each line (e.g. all increasing and peaking around the same time).

#### 4.1.5 Justification for a Volumetrically Filtered Approach

Differences in apparent stress variation between two seismogenic zones around the same stope highlight the need to spatially filter events. Figure 4-8 shows the filter volume for the events in the northwest corner of 1535-275-P1. The apparent stress variation in this volume will be compared to the apparent stress variation in the southeast corner of the stope. Beyond the spatial separation of events between these two groups, there are several physical aspects of the rock mass and mining geometry that may contribute to different stress and rock mass failure conditions:

- The NW corner is under the sill pillar where stresses are concentrated between the 1565 stopes and 1480 stopes and may be in a zone of lower confining stresses due to mining above and below.
- The SE corner is not underneath the 1480 stopes which may produce some degree of stress shadow beneath them and may have a more confined abutment state of stress rather than the sill pillar conditions in the NW corner.
- The SE corner is at the hanging wall limit of the stope which has a slight dip, making it more susceptible to gravity-driven failure than the vertical footwall limit near the northeast corner.
- The NW corner is near weaker, softer (SUBX and trunk vein).
- The SE corner is near stronger, stiffer FGN.
- There are possibly different rock mass conditions or geologic features present which might affect the stress field and failure mechanisms.

These differences in rock mass conditions between the two volumes may result in differences in their respective populations seismic events such as:

- Number of events.
- Seismic source mechanism.
- Energy-moment scaling.
- Size distribution of events.

These differences suggest that the populations should be separated to observe potentially different distributions of apparent stress. The manner in which the distributions change over time may also be different between the two volumes.

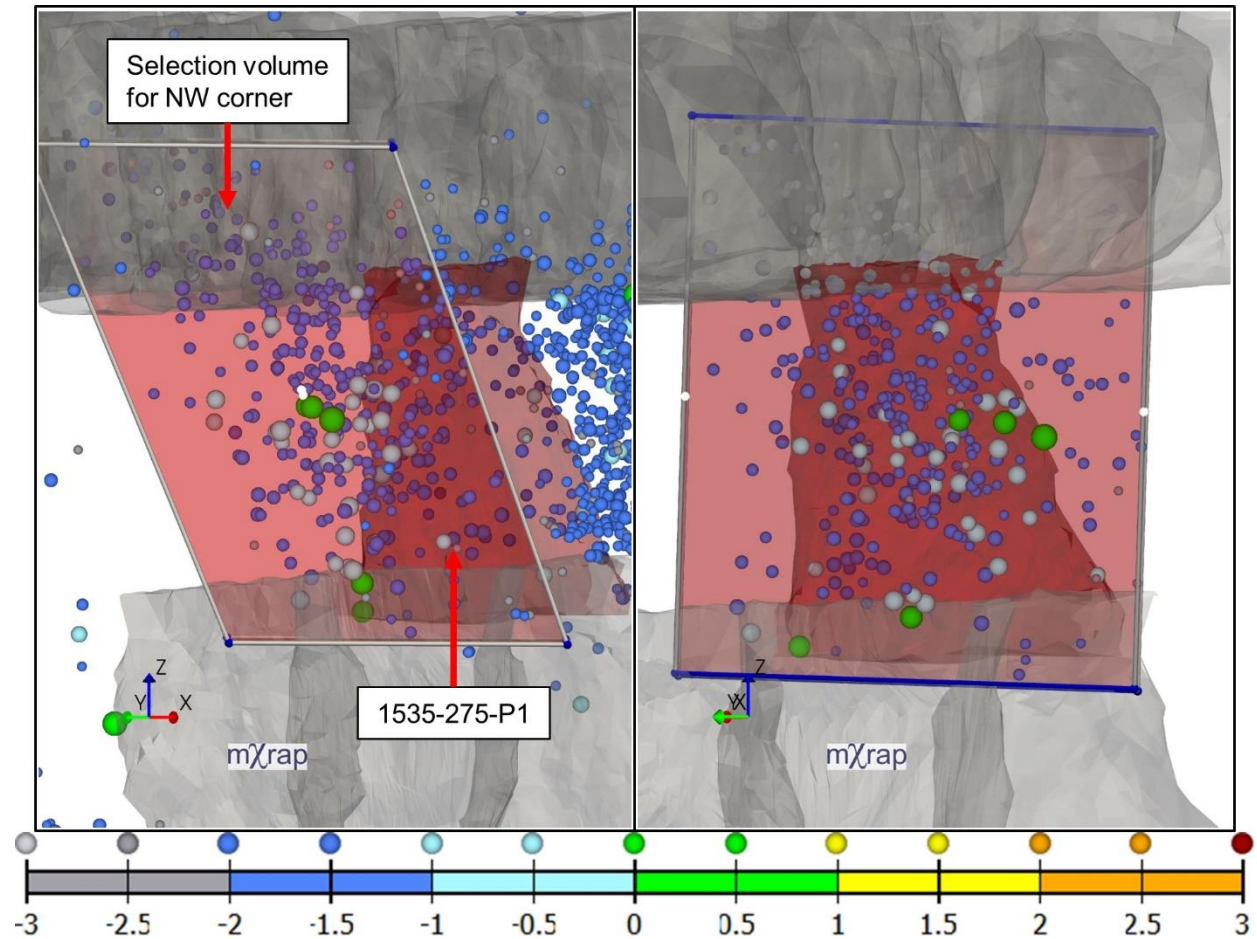


Figure 4-8: Events in 24 hours following 1535-275-P1 final blast (June 19<sup>th</sup>, 2013) showing NW corner selection volume looking NE (left) and SE (right) showing only events in volume

Figure 4-9 shows the apparent stress variations in the northwest and southeast corners over the same 12-hour period following the final blast. There are several differences between the trends in each volume:

- More events occur in the southeast corner.
- apparent stress is higher in the northwest corner (approximately 25 to 50% higher in each trend line).
- Phases 1 and 2 occur over longer periods of time in the northwest corner.
- Drop during Phase 2 is more gradual in the northwest than the southeast.

- The trendlines in the southeast have a larger percentage change between their initial values and their values at the end of Phase 2.

The levels of apparent stress and observed variation over time is clearly different in these two volumes. Combined analysis of the volumes may result in an interpretation that is biased towards behaviour in the southeast corner because there are more events there. Additionally, a combined analysis would fail to highlight the spatial variation in apparent stress around the stope. This example highlights how spatially distinct groups of seismic events occurring under different rock mass conditions have different patterns in the variation of apparent stress over time. Accordingly, these groups should be analysed separately by volumetrically filtering events.

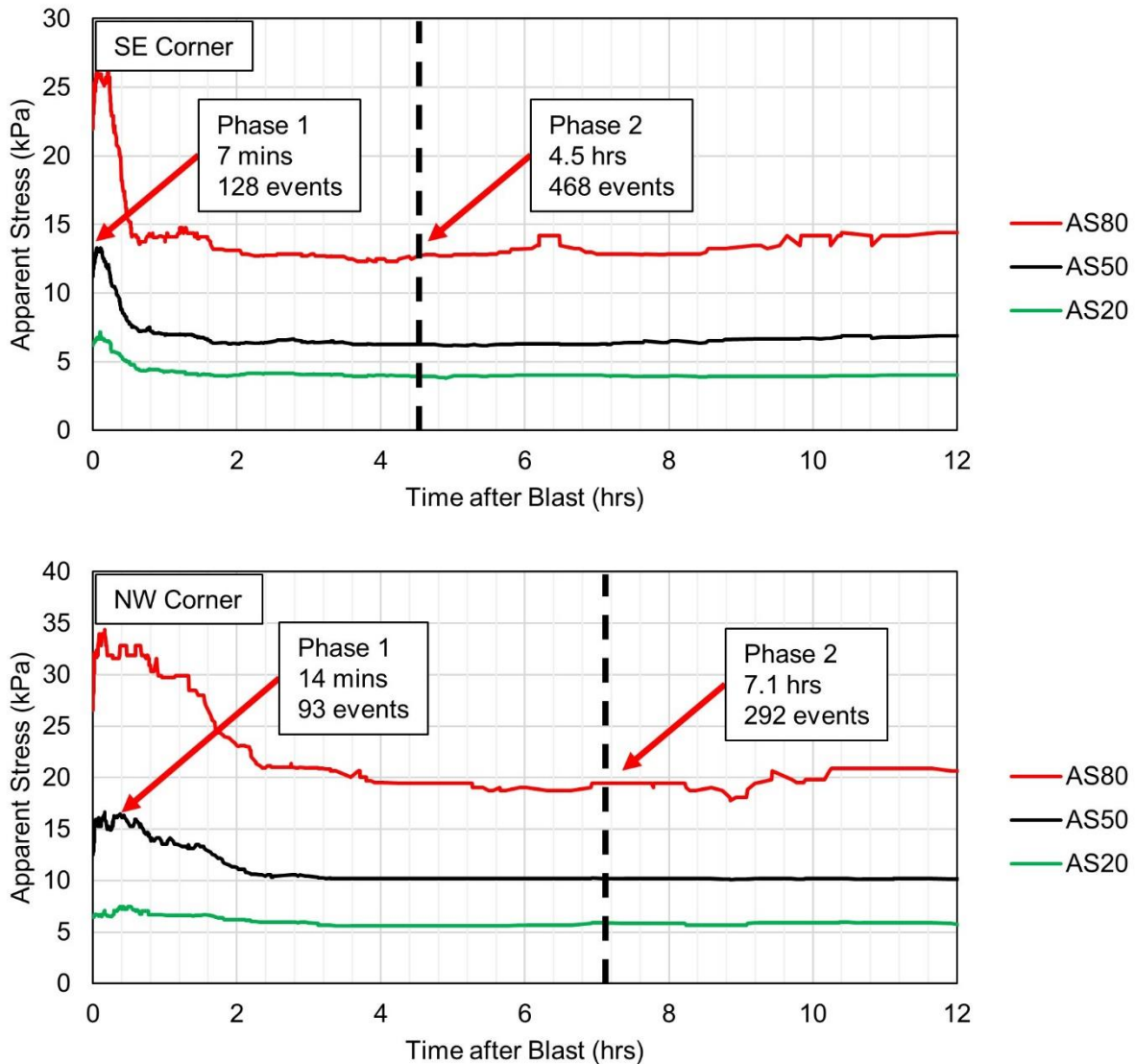


Figure 4-9: Comparison of apparent stress variation between SE and NW corners of 1535-275-P1 showing end times of phases and number of events in each phase

#### 4.1.6 Multiple Interpretations of Phases of Variation

Despite the robust approach to determining the end times of each phase, there are some cases where multiple phase interpretations are possible. One such case is the west sidewall of 1680-262-P2 which was blasted in late 2011. 1680-262-P2 was the second stope mined on 1680. In 2011, most of the stopes on 1660 were mined out, and mining on 1680 started a push into the lower abutment of what was then the deepest production level. A large seismic response was observed following the final blast, with most of the events locating in the stope's west sidewall.

Figure 4-10 shows a magnitude-time history and apparent stress percentiles over 12 hours after the final blast. The three phases of apparent stress variation are clearly identified and marked in the figure. Phase 2 occurs over about 400 events and drops about 35% from Phase 1, and Phase 3 occurs over about 200 events and climbs about 20% from Phase 2. The variations are visible in AS<sub>20</sub>, AS<sub>50</sub>, and AS<sub>80</sub>. Each phase occurs over a period of time longer than the last, indicating that changes in the rock mass are occurring more gradually over time.

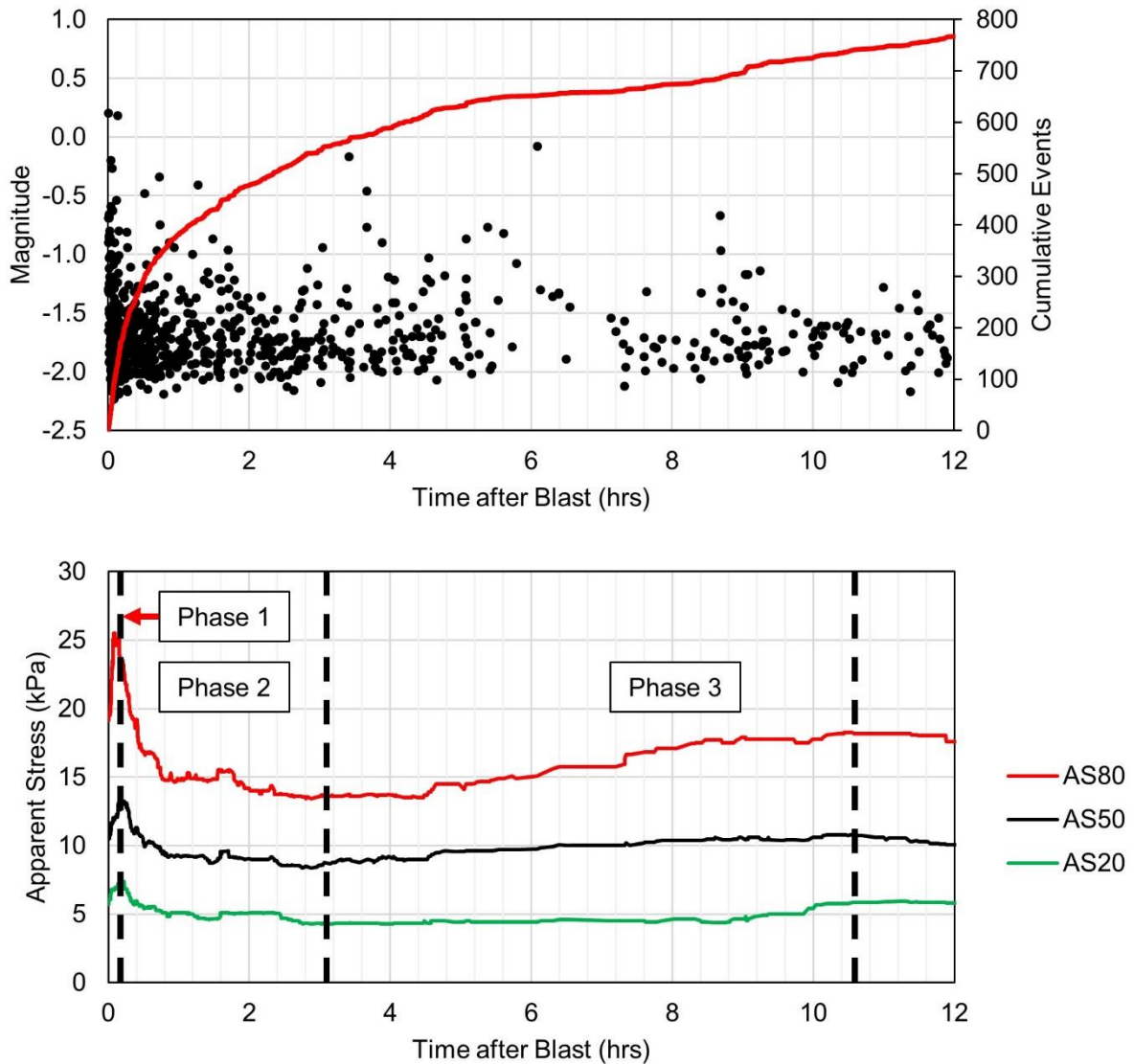


Figure 4-10: Three phases of apparent stress variation in the west sidewall of 1680-262-P2 (December 24<sup>th</sup>, 2011) ending 10.7 hours after blast

Figure 4-11 shows a magnitude-time history and apparent stress graph over 400 hours after the final blast in the same volume. The interpretation of Phase 1 is the same as in Figure 4-10, but this

graph shows a lower valley and a higher peak following the end of what was initially interpreted as Phase 3. This graph offers the interpretation that Phase 2 occurs over a longer period of time and ends around 25 hours after the blast, essentially ignoring the initially interpreted Phase 3. With this longer phase interpretation, Phase 3 ends around 370 hours after the blast. Several small drops during Phase 3 are visible in the AS<sub>80</sub> trend line, but the overall trend is still upwards. This interpretation shows apparent stress dropping and rising in a similar manner to previous examples and has each phase occurring over a longer period than the last.

It can be difficult to disregard the initial “short phase” interpretation. Noticeable changes in the trend lines occurred over several hundred events, indicating that the changes may be more significant. In such cases, both short and long phase interpretations may be considered valid. In the short phase interpretation, anything that occurs after the end of Phase 3 is considered a longer-term process with different behaviour (possibly a Phase 4 or 5 which is beyond the scope of this thesis). In the long phase interpretation, the peaks and valleys that defined the shorter phases are considered to be insignificant interruptions in larger scale process of rock mass failure. This larger scale process is still controlled by local conditions resulting from the final blast and occurs within the short term. Both interpretations are recorded for the purposes of analysing results.

In the magnitude-time history in Figure 4-11, there are several periods where the rate of events suddenly increases multiple days after the blast (most noticeably around 220 and 330 hours after the blast). While this thesis is primarily concerned with the apparent stress and locations of events, the rate at which events occur signifies an important aspect of the processes generating seismicity. Event rates are higher when the rock mass is adjusting at a faster rate. After a blast, it is expected that adjustments slow down over time (e.g. presentation of strain cell readings and modelled EDZ size in the hours after blasts in Chapter 2). When the rate of events suddenly increases at some period of time after the blast, it suggests that the rock mass is adjusting to another sudden stress change, such as one caused by a blast elsewhere in the mine. As discussed previously, the effects of distant blasts on local rock mass conditions are generally controlled by the rock mass conditions near that blast, the size of the blast, and its distance from the volume being analysed. Such effects present the inherent challenge of interpreting changes produced by a single, isolated blast several days after it took place. However, it is still possible to interpret localized changes and effects on an isolated volume of rock mass because:

1. The number of events in later sudden event rate increases is small compared to the number produced by the blast being studied.
2. The rate of events returns to the rate it was at before the sudden increase relatively quickly.
3. The variation in apparent stress percentiles is relatively small, and the overall longer term trend is still upwards throughout Phase 3.

To reiterate, this thesis is primarily concerned with space-time variations in apparent stress, so the rate of events is typically not considered in analysis. Of the above-mentioned factors, #3 is often the most relevant to interpreting the phases of apparent stress variation.

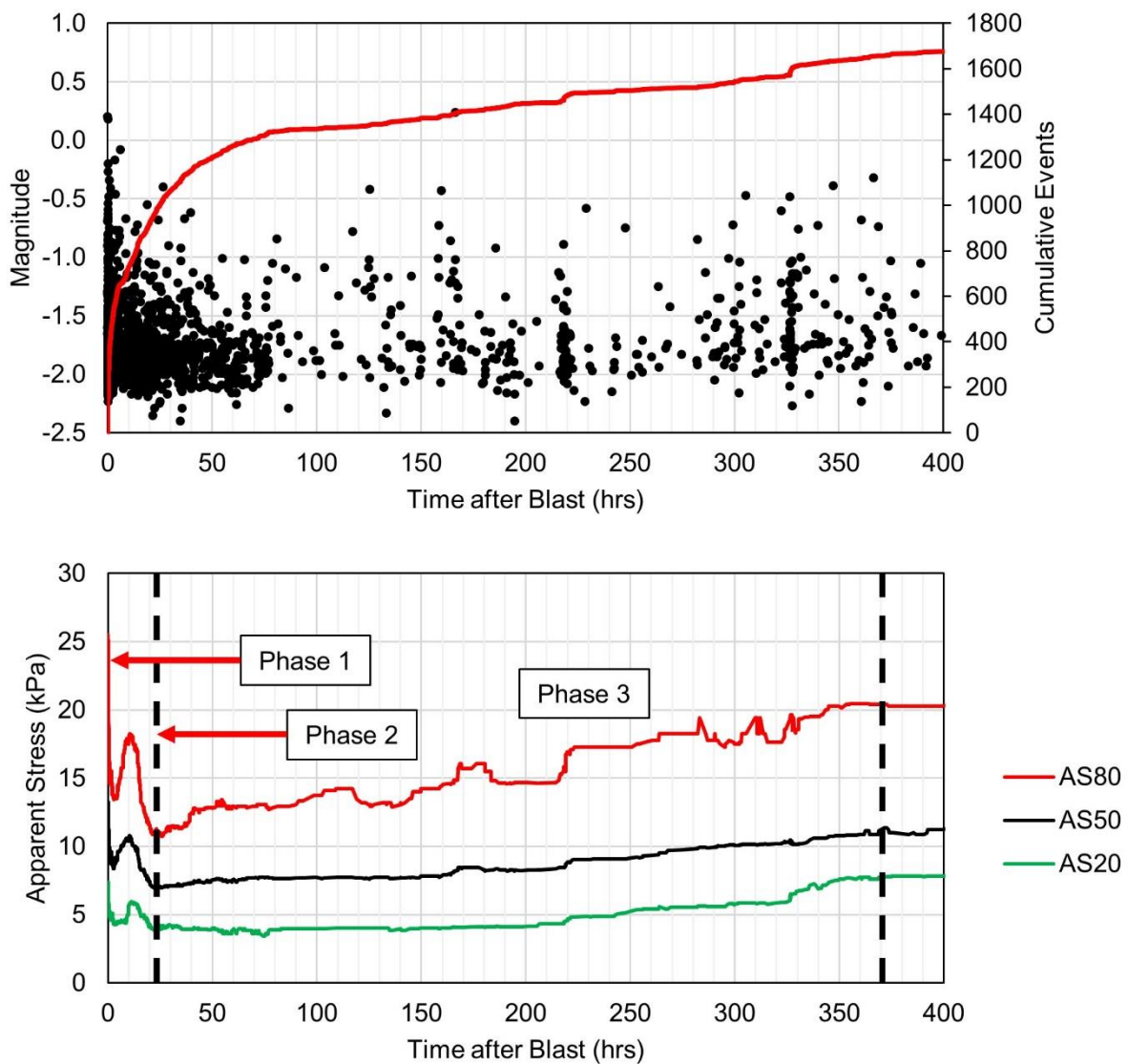


Figure 4-11: Three phases of apparent stress variation in west sidewall of 1680-262-P2 (December 24<sup>th</sup>, 2011) ending 370 hours after the final blast

## 4.2 Variations in Event Locations and Spatial Distribution of Apparent Stress

Event locations can be used to infer the locations of the rock mass under elevated stress where failure is occurring. This region of active rock mass yield, known as the seismogenic zone (after Duplancic, 2001), will migrate to areas where stress conditions result in local instability (high stress, low confinement). It will move away from excavations and damaged ground and towards more intact ground which has the capacity to store stress and release energy in the form of seismic events when it yields. Movement of the seismogenic zone will occur as incremental changes in induced stress occur (e.g. successive blasts in an advancing mining front) and as the rock mass yields and redistributes stress outside excavation damage zones. The locations of seismic events can be used to infer where the seismogenic zone (i.e. active rock mass yield) is, and if it is moving. Event source parameters can be used to infer different rock mass conditions (e.g. stress and confinement) within the seismogenic zone.

### 4.2.1 Methods of Tracking Variations in Event Locations

The goals of analyzing event locations in this thesis is to show how seismogenic zones migrate away from stopes, indicating stress redistribution and EDZ growth. Analysis of event locations will also show how apparent stress varies throughout a seismogenic zone, indicating spatial variation in local rock mass conditions. Previous studies have tracked median or average coordinates to illustrate migration of a seismogenic zone (e.g. work by Glazer (2016) on the Palabora block caving mine), but such approach alone does not show any variation in apparent stress. Maps and spatial plots are useful for visualizing spatial variations in a parameter but are less useful when trying to quantify change over time. Maps provide incremental snapshots which are difficult to employ when the time scales that changes occur over are unknown (i.e. changes that occur between mining steps rather than with each mining step). Consequently, this thesis will employ a different approach that makes certain simplifications to a multi-dimensional problem. This approach will enable visualization of changes in event locations and spatial variation in apparent stress over time.

First, an approach to measuring locations of populations of events must be chosen. The median has been selected again because the distributions of event locations and location error are not known. It is also a more robust but straightforward approach to finding the centre of a distribution. Event locations might be tracked by their median Cartesian coordinates (e.g. median X, Y, Z

coordinate within a group of seismic events). This approach provides a great deal of information that will be helpful considering the three-dimensional nature of the mining geometry and resulting seismic responses. However, the abundance of information has the potential to make the data too difficult to interpret and/or find consistent patterns. Furthermore, comparing different cases would be challenging because the stopes are in different locations and have different dimensions.

In order to simplify the analysis, each case was reduced to what is effectively a one-dimensional problem. The locations of events are reported in terms of their minimum distance from excavated stopes. The distance is determined by finding the shortest distance between events and three-dimensional surfaces of selected mine excavation surveys. The distances between events and surveyed stope surfaces were calculated using mXrap (Harris and Wesseloo, 2015). Conceptually, this approach simplifies the analysis to a single advancing mining front with an elevated stress region and seismogenic zone at the face. Syrek and Kijko (1988) performed a similar analysis of the distribution of events at varying distances from the face of a tabular excavation, a relatively simple mining geometry. This approach was illustrated in Figure 2-27.

Although a one-dimensional analysis significantly reduces the complexity compared to an environment with a three-dimensional geometry and stress regime, the analysis still provides meaningful information. Based on analytical solutions, numerical models, and field data presented in Chapter 2, an event's distance from excavations can be associated with varying degrees of stress, confinement, rock mass damage, and failure mechanisms. The manner in which events are grouped around stope faces and abutments is conducive to a one-dimensional analysis. Each volume of events essentially considers a single stress front around each face or corner of a stope. These volumes have a simplified mining geometry and relatively consistent rock mass properties and stress regimes. This approach is also applicable in mining pillars. Although there are two stopes forming the pillar, each with their own stress front, the geometry is mostly symmetrical and can therefore be simplified to a one-dimensional problem. This approach has been illustrated in Figure 4-12.

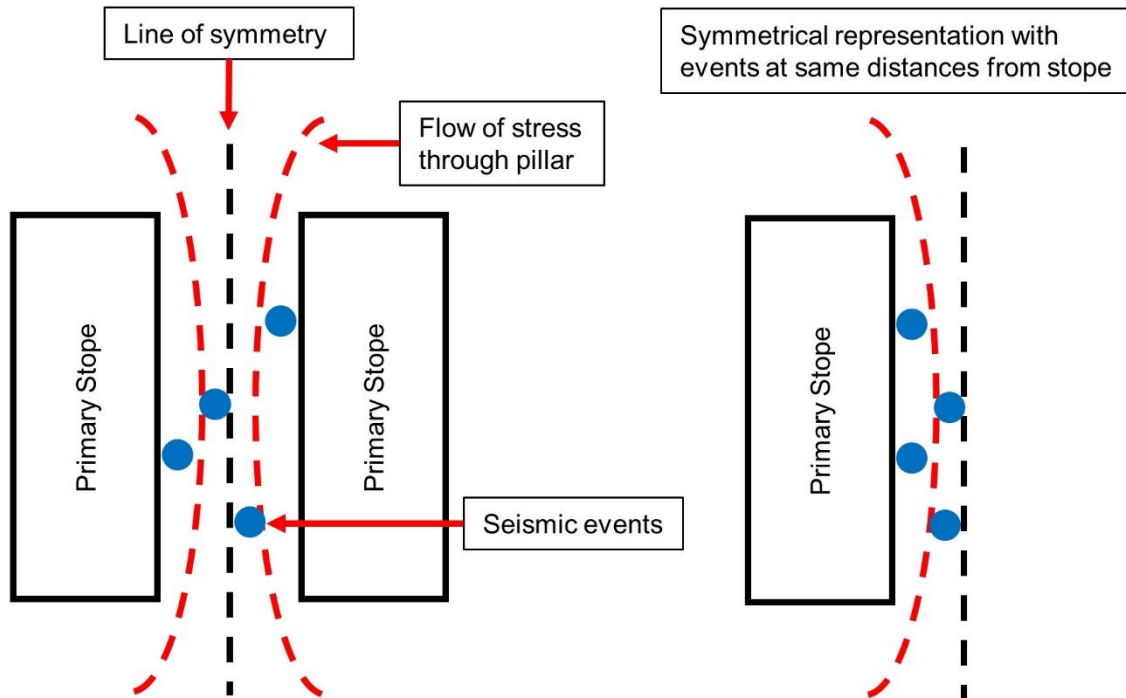


Figure 4-12: Plan view schematic of the use of symmetry in a pillar to simplify the analysis of event-stope distances

Only excavated stopes are considered for event-excavation distances. No drifts, stope accesses, or raises are accounted for. This approach assumes that the stress redistributions and excavation damage zones are controlled by conditions related to the distance from stopes only. This assumption is justifiable because stopes are the largest excavations. The volume of a single stope is approximately one hundred times larger than a development blast, and their greatest dimension (their height or length) is six times greater than the cross section of typical lateral development. Therefore, stopes have a much larger impact on induced stresses and confinement than smaller development. This is not to say that development does not have an influence, it is simply assumed to be negligible. Development voids may also not play a role in the majority of cases because seismic events from stope blasts typically locate in abutments or sidewalls. Development is usually not in place near these locations when the events occur (largely due to the just-in-time development strategy), so the closest excavation is usually a stope regardless of whether or not smaller excavations are considered.

#### 4.2.2 Phases of Change in Event-Stoppe Distances

As with the previous section, the southeast corner of 1535-275-P1 will be used as the primary example. The moving window used to find the median will be the same size (200 events) as with the apparent stress percentiles. Using the same window size ensures that this trend line will not respond to variations faster or slower than the apparent stress trend lines.

In Figure 4-13 the median event-stope distance (MESD), referred to symbolically as  $D_{50}$ , can be seen rising and falling for 80 hours after the blast. As with the variations in apparent stress, phases of variation in MESD are defined based on when the trend line is rising or falling. In Phase 1 the events quickly move away from the newly blasted stope for a period of about 4 hours. Phase 2 occurs as the events move towards the stope and ends around 14 hours after the blast. Finally, events move away from the stope again during Phase 3 which ends around 70 hours after the blast. As with the variations in apparent stress, the scope of this thesis is limited to these three phases.

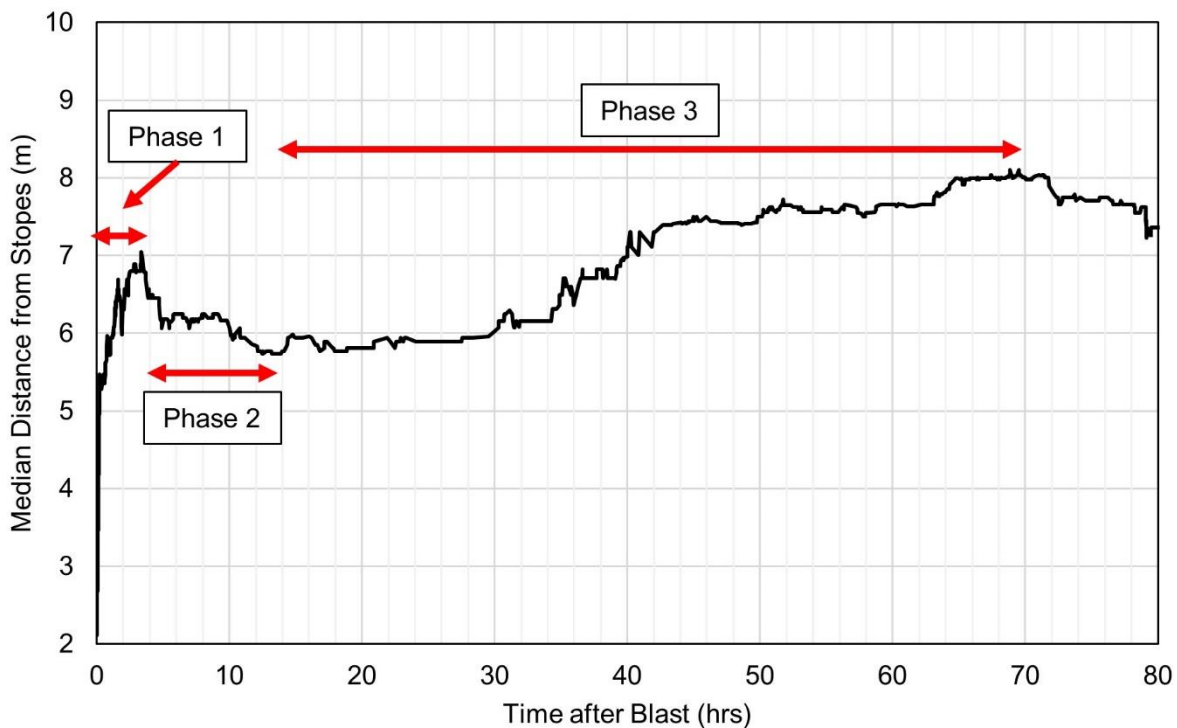


Figure 4-13: Median event-stope distance in 1535-275-P1 SE corner

The observed variations in MESD can be used to interpret rock mass behaviour around the stope. In each of the three phases, the following rock mass behaviour is inferred:

1. Stress redistribution around a new excavation and outside its excavation damage zone.

2. Continued rock mass yield closer to the stope in a region where stresses place the rock mass between stable and unstable states.
3. Growth of the excavation damage zone.

It is interesting that events move towards the stope some time after the blast. Conceptually, the formation of an excavation damage zone should begin immediately after the blast, and the zone should expand for some amount of time afterwards. As a result, seismic events should continuously move away from the stope so long as the excavation damage zone is expanding. However, there are numerous examples throughout the analysed cases where the MESD moves towards the stopes some time after the blast. Some examples of such behaviour observed in other cases is illustrated in Figure 4-14.

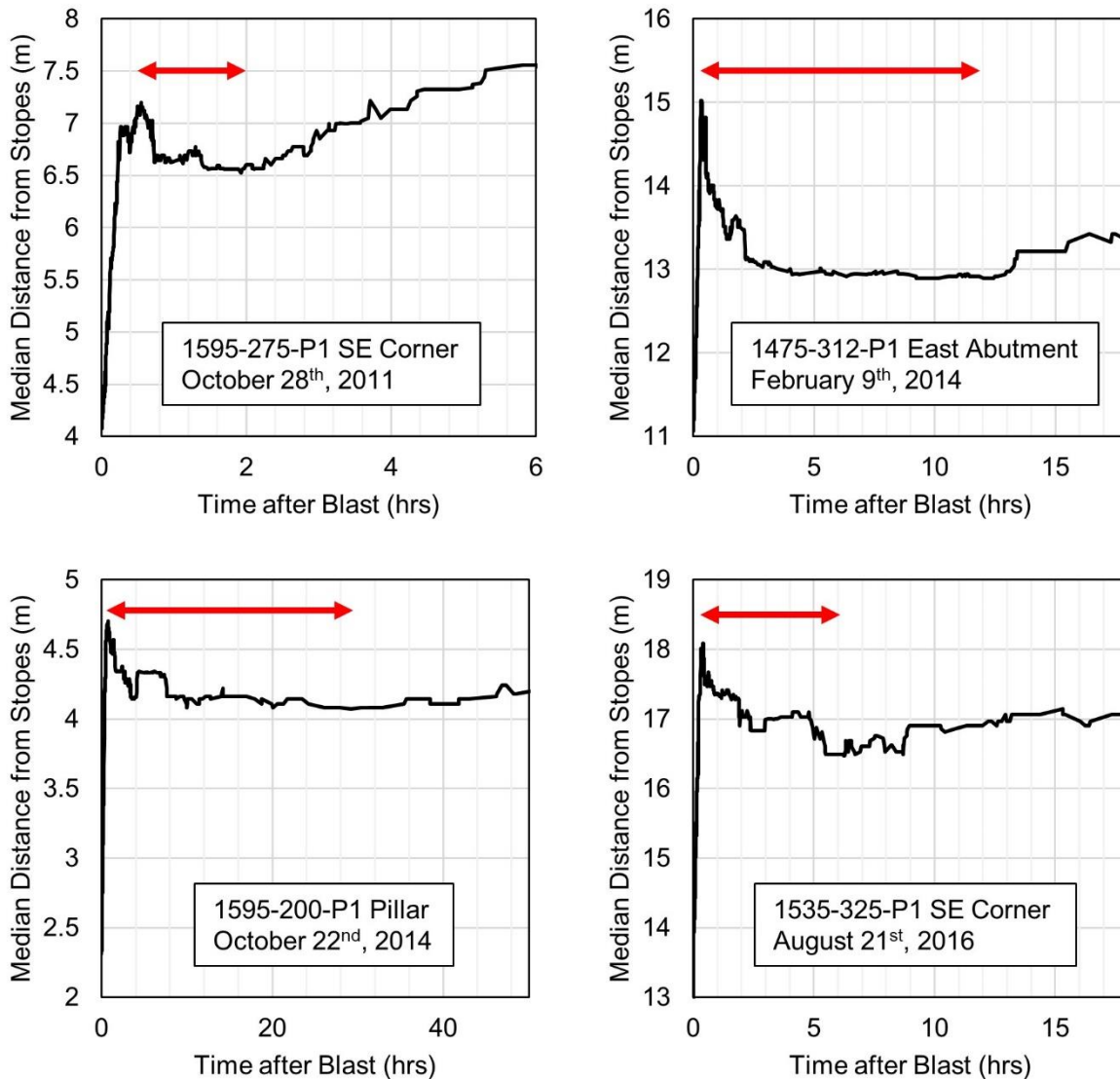


Figure 4-14: Examples of MESD decreasing some period after the blast, defining Phase 2 of MESD variation

The author believes there is a reasonable explanation as to why events may initially locate farther away from the stopes. Recalling Figure 2-5, a region of yielded rock mass near an excavation will shed stress onto more intact regions of the rock mass farther from the excavation. Figure 2-6 and Figure 2-7 illustrate how stress sheds away from a new excavation so long as yielding continues. Some aspects of seismicity and rock mass behaviour the author believes are relevant to the observed Phase 2 behaviour are:

- Seismic events may be associated with the rock mass closest to the excavation yielding, forming the EDZ, but may also be associated with yield in more intact regions onto which

stress is being shed. The presence of seismic events in a specific area does not necessarily imply local stress levels are decreasing (although a seismic event does represent a stress drop on a discrete fracture). Stress increases past the rock mass's yield point until the peak strength, a period during which seismic events occur. Seismic events will also occur in the post-peak when stress is dropping.

- Stress in one area increases as long as a nearby area continues to yield and shed stress onto it. These areas may generate seismic activity as long as local stress levels are increasing.
- Stress increases occur at greater distances from an excavation with more advanced yield or post-peak behaviour closer to the excavation. These stress changes may result in seismic activity at greater distances from the excavation.
- Stress decreases occur at greater distances from an excavation as stress shed from other regions pushes the local rock mass into the post-peak. These areas that are pushed into the post-peak will also generate seismic events at greater distances from the excavation.
- Stresses may not exceed the strength of the rock mass at greater distances from an excavation but may exceed the strength of discontinuities in the rock mass such as joints. Exceeding the strength of these discontinuities and giving them more kinematic freedom from the reduction in confinement results in structurally-controlled rock mass damage (Castro, 1996). This mechanism of rock mass damage may produce seismic events at greater distances from an excavation where induced stress changes are smaller. The mechanism of these events also differs from those related to damage to the intact rock.

Following a blast, the aforementioned behaviours contribute to events locating at progressively greater distances from the new excavation. A quasi-stable state is reached some time after the blast. At this time, stress changes and the migration of the elevated stress front has slowed, and with it the outward migration of seismicity. However, there is a region of the rock mass at some distance from the excavation that is in a delicate balance between being stable and unstable. With slowed yield and stress redistribution, this region becomes the dominant source of seismic events. This region is conceptually represented by the interface between the fractured and elastic domains around the excavation in Figure 2-5 (in realistic scenarios the region should not be considered a discrete envelope). This quasi-stable region will continue to yield and shed stress, and outward migration of the elevated stress front and seismicity will progress from its initial location. The migration should slow with time as the rock mass continues to search for a new stable state. The

gradual, ever slowing migration relies on further stress changes remaining gradual (unlike those caused sudden change in excavation geometry created by a blast) and rock mass properties remaining relatively consistent.

Phase 2 of MESD variation represents the transition from a yielding rock mass which is shedding stress and generating seismic events at ever increasing distances from a new excavation, to a rock mass in a quasi-stable state where yielding is slowed and seismicity occurs in a more consistent region. Growth of the EDZ progresses outwards from this initial quasi-stable region. Therefore, it is most accurate to define the growth of the EDZ based on the change in MESD during Phase 3. Of course, the EDZ has to some extent formed before this time, so Phase 3 does not represent the complete growth from immediately after the blast.

#### 4.2.3 Spatial Variations in Apparent Stress over Time

The analysis should also consider some indication of spatial variation in apparent stress. Within the 200-event window, the apparent stress percentiles provide some indication of the distribution of apparent stress. When considering spatial variations, the analysis should account for where events with higher or lower apparent stress are occurring. Figure 4-15 illustrates the process used to determine whether events with higher apparent stress occur closer or farther from stopes than events with lower apparent stress. Within the 200-event window, the events are separated into the 100 events with the highest and lowest apparent stress ( $\sigma_a > AS_{50}$  and  $\sigma_a < AS_{50}$ ). The median event-stope distance is found separately for each individual of high and low apparent stress events (referred to as  $D_{50H_{50}}$  and  $D_{50L_{50}}$  respectively). This approach creates consistent sample sizes for finding median distances.

It is important to note that the distribution of apparent stress changes over time, so what constitutes “high” or “low” apparent stress in this methodology will also change. An alternative approach would be to define high or low apparent stress based on a fixed threshold (e.g. above or below 20 kPa). However, a fixed threshold would result in variable sample sizes and trend lines that respond faster or slower depending on event rates and the distribution of apparent stress. Therefore, the approach illustrated in Figure 4-15 based on the distribution of apparent stress currently in the window is considered more favourable.

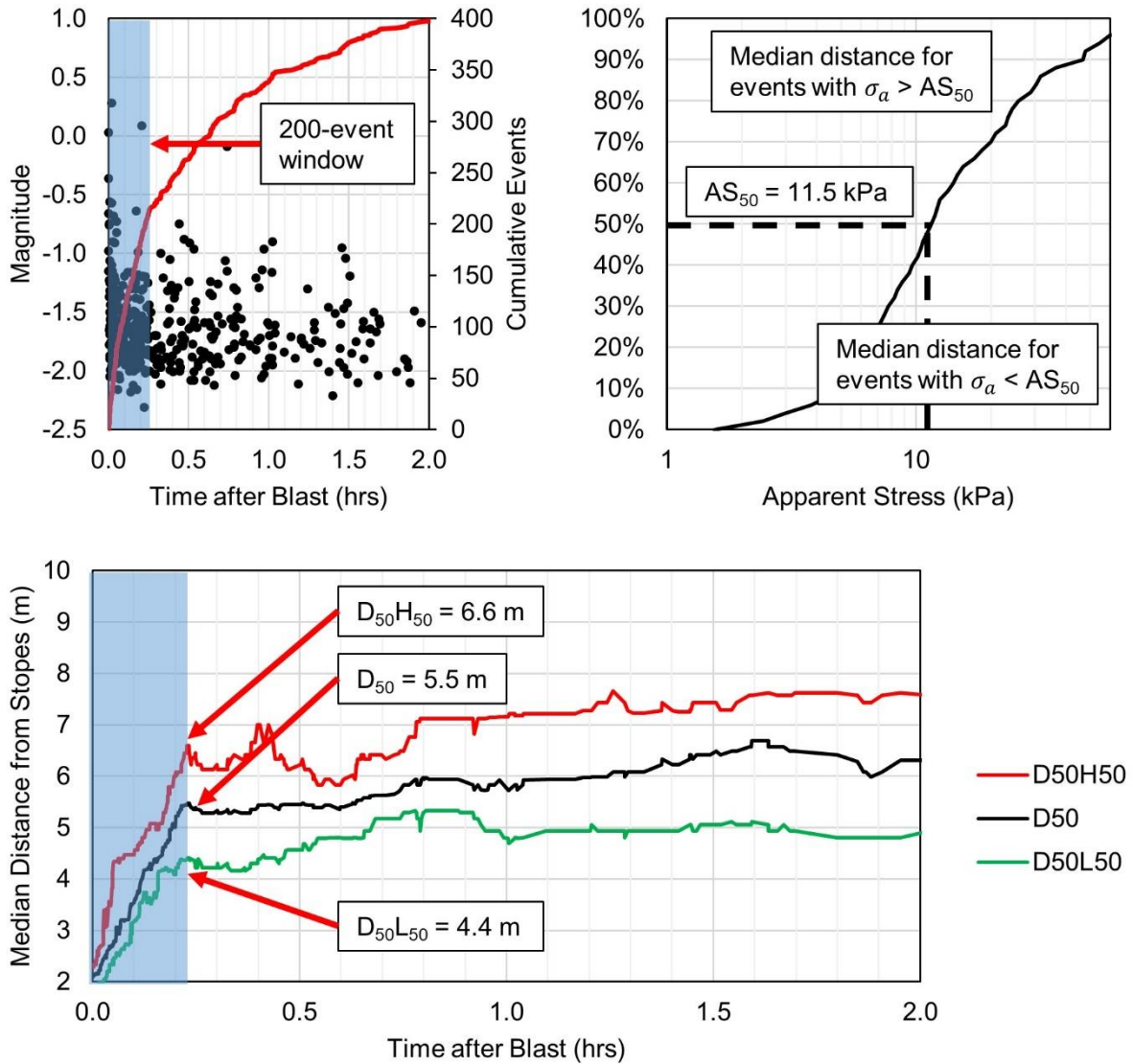


Figure 4-15: Determining  $D_{50}$ ,  $D_{50}H_{50}$ , and  $D_{50}L_{50}$  in 200-event window in 1535-275-P1 SE corner

In Figure 4-15, several features of the  $D_{50}L_{50}$  and  $D_{50}H_{50}$  trend lines can be used to enhance the interpretation of rock mass behaviour following the 1535-275-P1 final blast. Events with high and low apparent stress both move away from the stopes following the blast, which implies they are controlled by similar processes. However, there are short periods where  $D_{50}L_{50}$  and  $D_{50}H_{50}$  do not move in complete unison, such as 0.5 hours after the blast, which indicates they might be somewhat independent of each other. The graph also shows that events with higher apparent stress are farther away from the stopes than events with lower apparent stress, a result which is similar to those described by Abolfazlzadeh and Hudyma (2016) in the seismogenic zone of a sublevel caving mine. The separation between the trend lines is approximately 2.2 m after the first 200 events. This

behaviour indicates that events with higher and lower apparent stress occur under different conditions. Events with higher apparent stress occur farther from stopes where less damage and higher confinement is expected. Events with lower apparent stress occur closer to stopes where more damage and less confinement is expected.

#### 4.2.4 Determining Beginnings and Ends of Phases

The  $D_{50}H_{50}$  and  $D_{50}L_{50}$  trend lines can also be used to determine the end of each phase of MESD variation in a more robust manner. The method for defining the end of phases in event-stope distance variations is identical to the one used for apparent stress variations. In Figure 4-16, the three trend lines,  $D_{50}L_{50}$ ,  $D_{50}$ , and  $D_{50}H_{50}$ , all show an increase in event-stope distances but each peak at a different time. The average of the three times is used to define the end of Phase 1. The same process is used to determine the end of phases 2 and 3.

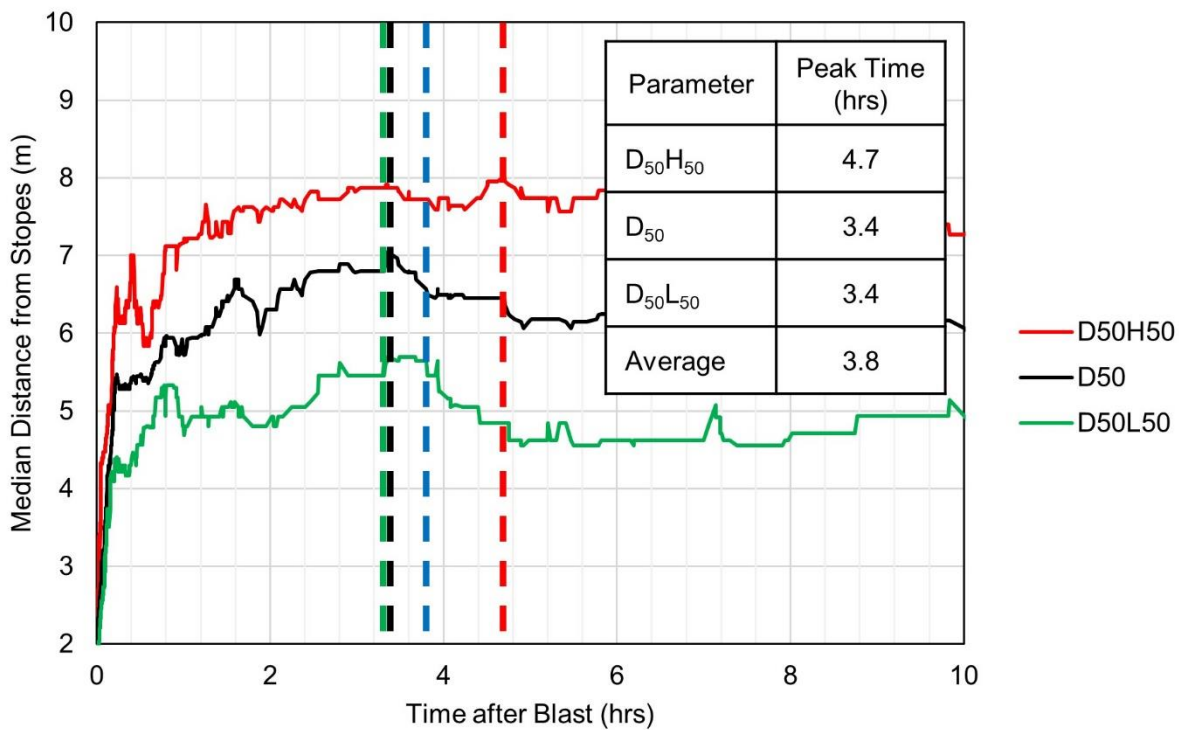


Figure 4-16: Determining end of Phase 1 in 1535-275-P1 SE corner using average peak time of MESDs

#### 4.2.5 Expanding the Interpretation of Spatial Variation in Apparent Stress

The approach to showing spatial variation in apparent stress can be expanded to show variation over a greater range of apparent stress values. The median distances for events in the top and bottom 20% of apparent stress add more detail to the analysis (i.e. showing any differences

between high and higher apparent stress, or low and lower apparent stress). These additional trend lines  $D_{50H80}$  and  $D_{50L20}$ , corresponding to the median distances for the top and bottom 20% of apparent stress respectively, are determined in the same manner shown in Figure 4-15.

The five trend lines are shown over a period of 2 hours in Figure 4-17. Events with the highest apparent stress, the top 20%, are even farther from the slope than events in the top 50% of apparent stress values. Similarly, events with the lowest apparent stress, the bottom 20%, are even closer to the slope than events in the bottom 50% of apparent stress values. Throughout the seismogenic zone, events with higher apparent stress will tend to locate farther away from the slope. Based on these results, it can be inferred that the rock mass closer to the stopes is more damaged and under lower stress, and the rock mass farther from the stopes is less damaged and under higher stress.

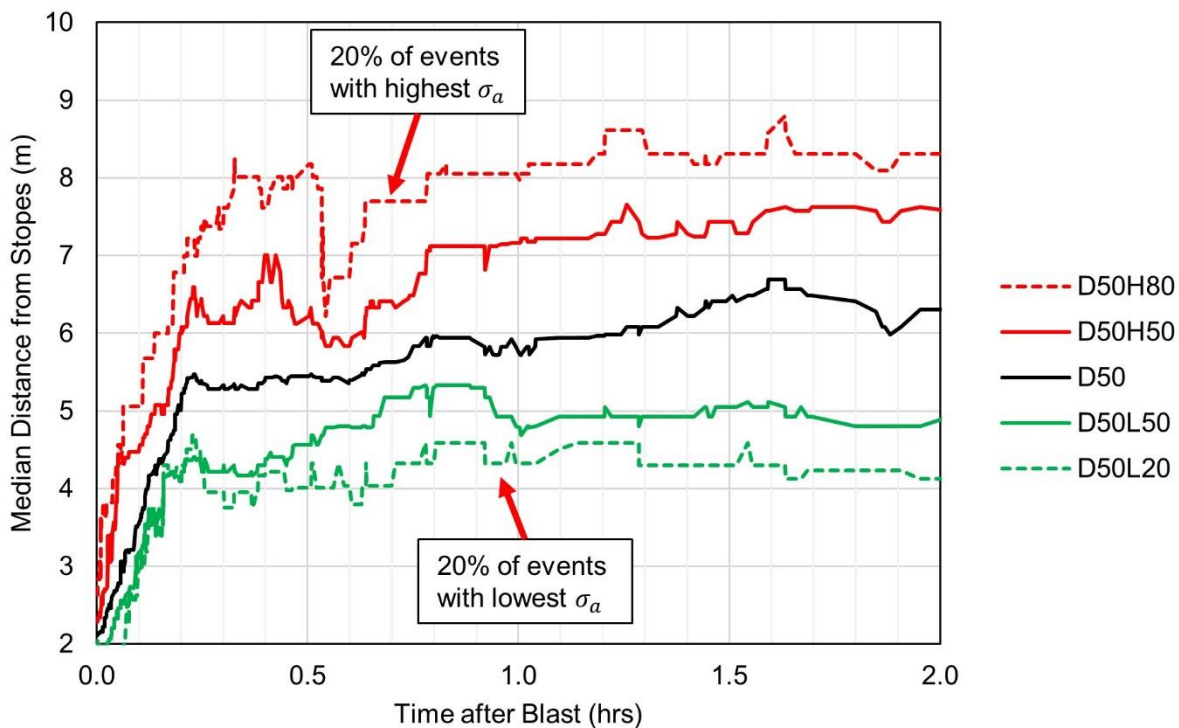


Figure 4-17: Use of  $D_{50H80}$  and  $D_{50L20}$  to enhance interpretation of spatial gradient of apparent stress in 1535-275-P1 SE corner

It should be noted that this approach further limits sample sizes, giving less confidence in the trend lines (i.e.  $D_{50H80}$  and  $D_{50L20}$  are only determined based on 40 events each). Therefore, there is a limit to how much detail can be gained from this analysis while still obtaining significant and reliable results (e.g. looking at the top and bottom 5% of apparent stress will make median distances based on only 10 events). Even with sample sizes of 40 events, some cases do not show

an ideal spatial gradient in apparent stress (e.g.  $D_{50}L_{20}$  may be farther from the stope than  $D_{50}$  and  $D_{50}H_{50}$ ).

This analysis does not give any indication of the size of the seismogenic zone (e.g. it does not show that 80% of the events lie within some distance of the stope). Rather, it simply indicates that there is variation in apparent stress throughout it. Greater difference between the median distances of higher and lower apparent stress events implies greater variation in stress and confinement conditions through the seismogenic zone. This variation may also scale with the size of the seismogenic zone (i.e. larger excavations may produce larger seismogenic zones with variations in stress conditions occurring over greater distances).

Also note that  $D_{50}H_{80}$  and  $D_{50}L_{20}$  are not used in the determining the end times of each phase. Only three trend lines,  $D_{50}L_{50}$ ,  $D_{50}$ , and  $D_{50}H_{50}$ , are used for that process, as is shown in Figure 4-16.

Spatial variation in apparent stress can be visualized in spatial plots as well. Figure 4-18 shows the locations of the first 200 events in the southeast corner of 1535-275-P1 following the final blast. The events are coloured by apparent stress, and  $AS_{20}$ ,  $AS_{50}$ , and  $AS_{80}$  are used as thresholds to show only events with high or low apparent stress in each view. These thresholds are 6.4, 11.5, and 25.7 kPa respectively.  $\sigma_a < AS_{50}$  events appear to be more densely distributed near the stope than  $\sigma_a > AS_{50}$  events.  $\sigma_a > AS_{80}$  events appear to be distributed farther away from the stope than  $\sigma_a > AS_{50}$  events. However, the  $\sigma_a < AS_{20}$  are not clearly closer to the stope than the  $\sigma_a < AS_{50}$  events. Figure 4-17 shows that the MESDs for these two groups of events,  $D_{50}L_{50}$  and  $D_{50}L_{20}$ , are relatively close (less than 1 m difference), so it is not surprising this variation in a scatterplot is difficult to visually quantify. Although events are located with relatively high accuracy, scatter in their locations makes spatial variations difficult to visualize in spatial plots.

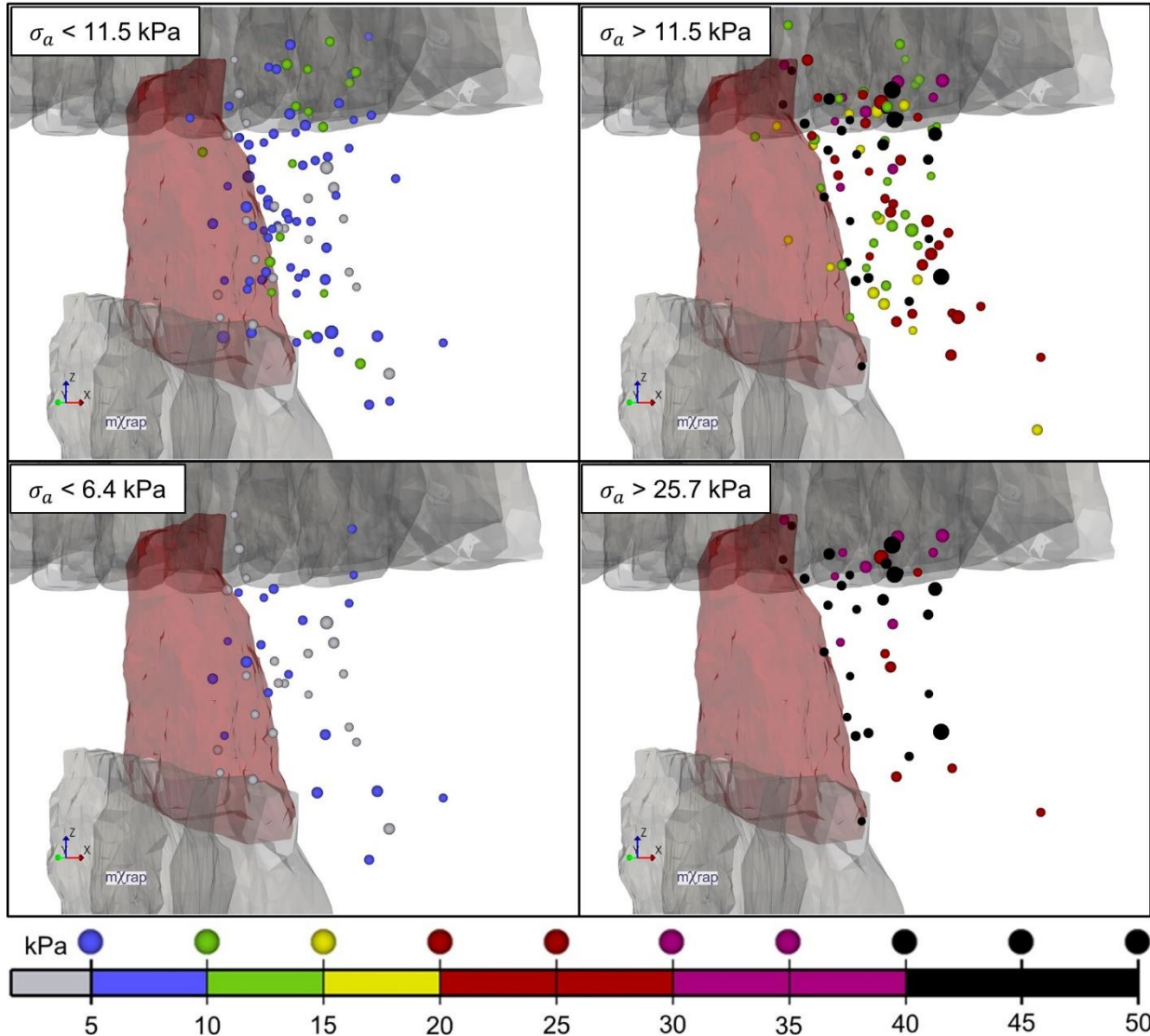


Figure 4-18: Locations of the first 200 events in 1535-275-P1 southeast corner (coloured apparent stress, sized by magnitude) separated by apparent stress

Visualization of spatial variation of apparent stress in spatial plots may be simplified by looking at a uniform slice of the event locations and stopes. The approach projects the mining geometry and seismogenic zone to a two-dimensional plane. Figure 4-19 shows plan views of a 10 m thick horizontal slice centered half way up the height of 1535-275-P1. A horizontal slice was selected because this particular seismogenic zone is interpreted to result from the horizontal major principal stress flowing around the stope. Similar to an approach taken by Abolfazlzadeh and Hudyma (2016) to describe the elevations of events above a sublevel cave, the events in the SE corner of 1535-275-P1 have been divided into four quartiles of event-stope distance (ESD). These quartiles were determined individually for each phase of MESD variation using all the events in the SE

corner volume (i.e. not just the events shown in the 10 m thick horizontal section). The first, second, and third (25%, 50%, and 75% respectively) quartile distances have been approximated around the stope with dashed lines. The boundaries between each quartile are relatively close together (around 2 to 3 m separation). The apparent stress of each event is indicated by a coloured marker. As in Figure 4-18, events with higher apparent stress tend to locate farther from the stope than events with lower apparent stress.

Further analysis of the events in each quartile indicates there is spatial variation in apparent stress throughout the seismogenic zone in each phase. Figure 4-19 shows cumulative distributions of apparent stress in each quartile of ESD for each phase. Note that these distributions are based on all the events in the SE corner, not just the ones shown in the plan views. In each phase, the distributions show that events farther away from the stope tend to have higher apparent stress than those closer to the stope. This analysis corroborates the results of the MESD graphs which show that events with higher apparent stress tend to locate farther away from mined stopes than events with lower apparent stress. The distributions of apparent stress for events in each ESD quartile show an inverse of the same result: events farther away from mined stopes tend to have higher apparent stress than events closer to mined stopes.

Also of interest in Figure 4-19 is that the events with higher apparent stress tend to locate farther to the south in the SE corner. There are several factors that might contribute to higher apparent stress in this part of the volume including:

- A stronger rock mass (closer to FGN hanging wall and farther from high grade copper), allowing for more energy storage.
- The corner of the stope offering more confinement than the sidewall, allowing the rock mass to reach a higher stress before yielding.
- Higher stress concentrations near the corner of the stope, causing yield to occur under higher stress conditions.

Therefore, localized effects within an analysis volume may also affect the spatial distribution of events and variation in apparent stress.

The spatial plots in Figure 4-19 further illustrate the challenge of analysing spatial variations in apparent stress in relatively small seismogenic zones. Variations occur over a scale of only a few

metres, which is difficult to visualize even with high-quality event locations and source parameter estimates. However, the interpretations are significantly aided with the use of graphs which can reveal subtle variations through somewhat scattered data.

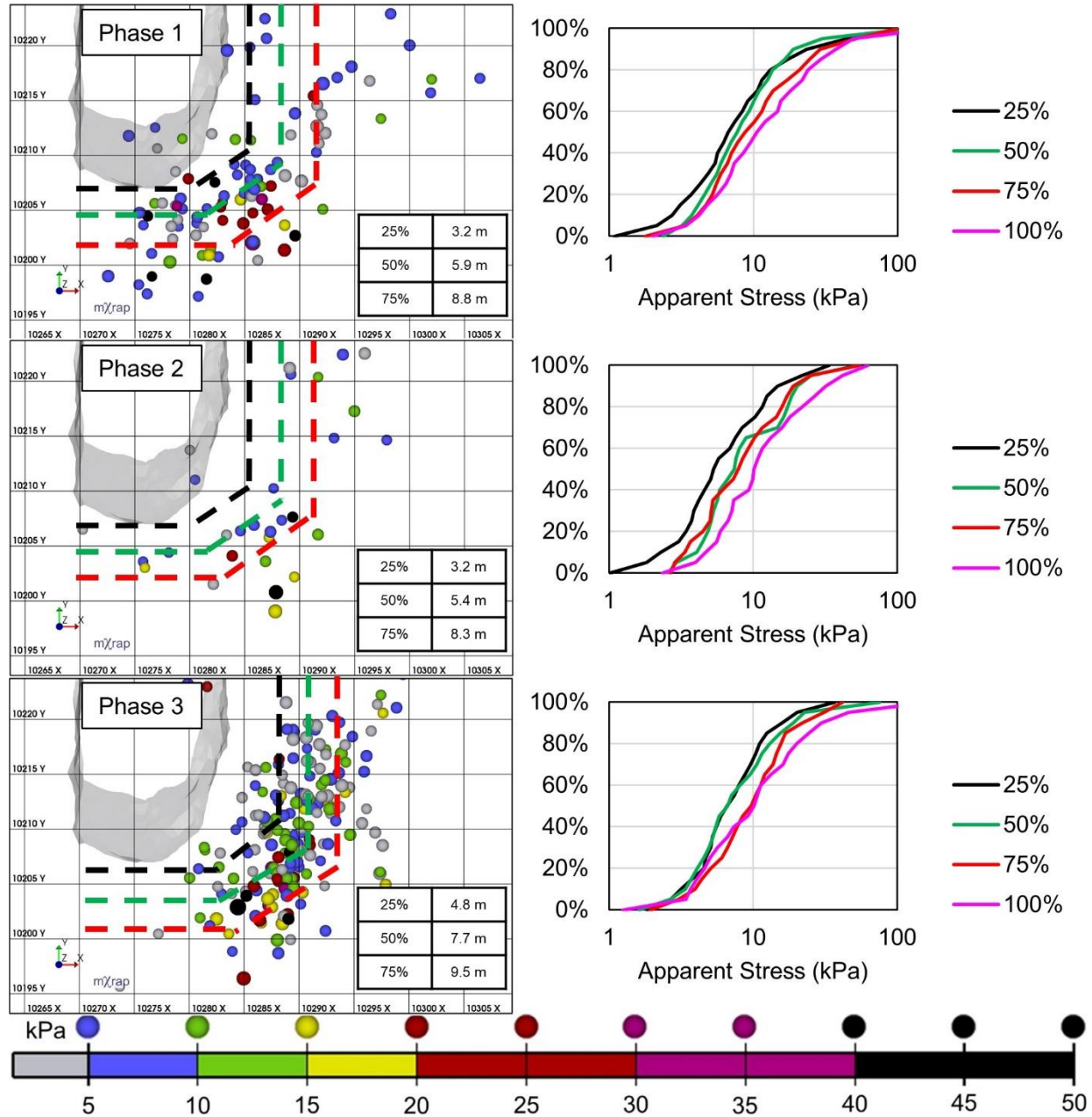


Figure 4-19: Plan view of 10 m thick horizontal section of 1535-275-P1 SE corner showing event locations (coloured by apparent stress) and cumulative distributions of apparent stress in four quartiles of event-stope distances

As discussed earlier in this section, maps and spatial plots of events may not effectively show variations in event locations if the time periods over which variations occur are unknown. Based on the graphs of MESD, relevant snapshots of event locations can now be made based on the

known times of each phase of MESD variation. Knowing the duration of each phase eliminates the need to take snapshots at arbitrary time intervals (e.g. 1-hour increments).

Figure 4-20 shows the locations of events coloured by apparent stress in each phase MESD variation. In each phase there is some spatial variation in apparent stress is visible (events with lower apparent stress closer to the stopes and events with higher apparent stress farther away). This variation is more apparent in Phase 1, and less apparent in phases 2 and 3. The graph shows that the MESDs for high and low apparent stress events are closer together after Phase 1, so logically it is more difficult to see the variation in the spatial plots.

It is also difficult to identify any movement of the events towards the stopes between phases 1 and 2. The graph shows that the MESD moves about 1 m closer to the stopes during Phase 2, so this variation would also be difficult to visualize. In Phase 3, the events are located in a group that is not immediately adjacent to the stopes, but there is still little obvious change from Phase 2. This example highlights the difficulties with using spatial plots or maps to visualize spatial variations that occur over relatively small distances.

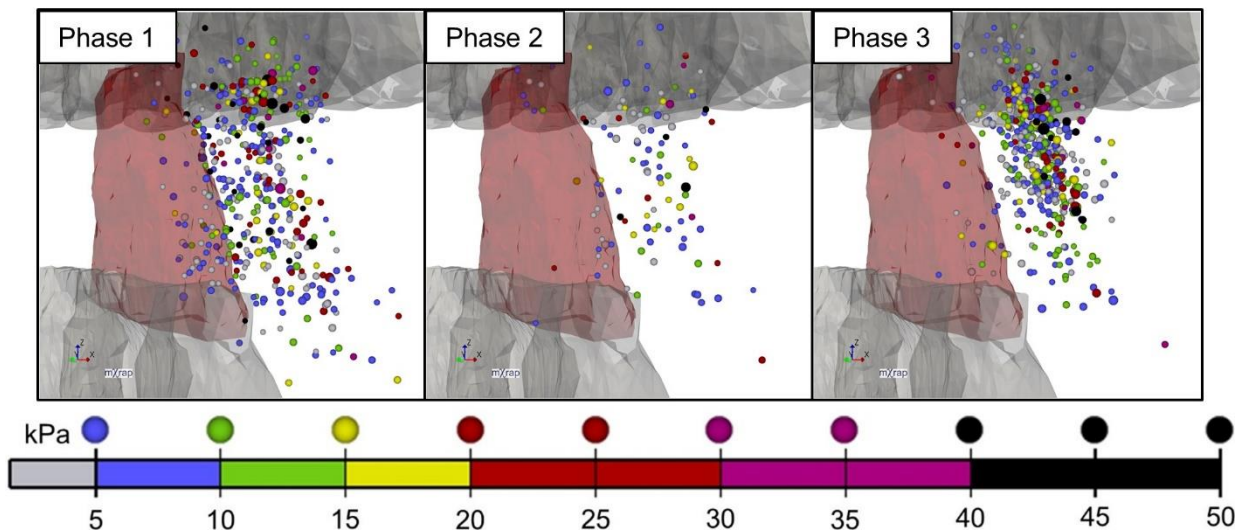
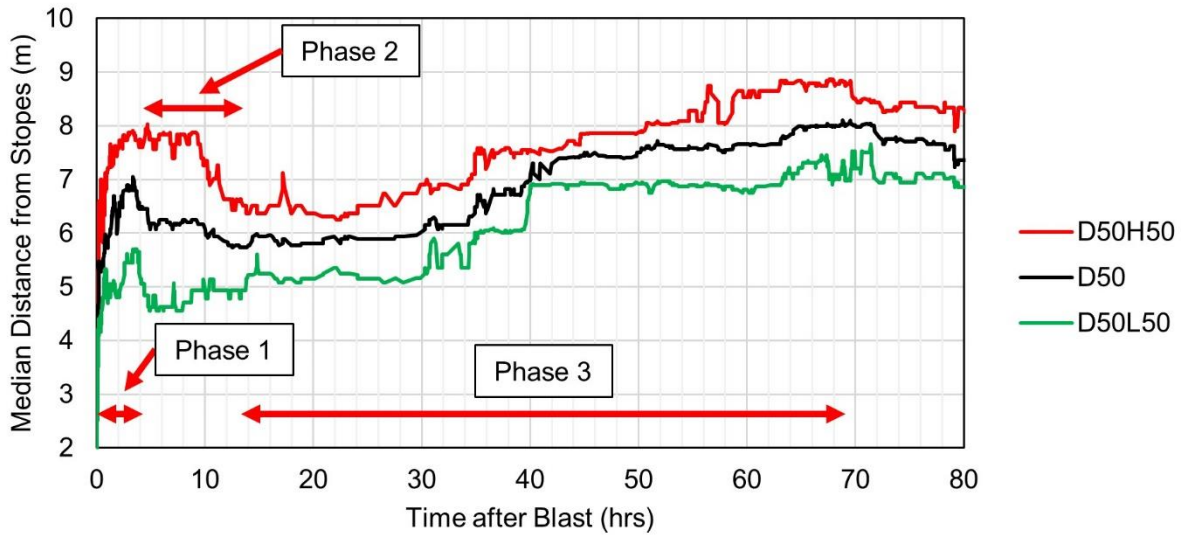


Figure 4-20: Spatial plots of events (coloured by apparent stress, sized by magnitude) occurring in three phases of MESD variation in 1535-275-P1 SE corner

#### 4.2.6 Justification for a Volumetrically Filtered Approach

Similar to how different regions of the rock mass around an open stope can exhibit different patterns in apparent stress variation, they may also exhibit different patterns in MESD variation. As discussed previously, these differences may be caused by the local conditions controlling rock mass yield (geology, stress, mining geometry, etc.) which are reflected in localized groups of seismic events.

Similar to the apparent stress variations in the previous section, the variations in MESD are compared between the SE and NW corners of 1535-275-P1. Several factors that might contribute to different modes of rock mass failure in each of these volumes have been discussed in the

previous section. Figure 4-21 shows the MESD graphs for both volumes. Within each volume, the three phases of event-stope distance variation (each indicated by vertical dashed lines) are present, and events with higher apparent stress tend to locate farther from mined stopes in each of the three phases. However, there are several differences between the observed variations in each volume:

- There are more events in the SE corner.
- Events are farther away from mined stopes in the SE corner.
- Phases occur over longer periods of time in the NW corner.
- MESDs increase more during Phase 3 in the SE corner.
- $D_{50L_{50}}$  varies less through all phases in the NW corner.

In addition to differences in apparent stress variations over time, the two principal seismogenic zones produced by this blast also have different variations in MESD. This example further justifies the need to spatially constrain analysis to observe unique behaviours of different seismogenic zones resulting from the same blast.

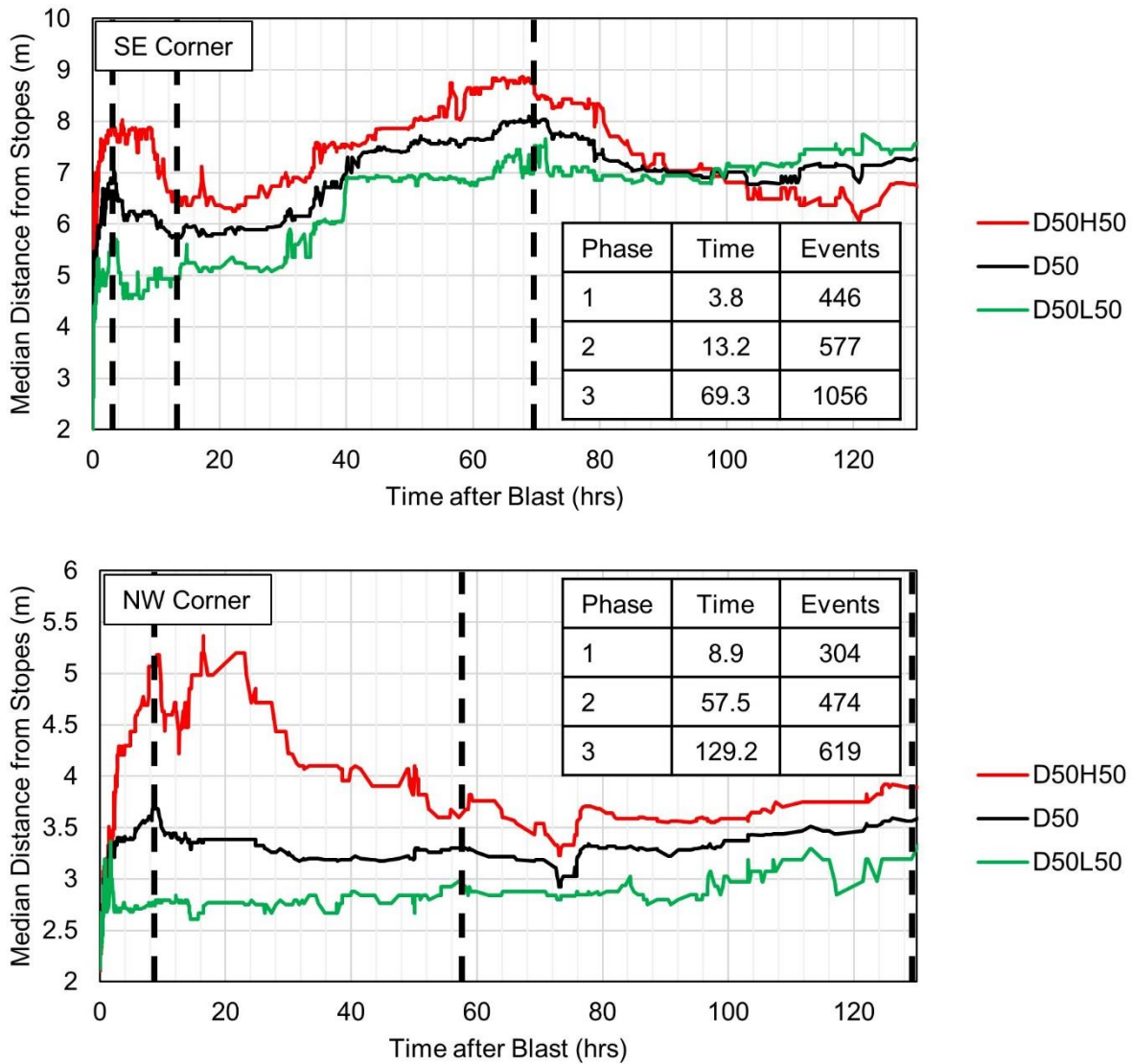


Figure 4-21: Comparison of MESD variation between SE and NW corner of 1535-275-P1 showing end times of phases and number of events in each phase

#### 4.2.7 Multiple Interpretations of Phases of Variation

As with variations in apparent stress over time, there may be multiple interpretations of MESD variations in the same volume. One such case is the SE corner of 1535-300-P1. This stope was mined in early 2014 and was the fourth stope mined in the lower sill pillar after the three 275 stope panels were mined along the centre of the level. Figure 4-22 shows a magnitude-time history and MESD graph for events in the SE corner in the first 40 hours after the blast. There is a short Phase 1 and 2, followed by a relatively longer Phase 3 which ends around 27 hours after the blast.

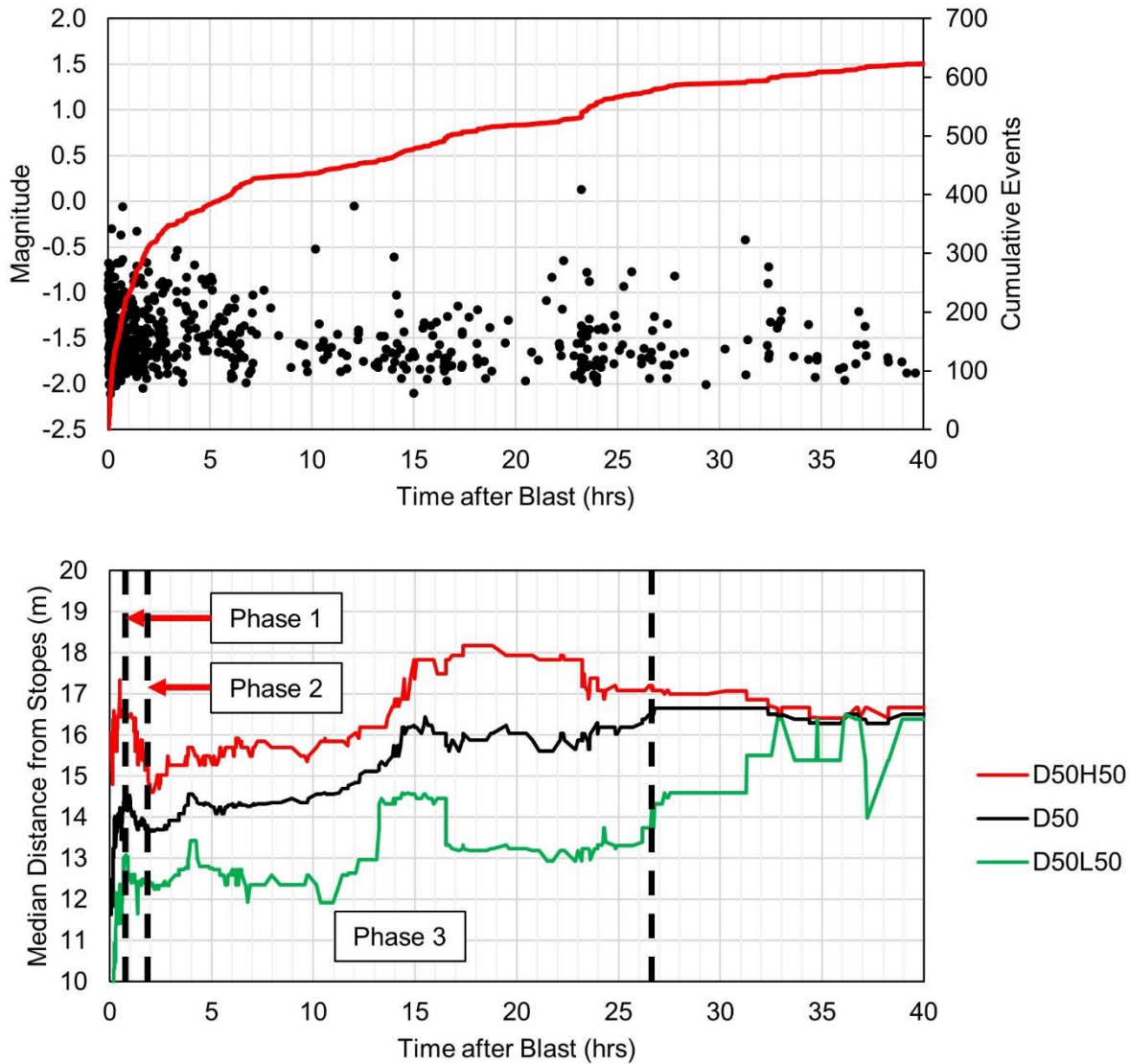


Figure 4-22: Three phases of event-stope distance variation in SE corner of 1535-300-P1 (April 9<sup>th</sup>, 2014) ending 26.8 hours after blast

Figure 4-23 shows a magnitude-time history and MESD graph of events in the same volume over 450 hours after the blast. In this time period, a different possible interpretation is apparent. The variations that defined Phase 1 and 2 in the initial interpretation may be disregarded, and what initially constituted the end of Phase 3 is now considered the end of Phase 1. In the longer-term interpretation, phases 2 and 3 occur over a span of several weeks rather than several hours, ending approximately 190 and 410 hours after the blast respectively. As with the apparent stress variations, both interpretations of MESD variation may be valid. The variations are noticeable in each of the trend lines and occur over several hundred events, so it is difficult to disregard one

interpretation as insignificant. Therefore, both interpretations are recorded for the purposes of analysing results.

As discussed in the previous section, interpreting localized variations in relation to an isolated, local blast becomes increasingly difficult at greater periods of time after that blast. This difficulty is associated with the complex structure of the rock mass and other stress changes occurring throughout the mine may also influence local conditions in the volume being studied. In Figure 4-23, sudden increases in event rate consistent with blasting can be seen in the magnitude time history at approximately 100 and 250 hours after the blast. However, the author believes variations resulting from a local blast some days earlier can still be interpreted throughout these periods because:

1. The number of events in later sudden event rate increases is small compared to the number produced by the blast being studied.
2. The rate of events returns to the rate it was at before the sudden increase relatively quickly.
3. The variation in MESD is relatively small, and the overall longer-term trend is still downwards during Phase 2, and upwards during Phase 3.

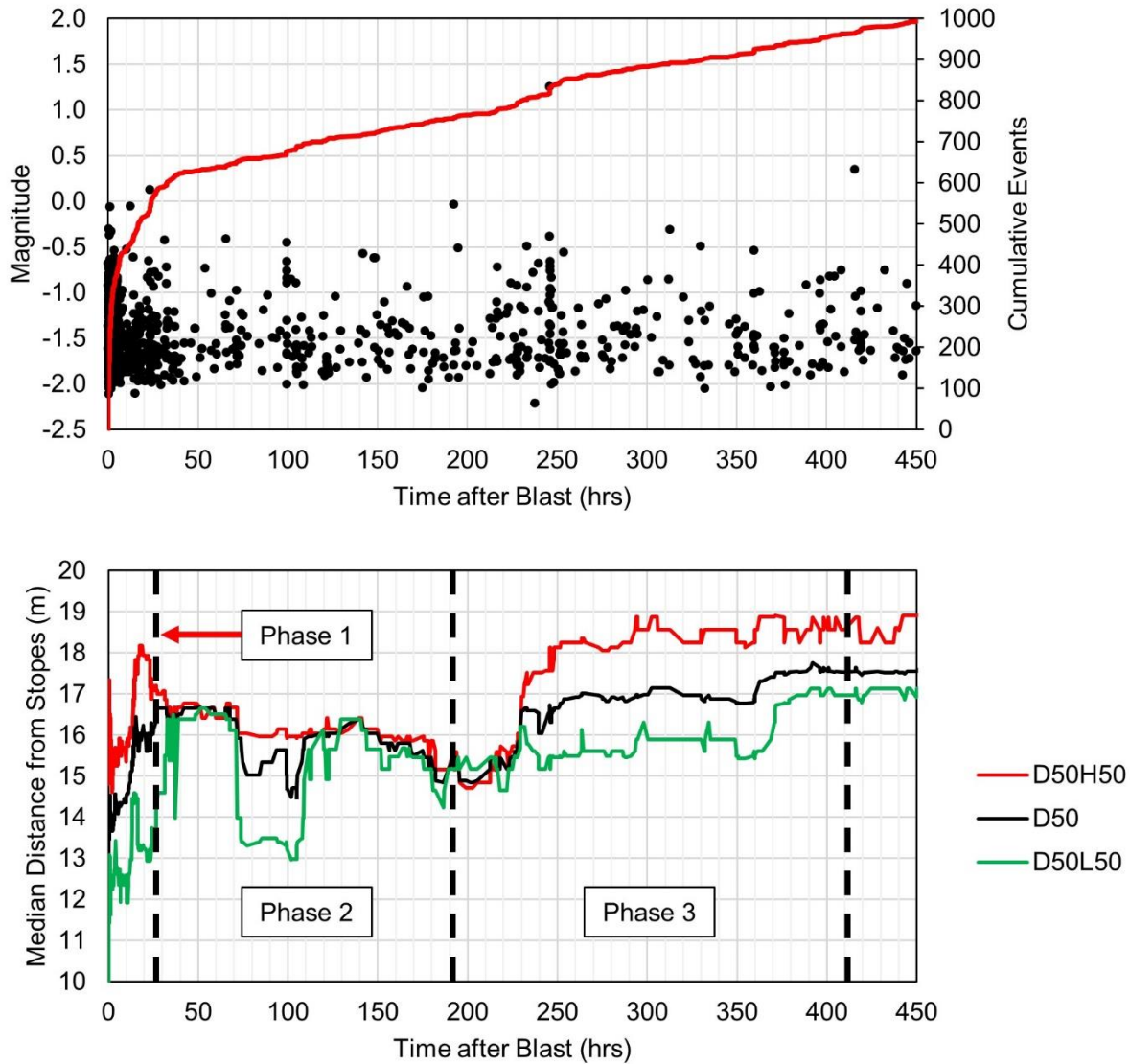


Figure 4-23: Three phases of event-stope distance variation in SE corner of 1535-300-P1 (April 9<sup>th</sup>, 2014) ending 411.7 hours after blast

#### 4.2.8 Coupled Interpretation of Apparent Stress and Event-Stope Distances

Some phases of variation in apparent stress and MESD correspond to similar inferred behaviour:

- Stress redistributing around new/existing openings and damaging the nearby rock mass.
- Rock mass near stopes yielding and losing capacity to store strain energy (i.e. the formation of an excavation damage zone).
- Stress shedding from yielded regions onto more intact regions under higher confinement.
- Growth of an EDZ into the rock mass further from an excavation.

Therefore, it would be logical if the phases of variation each behaviour is inferred from occurred simultaneously. These phases occurring simultaneously would corroborate the inferences drawn from each.

Recall the apparent stress variations in 1535-275-P1 SE corner which were presented in Chapter 4.1. The interpretation of Phase 3 was somewhat ambiguous because there was a drop in  $AS_{20}$ ,  $AS_{50}$ , and  $AS_{80}$  around 40 hours after the blast, but the percentiles begin to rise to a higher peak shortly after the short-lived drop. The apparent stress graph has been redrawn in Figure 4-24. This time, it is shown alongside the MESD graph. Phase 3 of MESD variation occurs from around 12 to 70 hours after the blast. The events continue to move away from the mined-out stopes when apparent stress drops at 40 hours. Based on the MESD graph, it is inferred that the EDZ is growing into what was previously less damaged ground during this time. Accordingly, events with elevated apparent stress are expected during this time as seismicity is occurring in what is supposedly more intact ground under higher confinement. Based on the coupled interpretation of MESD and apparent stress, Phase 3 in both graphs continues through this time period. Therefore, the drop in apparent stress at 40 hours is ignored for the purposes of this interpretation, and Phase 3 in apparent stress variation is considered to continue through this time period.

Also of interest in this example is that at the same time apparent stress drops at 40 hours, the events with lower apparent stress ( $D_{50}L_{50}$ ) suddenly move farther away from the stope. This behaviour suggests that the rock mass is yielding farther away from the stopes (i.e. the EDZ is growing). The low apparent stress events appear to be occurring in the recently yielded zone of the rock mass. This effect may be a result of sudden growth of the EDZ and further migration of the seismogenic zone. This example also highlights how maintaining consistent, gradual changes at greater lengths of time after a blast relies on consistent rock mass properties and the absence of sudden stress changes. Such requirements are increasingly difficult to meet with time in a naturally homogenous material subjected to some degree of human interference on a daily basis.

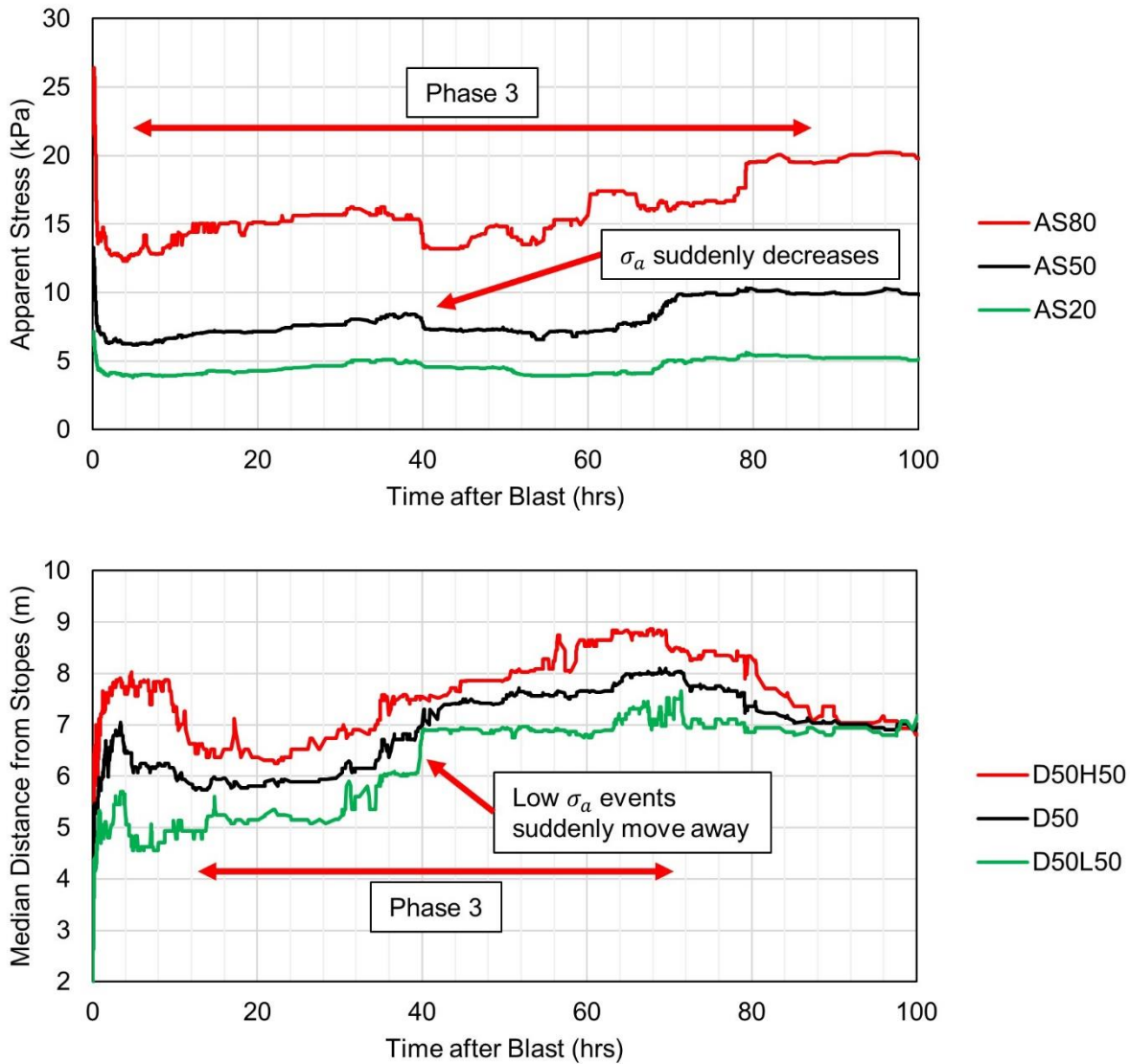


Figure 4-24: Apparent stress and MESD variation in 1535-275-P1 SE corner

Based on the coupled interpretation of apparent stress and MESD, cases with multiple interpretations for variations can be paired together. For example, an interpretation of apparent stress variations occurring over longer periods would correspond with an interpretation of MESD variations that also occur over a longer period of time. Such pairing is logical because the phases of apparent stress and MESD variation are assumed to be a result of a related processes of rock mass yield, and therefore should occur over similar time periods.

### 4.3 Selection of Cases and Compilation of Results

This thesis draws from case histories throughout NRSM between 2011 and late-2017. All cases are taken from individual spatially constrained areas of the rock mass that became seismically active immediately following a final blast. The objective was to find cases with the greatest quantity of available data (i.e. number of seismic events). With this approach, each case may have more potentially useful information to analyse. Event size and variations in microseismic array sensitivity throughout the mine were not considered in the selection of case histories. Accordingly, some cases are composed of large quantities of smaller events and few larger events (e.g. from a more sensitive part of the array), and some cases are composed of large quantities of larger events and fewer small events (e.g. from a less sensitive part of the array).

Initially, 79 blasts were considered for analysis based on the total number of events occurring within 2 sublevels (60 m) of the stope up to 24 hours after the blast. This approach was intended to consider a large area around the stope that might have become seismically active following the blast, and determine which blasts provided the more potentially useful data. Seismic responses following each blast were separated into spatially constrained volumes as per the typical seismic responses presented in Chapter 3.5.

From the 79 blasts initially considered, 162 volumes were created. In order to reduce the amount of cases to more manageable quantity for detailed analysis, only volumes containing at least 400 events in the month after the blast were retained. This reduction resulted in 85 volumes from 59 different final blasts being analysed. In each of these 89 volumes, variations in apparent stress were observed following the blast and interpreted into three phases of variation.

Only the 50 volumes with the greatest number of events across all three phases of apparent stress variation were retained in the results. The number of events in phases of MESD variations were not considered, as these variations were often more difficult to interpret in terms of the proposed three-phase model.

Twelve of the 50 cases had two interpretations for the phases of apparent stress variation. Five of these 12 also had two interpretations for the phases of MESD variation. The total number of interpretations is 62 across 50 volumes from 40 different final blasts.

## 5 Results

### 5.1 Selected Cases

This section summarizes the locations and times of the blasts, analysis volumes, and interpretations of variations from which results were obtained. Cases were not obtained from stope blasts in a specific area of the mine. However, stopes in certain parts of the mine which were extracted during certain time periods produced larger seismic responses than others, which led them to produce case histories that were selected over others. The larger seismic responses, measured by the total number of recorded events, result from a combination of stress, geology, mining sequence, and microseismic array sensitivity.

A total of 50 cases were analysed, resulting in 62 interpretations of apparent stress and MESD variation. This section summarizes the stope blasts (stopes) which resulted in one or more volumetrically isolated case studies. Each of those spatially-filtered case studies were analysed and resulted in one or more interpretations of apparent stress and MESD variation.

Figure 5-1 shows the time periods from which cases were selected. The years 2014 through 2016 produced more case histories than the other years. These years corresponded with significant amounts of primary stope extraction below and in the 1535 sill pillar which began in 2013, and the start of primary stope extraction in the 1355 sill pillar which began in 2015.

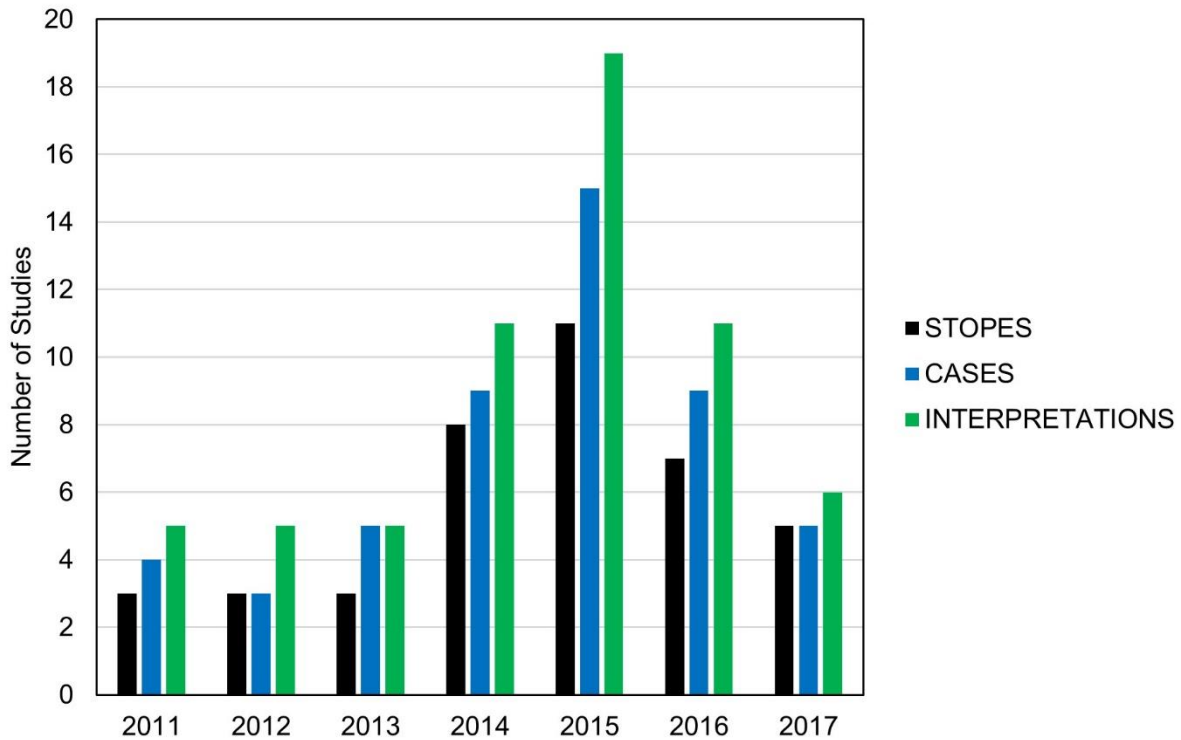


Figure 5-1: Number of stopes, cases, and interpretations by year

Figure 5-2 shows number of cases taken from each mine level. Cases primarily come from the lower part of the mine, where stopes are located in the footwall copper zone. Many cases come from stopes in the 1535 sill pillar and the levels immediately below it, 1565 and 1595. Primary stope mining in these locations corresponds with the dates for most of the cases. Primary extraction of 1535 started in 2013 and was near completion in 2017. Relatively few cases were obtained from the upper part of the mine, where stopes are located in the contact nickel zone. Extraction of this area commenced earlier in the mine life, so the majority of stopes mined in 2011 and later were secondaries and tertiaries which generally exhibit much smaller seismic responses than primary stopes. The microseismic array also has lower sensitivity in the upper part of the mine, leading to fewer small events being recorded and fewer attractive case studies being present.

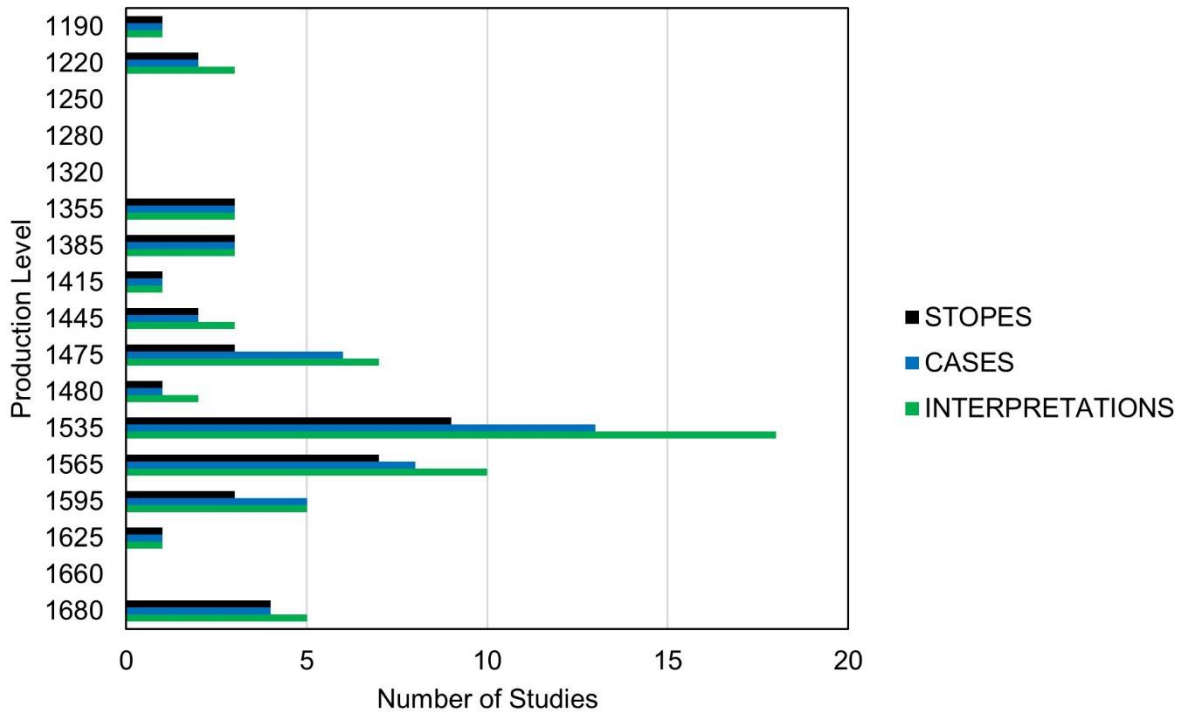


Figure 5-2: Number of stopes, cases, and interpretations by mine level

Figure 5-3 shows the number of cases by easting (stope access number). The majority of cases come from primary stopes (200, 225, 250, 275, 300, and 325). These stopes are intended to push stresses outwards and generate yielding pillars, so they are expected to generate larger seismic responses. Some cases were also generated by pillarless stopes in abutments (212 and 337), and the remainder were generated by secondary or tertiary stopes. The cases tend to come from the west side of the orebody. The microseismic array has higher sensitivity in this area, so more events are recorded which leads to more attractive cases.

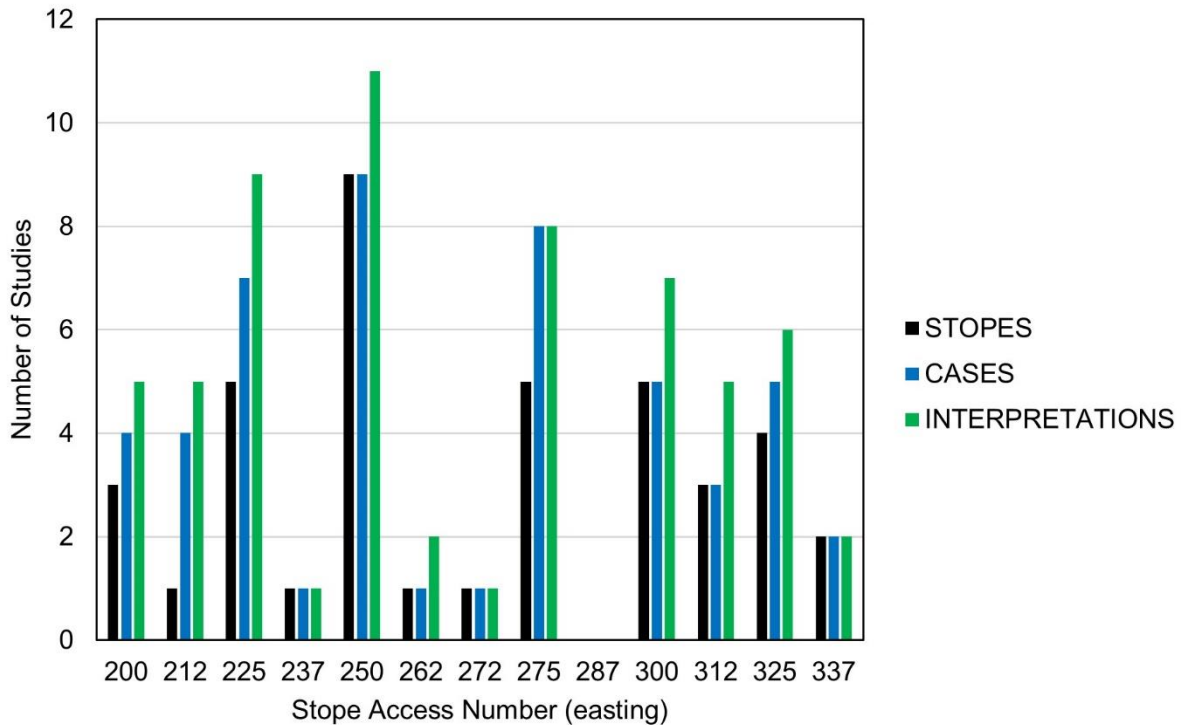


Figure 5-3: Number of stopes, cases, and interpretations by easting. Note that 272 corresponds to a line of tertiary stopes in the upper part of the mine only

Figure 5-4 summarizes the number of each type of seismic response (as discussed in Chapter 3.5) in the selected case histories. The majority of cases are immediately adjacent to an open stope (corners, sidewalls, pillars) rather than closer to previously mined stopes. A large number of cases are responses in the west sidewall. West sidewall responses are more common in the west side of the orebody due to the centre-out sequence. East sidewall cases are less abundant because the horseshoe shape of the orebody and orientation of the major principal stress trends to generate a SE corner response in the more easterly stopes. The higher microseismic array sensitivity in the western half of the orebody also contributes to the greater number of west sidewall responses.

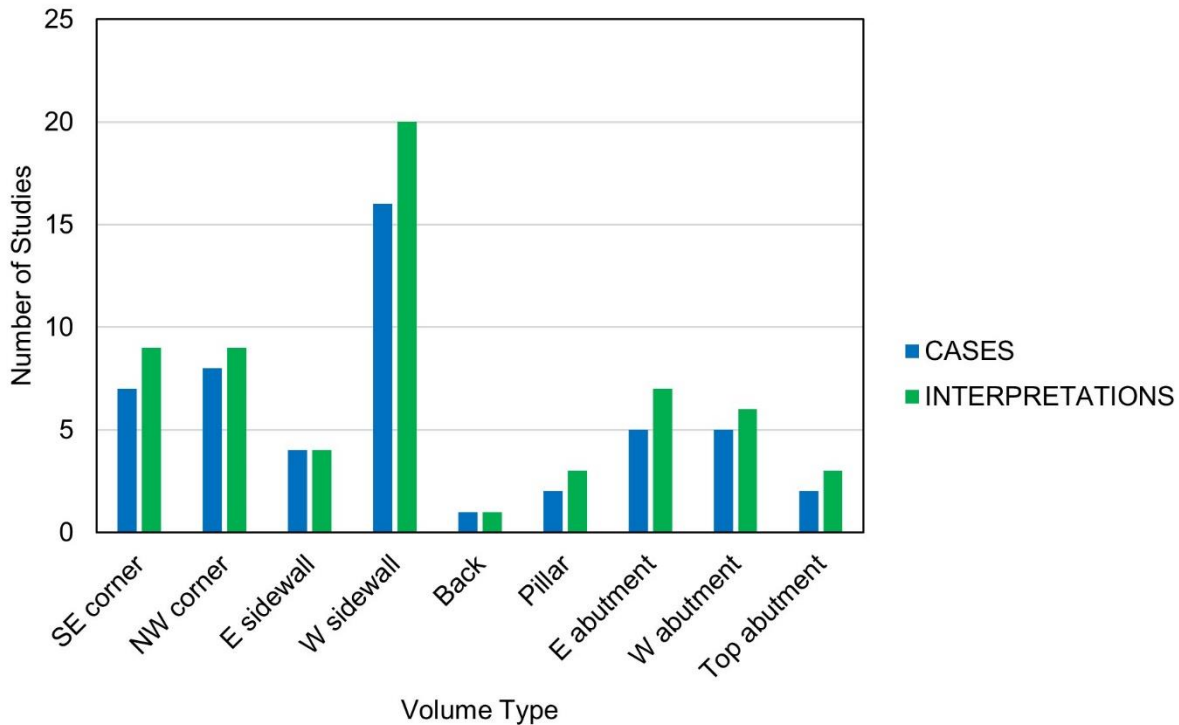


Figure 5-4: Number of cases and interpretations by type of seismic response

Figure 5-5 shows the distribution of final blast tonnages from the selected cases. The blasts that generated attractive case histories were slightly larger than most final blasts taken during the same time period but were not necessarily the largest blasts throughout the mine. Secondary stopes are slightly larger than primaries, so the distribution of final blast tonnages for the selected cases is also compared to primary stope final blasts in the middle and lower parts of the mine. The upper mine was excluded because primaries in the primary-secondary-tertiary sequences are slightly wider and the majority of cases came from primary stopes in the middle and lower mine. Again, the blasts that generated attractive case studies were slightly larger. However, the case history final blasts tend to be only 1,000 to 2,000 tonnes larger than a typical primary stope final blast. These differences correspond with the selected blasts being approximately 2 m longer across strike. Two metres is less than 10% variation from a typical stope length, so the apparent larger size of the case history final blasts may be purely coincidental.

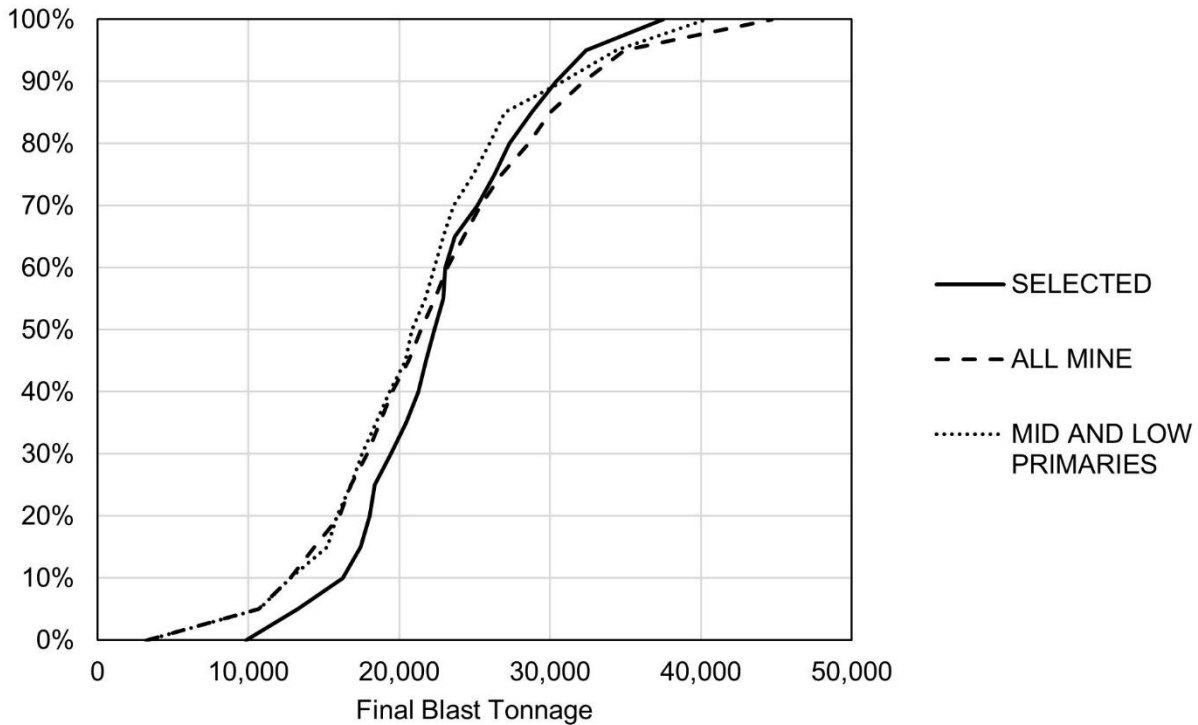


Figure 5-5: Distribution of final blast tonnages in selected cases compared to the tonnages of other final blasts taken in 2011 and later

## 5.2 Variations in Apparent Stress

### 5.2.1 Durations of Phases

The three phases of apparent stress variation over time occur over significantly different time scales. A distribution of the duration of each phase is shown in Figure 5-6. Phase 1 generally covers shorter periods of time, and Phase 3 generally covers longer periods of time. There is more than an order of magnitude of difference in duration from one phase to the next. Events occur more slowly over time, so it is logical that it might take longer for a change in the trend line to occur (i.e. filling the moving window with new events will take longer when the rate of events is slower). Based on the typical durations of each phase, it is inferred that:

- The rock mass can only maintain the stress increase produced by the blast for a matter of minutes before it begins to yield (Phase 1).
- Yield typically occurs over a matter of hours after a blast but may continue to occur for up to a day (Phase 2).

- Stress redistribution into more intact/confined ground and growth of the EDZ usually occurs over a period of at least a day but may continue for up to a month after the blast (Phase 3).

Phase 3 usually lasts longer than 12 hours. Development blasts are taken at the end of every shift, and one or two stope blasts are usually taken each week. Therefore, Phase 3 frequently overlaps with times that blasts are taken elsewhere in the mine at varying distances from the filter volume. The distance between a final blast and other blasts in the next month is typically more than 25 m for development blasts and more than 60 m for blasts in other stopes.

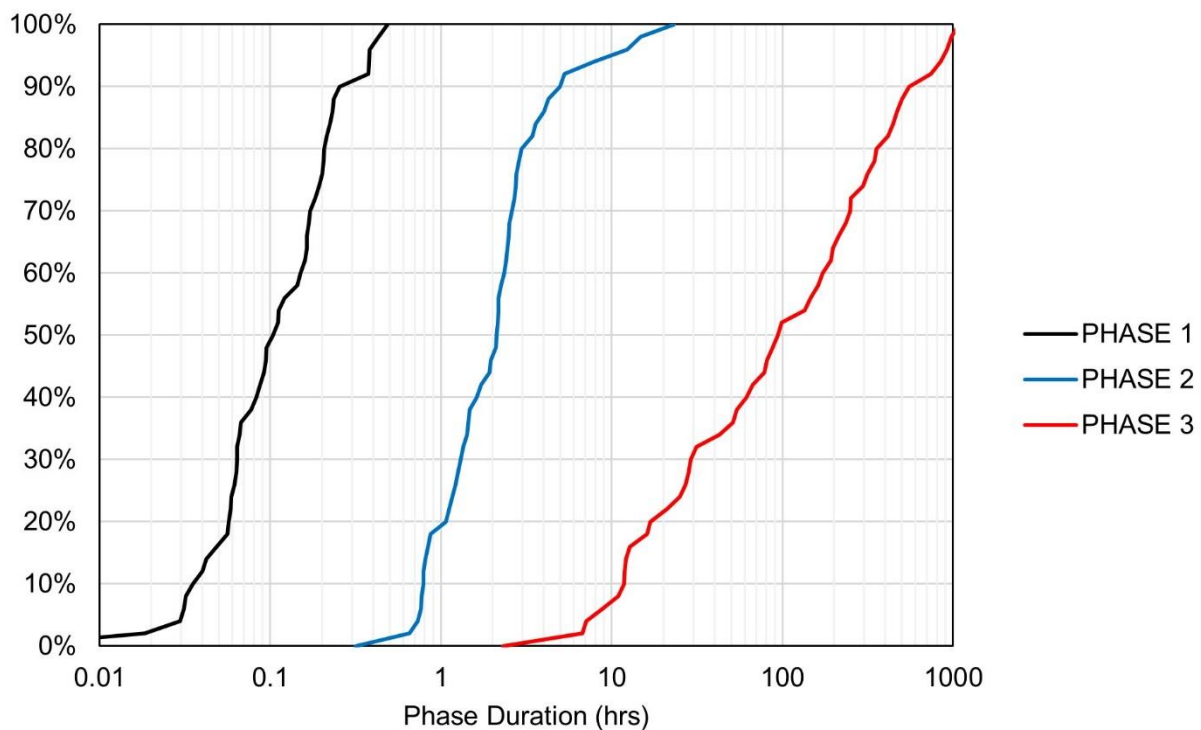


Figure 5-6: Distributions of phase durations for apparent stress variations

Figure 5-7 shows distributions of ratios of durations of each phase. Each phase is consistently longer than the last, often by an order of magnitude or more. This result suggests that there is some sort of proportionality that is maintained between the duration of each phase. It would be uncommon for there to be two or three phases with roughly equal durations.

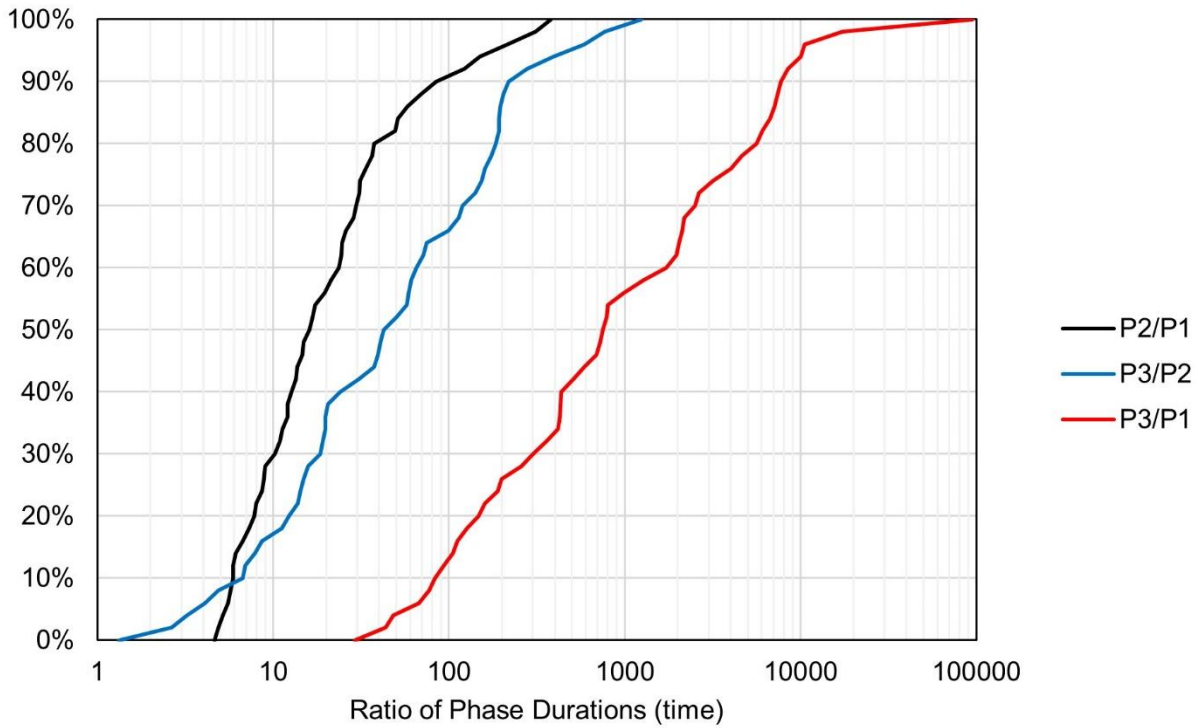


Figure 5-7: Distributions of ratios of phase durations for apparent stress variations

Figure 5-8 shows the distribution of the number of events in each phase. There are usually at least 100 events in each phase. There are often fewer than 100 events in Phase 1, which also occurs over a matter of minutes. However, the variations during Phase 1 are still clear. Similar numbers of events occur in Phase 2 and 3 despite Phase 3 covering a significantly longer period of time. Phases 2 and 3 often had more than 200 events in them, so the variations in these phases are quite clear.

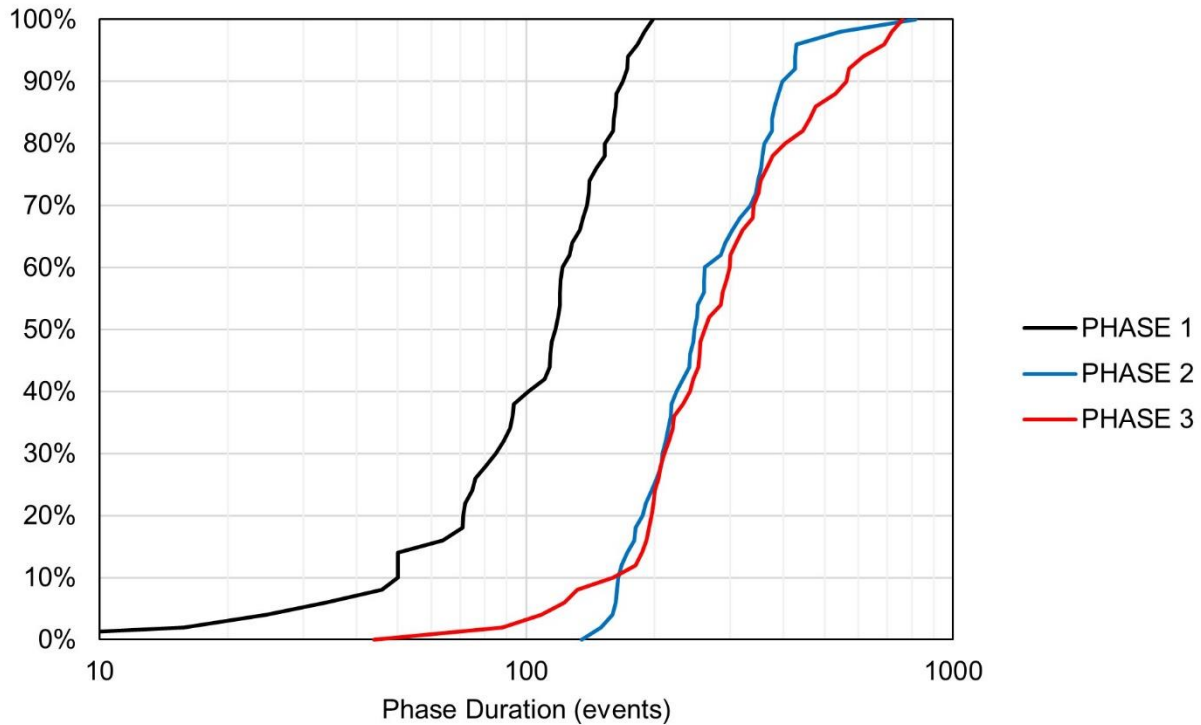


Figure 5-8: Distributions of the number of events in each phase of apparent stress variation

Figure 5-9 shows distributions of ratios of the number of events in one phase to a previous phase. In almost all cases, there are more events in phases 2 and 3 than Phase 1. Phases 2 and 3 usually have at least twice as many events as Phase 1. Phases 2 and 3 will often have a similar number of events (usually within 20%). More than half the events occurring within a few hours of the blast have lower apparent stress than events occurring immediately after the blast. If the events occurring within a few hours of the blasts are analysed in bulk (i.e. grouping all the events together and not accounting for the short variation that constitutes Phase 1), analysis may indicate an overall decrease in apparent stress. The quantity of events in each phase indicating increasing or decreasing apparent stress highlights the importance of accounting for variations which may occur over only several minutes.

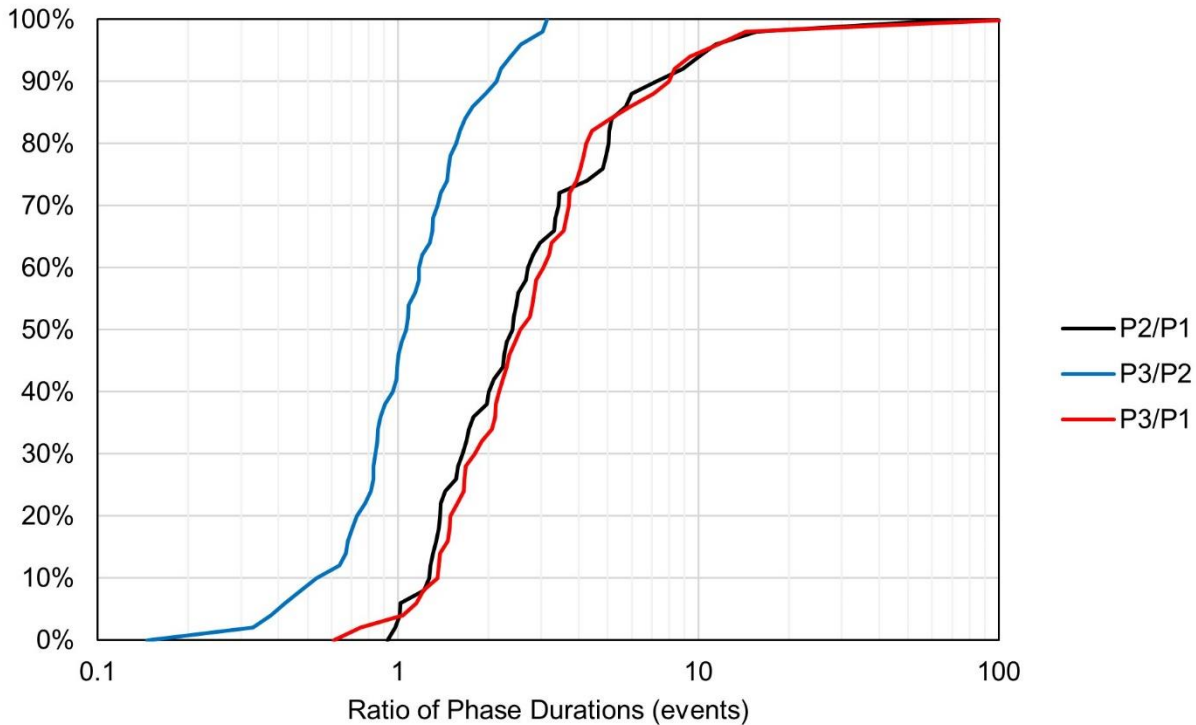


Figure 5-9: Distributions of ratios of numbers of events in each phase of apparent stress variation

### 5.2.2 Magnitude of Variations

This section presents the results of changes in apparent stress during each phase of variation with regard to increases and decreases in  $AS_{20}$ ,  $AS_{50}$ , and  $AS_{80}$ .

Figure 5-10 shows the percentage change in apparent stress observed during Phase 1.  $AS_{20}$ ,  $AS_{50}$ , and  $AS_{80}$  will typically increase by approximately 20% relative to their levels just before the final blast. Although the magnitude of increases in each percentile fall roughly within the same range, the distribution does not necessarily translate upwards and maintain the same variance. ASR may increase or decrease by approximately 20%, indicating that  $AS_{80}$  may move more or less than  $AS_{20}$  or vice versa. This result highlights the importance of considering multiple parts of the distribution in order to study more detailed aspects of how it changes over time.

It should be noted that Phase 1 included fewer than 200 events in all of the analyzed cases. Based on the behaviour exhibited by different moving window sizes demonstrated in Chapter 4, a shorter window might show a larger variation. Nevertheless, the variations during Phase 1 are still apparent with a 200-event window.

Note that some changes in individual trend lines may not correspond with the overall characterization of the phase (e.g. a decrease during Phase 1). Such results are caused by the methodology by which phases are defined (based on an average time of extreme values in multiple trend lines). The end times of each phase do not necessarily correspond with the times that any individual trend line is at its peak, resulting in this apparently contrary behaviour. For example, AS<sub>20</sub> may peak and start decreasing before the other trend lines. Based on the average peak time of all the trend lines, it may appear as if AS<sub>20</sub> decreased during Phase 1. Such effects are simply accepted as artefacts of the methodology.

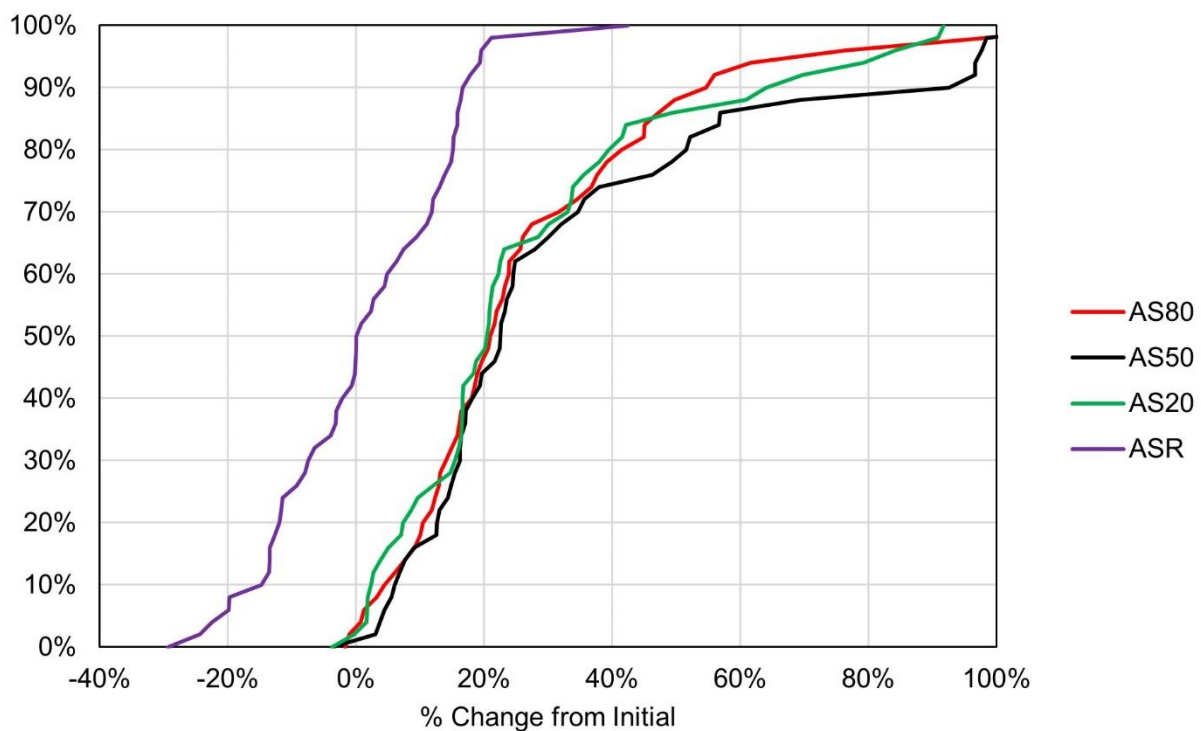


Figure 5-10: Distributions of percentage change in apparent stress observed during Phase 1 (relative to just before the final blast)

Figure 5-11 shows the percentage change in apparent stress observed between the end of Phase 1 and Phase 2. AS<sub>80</sub> will typically drop more than AS<sub>50</sub>, and AS<sub>50</sub> will typically drop more than AS<sub>20</sub>. These tendencies are reflected in ASR, which also tends to decrease during Phase 2.

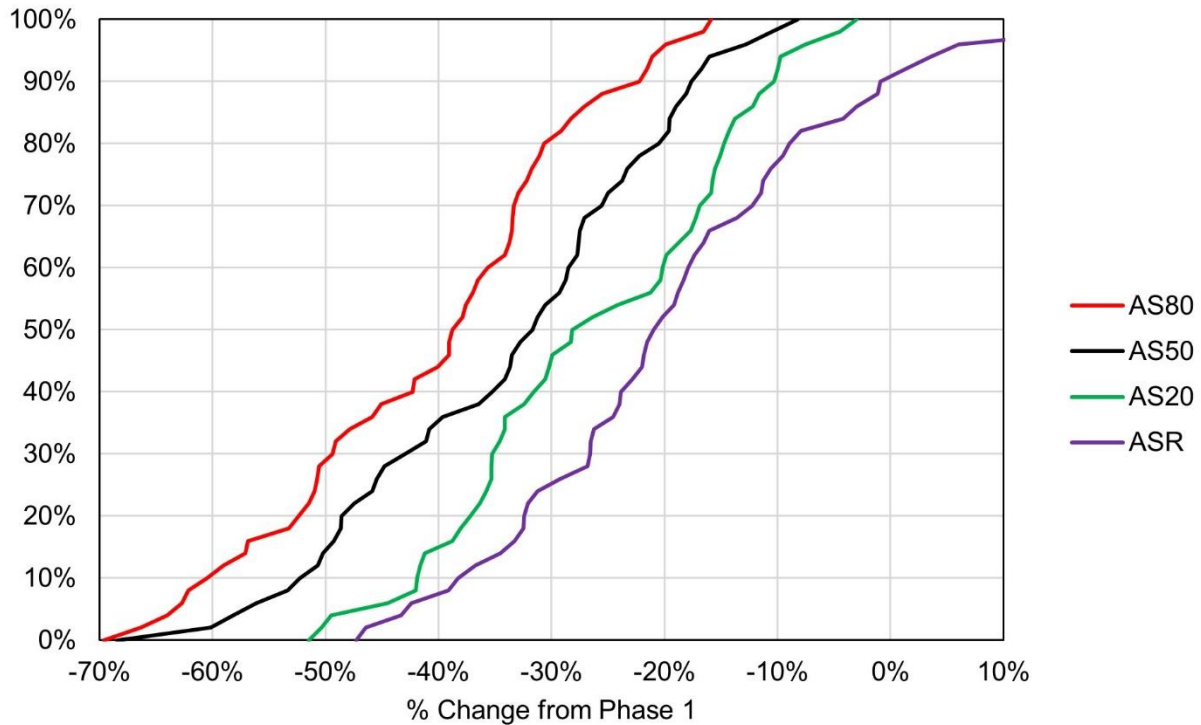


Figure 5-11: Distributions of percentage change in apparent stress observed during Phase 2 (relative to the end of Phase 1)

Figure 5-12 shows the percentage change in apparent stress at the end of Phase 2 relative to its level just before the final blast. By the end of Phase 2, the majority of the distribution usually lies below the initial level. Based on this behaviour, it can be inferred that seismic events are occurring under lower stress conditions at the end of Phase 2 than they were before a new, large excavation was created nearby. AS<sub>80</sub> tends to be farther below its initial level than AS<sub>50</sub>, and AS<sub>50</sub> tends to be farther below its initial level than AS<sub>20</sub>. As with the changes from the end of Phase 1 to Phase 2, these tendencies are also reflected in ASR which also tends to be below its initial levels. In around 35% of cases, AS<sub>20</sub> is above its initial levels at the end of Phase 2. In these cases, the final blast may have caused an upward shift in the lower end of the distribution that is more maintained throughout Phase 2 than the shift in the higher parts of the distribution.

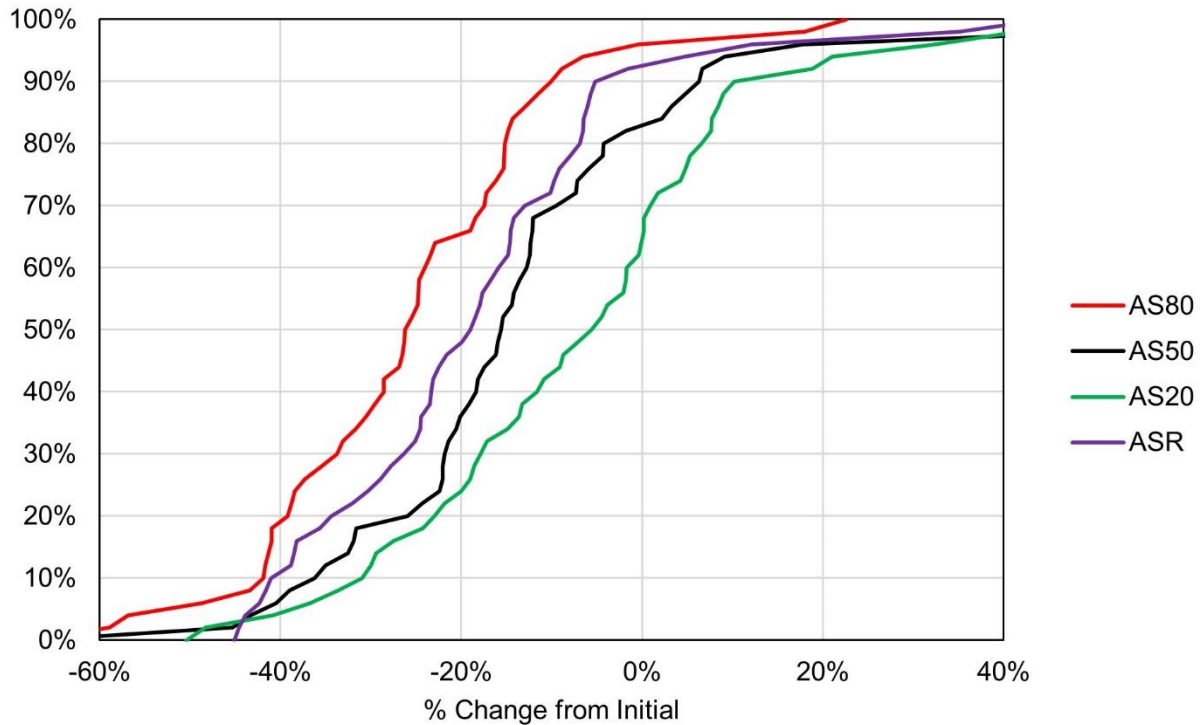


Figure 5-12: Distributions of percentage change in apparent stress observed during Phase 2 (relative to just before the final blast)

Figure 5-13 shows the percentage change in apparent stress observed between the end of Phase 2 and Phase 3. AS<sub>50</sub> tends to increase more than AS<sub>20</sub>, and AS<sub>80</sub> tends to increase more than AS<sub>50</sub>. The ASR shows that the variance of the distribution tends to increase, as there is a larger separation between AS<sub>80</sub> and AS<sub>20</sub>. However, ASR occasionally decreases during Phase 3, indicating that AS<sub>20</sub> may occasionally increase more than AS<sub>80</sub>.

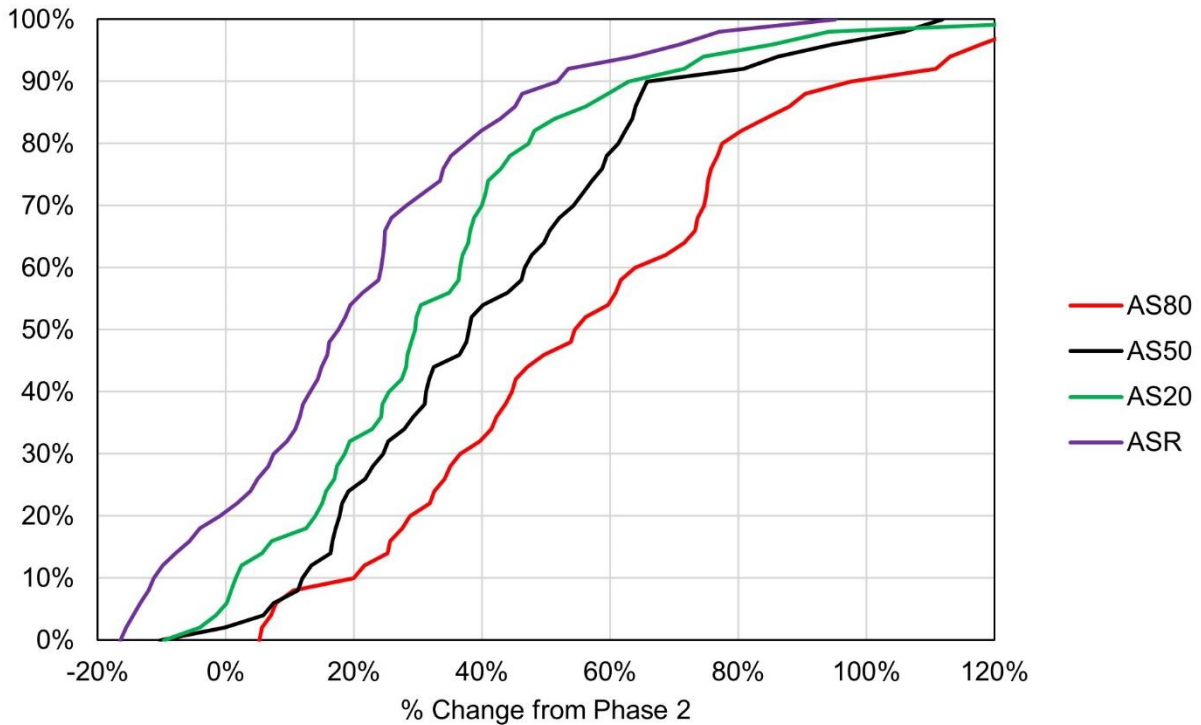


Figure 5-13: Distributions of percentage change in apparent stress observed during Phase 3 (relative to the end of Phase 2)

Figure 5-14 shows the percentage change in apparent stress at the end of Phase 3 relative to its level just before the final blast. AS<sub>20</sub>, AS<sub>50</sub>, and AS<sub>80</sub> all tend to be above their initial levels, indicating an increase in apparent stress as a result of the blast. AS<sub>20</sub> and AS<sub>50</sub> will increase slightly more often than AS<sub>80</sub>. As a result, ASR is usually lower than its initial levels. The variations in AS<sub>20</sub>, AS<sub>50</sub>, and AS<sub>80</sub> are less consistent with each other during Phase 3 than the first two phases.

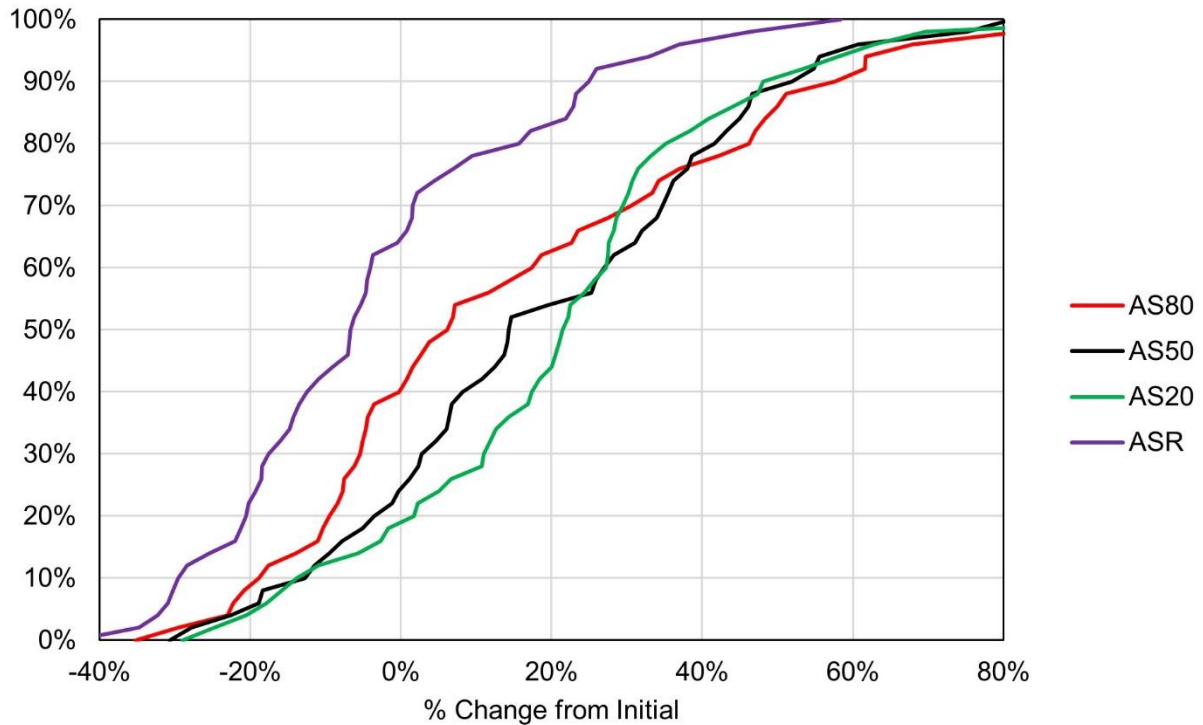


Figure 5-14: Distributions of percentage change in apparent stress observed during Phase 3 (relative to just before the final blast)

Figure 5-15 shows scatter plots of the number of events in each phase versus the change in apparent stress from one phase to the next. More events in a phase corresponds with a greater variation in apparent stress during that phase. In Phase 1, this result may be an artefact of the number of events in the moving window being greater than the number of events in the phase. The number of events in phases 2 and 3 was often greater than the size of the window. In these phases, the results indicate that a larger seismic response (measured by the number of events) corresponds with a greater change in the distribution of apparent stress. Consequently, it can be inferred that larger seismic responses are associated with greater changes in the state of stress in a rock mass. However, it should be noted that different sensitivities are not accounted for in the analysis. Cases with greater numbers of events may correspond with areas and times where and when the array has greater sensitivity. The detection of smaller events may lead to greater variations in apparent stress due to the parameter being scale-dependent (i.e. higher sensitivity leads to greater range in event sizes, greater ranges in apparent stress, and more events recorded overall).

Also of note is that there are a range of observed variations and numbers of events in each phase. Although the statistical significance of variations is not analysed in this thesis, it is important to note that smaller variations that occur over fewer numbers of events are less likely to be significant.

There are two cases where the observed change in apparent stress during Phase 2 does not align with the general trend of observed change versus number of events. These two cases have been indicated on the middle graph in Figure 5-15. In both of these cases, one of the interpretations of Phase 2 involved a longer-term drop during which there was an increase in apparent stress which was interpreted as a relatively insignificant variation within an overall longer-term Phase 2 with a larger variation. One of these cases was exemplified Figure 4-11. The disparity between these and the remainder of these cases suggests that those Phase 2's may have been incorrectly interpreted. The interpretations with shorter Phase 2's that do not disregard the increase in apparent stress might be more valid interpretations of these cases, in that the number of events is more proportional to the observed change in apparent stress.

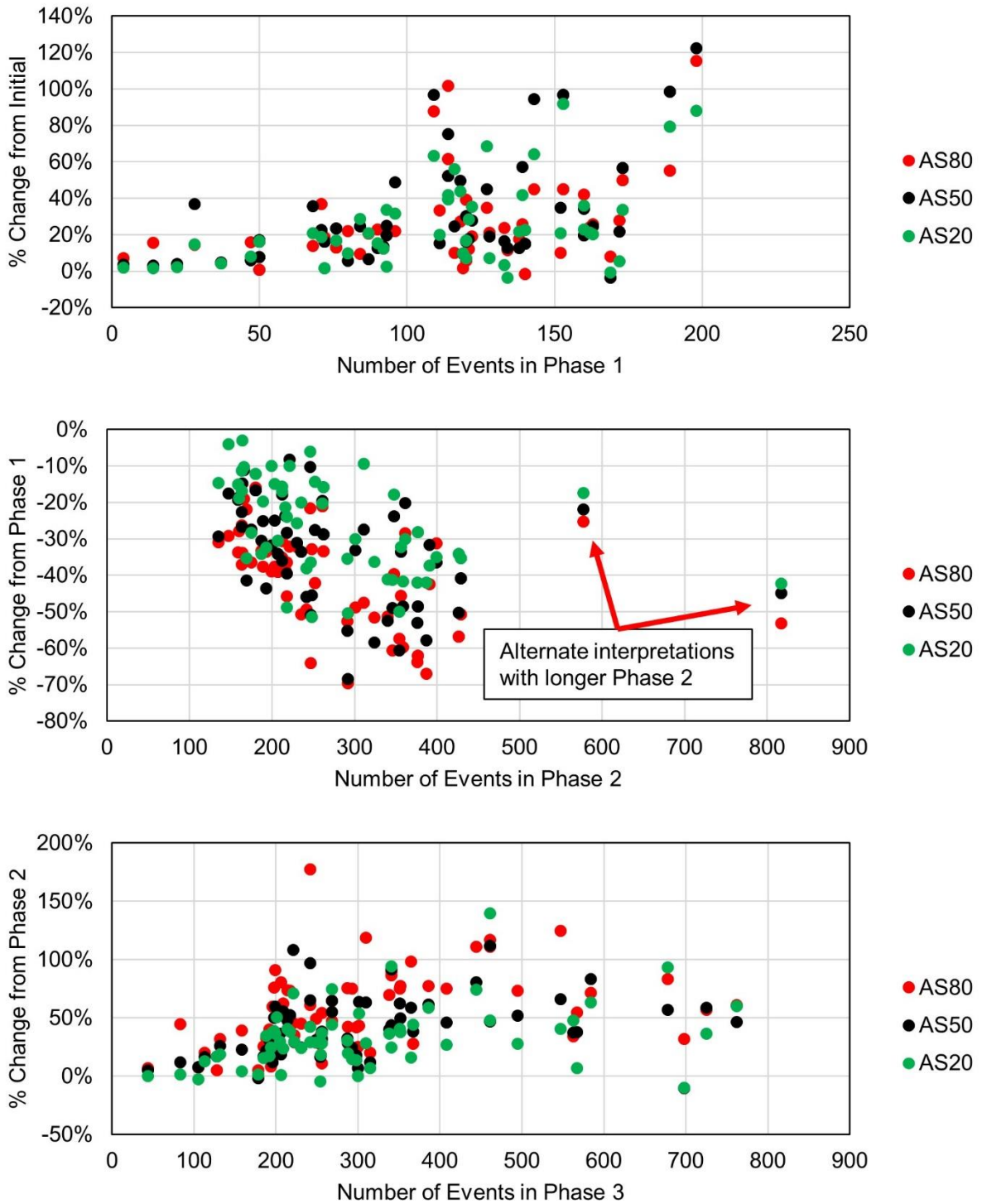


Figure 5-15: Percentage change in apparent stress from one phase to the next versus the number of events in that phase

### 5.2.3 Summary of Apparent Stress Variations

The behavior of the three phases of apparent stress variation can be summarized as follows:

- Phase 1
  - Lasts around 6 minutes.
  - Consists of less than 200 events.
  - All apparent stress percentiles increase around 20%.
  - ASR may indicate an increase or decrease in variance.
- Phase 2
  - Lasts around 2 hours.
  - Usually consists of at least 200 events.
  - Apparent stress percentiles decrease 30-40%, falling below their level before the blast.
  - ASR indicates that variance usually decreases.
- Phase 3
  - Lasts around 4 days but may be as short as 12 hours or longer than a month.
  - Usually consists of at least 200 events.
  - Apparent stress percentiles increase 30-50%, landing above their level before the blast.
  - ASR indicates that variance usually increases.

### 5.3 Variations in Event-Stop Distance

Variations in median event-stop distance (MESD) were often more difficult to interpret and showed less consistent behaviour than variations in apparent stress. Phases 1, 2, and 3 of MESD variation could not be interpreted for all cases. In such cases, the analysis was simply truncated at the last phase that could be interpreted. Of the 62 interpretations, 13 have no Phase 3, 7 have no Phase 2, and 4 have no Phase 1 (i.e. no interpretable variation that fits the three-phase model what so ever). There are 49 cases with a complete interpretation of all three phases. The results in this section include data from all the phases that could be interpreted for each case.

#### 5.3.1 Durations of Phases

Like the variations in apparent stress, the phases of variation in event-stop distances also occur over different time scales. Figure 5-16 shows distributions of the observed durations of the MESD phases of variation. Phase 1 occurs on the scale of a few hours, Phase 2 occurs on the scale of half

days, and Phase 3 occurs on the scale of multiple days. The typical durations of each phase imply that:

- Stress redistributes around the new excavation and out of the EDZ for approximately 1 hour after the blast (Phase 1).
- A region of the rock mass closer to the stopes in a quasi-stable state continues to yield throughout the next shift (approximately 12 hours) (Phase 2).
- The EDZ grows over the following days and weeks. (Phase 3).

Like Phase 3 of apparent stress variation, Phase 3 of MESD variations also frequently occurs over a period of several days. Multiple development and stope blasts occur throughout the mine at varying distances from the filter volume during this phase. Phase 2 of MESD variation also frequently overlaps with blasts in different areas of the mine on subsequent shifts.

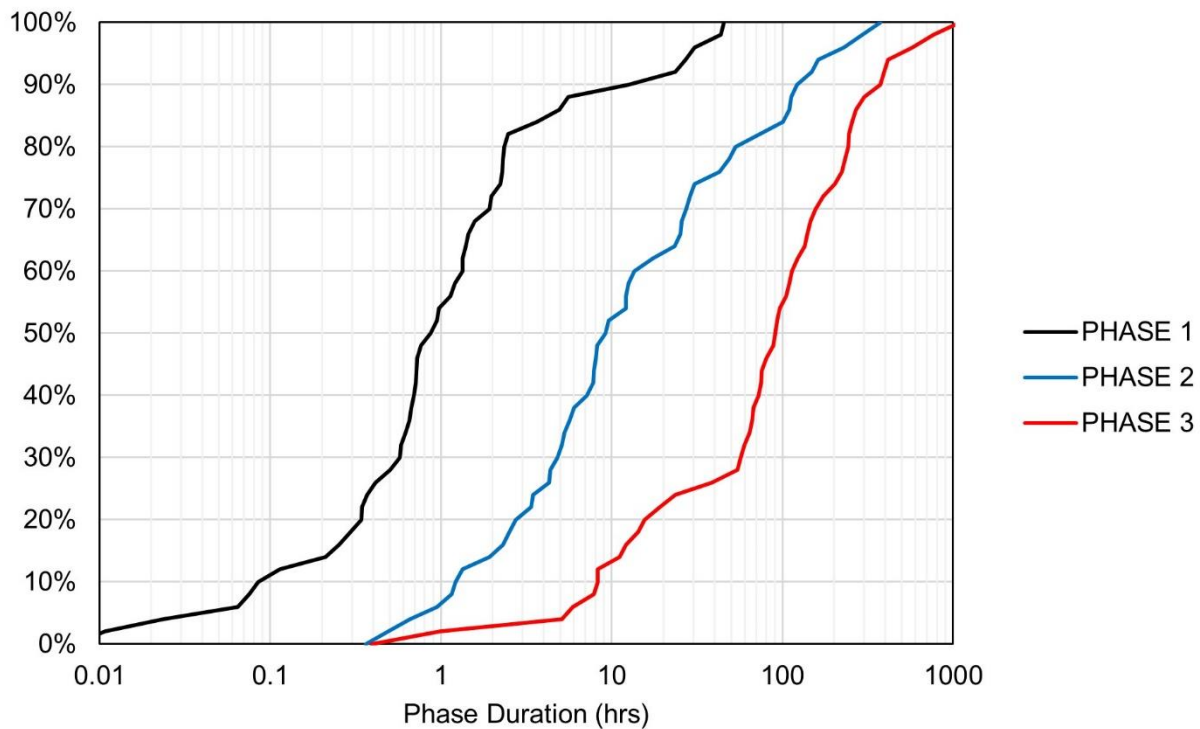


Figure 5-16: Distributions of phase durations for MESD variations

Figure 5-17 shows distributions of ratios of the durations of each phase. Each phase is usually at least as long as the previous one. However, the vast majority of phases are not an order of magnitude longer than the previous phase as they are with apparent stress variations.

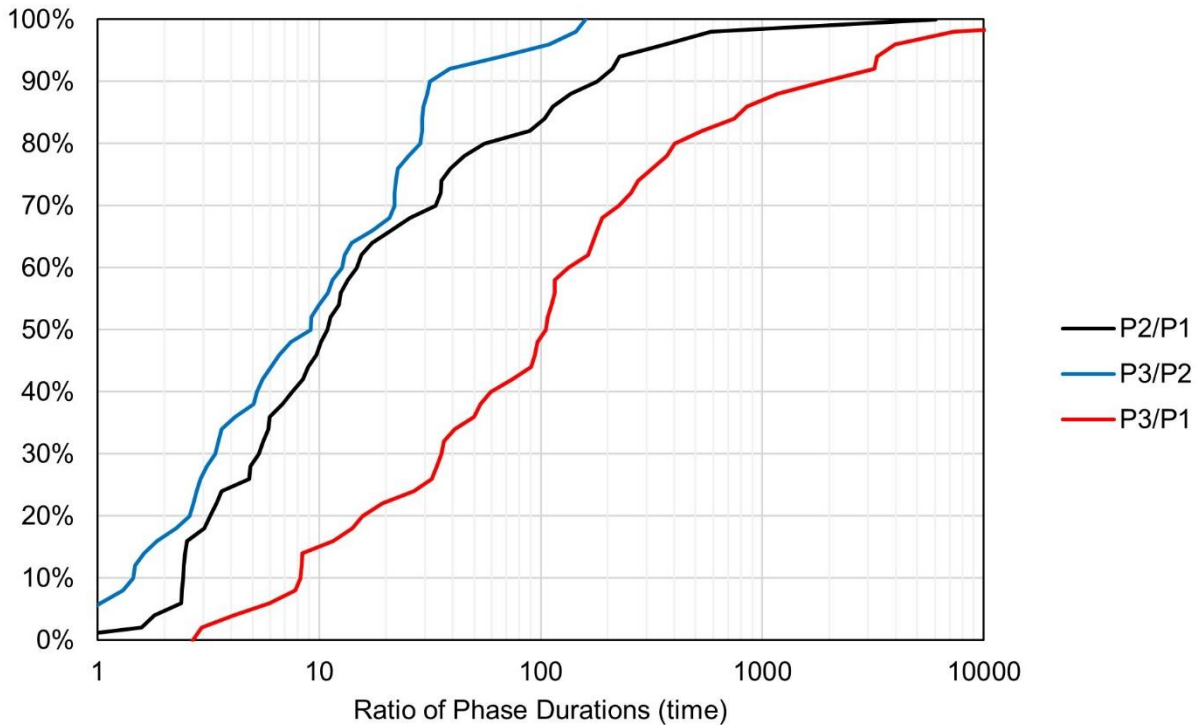


Figure 5-17: Distributions of ratios of phase durations for MESD variations

Figure 5-18 shows distributions of the number of events in each phase. There are often at least 100 events in each phase. Phase 1 tends to have slightly more events than Phase 2, and Phase 2 tends to have slightly more events than Phase 3. Also of note is that approximately half the Phase 2's and 60% of the Phase 3's have fewer than 200 events. Therefore, the variations that occur during these phases are often smoothed over by the 200-event window. The full extent of variation during these phases is less apparent in the trend lines.

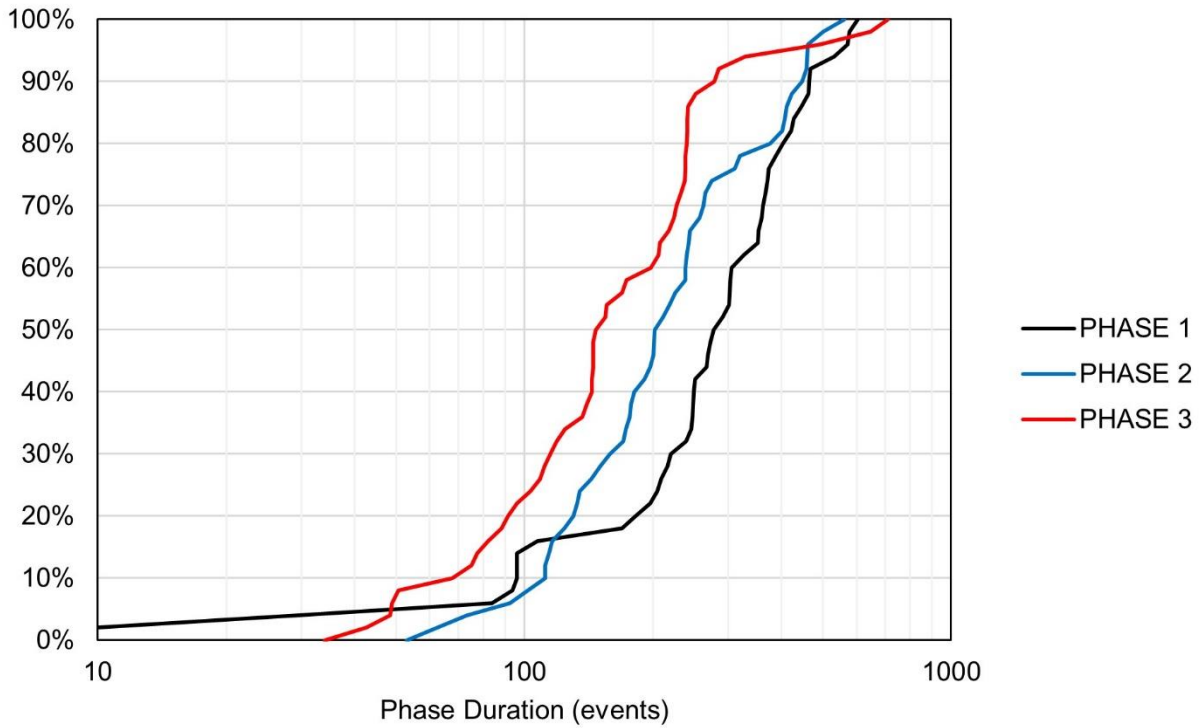


Figure 5-18: Distributions of the number of events in each phase of MESD variation

Figure 5-19 shows distributions of ratios of the number of events in one phase to a previous phase. Each phase tends to have fewer events than the last. This result is expected based on the decreasing event rate over time, and each phase not being significantly longer than the last.

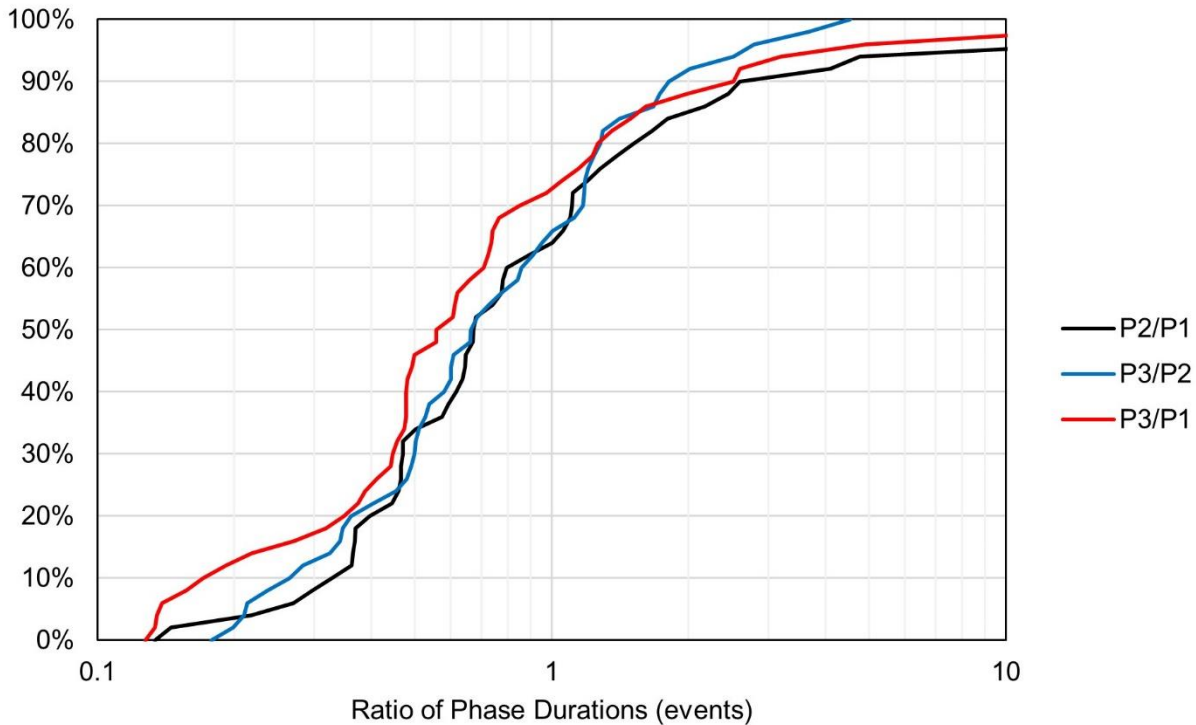


Figure 5-19: Distributions of ratios of numbers of events in each phase of MESD variation

### 5.3.2 Magnitude of Variations

This section presents the results of changes in apparent stress during each phase of variation with regard to increases and decreases in MESD of events with high and low apparent stress.

The largest changes in event-stope distances are usually observed during Phase 1. This result is largely driven by events redistributing around a new excavation (i.e. there is a sudden shift in event locations as a result of a new void being created). That is not to say that rock mass damage, excavation damage zone formation, and seismogenic zone migration do not occur during this phase. Rather, the aforementioned effects can not be distinguished from redistribution of stresses in short time periods after a blast. However, such effects may be more easily detected in cases where events do not locate closest to a newly formed excavation (e.g. in abutments). Unfortunately, such cases were often difficult to interpret, limiting the quantity of such results for analysis.

Figure 5-20 shows the distributions of observed changes in event-stope distances during Phase 1. The events with the highest apparent stress ( $D_{50H_{80}}$ ) show a slight tendency to move farther from the stopes than other events. However, the results do not show drastic differences between how far

high and low apparent stress events move away from the stopes during Phase 1. Recall that the changes are based on the trend line values at the averaged peak time, so actual maximum variations of each trend line are often larger.

As with the changes in apparent stress, a small portion of results exhibit the opposite behaviour to that which characterizes the phase (e.g. decreases during Phase 1). To reiterate, such results are an effect of the methodology by which phases are defined (based on multiple trend lines rather than individual peak values).

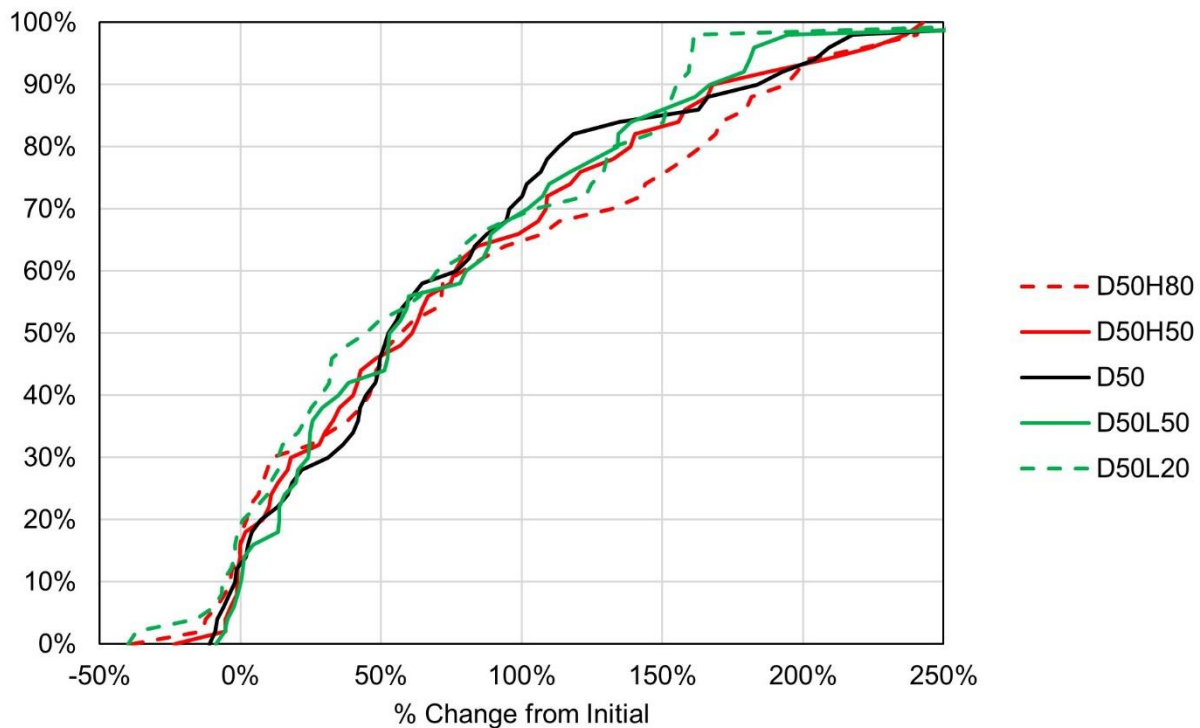


Figure 5-20: Distributions of percentage change in MESD observed during Phase 1 (relative to just before the final blast)

Despite there being no clear difference in whether high or low apparent stress events migrate further during Phase 1, there are examples where one moved significantly further than the other. One such example is the 1415-250-P1 west sidewall, the results of which are shown in Figure 5-21. Following the blast,  $D_{50H50}$  and  $D_{50H80}$  move noticeably further away from the stopes than  $D_{50L50}$  and  $D_{50L20}$ . The highest apparent stress events occurring at greater distances are associated with an elevated stress front outside of the EDZ, higher confinement conditions, and areas where stresses may not exceed the strength of the intact rock but may exceed the strength of discontinuities in the rock mass. The tendency for high apparent stress events to move farther from

the stopes than low apparent stress events implies that such mechanisms occur under conditions that are more widespread and distant from the stope. By contrast, low apparent stress events concentrate in supposedly low-confinement regions closer to the stopes soon after the blast. Such conditions may be more spatially limited to the rock mass near the stopes, resulting in less movement away from the stopes.

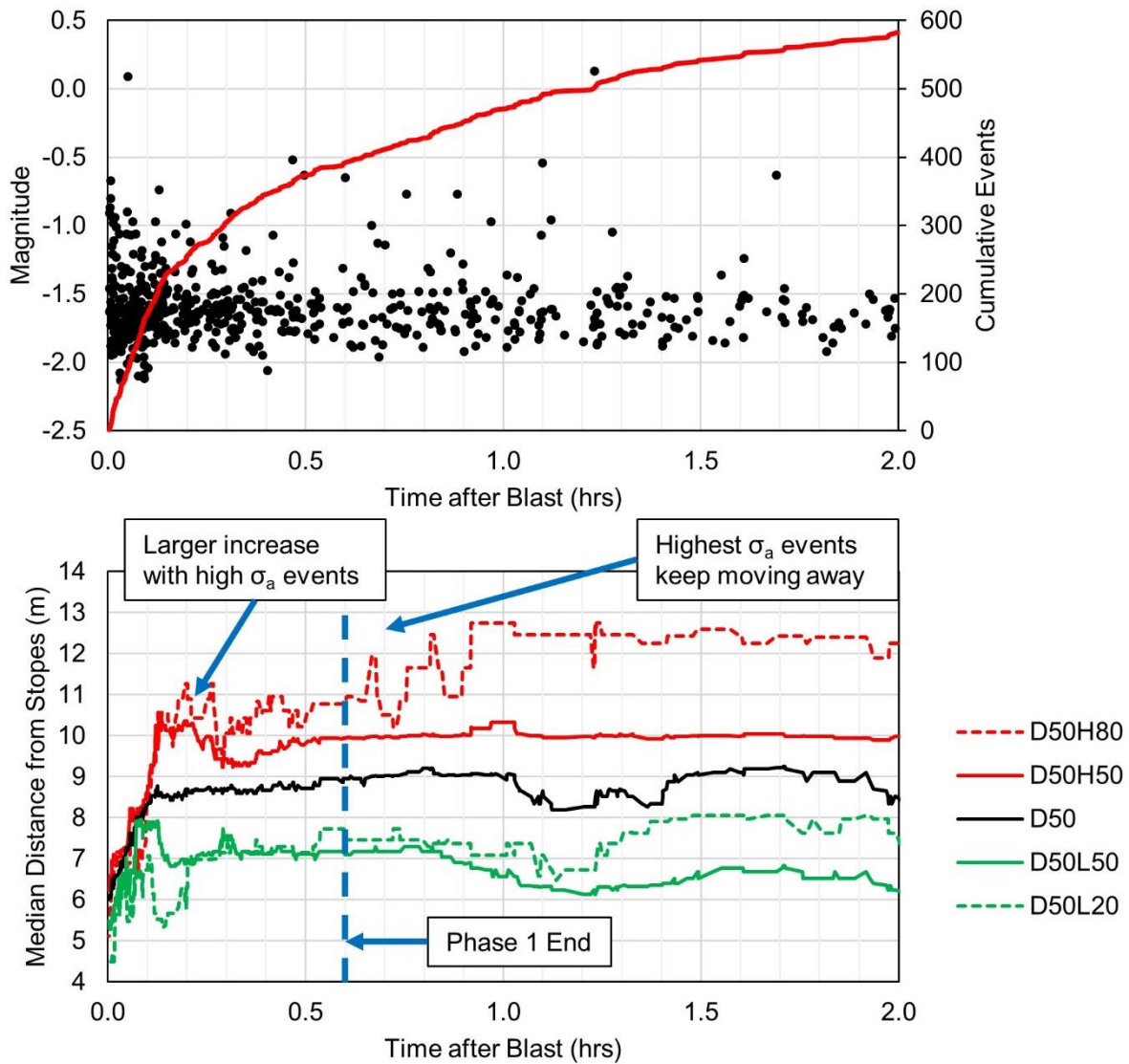


Figure 5-21: Example of high apparent stress events migrating further from stope than low apparent stress events (1415-250-P1 west sidewall, January 20<sup>th</sup>, 2015)

Figure 5-22 shows distributions of changes in MESD that occur during Phase 2. Events with higher apparent stress ( $D_{50}H_{50}$  and  $D_{50}H_{80}$ ) appear to have a slight tendency to move closer back towards the stope than events with lower apparent stress. Events with the lowest apparent stress ( $D_{50}L_{20}$ )

usually move towards the stope as well, but they also moved away from the stope in approximately 30% of interpretations.

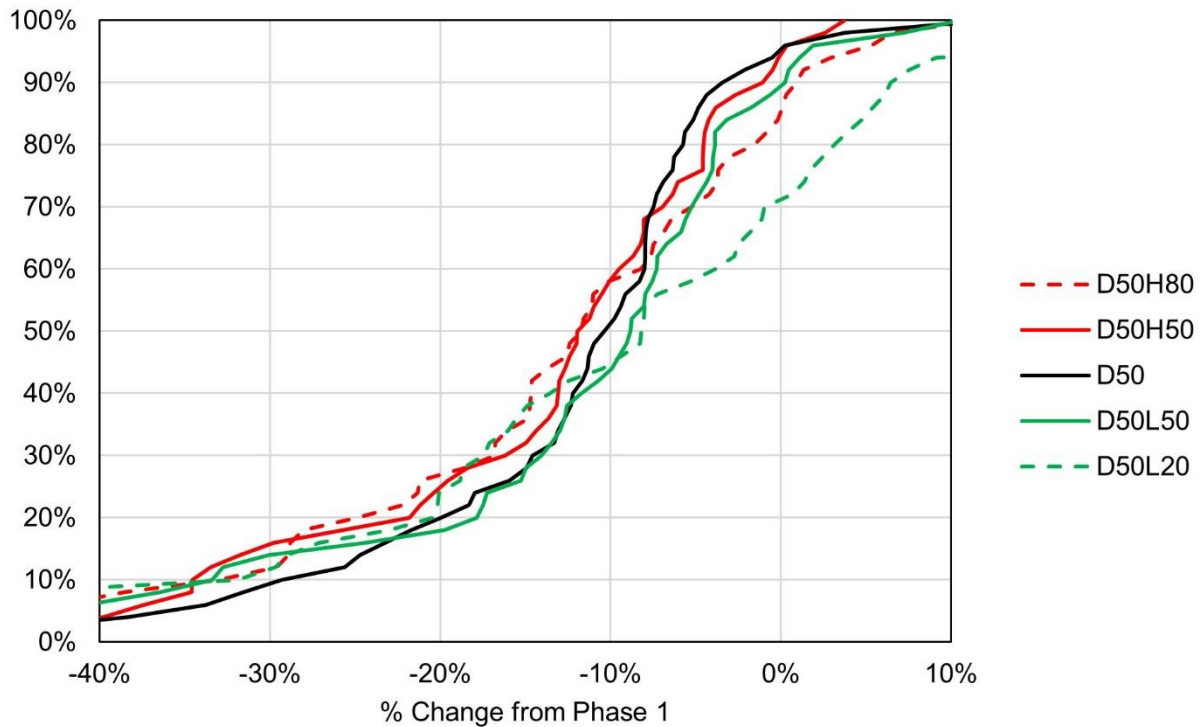


Figure 5-22: Distributions of percentage change in MESD observed during Phase 2 (relative to the end of Phase 1)

An example of typical Phase 2 behaviour is shown in Figure 5-23. In this example, high apparent stress events are consistently farther away from the stopes than lower apparent stress events, as is typically observed in other cases. During Phase 2, there is a much larger decrease in  $D_{50H50}$  than  $D_{50L50}$ . The lower apparent stress events do not move as far because they are supposedly associated with rock mass fracturing in the lower confinement areas closer to the stopes, which occurs in a consistent area around the stope and grows outwards. The higher apparent stress events are associated with rock mass yield in higher confinement conditions, the elevated stress front outside of the EDZ, and disturbance to discontinuities in the rock mass. The movement of higher apparent stress events back towards the stopes implies such mechanisms become less dominant over time. During Phase 2 rock mass yield begins to occur in a more consistent quasi-stable region at the interface of the EDZ and a more stable, less damaged region of the rock mass.

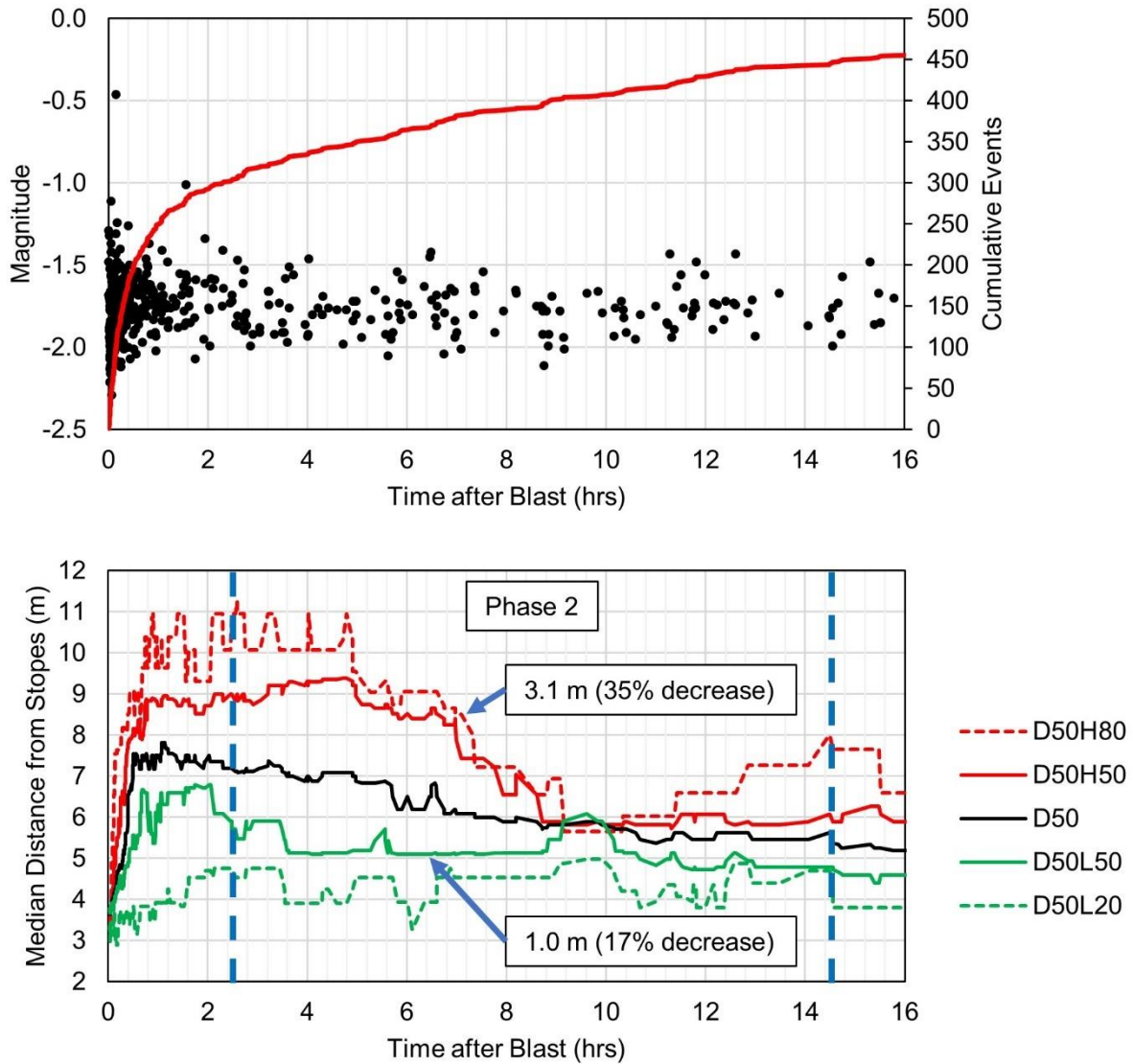


Figure 5-23: Example of high apparent stress events moving closer to the stopes than low apparent stress events during Phase 2 (1535-225-P1 west sidewall, June 30<sup>th</sup>, 2016)

The movement of the seismogenic zone towards the stopes during Phase 2 (Figure 5-22) is usually smaller than the migration away from them during Phase 1 (Figure 5-20). As a result, events are usually farther from the stopes at the end of Phase 2 than they were before the blast. The distributions of change in MESD at the end of Phase 2 relative to just before the final blast are shown in Figure 5-24. At the end of Phase 2, the events are farther away from the stopes than before the blast in approximately 80% of cases. Events may move closer to excavations in volumes where events were not grouping around an induced stress front associated with a single excavation before the blast. Rather, the events occurring before the blast may be part of a larger stress front

(e.g. a sill pillar) or seismically active feature (e.g. a fault) and the creation of an excavation near the volume results in a more distinct areas of rock mass failure close the to excavations.

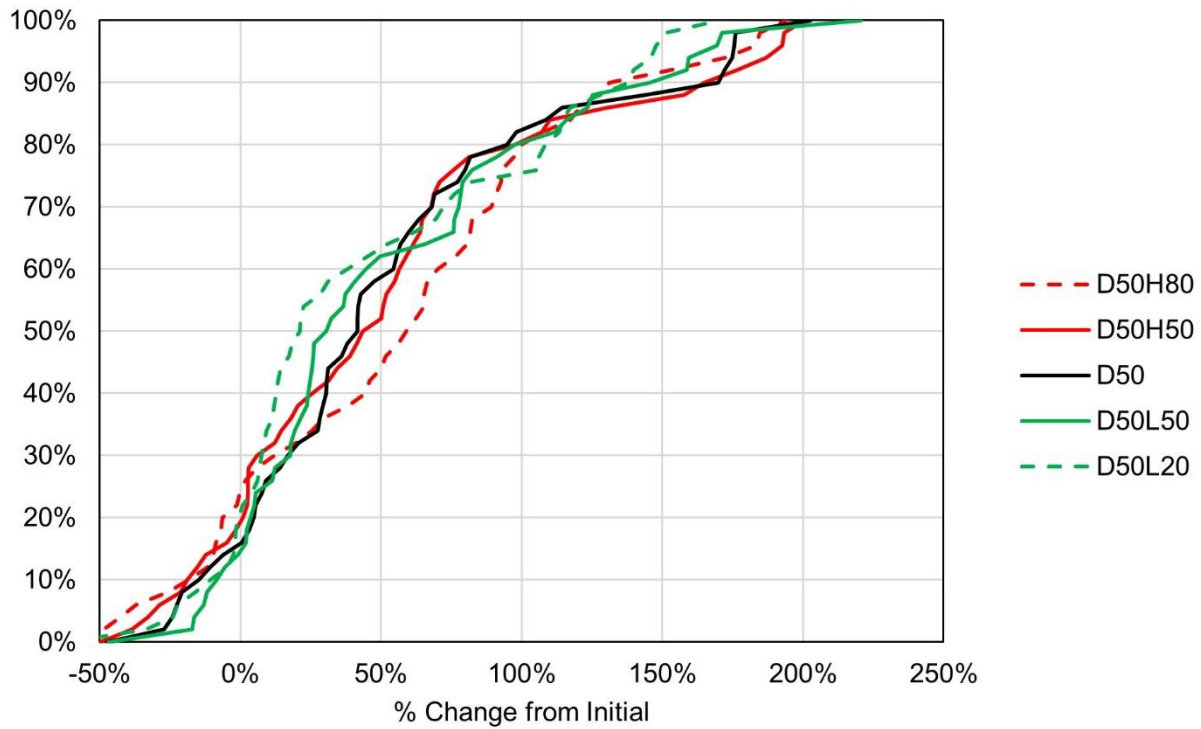


Figure 5-24: Distributions of percentage change in MESD observed during Phase 2 (relative to just before the final blast)

Figure 5-25 shows the distributions of change in MESD observed during Phase 3. Events with lower apparent stress ( $D_{50L50}$  and  $D_{50L20}$ ) move slightly farther from the stopes than events with higher apparent stress ( $D_{50H50}$  and  $D_{50H80}$ ) during Phase 3. Events with the highest and lowest apparent stress move towards the stopes in around 10 to 20% of interpretations.

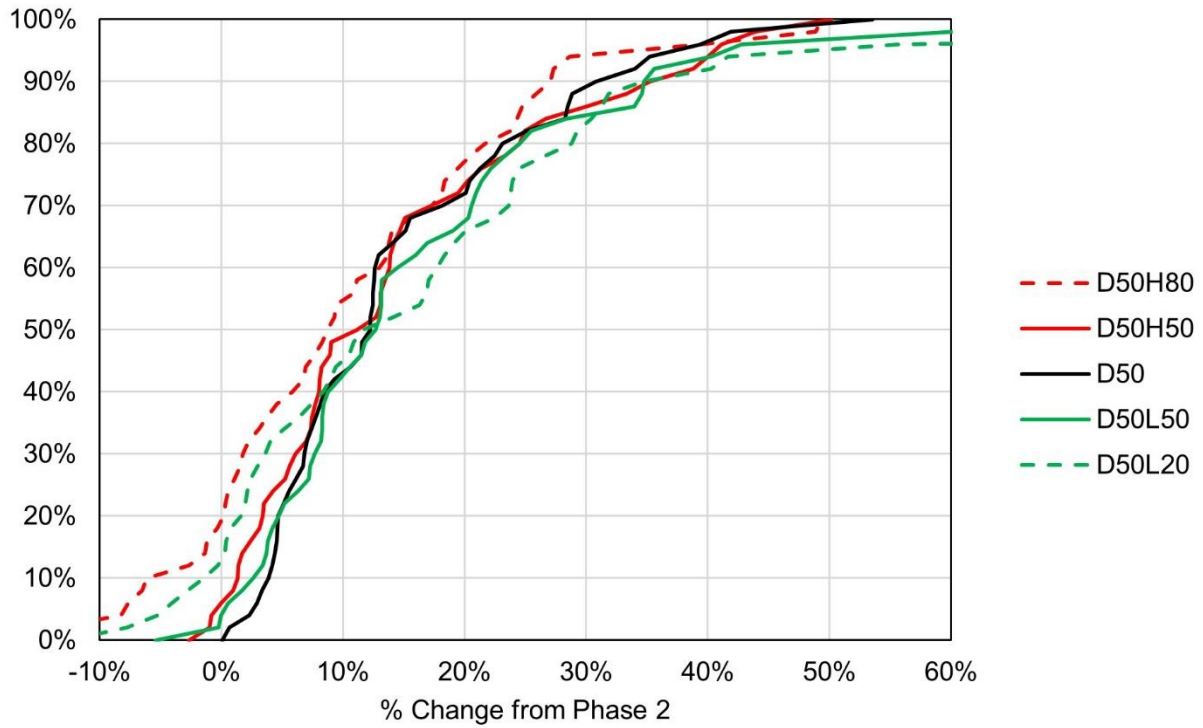


Figure 5-25: Distributions of percentage change in MESD observed during Phase 3 (relative to the end of Phase 2)

Figure 5-26 shows the distributions of the overall change in MESD observed from just before the final blast to the end of Phase 3. The distributions are similar to those observed during Phase 1 (Figure 5-20). This result implies that the position of the seismogenic zone at the end of Phase 3 is not consistently closer or farther from the stopes than it was at the end of Phase 1.

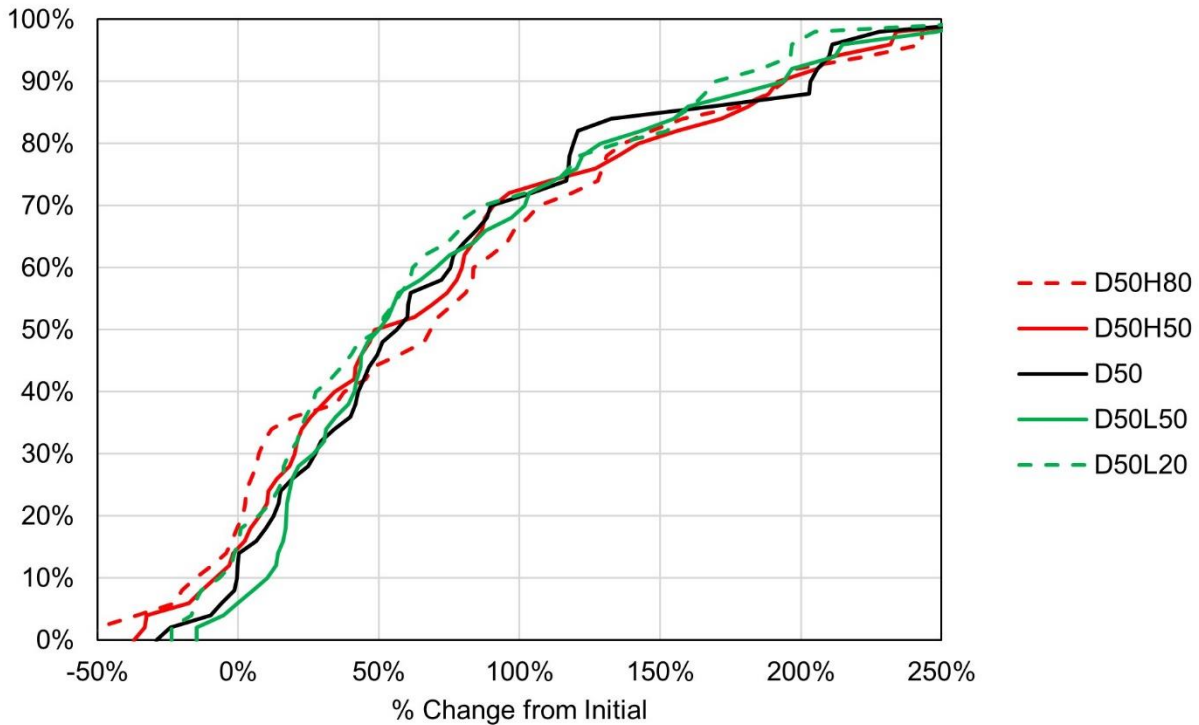


Figure 5-26: Distributions of percentage change in MESD observed during Phase 3 (relative to just before the final blast)

As discussed previously, the interpretation of Phase 2 is that events move towards the stopes because the redistribution of stress has slowed, and events are occurring in a more consistent quasi-stable region of rock mass yield. Accordingly, the interpretation of Phase 3 is that the seismogenic zone is migrating as the EDZ grows. Figure 5-27 shows the distributions of what is interpreted as growth of the EDZ between the end of Phase 1 to the end of Phase 3. As stated previously, the MESD is not consistently closer or farther from the stopes at the end of Phase 3 than it was at the end of Phase 1. Figure 5-22 and Figure 5-25 show that high apparent stress events have a stronger tendency to move towards the stopes during Phase 2, and low apparent stress events have a stronger tendency to move away from the stopes during Phase 3. Figure 5-27 shows there is little consistency in whether MESD is greater at the end of Phase 1 or Phase 3. However, it does indicate that low apparent stress events move farther from the stopes than high apparent stress events throughout phases 2 and 3. Based on this behaviour, it is inferred that the low apparent stress events associated with rock mass yield are moving away from the stopes as the EDZ grows. The seismogenic zone eventually reaches more confined, less yielded ground where high apparent stress events occur.

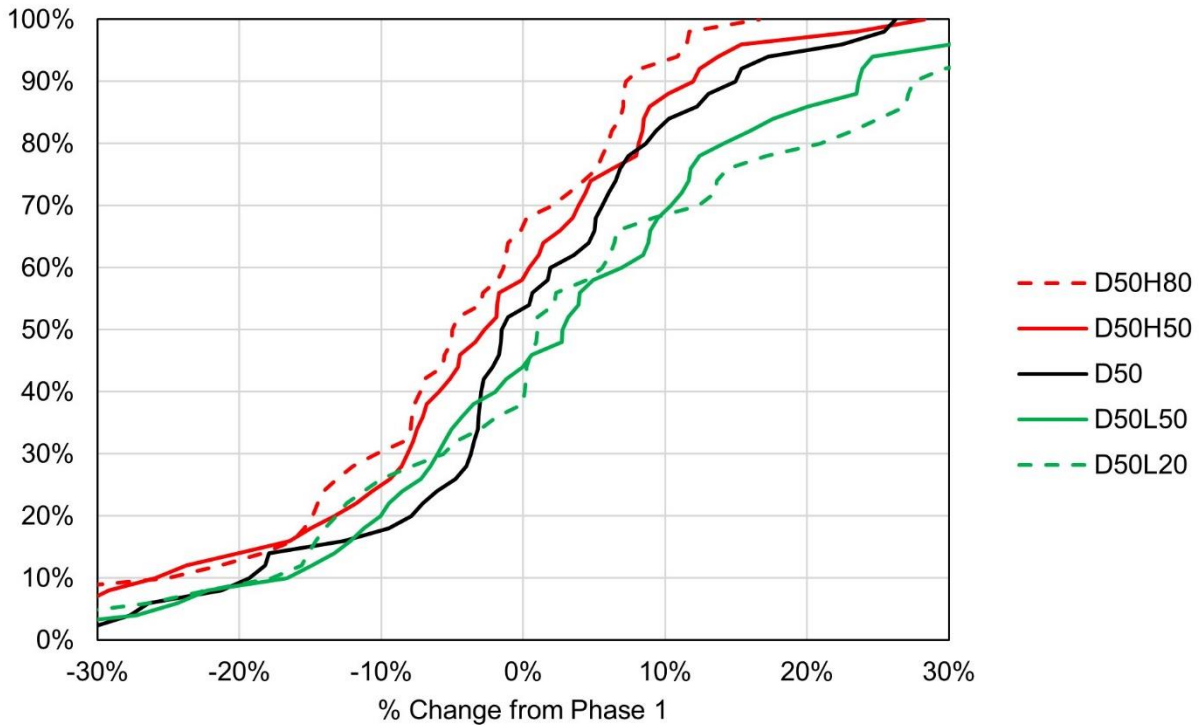


Figure 5-27: Distributions of percentage change in MESD between the ends of Phase 1 and 3 (change throughout Phase 2 and 3)

Figure 5-28 compares the number of events in each phase of MESD variation to the change in the trend lines observed during that phase. When there are fewer than 200 events in a phase, the window smooths over variations. Larger variations as the phases approach 200 events can therefore be attributed to events in that phase “taking over” the window. Beyond the first 200 events in a phase, larger changes in trend lines may be associated with larger seismic responses (measured by the number of events). The association between larger seismic responses and larger variations in MESD is not as apparent as with variations in apparent stress (Figure 5-15). In Phase 1, there appears to be a slight increase between 200 and 300 events, but the relation becomes quite scattered afterwards. However, more seismic events in phases 2 and 3 appear to be associated with larger variations in MESD during those phases.

As with the variations in apparent stress, there are some interpretations where there is a large number of events but a relatively small variation during one of the phases. Such results are apparent in two of the interpreted Phase 3’s. These cases have multiple interpretations of the phases of variations. The apparent outliers correspond to the “long phase” interpretation (note that these are not the same cases that produced outliers in variations in apparent stress). As with the variations

in apparent stress, the disparity between these interpretations and the others imply that those Phase 3's may have been interpreted incorrectly, and do not reflect the same process observed in the other interpretations of the same phase. Alternatively, there may be a secondary process of rock mass yield which resulted in the "short phase" interpretations. The events associated with that secondary process do not necessarily "count" towards the longer phase interpretation, resulting in the longer phase interpretation appearing as an outlier.

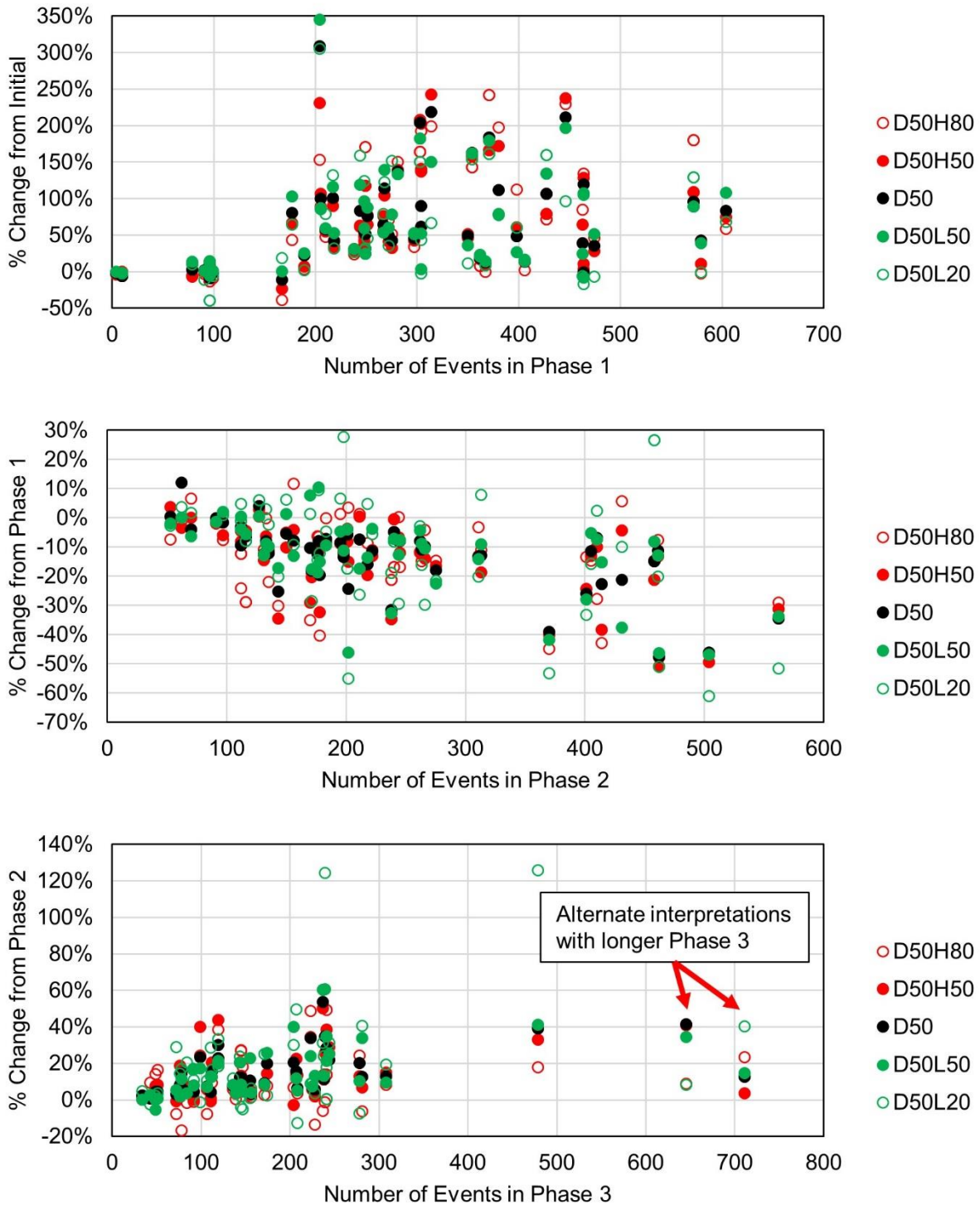


Figure 5-28: Percentage change in MESD from one phase to the next versus the number of events in that phase

### 5.3.3 Separation between Events with High and Low Apparent Stress

Spatial variations in apparent stress can be used to infer variation in rock mass conditions throughout the seismogenic zone. Figure 5-29 shows the variation in MESD for high and low

apparent stress events relative to the MESD for all events ( $D_{50}$ ) in the same interpretation. At the end of each phase of MESD variation,  $D_{50}H_{50}$  and  $D_{50}H_{80}$  are farther away from the stope than  $D_{50}$  in about 80% of interpretations. Similarly,  $D_{50}L_{50}$  and  $D_{50}L_{20}$  are closer to the stope than  $D_{50}$  at the end of each phase in about 80% of interpretations. Also,  $D_{50}H_{80}$  tends to be even farther from the stope than  $D_{50}H_{50}$ .  $D_{50}L_{20}$  appears to locate closer to the stope than  $D_{50}L_{50}$  during Phase 1, but in phases 2 and 3 it simply appears to have more variance in its position relative to  $D_{50}$ . These results indicate that throughout a seismogenic zone, events with higher apparent stress will tend to locate farther from mined out stopes than events with lower apparent stress. This tendency supports the notion that events with higher apparent stress occur in more intact ground with higher confinement, and events with lower apparent stress occur in more yielded ground with lower confinement. The increased separation of the higher apparent stress events ( $D_{50}H_{80}$  being farther than  $D_{50}H_{50}$ , but  $D_{50}L_{20}$  not being closer than  $D_{50}L_{50}$ ) indicates an increasing lack of similarity in the conditions that events with increasingly higher apparent stress occur under.

Also of note in Figure 5-29 is that  $D_{50}H_{50}$  and  $D_{50}H_{80}$  tend to become less separated from  $D_{50}$  at the end of each successive phase. Vertical blue lines in the figure indicate the position of the 80<sup>th</sup> percentile in each phase. In each successive phase, the 80<sup>th</sup> percentile has a lower difference relative to  $D_{50}$  than the previous phase. This result indicates that there is less spatial variation in apparent stress throughout the seismogenic zone at greater time periods after the blast. Because this data is presented relative to  $D_{50}$ , it can not be said for certain if this effect is driven by high apparent stress events moving towards the stope, or low apparent stress events moving away from the stope. However, the results of the previous section may shed some light on what drives the lower spatial variation over time. Results in the previous section indicated that  $D_{50}H_{50}$  moved more than  $D_{50}L_{50}$  towards the stopes during Phase 2. However,  $D_{50}L_{50}$  moved more than  $D_{50}H_{50}$  away from the stopes during Phase 3. Therefore, it is inferred that the reduced variation in apparent stress throughout the seismogenic zone over time is a result of events with high and low apparent stress moving towards each other.

It is important to recall that the distribution of apparent stress is also changing throughout this time. Therefore, what constitutes high and low apparent stress is not consistent between cases or from one phase to the next.

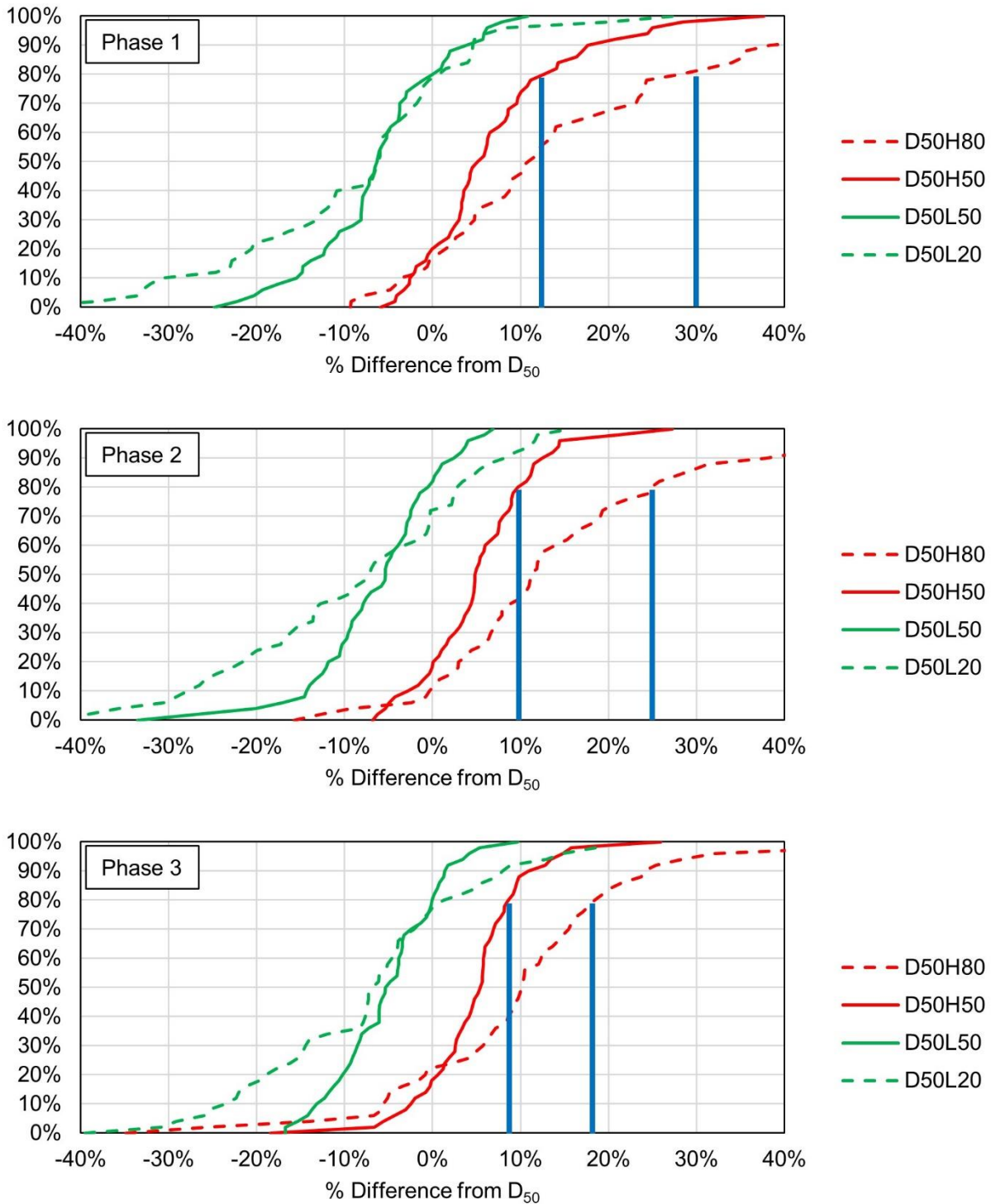


Figure 5-29: Distribution of percentage differences between MESD of events with high or low apparent stress and the MESD for all events at the end of each phase

Rather than measuring relative to  $D_{50}$ , spatial variation in apparent stress can also be shown by comparing MESDs of high and low apparent stress events. Figure 5-30 shows distributions of the

percentage difference between pairs of high and low apparent stress events in the same interpretation at the end of each phase (i.e. the higher apparent stress events are some percent further from the stopes than the lower apparent stress events). Throughout all three phases, the largest difference in MESD is found between the groups with the largest difference in apparent stress: the top 20% represented by  $D_{50}H_{80}$  and the bottom 20% represented by  $D_{50}L_{20}$ . The second largest difference is consistently between  $D_{50}H_{50}$  and  $D_{50}L_{50}$ . The smallest differences are consistently between events with closer levels of apparent stress. The top 20% is only slightly further away than the top 50%, and the bottom 50% is only slightly further away than the bottom 20%. In fact, there is often little consistency in the position of  $D_{50}L_{50}$  relative to  $D_{50}L_{20}$ .  $D_{50}L_{50}$  is usually farther from the stopes than  $D_{50}L_{20}$ , but in around 40 to 50% of interpretations  $D_{50}L_{20}$  is farther from the stopes than  $D_{50}L_{50}$ . This result indicates that while events with higher and the highest apparent stress may occur in different regions of the seismogenic zone, events with lower and the lowest apparent stress may occur in similar regions.

As with the comparison of the MESD of events with different levels of apparent stress to  $D_{50}$ , Figure 5-30 also shows that there is less separation between events with high and low apparent stress in later phases. The 80<sup>th</sup> percentiles of the difference between  $D_{50}H_{50}$  and  $D_{50}L_{50}$ , and  $D_{50}H_{80}$  and  $D_{50}L_{10}$  are indicated with vertical blue lines in each phase. The relative difference in MESD between events with high and low apparent stress becomes smaller in each successive phase. As discussed previously, this result is believed to be a combined effect of the low apparent stress events moving away from the stopes, and the high apparent stress events moving towards the stopes.

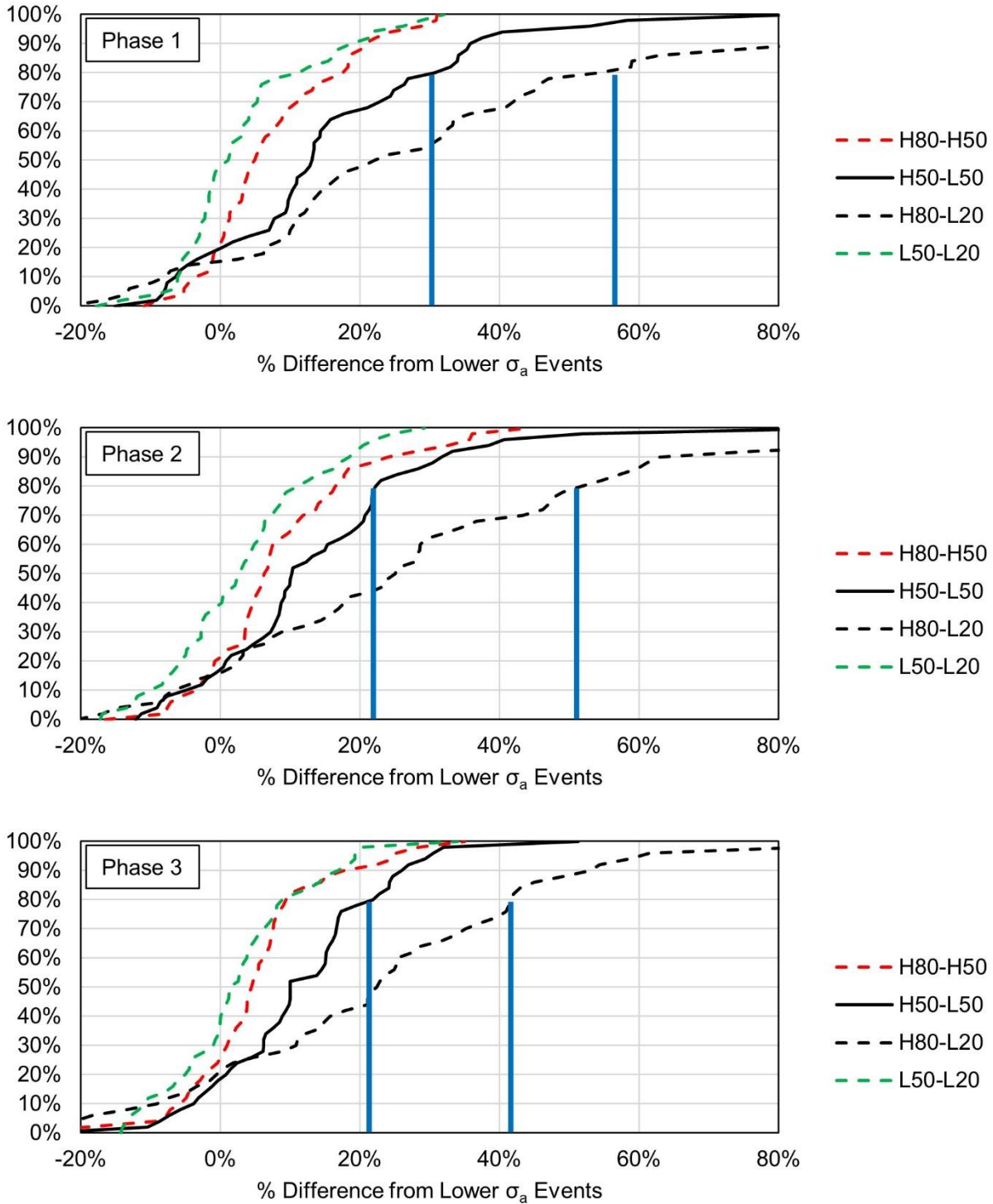


Figure 5-30: Distributions of percentage differences between MESD of higher and lower apparent stress events at the end of each phase

### 5.3.4 Summary of Event-Stope Distance Variations

The behavior of the three phases of median event-stope distance variation can be summarized as follows:

- Phase 1
  - Lasts around an hour.
  - Consists of around 300 events.
  - Events move 50% farther from stopes (related to stresses redistributing around a new excavation and outside of a zone of yielded ground closer to the excavation).
  - Higher apparent stress events tend to move slightly farther than lower apparent stress events.
- Phase 2
  - Lasts around 10 hours.
  - Consists of around 200 events.
  - Events move 10% closer to the stopes (still farther than they were before the blast, associated with a new quasi-stable region of the rock mass between the EDZ and a more intact region farther from the excavations).
  - Higher apparent stress events tend to move more towards the stopes than lower apparent stress events.
- Phase 3
  - Lasts around 4 days.
  - Consists of between 100 and 200 events.
  - Events move 10% farther from the stopes (growth of the EDZ).
  - Lower apparent stress events tend to move farther from the stopes than lower apparent stress events.
- There is more variability in the duration of each phase compared to the phases of apparent stress variation.
- Higher apparent stress events tend to locate farther from the stopes than lower apparent stress events in all phases.
- There is less separation between events with higher and lower apparent stress over time
- There are greater differences in MESD between events with higher apparent stress

## 5.4 Comparison of Variations in Apparent Stress and Event-Stop Distances

Certain variations in apparent stress and MESD are associated with similar inferred rock mass behaviour (e.g. yield, EDZ growth). Therefore, simultaneous variations in both apparent stress and MESD may corroborate certain inferred rock mass behaviours.

Figure 5-31 compares the end times of Phase 1 in apparent stress and MESD variation. The dashed black line indicates an equal end time for both apparent stress and MESD phases. The red and green dashed lines indicate an end time for the MESD phase that is half an order of magnitude of time later or earlier (respectively) than the apparent stress phase. Phase 1 of MESD often ends a substantial amount of time after Phase 1 of apparent stress. In many of the interpretations, events continue to move away from the stopes after apparent stress has peaked and begins to fall. This behaviour implies that co-seismic stress change and deformation continues to occur at increasing distances from the stopes as the rock mass yields following the blast.

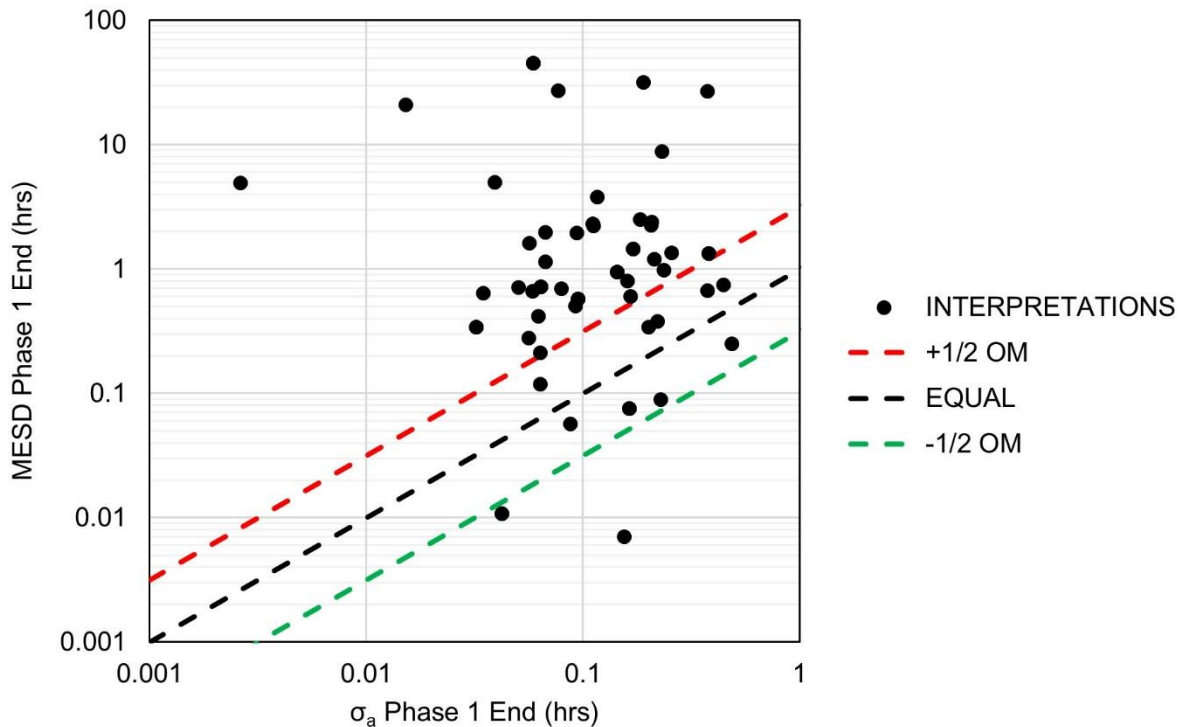


Figure 5-31: End time of Phase 1 of apparent stress variation versus end time of Phase 1 of MESD variation

Figure 5-32 compares the end times of Phase 2 in apparent stress, and Phase 1 and MESD variation. Phase 1 of MESD variations tends to end slightly before Phase 2 of apparent stress variation. Apparent stress reaches its low point slightly after the events stop moving away from the stopes.

This behaviour implies that seismicity will occur at progressively greater distances as the rock mass yields (as inferred by a decrease in apparent stress). As apparent stress stops dropping, it is inferred that the process of low-confinement yield is slowing down. Accordingly, the EDZ is not growing as rapidly, and the process of stress redistributing into less damaged parts of the rock mass, resulting in more distant events, is also slowed. The next phases of the process, Phase 3 of apparent stress and Phase 2 of MESD, involve events occurring in areas which are slightly closer to the stopes, but are more confined than the regions immediately adjacent to them. At this time, the slowed decrease in apparent stress suggests that rock mass yield has slowed. The active process of rock mass yield generating seismicity not occurs in a quasi-stable region outside of the EDZ.

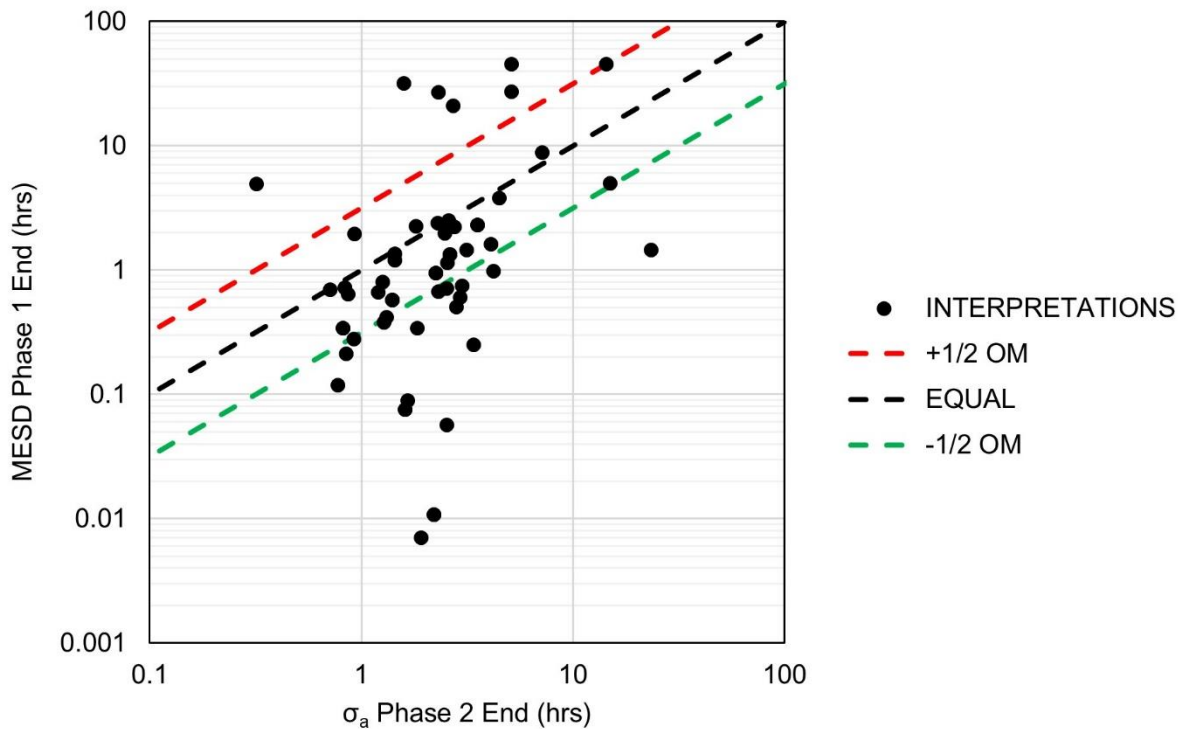


Figure 5-32: End time of Phase 2 of apparent stress variation versus end time of Phase 1 of MESD variation

Figure 5-33 compares the end times of Phase 3 in apparent stress, and Phase 2 and MESD variation. Phase 2 of MESD variation usually ends before Phase 3 of apparent stress variation. Therefore, apparent stress is usually rising as the events are occurring closer to the stopes. It is expected that events closer to the EDZ have lower apparent stress because they occur in more fractured ground under lower confinement conditions. However, the EDZ has already formed by this point, as suggested by the preceding drop in apparent stress during Phase 2 of the apparent stress variations,

so any further growth of the EDZ must now occur under higher confinement conditions. Consequently, these events will tend to have higher apparent stress.

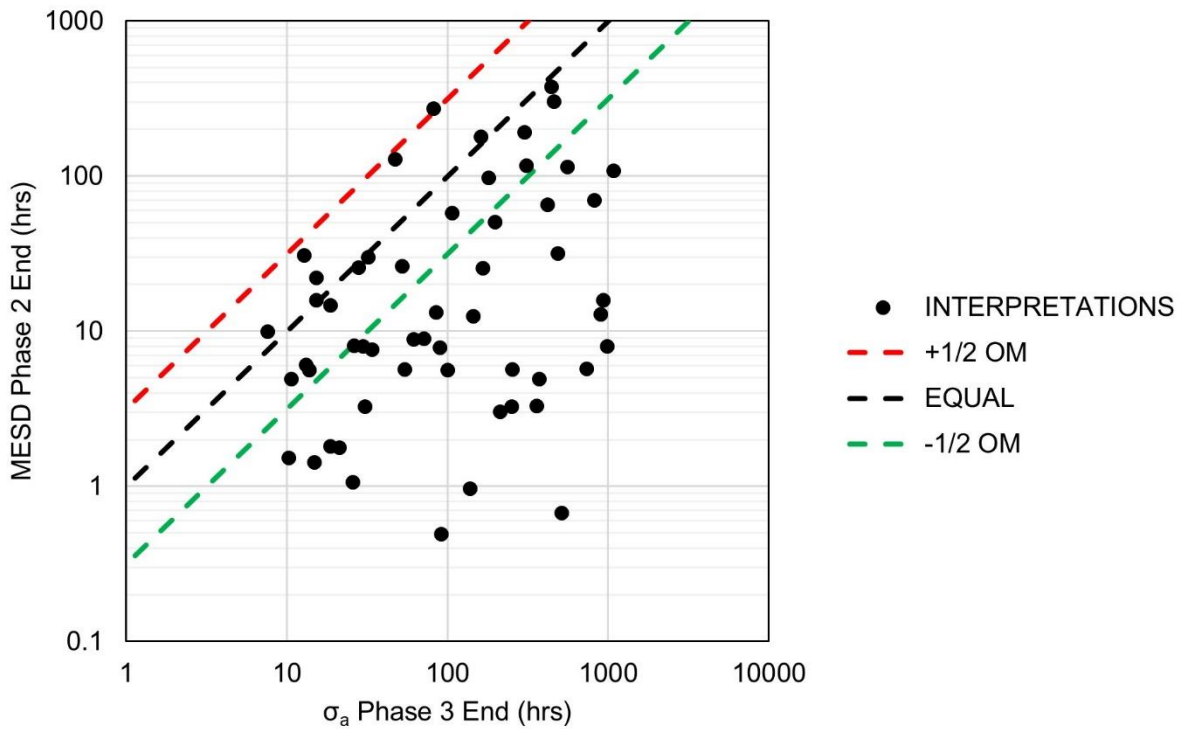


Figure 5-33: End time of Phase 3 of apparent stress variation versus end time of Phase 2 of MESD variation

Figure 5-34 compares the end times of Phase 3 in apparent stress, and Phase 3 and MESD variation. Phase 3 of both parameters ends around the same time (i.e. apparent stress stops rising as events stop moving away from the stopes). In other words, the occurrence of events with increasingly higher apparent stress ends around the same time that the seismogenic zone stops moving farther from the stopes, into more confined ground. This result supports the coupled interpretation of apparent stress and MESD.

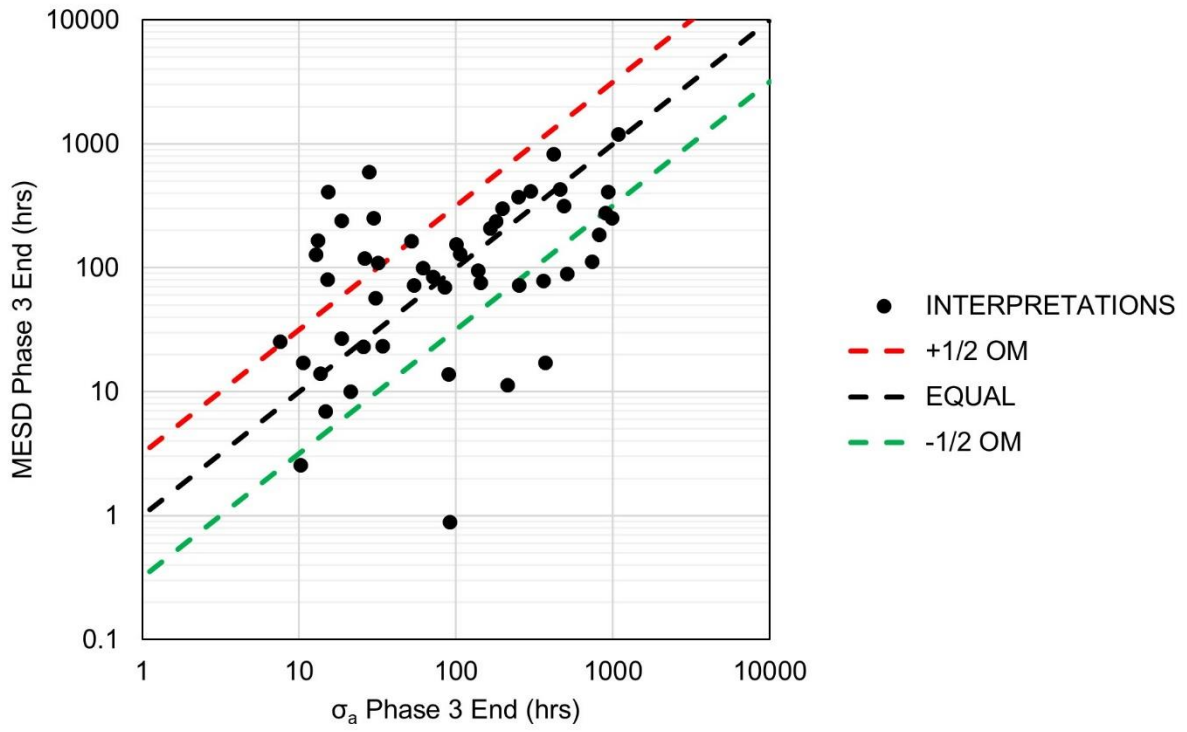


Figure 5-34: End time of Phase 3 of apparent stress variation versus end time of Phase 3 of MESD variation

## 6 Discussion

### 6.1 Inferred Rock Mass Behaviour and Dominant Seismic Responses

In general, apparent stress is used to infer stress conditions in a rock mass based on the assumption that larger co-seismic stress changes occur:

- In parts of the rock mass under higher stress.
- When the rock mass yields under higher stress conditions.

Therefore, there are both time and space dimensions to the analysis of apparent stress. Variation in both these dimensions is demonstrated in the majority of the 50 case studies analysed. Across these case studies, there is consistency in the variations observed in both dimensions (albeit less so in the space dimension as three phases of MESD variation could not be interpreted in every case).

Based on the observed variations in apparent stress and related inferences of local rock mass stress, the author has developed a model for rock mass yield in seismogenic zones of open stopes. The model accounts for the observed short-term variations in apparent stress throughout both space and time, and is presented graphically in Figure 6-1. Although three phases of variation were interpreted for time and space, the phase in each dimension do not occur simultaneously. For this reason, the proposed model for rock mass yield is presented in four stages. In the figure, a new excavation is represented by a black circle. While a circle is not consistent with the excavation geometry analysed in this thesis, it is used in this figure simply as a reference point for the position of the events relative to an excavation. The excavation damage zone is represented by a black dashed circle. Like the circle representing the excavation itself, this circle does not represent the shape or size of the EDZ under any specific stress or rock mass condition. There is no discrete boundary between damaged and undamaged rock. This envelope is only intended to function as a conceptual reference point. High and low apparent stress events are represented by red triangles and green circles respectively. Their quantities and positions are intended to generalize the overall distribution of apparent stress in the seismogenic zone, and the relative event-stope distances of events with higher or lower apparent stress.

The stages of rock mass yield following stope blasts as inferred from apparent stress can be summarized as follows:

1. Stress increase and the creation of a new zone of rock mass yield. This process occurs over a matter of minutes (Figure 6-1a).
2. Decreasing stress near the excavation as the rock mass yields and forms an excavation damage zone (Figure 6-1b). Stress migrates out of the EDZ, causing further stress redistribution and yield at greater distances from the excavation. This process occurs over a matter of hours.
3. Slowed redistribution of stress outside the yielded regions (Figure 6-1c). Yield occurs in a more consistent region of the rock mass where the stresses place it in a quasi-stable state. This process occurs over a matter of hours to days.
4. Progressive growth of the EDZ and rock mass yield occurring under higher stress conditions with greater confinement (Figure 6-1d). This process occurs over a matter of days to weeks.

The first two steps are reminiscent of a behaviour described by Mendecki (2016). Mendecki describes two stress related processes that occur in a rock mass following an incremental stress change caused by the creation of a new excavation or a sudden inelastic strain. First, there is an excitation phase in which stresses are elevated and the rock mass is loaded faster than it can dissipate strain energy. This phase is short lived and requires a relatively sensitive microseismic array to observe. With regard to the results of this thesis, the excitation phase corresponds with Phase 1 of apparent stress and the early stages of Phase 1 of MESD variation. The second phase described by Mendecki is the relaxation phase. This phase lasts longer than the excitation phase and generates the bulk of seismic activity. The relaxation phase involves the rock mass shedding stress away from excavations by deforming inelastically. This phase corresponds with Phase 2 in apparent stress variation and the later parts of Phase 1 of MESD variation. The inferred rock mass behaviour based on apparent stress and MESD presented in this thesis agree with Mendecki's descriptions of rock mass behaviour during the excitation and relaxation phases. The theorized model for rock mass yield in this thesis follows rock mass behaviour into a sort of late relaxation phase in which reloading of the surrounding rock mass becomes the dominant source of seismicity.

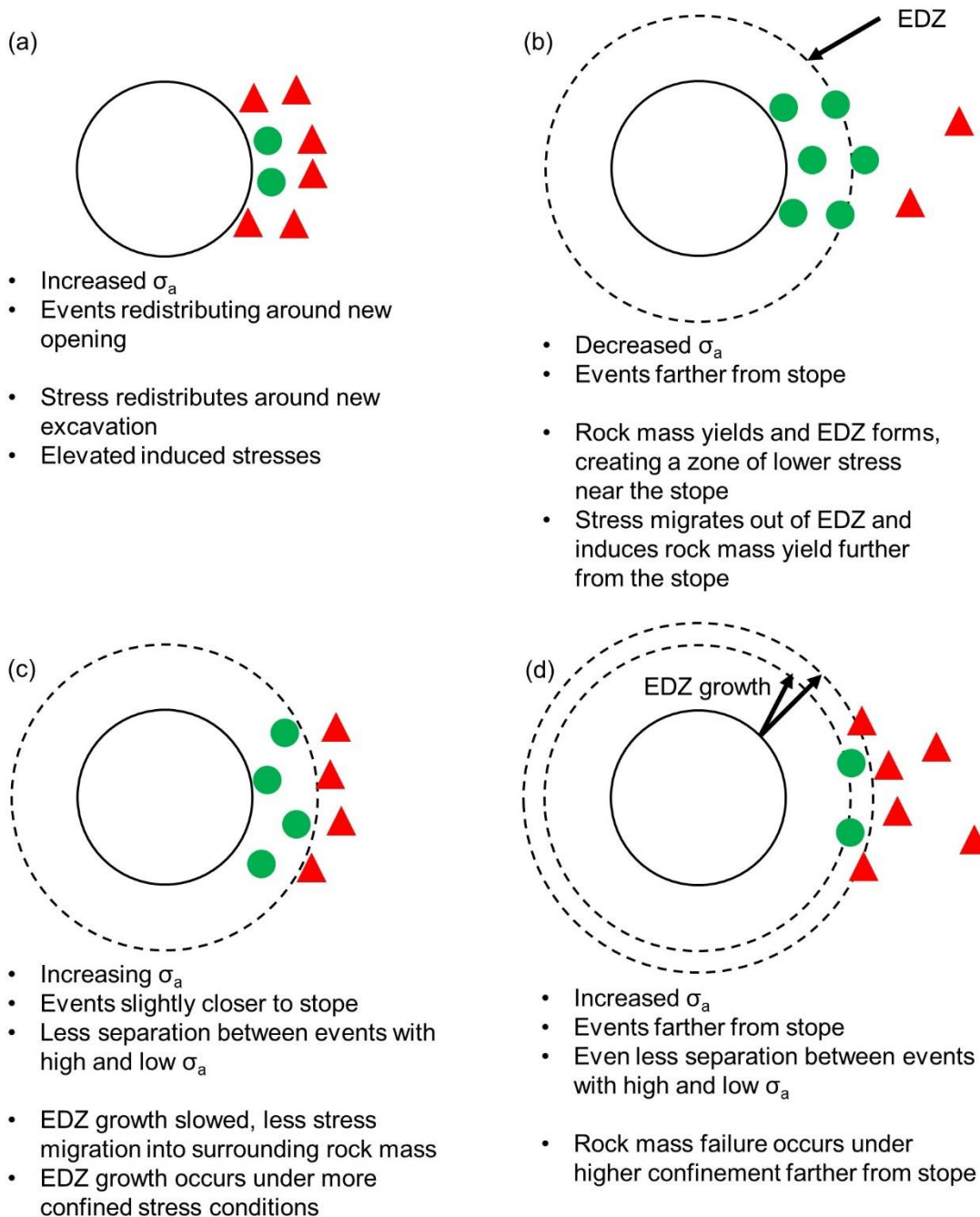


Figure 6-1: Schematic of interpreted typical behaviour and inferred rock mass response

One of the challenges with interpreting the rock mass response is inferring the nature of rock mass damage at different distances from the excavation. More damaged regions may host coalescing dilatational fractures which result in an overall decrease in stress in the post-peak. Less damaged regions may host more isolated fractures, corresponding with a rock mass that is yielding but still

accumulating strain energy as it approaches its peak strength. More complicated yet is the structurally-controlled damage which may occur at greater distances from an excavation. The results presented in this thesis elude to the complex behaviour of the rock mass within these damaged zones.

The initial movement of seismicity away from an open stope indicates that (1) stresses are redistributing around the new excavation and (2) there is a migration of rock mass yield which is progressing away from the excavation. However, the tendency for events to move back towards the stope some time after the blast (Phase 2 of MESD variation) indicates that the zone of active rock mass yield is not necessarily located as far away from the excavation as the first group of events following the blast would suggest. The more distant events (which tend to have higher apparent stress) may be more related to pre-peak strength and/or structurally-controlled damage. The stresses more distant from the excavation may not be great enough to induce failure of the rock mass into the post peak. However, the stresses in these more distant regions may start the process of yield or disturb structures such as joints or faults. The structural disturbance and yield (not necessarily in the post-peak) of the rock mass is what generates seismicity in the areas farther from an excavation which may not have visually-distinct damage.

The disturbance to the rock mass is what generates seismicity in regions outside the damage zone.

The damage zone grows with time, causing the seismogenic zone to gradually approach the areas where induced stresses initially resulted in a lesser degree of damage than closer to the excavation. There is a constant interaction between the growth of the EDZ and the disturbance of the adjacent rock mass. There will always be regions which are damaged and shed stress, and regions which are disturbed by stress redistributing outside of the damaged areas. These regions are not distinct, and a gradual transition occurs between them. The transitional nature between varying degrees of damage and disturbance throughout the rock mass makes specific information on the nature and degree of damage in any one area difficult to ascertain.

Inferences on rock mass behaviour are driven by the processes generating the greatest number of events in any given space and time. A single process may dominate the population of events in any space and time, making it challenging to identify, analyse, and describe other processes which are occurring simultaneously. For example, most events are generated when a rock mass enters its post-peak strength. As these regions shed stress, nearby regions are placed under higher stress

which may cause them to yield, but not yet pass their peak strength. These regions in an earlier state of yield may not generate as many events as those at a more advanced stage of strain and damage. Consequently, it is difficult to identify newly yielding regions of the rock mass when a large number of events is being generated by areas entering their post-peak strength. With regard to the observations in this thesis, it may be difficult to distinguish the regions of the rock mass that are starting to yield or where structures are being disturbed when the post-peak regions are generating larger numbers of events. Each phase of variation, be it in apparent stress or MESD, is driven by a dominant process (i.e. majority of events increasing/decreasing in apparent stress or moving towards/away from the stopes).

## 6.2 Typical Behaviour versus Analysed Cases

The inferred typical behaviour is only representative of the analysed cases. While the cases were taken from a variety of locations throughout the mine at different time periods, there are multiple similarities which dictate what the observed behaviour and inferred rock mass response is typical to:

- All cases are from large, open stope blasts, and are generally near the stope leading to low confinement conditions.
- The cases were selected based on having a minimum number of events, so the results are typical of seismic responses with greater numbers of events. Every seismic event represents an instantaneous, inelastic deformation in the rock mass, so a larger number of strains (generally greater than a certain size) in a finite volume of the rock mass implies that the volume has undergone more inelastic deformation. Consequently, a substantial yielding response is inferred in many of the analysed cases.
- The cases are all from Nickel Rim South (NRS) which has a unique set of properties which influence stress and yielding including:
  - Depth and stress conditions.
  - Rock mass properties.
  - Faults and other structures.
  - Mining geometry.
  - Mining sequence.
- The cases tend to be from specific places and times in the mining history of NRS:

- Areas with felsic gneiss (FGN) and Sudbury breccia (SUBX) lithologies.
- Later in the mine life with higher extraction and overall greater mining-induced stresses.

Several steps may be taken to broaden the analysis and verify that the proposed model for rock mass yield is more universal. The case studies can be diversified by analysing:

- Mines operating at different depths and in different stress conditions (e.g. different k-ratios).
- Rock masses with different levels of intact rock strength, jointing, and faulting.
- Mining methods and mining geometries which provide different levels of confinement (e.g. larger open stopes in a wider orebody or cut-and-fill mining in a narrow-vein deposit).
- Seismic responses from earlier in a mine's life where overall induced stresses are lower.
- Smaller seismic responses (fewer events).

### 6.3 Effects of Time Windows

#### 6.3.1 Effects of Different Window Sizes

A trendline shows change in some characteristic of a population of events. Different window sizes result in different populations of events being characterized at any given time. Accordingly, changing the size of a moving window can influence the analysis of a trend line. Chapter 4.1 presented an example of how different window sizes resulted in slightly different trendline behavior. In this section, the same example used previously, 1535-275-P1 SE corner, is analyzed quantitatively using varying window sizes. Using the same methodology applied throughout this thesis, the different window sizes produce slightly different results when analyzing MESD and apparent stress.

Table 6-1 summarizes the results of analyzing apparent stress variations in 1535-275-P1 SE corner using different window sizes. The results and observations are summarized as follows:

- Phase 1 appears to be anomalously short with a 50-event window and anomalously long with a 200-event window. These anomalies are caused by one of the trend lines peaking at a different time than the others and increasing or decreasing the average of all three.

- Phase 1 variations become smaller with larger window sizes. The small number of high apparent stress events carry less weight among larger populations. As a result, the increase in the trend lines is smaller.
- The durations of Phase 2 are relatively consistent for all the window sizes. The events occurring at the end of Phase 2 have consistently lower apparent stress than those occurring several tens to hundreds of events before or after. As a result, changing the window size by 100 events does not drastically change the duration of Phase 2.
- The average change during Phase 2 becomes smaller but more consistent with larger window sizes. The smaller window sizes reveal more erratic behavior, but the overall decrease is relatively consistent over several hundred events.
- The duration of Phase 3 increases with increasing window sizes. This change is attributed to the drop in apparent stress observed around 40 hours after the blast during Phase 3 (see Figure 4-5). This drop was interpreted as a relatively small inconsistency in what was an overall longer-term increase throughout Phase 3. The events occurring during this drop have consistently lower apparent stress than the events occurring after it. Larger windows cause these events to stay in the window for a longer period of time. Consequently, a larger window will cause the trendlines to increase for a longer time as these lower apparent stress events are still in the window.

Table 6-1: Analysis of apparent stress phases in 1535-275-P1 SE corner using various window sizes

Window Size	Events			Duration (hours)			Average Change (all trendlines)		
	P1	P2	P3	P1	P2	P3	P1	P2	P3
50	36	428	470	0.02	4.25	59.21	102%	-80%	71%
100	84	387	653	0.06	4.47	69.93	77%	-66%	76%
150	82	409	653	0.06	5.52	72.51	51%	-57%	43%
175	89	399	668	0.06	5.32	73.61	44%	-56%	50%
<b>200</b>	<b>128</b>	<b>340</b>	<b>725</b>	<b>0.12</b>	<b>4.37</b>	<b>80.11</b>	<b>16%</b>	<b>-48%</b>	<b>51%</b>
225	62	402	741	0.04	4.27	85.25	6%	-48%	53%
250	62	414	763	0.04	4.73	96.27	11%	-49%	49%
300	78	410	803	0.05	5.35	114.62	15%	-50%	42%

Table 6-2 summarizes the results of analyzing MESD variations in 1535-275-P1 SE corner using different moving window sizes. The results and observations are summarized as follows:

- The duration of Phase 1 increases and the average change decreases with increasing window sizes. Two processes occur during Phase 1: an initial redistribution of stress around a new excavation, and an outward migration. The migration back towards the excavation during Phase 2 is more gradual. Consequently, a longer moving window may cause Phase 1 to be longer because although events may start to move back towards the excavation, they are still farther from it than the events leaving the window. This behaviour represents a sort of artefact that is similar to the one observed in Phase 3 of apparent stress variation.
- There are anomalously low average changes during phases 2 and 3 when a 50-event window is used. The smaller windows result in more erratic trendline behaviour. This effect is exacerbated by dividing the moving window into events with high and low apparent stress, further decreasing the population size.
- The duration of Phase 2 and its average change decreases with increasing window size. Phase 2 is generally shorter than 150 events. Through a combination of time artefacts from Phase 1 events leaving the window and the relatively small number of events representing a smaller proportion of the population, a sufficiently large window may completely mask the occurrence of Phase 2.
- The duration of Phase 3 is relatively consistent, but the average change decreases with increasing window sizes. The migration away from the extracted stopes is slow but consistent throughout Phase 3. Phase 3 typically has a much larger number of events compared to Phase 2, giving it a consistent duration that is not significantly affected by artefacts. However, its average change becomes smaller when more distant events occurring later are grouped in a larger population where there are also events that occurred earlier and closer to the extracted stopes.

Table 6-2: Analysis of MESD phases in 1535-275-P1 SE corner using various window sizes

Window Size	Events			Duration (hours)			Average Change (all trendlines)		
	P1	P2	P3	P1	P2	P3	P1	P2	P3
50	392	139	484	1.86	6.18	59.82	260%	5%	9%
100	415	148	377	2.68	8.69	52.34	243%	-18%	46%
150	402	157	393	2.10	8.92	53.67	240%	-16%	45%
175	415	143	425	2.73	8.21	56.08	238%	-16%	44%
<b>200</b>	<b>446</b>	<b>134</b>	<b>476</b>	<b>3.80</b>	<b>9.57</b>	<b>55.91</b>	<b>215%</b>	<b>-13%</b>	<b>38%</b>
225	471	105	515	4.55	8.43	58.03	205%	-6%	33%
250	535	71	486	8.48	8.54	54.05	189%	-3%	28%
300	527	78	516	7.86	8.83	57.13	169%	-2%	24%

Different window sizes can cause small differences in the duration of phases and the magnitude of variations. However, the relative positions of high and low apparent stress events appear to be consistent with the results presented in Chapter 4 regardless of the window size. Table 6-3 summarizes the differences in MESD for events with high and low apparent stress relative to  $D_{50}$  using different window sizes. Three fundamental conclusions are consistent regardless of the window size used:

- High apparent stress events tend to locate farther from extracted stopes than low apparent stress events.
- Events with increasingly higher apparent stress tend to locate increasingly farther from extracted stopes (and vice versa for events with increasingly lower apparent stress).
- There is less separation between events with high and low apparent stress with each successive phase.

Table 6-3: Analysis of difference in MESD between high or low apparent stress events and  $D_{50}$  for 1535-275-P1 SE corner using different window sizes

Phase	Window Size	% Difference from $D_{50}$			
		$D_{50}L_{20}$	$D_{50}L_{50}$	$D_{50}H_{50}$	$D_{50}H_{80}$
Phase 1	50	-14%	-13%	5%	29%
	100	-38%	-15%	16%	36%
	150	-38%	-17%	11%	26%
	175	-40%	-20%	10%	23%
	<b>200</b>	<b>-39%</b>	<b>-14%</b>	<b>18%</b>	<b>31%</b>
	225	-41%	-21%	20%	30%
	250	-38%	-20%	25%	41%
	300	-37%	-20%	23%	35%
Phase 2	50	3%	-10%	11%	32%
	100	-21%	-22%	16%	40%
	150	-15%	-19%	13%	34%
	175	-37%	-21%	22%	36%
	<b>200</b>	<b>-41%</b>	<b>-14%</b>	<b>15%</b>	<b>34%</b>
	225	-38%	-12%	15%	33%
	250	-41%	-14%	16%	26%
	300	-33%	-17%	21%	33%
Phase 3	50	-25%	-13%	9%	17%
	100	-3%	-7%	11%	14%
	150	-9%	-12%	10%	21%
	175	-4%	-4%	9%	21%
	<b>200</b>	<b>-2%</b>	<b>-13%</b>	<b>9%</b>	<b>13%</b>
	225	-10%	-12%	8%	18%
	250	-9%	-10%	10%	14%
	300	-16%	-10%	11%	19%

Using different moving window sizes can alter the quantitative results of apparent stress and MESD variations. Conclusions drawn from quantitative results of a single case should be tested using different window sizes to reveal how they may have affected the interpretation of rock mass behaviour following the blast. For this reason, this thesis focused on the aggregated results of multiple cases analysed with the same moving window. Despite potentially small inconsistencies and artefacts within individual cases, this section demonstrated fundamental conclusions of this thesis remain consistent when the window size is varied:

- Three phases of apparent stress and MESD variation are consistently observed (so long as the window is not many times larger than the number of events in the phase).
- The individual variations occur over consistent time scales (i.e. minutes, hours, days), and each phase occurs over a different time scale than the others.
- Events with high apparent stress occur farther from extracted stopes where there is presumably more confinement and less rock mass damage (and vice versa for events with low apparent stress).

The example in this section demonstrated that a 200-event window is an appropriate middle ground for analysing the largest seismic responses at Nickel Rim South Mine. However, the results indicate that slightly smaller window sizes (between 100 and 200 events) may reveal more subtle and shorter-term behaviours (e.g. Phase 1 of apparent stress or Phase 2 of MESD variation). Smaller windows also enable the analysis of smaller seismic responses, enabling the methodology to incorporate a wider range of case studies. Ideally, a moving window should be shorter than the variations being analysed. However, it should not be so short that the trendlines become too erratic to interpret meaningful results.

### 6.3.2 Use of Fixed-Time Moving Windows

Based on the typical durations of phases of apparent stress and MESD variation, analysis of short-term variation in these parameters is less effective if performed with fixed length time windows (e.g. a 1-hour moving window). Each phase of variation occurs over significantly different durations of time than the others, despite all of them occurring in what was defined as the short term. Any fixed time window may be either too short or too long for at least one of the phases.

Furthermore, fixed time windows are susceptible to abrupt time artefacts which occur when events with drastically different characteristics that occurred over a short timeframe leave the window. These events leaving the window make it appear as if another sudden shift has occurred. The most prevalent source of time artefacts occurs during Phase 1 of apparent stress variations. Event rates are often highest, and events have elevated apparent stress immediately after the blast. This short period of high apparent stress events leaving the moving window creates an artefact during Phase 2. An example of this behaviour is shown in Figure 6-2. The figure shows a magnitude-time history which indicates the rate of events and apparent stress percentile graphs that use 1 and 2-hour moving windows. With both moving window sizes, there is a sudden drop (indicated on the figures)

at a time after the blast equal to the window length. In both graphs, this drop lasts around 10 minutes, and the percentiles exhibit little change for some period of time afterwards. This drop is not necessarily caused by low apparent stress events entering the window, rather, it is caused by high apparent stress events leaving it. This example also shows how a moving window longer than the duration of a phase can smooth out the variation. Phase 1 is shorter than 1 hour, so the Phase 1 events remain in both windows during Phase 2, making the variation seem less drastic until they leave the window.

Figure 6-2 also shows the number of events in the fixed-time moving windows at different times after the blast. The number of events in the moving window varies by more than an order of magnitude within several hours after the blast. The apparent stress percentiles also become noticeably more erratic as the number of events inside the window drops. The rapid variations in source parameters and event rates following blasts make fixed-time moving windows significantly less consistent and reliable for such short-term analyses.

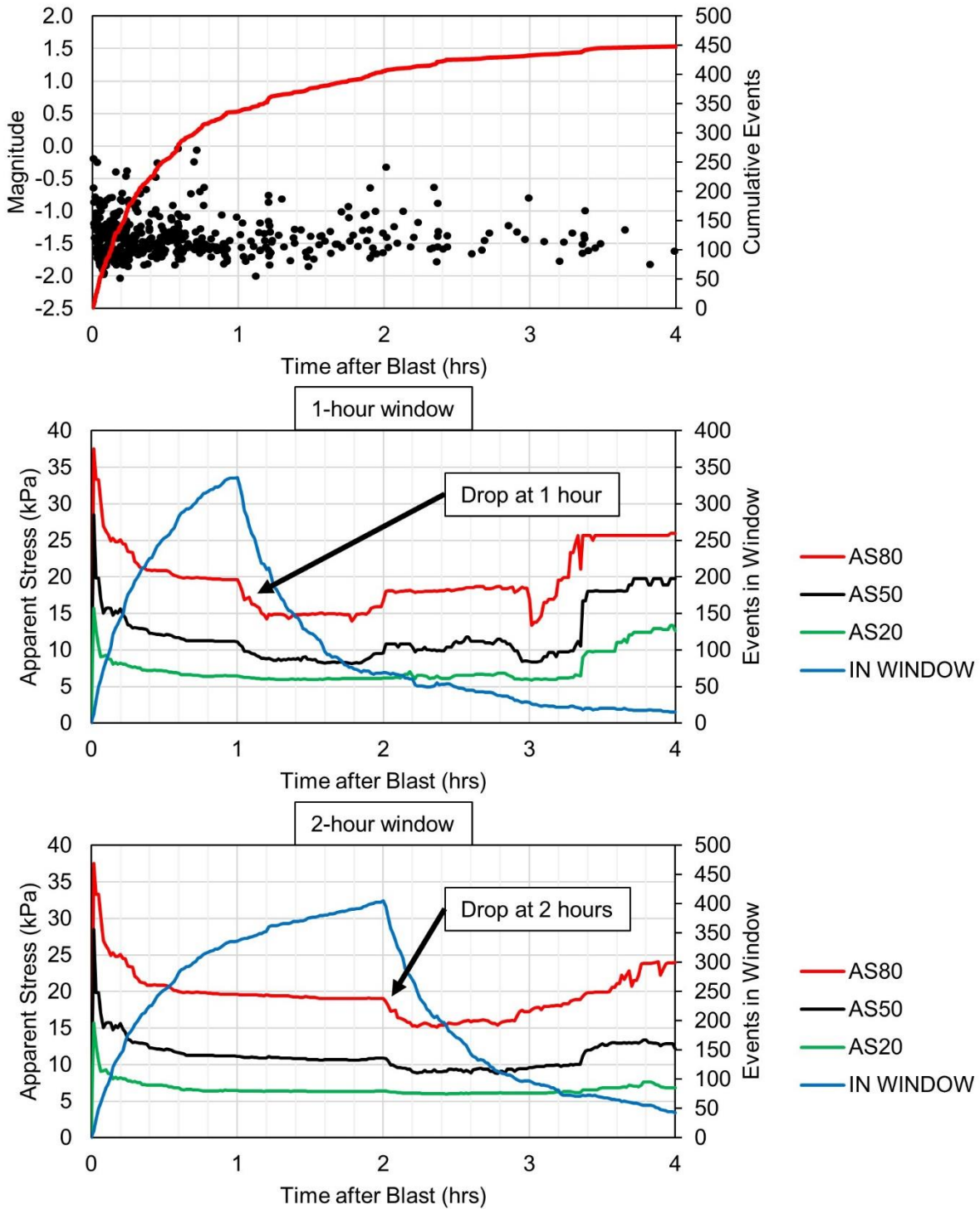


Figure 6-2: Example of time artefacts in apparent stress percentiles defined using fixed time moving windows following a final blast (1535-325-P1 SE corner, August 21<sup>st</sup>, 2016)

Moving windows defined by a fixed number of events (i.e. such as the ones used in this thesis) are less susceptible to time artefacts. It can be difficult to discern whether a change in a trend line is

more driven by the new events entering the window or the new ones leaving it. However, such behaviour is simply the nature of the methodology. At the very least, windows defined based on a fixed number of events are not affected by the rate of events, only the change in parameters for sequential events. This aspect of the methodology makes fixed-event moving windows less susceptible to time artefacts which may affect analysis of seismicity and corresponding inferences on rock mass behaviour.

#### 6.4 Inferring Brittle versus Softening Behaviour

As discussed previously, trend lines defined by moving windows can not only be affected by the events inside them, but the events leaving them as well. This aspect of moving windows makes it difficult to distinguish whether a variation is caused by a sudden shift from one distribution to another, or a more gradual transition with a sort of intermediate state between the end of one phase and the start of another. However, a more detailed analysis of the data can reveal which of the aforementioned behaviours is taking place, and the rate at which changes occur.

In terms of rock mass behaviour, the rate of change in apparent stress may indicate either brittle or softening behaviour. Recall from Chapter 2.1 that brittle failure results in a sudden drop in stress as rock yields, while strain softening involves a more gradual decrease in stress between the peak and residual strength. The number of events in phases 1 and 2 and the duration of and change observed during Phase 2 may be used to infer which constitutive behaviour is taking place.

Figure 6-3 compares apparent stress variations from two interpretations of different cases. Each interpretation has a similar number of events in phases 1 and 2. The ends of the first two phases are indicated on the graphs, and another indicator shows the time at which the Phase 1 events have left the 200-event window. The decrease at the beginning of Phase 2 may simply be attributed to the high apparent stress events that occurred during Phase 1 leaving the window. Any further variation that occurs during the Phase 2 is related to further decrease in apparent stress, rather than higher apparent stress leaving the window. With the 1535-275-P1 SE corner, most of the decrease observed during Phase 2 occurred while the Phase 1 events were leaving the moving window. This behaviour implies that stress suddenly dropped and remained constant after the rock mass yielded, similar to brittle post-peak behaviour. With the 1475-212-P1 back, only around half the decrease in apparent stress during Phase 2 occurred as the Phase 1 events left the moving window. Apparent stress continues to decrease for some period of time afterwards. This behaviour implies that the

rock mass transitioned more gradually from a high, to a moderate, and then to lower state of stress, similar to a strain softening response.

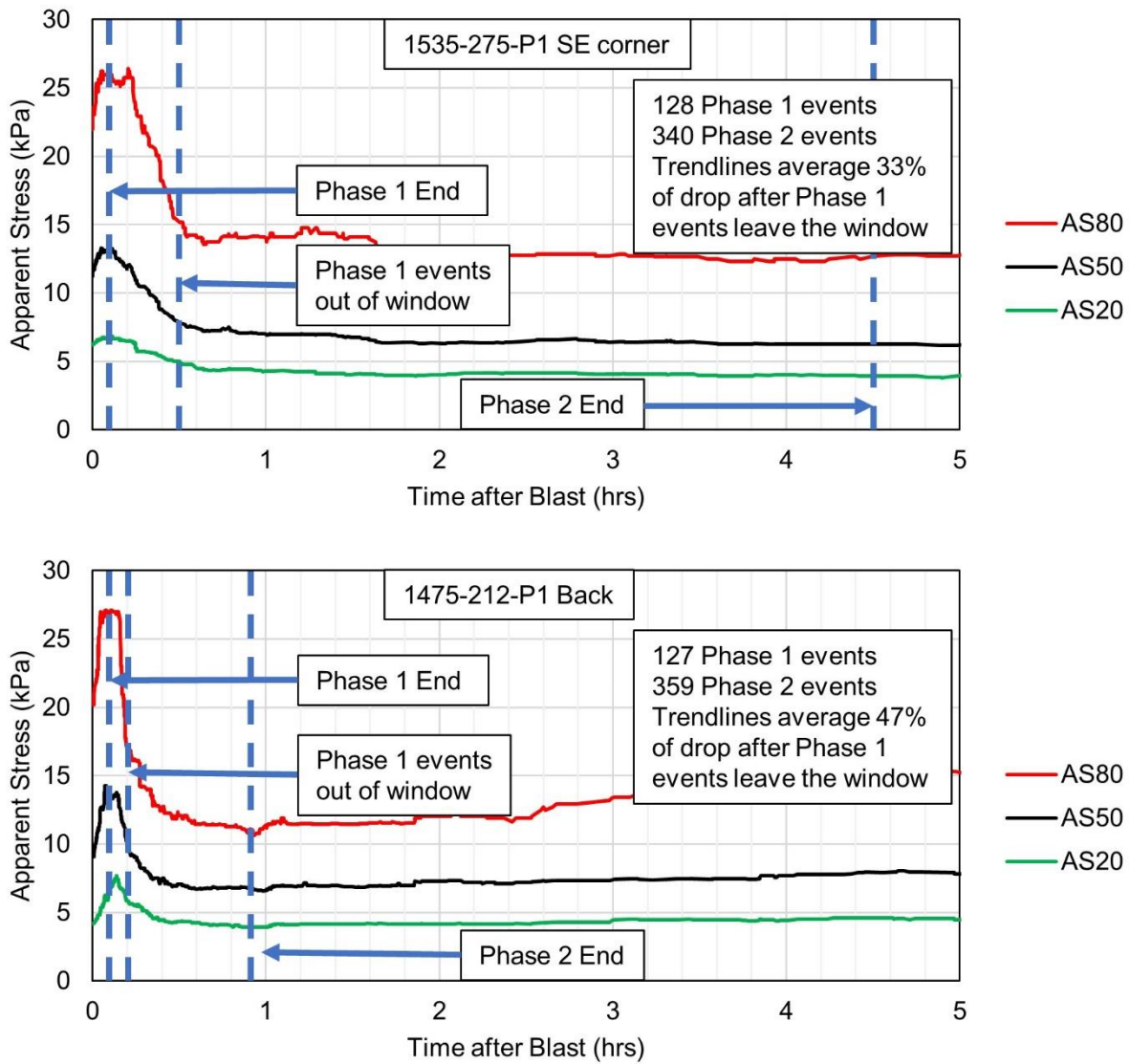


Figure 6-3: Comparison of apparent stress variation in 1535-275-P1 SE corner (June 19<sup>th</sup>, 2013) and 1475-212-P1 Back (December 29<sup>th</sup>, 2015) indicating duration of Phase 2 when Phase 1 events are leaving window

Chapter 6.3 demonstrated that specific quantitative results from individual cases should be tested using different moving window sizes. The analysis in Figure 6-3 indicated the 1535-275-P1 SE corner and 1475-212-P1 Back exhibit brittle and strain-softening behaviour respectively. However, more thorough analysis of these cases using different window sizes shows that this initial conclusion is erroneous. Table 6-4 and Table 6-5 show the portion of the Phase 2 drop that occurs after the Phase 1 events leave the moving window in each case. Using the same methodology

shown in Figure 6-3, the averaged results show that well over half the Phase 2 drop in 1535-275-P1 SE corner occurs after the Phase 1 events leave the moving window. The averaged results show that this case exhibits a more strain-softening response than 1475-212-P1 Back. In this volume, slightly less than half the Phase 2 drop occurs after the Phase 1 events leave the moving window. This result indicates a more brittle response than 1535-275-P1 SE corner.

Table 6-4: Proportion of decrease in apparent stress percentiles observed after Phase 1 events leave the moving window in 1535-275-P1 SE corner using various window sizes

Window Size	Events		% Drop after P1 events leave window			
	P1	P2	AS <sub>20</sub>	AS <sub>50</sub>	AS <sub>80</sub>	Average
50	36	428	78%	71%	61%	70%
100	84	387	24%	22%	13%	20%
150	82	409	46%	57%	70%	58%
175	89	399	50%	64%	81%	65%
<b>200</b>	<b>128</b>	<b>340</b>	<b>43%</b>	<b>29%</b>	<b>28%</b>	<b>33%</b>
225	62	402	96%	96%	104%	99%
250	62	414	93%	88%	94%	91%
300	78	410	85%	76%	71%	78%
	Average		64%	63%	65%	<b>64%</b>

Table 6-5: Proportion of decrease in apparent stress percentiles observed after Phase 1 events leave the moving window in 1475-212-P1 Back using various window sizes

Window Size	Events		% Drop after P1 events leave window			
	P1	P2	AS <sub>20</sub>	AS <sub>50</sub>	AS <sub>80</sub>	Average
50	43	368	49%	46%	56%	50%
100	85	362	40%	34%	31%	35%
150	140	316	22%	15%	19%	19%
175	143	333	35%	18%	20%	24%
<b>200</b>	<b>127</b>	<b>359</b>	<b>60%</b>	<b>44%</b>	<b>38%</b>	<b>47%</b>
225	149	328	69%	33%	32%	44%
250	165	322	42%	26%	26%	31%
300	143	408	130%*	89%	82%	100%
	Average		56%	38%	38%	<b>44%</b>

\* This drop is larger than 100% because AS<sub>20</sub> continued to increase after the end of Phase 1

The rate at which changes occur within each phase can be used to infer more detailed aspects of constitutive rock mass behaviour. In the example shown in this, the case with the inferred brittle response supposedly has lower confinement compared to the case with the inferred strain-softening

response. 1475-212-P1 was blasted as a pillarless stope against the extracted 1475-200-P1 and P2, and 1445-200-P1 stopes. Confinement in the back of this stope was reduced in two directions: vertically and along strike. The lower confinement may have contributed to the more brittle response. Conversely, 1535-275-P1 SE corner has reduced confinement in only one direction, perpendicular to the major principal stress and into the stope's corner. The comparatively high confinement in this case may have contributed to the inferred strain-softening response. Further consideration of rock mass and stress conditions near each case may elude to potential differences in the rate at which apparent stress and MESD variations occur.

## 6.5 Effects of Large Events

Seismic events are manifestations of the rock mass fracturing to relieve stress. In order to maintain equilibrium, stress must redistribute following an event. A large enough event might cause a significant stress redistribution, causing other events to occur nearby. Such phenomenon has been observed in both natural tectonic (King et al., 1994) and mining environments (Orlecka-Sikora, 2010). These subsequent events, known as aftershocks, tend to occur in areas which experience significant increases in shear stresses as a result of the large event (King et al., 1994; Orlecka-Sikora, 2010).

If a large event occurs within a seismogenic zone following a blast, the stress change caused by it and subsequent related seismic events may have a noticeable influence on apparent stress and MESD trend lines. One such example is found in the east sidewall of 1445-300-P1 on August 6<sup>th</sup> and 7<sup>th</sup>, 2012. Event rates decreased following the blast, but a  $M = 0.9$  occurred approximately 23.5 hours later. This event was followed by a  $M = 0.2$  and a  $M = 0.8$  in the next few minutes. These events occurred approximately 0.5 hours before the blasts at the end of that shift. Blasts at the end of the previous shift were development rounds located on 1190 and 1730, so there is assumed to be minimal additional induced stresses acting on the area following the stope blast.

Views of the stope and events locations over a period up to 25 hours after the blast are shown in Figure 6-4. Events that occur at a greater duration of time after the blast have larger markers. The large events were accompanied by around 50 events in the following hours. These events appear to occur farther from the stope than events that initially followed the blast. Several smaller events also occurred away from the east sidewall in a group designated as the east abutment.

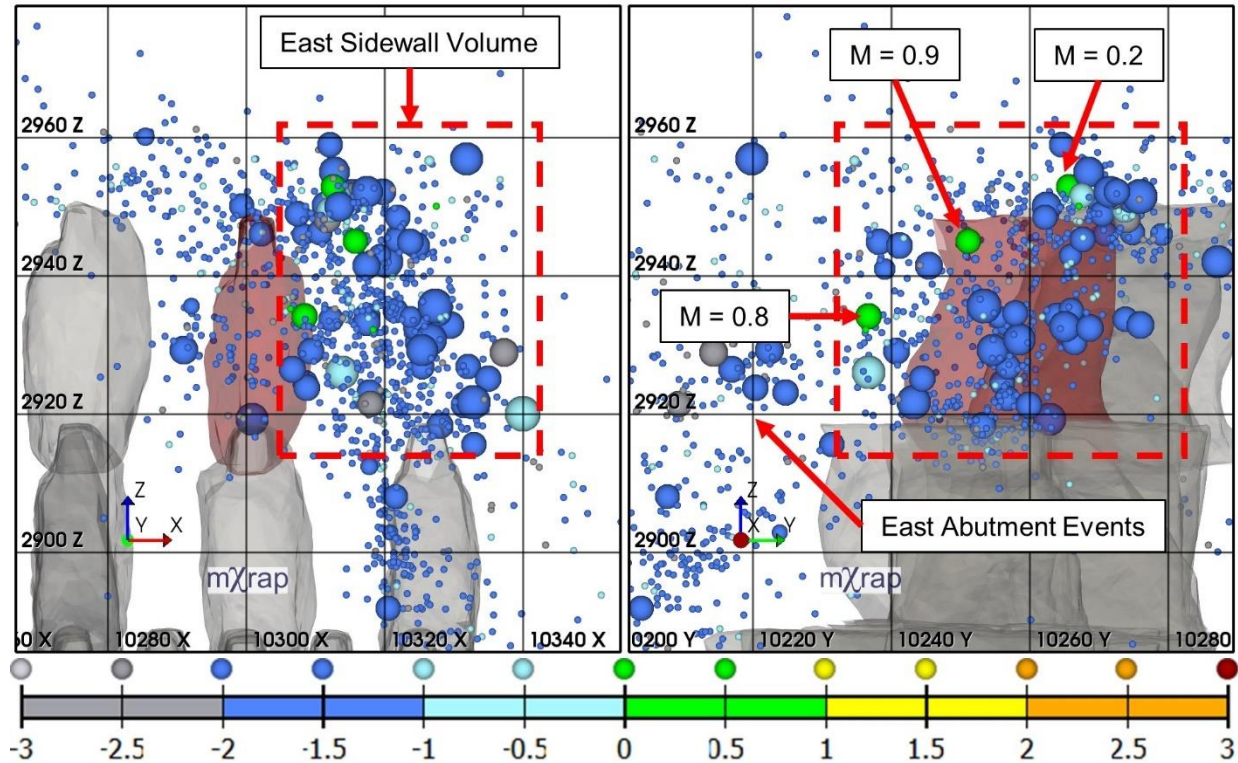


Figure 6-4: Longitudinal view looking north (left) and section view looking west (right) of event locations (coloured by magnitude and sized by time) in 25 hours following 1445-300-P1 final blast (August 6<sup>th</sup>, 2012)

Figure 6-5 shows magnitude-time, apparent stress, and MESD graphs from the east sidewall volume. The increased event rate following the large events is clearly visible in the magnitude-time graph around 23.5 hours after the blast. The event rate increase lasts a few hours and appears to have subsided by 28 hours after the blast. After this time, events occur at a nearly constant but slow rate. There is a spike in AS<sub>80</sub> and AS<sub>50</sub>, as well as in D<sub>50</sub>H<sub>50</sub>, D<sub>50</sub>, and D<sub>50</sub>L<sub>50</sub> following the large events. The large events and subsequent smaller events are interpreted to have occurred under higher stress conditions farther from the stope. However, it is not clear to what extent the elevated stress conditions were caused by large events versus the stope. Apparent stress and MESD are increasing before and after the increases in event rate which follow the large events. In this instance, the large events and subsequent flurry of seismic activity are interpreted to be a momentary occurrence in what is otherwise a continuous process of rock mass yield and stress redistribution resulting from the stope blast.

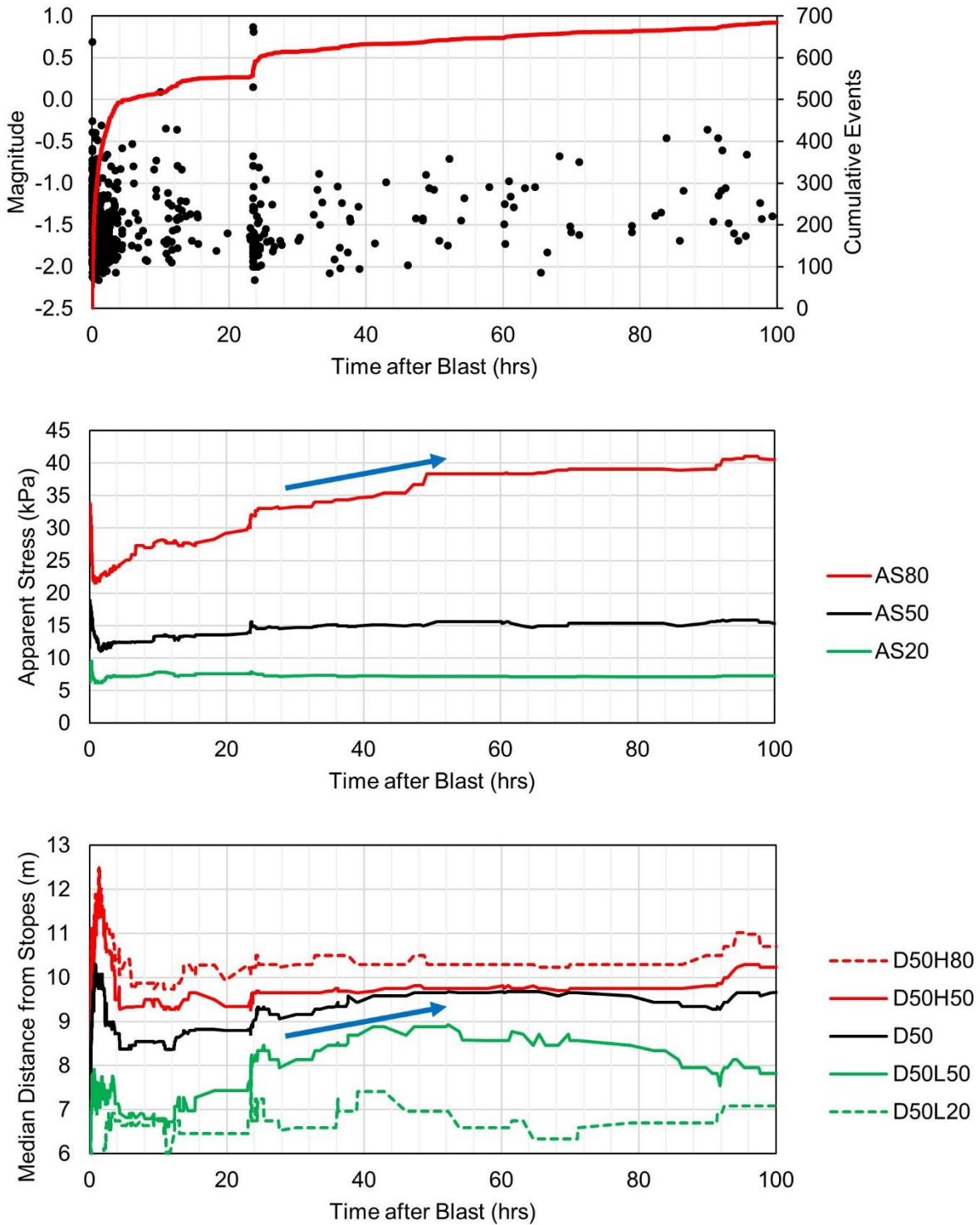


Figure 6-5: Magnitude-time, apparent stress, and MESD graphs of 1445-300-P1 east sidewall (August 6<sup>th</sup>, 2012)

There are however, examples of larger events and subsequent flurries of activity creating variations in apparent stress that mimic those that follow the studied blasts, but with greater amplitude. Figure

6-6 shows magnitude-time and apparent stress graphs of a population of events that covers a large volume in the eastern abutment of the orebody between the 1320 and 1445 levels. MESD analysis was not performed for this example because there were significant changes in the mining geometry which would alter event-stope distances over the period shown (3 stopes extracted on the abutment). The magnitude-time graph shows seismic responses produced by multiple stope blasts in that region of the mine over a period of 6 months. These blasts were between 4,000 and 40,000 tonnes, were followed by several hundred events each, and produced variations in apparent stress similar to those studied in this thesis (3 phases of apparent stress variation). In early September, a  $M = 2.9$  event occurred within a day of a stope blast. The large event was followed by several hundred smaller events and produced a variation in the apparent stress larger than any of the blasts in the past 6 months. The amplitude of the variation implies that the stress redistribution resulting from the  $M = 2.9$  event was larger than those caused by the stope blasts. It should be noted that the large event was followed by more events than any of the stope blasts. However, the stope blasts were often followed by several hundred events each. Therefore, it is not likely that the 200-event moving window smoothed over the variations in apparent stress resulting from those blasts.

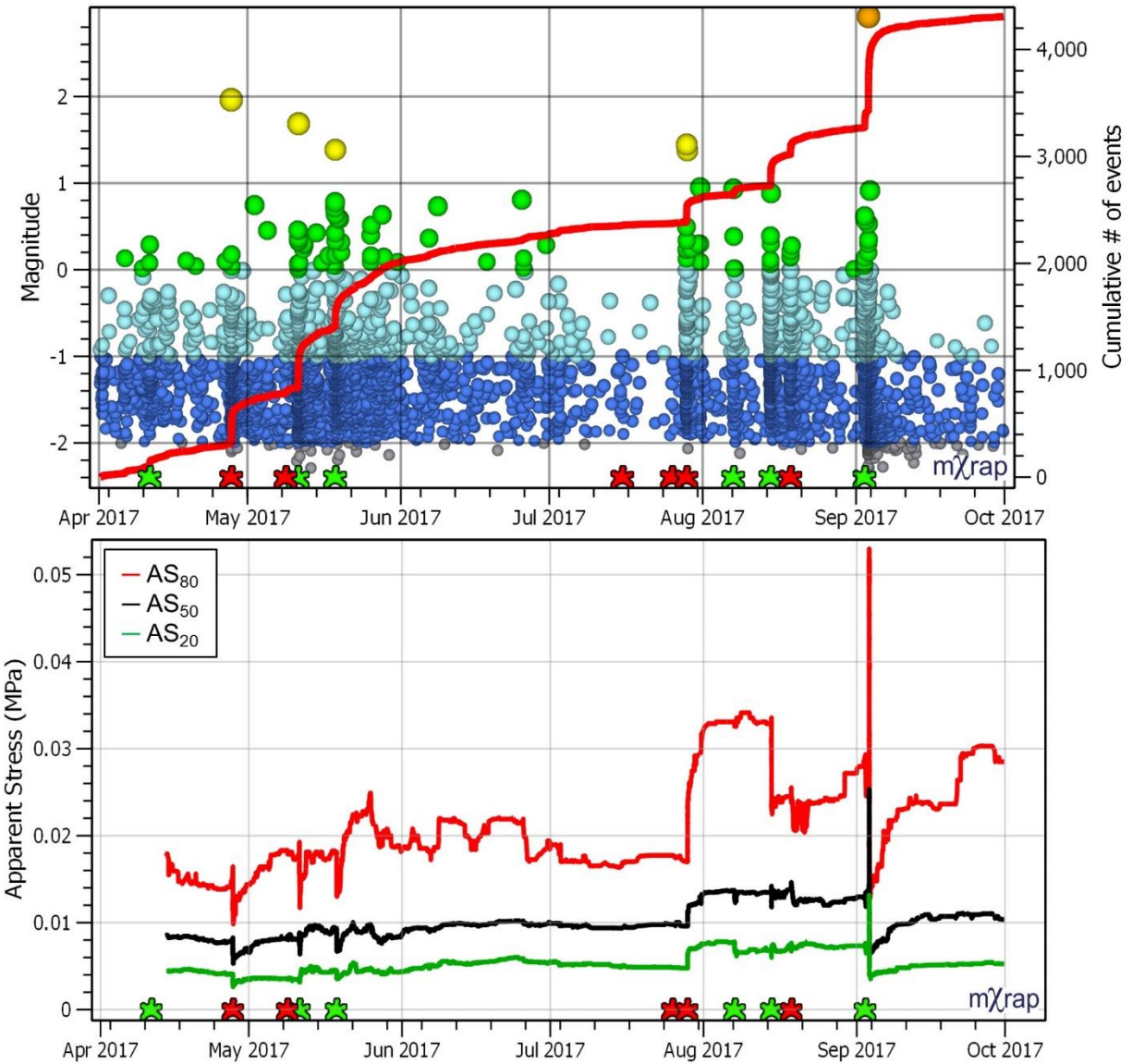


Figure 6-6: Magnitude-time and apparent stress percentiles in large volume between 1445 and 1320 east of 275 stopes (May to September 2017)

The time periods before and after the large event are shown in greater detail in Figure 6-7. The event occurred towards the end of Phase 2 or the beginning of Phase 3 of apparent stress variation. The variations in apparent stress following the large events are similar to those of the analysed final blasts. The variations imply that the large event caused stress to increase on the abutment, and then decrease over a period of several hours. Despite being associated with stress release, seismic events increase stress in some areas while causing it to decrease in others (King et al., 1994; Orlecka-Sikora, 2010). The resulting redistribution of stress may cause other areas of the rock mass to yield and relieve stress. The amplitude of the apparent stress variation caused by the

M = 2.9 event also eludes to the possibility that large events may cause stress redistributions and seismic responses on a scale larger than an individual blast. Therefore, there is the possibility that the stress redistribution caused by a blast may be smaller than the redistribution caused by a nearby large event that immediately follows it. Accordingly, the resulting space-time variation in apparent stress may be more of a reflection of stress change from the large event than the blast. Such effects may be difficult to investigate in seismic responses to stope blasts, which generate comparatively large stress changes. However, large events occurring near smaller blasts, such as development rounds which are on the order of a few hundred tonnes instead of several thousand, may demonstrate that the stress redistribution caused by an event may be larger than that caused by a blast.

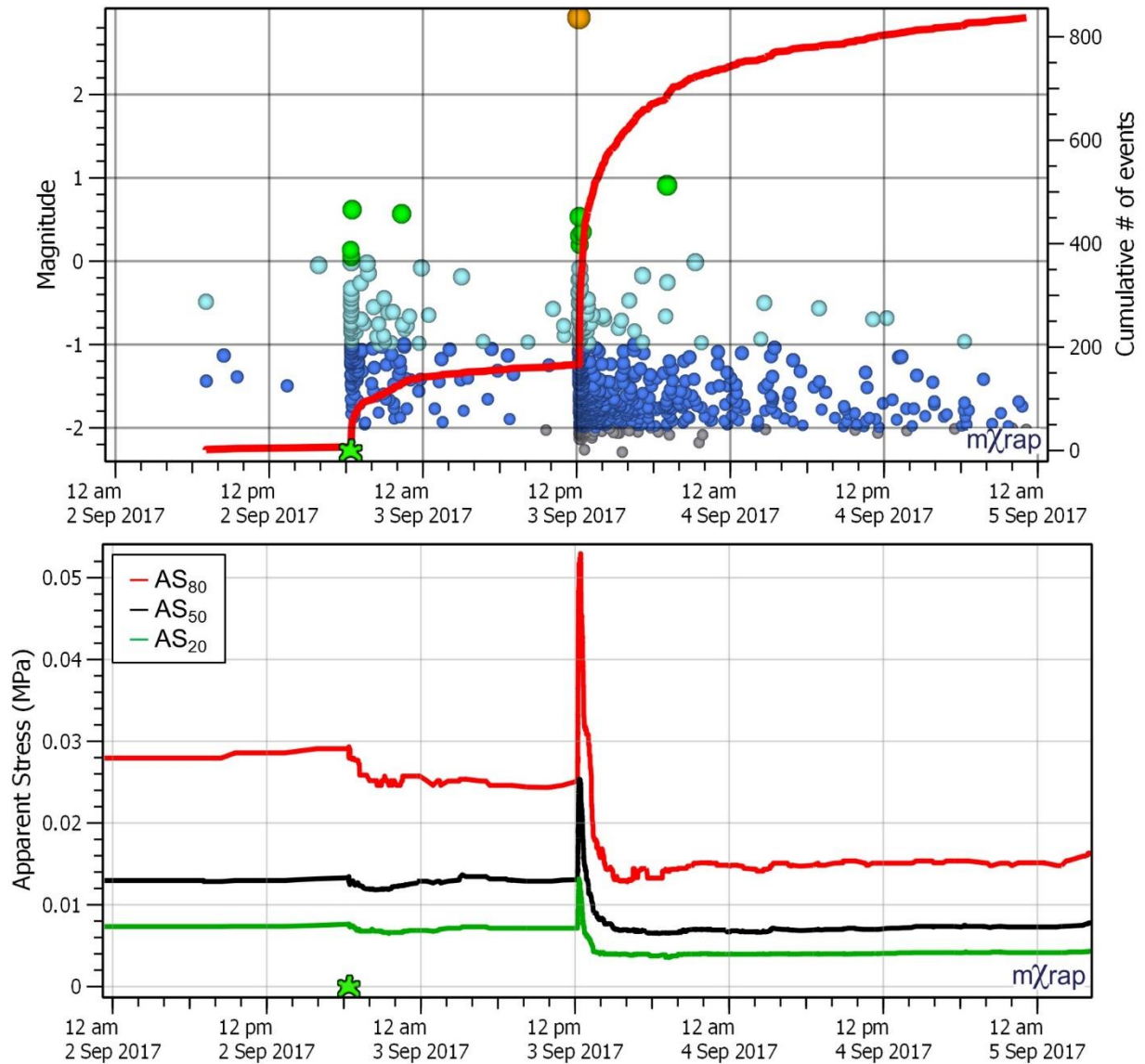


Figure 6-7: Magnitude-time and apparent stress percentiles in large volume between 1445 and 1320 east of 275 stopes (September 2<sup>nd</sup> to 5<sup>th</sup> 2017)

## 6.6 Additional Stress Changes in the Short Term

The methodology of analysing short-term variations in a spatially constrained volume was taken to isolate the effects of a single blast on a specific region of the rock mass. While many of the events and some substantial variations in apparent stress and event-stope distances occur within a matter of hours after the blast, other variations in these parameters occur over a period of several days. Blasts occur in various locations throughout the mine every 12 hours. One or more development blasts on the order of a few hundred tonnes are taken at the end of every shift, and stope blasts on the order of several thousand tonnes are taken every few days in order to maintain

the 3,000 tonnes per day production rate. Sequencing constraints and just-in-time development demand these blasts are located some distance away from other open stopes to maintain ground stability. However, these additional blasts inevitably induce some amount of stress change throughout the mine. These additional stress changes may affect a volume of the rock mass where seismicity is being analysed in the context of a previous blast. The degree to which these blasts may influence rock mass failure around other open stopes depends on their size and distance from the volume being studied, as well as pre-existing conditions within the volume being analysed.

The 1565-200-P1 west sidewall is an example of distant blasts inducing events and causing variations in apparent stress in a volume of the rock mass being studied in the context of a previous blast. 1565-200-P1 was blasted on May 6<sup>th</sup>, 2017. A few weeks later, a smaller stope was blasted on the same abutment two levels down: 1625-187-P1. 1625-187-P1 is an exceptionally small stope, with only a 3,200 t slash and an 8,000 t final blast. Figure 6-8 shows section views of event locations in 24 hours following the 1565-200-P1 final blast and the two blasts in 1625-187-P1. The 1625-187-P1 blasts are followed by events around that stope, as well as in the west sidewall of 1565-200-P1.

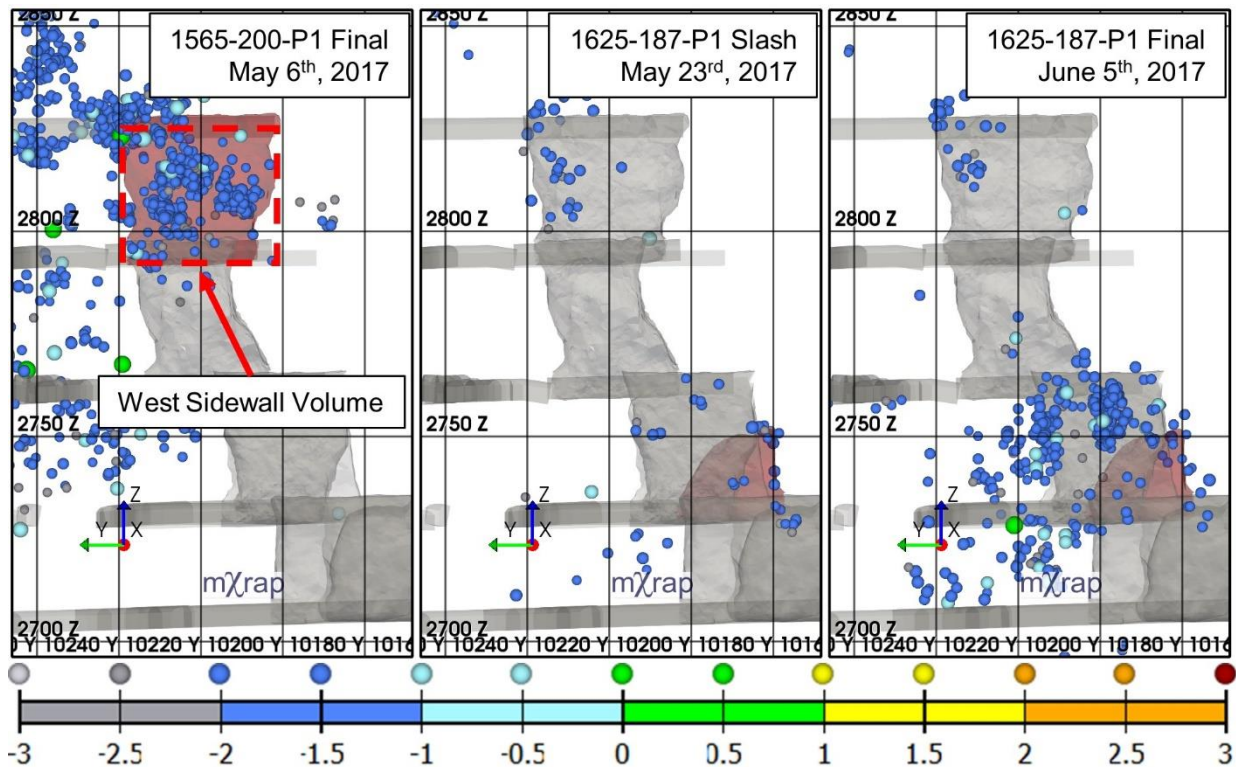


Figure 6-8: Section view looking east of event location (coloured and sized by magnitude) over 24 hour periods following blasts in 1565-200-P1 and 1625-187-P1

Figure 6-9 shows magnitude-time, apparent stress, and MESD graphs for the west sidewall volume. There are several times indicated in the charts where there is a sudden increase in event rate and corresponding sudden change in apparent stress and/or MESD. The indicated times correspond with:

- A.  $M = -0.7$  event and other smaller events
- B.  $M = 0.3$  event and other smaller events
- C. 1625-187-P1 slash (3,200 tonnes)
- D. 1625-187-P1 final blast (8,000 tonnes)

Variations produced by large events were discussed in the previous section and will not be addressed in the discussion of this example. The first blast in 1625-187-P1 produced a slight drop in  $AS_{20}$  and  $AS_{80}$  and caused events to move slightly farther away from the stope. The second blast caused an increase in  $AS_{20}$ , and no noticeable change in event-stope distances. The event rate increases and variations in apparent stress and MESD are small and short lived, much like those typically caused by larger events. However small these variations may be, they are potentially numerous, and not always easy to distinguish by a sudden increase in event rate (i.e. a distant blast or large event may only trigger one or two events near a distant stope). The implications of such effects are that variations occurring at greater lengths of time after a blast may be less related to the isolated effects of that original blast and become increasingly affected by the induced stress changes occurring throughout the mine. Therefore, the inferred stress increase and growth of the excavation damage zone observed during Phase 3 of apparent stress and MESD variation may not be driven solely by local effects of time-dependent yield in the rock mass, but also by small, cumulative increases in local stress levels resulting from distant blasts throughout the mine.

However, as stated in chapters 3 and 4, blasting near an open stope (be it on the same level or the level above or below it) is an uncommon practice at NRSM. Therefore, the effects of distant blasts are not believed to be a major factor in the observed Phase 3 behaviour. Furthermore, Phase 3 of apparent stress variation usually begins before any further blasting is performed. Phases 1 and 2 last approximately 6 minutes and 2 hours respectively, and the next set of blasts are taken 12 hours after the stope blast being studied. Apparent stress begins to increase before any new induced stresses are imposed on the volume being studied. Therefore, Phase 3 of apparent stress variation

can be attributed to localized effects of stress redistribution from rock mass damage near the open stope.

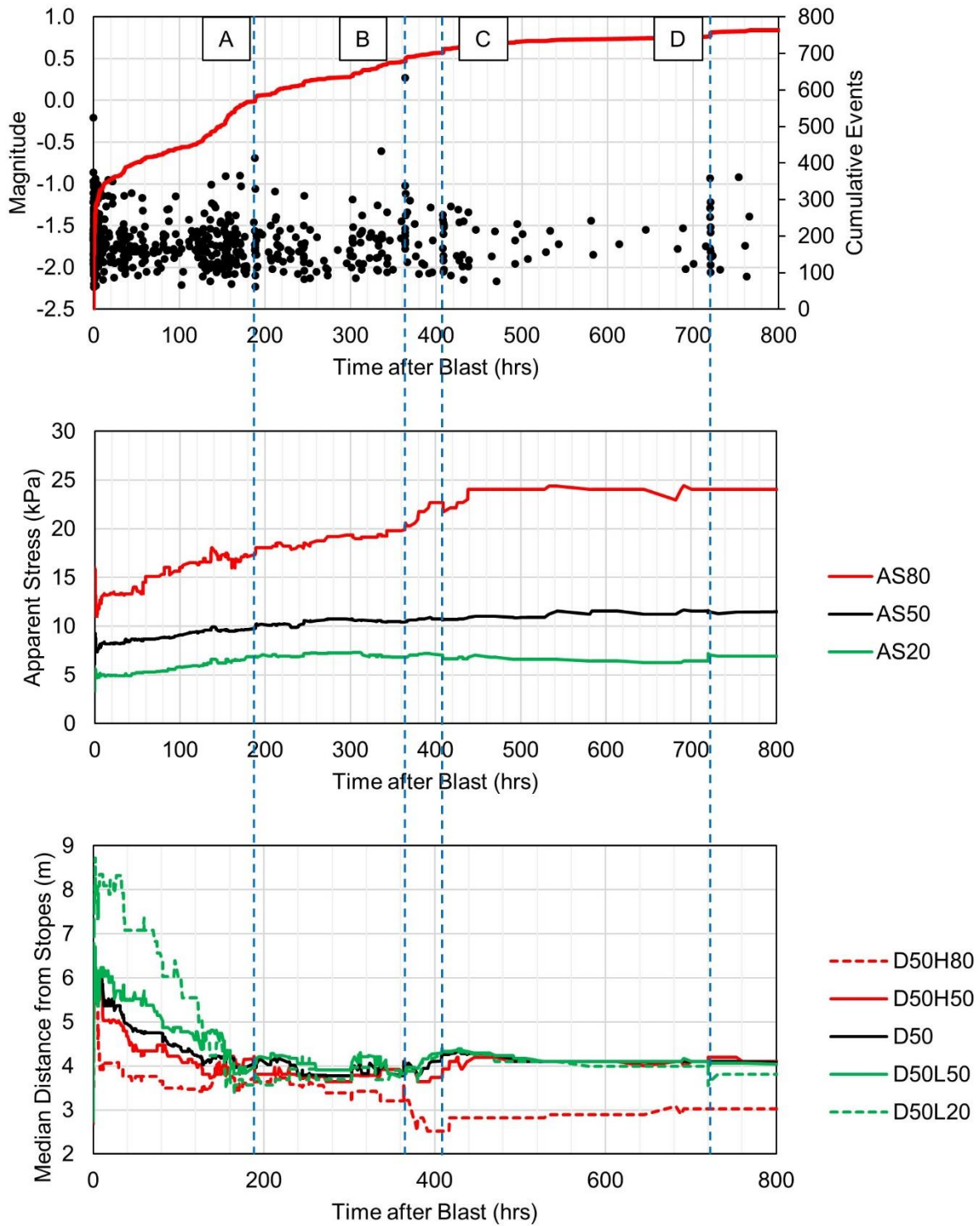


Figure 6-9: Magnitude-time, apparent stress, and MESD graphs of 1565-200-P1 west sidewall (May 6<sup>th</sup>, 2017)

Another potentially significant effect on the rock mass that occurs during Phase 3 of apparent stress and MESD variation may not be related to blasting at all. If the final blast is fired into the minimum required void, the muck pile will fill the stope to the upper stope access. While the blast significantly reduces confinement, the weight of the muck pile still exerts some outward pressure on the walls of the stope. Muck is removed from the stope at a rate between 500 and 1,000 tonnes per day (Xstrata, 2008). Since most Phase 3's in both apparent stress and MESD variation end several days after the blast, a significant amount of muck can be removed during the same period of time (several thousand tonnes constituting at least 5-10% of the tonnage of a final blast). The removal of muck may reduce confinement on the stope walls enough for additional yield to occur in the rock mass around the stope. This yield would occur at increasingly greater distances from the excavation under higher confinement than the events that initially formed the EDZ closer to the stope. As a result, apparent stress increases as the reduction in confinement from mucking causes events to occur at greater distances from the stopes. However, based on the density of blasted rock, the amount of pressure it exerts on the walls of the stope is relatively small compared to the overall redistribution of stress around the opening. Therefore, such effects are assumed to have a minimal impact on the results of this research.

Other non-blasting mining activities may also influence stress conditions and induce yield in areas of the rock mass distant from where the activities are performed. Drilling blasthole rings for other stopes creates "curtains" that stresses may have to travel around. Furthermore, empty stopes are backfilled with a hydraulic slurry that drains water into the surrounding rock mass which then percolates down through the mine, entering areas around other open stopes. Water lubricates faults and cracks and introduces pore pressure which acts against confinement of the rock mass, effectively reducing its strength. Inflow of water into an EDZ over a period of days or weeks may weaken the rock mass and allow for further yield to occur. As with the removal of muck from the stope, rock mass yield as a result of water inflow or ring drilling presumably occurs under higher confinement conditions than the initial formation of the EDZ near the stope, leading to increasing apparent stress over a period of days as the EDZ grows.

Small but numerous activities that influence stress and rock mass failure occur throughout the mine on a continuous basis. Furthermore, several other factors may contribute to localized rock mass yield in addition to the blast being studied in each case. For this reason, variations in apparent

stress and MESD among other parameters are increasingly difficult to associate with a single local induced stress change at greater time periods after it occurs. Accordingly, later phases of change in apparent stress and MESD occurring more than a matter of hours after a blast are increasingly difficult to interpret and relate to localized rock mass yield as a result of said blast.

## 6.7 Effect of Faults

The abundance of faults at Nickel Rim South inevitably results in some of the case studies occurring near these structures and potentially being affected by them. The variations in 1535-250-P2 west sidewall are an example of potential structural influences. The west sidewall of this stope is adjacent to the intersection of two major faults: NS-200 and LA5. Figure 6-10 shows longitudinal and plan views of event locations in the first day following the blast and the 30 days afterwards. NS-200 and LA5 faults are shown in brown and pink respectively. In the first 24 hours following the blast, several  $M > 0$  events occur in the west sidewall of the stope and along the western abutment. These large events and smaller ones tend to follow the strike of the NS-200 fault. The locations of these events suggest that they are somehow associated with this feature. The greatest number of events occurs close to the sidewall of the now open 1535-250-P2 stope. The events do not hug the stope's west wall and locate closer to the faults. The locations of the events indicate that they are associated with slip and fracturing near the stope, rather than rock mass yield immediately in the stope walls. This is not to say that rock mass yield does not occur immediately in the walls of the 1535-250-P2 stope (i.e. that region of the rock mass may have yielded before the final blast), rather the event locations following the final blast simply do not indicate that yield is occurring in that area.

In the weeks following the blast, events tend to have lower magnitudes ( $M < 0$ ). The seismicity appears to still follow the trend of the NS-200 fault, but the events tend to locate east of the geologist-interpreted fault plane rather than directly on it as they did during the day following the blast. The locations of events in the weeks following the blast indicate that they are not necessarily associated with slip along it but may be influenced by stresses near it.

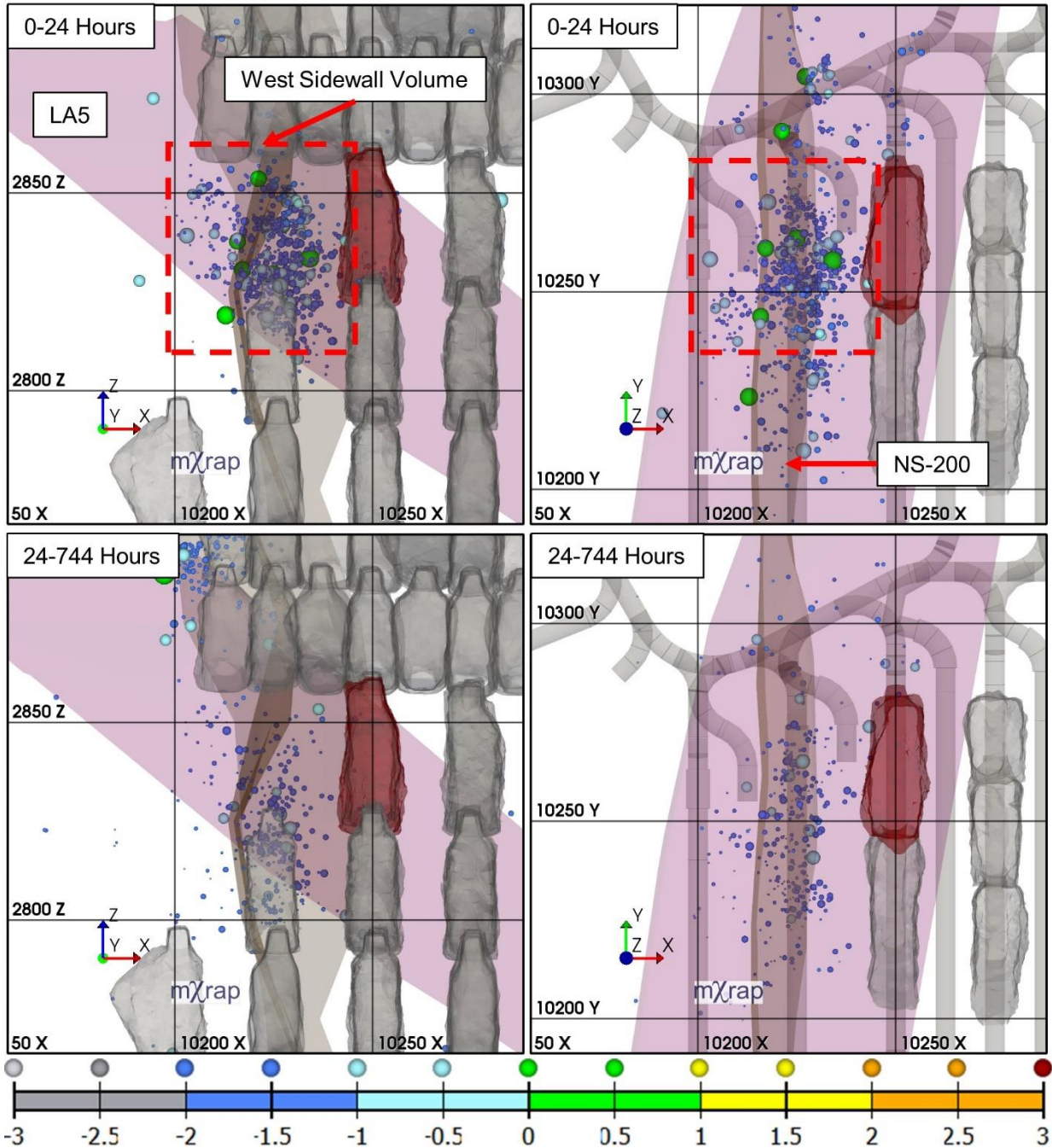


Figure 6-10: Longitudinal view looking north (left) and plan view (right) of event locations (coloured and sized by magnitude) in first day (top) and next 30 days (bottom) following 1535-250-P2 final blast (July 7<sup>th</sup>, 2015) showing LA5 (pink) and NS-200 (brown) faults

Figure 6-11 compares frequency-magnitude relations for events in the stope's west sidewall in the day after the blast, and the following 30 days. The frequency-magnitude relation for events in the 24 hours following the blasts is clearly bi-modal (Figure 6-11a). The bi-modal characteristics of the population indicate that that the nearby faults were the source of many of the larger events, and

rock mass fracturing was the source of many of the smaller events. In the following 30 days, the population has a substantially less bi-modal nature (Figure 6-11b). The b-value of the steep part of the relation is largely unchanged, but b-value for the larger events is steeper. The b-value for the population of events occurring longer after the blast indicates a more uniform, self-similar mechanism of rock mass fracturing. The bi-modal nature of the frequency-magnitude relation in the day following the blast also serves to reinforce that multiple processes are occurring in the seismogenic zone near an open stope: some that are related to fracturing of the rock mass, and some that are related to disturbing structures that are farther from the stope.

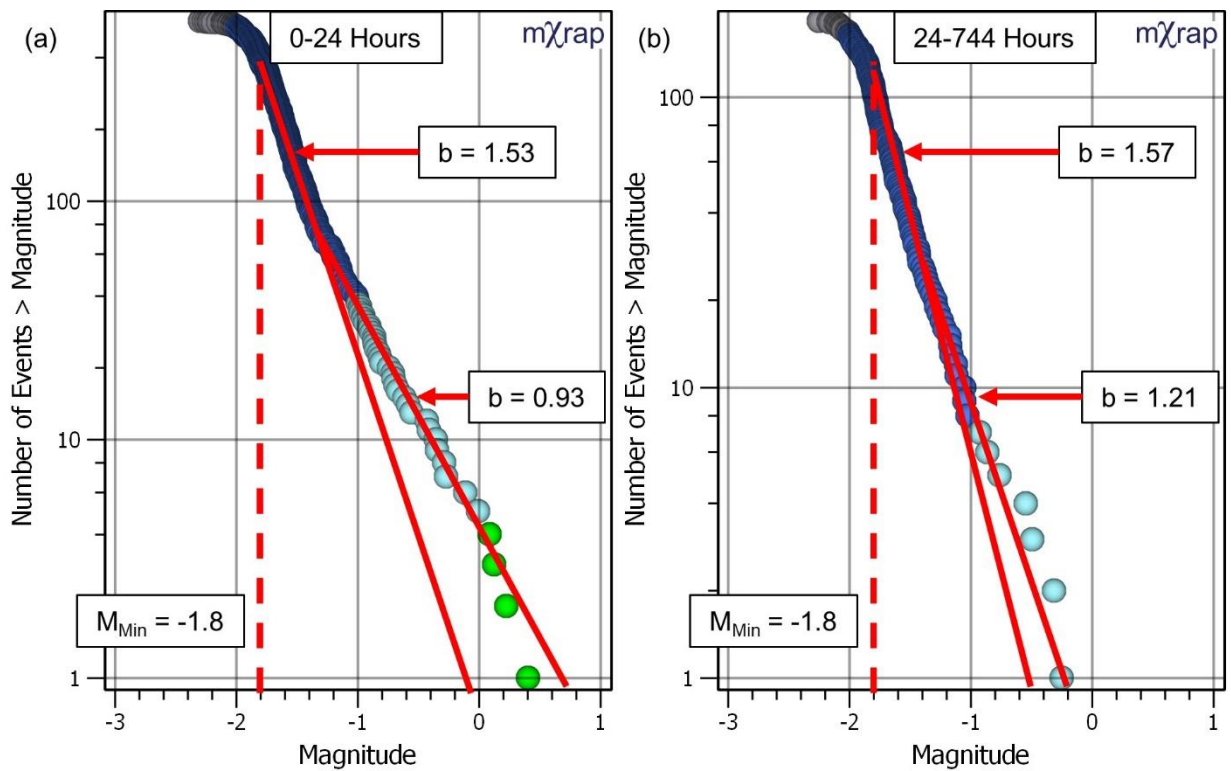


Figure 6-11: Comparison of frequency-magnitude relations for events in 1535-250-P2 west sidewall in first day following blast versus next 30 days

Figure 6-12 shows magnitude-time and apparent stress graphs up to 25 hours after the blast. Phase 2 ends around an hour after the blast.  $AS_{80}$  increases between 1 and 25 hours, but  $AS_{50}$  and  $AS_{20}$  are comparatively unchanged. It could be inferred that movement on the faults prevents the buildup of stress, causing the apparent stress of the majority of events in the population to remain low.

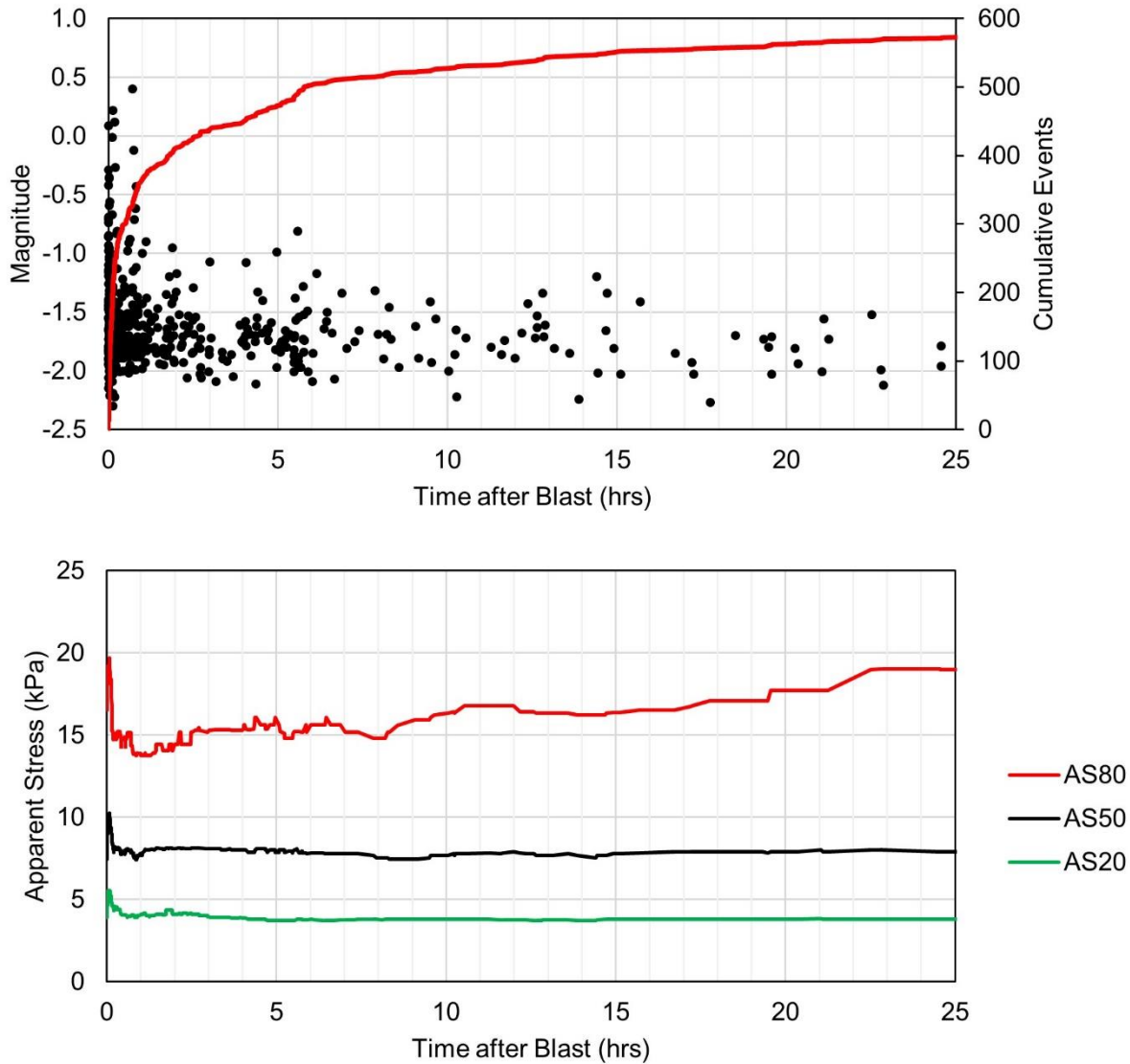


Figure 6-12: Magnitude-time and apparent stress graphs for 1535-250-P2 west sidewall up to 25 hours after blast (July 7<sup>th</sup>, 2015)

Figure 6-13 shows magnitude-time and apparent stress percentile graphs up to a month after the blast. Recall that the frequency-magnitude relation became less bi-modal following the first 24 hours, indicating a more uniform mechanism of rock mass yield. During this time, AS<sub>20</sub> and AS<sub>50</sub> rise along with AS<sub>80</sub>. Based on this behaviour, it is inferred that rock mass yield is occurring under higher stress conditions. During this time period, events also tended not to locate directly on the fault plane, indicating that the structure itself is no longer the dominant seismic source, but may still play a role in local seismicity. Recall that there is often a stress channeling effect observed between faults and excavations at NRSM. This example shows that such stress channeling effects may be influenced by slip on the faults, which may prevent stress buildup.

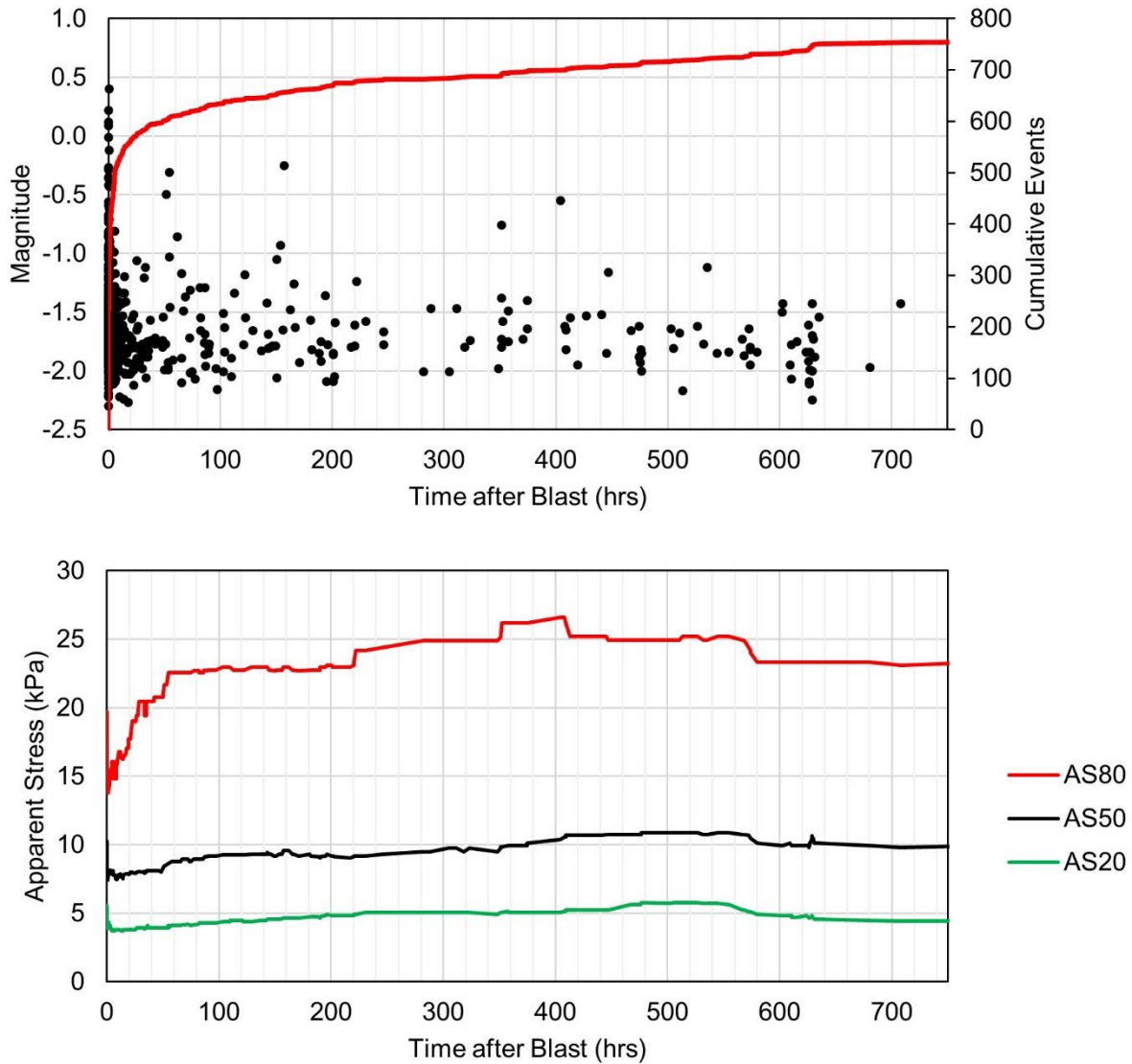


Figure 6-13: Magnitude-time and apparent stress graphs for 1535-250-P2 west sidewall up to 750 hours after blast (July 7<sup>th</sup>, 2015)

Geologic structures such as faults can influence local stress fields. The abundance of faults at NRSM implies that many of the case studies were taken from volumes of the rock mass where a fault was present. The influence of faults on space-time variations in apparent stress was not the subject of this thesis but may have significant implications on inferred stress changes in the rock mass. Therefore, further study is warranted on variations in apparent stress in less faulted environments.

## 6.8 Effects of Confinement

Most case studies in this thesis were taken from volumes of rock adjacent to open stopes (e.g. sidewalls and corners). The modelled behaviour of variations in apparent stress and MESD in this thesis are therefore most representative of rock mass yield in low-confinement conditions. The cases with the lowest confinement conditions are those taken from temporary pillars. Temporary pillars have reduced confinement on two sides of the volume (compared to usually only one side in sidewall and corner cases). Although only two pillar cases were analysed, they both exhibited the typical behaviour modelled in this thesis. One of these cases was 1595-200-P1 pillar which was formed with the adjacent 1595-225-P1 and P2 stopes on October 22<sup>nd</sup>, 2014. The magnitude-time, apparent stress, and MESD graphs for this case are shown in Figure 6-14. The graphs focus on Phase 3 of apparent stress and MESD variation, during which apparent stress is increasing and events are moving away from both adjacent stopes. Of note is that the MESD for the events with the highest apparent stress ( $D_{50}H_{80}$ ) moves to approximately 5.5 m away from the stopes. This MESD is within 1 m of the centre of this 12.5 m wide pillar, indicating that the events with the highest apparent stress, and inferred highest stress, are at the core of the pillar where the mining geometry suggests that rock mass has the most confinement.

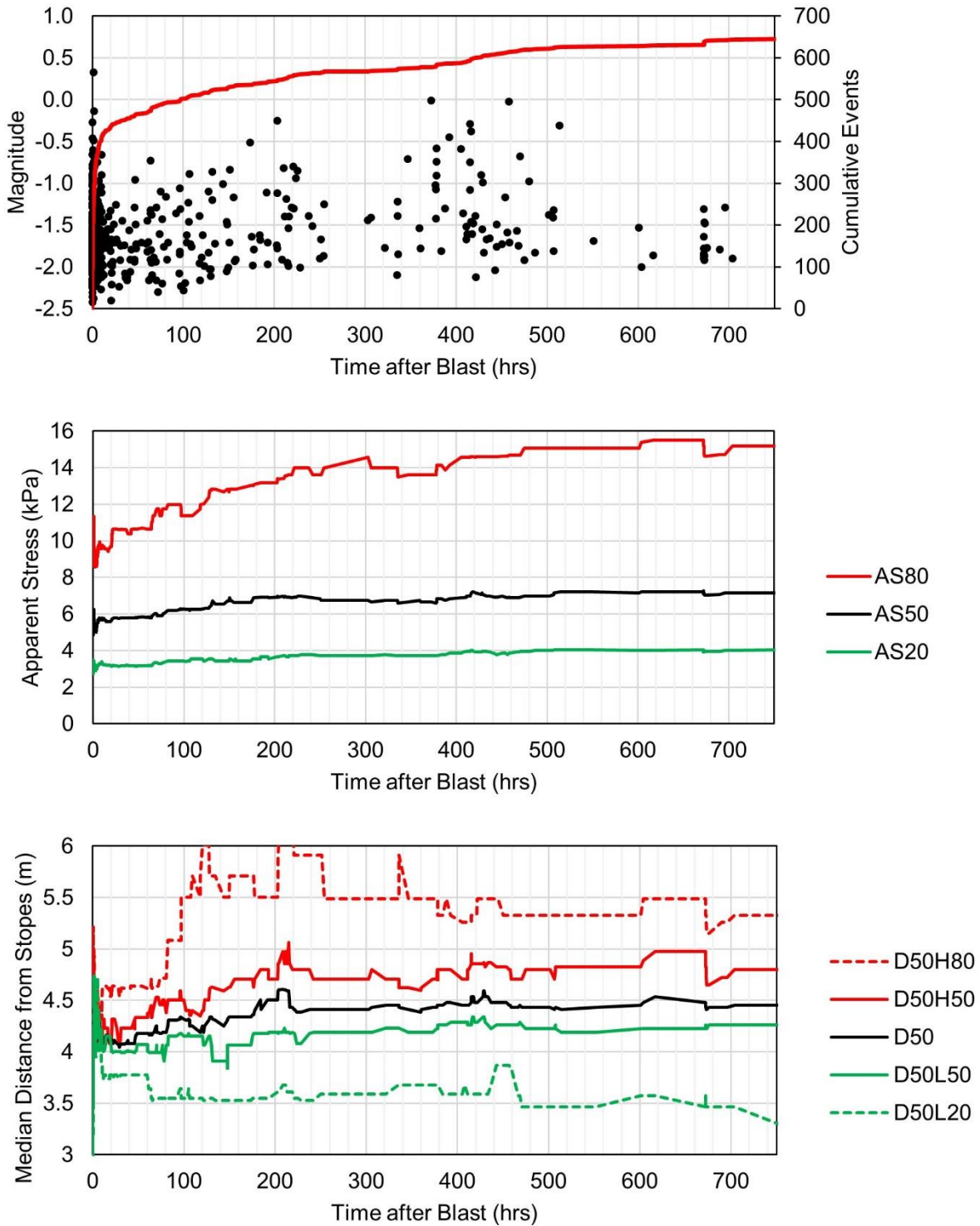


Figure 6-14: Magnitude-time, apparent stress, and MESD graphs for 1595-200-P1 pillar (October 22<sup>nd</sup>, 2014)

Figure 6-15 shows event locations in the pillar up to a month after the 1595-200-P1 final blast. The figure shows events coloured by both apparent stress and event-stope distance. The events

farthest from both stopes are located in the centre of the pillar. The figure also shows only events with apparent stress above  $AS_{80}$  at the end of Phase 3 (approximately 15 kPa). These events tend to locate towards the centre of the pillar, as indicated by the MESD graph. They also tend to locate higher up in the pillar, where there is a wider section of rock mass between the adjacent 1565-200 and 1565-225 stope accesses. The figure also shows views with only events below the  $AS_{20}$  at the end of Phase 2 (approximately 4 kPa). These events locate throughout the pillar and near the walls of the adjacent stopes. Conversely, the events with high apparent stress ( $\sigma_a > 15$  kPa) only locate at towards the core of the pillar. Based on the locations of events with high and low apparent stress, regions of the pillar with high confinement and high stress, and low confinement and low stress have been inferred. The middle and top of the pillar have the highest confinement and stress. Meanwhile, the sides of the pillar adjacent to the stope walls have the lowest confinement and stress. This example demonstrates the ideally interpreted rock mass behaviour, and corresponding inferred rock mass conditions.

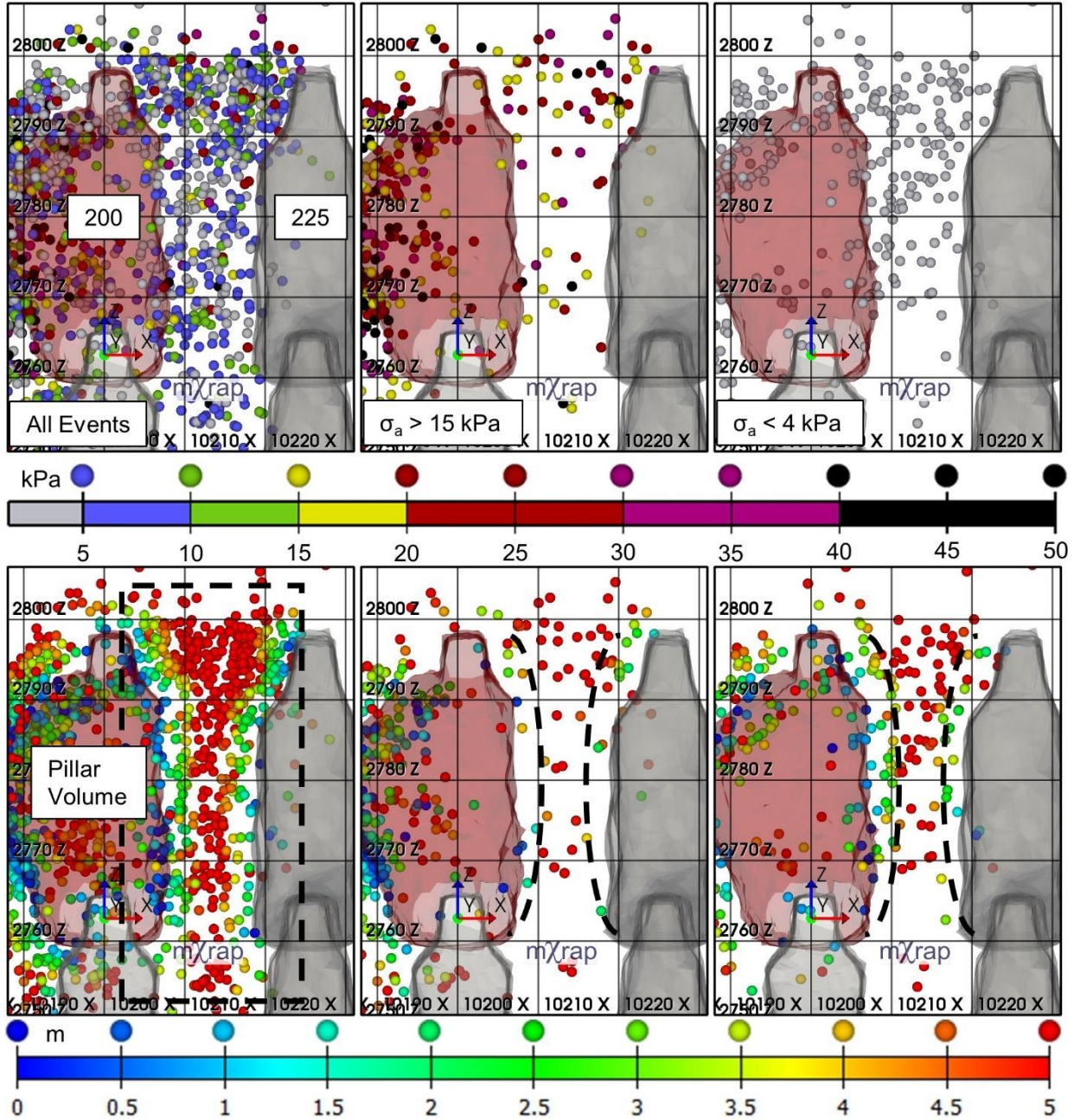


Figure 6-15: Longitudinal views looking north of event locations in pillar formed by 1595-200-P1 (October 22<sup>nd</sup>, 2014) up to one month after blast coloured by apparent stress (top) and event-stope distance (bottom) showing all events (left),  $\sigma_a > 15 \text{ kPa}$  (centre), and  $\sigma_a < 4 \text{ kPa}$  (right)

There is a minority of case studies taken from higher confinement conditions (e.g. abutments with no adjacent open stope). Seismic responses in abutments account for 12 out of 50 cases and 16 out of 62 interpretations of apparent stress and MESD variation analysed in this thesis. These cases were often more difficult to interpret using the three-phase models for apparent stress and MESD variation. In 4 of these cases a large event was associated with a noticeable sudden increase in

apparent stress during Phase 3. The sudden increases associated with large events indicate that these cases involve more complicated rock mass behaviours that incorporates other significant stress changes. At least one phase of MESD could not be interpreted in 6 out of the 12 abutment cases (and 8 out of the 16 interpretations). By comparison, only 5 out of the 46 interpretations not in an abutment had at one or more phases of MESD variation that could not be interpreted. The difficulty with fitting abutment cases with the proposed models of apparent stress and MESD variation implies that seismicity in these cases is unlike seismicity observed in the lower confinement conditions adjacent to open stopes. Accordingly, the processes controlling rock mass yield and generating seismic events may not be the same either.

Figure 6-16 shows magnitude-time, apparent stress, and MESD graphs for a response in the eastern abutment following the 1535-275-P2 blast. This case exemplifies the difficulties encountered when attempting to interpret variations in abutment volumes using the three-phase model. The apparent stress variations begin with the typical Phase 1 and 2 responses. During Phase 3, jumps in event rate around 7 and 8 hours after the blast occur and the apparent stress increases suddenly. Approximately 18 hours after the blast, a  $M = 1.9$  event occurs in the abutment and apparent stress increases significantly. The peak in the apparent stress following this event is greater than their highest levels over the next 100 hours, making it difficult to interpret whether this spike or the later, more gradual crest constitutes the end of Phase 3. In the MESD graph, there is no clear interpretation of the three-phase model.  $D_{50}$  is relatively consistent following the blast, increasing and decreasing erratically but staying around 10.5 m from the stopes. With the  $M = 1.9$  event, the MESD increases drastically, as the large event and subsequent flurry of smaller events occurs farther away from the stopes into the hanging wall. At the very least, this case is similar to the majority of others in that the events with higher apparent stress tend to locate farther from the stopes than events with lower apparent stress.

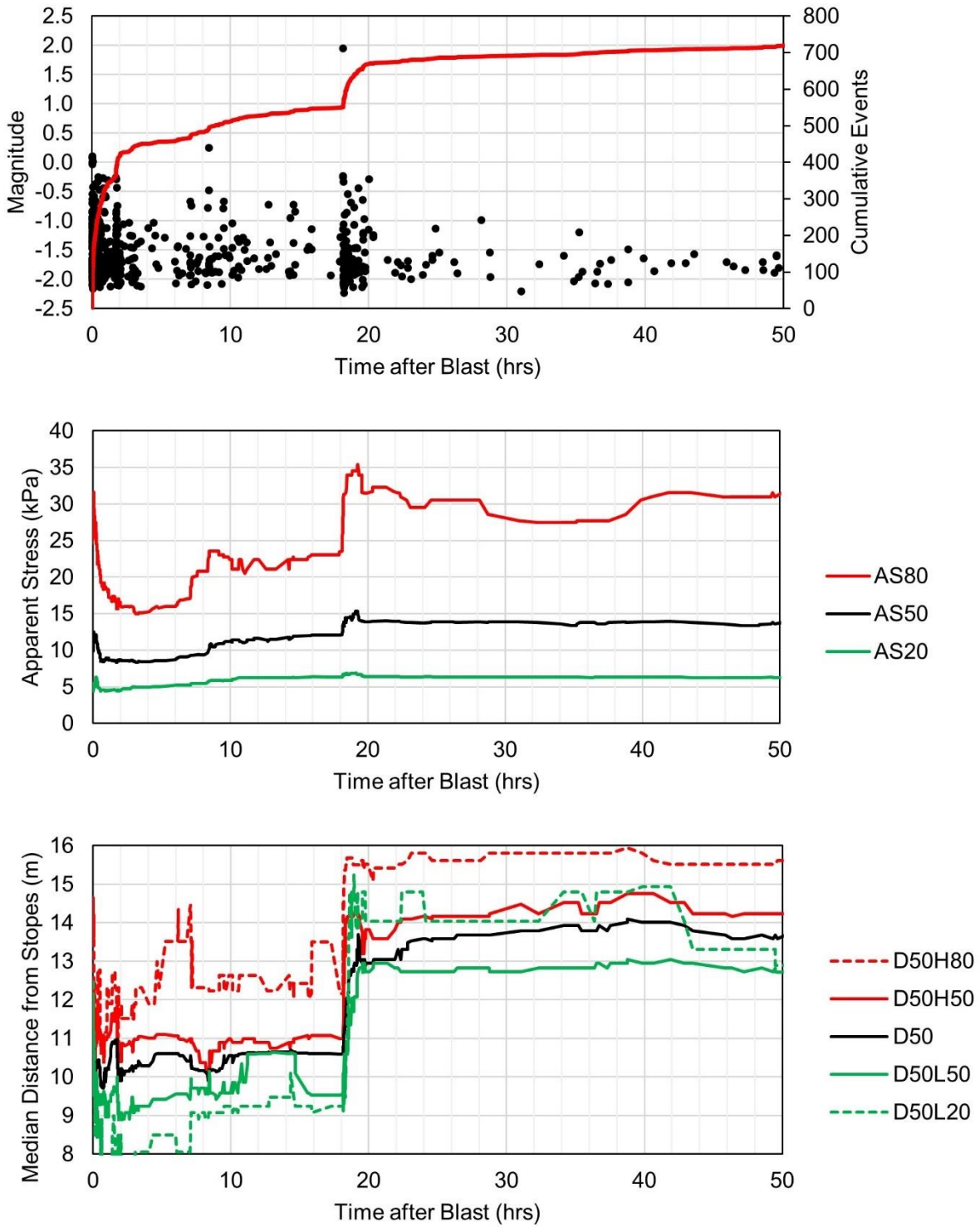


Figure 6-16: Magnitude-time, apparent stress, and MESD graphs for 1535-275-P2 east abutment (September 15<sup>th</sup>, 2013)

Compared to seismogenic zones adjacent to open stopes, there is minimal change in confinement in seismogenic zones in abutments. If not driven by a major loss of confinement, seismicity in these regions must be linked to one or more of the following mining or structural influences:

- An increase in one of the other major stresses from a nearby blast.
- Slip on a geological feature.
- A small perturbation in confinement driven by larger-scale convergence of the surrounding rock mass into the extracted stopes.

The seismic source mechanisms occurring in confined regions of the rock mass are inherently different from those occurring in less confined regions close to newly blasted stopes. As a result, the model for rock mass yield in high-confinement regions may differ from the model in low-confinement regions and be more complex.

## 6.9 Scale Effects and Impact on Analysis

Apparent stress is a scale-dependent parameter in many mining data sets. As a result, a change in the size distribution of a population of events, which can be indicated by the b-value of its frequency-magnitude relation, can change the distribution of apparent stress without any change in energy-moment scaling. Urbancic et al. (1992b) show examples from Strathcona Mine, Sudbury, Ontario where b-values are inversely correlated in space and time with the average apparent stress as well as other measures of co-seismic stress change. From these results, it follows that a low b-value indicates a greater proportion of larger events in a population, which in turn implies a larger proportion of events with higher apparent stress. This greater proportion of events with high apparent stress gives an overall higher distribution of apparent stress (and vice versa for higher b-values). If there is no change in energy-moment scaling, the methods in this thesis are potentially an indirect way of measuring variations in the size distribution of events following open stope blasts.

To address this issue, 1535-275-P1 SE corner, a familiar example from Chapter 4, will be re-analysed considering the size distribution of events in space and time. The results of the analysis using apparent stress will also be compared alongside results from an identical methodology that uses energy index (EI) in place of apparent stress. Recall that energy index (van Aswegen and Butler, 1993) is a scale-independent parameter that is conceptually similar to apparent stress, but

is relative to the energy-moment relation for the population of events rather than self-referential for each individual event. Use of EI enables the separation of variations in energy-moment scaling from variations in energy-moment scaling with event size distribution. This aspect of EI makes it useful for investigating the influences of scale effects on the analysis and interpretation of apparent stress

The occurrence of large events can be associated with periods of increasing apparent stress. Figure 6-17 shows a magnitude-time history of events in 1535-275-P1 SE corner along with the apparent stress percentiles up to the end of Phase 3 (approximately 85 hours after the blast). The magnitude-time history shows the cumulative number of  $M \geq -1$  events, and  $M \geq 0$  events are circled in pink. Larger events occur primarily during phases 1 and 3, when apparent stress is increasing. The occurrence of these larger events may be responsible for the increase in the apparent stress. However, there are relatively few of these larger events compared to the approximately 1,200 total events that occur in the same time frame. The size of the moving window is also sufficiently large that it is unlikely to cause a major shift (e.g. a single  $M \geq 0$  event would compose 0.5% of all the events in the moving window, and only 2.5% of events above  $AS_{80}$ ). Therefore, the size distribution of the entire population should be considered, rather than simply the timing of a limited number of large events.

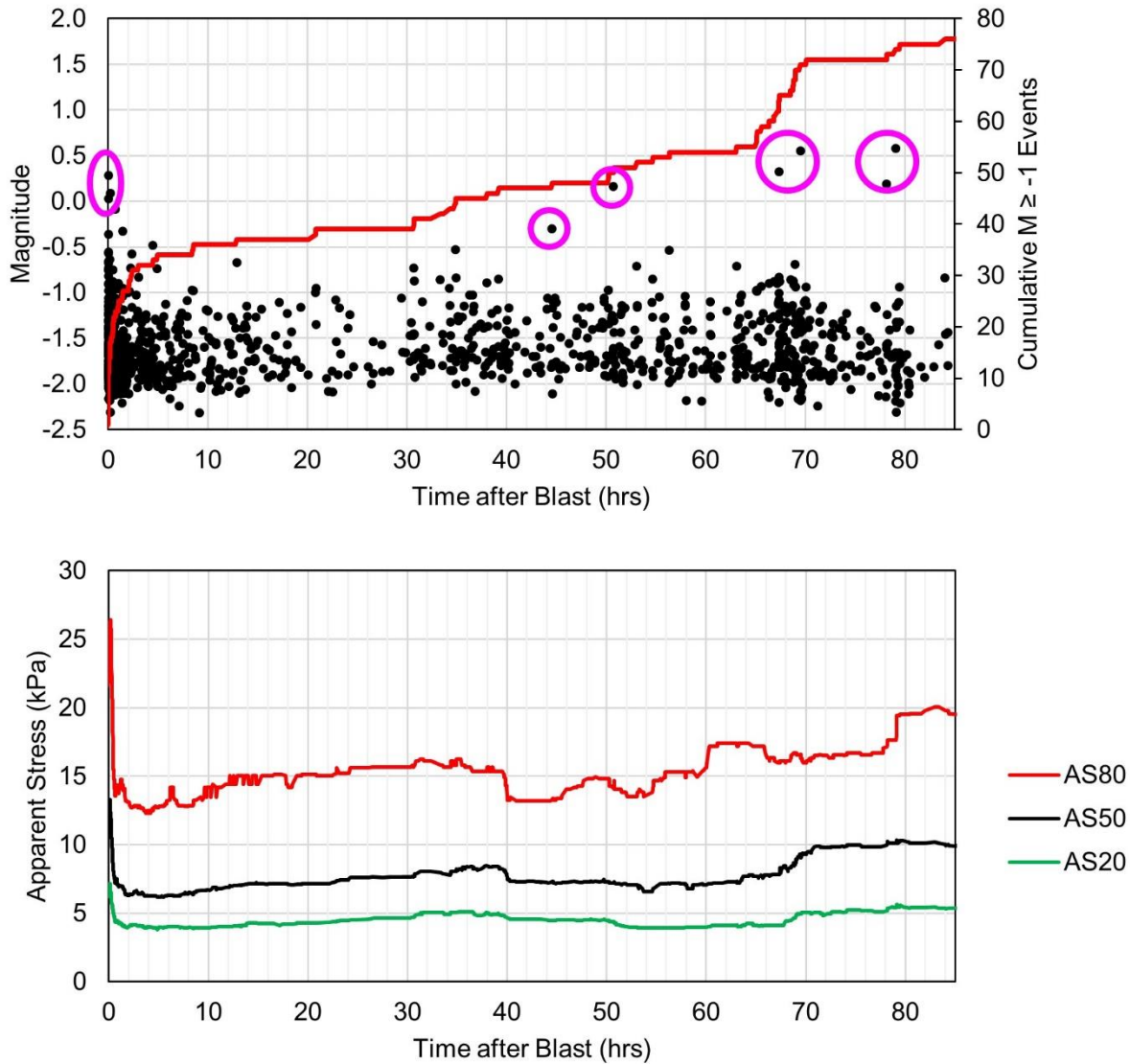


Figure 6-17: Magnitude-time and apparent stress graphs in 1535-275-P1 SE corner indicating times when larger events occur

Events in 1535-275-P1 SE corner were divided into separate populations for each phase of apparent stress variation, plus an additional population of the 200 events occurring in the volume before the final blast. The frequency-magnitude relations of these populations are shown in Figure 6-18. The b-value decreases during Phase 1, indicating an increase in the proportion of larger events which may be to some extent related to the increase in apparent stress observed during this phase. The b-value increases during Phase 2, which conversely may be responsible for the decrease in apparent stress observed during this phase. The frequency-magnitude relation for the Phase 3 events is difficult to interpret, and the b-value may increase or decrease from Phase 2 depending on the interpretation of the “linear” region of the data. If the b-value decreases from Phase 2, the

increase in apparent stress may again be attributed to the increase in proportion of larger events. Also of note is that the frequency-magnitude relations for the 200 events before the final blast and Phase 3 both show bi-modal characteristics, indicating a variety of mechanisms present during these periods. The variations in b-value between each phase support the notion that variations in apparent stress are driven by variations in the size distribution of events.

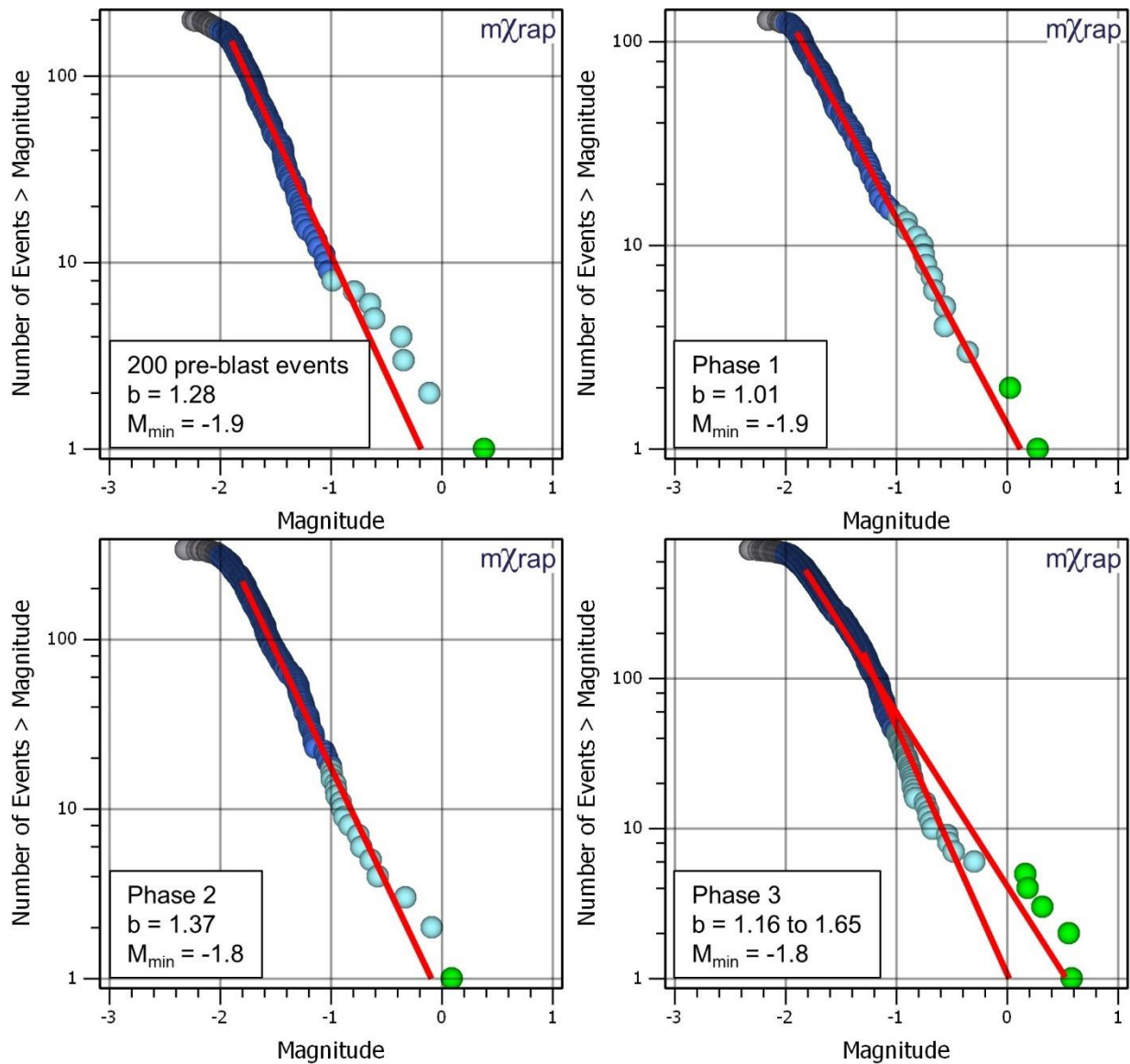


Figure 6-18: Frequency-magnitude relations for events in each phase of apparent stress variation in 1535-275-P1 SE corner and 200 events in SE corner prior to blast

Figure 6-19 shows energy-moment relations for each phase of apparent stress variation and the 200 events before the final blast. There are variations in the slope (d) and/or the intercept (c) of the relation between each phase. The slope of all the relations is greater than 1, indicating that

apparent stress is scale-dependent throughout each phase. However, the changes in these relations are independent of the changes in the frequency-magnitude relations, which indicates that some portion of the variation in apparent stress may be driven by changes in energy-moment scaling rather than solely by changes in event size distributions.

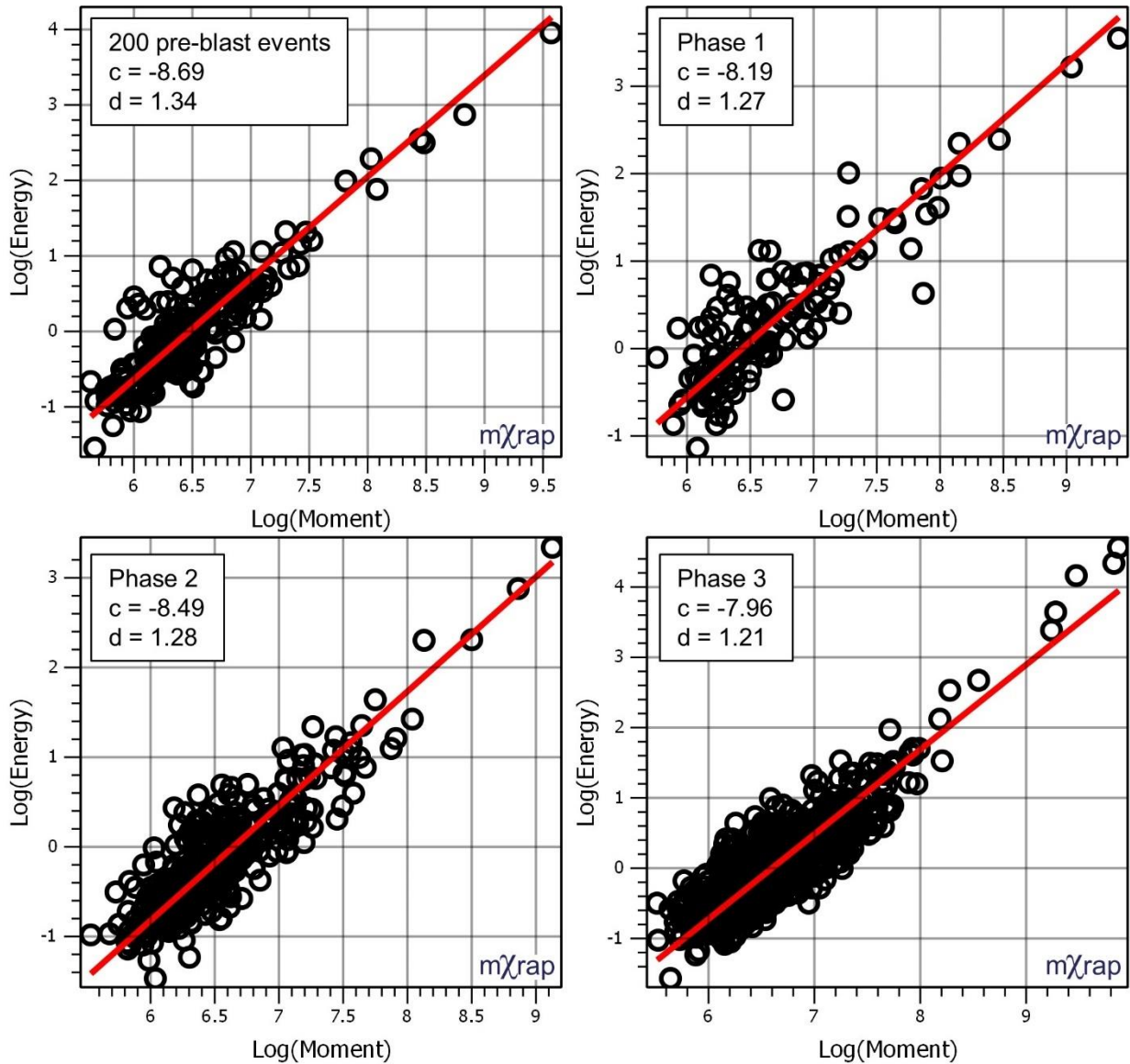


Figure 6-19: Energy-moment relations for events in each phase of apparent stress variation in 1535-275-P1 SE corner and 200 events in SE corner prior to blast

Having established that there is variation in both the size distribution of events and energy-moment scaling from one phase to the next, variations in apparent stress and EI will be compared to investigate if similar variations are observed. The energy index of any event is relative to the energy-moment relation for a population of events. The energy moment relation for this example

was defined using events in the SE corner of 1535-275-P1. Events up to the end of Phase 3 of apparent stress variation and the 200 events occurring in the volume before the blast were used to define the relation. By selecting these events to define the energy-moment relation, their EI values will be relative to the same population for which any trends they exhibit are being compared to.

Figure 6-20 compares the variations in  $AS_{20}$ ,  $AS_{50}$ , and  $AS_{80}$  observed in the first 5 hours following the final blast to variations in the same percentiles of  $\log(EI)$ :  $EI_{20}$ ,  $EI_{50}$ , and  $EI_{80}$ . There are several similarities between the two parameters:

- Both increase immediately after the blast and peak around the same time
- Both decrease for some hours after the blast
- All trend lines in both parameters are below their initial pre-blast values some hours after the blast

The similarities between variations of scale-dependent and independent parameters suggest that the increase in apparent stress during Phase 1 and the decrease during Phase 2 are not entirely a result of variations in the size distribution of events. However, the increase in apparent stress immediately after the blast is larger than the increase in  $\log(EI)$ , most noticeably when comparing  $AS_{80}$  and  $EI_{80}$ . This result indicates that some of the variation in the distribution of apparent stress is driven by variations in the size distribution of events (i.e. the decrease in b-value between the 200 events before the blast and the events in Phase 1 of apparent stress variation).

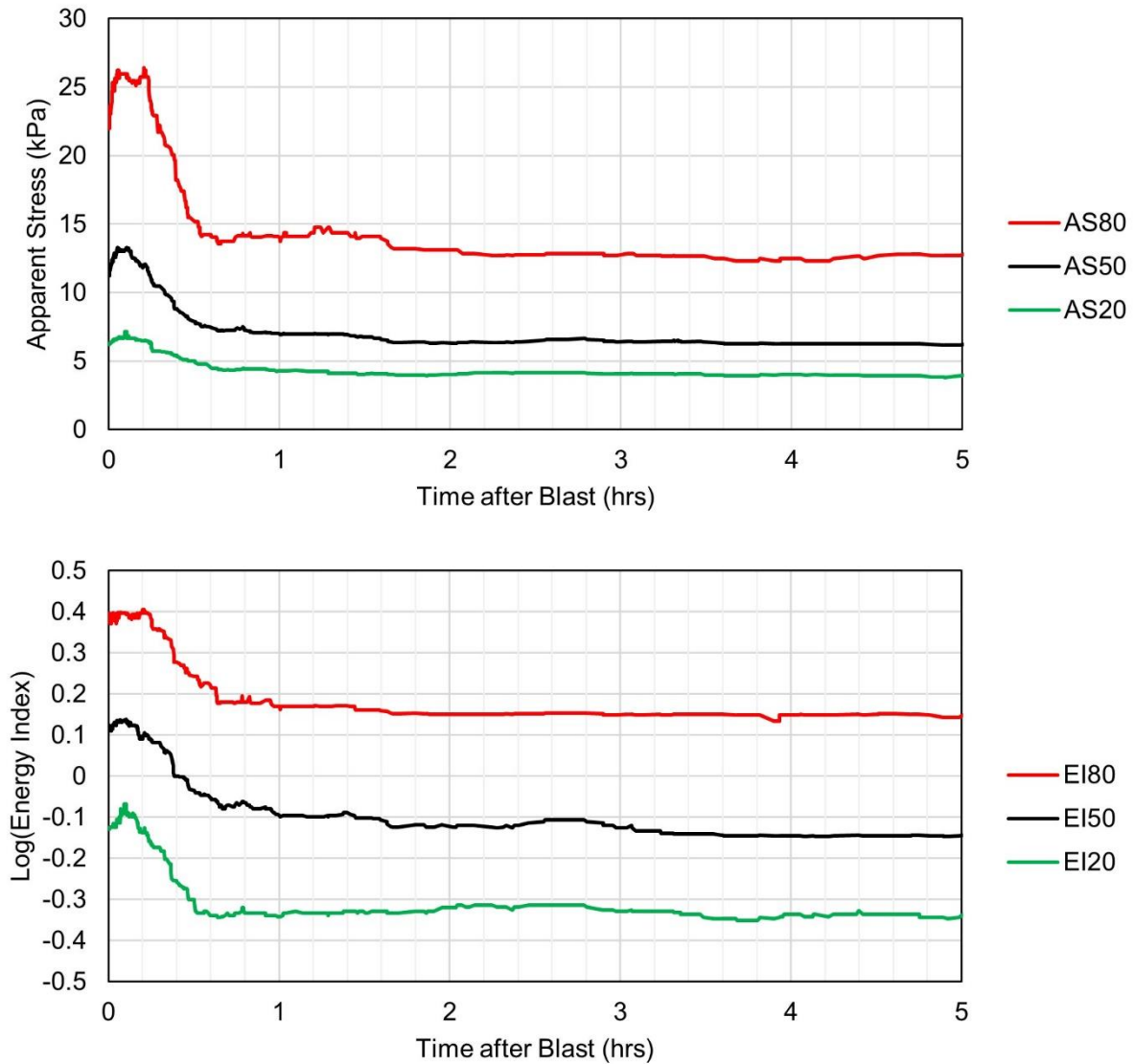


Figure 6-20: Apparent stress and log(EI) percentiles in first 5 hours after blast in 1535-275-P1 SE corner

Figure 6-21 compares the apparent stress and log(EI) percentiles up to 85 hours after the blast, approximately the time that Phase 3 of apparent stress variation ends. Both apparent stress and log(EI) increase between approximately 4 and 85 hours after the blast, indicating that like phases 1 and 2, Phase 3 of apparent stress variation is not purely a result of variations in the size distribution of events. The drop in apparent stress around 40 hours that was disregarded in the interpretation of the apparent stress phases is more drastic and prolonged in the log(EI) percentiles. The drop in the log(EI) percentiles during Phase 3 starts gradually around 35 hours, rather than appearing as a sudden shift at 40 hours as it does in the apparent stress percentiles. These

differences may lead to different interpretations of Phase 3 between the two parameters when they are analysed independently.

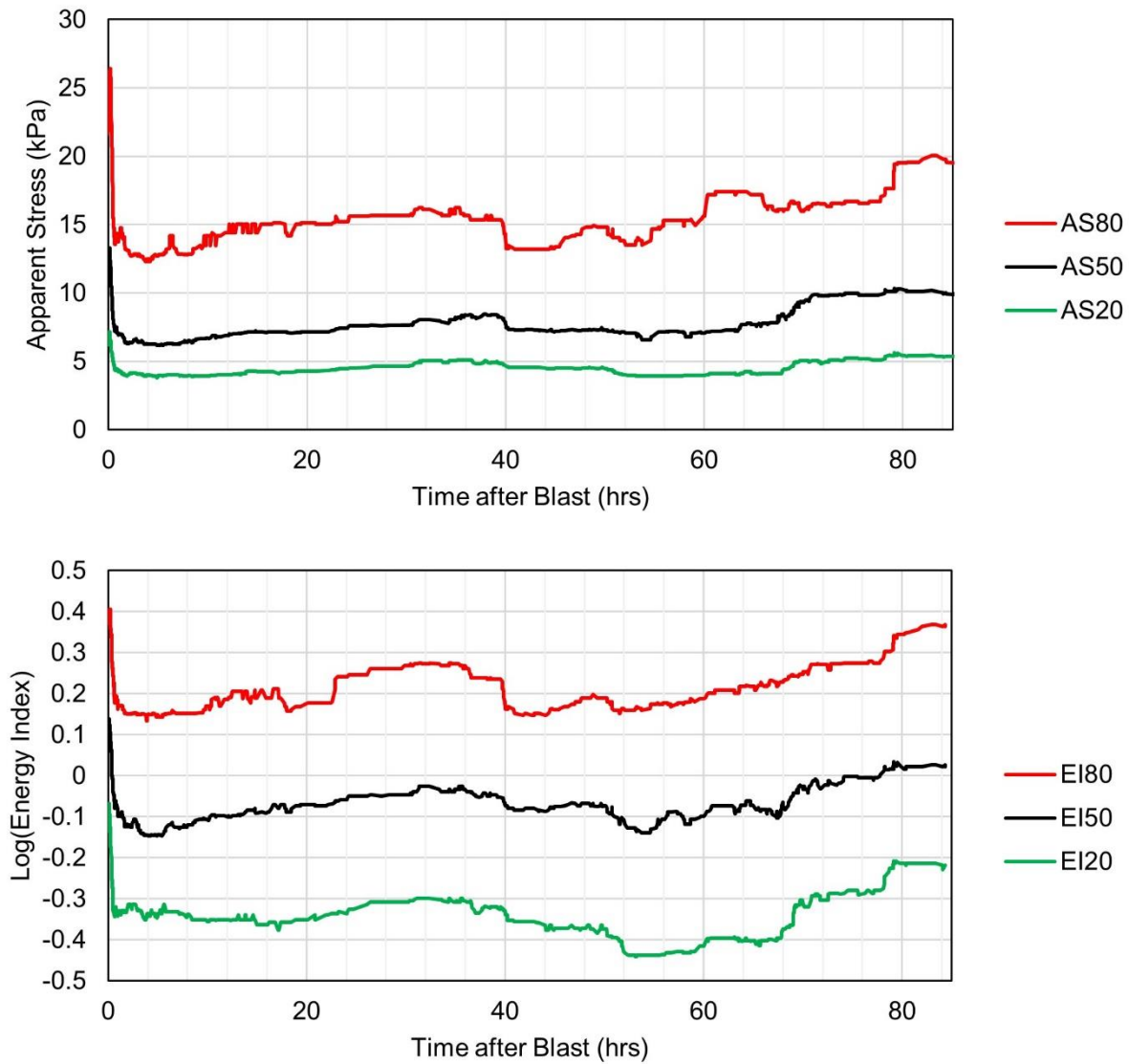


Figure 6-21: apparent stress and log(EI) percentiles in first 85 hours after blast in 1535-275-P1 SE corner

Scale effects may also be responsible for spatial variations in the distribution of apparent stress.  $b$ -values vary spatially in mining environments, indicating different seismic source mechanisms and stress regimes (Hudyma, 2008; Urbancic et al., 1992b; Wesseloo, 2014). Based on the variety of rock mass failure and seismic source mechanisms present near open stopes, it is logical that  $b$ -value may vary throughout a seismogenic zone and therefore may influence the distribution of apparent stress at different distances from stopes.

To address this possibility, events in the 1535-275-P1 SE corner case have been separated into populations occurring within each phase of MESD variation. The population of events in each phase was divided into two groups of the 50% of events closest to the mined stopes (“near” events) and the 50% of events farthest from the mined stopes (“far” events). Note that because the MESD changes over time, the event-stope distance at which the populations are separated is not consistent between each phase. The frequency-magnitude relations for each population are shown in Figure 6-22. In each phase, the events closer to the stope have higher b-values and fewer large events than the events farther from the stope. The higher b-values close to the stopes indicate a population composed of more stress-driven source mechanisms, while the lower b-values farther from the stopes indicate a population composed of more structure-related source mechanisms. The greater proportion of large events farther from the stopes may be the cause of the tendency for events with higher apparent stress to locate farther from the stopes.

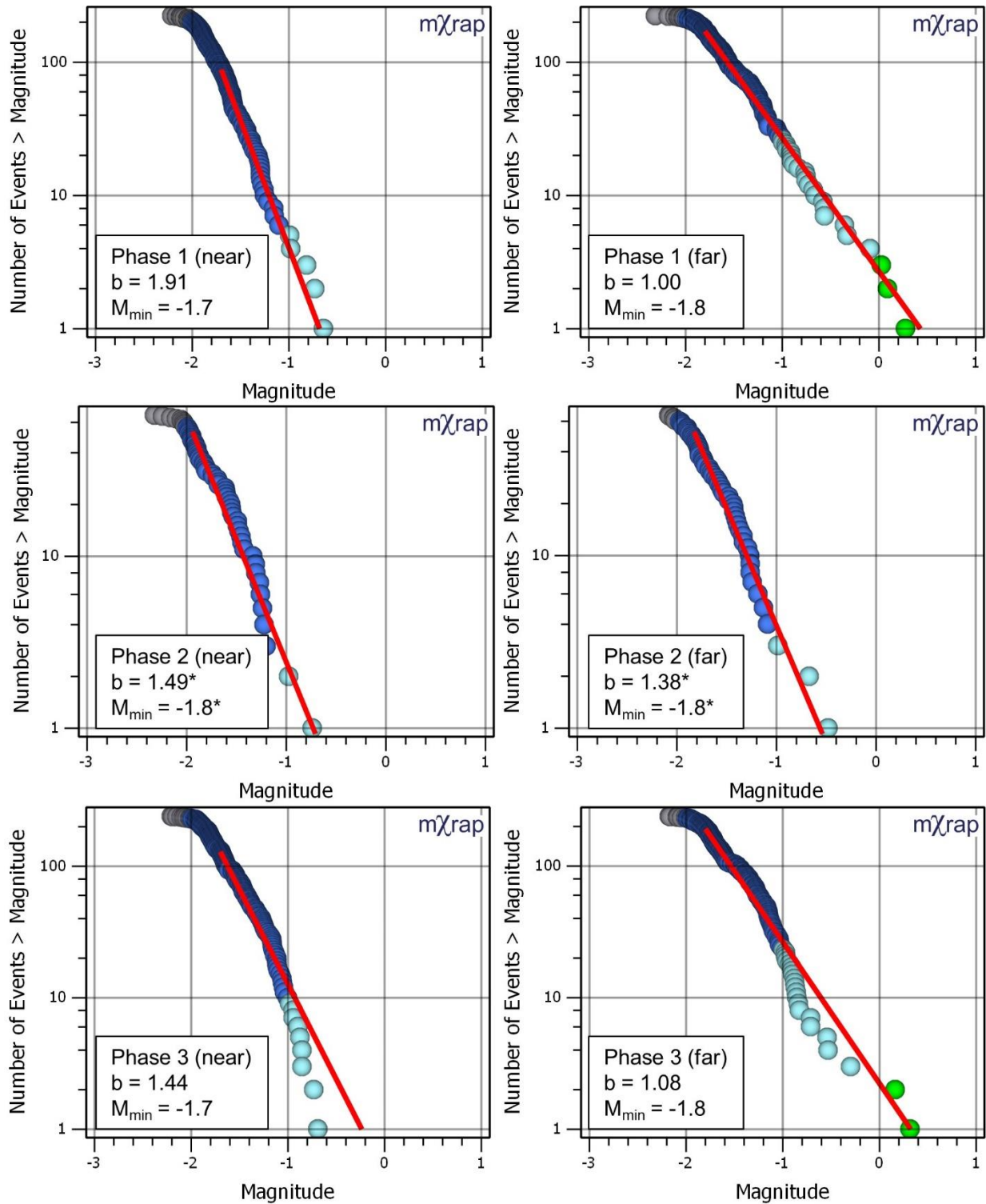


Figure 6-22: Comparison of frequency-magnitude relations of events closest and farthest from stopes in each phase of MESD variation in 1535-275-P1 SE corner. \*Phase 2 frequency-magnitude relations were determined by inspection due to lack of events for algorithmic determination in mχrap

Figure 6-23 shows the energy-moment relations for the same “near” and “far” groups of events in each phase of MESD variation. The slope of each energy-moment relation is greater than 1, which

indicates that apparent stress is scale-dependent throughout each phase and at different distances from the stopes. Within each phase, there is also variation in energy-moment scaling which indicates different distributions of apparent stress. As with the phases of apparent stress variation, the energy-moment relations are independent of the frequency-magnitude relations, so the size distribution of events is not the only factor influencing the distribution of apparent stress at different distances from the stopes.

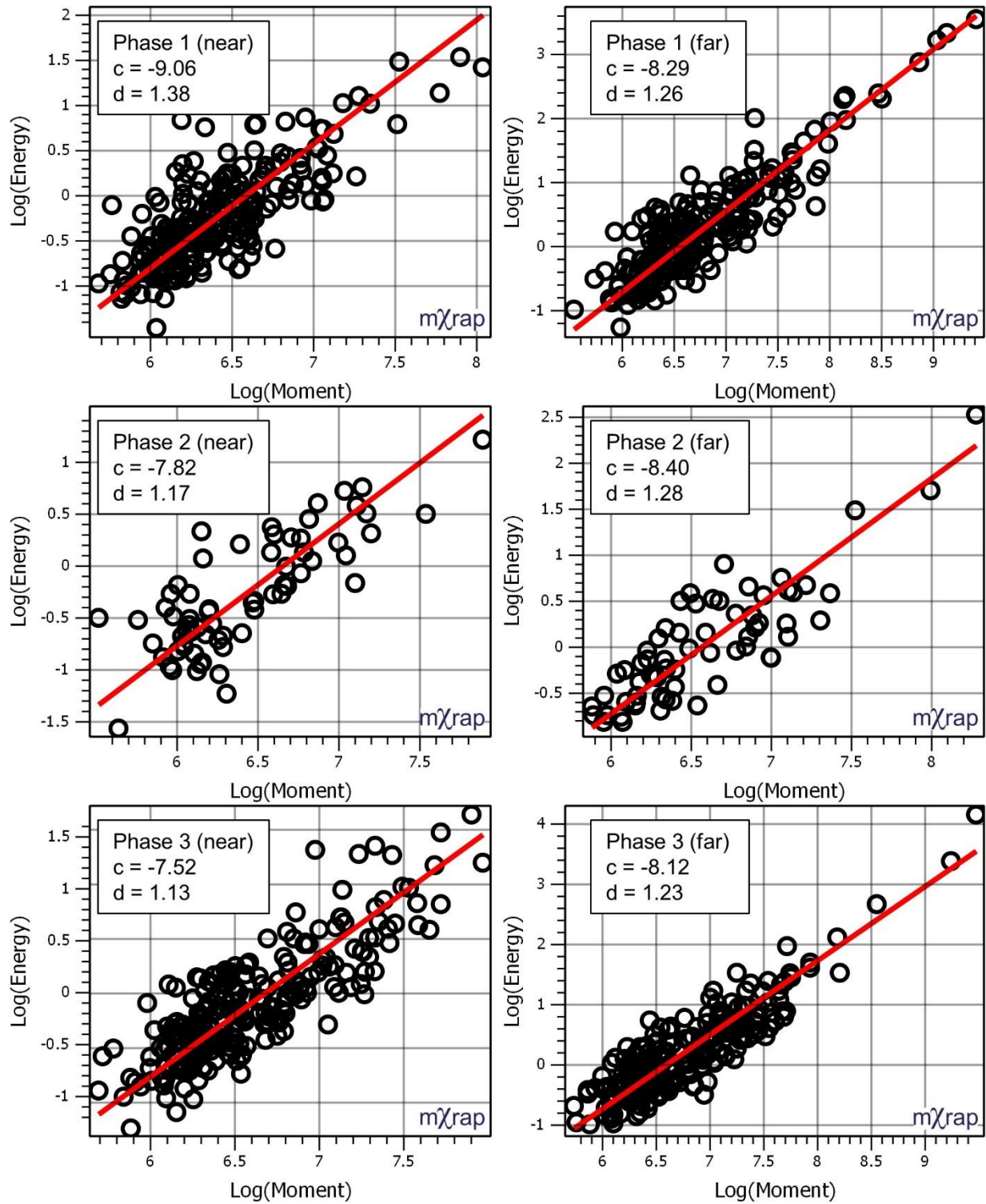


Figure 6-23: Comparison of energy-moment relations of events closest and farthest from stopes in each phase of MESD variation in 1535-275-P1 SE corner

As stated previously, energy index is relative to the energy-moment relation for a population of events, so the EI of any single event depends on the other events it is being compared relative to.

For the purposes of consistency with the comparison of apparent stress and  $\log(EI)$  variations over time, the same population has been used for comparison of MESD variations: events in the SE corner volume from 200 events before the blast up to the end of Phase 3 of apparent stress variation. The methodology for MESD analysis using  $\log(EI)$  is identical to that used for apparent stress, the former parameter simply replaces the latter. The results of the two MESD analyses are shown in Figure 6-24. Similar behaviours between the two analyses indicate that similar conclusions might be drawn from either parameter. Three phases of MESD variation are apparent in both graphs. These phases also appear to have similar durations. Furthermore, events with parameters that are used to infer higher stress (higher apparent stress and  $\log(EI)$ ) are consistently farther from the stopes than events with parameters that are used to infer lower stress (lower apparent stress and  $\log(EI)$ ). The MESD for the high apparent stress events are around the same distance from the stopes as the MESD for the high  $\log(EI)$  events (and the same for the low apparent stress and  $\log(EI)$  events). The differences between the analyses are mostly related to the spatial variation in the parameters. For example, in the  $\log(EI)$  analysis there appears to be:

- Less separation between  $D_{50}H_{50}$  and  $D_{50}L_{50}$  up to 85 hours after the blast
- Less separation between  $D_{50}H_{50}$  and  $D_{50}H_{80}$  up to 85 hours after the blast
- Less separation between  $D_{50}L_{50}$  and  $D_{50}L_{20}$  between 5 and 20 hours after the blast

These differences lead to the conclusion that interpretation of spatial variations in stress is partially affected by the scale dependence of apparent stress.

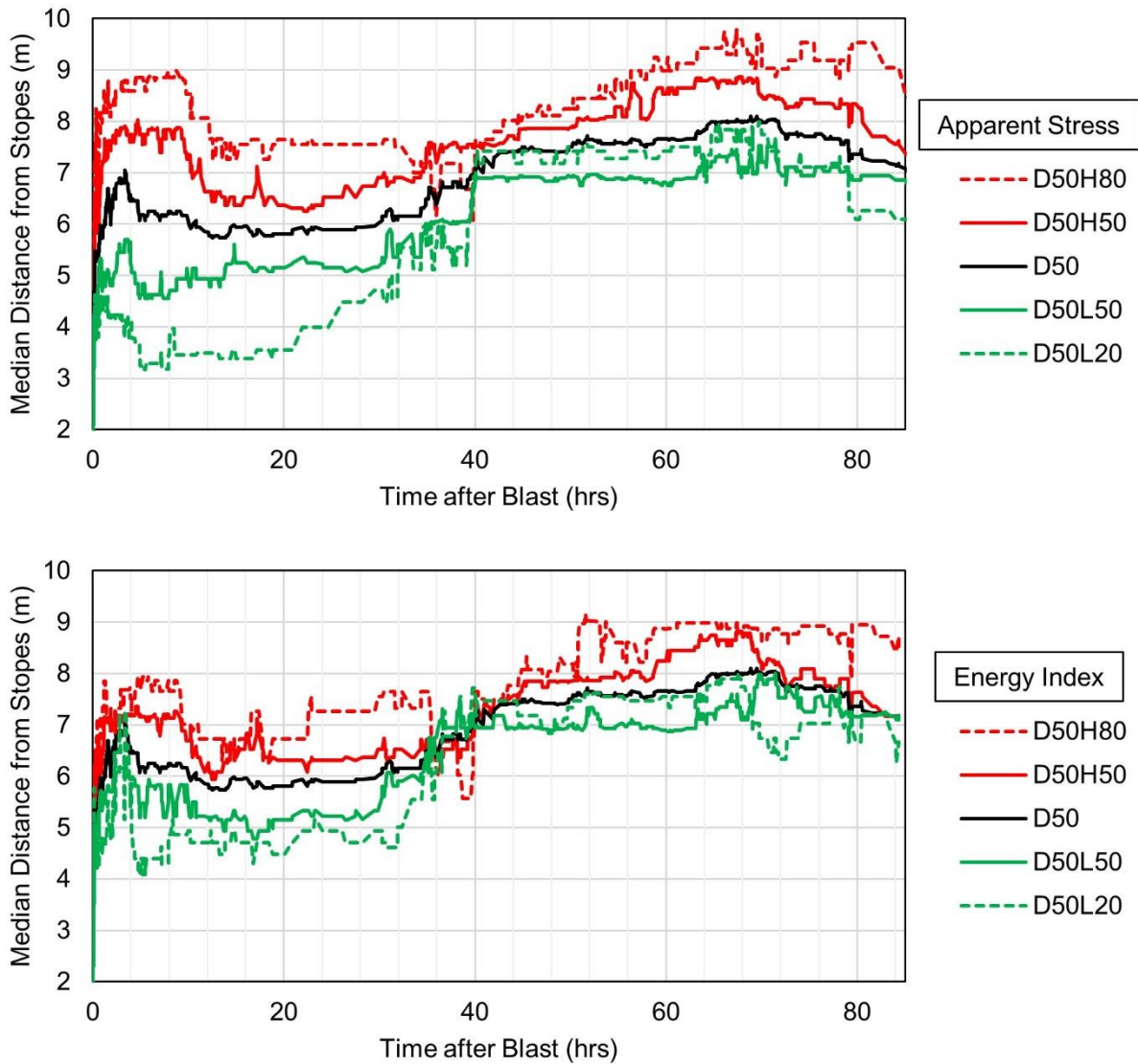


Figure 6-24: MESD graphs using apparent stress (top) and  $\log(EI)$  (bottom) in 1535-275-P1 SE corner in the first 85 hours following the final blast

The differences in these examples show that although apparent stress and energy index are conceptually similar, differences brought about by scale dependence may lead to different interpretations of trends and consequently different interpretations of rock mass behaviour. However, an identical methodology using scale-dependent and scale-independent parameters reveals largely similar behaviours in the examples shown. The analysis of this case leads to the conclusion that the variations in apparent stress over space and time following the final blast are driven in part by scale effects, and in part by variations in energy-moment scaling. The most

appropriate parameter to use then depends on the extent to which either parameter can be used to infer a certain level of stress in the rock mass.

## 6.10 Non-Similar Behaviour in Mining-Induced Seismogenic Zones

Several results in this thesis elude to the breakdown of self-similarity between seismic sources, that is, not all events in the data set are related to similar processes of rock mass yield. Different seismic source mechanisms exist throughout any one mine and within the vicinity of a single stope. Seismic events may be associated with fracture of intact rock, disturbance of joints in the rock mass, or slip on a geologic feature. All these mechanisms have been inferred from the case studies analysed in this thesis.

With regard to apparent stress, the results of this thesis elude to the breakdown on self-similarity in a number of ways including:

- Local blasting to temporarily elevates apparent stress (i.e. a sudden, mining-induced stress change can alter the local energy-moment scaling relation)
- Large quantities of events with low apparent stress occurring within a few hours of the blast, and apparent stress rising afterwards (i.e. the low apparent stress events associated with rock mass yield tend to occur more frequently after blasts, certain conditions exist in a limited space and time following a blast that permit events with such properties to occur)
- Events with higher and lower apparent stress tend to occur at different distances from stopes (i.e. there is different energy-moment scaling relation behaviour under different levels of rock mass confinement, and where different seismic sources and rock mass failure mechanisms are expected to occur)

Apparent stress percentiles do not move uniformly. Figure 6-25 shows an apparent stress graph where  $AS_{80}$  increases for several hours while  $AS_{50}$  and  $AS_{20}$  are decreasing. This example demonstrates a lack of connection between different parts of the distribution of apparent stress (i.e. they may move independently of one another). Changes in higher percentiles may not correlate with lower percentiles, and different rock mass behaviour (i.e. increasing or decreasing stress) may be inferred from events with different apparent stress.

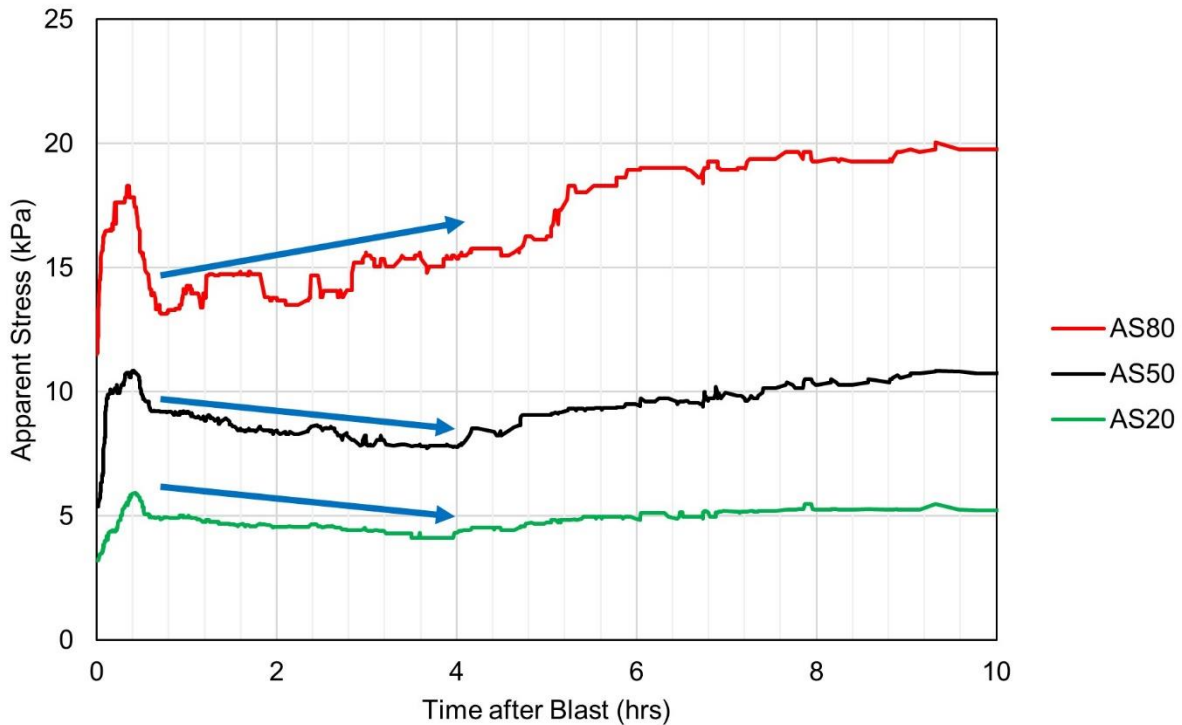


Figure 6-25: Apparent stress percentiles in 1535-225-P1 NW corner (June 30<sup>th</sup>, 2016)

In addition to events with high and low apparent stress occurring at different distances from stopes, MESD graphs may show other aspects of non-similar behaviour between events with high and low apparent stress. Figure 6-26 shows an example of a MESD graph that could not be interpreted using the three-phase model. In this graph,  $D_{50}H_{50}$  and  $D_{50}H_{80}$  increase for a period of approximately 30 hours while  $D_{50}L_{50}$  and  $D_{50}L_{20}$  are decreasing.  $D_{50}$  is largely unchanged during this time which indicates that the seismogenic zone as a whole is stationary, but events with higher and lower apparent stress are migrating independently of each other.

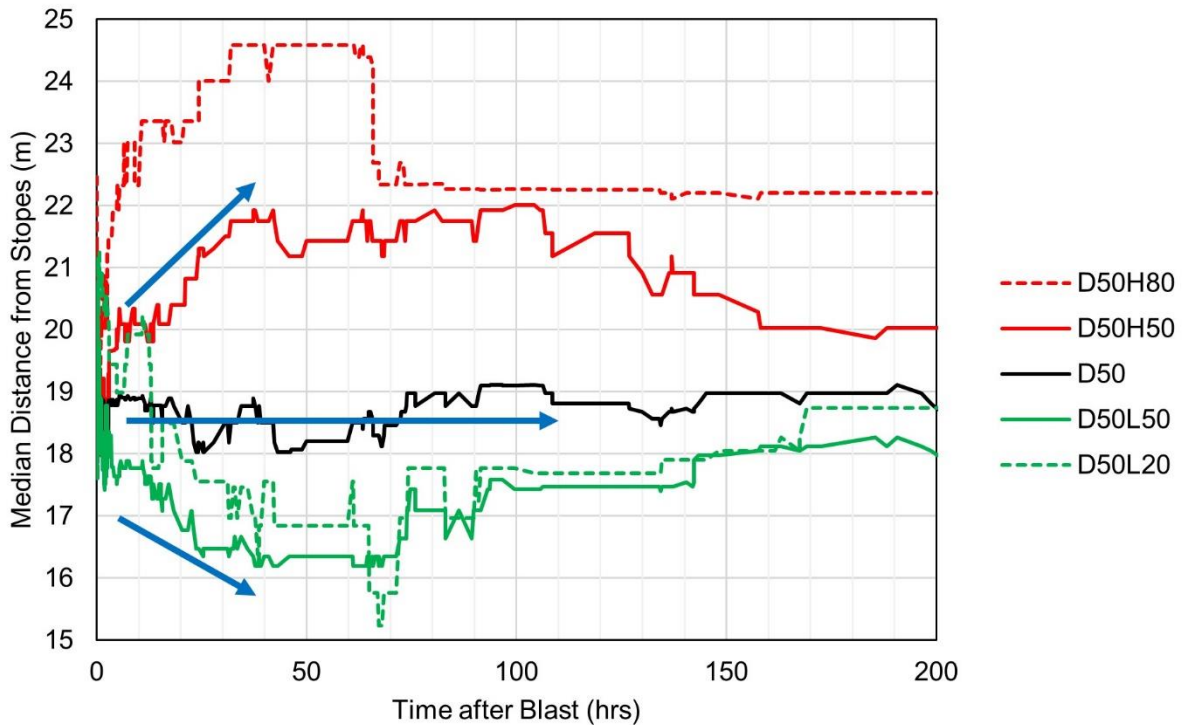


Figure 6-26: MESD in 1355-275-P3 west abutment (October 7<sup>th</sup>, 2015)

The results in this thesis demonstrate a number of aspects of non-similar behaviour in mining-induced seismic events. This author believes that areas of a jointed rock mass which are subjected to elevated stress and reduced confinement from open stope blasts are ideal case studies for investigating the self-similarity (or lack thereof) of mining-induced seismic events. Some characteristics of such rock mass and mining environments that may contribute to a lack of self-similarity include:

- A transition from a damaged to a less damaged rock mass.
- Different damage mechanisms within an EDZ (coalesced, dilating fractures versus isolated fractures lacking significant dilation).
- Heterogeneities and structures in the rock mass which favour different source mechanisms.

## 7 Conclusion

This thesis investigates the use of the seismic source parameter apparent stress to infer short-term variations in local stress conditions following large open stope blasts at Nickel Rim South mine. Open stope blasts produce sudden, large stress increases and loss of confinement in the surrounding rock mass. These changes result varying degrees of damage and disturbance to the rock mass at different distances from the excavation. Yield of the rock mass near the open stope results in the migration of stress away from more damaged areas and into what were previously less damaged and disturbed regions. The formation of excavation damage zones is time dependent, with the damaged zone growing more gradually with time. This behaviour is reflected in space-time variations in apparent stress in seismogenic zones.

### 7.1 Contributions

The main contributions of this thesis are related to how populations of mining-induced seismic events can be used to infer short-term stress changes in a rock mass that result from the creation of an excavation.

This thesis presents:

- A discussion of seismic source parameter apparent stress, how it varies in space and time, and how it can be related to stress change in a rock mass.
- A robust method for analysing variations in apparent stress over time that uses multiple percentiles of a population to analyse its distribution.
- A method for analysing variations in event-stope distances that also indicates whether there is spatial variation in apparent stress.

Using the methods developed to analyse space-time variations in apparent stress, numerous case studies of seismogenic zones following open stope blasts at Nickel Rim South were analysed. The analysis revealed three phases of variation in apparent stress and median event-stope distance (MESD) that occur in the majority of analysed cases. The three phases of variation in apparent stress and MESD are used to interpret different phases of rock mass short-term response following the blast. The inferred rock mass behaviours from the three phases of apparent stress variation are:

1. Increasing stress immediately after the blast.
2. Decreasing stress inside the stope's excavation damage zone (EDZ) as it forms.

3. Increasing stress as load sheds from the EDZ onto more intact and confined ground.

The inferred rock mass behaviours from the three phases of MESD variation are:

1. Stress redistribution around a new excavation and outside its excavation damage zone.
2. Continued rock mass yield closer to the stope in a region where stresses place the rock mass between stable and unstable states.
3. Growth of the excavation damage zone.

Compilation of the results from multiple case studies indicate typical characteristics for each phase of variation. The key findings from the compilation of the results are:

- The time periods over which stress change and rock mass yield occur:
  - The rock mass is subject to the stress increase caused by the stope blast for a matter of minutes.
  - Formation of an excavation damage zone and stress rapidly shedding out of it occurs over a matter of hours.
  - Gradual redistribution of stress outside the more damaged regions and into less damaged regions occurs over a matter of days.
- Events continue to migrate away from stopes as the rock mass yields, which eludes to redistribution of stress outside the yielded zone causing disturbance to the rock mass at greater distances.
- There is a spatial gradient in apparent stress throughout all phases of variation:
  - Events with lower apparent stress tend to locate closer to stopes where there is less confinement and the rock mass has less capacity to store stress.
  - Events with higher apparent stress tend to locate farther from stopes where there is more confinement and the rock mass has more capacity to store stress.

Additional analysis and discussion of selected case histories also demonstrates that:

- The use of different moving windows may affect the results of the analysis and inferences on rock mass behaviour.
- Large events also cause stress changes which may influence variations in apparent stress and MESD.

- Additional stress changes occur throughout the mine in what is defined as the short term, and these stress changes may influence variations in apparent stress near distant open stopes.
- Geologic structures such as faults may influence variations apparent stress.
- Space-time variations in apparent stress in seismogenic zones that are not adjacent to an open stope may not be adequately described by the three-phase model proposed in this thesis.
- Although apparent stress is a scale-dependent source parameter, the observed variations in space and time are not solely driven by variations in event size distribution. Similar variations are also observed in scale-independent measures energy-moment scaling.
- Space-time variations in apparent stress following stope blasts elude to a non-self-similar nature of mining induced seismicity.

## 7.2 Future Work

Further analysis of apparent stress using similar methodologies can be refined in the following ways:

- Examine the possibility of using shorter moving windows to avoid smoothing over variations that occur over smaller numbers of events but being mindful of conclusions drawn from smaller sample sizes.
- Compensate for scale effects in the comparison of case studies by limiting analysis to events larger than a magnitude that is consistently observed across all case studies (e.g.  $M \geq -1.5$  events only).
- Consider peak changes in individual trend lines rather than their values at the averaged phase end time.
- Characterize the distributions of apparent stress and MESD and perform some statistical treatment to establish the significance of variations.

The striking consistency of the three-phase models across the analysed cases warrants further study of this behaviour. Such consistent observations indicate that there may be a common seismogenic process following open stope blasts which can be used to infer rock mass behaviour, leading to an improved understanding of the constitutive behaviour of rock masses. Further study of the behaviours observed in this thesis may involve:

- Correlating variations in each trend line.
- Describing the variation in spatial distributions of events around stopes over time in greater detail.
  - Distribution of event-stope distances.
  - Three-dimensional analysis of event distribution.
- Revisiting results with added context of rock mass conditions, modelled stresses, and stress change produced by individual blasts.
- Investigating the influence of geologic features on non-similar behaviour of events with high and low apparent stress.
- Analysing variations in other seismic source parameters.
  - Other measures of co-seismic stress change.
  - Scale-independent analysis (energy index).
  - Indicators of seismic source mechanism or fracture complexity.
- Analysis of co-seismic deformation in different regions around the stope and their relation to the inferred stress change.

There are also other broad genres of seismicity and rock mechanics research which may stem from the results demonstrated in this thesis. These areas include:

- Calibration of constitutive rock mass behaviour:
  - Rock mass strength.
  - EDZ/seismogenic zones.
  - Brittle versus softening.
  - Viscoplastic creep.
- Seismic hazard forecasting:
  - Compare inferences on rock mass stress and yield to occurrence of large events in space and time.
  - Compare to existing theories/methods based on the rates of events and their magnitudes.

## References

- Abolfazlzadeh, Y., 2013. Application of seismic monitoring in caving mines - case study of Telfer Gold Mine (MASC Thesis). Laurentian University, Sudbury, ON.
- Abolfazlzadeh, Y., Hudyma, M., 2016. Identifying and describing a seismogenic zone in a sublevel caving mine. *Rock Mech. Rock Eng.* 49, 3735–3751.
- Abolfazlzadeh, Y., McKinnon, S.D., 2017. Stress field characterisation in Nickel Rim South Mine using seismic stress inversion, in: Wesseloo, J. (Ed.), *Deep Mining 2017: Eighth International Conference on Deep and High Stress Mining*. Australian Centre for Geomechanics, Perth, WA, pp. 247–256.
- Aki, K., Richards, P.G., 1980. *Quantitative seismology, theory and methods*. Freeman, San Francisco, CA.
- Amidzic, D., 2001. Energy-moment relation and its application, in: van Aswegen, G., Durrheim, R.J., Ortlepp, W.D. (Eds.), *Proceedings of the Fifth International Symposium on Rockbursts and Seismicity in Mines - RaSiM 5*. South African Institute of Mining and Metallurgy, Johannesburg, South Africa, pp. 509–513.
- Andrieux, P., Simser, B., 2001. Chapter 21: Ground-stability-based mine design guidelines at the Brunswick Mine, in: Hustrulid, W.A., Bullock (Eds.), *Underground Mining Methods: Engineering Fundamentals and International Case Studies*. Society for Mining, Metallurgy, and Exploration, Englewood, CO, pp. 207–214.
- Andrieux, P.P., Hudyma, M.R., O'Connor, C.P., Li, H., Cotesta, L., Brummer, R.K., 2008. Calibration of large-scale three-dimensional non-linear numerical models of underground mines using microseismic data, in: *Continuum and Distinct Element Numerical Modelling in Geo-Engineering*. Itasca Consulting Group Inc., Minneapolis, MN.
- Bawden, W.F., Mercer, R.A., 1994. Some thoughts on hazard assessment for improved mine design, in: *Proceedings for Risk Assessment in Extractive Industries*. University of Exeter, United Kingdom.
- Beck, D., Levkovitch, V., Simser, B., 2012. Explicit discontinuum simulation for probabilistic forecasting of fault slip and rock mass seismic potential, in: Potvin, Y. (Ed.), *Deep Mining 2012: Proceedings of the Sixth International Seminar on Deep and High Stress Mining*. Australian Centre for Geomechanics, Perth, WA, pp. 373–388.
- Beeler, N.M., Wong, T.-F., Hickman, S.H., 2003. On the expected relationships among apparent stress, static stress drop, effective shear fracture energy, and efficiency. *Bull. Seismol. Soc. Am.* 93, 1381–1389.
- Bieniawski, Z.T., 1974. Estimating the strength of rock materials. *J. South. Afr. Inst. Min. Metall.* 74, 312–320.
- Boatwright, J., Fletcher, J.B., 1984. The partition of radiated energy between P and S waves. *Bull. Seismol. Soc. Am.* 74, 361–376.
- Brady, B.H., Brown, E.T., 2006. *Rock Mechanics for underground mining*, 3rd ed. Springer, Dordrecht, The Netherlands.
- Brown, E.T., Hoek, E., 1978. Trends and relationships between measured in-situ stresses and depth. *Int. J. Rock Mech. Min. Sci. Geomech. Abstr.* 15, 211–215.
- Brown, L., Hudyma, M., 2017a. Identification of stress change within a rock mass through apparent stress of local seismic events. *Rock Mech. Rock Eng.* 50, 81–88.
- Brown, L., Hudyma, M., 2017b. Identifying local stress increase using a relative apparent stress ratio for populations of mining-induced seismic events. *Can. Geotech. J.* 54, 128–137.

- Brown, L.G., 2015. Seismic hazard evaluation using apparent stress ratio for mining-induced seismic events (MASc Thesis). Laurentian University, Sudbury, ON.
- Castro, L.A.M., 1996. Analysis of stress-induced damage initiation around deep openings in a moderately jointed brittle rock mass (PhD Thesis). University of Toronto, Toronto, ON.
- Cichowicz, A., Green, R.W.E., van Zyl Brink, A., Grobler, P., Mountfort, P.I., 1990. The space and time variation of micro-event parameters occurring in front of an active stope, in: Fairhurst, C. (Ed.), *Rockbursts and Seismicity in Mines*. A.A. Balkema, Minneapolis, MN, pp. 171–175.
- Collins, D.S., Toya, Y., Pinnock, I., Shumila, V., Hosseini, Z., 2014. 3D velocity model with complex geology and voids for microseismic location and mechanism, in: Hudyma, M., Potvin, Y. (Eds.), *Deep Mining 2014: Proceedings of the Seventh International Seminar on Deep and High Stress Mining*. Australian Centre for Geomechanics, Sudbury, ON, pp. 681–688.
- Cook, N.G.W., 1976. Seismicity associated with mining. *Eng. Geol.* 10, 99–122.
- Costin, L.S., 1987. Chapter 5: Time-dependent deformation and failure, in: Atkinson, B.K. (Ed.), *Fracture Mechanics of Rock*. Academic Press, London, pp. 167–215.
- Cotesta, L., O'Connor, C.P., Brummer, R.K., Punkkinen, A.R., 2014. Numerical modelling and scientific visualisation - integration of geomechanics into modern mine designs, in: Hudyma, M., Potvin, Y. (Eds.), *Deep Mining 2014: Proceedings of the Seventh International Seminar on Deep and High Stress Mining*. Australian Centre for Geomechanics, Sudbury, ON, pp. 377–394.
- Coulomb, C.A., 1776. Essai sur une application des regles de maximis et minimis a quelques problemes de statique, relatifs a l'architecture. *Memoires Math. Phys.* 7, 343–382.
- Coulson, A.L., 2009. Investigation of the pre to post peak strength state and behaviour of confined rock masses using mine induced microseismicity (PhD Thesis). University of Toronto, Toronto, ON.
- Deneka, E., 2014. Digital photograph of 1680 level burst (Unpublished Internal Document).
- Diederichs, M.S., 2003. Rock fracture and collapse under low confinement conditions. *Rock Mech. Rock Eng.* 36, 339–381.
- Disley, N.V., 2014. Seismic risk and hazard management at Kidd Mine, in: *Deep Mining 2014: Proceedings of the Seventh International Seminar on Deep and High Stress Mining*. Australian Centre for Geomechanics, Sudbury, ON, pp. 107–122.
- Dressler, B.O., 1984. Chapter 4: General geology of the Sudbury area, in: Pye, E.G., Naldrett, A.J., Giblin, P.E. (Eds.), *The Geology and Ore Deposits of the Sudbury Structure*. Ontario Geological Survey, pp. 57–82.
- Dunn, M.J., 2005. Seismicity in a scattered mining environment - a rock engineering interpretation, in: Potvin, Y., Hudyma, M. (Eds.), *Controlling Seismic Risk: Proceedings of the Sixth International Symposium on Rockbursts and Seismicity in Mines*. Australian Centre for Geomechanics, Perth, WA, pp. 337–346.
- Duplancic, P., 2001. Characterisation of caving mechanisms through analysis of stress and seismicity (Unpublished PhD Thesis). University of Western Australia, Perth, WA.
- Duplancic, P., Brady, B.H., 1999. Characterization of caving mechanisms by analysis of seismicity and rock stress, in: Vouille, G., Berest, P. (Eds.), *Proceedings of the 9th International Congress on Rock Mechanics*. Balkema: Rotterdam, Paris, pp. 1049–1053.
- Ecobichon, D., Hudyma, M., Laplante, B., 1992. Understanding geomechanics problems through microseismic monitoring at Lac Shortt, in: *Proceedings of the 94th Annual General*

- Meeting of the Canadian Institute of Mining, Metallurgy, and Petroleum. Montreal, QC, pp. 1–13.
- Fairhurst, C., 2004. Nuclear waste disposal and rock mechanics: contributions of the Underground Research Laboratory (URL), Pinawa, Manitoba, Canada. *Int. J. Rock Mech. Min. Sci.* 41, 1221–1227.
- Falmagne, V., Gagnon, G., Ouellet, D., Simser, B., 2004. Mining strategy for the Retreat Zone at Noranda's Bell-Allard mine. *CIM Bull.* 97, 42–46.
- Gibowicz, S.J., Harjes, H.-P., Schafer, M., 1990. Source parameters of seismic events at Heinrich Robert Mine, Ruhr Basin, Federal Republic of Germany: evidence for nondouble-couple events. *Bull. Seismol. Soc. Am.* 80, 88–109.
- Gibowicz, S.J., Kijko, A., 1994. *An introduction to mining seismology*. Academic Press, San Diego, CA.
- Gibowicz, S.J., Young, R.P., Talebi, S., Rawlence, D.J., 1991. Source parameters of seismic events at the Underground Research Laboratory in Manitoba, Canada: Scaling relations for the events with moment magnitude smaller than -2. *Bull. Seismol. Soc. Am.* 81, 1157–1182.
- Glazer, S.N., 2016. *Mine seismology: data analysis and interpretation - Palabora Mine caving process as revealed by induced seismicity*. Springer, Switzerland.
- Glencore, 2017a. 1445 interpreted geology contacts (Unpublished Internal Document). Sudbury, ON.
- Glencore, 2017b. 1625 interpreted geology contacts (Unpublished Internal Document). Sudbury, ON.
- Glencore, 2013. 1565-300-P1 drill package (Unpublished Internal Document). Sudbury, ON.
- Goodfellow, S.D., Simser, B., Drielsma, C., Gerrie, V., 2017. In situ stress estimation using acoustic televiewer data, in: Hudyma, M., Potvin, Y. (Eds.), *Underground Mining Technology 2017: Proceedings of the First International Conference on Underground Mining Technology*. Australian Centre for Geomechanics, Sudbury, ON, pp. 487–496.
- Griffith, A.A., 1924. Theory of rupture, in: *Proceedings of the 1st International Congress on Applied Mechanics*. Delft, Netherlands, pp. 55–63.
- Hajiabdolmajid, V., Kaiser, P.K., Martin, C.D., 2002. Modelling brittle failure of rock. *Int. J. Rock Mech. Min. Sci.* 39, 731–741.
- Hanks, T.C., Kanamori, H., 1979. A moment magnitude scale. *J. Geophys. Res.* 84, 2348–2350.
- Harris, P., Wesseloo, J., 2015. *mXrap Version 5*. Australian Centre for Geomechanics, University of Western Australia, Perth, WA.
- Hasegawa, H.S., Wetmiller, R.J., Gendzwill, D.J., 1989. Induced seismicity in mines in Canada - an overview. *Pure Appl. Geophys.* 129, 423–453.
- Heal, D., Hudyma, M., Vézina, F., 2005. Seismic hazard at Agnico-Eagle's LaRonde Mine using MS-RAP. Presented at the Maintenance Engineering and Mine Operators Conference, Sudbury, ON.
- Hedley, D.G.F. (Ed.), 1992. *Rockburst handbook for Ontario hardrock mines*. CANMET Special Report SP92-1E. Canada Communication Group, Ottawa, ON.
- Herget, G., 1973. Variation of rock stresses with depth at a Canadian iron mine. *Int. J. Rock Mech. Min. Sci. Geomech. Abstr.* 10, 37–51.
- Hoek, E., 2006. *Practical Rock Engineering*.
- Hoek, E., Brown, E.T., 1997. Practical estimates of rock mass strength. *Int. J. Rock Mech. Min. Sci.* 34, 1165–1186.

- Hoek, E., Brown, E.T., 1980. *Underground excavations in rock*. The Institution of Mining and Metallurgy, London.
- Hoek, E., Diederichs, M.S., 2006. Empirical estimation of rock mass modulus. *Int. J. Rock Mech. Min. Sci.* 43, 203–215.
- Hudyma, M., Heal, D., Mikula, P., 2003. Seismic monitoring in mines - Old technology - New applications, in: *Proceedings of the 1st Australasian Ground Control in Mining Conference*. Presented at the 1st Australasian Ground Control in Mining Conference, University of NSW, Sydney, NSW.
- Hudyma, M., Potvin, Y., Allison, D., 2008a. Seismic monitoring of the Northparkes lift 2 block cave—part I undercutting. *J. South. Afr. Inst. Min. Metall.* 108, 405–419.
- Hudyma, M., Potvin, Y., Allison, D., 2008b. Seismic monitoring of the Northparkes Lift 2 block cave—part 2 production caving. *J. South. Afr. Inst. Min. Metall.* 108, 421–430.
- Hudyma, M.R., 2008. *Analysis and interpretation of clusters of seismic events in mines* (PhD Thesis). University of Western Australia, Perth, WA.
- Hudyma, M.R., Frenette, P., Leslie, I., 2010. Monitoring open stope caving at Goldex Mine. *Min. Technol.* 119, 142–150.
- Hudyma, M.R., Potvin, Y., Grant, D.R., Milne, D., Brummer, R.K., Board, M., 1994. Geomechanics of sill pillar mining, in: Nelson, P.P., Laubach, S.E. (Eds.), *Rock Mechanics Models and Measurements Challenges from Industry*. A.A. Balkema, Austin, TX, pp. 969–976.
- Ide, S., Beroza, G.C., 2001. Does apparent stress vary with earthquake size? *Geophys. Res. Lett.* 28, 3349–3352.
- Jalbout, A., Simser, B., 2014. Rock mechanics tools for mining in high stress ground conditions at Nickel Rim South Mine, in: Hudyma, M., Potvin, Y. (Eds.), *Deep Mining 2014: Proceedings of the Seventh International Seminar on Deep and High Stress Mining*. Australian Centre for Geomechanics, Sudbury, ON, pp. 189–208.
- King, G.C.P., Stein, R.S., Lin, J., 1994. Static stress changes and the triggering of earthquakes. *Bull. Seismol. Soc. Am.* 84, 935–953.
- Kwiatek, G., Plenkers, K., Dresen, G., 2011. Source Parameters of Picoseismicity Recorded at Mponeng Deep Gold Mine, South Africa: Implications for Scaling Relations. *Bull. Seismol. Soc. Am.* 101, 2592–2608.
- Madariaga, R., 1976. Dynamics of an expanding circular fault. *Bull. Seismol. Soc. Am.* 66, 639–666.
- Malan, D.F., 1999. Time-dependent behaviour of deep level tabular excavations in hard rock. *Rock Mech. Rock Eng.* 32, 123–155.
- Martino, J.B., Chandler, N.A., 2004. Excavation-induced damage studies at the Underground Research Laboratory. *Int. J. Rock Mech. Min. Sci.* 41, 1413–1426.
- Mayeda, K., Gok, R., Walter, W.R., Hofsterrer, A., 2005. Evidence for non-constant energy//moment scaling from coda-derived source spectra. *Geophys. Res. Lett.* 32.
- McCreary, R., McGaughey, J., Potvin, Y., Ecobichon, D., Hudyma, M., Kanduth, H., Coulombe, A., 1992. Results from microseismic monitoring, conventional instrumentation, and tomography surveys in the creation and thinning of a burst-prone sill pillar. *Pure Appl. Geophys.* 139, 349–373.
- McGarr, A., 2005. Observations concerning diverse mechanisms for mining-induced earthquakes, in: Potvin, Y., Hudyma, M. (Eds.), *Controlling Seismic Risk: Proceedings of the Sixth*

- International Symposium on Rockbursts and Seismicity in Mines. Australian Centre for Geomechanics, Perth, WA, pp. 107–111.
- McGarr, A., 1999. On relating apparent stress to the stress causing earthquake fault slip. *J. Geophys. Res.* 104, 3003–3011.
- McGarr, A., 1994. Some comparisons between mining-induced and laboratory earthquakes. *Pure Appl. Geophys.* 142, 467–289.
- McGarr, A., 1976. Seismic moments and volume changes. *J. Geophys. Res.* 81, 1487–1494.
- McGarr, A., Spottiswoode, S.M., Gay, N.C., 1975. Relationship of mine tremors to induced stresses and rock properties in the focal region. *Bull. Seismol. Soc. Am.* 65, 981–993.
- McGarr, A., Spottiswoode, S.M., Gay, N.C., Ortlepp, W.D., 1979. Observations relevant to seismic driving stress, stress drop, and efficiency. *J. Geophys. Res.* 84, 2251–2261.
- McKinnon, S.D., Garrido de la Barra, I., 1998. Fracture initiation, growth and effect on stress field: a numerical investigation. *J. Struct. Geol.* 20, 1673–1689.
- McLean, S.A., Straub, K.H., Stevens, K.M., 2005. Chapter 16: The discovery and characterization of the Nickel Rim South deposit, Sudbury, Ontario, in: Mungall, J.E. (Ed.), *Exploration for Platinum-Group Elements Deposits*. Mineralogical Association of Canada, Oulu, Finland, pp. 359–368.
- Mendecki, A.J., 2016. *Mine seismology reference book: seismic hazard*. Institute of Mine Seismology.
- Mendecki, A.J. (Ed.), 1997. *Seismic monitoring in mines*. Chapman & Hall, London.
- Mendecki, A.J., 1993. Keynote address: real time quantitative seismology in mines, in: Young, R.P. (Ed.), *Rockbursts and Seismicity in Mines 93: Proceedings of the 3rd International Symposium*. CRC Press, Kingston, ON, pp. 287–295.
- Mendecki, A.J., van Aswegen, G., Mountfort, P., 1999. A guide to routine seismic monitoring in mines, in: Jager, A.J., Ryder, J.A. (Eds.), *A Handbook on Rock Engineering Practice for Tabular Hard Rock Mines*. Creda Communications, Cape Town, South Africa.
- Mercer, R.A., 1999. *The quantitative analysis of integrated seismic and numerical modelling data at Creighton mine, Sudbury, Ontario (PhD Thesis)*. Queen's University, Kingston, ON.
- Mercer, R.A., Bawden, W.F., 2005. A statistical approach for the integrated analysis of mine-induced seismicity and numerical stress estimates, a case study — Part I: developing the relations. *Int. J. Rock Mech. Min. Sci.* 42, 47–72.
- Nuttli, O.W., 1973. Seismic wave attenuation and magnitude relations for eastern North America. *J. Geophys. Res.* 78, 876–885.
- Orlecka-Sikora, B., 2010. The role of static stress transfer in mining induced seismic events occurrence, a case study of the Rudna mine in the Legnica-Glogow Copper District in Poland. *Geophys. J. Int.* 182, 1087–1095.
- Perez-Campos, X., Beroza, G.C., 2001. An apparent mechanism dependence of radiated seismic energy. *J. Geophys. Res.* 106, 11,127–11,136.
- Perras, M.A., Diederichs, M.S., 2016. Predicting excavation damage zone depths in brittle rocks. *J. Rock Mech. Geotech. Eng.* 8, 60–74.
- Richter, C.F., 1935. An instrumental earthquake magnitude scale. *Bull. Seismol. Soc. Am.* 25, 1–32.
- Rousell, D.H., 2009. Chapter 9: Structural geology, in: Rousell, D.H., Brown, G.H. (Eds.), *A Field Guide to the Geology of Sudbury, Ontario*. Ontario Geological Survey, Open File Report 6423, pp. 75–94.

- Rousell, D.H., Card, K.D., 2009. Chapter 1: Geological setting, in: Rousell, D.H., Brown, G.H. (Eds.), *A Field Guide to the Geology of Sudbury, Ontario*. Ontario Geological Survey, Open File Report 6423, pp. 1–6.
- Savage, J.C., Wood, M.D., 1971. The relation between apparent stress and stress drop. *Bull. Seismol. Soc. Am.* 61, 1381–1388.
- Sharan, S.K., 2008. Analytical solutions for stresses and displacements around a circular opening in a generalized Hoek-Brown rock. *Int. J. Rock Mech. Min. Sci.* 45, 78–85.
- Simser, B., 2017. Use of micro seismic data for numerical model calibration: stress inputs, yield zones, influence of faults and forecasting future behaviour. Examples from Nickel Rim South Mine.
- Simser, B., 2016. Sudbury Integrated Nickel Operations - a Glencore Company.
- Simser, B., 2013. Seismic damage to rib pillar (Unpublished Internal Document). Sudbury, ON.
- Simser, B., Deredin, R., Jalbout, A., Butler, T., 2015a. Use of microseismic monitoring data as an aid to rock mechanics decision making and mine design verification. Presented at the 49th US Rock Mechanics/Geomechanics Symposium, American Rock Mechanics Association, San Francisco, CA, p. NA.
- Simser, B., Falmagne, V., 2004. Seismic source parameters used to monitor rockmass response at Brunswick mine. *CIM Bull.* 97, 58–63.
- Simser, B., Falmagne, V., Gaudreau, D., MacDonald, T., 2003. Seismic response to mining at the Brunswick No.12 Mine. Presented at the Canadian Institute of Mining and Metallurgy Annual General Meeting, Montreal, QC.
- Simser, B., Pawlowicz, C., Falconer, S., 2015b. Nickel Rim South mine design document (Unpublished Internal Document). Glencore, Sudbury, ON.
- Simser, B.P., Andrieux, P.P., Peterson, D.A., MacDonald, T.A., Alcott, J.M., 1998. Advanced monitoring and analysis of microseismic activity as an aid to mining at Brunswick Mines. *Int. J. Rock Mech. Min. Sci.* 35, Paper No. 73.
- Smith-Boughner, L.T., Urbancic, T.I., Baig, A.M., 2017. Resolving sill pillar stress behaviour associated with blasts and rockbursts, in: *Deep Mining 2017: Eighth International Conference on Deep and High Stress Mining*. Australian Centre for Geomechanics, Perth, WA.
- Snelling, P.E., Godin, L., McKinnon, S.D., 2013. The role of geologic structure and stress in triggering remote seismicity in Creighton Mine, Sudbury, Canada. *Int. J. Rock Mech. Min. Sci.* 58, 166–179.
- Souley, M., Homand, F., Pepa, S., Hoxha, D., 2001. Damage-induced permeability changes in granite: a case example at the URL in Canada. *Int. J. Rock Mech. Min. Sci.* 38, 297–310.
- Syrek, B., Kijko, A., 1988. Energy and frequency distribution of mining tremors and their relation to rockburst hazard in the Wujek coal mine, Poland. *Acta Geophys. Pol.* 36, 189–201.
- Tsang, C.F., Bernier, F., Davies, C., 2005. Geohydromechanical processes in the Excavation Damaged Zone in crystalline rock, rock salt, and indurated and plastic clays—in the context of radioactive waste disposal. *Int. J. Rock Mech. Min. Sci.* 42, 109–125.
- Urbancic, T.I., 1991. Source studies of mining-induced microseismicity at Strathcona Mine, Sudbury, Canada: a spatial and temporal analysis (PhD Thesis). Queen's University, Kingston, ON.
- Urbancic, T.I., Feignier, B., Young, R.P., 1992a. Influence of source region properties on scaling relations for  $M < 0$  events. *Pure Appl. Geophys.* 139, 721–739.

- Urbancic, T.I., Trifu, C.-I., 1998. Shear zone stress release heterogeneity associated with two mining-induced events of M 1.7 and 2.2. *Tectonophysics* 289, 75–89.
- Urbancic, T.I., Trifu, C.-I., 1996. Effects of rupture complexity and stress regime on scaling relations of induced microseismic events. *Pure Appl. Geophys.* 147, 319–343.
- Urbancic, T.I., Trifu, C.-I., Long, J.M., Young, R.P., 1992b. Space-time correlations of b values with stress release. *Pure Appl. Geophys.* 139, 449–462.
- Urbancic, T.I., Young, R.P., 1993. Space-time variations in source parameters of mining-induced seismic events with  $M < 0$ . *Bull. Seismol. Soc. Am.* 83, 378–397.
- van Aswegen, G., 2005. Routine seismic hazard assessment in some South African mines, in: *Controlling Seismic Risk: Proceedings of the Sixth International Symposium on Rockburst and Seismicity in Mines*. Australian Centre for Geomechanics, Perth, WA, pp. 437–444.
- van Aswegen, G., Butler, A.G., 1993. Applications of quantitative seismology in South African gold mines, in: Young, R.P. (Ed.), *Rockbursts and Seismicity in Mines 93: Proceedings of the 3rd International Symposium*. CRC Press, Kingston, ON, pp. 261–266.
- van Aswegen, G., Mendecki, A.J., 1999. Mine layout, geological features and seismic hazard (No. GAP303). Safety in Mines Research Advisory Committee, South Africa.
- Wawersik, W.R., Fairhurst, C., 1970. A study of brittle rock fracture in laboratory compression experiments. *Int. J. Rock Mech. Min. Sci.* 7, 561–575.
- Wesseloo, J., 2014. Evaluation of the spatial variation of b-value. *J. South. Afr. Inst. Min. Metall.* 114, 823–828.
- Wesseloo, J., Woodward, K., Pereira, J., 2014. Grid-based analysis of seismic data. *J. South. Afr. Inst. Min. Metall.* 114, 815–822.
- Wyss, M., Brune, J.N., 1968. Seismic moment, stress and source dimensions for earthquakes in the California-Nevada region. *J. Geophys. Res.* 73, 4681–4694.
- Xstrata, 2008. Nickel Rim South full mine phase feasibility study (Unpublished Internal Document). Sudbury, ON.
- Young, D.P., 2012. Energy variations in mining-induced seismic events using apparent stress (MAsc Thesis). Laurentian University, Sudbury, ON.
- Young, R.P., Maxwell, S.C., Urbancic, T.I., Feignier, B., 1992. Mining-induced microseismicity: monitoring and applications of imaging and source mechanism techniques. *Pure Appl. Geophys.* 139, 697–719.

## Appendix A: Source of Seismic Data

All seismic data analysed in this thesis is taken from NRSM's seismic monitoring system. This system is supplied by Engineering Seismology Group (ESG) and uses their Paladin monitoring units. The database is cleared of blast vibrations and noise but has otherwise been unaltered in any way. The majority of this data is also automatically processed by ESG's software. Site practices typically involve manually picking wave arrivals for larger events ( $M \geq -1$ ). Values of apparent stress are based on the system's estimates of seismic energy and moment (Equation 2.3). Specific constants for source parameter estimates and calibration data are not available.

## Appendix B: Summary of Apparent Stress and MESD Parameters Preceding Blasts

Times are given in hours, apparent stress is stated in kPa, and event-stope distances are stated in metres

INTERPRETATION	BLAST	DATE-TIME	VOLUME	INITIALS								
				AS <sub>20</sub>	AS <sub>50</sub>	AS <sub>80</sub>	D <sub>50</sub>	D <sub>50H50</sub>	D <sub>50H80</sub>	D <sub>50L50</sub>	D <sub>50L20</sub>	
1	1595-275-P1	2011-10-28 5:24	NW corner	5.1	10.2	22.2	3.0	3.0	3.0	2.9	3.1	
2	1595-275-P1	2011-10-28 5:24	SE corner	6.7	12.3	25.1	4.1	4.5	4.4	3.5	3.9	
3	1595-225-P1	2011-12-13 18:22	W sidewall	3.9	8.6	18.7	3.6	3.6	3.2	3.6	3.4	
4	1680-262-P2	2011-12-24 3:54	W sidewall	5.7	10.5	19.1	5.7	7.0	7.2	4.7	4.5	
5	1680-262-P2	2011-12-24 3:54	W sidewall	5.7	10.5	19.1	5.7	7.0	7.2	4.7	4.5	
6	1445-250-P1	2012-01-05 6:17	Pillar	4.6	8.6	16.7	4.3	3.1	3.3	5.0	5.0	
7	1445-250-P1	2012-01-05 6:17	Pillar	4.6	8.6	16.7	4.3	3.1	3.3	5.0	5.0	
8	1480-312-P1	2012-01-13 18:26	E abutment	7.8	19.0	50.8	19.2	22.8	27.0	17.0	17.3	
9	1480-312-P1	2012-01-13 18:26	E abutment	7.8	19.0	50.8	19.2	22.8	27.0	17.0	17.3	
10	1445-300-P1	2012-08-06 18:24	E sidewall	5.9	11.4	26.2	3.1	3.2	3.7	3.1	3.1	
11	1535-275-P1	2013-06-19 14:56	NW corner	6.4	12.5	26.4	2.3	2.1	2.1	2.7	2.9	
12	1535-275-P1	2013-06-19 14:56	SE corner	6.2	11.0	21.2	2.1	2.3	2.6	1.9	2.0	
13	1565-300-P1	2013-08-03 10:46	E sidewall	5.9	10.6	21.9	8.6	8.8	9.1	8.6	8.6	
14	1535-275-P2	2013-09-15 18:24	E abutment	4.5	10.2	25.6	10.9	11.4	13.6	10.4	11.8	
15	1535-275-P2	2013-09-15 18:24	NW corner	6.7	12.8	25.2	9.9	10.9	10.9	9.2	10.2	
16	1475-312-P1	2014-02-09 6:12	E abutment	9.0	15.4	29.1	11.1	11.8	12.8	10.7	10.7	
17	1535-300-P1	2014-04-09 18:22	SE corner	5.3	10.9	22.8	11.6	15.4	18.7	9.9	11.6	
18	1535-300-P1	2014-04-09 18:22	SE corner	5.3	10.9	22.8	11.6	15.4	18.7	9.9	11.6	
19	1625-337-P1	2014-05-17 18:16	E sidewall	5.4	9.2	18.1	9.0	9.2	9.3	8.5	10.4	
20	1565-250-P2	2014-05-19 20:06	NW corner	4.7	9.8	21.8	12.9	14.5	16.3	11.0	11.9	
21	1535-300-P2	2014-08-11 9:26	E abutment	5.2	8.9	17.0	19.0	19.2	23.4	18.7	19.5	
22	1535-300-P2	2014-08-11 9:26	E abutment	5.2	8.9	17.0	19.0	19.2	23.4	18.7	19.5	
23	1565-250-P3	2014-09-05 18:15	NW corner	4.3	8.9	19.5	4.8	4.8	5.5	4.7	4.2	
24	1595-200-P1	2014-10-22 18:19	W sidewall	3.6	7.6	15.4	4.2	4.7	5.7	3.7	4.1	
25	1595-200-P1	2014-10-22 18:19	Pillar	2.7	4.9	9.0	2.3	2.4	2.8	2.2	2.1	
26	1190-325-P1	2014-11-14 6:06	W sidewall	4.1	9.0	22.5	16.1	18.7	18.2	14.5	15.0	
27	1475-337-P1	2015-01-03 18:20	SE corner	7.5	11.4	24.5	12.5	13.3	14.8	12.0	14.0	
28	1565-325-P1	2015-01-07 18:22	SE corner	4.7	8.0	15.5	5.0	5.0	5.9	4.9	5.7	
29	1565-325-P1	2015-01-07 18:22	SE corner	4.7	8.0	15.5	5.0	5.0	5.9	4.9	5.7	
30	1415-250-P1	2015-01-20 18:12	W sidewall	6.8	13.7	36.6	6.0	6.2	5.1	5.7	4.7	
31	1535-250-P1	2015-02-14 18:18	W abutment	4.4	8.6	21.5	17.8	18.7	19.4	16.5	17.1	
32	1535-250-P1	2015-02-14 18:18	W abutment	4.4	8.6	21.5	17.8	18.7	19.4	16.5	17.1	
33	1565-225-P1	2015-04-09 18:15	W sidewall	2.4	4.2	8.1	3.8	4.0	3.7	3.5	4.4	

INTERPRETATION	BLAST	DATE-TIME	VOLUME	INITIALS							
				AS <sub>20</sub>	AS <sub>50</sub>	AS <sub>80</sub>	D <sub>50</sub>	D <sub>50H50</sub>	D <sub>50H80</sub>	D <sub>50L50</sub>	D <sub>50L20</sub>
34	1355-275-P2	2015-06-01 18:17	W sidewall	5.1	9.2	18.0	9.8	12.0	11.6	6.8	5.2
35	1680-325-P1	2015-06-08 18:45	SE corner	5.4	8.0	15.8	10.4	10.6	11.1	10.3	9.6
36	1535-250-P2	2015-07-07 18:16	W sidewall	4.1	7.3	16.0	14.8	15.7	17.8	13.8	13.6
37	1565-225-P2	2015-09-09 18:08	W sidewall	2.9	6.3	16.2	6.6	6.9	6.8	5.4	6.7
38	1565-225-P2	2015-09-09 18:08	W sidewall	2.9	6.3	16.2	6.6	6.9	6.8	5.4	6.7
39	1565-225-P2	2015-09-09 18:08	W sidewall	3.6	7.9	18.4	3.3	3.6	3.6	3.0	3.4
40	1355-275-P3	2015-10-07 6:06	W abutment	4.1	8.2	18.6	19.5	19.3	22.5	19.6	21.0
41	1475-212-P1	2015-12-29 18:09	W sidewall	3.3	7.3	16.9	2.3	2.6	2.4	2.1	2.2
42	1475-212-P1	2015-12-29 18:09	W sidewall	3.3	7.3	16.9	2.3	2.6	2.4	2.1	2.2
43	1475-212-P1	2015-12-29 18:09	W abutment	3.3	6.9	14.6	3.2	3.7	4.4	3.0	3.0
44	1475-212-P1	2015-12-29 18:09	NW corner	3.7	8.2	26.5	2.0	1.8	2.1	2.0	2.1
45	1475-212-P1	2015-12-29 18:09	Back	4.0	9.0	19.9	3.9	4.2	4.6	3.3	4.1
46	1680-250-P2	2016-04-12 6:08	W abutment	4.6	8.3	15.6	13.6	13.6	14.7	13.7	14.0
47	1385-250-P1	2016-05-29 18:14	NW corner	5.3	11.0	19.8	5.5	6.7	7.0	4.1	2.9
48	1220-312-P1	2016-06-24 6:07	Top abutment	4.8	10.7	23.4	31.3	30.9	33.1	32.5	31.5
49	1220-312-P1	2016-06-24 6:07	Top abutment	4.8	10.7	23.4	31.3	30.9	33.1	32.5	31.5
50	1535-225-P1	2016-06-30 18:23	W sidewall	2.6	6.0	13.8	3.8	3.8	3.7	3.8	3.3
51	1535-225-P1	2016-06-30 18:23	NW corner	3.2	5.3	11.5	3.3	3.7	4.4	3.2	3.2
52	1535-225-P1	2016-06-30 18:23	NW corner	3.2	5.3	11.5	3.3	3.7	4.4	3.2	3.2
53	1385-300-P3	2016-07-26 18:15	E sidewall	5.2	9.1	17.0	4.5	6.2	7.4	3.7	4.1
54	1535-325-P1	2016-08-21 6:01	SE corner	6.0	10.0	20.6	12.6	14.1	13.7	11.3	13.2
55	1535-325-P1	2016-08-21 6:01	E abutment	5.6	9.1	17.4	15.9	15.8	16.9	16.0	17.3
56	1680-237-P1	2016-11-25 18:07	W abutment	4.2	8.5	15.2	18.7	22.8	29.6	15.7	13.5
57	1355-250-P1	2017-03-23 18:19	W sidewall	3.8	7.6	13.9	6.9	8.1	9.2	5.6	4.6
58	1220-272-P1	2017-04-21 18:20	Top abutment	2.5	7.0	14.5	29.7	26.8	29.8	31.9	33.8
59	1565-200-P1	2017-05-06 18:20	W sidewall	3.4	6.1	12.3	2.9	3.0	2.9	2.8	3.5
60	1535-200-P1	2017-10-08 18:20	W sidewall	5.3	8.4	16.0	4.4	4.5	3.4	4.3	3.8
61	1535-200-P1	2017-10-08 18:20	W sidewall	5.3	8.4	16.0	4.4	4.5	3.4	4.3	3.8
62	1385-225-P1	2017-10-27 18:20	W sidewall	4.3	7.6	15.9	6.7	6.7	7.6	6.7	5.4

## Appendix C: Summary of Parameters Taken from Interpretations of Variation in Apparent Stress

Times are given in hours and apparent stress is stated in kPa

### Phase 1

INTERPRETATION	EXTREMES			TIMES				VALUE AT AVERAGE TIME				
	AS <sub>20</sub>	AS <sub>50</sub>	AS <sub>80</sub>	AS <sub>20</sub>	AS <sub>50</sub>	AS <sub>80</sub>	AVG TIME	AS <sub>20</sub>	AS <sub>50</sub>	AS <sub>80</sub>	EVENT #	EVENTS
1	5.5	10.6	25.9	0.04	0.04	0.03	0.04	5.2	10.5	25.6	14	14
2	8.7	15.4	28.1	0.11	0.09	0.08	0.09	8.6	15.4	27.5	84	84
3	4.2	9.8	22.0	0.06	0.04	0.07	0.06	4.2	9.1	21.7	47	47
4	7.4	13.2	25.5	0.23	0.21	0.08	0.17	6.9	12.9	23.7	162	162
5	7.4	13.2	25.5	0.23	0.21	0.08	0.17	6.9	12.9	23.7	162	162
6	5.7	10.9	19.0	0.27	0.12	0.04	0.14	5.3	10.6	18.9	76	76
7	5.7	10.9	19.0	0.27	0.12	0.04	0.14	5.3	10.6	18.9	76	76
8	11.3	22.5	54.8	0.07	0.03	0.03	0.04	9.1	20.4	51.2	50	50
9	11.3	22.5	54.8	0.07	0.03	0.03	0.04	9.1	20.4	51.2	50	50
10	9.6	18.8	33.8	0.27	0.11	0.10	0.16	8.4	17.9	32.9	139	139
11	7.5	16.6	34.4	0.37	0.17	0.17	0.23	6.6	15.0	31.8	93	93
12	7.2	13.3	26.4	0.09	0.05	0.21	0.12	6.7	13.1	25.7	128	128
13	7.1	12.6	27.9	0.11	0.38	0.08	0.19	6.5	11.6	22.3	119	119
14	6.3	12.7	31.7	0.21	0.02	0.03	0.09	5.5	11.5	30.1	138	138
15	7.0	13.8	27.0	0.01	0.01	0.02	0.02	6.9	13.3	26.1	22	22
16	9.5	16.7	30.7	0.09	0.05	0.05	0.06	9.3	16.1	30.4	37	37
17	6.9	13.4	26.8	0.31	0.72	0.10	0.38	6.5	12.5	22.4	140	140
18	6.9	13.4	26.8	0.31	0.72	0.10	0.38	6.5	12.5	22.4	140	140
19	6.3	10.5	21.8	0.32	0.18	0.14	0.21	6.1	10.4	20.3	92	92
20	4.8	11.4	25.7	0.35	0.06	0.28	0.23	4.5	11.1	24.3	134	134
21	6.0	10.4	20.2	0.03	0.03	0.03	0.03	6.0	10.4	19.7	50	50
22	6.0	10.4	20.2	0.03	0.03	0.03	0.03	6.0	10.4	19.7	50	50
23	6.0	13.7	24.3	0.09	0.07	0.03	0.06	5.7	13.2	23.8	96	96
24	6.9	17.0	34.0	0.15	0.16	0.16	0.16	6.9	16.8	33.1	198	198
25	3.8	6.3	11.4	0.30	0.50	0.54	0.44	3.3	6.1	11.3	163	163
26	5.6	12.1	29.0	0.71	0.71	0.04	0.49	5.2	10.5	25.2	121	121
27	8.4	13.5	26.2	0.08	0.08	0.11	0.09	8.1	13.3	25.9	120	120
28	5.6	10.5	22.0	0.10	0.09	0.14	0.11	5.5	10.4	21.6	120	120
29	5.6	10.5	22.0	0.10	0.09	0.14	0.11	5.5	10.4	21.6	120	120
30	9.4	18.9	42.0	0.05	0.03	0.02	0.03	8.3	18.6	41.7	68	68
31	4.9	10.5	25.9	0.09	0.06	0.03	0.06	4.4	10.0	25.5	72	72
32	4.9	10.5	25.9	0.09	0.06	0.03	0.06	4.4	10.0	25.5	72	72

INTERPRETATION	EXTREMES			TIMES				VALUE AT AVERAGE TIME				
	AS <sub>20</sub>	AS <sub>50</sub>	AS <sub>80</sub>	AS <sub>20</sub>	AS <sub>50</sub>	AS <sub>80</sub>	AVG TIME	AS <sub>20</sub>	AS <sub>50</sub>	AS <sub>80</sub>	EVENT #	EVENTS
33	3.5	7.4	16.4	0.07	0.07	0.06	0.07	3.4	7.4	16.4	114	114
34	5.8	9.4	23.4	0.35	0.34	0.03	0.24	5.0	8.9	19.5	169	169
35	6.0	10.0	20.4	0.14	0.20	0.26	0.20	5.7	9.7	20.2	172	172
36	5.6	9.8	19.9	0.04	0.08	0.03	0.05	5.5	9.4	19.1	122	122
37	5.8	12.5	23.4	0.17	0.17	0.15	0.16	5.6	12.4	23.4	153	153
38	5.8	12.5	23.4	0.17	0.17	0.15	0.16	5.6	12.4	23.4	153	153
39	7.1	15.6	28.8	0.12	0.10	0.02	0.08	6.0	15.3	26.7	143	143
40	5.7	11.0	24.1	0.32	0.26	0.03	0.20	5.0	9.8	22.3	160	160
41	5.6	11.9	27.8	0.17	0.06	0.05	0.10	4.6	11.1	27.3	114	114
42	5.6	11.9	27.8	0.17	0.06	0.05	0.10	4.6	11.1	27.3	114	114
43	5.6	13.7	27.5	0.17	0.17	0.16	0.17	5.5	13.5	27.5	109	109
44	4.4	11.5	30.7	0.11	0.06	0.06	0.08	4.2	11.2	30.3	28	28
45	7.7	14.3	27.1	0.14	0.07	0.07	0.09	6.7	13.0	26.8	127	127
46	4.8	10.2	19.4	0.25	0.25	0.27	0.26	4.8	9.7	19.3	133	133
47	6.0	12.1	27.3	0.02	0.07	0.08	0.06	5.8	11.6	24.2	80	80
48	5.7	13.4	32.1	0.03	0.03	0.03	0.03	5.7	13.2	32.0	71	71
49	5.7	13.4	32.1	0.03	0.03	0.03	0.03	5.7	13.2	32.0	71	71
50	4.3	7.8	17.4	0.25	0.25	0.05	0.18	4.1	7.4	15.3	116	116
51	5.9	10.8	18.3	0.41	0.39	0.34	0.38	5.8	10.6	17.8	189	189
52	5.9	10.8	18.3	0.41	0.39	0.34	0.38	5.8	10.6	17.8	189	189
53	6.2	10.4	21.1	0.07	0.06	0.03	0.06	5.9	10.3	20.8	90	90
54	7.7	13.5	23.6	0.30	0.21	0.15	0.22	7.3	13.5	22.6	152	152
55	8.6	12.6	25.1	0.29	0.26	0.07	0.21	7.6	12.2	24.8	160	160
56	5.0	9.9	20.2	0.06	0.07	0.06	0.06	5.0	9.8	20.2	111	111
57	4.6	8.3	17.7	0.11	0.05	0.05	0.07	4.6	8.2	16.8	87	87
58	2.5	7.2	15.5	0.00	0.00	0.00	0.00	2.5	7.2	15.5	4	4
59	5.6	9.3	16.0	0.28	0.28	0.06	0.21	4.9	9.1	15.6	118	118
60	7.2	14.2	24.7	0.08	0.05	0.05	0.06	7.0	13.1	24.0	173	173
61	7.2	14.2	24.7	0.08	0.05	0.05	0.06	7.0	13.1	24.0	173	173
62	6.0	9.7	19.6	0.10	0.13	0.11	0.11	5.8	9.5	19.6	93	93

## Phase 2

INTERPRETATION	EXTREMES			TIMES				VALUE AT AVERAGE TIME				
	AS <sub>20</sub>	AS <sub>50</sub>	AS <sub>80</sub>	AS <sub>20</sub>	AS <sub>50</sub>	AS <sub>80</sub>	AVG TIME	AS <sub>20</sub>	AS <sub>50</sub>	AS <sub>80</sub>	EVENT #	EVENTS
1	4.0	6.9	12.1	11.74	21.16	11.90	14.93	4.1	7.0	12.6	249	235
2	5.6	9.6	18.4	2.25	1.84	4.36	2.81	5.6	9.8	18.9	483	399
3	2.3	4.5	8.3	1.47	1.14	0.99	1.20	2.5	4.7	8.5	393	346
4	4.3	8.4	13.4	3.88	2.75	2.80	3.14	4.3	8.8	13.7	553	391

INTERPRETATION	EXTREMES			TIMES				VALUE AT AVERAGE TIME				
	AS <sub>20</sub>	AS <sub>50</sub>	AS <sub>80</sub>	AS <sub>20</sub>	AS <sub>50</sub>	AS <sub>80</sub>	AVG TIME	AS <sub>20</sub>	AS <sub>50</sub>	AS <sub>80</sub>	EVENT #	EVENTS
5	3.8	7.0	10.8	22.17	22.06	25.86	23.36	4.0	7.1	11.1	979	817
6	4.5	7.4	12.3	1.97	0.94	3.85	2.25	4.5	7.5	12.6	338	262
7	4.5	7.4	12.3	1.97	0.94	3.85	2.25	4.5	7.5	12.6	338	262
8	7.8	14.7	28.4	2.07	2.31	2.24	2.21	7.8	14.8	29.6	302	252
9	7.8	14.7	28.4	2.07	2.31	2.24	2.21	7.8	14.8	29.6	302	252
10	6.2	11.0	21.6	1.38	1.65	0.75	1.26	6.2	12.3	22.3	369	230
11	5.6	10.1	17.8	3.71	8.86	8.86	7.14	5.9	10.2	19.4	292	199
12	3.8	6.2	12.3	4.90	4.90	3.68	4.49	3.9	6.2	12.5	468	340
13	5.3	8.9	15.6	1.65	1.74	1.36	1.58	5.4	9.0	16.4	282	163
14	4.6	8.3	15.0	2.03	3.27	3.30	2.87	5.0	8.3	15.8	449	311
15	3.1	7.3	17.5	3.43	2.36	2.36	2.72	3.3	7.3	17.5	270	248
16	7.6	12.1	18.3	1.26	1.36	1.32	1.31	7.7	12.3	18.3	385	348
17	5.7	10.2	18.6	2.44	2.49	2.04	2.32	5.7	10.4	18.8	320	180
18	5.7	10.2	18.6	2.44	2.49	2.04	2.32	5.7	10.4	18.8	320	180
19	5.1	9.2	13.8	1.57	1.31	1.43	1.44	5.5	9.6	13.8	313	221
20	3.8	7.8	16.6	1.48	1.48	1.99	1.65	3.9	7.8	16.8	269	135
21	5.2	8.5	14.9	0.38	0.51	1.44	0.78	5.6	9.3	15.5	296	246
22	4.8	8.1	14.5	9.02	9.78	10.43	9.74	4.9	8.1	14.8	627	577
23	3.8	7.2	15.4	0.65	1.24	0.67	0.85	3.8	7.4	15.8	289	193
24	3.4	6.6	13.5	1.84	1.98	1.94	1.92	3.4	6.6	14.1	552	354
25	2.9	5.0	8.6	2.63	2.51	3.84	2.99	3.0	5.4	9.1	329	166
26	4.2	8.3	17.6	2.53	5.83	1.80	3.39	4.2	8.6	18.2	281	160
27	5.8	9.6	16.3	2.44	2.61	2.56	2.54	5.8	9.6	16.5	295	175
28	3.8	6.8	12.6	3.95	2.76	3.95	3.55	3.8	6.8	13.2	327	207
29	3.8	6.8	12.6	3.95	2.76	3.95	3.55	3.8	6.8	13.2	327	207
30	4.6	8.3	15.0	1.40	0.71	0.48	0.86	4.8	8.7	15.1	444	376
31	3.1	6.6	12.8	4.66	5.38	5.38	5.14	3.1	6.7	13.0	373	301
32	3.0	6.6	12.8	19.10	18.67	5.38	14.38	3.0	6.7	13.8	428	356
33	1.9	3.1	5.3	1.37	2.91	3.17	2.48	2.0	3.1	5.4	501	387
34	4.6	7.4	11.8	1.54	9.13	1.94	4.20	4.9	7.6	12.9	333	164
35	4.6	7.6	12.3	0.88	1.27	3.37	1.84	4.8	7.9	13.4	331	159
36	3.7	7.2	13.5	6.37	0.60	0.65	2.54	3.9	7.5	13.6	483	361
37	3.4	6.3	11.5	0.88	1.99	1.95	1.61	3.5	6.7	11.9	395	242
38	3.4	6.3	11.5	0.88	1.99	1.95	1.61	3.5	6.7	11.9	395	242
39	3.7	6.2	11.8	0.93	0.61	0.60	0.71	3.8	6.4	12.9	467	324
40	4.4	7.1	14.0	2.40	2.43	2.26	2.36	4.4	7.2	14.0	323	163
41	3.1	5.2	8.9	2.03	1.07	1.10	1.40	3.3	5.7	10.4	491	377
42	3.1	5.2	8.9	2.03	1.07	1.10	1.40	3.3	5.7	10.4	491	377
43	3.2	6.0	12.2	5.33	1.16	2.31	2.93	3.5	6.1	13.0	400	291

INTERPRETATION	EXTREMES			TIMES				VALUE AT AVERAGE TIME				
	AS <sub>20</sub>	AS <sub>50</sub>	AS <sub>80</sub>	AS <sub>20</sub>	AS <sub>50</sub>	AS <sub>80</sub>	AVG TIME	AS <sub>20</sub>	AS <sub>50</sub>	AS <sub>80</sub>	EVENT #	EVENTS
44	2.6	5.4	10.9	3.97	5.71	5.71	5.13	2.7	5.5	10.9	275	247
45	3.9	6.6	10.6	0.88	0.98	0.93	0.93	3.9	6.7	10.8	486	359
46	3.1	5.7	15.0	1.41	1.49	1.41	1.44	3.1	5.7	15.0	302	169
47	2.9	6.6	12.7	3.84	6.28	2.19	4.10	2.9	7.0	13.1	298	218
48	3.5	6.3	13.1	0.93	0.46	1.06	0.82	3.8	6.6	13.8	497	426
49	3.5	6.3	13.1	0.93	0.46	1.06	0.82	3.8	6.6	13.8	497	426
50	3.2	5.4	9.3	3.59	2.75	1.43	2.59	3.3	5.6	9.5	305	189
51	4.1	7.7	13.1	3.50	3.67	0.72	2.63	4.6	8.5	14.1	450	261
52	4.1	7.7	13.1	3.50	3.67	0.72	2.63	4.6	8.5	14.1	450	261
53	5.0	7.7	13.0	1.01	0.92	0.84	0.93	5.0	7.7	13.0	293	203
54	6.0	8.4	13.9	1.14	1.56	1.14	1.28	6.0	8.6	14.7	364	212
55	5.9	9.0	15.0	1.65	1.89	1.91	1.82	6.0	9.3	15.2	376	216
56	3.8	7.0	12.6	0.69	0.75	0.89	0.77	3.8	7.0	12.8	329	218
57	3.8	6.5	11.6	2.31	3.24	2.09	2.55	3.8	6.7	11.6	299	212
58	1.2	2.2	4.7	0.34	0.28	0.34	0.32	1.2	2.3	4.7	296	292
59	4.7	7.4	11.1	2.38	2.41	2.10	2.30	4.7	7.5	11.1	265	147
60	4.4	7.5	11.5	1.21	0.71	0.59	0.83	4.6	7.8	11.8	602	429
61	4.4	7.5	11.5	1.21	0.71	0.59	0.83	4.6	7.8	11.8	602	429
62	3.7	6.3	12.8	3.26	3.26	1.71	2.75	3.8	6.6	13.0	280	187

### Phase 3

INTERPRETATION	EXTREMES			TIMES				VALUE AT AVERAGE TIME				
	AS <sub>20</sub>	AS <sub>50</sub>	AS <sub>80</sub>	AS <sub>20</sub>	AS <sub>50</sub>	AS <sub>80</sub>	AVG TIME	AS <sub>20</sub>	AS <sub>50</sub>	AS <sub>80</sub>	EVENT #	EVENTS
1	4.2	8.3	23.0	310.9	310.9	311.0	310.9	4.2	8.3	22.8	455	206
2	6.7	11.9	22.1	22.5	11.8	29.5	21.3	6.5	11.4	19.9	611	128
3	3.6	7.1	15.7	57.1	30.5	97.8	61.8	3.4	7.0	15.2	745	352
4	6.0	10.8	18.3	11.2	10.3	10.4	10.7	5.8	10.7	18.2	741	188
5	7.8	11.4	20.4	385.6	371.4	355.0	370.7	7.8	11.1	20.4	1657	678
6	5.2	8.8	15.1	40.3	21.5	30.5	30.8	5.1	8.8	15.1	451	113
7	6.0	9.8	17.4	224.9	230.7	297.8	251.2	5.8	9.7	17.0	560	222
8	9.7	18.7	41.0	61.5	69.1	144.3	91.6	9.3	18.6	39.1	434	132
9	10.3	20.9	46.2	385.2	385.2	484.0	418.1	10.2	20.2	45.5	507	205
10	7.9	15.8	41.0	23.7	95.4	95.6	71.6	7.2	15.3	39.0	662	293
11	6.4	12.2	26.1	139.5	139.0	40.6	106.4	5.9	10.9	24.3	592	300
12	5.7	10.3	20.2	79.1	79.1	95.5	84.6	5.4	9.9	19.6	1193	725
13	7.6	13.9	29.4	57.7	101.3	87.5	82.1	7.6	13.3	28.6	496	214
14	6.4	13.9	35.0	69.1	56.9	69.1	65.0	6.4	13.6	34.5	759	310
15	5.3	10.1	23.5	178.2	180.2	127.4	161.9	5.0	9.6	22.1	471	201

INTERPRETATION	EXTREMES			TIMES				VALUE AT AVERAGE TIME				
	AS <sub>20</sub>	AS <sub>50</sub>	AS <sub>80</sub>	AS <sub>20</sub>	AS <sub>50</sub>	AS <sub>80</sub>	AVG TIME	AS <sub>20</sub>	AS <sub>50</sub>	AS <sub>80</sub>	EVENT #	EVENTS
16	10.3	16.4	29.1	23.6	24.2	30.7	26.1	9.5	15.3	26.6	616	231
17	7.4	12.6	21.4	15.8	15.8	24.4	18.7	7.1	12.5	20.4	514	194
18	9.2	15.0	27.3	334.3	320.2	246.0	300.1	8.5	14.3	25.3	883	563
19	7.2	12.8	24.2	34.0	34.0	33.9	34.0	7.1	12.7	24.2	600	287
20	5.3	13.6	32.7	145.7	152.9	116.3	138.3	5.3	12.5	32.1	468	199
21	6.0	9.7	16.9	2.1	3.4	3.7	3.1	5.7	9.2	16.3	474	178
22	6.5	13.0	26.0	260.9	156.3	197.9	205.0	6.3	12.3	25.6	1122	495
23	5.6	12.2	26.4	45.9	46.6	48.9	47.1	5.6	12.2	26.1	557	268
24	4.8	11.5	23.8	10.6	10.6	23.2	14.8	4.4	10.9	22.7	794	242
25	4.2	7.7	15.7	1140.9	949.3	616.6	902.3	4.0	7.6	15.5	667	338
26	7.1	13.9	32.6	215.1	208.6	215.6	213.1	6.7	13.9	32.2	667	386
27	8.1	14.6	29.3	459.6	515.0	561.9	512.2	8.0	14.5	29.0	493	198
28	4.0	8.1	19.0	18.0	15.6	12.3	15.3	3.9	7.7	19.0	410	83
29	7.5	13.4	25.5	706.0	1017.6	1068.4	930.7	7.4	13.1	24.6	668	341
30	7.0	15.1	34.1	170.7	170.8	154.3	165.3	6.7	14.5	33.8	991	547
31	3.3	7.2	14.2	7.3	8.4	19.9	11.9	3.1	7.1	13.9	417	44
32	5.7	11.5	22.4	190.2	260.3	260.3	236.9	5.3	10.3	20.4	696	268
33	2.8	6.4	15.7	176.9	212.5	150.1	179.8	2.8	6.1	15.1	743	242
34	5.8	10.2	18.3	725.9	628.0	854.7	736.2	5.7	9.9	18.0	525	192
35	6.8	11.2	21.5	266.8	163.5	163.5	198.0	6.6	10.9	20.6	587	256
36	5.3	12.2	27.0	419.4	412.9	245.9	359.4	4.8	10.8	25.9	824	341
37	4.6	8.6	16.5	22.4	20.9	46.2	29.8	4.1	7.9	16.1	650	255
38	4.0	9.7	18.9	1198.7	1133.4	631.1	987.7	3.7	9.3	18.4	962	567
39	5.7	11.3	24.0	19.8	20.0	37.1	25.7	5.4	10.3	22.6	818	351
40	5.7	9.7	20.3	469.3	140.5	434.6	348.1	5.3	9.3	20.0	611	288
41	3.4	6.9	14.5	30.5	44.4	87.5	54.2	3.2	6.6	13.2	745	254
42	4.2	8.5	18.1	251.6	253.8	250.8	252.0	4.2	8.3	18.1	899	408
43	3.5	6.9	14.1	10.9	17.4	17.4	15.2	3.4	6.5	14.0	505	105
44	3.2	8.9	21.9	726.1	856.2	872.2	818.2	3.1	8.7	21.6	640	365
45	4.7	8.2	16.7	7.8	20.6	10.2	12.8	4.5	7.9	15.3	784	298
46	5.5	11.9	22.4	574.9	518.5	574.9	556.1	5.3	11.8	21.9	523	221
47	4.1	8.0	21.5	477.5	477.5	373.5	442.9	4.1	7.8	21.0	494	196
48	5.8	10.9	19.8	10.2	10.6	10.0	10.2	5.8	10.7	19.8	798	301
49	6.4	12.2	25.5	107.8	154.9	169.5	144.1	6.1	12.0	23.7	1081	584
50	3.6	7.5	13.5	10.3	22.9	22.9	18.7	3.4	6.8	13.2	463	158
51	5.7	10.9	20.3	11.1	19.6	10.6	13.7	4.9	9.5	16.9	765	315
52	4.6	8.8	21.0	121.1	50.1	129.4	100.2	4.1	7.6	18.5	1148	698
53	8.9	14.1	27.8	1027.6	1047.4	1164.5	1079.8	8.8	13.9	27.4	737	444
54	8.1	13.6	23.9	21.4	9.0	9.0	13.2	7.5	13.4	23.9	573	209

INTERPRETATION	EXTREMES			TIMES				VALUE AT AVERAGE TIME				
	AS <sub>20</sub>	AS <sub>50</sub>	AS <sub>80</sub>	AS <sub>20</sub>	AS <sub>50</sub>	AS <sub>80</sub>	AVG TIME	AS <sub>20</sub>	AS <sub>50</sub>	AS <sub>80</sub>	EVENT #	EVENTS
55	8.9	14.6	27.4	23.9	25.6	46.3	31.9	8.3	14.2	26.4	593	217
56	5.2	9.7	15.1	14.4	16.1	53.5	28.0	4.9	9.3	14.2	585	256
57	5.1	9.2	19.5	587.1	587.1	282.7	485.7	4.9	8.8	17.4	548	249
58	3.1	5.0	10.8	112.5	313.9	327.9	251.4	3.0	4.8	10.0	757	461
59	7.3	11.6	24.4	302.7	542.9	533.3	459.7	7.0	11.0	24.0	726	461
60	6.7	11.0	15.8	6.6	6.5	9.5	7.6	6.6	10.8	15.1	969	367
61	7.3	11.6	19.0	50.3	58.7	47.3	52.1	7.3	11.4	19.0	1364	762
62	4.6	7.9	17.0	98.9	98.5	72.1	89.8	4.4	7.7	16.4	465	185

# Appendix D: Summary of Parameters Taken from Interpretations of Variation in Event-Stop Distance

Times are given in hours and event-stop distances are stated in metres

## Phase 1

INTER PRETA TION	EXTREMES			TIMES				VALUE AT AVERAGE TIME						
	D <sub>50</sub> L <sub>50</sub>	D <sub>50</sub>	D <sub>50</sub> H <sub>50</sub>	D <sub>50</sub> L <sub>50</sub>	D <sub>50</sub>	D <sub>50</sub> H <sub>50</sub>	AVG TIME	EVENT #	EVENTS	D <sub>50</sub>	D <sub>50</sub> H <sub>50</sub>	D <sub>50</sub> H <sub>80</sub>	D <sub>50</sub> L <sub>50</sub>	D <sub>50</sub> L <sub>20</sub>
1	6.4	5.9	5.8	5.6	4.6	4.6	5.0	217	217	5.9	5.8	6.0	6.3	7.2
2	6.8	7.2	7.7	0.7	0.5	0.3	0.5	251	251	7.2	7.4	7.8	6.5	5.7
3	8.6	8.6	9.4	0.4	0.8	0.8	0.7	281	281	8.5	8.5	8.1	8.4	8.0
4	11.2	11.9	12.9	1.9	1.2	1.2	1.4	427	427	11.8	12.5	12.4	11.0	11.7
5	11.2	11.9	12.9	1.9	1.2	1.2	1.4	427	427	11.8	12.5	12.4	11.0	11.7
6	6.7	6.7	8.1	0.7	0.8	1.3	0.9	249	249	6.5	6.8	8.8	6.3	6.6
7	6.7	6.7	8.1	0.7	0.8	1.3	0.9	249	249	6.5	6.8	8.8	6.3	6.6
8	16.9	18.6	22.8	0.0	0.0	0.0	0.0	10	10	18.1	22.5	27.0	16.6	17.0
9	16.9	18.6	22.8	0.0	0.0	0.0	0.0	10	10	18.1	22.5	27.0	16.6	17.0
10	7.9	10.3	11.6	0.7	0.8	0.9	0.8	314	314	9.9	10.8	11.2	7.6	5.2
11	3.4	3.7	5.4	1.7	8.4	16.5	8.9	304	304	3.7	5.1	6.4	2.8	2.8
12	5.7	7.0	8.0	3.4	3.4	4.7	3.8	446	446	6.6	7.7	8.6	5.6	4.0
13	18.2	19.1	20.4	41.0	26.7	27.4	31.7	464	464	18.9	20.1	21.3	17.9	17.6
14	-	-	-	-	-	-	-	-	-	-	-	-	-	-
15	14.4	15.7	16.9	0.4	36.5	26.1	21.0	350	350	14.7	16.0	16.5	12.5	11.4
16	15.0	15.0	15.7	0.3	0.3	0.6	0.4	238	238	14.5	15.2	15.8	13.9	13.5
17	13.1	14.5	17.3	0.8	0.7	0.5	0.7	189	189	14.2	16.5	19.3	12.4	11.8
18	16.5	16.6	18.2	36.1	26.8	17.4	26.8	579	579	16.5	17.1	18.2	13.7	11.5
19	14.0	13.7	13.8	1.1	1.1	1.3	1.2	272	272	13.5	13.0	16.0	13.7	14.1
20	12.8	13.5	14.4	0.2	0.1	0.0	0.1	79	79	13.3	13.7	15.1	12.4	13.0
21	-	-	-	-	-	-	-	-	-	-	-	-	-	-
22	-	-	-	-	-	-	-	-	-	-	-	-	-	-
23	9.7	8.6	8.2	0.2	0.2	0.2	0.2	177	177	8.6	8.1	7.8	9.5	6.9
24	3.9	4.2	4.6	0.0	0.0	0.0	0.0	4	4	4.2	4.6	5.5	3.7	4.1
25	4.2	4.7	5.1	0.7	0.8	0.8	0.7	205	205	4.7	5.0	5.2	4.2	4.0
26	14.8	15.9	18.8	0.3	0.2	0.2	0.2	99	99	15.9	18.5	16.5	14.7	14.1
27	12.8	13.2	13.6	0.1	0.1	0.0	0.1	91	91	12.7	13.2	14.3	12.1	12.4
28	14.2	15.2	15.5	2.4	2.2	2.3	2.3	303	303	15.2	15.5	15.6	14.0	14.2
29	14.2	15.2	15.5	2.4	2.2	2.3	2.3	303	303	15.2	15.5	15.6	14.0	14.2
30	8.0	9.3	10.3	0.1	1.7	0.1	0.6	398	398	9.0	9.9	10.8	7.2	7.5
31	19.0	18.8	19.0	26.2	58.0	52.2	45.5	484	96	18.5	17.7	16.8	18.8	19.4
32	19.0	18.8	19.0	26.2	58.0	52.2	45.5	484	96	18.5	17.7	16.8	18.8	19.4

INTER PRETA TION	EXTREMES			TIMES				VALUE AT AVERAGE TIME						
	D50L50	D50	D50H50	D50L50	D50	D50H50	AVG TIME	EVENT #	EVENTS	D50	D50H50	D50H80	D50L50	D50L20
33	5.3	5.3	5.4	2.5	2.7	0.6	2.0	474	474	5.2	5.1	5.4	5.2	4.1
34	13.8	15.6	16.9	0.4	0.5	2.0	1.0	248	248	15.2	16.4	17.3	13.3	11.7
35	16.7	16.5	16.5	0.3	0.4	0.4	0.3	210	210	16.4	16.3	16.3	16.5	17.1
36	15.9	16.7	17.2	0.8	0.7	0.7	0.7	367	367	16.7	17.2	17.7	15.7	14.8
37	5.5	6.5	7.3	0.2	0.0	0.0	0.1	96	96	6.0	6.9	7.5	5.1	4.0
38	5.5	6.5	7.3	0.2	0.0	0.0	0.1	96	96	6.0	6.9	7.5	5.1	4.0
39	4.6	5.1	6.0	0.4	1.0	0.7	0.7	463	463	4.6	5.9	6.6	3.8	3.2
40	-	-	-	-	-	-	-	-	-	-	-	-	-	-
41	6.4	6.8	7.3	0.2	0.8	0.8	0.6	371	371	6.5	6.8	8.1	6.0	5.7
42	6.4	6.8	7.3	0.2	0.8	0.8	0.6	371	371	6.5	6.8	8.1	6.0	5.7
43	5.0	5.1	5.5	0.4	0.6	0.9	0.6	248	248	5.0	5.3	5.7	4.7	3.9
44	3.8	4.2	5.4	17.4	14.8	49.2	27.1	380	380	4.1	4.9	6.3	3.7	3.7
45	7.3	7.3	7.8	1.0	1.0	3.9	2.0	604	604	7.1	7.3	7.3	7.0	6.8
46	21.5	20.7	20.4	0.8	1.6	1.6	1.4	297	297	19.8	19.4	19.6	20.9	21.1
47	7.3	7.9	8.9	1.6	1.7	1.5	1.6	275	275	7.8	8.9	10.5	7.3	7.4
48	39.8	37.1	36.3	0.3	0.3	0.3	0.3	362	362	37.1	36.1	35.7	39.2	38.8
49	39.8	37.1	36.3	0.3	0.3	0.3	0.3	362	362	37.1	36.1	35.7	39.2	38.8
50	6.8	7.8	9.4	1.7	1.1	4.7	2.5	304	304	7.2	9.0	11.0	5.7	4.8
51	9.1	8.9	9.8	1.8	1.0	1.3	1.3	354	354	8.7	9.5	10.8	8.4	8.2
52	9.1	8.9	9.8	1.8	1.0	1.3	1.3	354	354	8.7	9.5	10.8	8.4	8.2
53	16.8	19.5	20.5	0.3	0.2	0.3	0.3	204	204	18.6	20.5	18.6	16.3	16.5
54	17.3	18.1	19.5	0.3	0.4	0.4	0.4	218	218	17.9	18.9	19.5	17.2	17.4
55	19.1	18.3	18.4	4.1	2.0	0.7	2.3	406	406	18.1	18.0	17.2	18.6	19.7
56	17.9	18.7	22.8	0.3	0.0	0.0	0.1	167	167	16.7	17.4	18.1	15.8	16.1
57	12.4	12.7	13.3	1.2	1.1	1.1	1.1	244	244	12.7	13.1	15.0	12.2	12.0
58	30.8	30.5	30.7	5.3	5.1	4.3	4.9	550	464	29.3	29.7	30.7	29.1	27.9
59	6.7	6.2	6.1	2.4	2.4	2.4	2.4	268	268	6.2	6.1	6.1	6.7	7.9
60	8.5	9.3	10.1	0.6	0.5	1.0	0.7	572	572	8.7	9.4	9.5	8.1	8.6
61	8.5	9.3	10.1	0.6	0.5	1.0	0.7	572	572	8.7	9.4	9.5	8.1	8.6
62	10.4	11.1	12.0	2.1	2.3	2.3	2.2	267	267	11.0	11.8	11.9	10.3	9.7

## Phase 2

INTER PRETA TION	EXTREMES			TIMES				VALUE AT AVERAGE TIME						
	D50L50	D50	D50H50	D50L50	D50	D50H50	AVG TIME	EVENT #	EVENTS	D50	D50H50	D50H80	D50L50	D50L20
1	4.9	4.8	4.4	146.5	108.2	95.5	116.8	388	171	4.9	4.6	4.9	5.2	5.2
2	5.8	6.5	6.6	1.9	1.9	1.5	1.8	446	195	6.6	6.7	7.9	6.2	6.1
3	7.6	7.3	6.9	9.3	9.3	7.9	8.9	594	313	7.4	7.0	7.2	7.7	8.6
4	9.6	11.0	11.1	6.1	4.3	4.3	4.9	628	201	11.1	11.5	11.9	10.6	9.6

INTER PRETA TION	EXTREMES			TIMES				VALUE AT AVERAGE TIME						
	D50L50	D50	D50H50	D50L50	D50	D50H50	AVG TIME	EVENT #	EVENTS	D50	D50H50	D50H80	D50L50	D50L20
5	9.6	11.0	11.1	6.1	4.3	4.3	4.9	628	201	11.1	11.5	11.9	10.6	9.6
6	5.9	6.1	6.3	2.7	3.4	3.6	3.2	365	116	6.1	6.4	6.3	5.9	6.1
7	5.9	6.1	6.3	2.7	3.4	3.6	3.2	365	116	6.1	6.4	6.3	5.9	6.1
8	13.7	14.3	14.6	0.3	0.5	0.6	0.5	188	178	14.5	15.2	16.1	14.1	14.9
9	13.8	14.0	13.9	72.4	61.8	61.8	65.4	424	414	14.0	13.9	15.4	14.1	14.4
10	6.6	8.4	9.3	11.2	11.2	4.4	8.9	512	198	8.5	9.5	9.9	6.8	6.6
11	2.7	2.9	3.2	26.3	73.1	73.1	57.5	474	170	3.3	3.6	4.1	3.0	2.9
12	4.6	5.7	6.2	4.9	12.5	22.1	13.2	577	131	5.8	6.6	7.7	4.9	3.5
13	18.2	18.5	18.9	299.7	273.7	240.7	271.4	561	97	18.6	18.9	19.7	18.2	17.7
14	-	-	-	-	-	-	-	-	-	-	-	-	-	-
15	12.0	14.6	16.3	152.8	220.6	161.3	178.2	477	127	15.3	16.4	16.5	12.6	12.0
16	12.4	12.9	13.0	9.2	9.2	5.7	8.1	501	263	12.9	13.3	13.5	12.7	11.4
17	11.7	13.7	14.6	1.4	2.0	2.0	1.8	301	112	13.7	15.2	14.6	12.4	12.4
18	14.2	14.8	14.7	186.6	186.6	199.3	190.8	756	177	15.2	15.2	17.0	15.2	12.6
19	11.0	12.4	12.5	5.8	3.8	13.1	7.6	483	211	12.5	13.1	16.2	11.3	10.4
20	11.2	11.5	11.5	0.7	1.1	1.1	1.0	214	135	11.7	12.2	11.8	11.2	12.7
21	-	-	-	-	-	-	-	-	-	-	-	-	-	-
22	-	-	-	-	-	-	-	-	-	-	-	-	-	-
23	5.8	6.6	7.3	65.7	199.9	119.5	128.4	608	431	6.8	7.7	8.3	5.9	6.2
24	1.6	1.9	2.0	0.9	0.9	2.5	1.4	508	504	2.2	2.3	2.9	2.0	1.6
25	3.9	4.1	4.1	0.5	29.2	8.7	12.8	427	222	4.1	4.3	4.6	4.0	3.8
26	13.0	14.1	14.6	2.6	4.8	1.7	3.0	269	266	14.3	15.9	15.8	13.1	9.9
27	11.8	11.9	11.6	0.5	0.8	0.8	0.7	241	150	12.1	11.9	13.6	12.2	13.2
28	13.4	13.7	14.6	15.5	16.0	16.0	15.8	415	112	13.8	14.8	13.7	13.4	14.1
29	13.4	13.7	14.6	15.5	16.0	16.0	15.8	415	112	13.8	14.8	13.7	13.4	14.1
30	5.9	7.6	8.4	12.0	13.1	51.3	25.5	803	405	7.9	8.6	9.3	6.8	6.3
31	-	-	-	-	-	-	-	-	-	-	-	-	-	-
32	-	-	-	-	-	-	-	-	-	-	-	-	-	-
33	4.0	4.1	3.8	140.3	47.4	105.0	97.6	692	218	4.4	4.1	4.9	4.5	4.3
34	13.0	15.1	16.0	1.8	9.0	6.4	5.7	339	91	15.1	16.1	17.0	13.1	11.5
35	13.8	14.0	13.9	71.8	39.6	39.6	50.3	521	311	14.2	14.2	15.8	14.1	13.7
36	14.2	15.2	15.5	1.9	3.4	4.5	3.3	500	133	15.4	16.1	17.7	14.3	15.2
37	4.5	5.0	5.2	1.5	11.0	11.3	7.9	554	458	5.1	5.4	6.4	4.7	5.1
38	4.5	5.0	5.2	1.5	11.0	11.3	7.9	554	458	5.1	5.4	6.4	4.7	5.1
39	3.5	4.6	5.3	0.8	0.7	1.7	1.1	525	62	5.2	5.7	6.5	3.8	3.3
40	-	-	-	-	-	-	-	-	-	-	-	-	-	-
41	5.5	6.2	6.6	5.3	5.3	6.5	5.7	611	240	6.2	6.8	6.7	5.6	5.2
42	5.5	6.2	6.6	5.3	5.3	6.5	5.7	611	240	6.2	6.8	6.7	5.6	5.2
43	3.3	4.0	4.2	13.6	26.4	26.4	22.1	523	275	4.1	4.4	4.9	3.7	3.1

INTER PRETA TION	EXTREMES			TIMES				VALUE AT AVERAGE TIME						
	D50L50	D50	D50H50	D50L50	D50	D50H50	AVG TIME	EVENT #	EVENTS	D50	D50H50	D50H80	D50L50	D50L20
44	3.3	4.0	4.5	87.1	87.1	34.4	69.5	433	53	4.2	5.1	5.9	3.6	3.6
45	5.9	6.4	6.7	20.7	36.0	36.0	30.9	848	244	6.6	6.8	7.3	6.1	4.8
46	16.7	17.1	17.2	118.2	173.0	52.2	114.5	473	176	17.3	17.3	18.4	17.0	18.1
47	3.8	5.6	7.1	329.5	404.7	391.4	375.2	477	202	5.9	7.6	10.9	3.9	3.3
48	35.6	34.0	31.8	1.6	1.6	1.5	1.5	607	245	34.1	31.8	29.7	36.2	35.7
49	33.0	32.8	30.4	10.2	13.8	13.4	12.5	823	461	32.9	31.4	33.0	34.2	31.0
50	4.4	5.2	5.7	15.4	17.2	11.3	14.6	447	143	5.4	5.9	7.7	4.7	3.8
51	5.3	5.9	6.0	6.8	5.7	4.5	5.6	592	238	5.9	6.2	8.5	5.7	6.6
52	5.3	5.9	6.0	6.8	5.7	4.5	5.6	592	238	5.9	6.2	8.5	5.7	6.6
53	11.7	13.1	14.6	86.8	119.5	119.5	108.6	605	401	13.7	15.5	16.1	11.7	11.0
54	16.0	16.5	16.5	6.3	6.3	5.6	6.0	480	262	16.5	16.6	17.2	16.5	16.9
55	16.7	16.6	16.3	20.1	31.1	38.5	29.9	589	183	16.8	16.4	17.2	16.9	18.8
56	13.3	14.7	15.0	11.6	34.5	31.4	25.8	577	410	15.5	15.7	13.1	14.6	16.5
57	10.2	11.4	12.4	65.5	24.8	5.1	31.8	400	156	11.7	12.6	16.8	10.6	10.9
58	-	-	-	-	-	-	-	-	-	-	-	-	-	-
59	3.7	3.8	3.6	358.8	273.1	273.1	301.7	638	370	3.8	3.6	3.4	3.9	3.7
60	4.3	4.5	4.4	10.1	10.1	9.5	9.9	1034	462	4.5	4.6	5.0	4.4	4.2
61	4.3	4.5	4.3	34.7	10.1	33.4	26.1	1134	562	5.7	6.5	6.8	5.4	4.2
62	9.1	10.4	11.5	10.7	8.8	4.0	7.8	337	70	10.6	11.8	12.6	9.6	9.8

### Phase 3

INTER PRETA TION	EXTREMES			TIMES				VALUE AT AVERAGE TIME						
	D50L50	D50	D50H50	D50L50	D50	D50H50	AVG TIME	EVENT #	EVENTS	D50	D50H50	D50H80	D50L50	D50L20
1	-	-	-	-	-	-	-	-	-	-	-	-	-	-
2	7.1	7.6	8.3	6.1	7.7	16.3	10.1	558	112	7.6	8.1	8.6	7.0	7.1
3	8.1	8.0	8.1	73.3	94.1	131.4	99.6	802	208	7.9	7.9	7.5	8.0	7.5
4	12.2	12.6	13.6	14.5	18.3	18.3	17.0	866	238	12.4	13.1	13.3	11.9	11.9
5	12.2	12.6	13.6	14.5	18.3	18.3	17.0	866	238	12.4	13.1	13.3	11.9	11.9
6	7.2	7.6	7.8	25.4	73.5	70.6	56.5	484	119	7.5	7.7	7.5	7.1	8.1
7	7.6	8.3	8.7	383.5	383.5	345.2	370.7	588	223	8.2	8.7	9.4	7.4	6.6
8	14.5	14.9	15.6	0.8	0.9	1.0	0.9	231	43	14.6	15.4	17.7	14.5	14.5
9	17.1	18.6	20.6	732.0	839.3	893.0	821.4	543	119	18.2	19.9	21.4	17.1	17.1
10	8.9	9.7	10.3	52.2	103.9	95.4	83.9	667	155	9.4	9.8	10.3	8.3	6.7
11	3.3	3.6	3.9	130.3	132.3	124.9	129.2	619	145	3.6	3.9	5.3	3.2	2.7
12	7.7	8.1	8.9	71.4	68.8	67.6	69.3	1056	479	8.0	8.8	9.0	7.0	7.9
13	-	-	-	-	-	-	-	-	-	-	-	-	-	-
14	-	-	-	-	-	-	-	-	-	-	-	-	-	-
15	-	-	-	-	-	-	-	-	-	-	-	-	-	-

INTER PRETA TION	EXTREMES			TIMES				VALUE AT AVERAGE TIME						
	D50L50	D50	D50H50	D50L50	D50	D50H50	AVG TIME	EVENT #	EVENTS	D50	D50H50	D50H80	D50L50	D50L20
16	14.5	14.9	15.4	131.5	122.0	101.6	118.4	809	308	14.6	15.3	14.6	13.9	13.6
17	16.5	16.6	18.2	36.1	26.8	17.4	26.8	579	278	16.5	17.1	18.2	13.7	11.5
18	17.1	17.8	19.0	391.0	392.1	452.0	411.7	963	207	17.5	18.6	19.3	17.0	18.8
19	13.3	13.5	14.3	15.1	25.8	28.9	23.3	574	91	13.2	13.5	16.5	13.1	12.1
20	13.6	15.0	17.0	87.6	113.5	81.9	94.3	455	241	14.9	16.9	17.6	13.6	15.0
21	-	-	-	-	-	-	-	-	-	-	-	-	-	-
22	-	-	-	-	-	-	-	-	-	-	-	-	-	-
23	-	-	-	-	-	-	-	-	-	-	-	-	-	-
24	3.3	3.0	3.0	6.5	7.2	7.0	6.9	747	239	3.0	2.9	2.9	3.2	3.6
25	4.4	4.6	5.1	415.5	203.3	211.5	276.8	574	147	4.4	4.8	5.5	4.2	3.6
26	14.5	15.0	16.4	9.1	11.8	12.8	11.2	341	72	14.7	15.8	14.6	13.8	12.7
27	12.9	12.7	12.8	48.8	105.6	112.9	89.1	380	139	12.5	12.3	13.6	12.7	14.1
28	14.7	15.5	16.7	428.7	409.5	389.7	409.3	560	145	15.5	16.7	17.4	14.5	14.4
29	14.7	15.5	16.7	428.7	409.5	389.7	409.3	560	145	15.5	16.7	17.4	14.5	14.4
30	8.6	9.7	11.2	216.6	204.5	204.7	208.6	1047	244	9.7	11.1	11.6	8.5	8.3
31	-	-	-	-	-	-	-	-	-	-	-	-	-	-
32	-	-	-	-	-	-	-	-	-	-	-	-	-	-
33	4.7	4.7	5.0	243.5	215.4	255.3	238.1	768	76	4.7	4.9	5.0	4.6	4.9
34	15.7	15.9	16.9	156.4	155.3	23.2	111.6	450	111	15.8	15.9	17.1	14.9	14.8
35	14.9	14.9	15.6	281.6	311.0	312.5	301.7	677	156	14.7	14.9	16.0	14.7	14.5
36	16.2	16.3	16.6	61.5	87.1	87.1	78.6	728	228	16.2	16.4	15.3	16.2	15.8
37	6.7	6.8	6.9	203.5	274.3	274.2	250.7	795	241	6.6	6.8	7.3	6.4	5.1
38	6.7	6.8	6.9	203.5	274.3	274.2	250.7	795	241	6.6	6.8	7.3	6.4	5.1
39	5.2	5.8	6.3	40.1	22.9	6.1	23.1	806	281	5.8	6.1	6.1	5.0	4.6
40	-	-	-	-	-	-	-	-	-	-	-	-	-	-
41	6.7	7.0	7.4	85.3	65.9	65.2	72.1	755	144	7.0	7.4	8.1	6.7	6.4
42	6.7	7.0	7.4	85.3	65.9	65.2	72.1	755	144	7.0	7.4	8.1	6.7	6.4
43	3.7	4.2	4.6	88.4	54.5	98.4	80.4	572	49	4.1	4.5	4.9	3.5	3.1
44	3.6	4.4	5.5	152.2	217.0	182.3	183.8	484	51	4.3	5.5	6.8	3.6	3.7
45	6.5	7.0	7.4	74.0	138.6	169.5	127.3	932	84	6.9	7.3	7.2	6.3	5.8
46	-	-	-	-	-	-	-	-	-	-	-	-	-	-
47	-	-	-	-	-	-	-	-	-	-	-	-	-	-
48	36.3	35.9	35.0	2.4	2.7	2.6	2.5	656	49	35.7	34.2	33.9	36.2	36.6
49	39.5	36.6	35.3	69.5	61.9	94.4	75.2	994	171	35.9	33.9	33.9	37.1	38.7
50	7.8	8.3	8.8	242.1	239.9	239.9	240.7	684	237	8.3	8.8	7.2	7.6	5.0
51	7.3	7.3	8.5	15.0	15.6	11.2	13.9	766	174	7.1	7.1	9.1	7.1	6.8
52	8.1	8.5	9.2	191.4	192.1	82.0	155.2	1237	645	8.4	8.8	9.2	7.6	7.2
53	12.7	14.8	16.9	1211.4	1164.5	1206.9	1194.2	741	136	14.8	16.7	17.0	12.7	12.3
54	18.2	17.7	18.0	134.3	134.3	228.6	165.7	705	225	17.6	17.6	18.4	17.7	18.5

INTER PRETA TION	EXTREMES			TIMES				VALUE AT AVERAGE TIME						
	D <sub>50</sub> L <sub>50</sub>	D <sub>50</sub>	D <sub>50</sub> H <sub>50</sub>	D <sub>50</sub> L <sub>50</sub>	D <sub>50</sub>	D <sub>50</sub> H <sub>50</sub>	AVG TIME	EVENT #	EVENTS	D <sub>50</sub>	D <sub>50</sub> H <sub>50</sub>	D <sub>50</sub> H <sub>80</sub>	D <sub>50</sub> L <sub>50</sub>	D <sub>50</sub> L <sub>20</sub>
55	18.3	17.8	16.8	114.2	155.3	58.9	109.5	681	92	17.5	16.5	17.0	18.2	20.8
56	22.2	19.1	16.4	296.2	673.8	793.8	587.9	781	204	18.7	15.3	14.0	20.5	21.4
57	11.4	12.5	13.4	311.6	304.1	323.7	313.1	507	107	12.5	13.3	15.5	11.4	12.0
58	-	-	-	-	-	-	-	-	-	-	-	-	-	-
59	4.4	4.4	4.2	427.0	427.0	425.8	426.6	716	78	4.3	4.2	2.8	4.4	4.3
60	5.8	5.7	6.5	27.6	25.8	22.8	25.4	1133	99	5.6	6.5	6.2	5.1	4.2
61	7.2	7.1	7.6	160.1	159.5	174.4	164.6	1845	711	6.4	6.7	8.4	6.2	5.9
62	9.6	10.9	12.1	13.4	13.4	14.7	13.8	371	34	10.9	12.0	12.7	9.6	10.3